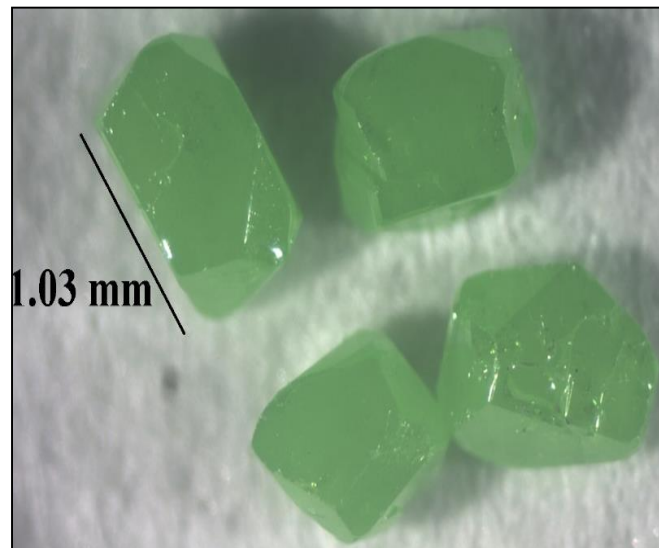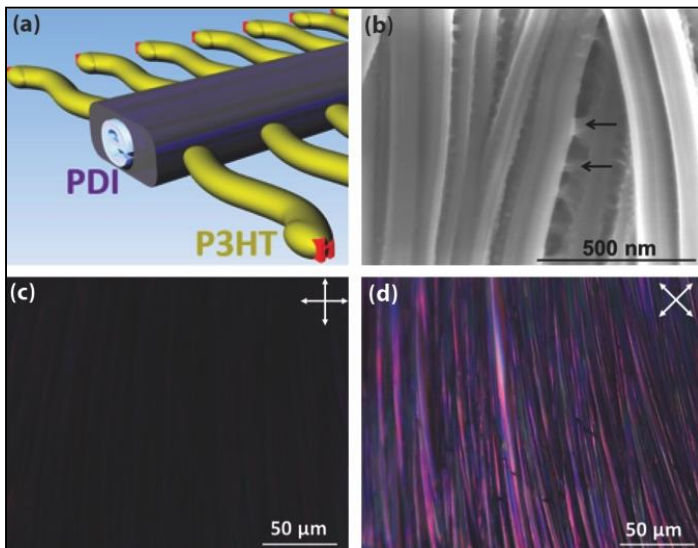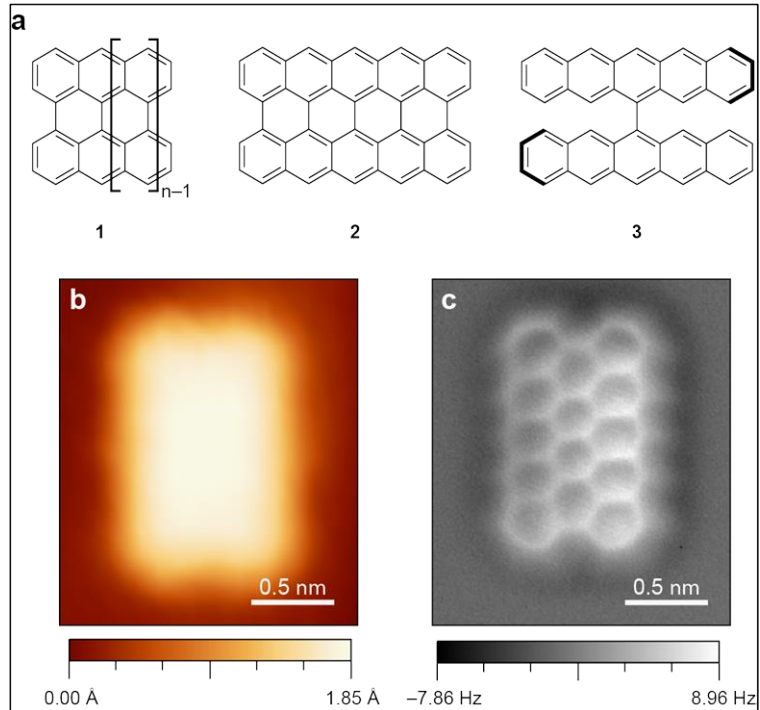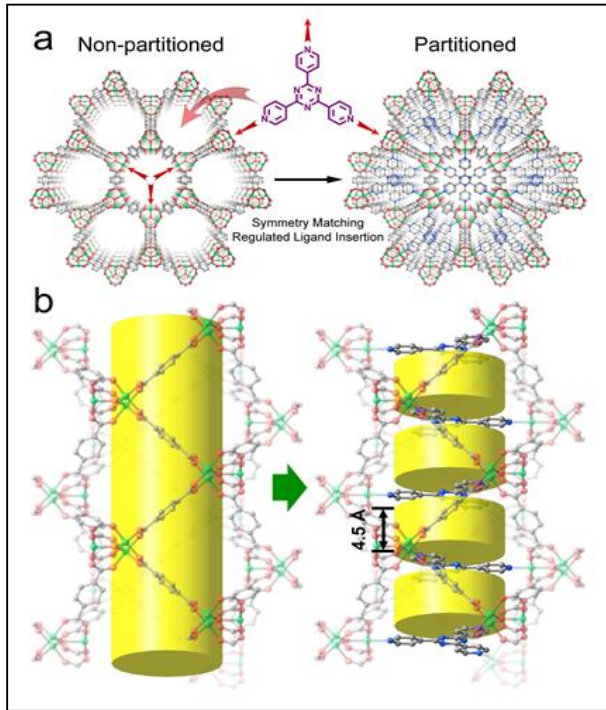# Materials Chemistry
Principal Investigators' Meeting–2016
July 12-14, 2016
Hilton Washington DC North Hotel, Gaithersburg, MD

U.S. DEPARTMENT OF ENERGY

Office of Basic Energy Sciences
Materials Sciences and Engineering Division

On the Cover

Top Left: Illustration of pore space partition in a metal organic framework (MOF) compound achieved through symmetry matching regulated ligand insertion. (a) Viewed along c axis and (b) Side view of the channels showing the cylindrical channel before and after partition. (green: Ni, red: O, blue: N, grey: C).
Pingyun Feng, UC Riverside

Top Right: (a) Chemical structure of n-periacene (1), peripentacene (2), and 6,6'-bipentacene (3). (b) Constant-current STM image of 2. (c) nc-AFM image of 2.
Felix Fischer, UC Berkeley

Bottom Left: (a) Schematic illustration of P3HT/PDI hybrid shish-kebab structures; (b) Scanning electron micrograph of aligned shish-kebab films: arrows denote bundles of P3HT nanowires; (c-d) Polarized optical micrographs showing a high degree of orientation in aligned shish-kebab films.
Ryan Hayward, University of Massachusetts, Amherst

Bottom Right: Example of products from hydrothermal reactions. Single crystals of $Pr_2TaO_5(OH)$ 1mm/edge.
Joseph Kolis, Clemson University

Table of Contents

i

University Grant Projects

Foreword

This document is a collection of abstracts of the presentations made at the Principal Investigators' Meeting of the Materials Chemistry program, sponsored by the Materials Sciences and Engineering (MSE) division in the Office of Basic Energy Sciences (BES) of the U. S. Department of Energy (DOE). The meeting was held on July 12–14, 2016, at the Hilton Washington DC North Hotel in Gaithersburg, Maryland, and is one of a series of principal investigators' meetings organized by BES. The purpose of the meeting is to bring together all the Principal Investigators with currently active projects in the Materials Chemistry program for the multiple purposes of raising awareness among PIs of the overall program content and of each other's research, encouraging exchange of ideas, promoting collaboration and stimulating innovation. The meeting also provides an opportunity for the Program Managers and MSE/BES management to get a comprehensive overview of the program on a periodic basis, which provides opportunities to identify program needs and potential new research directions. The meeting agenda is organized in nine sessions around topical areas in materials research that encompass many of the projects in the current Materials Chemistry portfolio. These include Porous Media; Materials for Energy Storage/Conversion (I and II); Self-Assembly/Soft Matter (I and II); Synthesis and Crystal Growth; Surfaces, Liquids, and Nanomaterials; Hybrid Materials; and Interfacial Chemistry.

Recent BES workshops and other reports have identified as a Grand Challenge goal the ability to design and synthesize new materials having specific properties tailored and optimized for use in next-generation technologies. In support of this objective, the Materials Chemistry program supports basic research in the discovery, design and synthesis of materials with an emphasis on elucidating the complex relationships between a material's functional properties and its composition, atomic and molecular structure and higher-order morphology. Major focus areas of the program include the discovery, synthesis and characterization of new materials and the manipulation of materials' structure across a range of length scales using *chemistry*.

We thank all of the meeting attendees, including the invited speakers, for their active participation and for sharing their ideas and new research results. The assistance of the Meeting Chairs, Svilen Bobev and Nicholas Melosh, in organizing this meeting is greatly appreciated. Sincere thanks also go to Teresa Crockett in MSE and Linda Severs and her colleagues at the Oak Ridge Institute for Science and Education (ORISE) for their excellent work providing all the logistical support for the meeting.

Michael Sennett
Craig Henderson
Program Managers, Materials Chemistry
Materials Sciences and Engineering Division
Office of Basic Energy Sciences
U.S. Department of Energy

AGENDA
2016 Materials Chemistry PI Meeting
Hilton Gaithersburg, 620 Perry Parkway, Gaithersburg, MD

Day 1 (Tuesday, July 12, 2016)

7:30 – 8:30 am *Breakfast*

8:30 – 8:45 am *Welcome*
Linda Horton, Director, Materials Sciences and Engineering Division, Basic Energy Sciences

8:45 – 9:00 am *Introductory Remarks*
Michael Sennett and Craig Henderson, Program Managers, Materials Chemistry
Meeting Chairs: **Svilen Bobev**, University of Delaware, and **Nicholas Melosh**
SLAC National Accelerator Laboratory

9:00 – 9:30 am **James De Yoreo** (Invited), Pacific Northwest National Laboratory
2016 Basic Research Needs for Synthesis Science for Energy Relevant Technology Workshop

Session I ***Porous Media. Metal and Covalent Organic Frameworks***
<u>Chair</u>*: Svilen Bobev, University of Delaware*

9:30 – 9:50 am **Yves J. Chabal**, University of Texas, Dallas (talk given by Timo Thonhauser)
Synthesizing New Metal Organic Frameworks with Tailored Physical and Chemical Properties

9:50 – 10:10 am **Adam J. Matzger**, University of Michigan
Leveraging Kinetic Control in the Assembly and Sorption Properties of Nanostructured Porous Material

10:10 – 10:30 am Break

10:30 – 10:50 am **Seth Cohen**, University of California, San Diego
Functionalization of Metal-Organic Frameworks - PolyMOFs

10:50 – 11:10 am **Pingyun Feng**, University of California, Riverside
Pore Space Engineering and Functionalization in Porous Metal-Organic Framework Materials

11:10 – 11:30 am **Sarah H. Tolbert**, University of California, Los Angeles
Using Nanoporous Materials to Understand Kinetic Constraints in Pseudocapacitive Energy Storage

11:30 – 12:50 pm Working Lunch
Informal discussions and poster introductions

Session II   *Materials for Energy Storage/Conversion I*
<u>Chair</u>: *Larry Curtiss, Argonne National Laboratory*

12:50 – 1:20 pm   **Nenad M. Markovic**, Argonne National Laboratory
Energy and Fuels from Multifunctional Electrochemical Interfaces

1:20 – 1:40 pm   **Arumugam Manthiram**, University of Texas, Austin
Materials and Interfacial Chemistry for Next-Generation Electrical Energy
Storage

1:40 – 2:00 pm   **Sheng Dai**, Oak Ridge National Laboratory
Materials and Interfacial Chemistry for Next Generation Electrical Energy
Storage

2:00 – 2:20 pm   **Jodie L. Lutkenhaus**, Texas A&M University
The Nature of Charge Storage in Nitroxide Radical Polymers

2:20 – 2:40 pm   **Christopher Ober**, Cornell University
Engineering Transport in Confined Environments of Self-Assembled Stable
Radical Polymers

2:40 – 3:00 pm   Break

Session III   *Self-Assembly, Soft Matter I*
<u>Chair</u>: *Thomas Gennett, National Renewable Energy Laboratory*

3:00 – 3:30 pm   **Vera Bocharova**, Oak Ridge National Laboratory
Dynamics in Multicomponent Polymeric Materials

3:30 – 3:50 pm   **Lisa M. Hall**, Ohio State University
Designing Efficient Nanostructured Polymer Electrolytes Using Tapered Block
Polymers - Joint Experiment and Theory Effort in Controlled Interface Design

3:50 – 4:10 pm   **Gregory M. Grason**, University of Massachusetts, Amherst
Ordered Phases of Chiral Block Copolymers: Mesochiral, Periodic
Nanostructures via Self-Assembly

4:10 – 6:00 pm   Poster Session 1

6:00 – 8:00 pm   Working Dinner

Day 2 (Wednesday, July 13, 2016)

7:30 – 8:30 am   Breakfast

8:30 – 9:00 am   **John Sarrao** (Invited), Los Alamos National Laboratory
BESAC report "Challenges at the Frontiers of Matter and Energy:
Transformative Opportunities for Discovery Science"

Session IV   ***Synthesis and Crystal Growth***
<u>Chair</u>: ***Hanno zur Loye, University of South Carolina***

9:00 – 9:20 am   **Mercouri G. Kanatzidis**, Argonne National Laboratory
Rational Synthesis of Superconductors

9:20 – 9:40 am   **Joseph W. Kolis**, Clemson University
Synthesis and Single Crystals of Refractory Oxides of Lanthanides and Thorium

9:40 – 10:00 am   **Svilen Bobev**, University of Delaware
Novel Pnictides with *d*- and *f*-Metals as Prospective Materials for Thermal
Energy Conversion

10:00 – 10:20 am   Break

Session V   ***Materials for Energy Storage/Conversion II***
<u>Chair</u>: ***Kirill Kovnir, University of California, Davis***

10:20 – 10:50 am   **Song Jin**, University of Wisconsin
Fundamental Studies of Charge Transfer in Nanoscale Heterostructures of Earth-
Abundant Semiconductors for Solar Energy Conversion

10:50 – 11:10 am   **Howard E. Katz**, Johns Hopkins University
Statically Polarized Polymer Heterostructures for Charge Carrier Density Control
in Energy-Relevant Semiconductors

11:10 – 11:30 am   **Shyue Ping Ong**, University of California, San Diego
Elucidating the Determinants of Alkali Ionic Conductivity in Oxide and Sulfide
Frameworks

11:30 – 11:50 am   **Vinayak P. Dravid**, Northwestern University
Design of Next Generation Thermoelectrics

11:50 – 1:10 pm   Working Lunch - Informal discussions and poster introductions

1:10 – 1:30 pm   **Craig Henderson** and **Michael Sennett**
BES Presentation on Programmatic Issues

Session VI   ***Self-Assembly, Soft Matter II***
                                 Chair: ***Ryan Hayward, University of Massachusetts, Amherst***

1:30 – 2:00 pm   **Paul Braun**, University of Illinois, Urbana-Champaign
                                 Programming Function via Soft Materials

2:00 – 2:20 pm   **Bryan Pivovar**, National Renewable Energy Laboratory
                                 Hydroxide Conductors for Energy Conversion Devices

2:20 – 2:40 pm   **Juan de Pablo**, Argonne National Laboratory (talk given by Paul Nealey)
                                 Solvent-Assisted Non-Equilibrium Directed Self-Assembly of Complex Polymeric
                                 Materials

2:40 – 3:00 pm   Break

Session VII   ***Surfaces, Liquids, and Nanomaterials***
                                 Chair: ***Sarah Tolbert, University of California, Los Angeles***

3:00 – 3:30 pm   **Miquel B. Salmeron**, Lawrence Berkeley National Laboratory
                                 Chemical and Mechanical Properties of Surfaces, Interfaces and Nanostructures

3:30 – 3:50 pm   **Jacob Israelachvili**, University of California, Santa Barbara
                                 Relationships between the Chemistry and Physical Interaction Forces (Adhesion,
                                 Friction & Lubrication) between Closely Apposed Surfaces in Liquids

3:50 – 4:10 pm   **Felix R Fischer**, University of California, Berkeley
                                 Atomically Defined Doping of Graphene Nanoribbons for Mesoscale Electronics

4:10 – 4:30 pm   **Richard L. Brutchey**, University of Southern California
                                 Low-Temperature Chemical Routes to Functional Complex Oxide Nanocrystals

4:30 – 6:00 pm   Poster Session 2

6:00 – 8:00 pm   Working Dinner

Day 3 (Thursday, July 14, 2016)

7:15 – 8:15 am   Breakfast

Session VIII   *Hybrid Materials*
<u>Chair</u>: *Miquel Salmeron, Lawrence Berkeley National Laboratory*

8:15 – 8:45 am   **Ram Seshadri**, University of California, Santa Barbara
Hybrid Halide Perovskites: Advancing Optoelectronic Materials

8:45 – 9:05 am   **Rebekka S. Klausen**, Johns Hopkins University
Mesoscale Fragments of Crystalline Silicon by Chemical Synthesis

9:05 – 9:25 am   **Xiangfeng Duan**, University of California, Los Angeles
Scalable Growth and Charge Transport Properties of Perovskite Microplate
Crystal Array

9:25 – 9:55 am   **Vladimir V. Tsukruk**, Georgia Institute of Technology
Mesoscale Photophysical Properties of Anisotropic Hybrid Nanostructure
Assemblies

9:55 – 10:10 am   Break

Session IX   *Interfacial Chemistry*
<u>Chair</u>: *Nicholas Melosh, SLAC National Accelerator Laboratory*

10:10 – 10:40 am   **Paul Alivisatos**, Lawrence Berkeley National Laboratory
Synthesis and Properties of Perovskite Nanostructures

10:40 – 11:00 am   **Xiaoyang Zhu**, Columbia University
Charge Carrier Dynamics in Hybrid Organic-Inorganic Semiconductors

11:00 – 11:30 am   **Ting Xu**, Lawrence Berkeley National Laboratory
Organic/inorganic Nanocomposites

11:30 – 12:00 pm   Program Managers and Meeting Chairs
Wrap-up, debriefing, evaluation

12:00 pm   Departure

LABORATORY PROJECTS

Synthesis and Properties of Perovskite Nanostructures

A. P. Alivisatos, S. Leone, and P. Yang

Lawrence Berkeley National Lab

Program Scope

The resurgence of interest in perovskite materials has prompted us to initiate a program to synthesize and characterize perovskite nanostructures with controlled dimensionality. We have prepared one, two and three-dimensionally confined nanoparticles with narrow control over the confined dimensions. We have studied the structural and photophysical properties of these materials. Current work is directed towards investigations of electron transfer processes in these new materials and to the processes of charge injection.

Recent Progress

We have reported synthesis of ultrathin two-dimensional (2D) $(C_4H_9NH_3)_2PbX_4$ (X = Cl, Br, I) organic-inorganic materials which represents the first well-controlled ultrathin 2D ionic materials to be created.[1] This material consists of ideal quantum wells with monolayers of PbX_4^{2-} sheets sandwiched between layers of organic chains, with thicknesses down to a single monolayer, exhibiting blue-shifted photoluminescence and

structural relaxation relative to the bulk analogue. A related study focused on all-inorganic colloidal $CsPbBr_3$ 2D plates
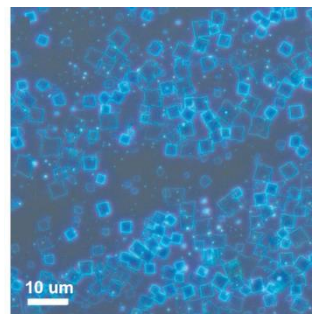
Figure 1: 2D Hybrid Perovskites.

and 1D wires.[2-3] The incorporation of Cs^+ to replace the organic cation increases the melting point and the overall thermal stability of the crystal. Band gap tunability was exhibited through taking advantage of quantum confinement *via* modulation of 2D plate thickness. Furthermore, halide-exchange reactions were used to systematically replace the Br halide component with Cl or I to attain band gaps spanning from the ultraviolet to the infrared region both in the 2D and 1D crystals[4]. A kinetic study of the halide exchange process have shown, desperate exchange mechanisms with I replacing Br significantly faster than the Br to Cl anion exchange. These findings are important for developing better understanding of anion migration and segregation in lead-halide perovskite devices.

Future Plans

In our future research, the transformation between different perovskite phases of the halide perovskite NCs will be systematically investigated. Due to the relatively weak bonding in halide perovskites, lattice distortion and atom displacement are very common. These characteristics lead to rich phase diagrams in halide perovskites, especially on the nanoscale. The exact structure and phase of the crystal influence the optoelectronic properties of the materials strongly. Therefore, understanding the phase transformation of the halide perovskites

nanostructures is scientifically important. In addition to crystal structure changes, changes are anticipated in band gap and, as a result, in the photoluminescence wavelength, quantum yield, charge carrier density, mobility, and other related optoelectronic properties. The carrier dynamics will be investigated in different crystal phases using ultrafast optical spectroscopy. Such properties directly determine the performance of related optoelectronic devices based on halide perovskite NCs.

The surprising thin film device performance and high PLQY in perovskite nanostructures suggest a high tolerance to defects and non-trivial charge carrier dynamics. A study of trap charge carrier dynamics is important, in which these trap states are characterized spectroscopically and the real time charge trapping/de-trapping dynamics are observed. By combining expertise in interfacial synthetic methods, device fabrication, and ultrafast X-ray spectroscopy, the transient dynamics of charges will be observed with chemical specificity. These experiments will investigate the roles of both bulk and surface states, correlate these dynamics with the performance of devices, and develop perovskite synthetic methods for controlling bulk and surface properties. Two interesting aspects of this study are achieving a better understanding of whether lead (Pb) plays a role in increasing the electronic tolerance to defects in these materials, as well as exploring alternative, less toxic compounds that demonstrate similar properties.

Synthesis of lead-free perovskite materials by replacement of Pb^{2+} with Sn^{2+} or Ge^{2+} represents an important area we would like to explore. In particular, $CsSnI_3$ is a material known to be highly conductive with a solar relevant band-gap of 1.3 eV and strong photoluminescence in the near IR. The synthesis of low dimensionality lead free QDs, NWs and ultrathin sheets present another model system to explore fundamental properties such as charge transfer and charge injection at the nanoscale.

Trapping of charges at localized defect states in semiconductor NCs impedes both charge transport and radiative recombination, limiting the efficiency of any NC-based optoelectronic device. On the single NC level, charge carrier trapping leads to intermittencies in the emitted fluorescence, known as blinking; thus, the study of fluorescence blinking in individual NCs provides a unique probe of the charge trapping processes that ultimately govern device performance. Referred to as defect-tolerant semiconductors, lead halide perovskites are thought to have no inter-band trap states, but they instead possess a distribution of trap states in resonance with the valence band states.[5] As such, the nature and energetics of trap states in perovskite confined systems are likely very different than in the more traditional, colloidal QDs that do suffer from the presence of deep trap energy levels. The investigation of single particle perovskite nanoparticles blinking properties, will contribute to the fundamental understanding of how this new class of materials differs from typical semiconductors.

References

(1) Dou, L.; Wong, A. B.; Yu, Y.; Lai, M.; Kornienko, N.; Eaton, S. W.; Fu, A.; Bischak, C. G.; Ma, J.; Ding, T. Science 2015, 349, 1518.

(2) Bekenstein, Y.; Koscher, B. A.; Eaton, S. W.; Yang, P.; Alivisatos, A. P. J. Am. Chem. Soc. 2015.

(3) Zhang, D.; Eaton, S. W.; Yu, Y.; Dou, L.; Yang, P. J. Am. Chem. Soc. 2015, 137, 9230.

(4) Zhang, D., Yang, Y, Bekenstein, Y, Yu, Y, Gibson, N, Eaton, S, Kornienko, N, Lai, M, Kong, Q, Alivisatos, A. P, Leone, S, Yang, P . J. Am. Chem. Soc. 2016.

(5) Brandt, R. E.; Stevanović, V.; Ginley, D. S.; Buonassisi, T. MRS Comm. 2015, 5, 265.

Publications

SW Eaton, M Lai, N Gibson, AB Wong, L Dou, J Ma, LW Wang, SR Leone and P Yang. "Lasing in Robust Cesium Lead Halide Nanowires," *Proc. Natl. Acad. Sci. U.S.A.* 113 (8), pp 1993-1998 (2016).

KK Sakimoto, AB Wong and P Yang. "Self-photosensitization of Non-photosynthetic Bacteria for Solar-to-chemical Production," *Science* 351 (6268), pp 74-77 (2016).

J Resasco, H Zhang, N Kornienko, N Becknell, H Lee, J Guo, A Briseno, P Yang. "TiO2/BiVO4 Nanowire Heterostructure Photoanodes Based on Type II Band Alignment", *ACS Central Science* 2 (2), pp 80-88 (2016).

D Zhang, SW Eaton, Y Yu, L Dou, P Yang. "Solution-phase Synthesis of Cesium Lead Halide Perovskite Nanowires," *J. Am. Chem. Soc.* 137 (29), pp 9230–9233 (2015).

AB Wong, M Lai, SW Eaton, Y Yu, E Lin, L Dou, A Fu, P Yang. "Growth and Anion Exchange Conversion of $CH_3NH_3PbX_3$ Nanorod Arrays for Light-Emitting Diodes," *Nano. Lett*. 15 (8), pp 5519–5524 (2015).

J Park, H Elmlund, P Ercius, JM Yuk, DT Limmer, Q Chen, K Kim, SH Han, DA Weitz, A Zettl, AP Alivisatos. "3D Structure of Individual Nanocrystals in Solution by Electron Microscopy," *Science* 349 (6245), pp 290-295 (2015).

C Liu, JJ Gallagher, KK Sakimoto, EM Nichols, CJ Chang, MCY Chang, P Yang. "Nanowire-Bacteria Hybrids for Unassisted Solar Carbon Dioxide Fixation to Value-Added Chemicals," *Nano Lett.* 15 (5), pp 3634–3639 (2015).

N Kornienko, J Resasco, N Becknell, CM Jiang, YS Liu, K Nie, X Sun, J Guo, SR Leone, P Yang. "*Operando* Spectroscopic Analysis of an Amorphous Cobalt Sulfide Hydrogen Evolution Electrocatalyst*," J. Am. Chem. Soc.* 137 (23), pp 7448–7455 (2015).

N Kornienko, DD Whitmore, Y Yu, SR Leone, P Yang. "Solution Phase Synthesis of Indium Gallium Phosphide Alloy Nanowires," *ACS Nano* 9 (4), pp 3951–3960 (2015).

L Amirav, F Oba, S Aloni, AP Alivisatos. "Modular Synthesis of a Dual Metal-Dual Semiconductor Nano-Heterostructure," *Angew. Chem. Int. Ed.* 54 (24), pp 7007-7011 (2015).

TX Ding, JH Olshansky, SR Leone, AP Alivisatos. "Efficiency of Hole Transfer from Photoexcited Quantum Dots to Covalently Linked Molecular Species," *J. Am. Chem. Soc.* 137 (5), pp 2021-2029 (2015).

D Kim, KK Sakimoto, D Hong, P Yang. "Artificial Photosynthesis for Sustainable Fuel and Chemical Production," *Angew. Chem. Int. Ed.* 54 (11), pp 3259-3266 (2015).

L Zhang, C Liu, AB Wong, J Resasco, P Yang. "MoS_2-wrapped Silicon Nanowires for Photoelectrochemical Water Reduction," *Nano Research* 8 (1), pp 281-287 (2015).

B Liu, CH Wu, J Miao, P Yang. "All Inorganic Semiconductor Nanowire Mesh for Direct Solar Water Splitting," *ACS Nano* 8 (11), pp 11739-11744 (2014).

L Zhang, K Liu, AB Wong, J Kim, X Hong, C Liu, T Cao, SG Louie, F Wang, P Yang. "Three-Dimensional Spirals of Atomic Layered MoS_2," *Nano Letters* 14 (11), pp 6418-6423 (2014).

CM Jiang, LR Baker, JM Lucas, J Vura-Weis, AP Alivisatos, SR Leone. "Characterization of Photo-Induced Charge Transfer and Hot Carrier Relaxation Pathways in Spinel Cobalt Oxide (Co_3O_4)," *J. Phys. Chem.* 118 (39), pp 22774-22784 (2014).

LR Baker, CM Jiang, ST Kelly, JM Lucas, J Vura-Weis, MK Gilles, AP Alivisatos, SR Leone. "Charge Carrier Dynamics of Photoexcited Co_3O_4 in Methanol: Extending High Harmonic Transient Absorption Spectroscopy to Liquid Environments," *Nano Letters* 14 (10), pp 5883-5890 (2014).

D Zhang, AB Wong, Y Yu, S Brittman, J Sun, A Fu, B Beberwyck, AP Alivisatos, P Yang. "Phase-Selective Cation-Exchange Chemistry in Sulfide Nanowire Systems," *J. Am. Chem. Soc.* 136 (50), pp 17430-17433 (2014).

C Liu, P Yang. "Introductory Lecture: Systems Materials Engineering Approach for Solar-to-Chemical Conversion," *Faraday Discussions* 176, pp 9-16 (2015).

L Dou, AB Wong, Y Yu, M Lai, N Kornienko, SW Eaton, A Fu, CG Bischak, J Ma, T Ding, NS Ginsberg, LW Wang, AP Alivisatos, P Yang, "Atomically Thin Two-dimensional Organic-inorganic Hybrid Perovskites," *Science* 349 (6255), pp 1518-1521 (2015).

J Sun, F Cui, C Kisielowski, Y Yu, N Kornienko, and P Yang, "Low-Temperature Solution-Phase Growth of Silicon and Silicon-Containing Alloy Nanowires," *J. Phys. Chem. C* Article ASAP (2015).

Liu C, Dasgupta NP and Yang P, "Semiconductor Nanowires for Artificial Photosynthesis," *Chem. Mater.* 26(1), 415-422 (2014).

Resasco J, Dasgupta NP, Rosell JR, Guo J and Yang P., "Uniform doping of metal oxide nanowires using solid state diffusion," *J Am Chem Soc.* 136(29), 10521-6 (2014).

Sakimoto KK, Liu C, Lim J and Yang P., "Salt-induced self-assembly of bacteria on nanowire arrays," *Nano Lett.* 14(9), 5471-6 (2014).

Tarafder K, Surendranath Y, Olshansky JH, Alivisatos PA and Lin-Wang Wang, "Hole Transfer Dynamics from a CdSe/CdS Quantum Rod to a Tethered Ferrocene Derivative," *JACS* 136, 5121-5131 (2014).

Wittenberg JS, Miller TA, Szilagyi E, Lutker K, Quirin F, Lu W, Lemke H, Zhu D, Chollet M, Robinson J, Wen H, Sokolowski-Tinten K and Alivisatos AP, and Lindenberg AM, "Real-Time Visualization of Nanocrystal Solid-Solid Transformation Pathways," *Nano Lett*. 14(4), 1995-9 (2014).

Rao PM, Cai L, Liu C, Cho I, Lee C, Weisse JM, Yang P and Zheng X., "Simultaneously Efficient Light Absorption and Charge Separation in WO3/BiVO4 Core/Shell Nanowire Photoanode for Photoelectrochemical Water Oxidation," *Nano. Lett.* 14, 1099 (2014).

Dynamics in Multicomponent Polymeric Materials

Lead PI: A. P. Sokolov,[1,2]
PIs: B. Sumpter,[3,4] **T. Saito,**[1] <u>**V. Bocharova**</u>,[1] **J. Mays,**[2] **M. Dadmun,**[2] **K. Schweizer**[5]

[1]**Chemical Sciences Division, Oak Ridge National Laboratory, Oak Ridge, Tennessee 37831, USA**
[2]**Department of Chemistry, University of Tennessee, Knoxville, Tennessee 37996, USA**
[3]**Center for Nanophase Materials Sciences, Oak Ridge National Laboratory, Oak Ridge, Tennessee 37831, United States**
[4]**Computer Science and Mathematics Division, Oak Ridge National Laboratory, Oak Ridge, Tennessee 37831, United States**
[5]**Department of Materials Science and Chemistry, Frederick Seitz Materials Research Laboratory, University of Illinois, Urbana, Illinois 61801, USA**

Program Scope

The overarching goal of the proposed research is to develop a fundamental, predictive understanding of dynamics in multicomponent polymeric materials, and establish how interfacial structure, properties and interactions, combined with mesoscale confinement, affect molecular motions and macroscopic properties in these intrinsically heterogeneous materials. The pervasive presence of interfaces between different phases or species in multicomponent systems, and their effect on bulk properties, is the unifying aspect of our research. We address the following fundamental issues: How do the nanoparticle-polymer interactions and polymer rigidity affect the structure and dynamics in the interfacial region? How do confinement and interactions affect polymer and nanoparticles diffusion? How are viscoelastic properties of composites affected by nanoparticle size, softness and surface fluctuations? How do molecular architecture and morphology of segregated block copolymers affect structure and dynamics of the interfacial region and macroscopic viscoelastic properties of these materials? We will pursue a comprehensive interdisciplinary approach led by advanced theory and simulations, precise synthesis and state-of-the-art characterization (with special emphasis on neutron scattering). The proposed research connects well to the priority research directions formulated in the BESAC report on Mesoscale Science and the DOE report on Computational Materials Science and Chemistry. The fundamental knowledge developed in this program will contribute to the scientific foundation for the rational design of multicomponent polymer based materials with superior properties and function that can address many DOE challenges.

Recent Progress

Recently, it has been realized that macroscopic properties of multicomponent materials such as e.g. polymer nanocomposites and block copolymers are strongly affected by the interfacial layer formed between different components. In particular case of polymer

nanocomposites (PNC), the presence of an interfacial layer around nanoparticles has been demonstrated in experimental studies of static and dynamic properties, and it became clear that the interfacial layer is the key to control macroscopic properties of these materials. However, there is no clear understanding of the major parameters controlling the structure and properties of the interfacial layer in PNC.

Here, we present detailed studies of structure and dynamics of the interfacial layer in several model nanocomposites [1-5]. We employed Small-angle X-ray scattering (SAXS), Broadband dielectric spectroscopy (BDS), Brillion light scattering (BLS), advanced atomic force microscopy (AFM), and several other techniques to study the structure and dynamic properties of the interfacial layer. Our experimental studies were coupled to theory [1] and simulations [4] to reveal macroscopic details of the underlying phenomena. These studies developed new approaches to analyze segmental dynamics and mechanical properties of the interfacial layer at the nanoscale [1,3]. We discovered that an increase in molecular weight (MW) of a polymer decreases the thickness of the interfacial layer and diminishes changes in its properties [2]. This result contradicts to theoretical predictions, and we ascribe it to frustration in chain packing in the interfacial layer that increases with MW. Our studies revealed that the mechanical modulus of the interfacial layer is more than two times higher than the modulus of a neat polymer [3]. Moreover, using advanced AFM technique we were able to map the nanoscale gradient of mechanical properties in PNC [3]. Detailed coarse-grained simulation studies helped us to demonstrate the increase in the interfacial layer thickness with increase in chain rigidity [4]. Analysis of composites with chemically grafted chains revealed that the way of chain attachments (chemically bonded or physically adsorbed) plays no important role in segmental dynamics, and chain stretching induced by the nanoparticles in the interfacial layer plays the major role [5]. The presented results deepen our fundamental understanding of structure and dynamics of polymeric nanocomposites, and provide novel insight that can be used to optimize the design of polymeric materials for many applications, including gas separation and electrical energy storage devices.

Future Plans

Experimental studies and theoretical developments to understand factors affecting structure and properties of the interfacial layer in composite materials, the role of chain rigidity and nanoparticle size and softness, and the role of interfacial layer in macroscopic properties. Specific focus is on synthesis and characterization of polymers with complex architectures including star-like and grafted block-copolymers to address the role of architecture in formation of interfacial layer. Furthermore, experimental and theoretical studies of diffusion of polymers and nanoparticles in nanocomposite materials will be pursued in future.

References

1. S. Cheng, et al., **J. Chem. Phys. 143**, 194704 (2015).

2. Cheng, et al., **Phys. Rev. Lett 116**, 038302 (2016).
3. Cheng, S., et al. **Nano Lett.** (2016. in press), DOI: 10.1021/acs.nanolett.6b00766
4. J.M.Y. Carrillo, et al., **Macromolecules 48**, 4207 (2015).
5. A. P. Holt, et al., **ACS Nano** (2016, in press).

Publications

1.   D.Banerjee et al., Macromolecules 46, 8732 (2013).
2.   S.Mirigian et al., J.Phys.Chem.Lett. 4, 3648 (2013).
3.   D.W. Holley et al., Polymer 55, 58-65 (2014).
4.   Holt, Adam et al., Macromolecules 47, 1837-1843 (2014).
5.   J.G. Kennemur et al.,, Macromolecules 47, 1411-1418 (20014).
6.   S.Mirigian et al., J.Chemical Physics 140, 194506 (2014).
7.   S.Mirigian et al.,J.Chemical Physics 140, 194507 (2014).
8.   H. Chen et al.,J. Mat. Chem. A 2, 9883-9890 (2014).
9.   Jan-Michael Y. Carrillo, et al.,J. Chem. Phys. 141, 074904 (2014).
10.   Y. Wang, et al.,Polymer, 55, 4067 - 4076 (2014).
11.   S. Bobade, et al.,Macromolecules, 47, 5040 - 5050 (2014).
12.   H. Chen, et al.,Chemistry of Materials, 26, 3993−4003 (2014).
13.   H. Chen, et al., Adv. Funct. Mat., 24, 5129-5136 (2014).
14.   P. J. Griffin, et al., Soft Matter 9, 10373-10380 (2013).
15.   Clemens Liedel, et al., Small 9, 3276-3281 (2013).
16.   D.M.Sussman et al.,J. Chemical Physics 139, 234904 (2013).
17.   Dergunov, Sergey; et al.,Chem. Commun., 49 (94), 11026 – 11028 (2013).
18.   Y. M. Shulga, et al.,RSC Advances 4, 587-592 (2014).
19.   Kim, Mariya et al., Langmuir 30, 7061−7069 (2014
20.   V. K. Srivastava, et al., Adv. Func. Mater., 24, 4969 – 4977 (2014).
21.   Yangyang Wang, et al.,Sol. St. Ionics 262, 782-784 (2014).
22.   H. Chen, et al.,Adv. Funct. Mat., 24, 140-150 (2014).
23.   D.N. Voylov, et al., Carbon 69, 563-570 (2014).
24.   J.T. Kalathi, et al.,Phys.Rev.Lett., 112, 108301 (2014).
25.   D.M.Sussman, et al.,Macromolecules, 47 (18), p. 6462–6472 (2014).
26.   Bing Huang, et al., Phys. Rev. X, 4, 021029 (2014).
27.   Vikram K. Srivastava, et al.,Ind. & Eng. Chem. Res., 53, 9781 – 9791 (2014).
28.   Y. Matsuda, et al., Polymer, 55, 4369 - 4378 (2014).
29.   S. Mirigian et al., J. Chemical Physics-Communications 141, 161103 (2014).
30.   S. Mirigian, et al., Macromolecules 48, 1901 (2015).
31.   Jan-Michael Y. Carrillo, et al., Macromolecules 48, 4207−4219 (2015).
32.   D. Banerjee J. et al., Chemical Physics 142, 214903 (2015).
33.   D. Banerjee J. et al., Polymer Science Polymer Physics 53, 1098 (2015).
34.   Beom-Goo Kang, et al., Polymer Chemistry 6, 6732 - 6738 (2015).

35.   A. Imel, et al., Polymer 75, 134-140 (2015).
36.   T. Etampawala, et al., Polymer, 61, 155-162 (2015).
37.   H. Chen, et al., Adv. Funct. Mater. 24, 7284–7290 (2014).
38.   Bocharova, V et al., Adv. Funct. Mater 25, 805-811 (2015).
39.   Kumar, R et al., Nanoscale 7, 947-955 (2015). DOI: 10.1039/c4nr05491a
40.   T. Wu, et al., J. Phys. Chem. C 119, 2727 - 2732 (2015). DOI: 10.1021/acs/jpcc.5b0082
41.   Y. Matsuda, et al., Polym. J. 47, 282 - 285 (2015). DOI: 10.1038/pj.2014.102
42.   Y. Wang, et al., Curr. Opinion in Chem. Engineering 7, 113-119 (2015).
43.   Y. M. Shulga et al., RSC Advances 5, 9865-9874 (2015).
44.   Olga S. Ovchinnikova , et al., ACS Nano 9, 4260–4269 (2015).
45.   Hao Sun, et al., J. Rheology 59, 751 - 767 (2015).
46.   J. Liu, et al., ACS Macroletters 4, 1072-1076 (2015
47.   C.S. Lee, et al., Advanced Functional Materials 25, 5848-5857 (2015).
48.   Fan, Fei; et al., Macromolecules 48, 4461-4470 (2015).

Two-Dimensional Chalcogenide Nanomaterials

Yi Cui (Lead), Harold Hwang, Jun-Sik Lee, Shoucheng Zhang.

Stanford Institute for Materials and Energy Sciences, SLAC National Accelerator Laboratory

1. Program Scope

Our vision is to build a cutting-edge interdisciplinary program on two-dimensional (2D) chalcogenide (O, S, Se, Te) nanomaterials, with emphasis on their design, growth, and basic electronic, spintronics, electrochemical and catalytic properties. We envision that our research can lead to the rational design and creation of "2D Artificial Materials" with exciting properties. They will form a basis for new materials approaches to charge storage and transfer for advanced batteries and fuel cells, novel electronics/spintronics, catalysis, thermoelectrics, and hybrid functionalities.

2. Recent Progress

With the support in past two years, we have focused on electrostatic, chemical and electrochemical tuning of three types of layer-structured chalcogenides, (Bi_2Se_3, MoS_2 and BiTeI) and demonstrate that novel electronic, optoelectronic and catalytic properties can be designed rationally. For oxides, we have successfully realized the technique development for generating free-standing films. We summarize the key achievements during of the past two years as below.

2.1 Progress on novel 2D materials synthesis

Vertically aligned 2D layered materials and their heterostructures: (Fig. 1a to d, *JACS*, **136**, 4897 (2014); *ACS Nano*, **8**, 4940 (2014)) Most 2D materials studied in the literature including binary dichalcogenides such as MoS_2 and graphene are inclined to be terminated by the basal planes to reduce the exposed edges due to their inherently high surface energy. However, exposing the edges of 2D materials can provide exciting control opportunities of their electronic and catalytic properties. We have successfully developed the synthesis and structural characterization of a family of 2D-layered metal dichalcogenide nanofilms (MoS_2, $MoSe_2$, WS_2, WSe_2) whose crystal layers are perpendicular to the substrate surface.

Vertical and lateral heterostructures (Manuscripts in preparation) We report an *in situ* two-step synthesis process to form TI lateral heterostructures. We demonstrated the novel exciton states obtained from the heterostructure. This novel device geometry opens up exciting opportunities for a variety of electronic and optoelectronic devices, complementary to the recent interesting vertical heterostructures with horizontal atomic layers.

Free standing perosvkite oxide films (Fig. 1e, Nature Materials, accepted): Many important complex oxides do not have van der Waals interfaces, and thus cannot be exfoliated in 2D

nanomaterials form. If we could create such structures, however, this would greatly expand the available properties for incorporation in stacked structures. They would also enable many new experimental techniques (transmission x-ray/electron microscopy/spectroscopy) and devices. Here we demonstrate a general method to create freestanding oxide membranes based on a thin film growth technique.

2.2 Progress on electronic property and tuning

The 2D nanomaterials are interesting materials for novel electronic properties and afford the opportunity to tune them chemically and electrochemically. We have achieved four stages of interesting results, paving the road for our vision for the rational design and creation of a family of "2D Artificial Materials".
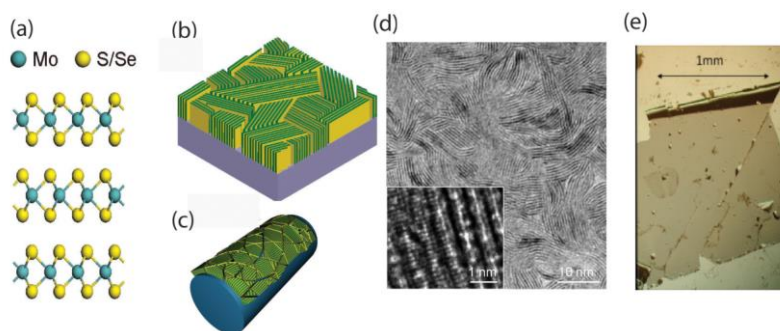
Figure 1: a) Crystal structure of MoS_2 and $MoSe_2$. Schematic of vertically aligned 2D layered materials on b) flat substrate and c) rough substrate. d) Transmission electron microscopy image of MoS_2 vertical layers. e) Optical microscope image of a $Nd_{0.5}Sr_{0.5}MnO_3$ free-standing epitaxial film transferred onto a sapphire substrate.

Electronic structure of layered chalcogenides: (Fig. 2a, b, *Nano Letters* 2016 in press). Layered transition metal chalcogenides with large spin orbit coupling have recently sparked much interest due to their potential applications for electronic, optoelectronic, spintronics and valleytronics. However, most current understanding of the electronic structure near band valleys in momentum space is based on either theoretical investigations or optical measurements, leaving the detailed band structure elusive. For example, the exact position of the conduction band valley of bulk MoS_2 remains controversial. Using angle-resolved photoemission spectroscopy with sub-micron spatial resolution (micro-ARPES), we systematically imaged the conduction/valence band structure evolution across representative chalcogenides MoS_2, WS_2 and WSe_2, as well as the thickness dependent electronic structure from bulk to the monolayer limit.

Superconductivity of mono- and bilayer MoS_2 by ionic liquid gating: (Fig. 2 d, e, Manuscript in preparation) Superconductors at the atomic two-dimensional (2D) limit are the focus of an enduring fascination in the condensed matter community. This is majorly because, with the reduced dimensions, the effects of disorders, fluctuations, and correlations in superconductors become particularly prominent at the atomic 2D limit; thus such superconductors provide opportunities to tackle tough theoretical and experimental challenges. We report the observation of ultrathin 2D superconductivity in mono- and bilayer molybdenum disulfide (MoS_2) with electric-double-layer (EDL) gating.
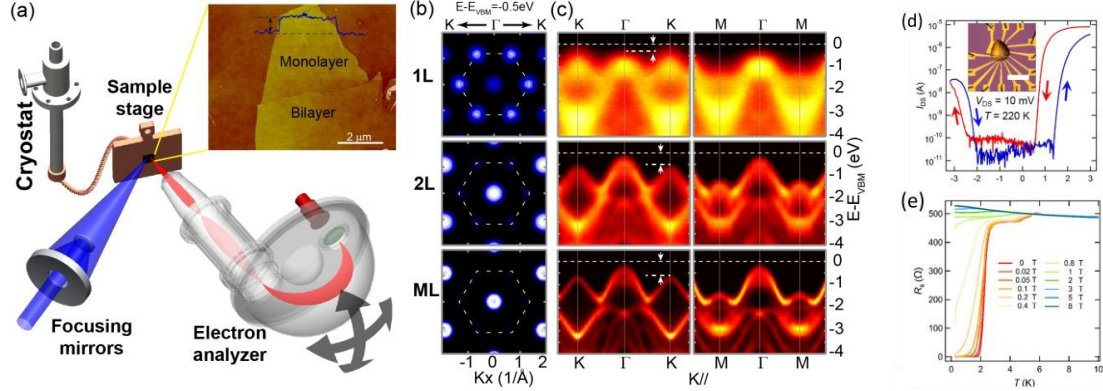
Figure 2. (a) Schematic drawing of ARPES apparatus examining at MoS_2 thin layer samples, (b) and (c) Electronic band structure plot for monolayer (1L), bilayer (2L) and multilayer (ML) MoS_2. (d) Typical ambipolar transfer curves obtained from a bilayer MoS_2 EDLT device at 220 K (blue: scanning V_{LG} forward; red: scanning V_{LG} backward). V_{DS} was fixed at 10 mV. Inset: optical microscope image of a bilayer MoS_2 EDLT device. T dependent R_s of a bilayer MoS_2 device under different perpendicular magnetic fields.

Electrical control of spin coupled valley current in WSe₂: (*Nature Nanotech.* 9, 851–857 (2014)) The valley degree of freedom in layered transition-metal dichalcogenides (MX_2) provides the opportunity to extend functionalities of novel spintronics and valleytronics devices. Due to spin splitting induced by spin-orbital coupling (SOC), the non-equilibrium charge carrier imbalance between two degenerate and inequivalent valleys to realize valley/spin polarization has been successfully demonstrated theoretically and supported by optical experiments. However, the generation of a valley/spin current by the valley polarization in MX_2 remains elusive and a great challenge. Here, within an electric-double-layer transistor based on WSe_2, we demonstrated a spin-coupled valley photocurrent whose direction and magnitude depend on the degree of circular polarization of the incident radiation and can be further greatly modulated with an external electric field.

Direct imaging of nanoscale conductance evolution in gel-gated oxide transistors (Nano Lett. 15, 4730 (2015)) Electrostatic modification of functional materials by electrolytic gating has demonstrated a remarkably wide range of density modulation, a condition crucial for developing novel electronic phases in systems ranging from complex oxides to layered chalcogenides. Yet little is known microscopically when carriers are modulated in electrolyte-gated electric double-layer transistors (EDLTs) due to the technical challenge of imaging the buried electrolyte-semiconductor interface. We demonstrate the real-space mapping of the channel conductance in ZnO EDLTs using a cryogenic microwave impedance microscope.

Extraordinary optical transmission of 2D Bi₂Se₃ nanoplates by chemical tuning: (*Nature Commun.* 5, 5670 (2014), *Nano Lett.* 15, 6777 (2015)) Tuning the optical property is a new direction of our nanomaterials research. We discovered extraordinary light transmission through thin nanoplates of layered *Bi₂Se₃* and *Bi₂Te₃* nanoplates by chemical intercalation of copper atoms, which is contrary to most bulk materials in which doping reduces the light transmission. We explained this surprising behavior with two combined mechanisms: a chemical tuning effect of substantial reduction of material absorption after intercalation, and a nanophotonic effect of zero-wave antireflection unique to the ultra-small thickness of our nanoplates. We demonstrated that the synergy of these two effects in 2D nanostructures can be exploited for various optoelectronic applications including transparent electrodes.

13

Photodetection in black phosphorus and ReS₂: (*Nature Nanotech* 10, 419 (2015), *Adv. Funct. Mater.* 26, 1938 (2015)) Two-dimensional transition metal dichalcogenides are emerging with tremendous potentials for many optoelectronic applications due to strong light-matter interaction and p-n junction geometry. We have demonstrate a broadband photodetector using layered black phosphorus transistors which is polarization sensitive over a broad bandwidth from about 400 nm to 3750 nm. The polarization-sensitivity is due to the strong intrinsic linear dichroism, which arises from the in-plane optical anisotropy of this material.

High pressure induced insulator to metal transition: (*Nature Commun.* 6, 6991 (2015)) We investigated the insulator-metal phase transition behavior of layered 2H-MoSe₂ using pressure generated by a Diamond Anvil Cell. We found that pressure allows MoSe₂ to change from a highly anisotropic 2D layered network to an isotropic 3D solid where the van der Waals gap is effectively closed. With continuous contractions in lattice parameters under pressure, MoSe₂ evolves from a semiconductor to a metal with the "indirect" feature of its band structure being well preserved.
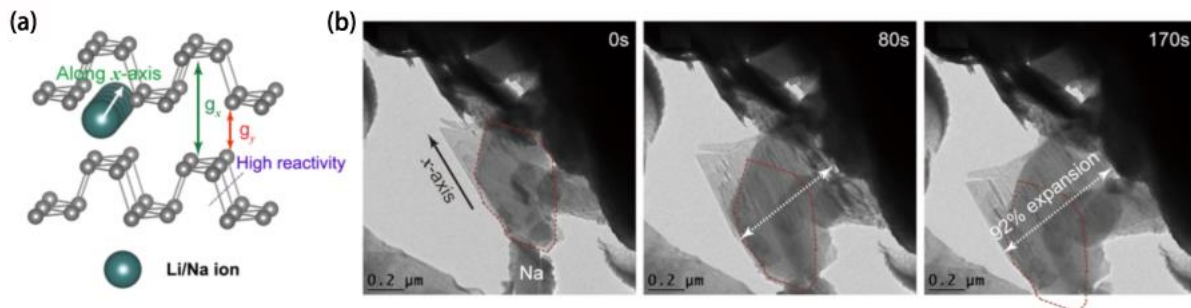
Figure 4. (a) Schematics of black phosphorus for lithiation or sodiation, (b) Time-lapse TEM images of the sodiation in black phosphorus.

Layered black phosphorus for negative electrode (Fig. 4, *Nature Nanotech.* 10, 980 (2015)) Phosphorus is an attractive negative electrode material for sodium ion batteries due to its high theoretical specific capacity of 2596 mAh g^{-1}. However, it suffers poor conductivity (10^{-12} S m^{-1}), slow reaction dynamics, and large volume expansion (440%) during the sodiation process, leading to rapid capacity decay upon cycling. We developed hydrids of layered graphene and black phosphorus to overcome this problem.

3. Future Plan

During the past two years of funded research, we have produced exciting results to lay down the foundation for a vision of "2D Artificial Materials" in the MSD at SLAC. We will continue our exciting directions outlined during the remainder of the 1st year. Specifically, we will continue our effort on synthesizing unique 2D layered materials and freestanding oxide nano-films and extend our research into layered structure-oxide hybrid materials from these components. We will continue electron transport, ARPES and optical property measurement on chimerically/electrochemically tuned 2D nanomaterials and elucidate their microscopic physics. In coming year, a key additional effort will to combine chalcogenide and oxide synthesis techniques together to pursue hybrid structures grown *in situ*.

4. Publications

1.   J. Yao, K. J. Koski, W. Luo, J. J. Cha, L. Hu, D. Kong, V. K. Narasimhan, K. Huo, and Y. Cui, *Nature Communications* **5**, 5670 (2014).
2.   S. S. Hong, Y. Zhang, J. J. Cha, X.-L. Qi, and Y. Cui, , *Nano Letters* **14**, 2815 (2014).
3.   H. Wang, Z. Lu, D. Kong, J. Sun, T. M. Hymel, and Y. Cui, *ACS Nano* **8**, 4940-4947(2014).
4.   D. Kong, H. Wang, Z. Lu, and Y. Cui, *Journal of the American Chemical Society* **136**, 4897-4900 (2014).
5.   J. P. Motter, K. J. Koski, and Y. Cui, *Chemistry of Materials* **26**, 2313-2317 (2014).
6.   H. Wang, C. Tsai, D. Kong, K. Chan, F. Abild-Pedersen, J. K. Norskov, and Y. Cui, *Nano Research* **8**, 566-575 (2015).
7.   H. T. Yuan, X. Q. Wang, B. Lian, H. Zhang, X. Fang, B. Shen, G. Xu, Y. Xu, S. C. Zhang, H. Y. Hwang, and Y. Cui, *Nature Nanotechnology* **9**, 851–857 (2014).
8.   H. T. Yuan, X. G. Liu, F. Afshinmanesh, W. Li, G. Xu, J. Sun, B. Lian, G. J. Ye, Y. Hikita, Z. X. Shen, S.-C. Zhang, X. H. Chen, M. Brongersma, H. Y. Hwang, Y. Cui, *Nature Nanotechnology* **10**, 419 (2015).
9.   H. T. Yuan, H. T. Wang, Y. Cui, *Accounts of Chemical Research* **48**, 81-90 (2015).
10.   H. T. Wang, H. T. Yuan, S. S. Hong, Y.B. Li, Y. Cui, *Chemical Society Reviews* **44**, 2664-80 (2015).
11.   Z. Zhao, H. J. Zhang, H. T. Yuan, S. B. Wang, Y. Lin, Q. S. Zeng, Z. Liu, K. D. Patel, G. K. Solanki, Y. Cui, H. Y. Hwang, W. L. Mao,   *Nature Communications* **6**, 6991 (2015).
12.   E. Liu, Y. Fu, Y. Wang, Y. Feng, Y. Pan, H. Liu, X. Wan, W. Zhou, B. Wang, Z. Cao, L. Wang, A. Li, J. Zeng, F. Song, X. Wang, Y. Shi, H. T. Yuan, H. Y. Hwang, Y. Cui, F. Miao & D. Xing. *Nature Communications* **6**, 7312 (2015).
13.   S. S. Hong, D. Kong, and Y. Cui, *MRS Bulletin* **39**, 873 (2014)
14.   H. Wang, Q. Zhang, H. Yao, Z. Liang, H.-W. Lee, P.-C. Hsu, G. Zheng, and Y. Cui, *Nano Letters* (2014) DOI:10.1021/NL503730C.
15.   J. H. Yu, H. R. Lee, S. S. Hong, D. Kong, H.-W. Lee, H. Wang, F. Xiong, S. Wang, and Y. Cui, *Nano Letters* (2015) DOI:10.1021/NL503897H.
16.   J. Sun, H.-W. Lee, M. Pasta, H. T. Yuan, G. Zheng, Y. Sun, Y. Li & Y. Cui. *Nature Nanotechnology* **10**, 980–985 (2015).
17.   F. Xiong, H. T. Wang, X. G. Liu, J. Sun, M. Brongersma, E. Pop, & Yi Cui. *Nano Letters* **15**, 6777–6784 (2015).
18.   Y. Li, J. Zhang, G. Zheng, Y. Sun, S. S. Hong, F. Xiong, S. Wang, H. R. Lee, and Y. Cui, *ACS Nano* **9**, 10916-10921 (2015).
19.   W. Chen, H. Wang, Y. Li, Y. Liu, J. Sun, S. Lee, J.-S. Lee, and Y. Cui, *ACS Central Science* (2015) DOI:10.1021/acscentsci.5b00227
20.   Haotian Wang, Hyun-Wook Lee, Yong Deng, Zhiyi Lu, Po-Chun Hsu, Yayuan Liu, Dingchang Lin and Yi Cui, *Nature Communications* **6**, 7261 (2015).
21.   J. Sun, H.-W. Lee, M. Pastac, Y. M. Sun, W. Liu, Y. B. Li, H. R. Lee, N. Liu, Y. Cui, *Energy Storage Materials* **4**, 130–136 (2016).
22.   Y. Ren, H. T. Yuan, X. Y. Wu, Z. Y. Chen, Y. Iwasa, Y. Cui, H. Y. Hwang, K. J. Lai, *Nano Letters* **15**, 4730-4736 (2015).
23.   V. Thareja, J. H. Kang, Hongtao Yuan, K. M. Milaninia, H. Y. Hwang, Y. Cui, P. G. Kik, M. L. Brongersma, *Nano Letters* **15**, 1570-1576 (2015).

24.   E. Liu, M. Long, J. Zeng, W. Luo, Y. Wang, Y. Pan, W. Zhou, B. Wang, W. Hu, Z. Ni, Y. You, X. Zhang, S. Qin, Y. Shi, Z. Liang, K. Watanabe, T. Taniguchi, H. T. Yuan, H. Y. Hwang, Y. Cui, F. Miao & D. Xing, *Adv. Funct. Mater*, **26**, 1938–1944 (2016).

25.   H. T. Yuan, B. Zhou, G. Xu, Z. K. Liu, S. F. Wu, D. Dumcenco, K. Yan, Y. Zhang, S. K. Mo, P. Dudin, V. Kandyba, M. Yablonskikh, A. Barinov, Z. X. Shen, S. C. Zhang, Y. S. Huang, X. D. Xu, Z. Hussain, H. Y. Hwang, Y. Cui, and Y. L. Chen, , *Nano Letters*, accepted.

Cluster/Carbon Composite Materials for Energy

Larry A. Curtiss, Stefan Vajda, Peter Zapol, and Michael J. Pellin
Materials Science Division
Argonne National Laboratory
Argonne, Il 60516

Program Scope
In this program we seek a fundamental understanding of a novel class of materials based on supported subnanometer clusters and support materials under electrochemical conditions. We use our unique capabilities to synthesize well-defined small clusters of specific size and composition, which we have demonstrated that can be stable, highly active, and selective on the right type of support for a variety of catalytic reactions. Materials based on size-specific subnanometer clusters are attractive for catalysis because (1) they have well-defined and identical catalytic sites, (2) the number of sites can be precisely controlled, (3) their activity can provide valuable insights into catalytic mechanisms, and (4) calculations can be done at sufficient accuracy to allow guidance for design of optimal clusters. A key part of the program is the support material. One of the supports that we are using is a form of diamond referred to as ultrananocrystalline diamond (UNCD), which has many unique properties due to combining sp^3 diamond grains with sp^2–like carbon grain boundaries in one material. We also use our capabilities to synthesize metal oxide supports for the clusters. Another key part of this program is the use of characterization and computational capabilities to both understand the properties of the new cluster/nanocarbon composites as well as to perform screening to find optimal candidate clusters to be used on the supports. Here size-specific subnanometer cluster samples provide a unique test environment for synchrotron and mass spectrometric based analysis.

Recent Progress
Supported Cu Clusters for CO₂ Reduction
The activation of CO_2 and its hydrogenation to methanol is of much interest as a way to utilize captured CO_2. In this work we investigate the use of size-selected Cu_4 clusters supported on Al_2O_3 thin films for CO_2 reduction in the presence of hydrogen.[1] Cu_4 clusters were synthesized using a size-selected cluster source, which enables single-size mass selection with atomic precision without fragmentation. The Cu_4 cluster was chosen based on preliminary density functional (DFT) calculations indicating they are active for methanol formation. The catalytic activity was measured under near-atmospheric reaction conditions with a low CO_2 partial pressure, and the oxidation state of the clusters was investigated by in situ grazing incidence X-ray absorption spectroscopy. The results indicate that size-selected Cu_4 clusters are the most active low-pressure catalyst for catalytic CO_2 conversion to CH_3OH. Density functional theory calculations were carried out for the reaction pathways on Cu_4 clusters as shown in Figure 1 and revealed low activation barriers for conversion of CO_2 to CH_3OH. The low reaction barrier for Cu_4 can be explained by the adsorption strength of the adsorbate species to the catalyst. To the best of knowledge the Al_2O_3 supported size-selected Cu_4 clusters exhibit the highest reported activity to date for CO_2 reduction to CH_3OH at a low CO_2 partial pressure. These results for size-selected Cu clusters demonstrate their great potential for the development of novel low-pressure

catalysts for CH₃OH synthesis from catalytic conversion of CO_2 using alternative feed streams with low CO_2 concentration.
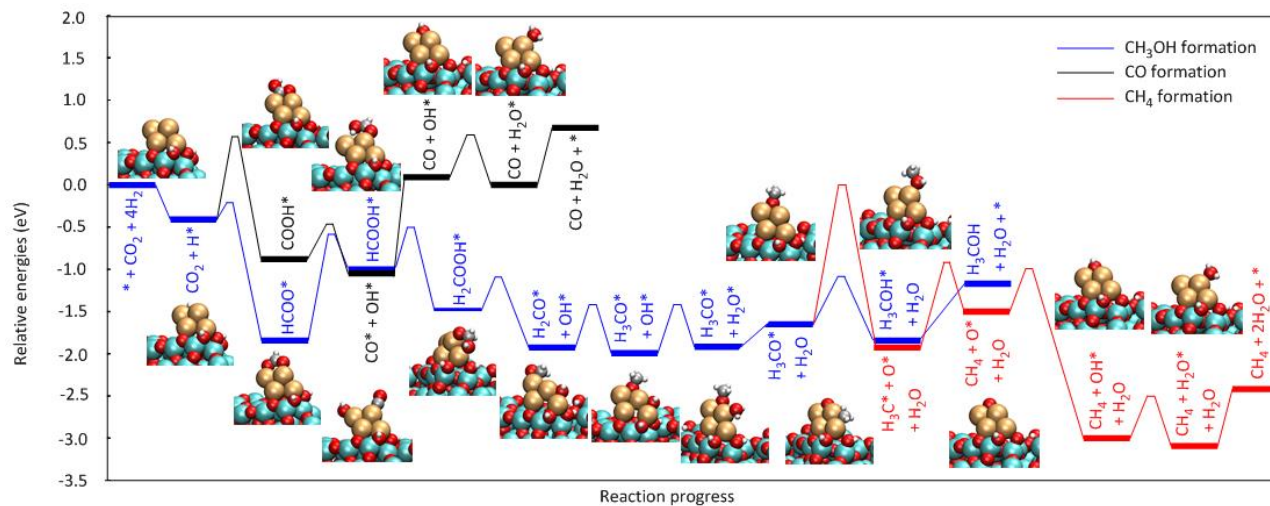
Figure 1. Calculated reaction pathways of CO_2 reduction to CH_3OH, CO and CH_4 on Al_2O_3 supported Cu_4 clusters. The catalyst surface site is labeled as "*". To improve legibility, "H_2" was omitted from the labels after the initial state.

Subnanometer copper clusters have been suggested by computational studies from this project to be a good candidate material for CO_2 electrochemical reduction, being able to lower the overpotential in the reaction. In collaboration with G. Centi's group (University of Messina) experimental measurements have been carried out on the electrochemical behavior (in the presence of N_2 or CO_2) of size-controlled naked Cu_5 and Cu_{20} nanoclusters, prepared using a combination of gas-phase cluster ion sources, mass spectrometry, and soft-landing techniques[2]. Cu_{20} nanoclusters show anodic redox processes occurring at much lower potential with respect to Cu_5 nanoclusters, which behave relatively similar to much larger Cu particles. However, Cu_5 nanocluster coordinate effectively CO_2 (hydrogen carbonate) in solution differently from Cu_{20} nanoclusters and larger Cu particles. This effect, rather than the redox behavior, is apparently connected to the ability of Cu_5 nanoclusters to reduce CO_2 under cathodic conditions at low overpotential. Although preliminary, these results provide rather exciting indications on the possibility to realize low overpotential electrocatalytic conversion of CO_2 using clusters.

Supported Co Clusters for Water Oxidation

The complexity of the water oxidation reaction makes understanding the role of individual catalytic sites critical to improving the process. Recently, size selected Co_{27} metal clusters deposited on Fe_2O_3 anodes were tested for water oxidation activity as shown in Figure 2.[3] The uniformity of these anodes containing isolated Co_{27} catalytic sites allows measurement of the activity of catalytic sites of known nuclearity and known density. Grazing Incidence X-ray Absorption Spectroscopy (GIXAS) investigation of the anodes before and after electrochemical and/or photochemical (0.4 suns) cycling demonstrate that these Co_{27} clusters are stable (both to dissolution and to aggregation) even in the harsh water oxidation electrochemical environment. The clusters show turnover frequencies per cobalt atom for water oxidation that are significantly

higher than the Atomic Layer Deposition (ALD) grown Fe_2O_3 alone. Moreover, annealing under controlled oxidation conditions significantly improves the turnover rates.

Figure 2. Electrochemical behavior of a Si electrode (grey dashed curve), Fe_2O_3 ALD coated Si electrode (green curve) and a heat treated Co_{27} covered Fe_2O_3 ALD coated Si electrode (red curve) in the dark (left) and under illumination (right).
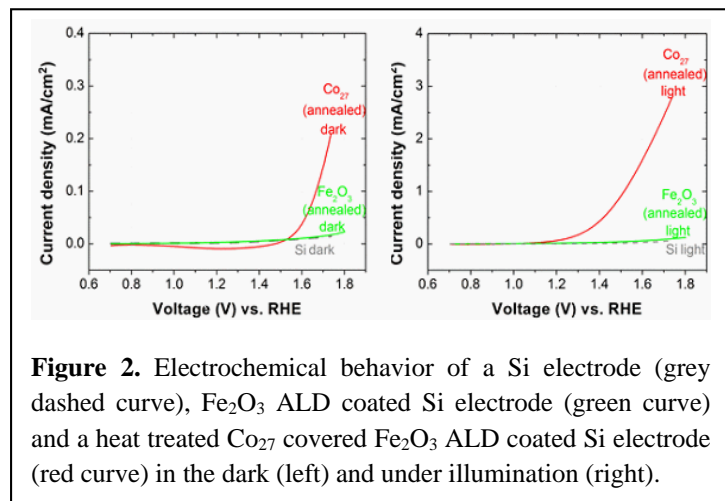
Supported Ag and Ir Clusters for Li-O_2 Electrochemistry

The Li-O_2 battery has the potential for the very high energy densities needed for long range electric vehicles, but the charge and discharge chemistries are complex and not well understood. The active sites on cathode surfaces and their role in the electrochemical reactions in aprotic Li-O_2 cells are difficult to ascertain because the exact nature of the sites are unknown.

Deposition of subnanometer Ir clusters of exact size and number on a carbon surface was used to study the discharge process in Li-O_2 cells. The results reveal dramatically different morphologies (films vs toroids) of the electrochemically grown discharge product compared to our previously studied Ag clusters.[4] This is believed to be due to differences in nucleation and growth mechanisms of the two types of clusters.

Characterization of Supported Clusters

The careful characterization of the precisely synthesized catalytic materials both before during and after catalytic study is a key strength of this FWP. These characterization tools range from a variety of synchrotron methods to advanced mass based tools that use sputtering or laser desorption followed by post-ionization of the desorbing flux to characterize cluster samples. Recently we have been able to compare Ir samples (Ir$_6$ supported on Au) such as those produced for Li-O_2 electrochemistry with pure metal Ir standards using 157 nm post-ionization (Fig. 3). The standard materials produce the expected log normal series of clusters ranging to very high masses (>Ir$_{12}$). The cluster samples show a much narrower size distribution with a far steeper slope versus cluster size.

Figure 3. Ir nanoparticles annealed from Ir8 size-selected clusters on a reduced graphene oxide substrate.

We note a few Ir$_6^+$ clusters can be detected. We are currently exploring several cluster based samples and hope to develop models to use this mass based methodology to interrogate the unique cluster based samples produced in this FWP.

We are also using these tools to develop chemistries for support materials. In particular we are developing epitaxial and chemical Atomic Layer Deposition methods capable of producing phase controlled and single crystal supports for clusters [5]. We have clear evidence from earlier studies that deposited clusters tend to cover active support catalysis sites. Thus synthesis of
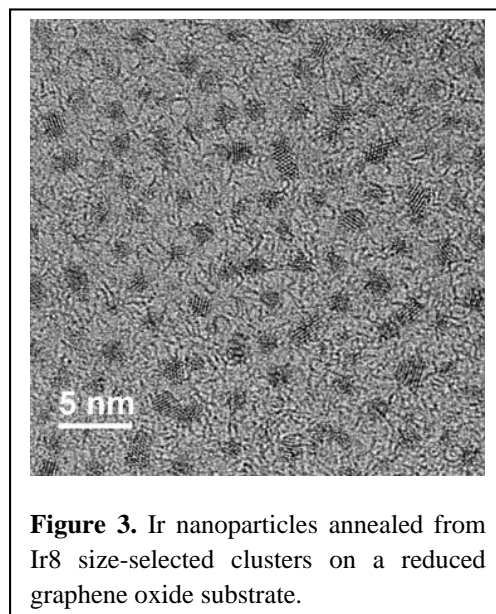
crystalline supports with controlled production of defect sites may allow exploration of support sites as well as cluster dependencies.
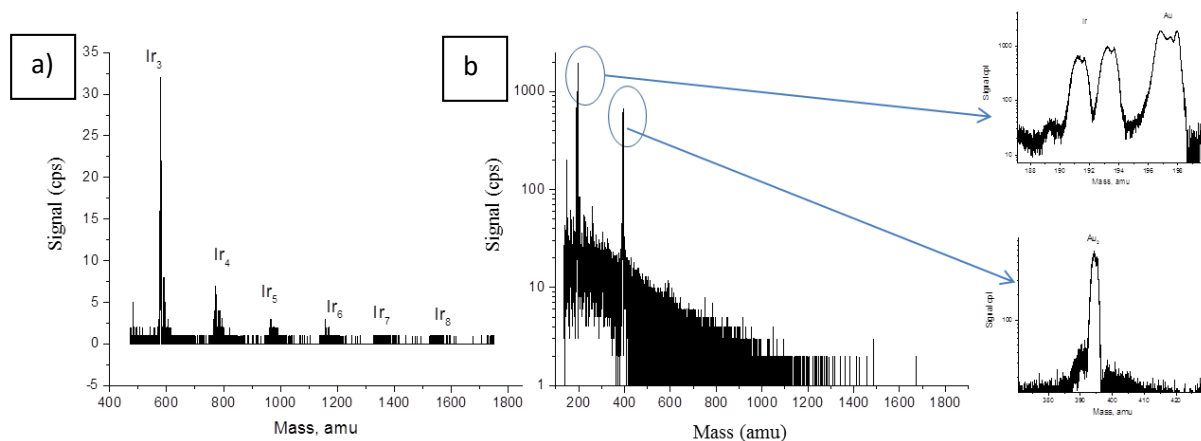
Figure 3. One Photon post-ionized mass spectrum of a) iridium metal and b) Ir_6 clusters supported on a Au substrate. The cluster size distribution gives a window into the size and structure of the sample measured. We also see significant changes for oxidized versus reduced clusters and suggest that this might be a unique, facile method to measure the oxygen atom nuclearity of the clusters.

Future Plans

Our plans for fundamental studies for design and discovery of novel materials based on supported size-specific clusters will focus on new strategies for materials synthesis including (1) extending our capabilities in generating size- and composition- specific clusters to a larger range of clusters based on deposition as well as annealing, (2) metal sulfur and metal oxide clusters, and (3) new concepts in metal oxide supports for controlling stability and activity. This work will be supported by continued development of both synchrotron and mass based analytical methods for understanding both the as synthesized catalytic materials and their evolution during electrochemical reaction. In addition we will carry out first principles for materials design and understanding of the cluster-based materials for key catalytic reactions.

 References
[1]"Carbon Dioxide Conversion to Methanol over Size-selected Cu_4 Clusters at Low Pressures", C. Liu, et al *J. Am. Chem. Soc.* **137**, 8676−8679 (2015)
[2]"Electrochemical behaviour of naked sub-nanometre sized copper clusters and effect of CO_2" R. Passalacqua, et al *Catal. Sci. Technol.,* submitted.
[3] "Water oxidation: Size selected Co_{27} Clusters on Fe_2O_3", Pellin et al, *ChemSusChem*, submitted
 [4] Effect of the Size-selective Silver Clusters on Li_2O_2 Morphology in Lithium-Oxygen Batteries, J. Lu, et al *Nature Communications*, **5**, 4895 (2014)
[5] "Atomic Layer Deposition of MnS: Phase Control and Electrochemical Applications." S. C.:Riha, et al A. B. F. Martinson, *ACS Applied Materials & Interfaces* **8**: 2774 (2016).

Publications

1. Computational studies of electrochemical CO_2 reduction on subnanometer transition metal clusters, C. Liu, H. He, P. Zapol and L. A. Curtiss, *Phys. Chem. Chem. Phys*., **16**(48):26584-99 (2014).
2. Combination of imaging mass spectrometry and electron microscopy for quasi nondestructive surface analysis Baryshev, SV Zinovev, AV Tripa, CE Veryovkin, IV NIMB **332**, 364-367 (2014).
3. Editorial: Size-Selected Clusters and Particles: From Physical Chemistry and Chemical Physics to Catalysis" J. A. Van Bokhoven and S. Vajda *Phys. Chem. Chem. Phys*. **16**, 26418-26420 (2014).
4. Ambient pressure XPS study of silver clusters on Al_2O_3 and TiO_2 ultrathin film supports, B. H. Mao, R. Chang, L. Shi, Q. Q. Zhuo, S. Rani, X. S. Liu, E. C. Tyo, S. Vajda, S. D. Wang, and Z. Liu *Phys. Chem. Chem. Phys*.**16**, 26645-26652 (2014).
5. TOF SIMS characterization of SEI layer on battery electrodes Veryovkin, IV ; Tripa, CE Zinovev, AV Baryshev, SV Li, Y Abraham, NIMB **332**, 368-372 (2014).
6. Physical Fabrication of Nanostructured Heterogeneous Catalysts" C. Yin, E. Tyo and S. Vajda Chapter 3 in "Heterogeneous Catalysis at the Nanoscale for Energy Applications", Eds. F. Tao, W. Schneider, and P. Kamat, Wiley-VCH, ISBN 0470952601, ISBN 978-0470952603, invited chapter (December 2014).
7. Depth profile of oxide volume fractions of Zircaloy-2 in. high-temperature steam: An in-situ synchrotron radiation study." W. Mohamed, D. Yun, K. Mo, M. J. Pellin, M. C. Billone, J. Almer and A. M. Yacout, *J. Nucl. M*ater, **454**(1-3), 192-199 (2014).
8. Size and Support Dependent Evolution of the Oxidation State and Structure by Oxidation of Subnanometer Cobalt Clusters, C. Yin, F. Zheng, S. Lee, J. Guo, W.C. Wang, G. Kwon, V. Vajda, H. Wang, B. Lee, J. DeBartolo, S. Seifert, R. E. Winans, and S. Vajda, *J. Phys. Chem.* A 118, 8477−8484 (2014).
9. Carbon Dioxide Conversion to Methanol over Size-selected Cu_4 Clusters at Low Pressures C. Liu, B. Yang, E. Tyo, S. Seifert, J. E. Ernst, B. von Issendorff, P. Zapol, S. Vajda and L. A. Curtiss *J. Am. Chem. Soc.* 137, 8676−8679 (2015).
10. Solar Absorber Cu_2ZnSnS_4 and its Parent Multilayers $ZnS/SnS_2/Cu_2S$ Synthesized by Atomic Layer Deposition and Analyzed by X-ray Photoelectron Spectroscopy, S. V. Baryshev, S. C. Riha and A. V. Zinovev *Surf. Sci.* **22**, 81 (2015);
11. Pronounced Size Dependence in Structural and Morphological Transitions of Gas-Phase Produced and Partially Oxidized Co Nanoparticles under Catalytic Reaction Conditions, S. Bartling, C. Yin, I. Barke, K. Oldenburg, H. Hartmann, V. von Oeynhausen, M.-. Pohl, K. Houben, E. C. Tyo, S. Seifert, P. Lievens, K.-H. Meiwes-Broer and S. Vajda, *ACS Nano* **9**, 5984–5998, (2015).
12. Nanoscale friction properties of graphene and graphene oxide." Berman, D ; Erdemir, A Zinovev, AV; Sumant, AV. *Diamond and related materials*, **54**, 91-96 (2015).
13. "Irradiation behavior study of U–Mo/Al dispersion fuel with high energy Xe." B. Ye, S. Bhattacharya, K. Mo, D. Yun, W. Mohamed, M. J. Pellin, J. Fortner, Y. S. Kim, G. L. Hoffman, A. M. Yacout, T. Wiencek, S. Van den Berghe, and A. Leenaers, *J. Nucl. Mater*, 464(1), 236-244(2015).
14. Cluster Catalysis," M. White and S. Vajda, *ACS Catalysis*, 7152-7176 (2015).
15. Fischer−Tropsch Synthesis at a Low Pressure on Subnanometer Cobalt Oxide Clusters: The Effect of Cluster Size and Support on Activity and Selectivity" S. Lee, B. Lee, S. Seifert, R.E. Winans and S. Vajda *J. Phys. Chem*. C 119, 11210–11216 (2015).

16. Catalysis by Clusters with Precise Number of Atoms" E. C Tyo and S. Vajda, *Nat. Nanotech.*10, 577-588 (2015), invited review.

17. Understanding and mitigating some of the key factors that limit non-aqueous lithium-air battery performance," J. Lu, K. C. Lau, Y.-K. Sun, L A Curtiss and K. Amine, *Journal of the Electrochemical Society*, 162, A1-A8 (2015).

18. Migration of Single Iridium Atoms and Tri-iridium Clusters on MgO Surfaces: Aberration-Corrected STEM Imaging and Ab Initio Calculations," C. W. Han, H. Iddir, A. Uzun, L. A. Curtiss, N. D. Browning, B. C. Gates, and V. Ortalan, *J. Phys. Chem. Lett*., 6 (23), 4675–4679 (2015).

19. Water as promoter and catalyst in dioxygen electrochemistry at aqueous and organic electrified interfaces, J. S. Jirkovsk, R. Subbaraman, D. Strmcnik, K. L. Harrison, C. E. Diesendruck, R. Assary, O. Frank , L. Kobr, G. K. H. Wiberg, B. Genorio, V. R. Stamenkovic, L. A. Curtiss, Jeffrey S. Moore, K. R. Zavadil, and N. M. Markovic, *ACS Catalysis*, **5**, 6600−6607 (2015).

20. Characterization of high energy Xe ion irradiation effects in single crystal molybdenum with depth-resolved synchrotron microbeam diffraction, D. Yun, Y. Miao, R. Xu, Z. Mei, K. Mo, W. Mohamed, B. Ye, M. J. Pellin, A. M. Yacout, *Journal of Nuclear Materials*, 471, 272-279 (2016).

21. High-mass heterogeneous cluster formation by ion bombardment of the ternary alloy $Au_7Cu_5Al_4$ Alexander V. Zinovev, Bruce V. King, Igor V. Veryovkin and Michael J. Pellin *J. Vac. Sci. Technol*. B **34**, (2016).

22. Atomic Layer Deposition of MnS: Phase Control and Electrochemical Applications." S. C.:Riha, A. A. Koege,Y. Q. Cao, M. J. Pellin, J. W. ElamA. B. F. Martinson, *ACS Applied Materials & Interfaces* **8**(4): 2774-2780 (2016).

23. Investigation of High-Energy Ion-Irradiated MA957 Using Synchrotron Radiation under In-Situ Tension K. Mo, D. Yun, Y. B. Miao, X. Liu, M. Pellin, J. Almer, J. S. Park, J. F. Stubbins, S. F. Zhu A. M. Yacout, *Materials*, **9**(1), 1-11 (2016).

24. A Molybdenum Disulfide/ and Ionic Liquid Bi-functional Co-catalyst for Lithium–Oxygen Batteries, M. Asadi, B. Kumar, C. Liu, P. Phillips, P. Yasaei, A. Behranginia, P. Zapol, R. F. Klie, L. A. Curtiss, A. Salehi-Khojin, *ACSNano*, **10** (2), pp 2167–2175 (2016).

25. MeV per nucleon ion irradiation of nuclear materials with high energy synchrotron X-ray characterization. M. J. Pellin, A. M. Yacout, K. Mo, J. Almer, S. Bhattacharya, W. Mohamed, D. Seidman, B. Ye, D. Yun, R. Xu, S. Zhu, *Journal of Nuclear Materials 471,266-271* (2016).

26. Atomistic and Electronic Structure Methods for Nanostructured Oxide Interfaces" G. Barcaro, L. Sementa, F. Ribeiro Negreiros, I. O. Thomas, S. Vajda, A. Fortunelli In "Oxide Materials at the Two-dimensional Limit", Springer, Eds: F. P. Netzer and A. Fortunelli, DOI 10.1007/978-3-319-28332-6-2, *invited chapter* (2016)

27. Highly Efficient Hydrogen Evolution Reaction Using Crystalline Layered Three-Dimensional Molybdenum Disulfides Grown on Graphene Film, A. Behranginia ; M. Asadi ; C. Liu ; P. Yasaei ; B. Kumar ; P. Phillips ; T. Foroozan ; J. C. Waranius ; K. Kim ; J. Abiade ; R. F. Klie ; L. A. Curtiss ; A. Salehi-Khojin, *Materials Chemistry*, **28**, 549 (2015).

28. Superoxide (electro)chemistry on well-defined surfaces in organic environments, B. Genorio, J. S. Jirkovský, R. S. Assary, J. G. Connell, D. Strmcnik, C. E. Diesendruck, V. R. Stamenkovic, J. S. Moore, L. A. Curtiss, and N. M. Markovic, *J. Phys. Chem. C*, ASAP (2016) DOI: 10.1021/acs.jpcc.5b12230

29. Electrochemical behaviour of naked sub-nanometre sized copper clusters and effect of CO_2", R. Passalacqua, S. Parathoner, G. Centi, A. Halder, E. C. Tyo, S. Seifert and S. Vajda, *Catal. Sci. Technol., submitted.*
30. Transition metal dichalcogenides as highly active catalysts for carbon dioxide reduction, Salehi, Liu, Zapol, Curtiss, et al, Science, submitted
31. In situ study of electronic structure of atomic layer deposited oxide ultrathin films upon oxygen adsorption using ambient pressure XPS**,** B.H. Mao, E. Crumlin, M. J. Pellin, E. C. Tyo, S. Vajda, Y. Li, S.-D. Wang, and Zhi Liu, *Catal. Sci, Technol., submitted.*
32. Modification of Gas Aggregation Sources: High Pressure and Reactive Gas Magnetron Sputtering, L. Kolipaka and S. Vajda, in "*Gas Phase Synthesis of Nanoparticles",* Wiley-VCH, Ed.: Y. Huttel, *, submitted.*
33. Bridging the Pressure Gap: CO oxidation by Pt_{10} clusters, C. Yin, F. R. Negreiros, G. Barcaro, L. Sementa, E. C. Tyo, S. Bartling, K.-H. Meiwes-Broer, S. Seifert, A. Beniya, H. Hirata, N. Isomura, S, Nigam, C.Majumder, Y. Watanabe, A. Fortunelli, and S. Vajda, *submitted.*
34. Water oxidation: Size selected Co_{27} Clusters on Fe_2O_3, M. J. Pellin, S. C. Riha, E. C. Tyo, G. Kwon, J. A. Libera, J. W. Elam, S. Seifert, S. Lee, and S. Vajda, ChemSusChem, *submitted*.

Materials and Interfacial Chemistry for Next Generation Electrical Energy Storage

S. Dai, M. P. Paranthaman, C. A. Bridges, X. G. Sun, G. M. Veith
Oak Ridge National Laboratory, Oak Ridge, TN 37831
J. B. Goodenough, A. Manthiram – The University of Texas at Austin, Austin, TX 78712

Program Scope

The overarching goal is t*o investigate fundamental principles governing energy storage through integrated synthesis and advanced characterization.* Our current research is focused on fundamental investigation of electrolytes based on ionic liquids and rational synthesis of novel electrode architectures through Fermi level engineering of anode and cathode redox levels by employing porous structures and surface modifications as well as advanced operando characterization techniques including neutron diffraction and scattering. The key scientific question concerns the relationship between chemical structures and their energy-storage efficacies.

Recent Progress

- A new orthochelated salt, lithium bis(methylfluoromalonato)borate (LiMBFMB), was synthesized and purified for controlling SEI layers in lithium-ion batteries. The replacement of acidic hydrogen with methyl group at the C-2 position of the anion MBFMB significantly improved the stability of the salt under both reduction and oxidation conditions, which was evidenced by the long cycling stability of the half cells based on graphite and 5.0 V lithium nickel manganese oxide ($LiNi_{0.5}Mn_{1.5}O_4$), respectively.
- We reported a strategy of mixing both the ionic liquid and sulfone which shows synergistic effects of reducing viscosity, increasing ionic conductivity, and reducing the polysulfide dissolution. The mixtures of the ionic liquid and sulfone also show distinctly different physicochemical properties than either of the pure components, including the thermal properties and crystallization behavior. Lithium sulfur batteries exhibit an excellent cycling stability and remains as high as 655 mAh g^{-1} even after 50 cycles. Our strategy provides a method to alleviate the polysulfide dissolution and redox shuttle phenomena, while improve the ionic conductivity at the same time.
- The increasing demand for a safe rechargeable battery with a high energy density per cell is driving a search for a novel solid electrolyte with a high Li^+ or Na^+ conductivity that is chemically stable in a working Li-ion or Na-ion battery. $Li_6ZnNb_4O_{14}$ has been reported to exhibit a $\sigma_{Li} > 10^{-2}$ S cm^{-1} at 250°C, but to disproportionate into multiple phases on cooling from 850°C to room temperature. An investigation of the room-temperature Li-ion conductivity in a porous pellet of a multiphase product of a nominal $Li_6ZnNb_4O_{14}$ composition is shown to have bulk $\sigma_{Li} \approx 3.3$ x 10^{-5} S cm^{-1} at room temperature that increases to 1.4 x 10^{-4} S cm^{-1} by 50°C.
- The program successfully followed and understood the SEI formation process over silicon anodes. The data showed a "living" SEI layer that changed chemistry and thickness with cycling. More importantly we demonstrated the SEI is only 30 nm thick over silicon. This was in contrast to the thickness of the SEI over a cathode (3 nm).
- The program explored the phase Na-Sn phase diagram and compared the chemistry and structure of the thermodynamically stable compounds to the electrochemically prepared

materials. The data showed the formation of new Na-Sn structures not previously identified. In addition the data showed that the electrochemically prepared Na-Sn structures contained a high concentration of Sn-Sn bonding. The resulting structures were predominantly Zintl chemistry like.

- A new quasi solid electrolyte was developed using nanoarchitectures of hollow silica spheres to confine liquid electrolytes in hollow space to afford high conductivities (2.5 mS cm^{-1}). In a symmetric lithium/lithium cell, the solid-like electrolytes demonstrate a robust performance against the Li dendrite problem, preventing the cell from short circuiting at current densities ranging from 0.16 to 0.32 mA cm-2 over an extended period of time. The high flexibility and compatibility of HS nanoarchitectures enables broad tunability to choose desired liquids for the fabrication of other kinds of solid-like electrolytes, providing a useful alternative strategy for the development of next generation rechargeable batteries.

Future Plans

- Further understand the structure-property relationship of ionic liquids and design new ionic liquids with good SEI formation ability to be compatibility with graphite and high voltage cathodes.
- Understanding the limiting factors in rate performance of anode and cathode materials and design novel electrode materials with enhanced rate capability.
- Further explore the understanding gained from small angle neutron scattering (SANS) on the electrochemical processes occurring at the surface and in the bulk of both anode and cathode electrode materials
- Continue to work with UT-Austin to develop a more comprehensive picture of next-generation electrode and electrolyte materials being investigated as a part of this project
- Investigate and characterize nanocomposite solid electrolytes for ion transport
- Explore the synthesis of Na-intercalation batteries and understand how the surface reactivity of these materials changes in comparison with their Li analogs.

Publications (2015-2016)
1. X. G. Sun, Z. Bi, H. Liu, Y. Fang, C. A. Bridges, M. P. Paranthaman, S. Dai, G. M. Brown, "A high performance hybrid battery based on aluminum anode and LiFePO$_4$ cathode," *Chem. Comm.* 52(8), 1713-1716 (2016).
2. Loic Baggetto, Cedric Charvillat, Yannick Thebault, Jerome Esvan, Marie-Christine Lafont, Emmanuel Scheid, Gabriel M. Veith, and Constantin Vahlas, "Amorphous alumina thin films deposited on titanium: Interfacial chemistry and thermal oxidation barrier properties", *Physica Status Solidi A* 213 (2), pg. 470–480 (2016).
3. Wan, N.; Lu, X.; Wang, Y. S.; Zhang, W. F.; Bai, Y.; Hu, Y. S.; Dai, S. Improved Li storage performance in SnO2 nanocrystals by a synergetic doping. *Sci Rep* **2016**, *6*.
4. Matthew S. Rager, Tolga Aytug, Gabriel M. Veith, Pooran Joshi, "Low-Thermal-Budget Photonic Processing of Highly Conductive Cu Interconnects Based on CuO Nanoinks: Potential for Flexible Printed Electronics", *ACS Applied Materials & Interfaces,* 8 (3), 2441–2448 (2016).
5. Alberto Villa, Simon J. Freakley, Marco Schiavoni, Jennifer K. Edwards, Ceri Hammond, Gabriel M. Veith, Wu Wang, Di Wang, Laura Prati, Nikolaos Dimitratos, Graham J. Hutchings, "Depressing the hydrogenation and decomposition

reaction in H_2O_2 synthesis by supporting gold-palladium nanoparticles on oxygen functionalized carbon nanofibers", *Catalysis Science and Technology* 6(3), 694-697 (2016).

6. Z. D. Hood, H. Wang, Y. Li, A. S. Pandian, M. P. Paranthaman, and C. Liang, "The filler effect": A study of solid oxide fillers with beta-Li_3PS_4 for lithium conducting electrolytes", *Solid State Ionics* 283, 75-80 (2015).

7. Li, Y. C.; Paranthaman, M. P.; Gill, L. W.; Hagaman, E. W.; Wang, Y. Y.; Sokolov, A. P.; Dai, S.; Ma, C.; Chi, M. F.; Veith, G. M.; Manthiram, A.; Goodenough, J. B. Conduction below 100 degrees C in nominal Li6ZnNb4O14. *J. Mater. Sci.* **2016**, *51*, 854-860.

8. Li, Y. C.; Paranthaman, M. P.; Akato, K.; Naskar, A. K.; Levine, A. M.; Lee, R. J.; Kim, S. O.; Zhang, J. S.; Dai, S.; Manthiram, A. Tire-derived carbon composite anodes for sodium-ion batteries. *J. Power Sources* **2016**, *316*, 232-238.

9. Bai, Y.; Yan, D.; Yu, C. Y.; Cao, L. N.; Wang, C. L.; Zhang, J. S.; Zhu, H. Y.; Hu, Y. S.; Dai, S.; Lu, J. L.; Zhang, W. F. Core-shell Si@TiO2 nanosphere anode by atomic layer deposition for Li-ion batteries. *J. Power Sources* **2016**, *308*, 75-82.

10. S. M. Yang, M. P. Paranthaman, T. W. Noh, S. V. Kalinin, and E. Strelcovt, "Nanoparticle Shape Evolution and Proximity Effects During Tip-Induced Electrochemical Processes", *ACS Nano* 10 (1), 663-671 (2016).

11. S. Wan, X. G. Jiang, B. K. Guo, S. Dai, J. B. Goodenough, and X. G. Sun, "A Stable Fluorinated and Alkylated Lithium Malonatoborate Salt for Lithium Ion Battery Application," *Chem. Comm.* **51**(48), 9817–9820 (2015).

12. J. S. Zhang, Y. Bai, X. G. Sun, Y. C. Li, B. K. Guo, J. H. Chen, G. M. Veith, D. K. Hensley, M. P. Paranthaman, J. B. Goodenough, and S. Dai, "Superior Lithium Conductive Solid-like Electrolytes: Nanoconfining Liquids within the Hollow Structures," *Nano Lett.* **15**(5), 3398–3402 (2015).

13. C. Liao, B. K. Guo, X. G. Sun, and S. Dai, "Synergistic Effects of Mixing Sulfone and Ionic Liquid as Safe Electrolytes for Lithium Sulfur Batteries," *ChemSusChem* **8**(2), 353–360 (2015).

14. G. He, C. A. Bridges, and A. Manthiram, "Crystal Chemistry of Electrochemically and Chemically Lithiated Layered αI‑LiVOPO4," *Chem. Mater.* **27**, 6699–6707 (2015).

15. G. M. Veith, M. Doucet, J. Baldwin, R. L. Sacci, T. M. Fears, Y. Wang, and J. F. Browning, "Direct Determination of Solid-Electrolyte Interphase Thickness and Composition as a Function of State of Charge on a Silicon Anode," *J. Phys. Chem. C* **119** (35), 20339–20349 (2015).

16. J. Gorka, L. Baggetto, J. K Keum, S. M Mahurin, R. T Mayes, S. Dai, and G. M. Veith, "The Electrochemical Reactions of SnO_2 with Li and Na: A Study Using Thin Films and Mesoporous Carbons," *J. Power Sources* **284**(1), 1–9 (2015).

17. L. Torres-Castro, J. Shojan, C. M. Julien, A. Huq, C. Dhital, M. P. Paranthaman, R. S. Katiyar, and A. Manivannan, "Synthesis, Characterization and Electrochemical Performance of Al-Substituted Li2MnO3," *Mater. Sci. Eng., B* **201**, 13–22 2015.

18. S. M. Yang, E. Strelcov, M. P. Paranthaman, A. Tselev, T. W. Noh, and S. V. Kalinin, "Humidity Effect of Nanoscale Electrochemistry in Solid Silver Ion Conductors and the Dual Nature of Its Locality," *Nano Lett.* **15**, 1062–1069 (2015).

19. H. D. Liu, D. Qian, M. G. Verde, M. H. Zhang, L. Baggetto, K. An, Y. Chen, K. J. Carroll, D. Lau, M. F. Chi, G. M. Veith, and Y. S. Meng, "Understanding the Role of NH4F and Al2O3 Surface Co-modification on Lithium-Excess Layered Oxide Li1.2Ni0.2Mn0.6O2," *ACS Appl. Mater. Interfaces* **7**(34), 19189–19200 (2015).

20. A. Villa, M. Schiavoni, C. E. C.-Thaw, P. F. Fulvio, R. T. Mayes, S. Dai, K. L. More, G. M. Veith, and L. Prati, "Acid-Functionalized Mesoporous Carbon: An Efficient Support for Ruthenium-Catalyzed □-Valerolactone Production," *ChemSusChem* **8**(15), 2520–2528 (2015).

21. C. E. Chan-Thaw, A. Villa, and G. M. Veith**,** L. Prati, "Identifying the Role of N-Heteroatom Location in the Activity of Metal Catalysts for Alcohol Oxidation," *ChemCatChem* **7**(8), 1338–1346 (2015).

22. R. Younesi, G. M. Veith, P. Johansson, K. Edström, and T. Vegge, "Lithium Salts for Advanced Lithium Batteries: Li–metal, Li–O$_2$, and Li–S," *Energy Environ. Sci.* **8**(7), 1905–1922 (2015).

23. A. M. Pezeshki, J. T. Clement, G. M. Veith, T. A. Zawodzinski, and M. M. Mench, "High Performance Electrodes in Vanadium Redox Flow Batteries through Oxygen-Enriched Thermal Activation," *J. Power Sources* **294**(1), 333–338 (2015).

24. H. Y. Zhu, Z. L. Wu, D. Su, G. M. Veith, H. F. Lu, P. F. Zhang, S. H. Chai, and S. Dai, "Constructing Hiearchial Interfaces: TiO$_2$-supported PtFe-FeO$_x$ Nanowires for Room Temperature CO Oxidation," *J. Am. Chem. Soc.* **137**(32)*,* 10156–10159 (2015).

25. R. L Sacci, J. L. Bañuelos, G. M. Veith, K. C Littrell, Y. Cheng, C. U Wildgruber, L. L Jones, A. J. Ramirez-Cuesta, G. Rother, and N. J Dudney, "Structure of Spontaneously Formed Solid-Electrolyte Interphase on Lithated Graphite Determined Using Small-Angle Neutron Scattering," *J. Phys. Chem. C* **119** (18), 9816–9823 (2015).

26. R. W. Atkinson, III, R. R. Unocic, K. A. Unocic, G. M. Veith, T. A. Zawodzinski, Jr., and A. B. Papandrew, "Vapor Synthesis and Thermal Modification of Supportless Platinum-Ruthenium Nanotubes and Applications as Methanol Electroxidation Catalyst," *ACS Appl. Mater. Interfaces*, **7**(19), 10112–10124 (2015).

27. Y. Li, R. Raghavan, N. A. Wagner, S. K. Davidowski, L. Baggetto, R. Zhao, Q. Cheng, J. L. Yarger, G. M. Veith, C. Ellis-Terrell, M. A. Miller, K. S. Chan, and C. K. Chan, "Type I Clathrates as Novel Silicon Anodes: An Electrochemical and Structural Investigation," *Adv. Sci.* **2**, 1500057 (2015).

28. P. F. Zhang, H. Li, G. M. Veith, and S. Dai, "Soluble Porous Coordination Polymers by Mechanochemistry: From Metal-Containing Films/Membranes to Active Catalysts for Aerobic Oxidation," *Adv. Mater*. **27**(2), 234–239 (2015).

29. P. F. Zhang, Z. A. Qiao, X. G. Jiang, G. M. Veith, and S. Dai, "Nanoporous Ionic Organic Networks: Stabilizing and Supporting Gold Nanoparticles for Catalysis," *Nano Lett.* **15**(2), 823–828, (2015).

30. H. Zhou, R. E. Ruther, J. Adcock, W. Zhou, S. Dai**,** and J. Nanda, "Controlled Formation of Mixed Nanoscale Domains of High Capacity Fe$_2$O$_3$-FeF$_3$ Conversion Compounds by Direct Fluorination," *ACS Nano* **9**, 2530–2539 (2015).

31. P. A. Ward, J. A. Teprovich Jr., R. N. Compton, V. Schwartz, G. M. Veith**,** and R. Zidan, "Evaluation of the physi- and chemisorption of hydrogen in alkali (Na, Li) doped fullerenes," *Int. J. Hydrogen Energy* **40**(6), 2710–2716 (2015).

32. C. E. Chan-Thaw, A. Villa, D. Wang, V. Dal Santo, A. O. Biroli, G. M. Veith, A. Thomas, and L. Prati, "PdHx Entrapped in Covalent Triazine Framework Modulates Selectivity in Glycerol Oxidation," *ChemCatChem* 7(14), 2149–2154 (2015).

Solvent-Assisted Non-Equilibrium Directed Self-Assembly of Complex Polymeric Materials

Juan J. de Pablo – Paul F. Nealey – M. Tirrell

Institute for Molecular Engineering
Argonne National Laboratory
University of Chicago

Program Scope

The aim of this program is to direct the assembly and function of polymeric materials through the application of external fields. Such fields can be templating patterns on a surface, solvent gradients, or voltage acting on charges, to name some of the examples that have been considered under this program. As our ability to control assembly on smaller and smaller length scales has increased, we have gradually shifted our focus to two specific challenges, where we have identified a range of opportunities for major advances. The first has to do with the incorporation of charges in polymeric materials as a means to add function and manipulate assembly. The second has to do with development of multimodal experimental techniques that will enable efficient and reliable characterization of hierarchical, self-assembled polymeric materials over a wide range of length scales.

Recent Progress

Charge-driven complexation of polymeric materials: In past work we demonstrated that by controlling the chirality of polymeric materials of opposite charge, it was possible to manipulate the phase behavior of aqueous solutions of such polymers, and whether complex coacervation (the formation of a second liquid phase) or precipitation occurs (1,2). In that example, our efforts to manipulate structure focused on truly small length scales, and how monomers of different chirality arranged in different sequences influence the structure and properties of the corresponding solutions (1-4). In more recent work, we have examined how the mesoscale structure of charged polymeric materials influences self-assembly in solution. To that end, we have prepared multi-block polymers (primarily diblocks and triblocks) consisting of various combinations of charged and neutral blocks. We have found that, depending on sequence, such materials can form spherical micelles, or percolating networks that phase separate into a new, previously unknown hierarchical
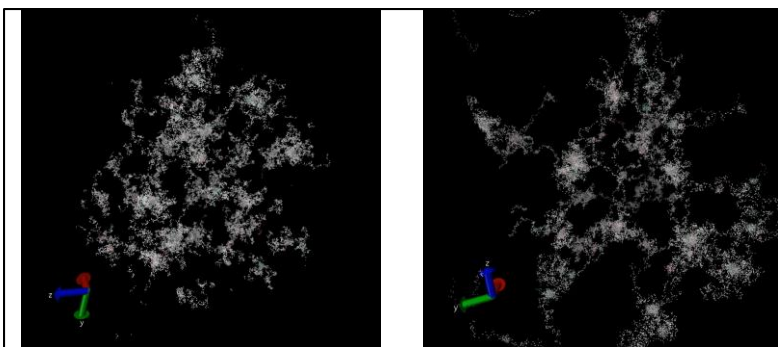
Simulated charged diblock copolymer solution (left) and triblock copolymer solution (right). Diblocks formed spherical micelles. Triblocks for a network in which some of the chains connect adjacent charged domains, and others fold onto themselves within the same domain.

networks with well-defined structure. Our experimental predictions have been interpreted in terms of multiscale models and novel simulation techniques (5-11), which help explain the origin of such phase behavior, and how it can be manipulated by controlling molecular architecture and solution conditions. Indeed, as part of this project we have developed closed-form mathematical models capable of describing the coacervation of polyelectrolyte molecules of arbitrary stiffness and fractal dimension. We have also developed an analytical theory capable of describing the polarization of charged macromolecular objects, and the polarization-induced forces that are generated in such materials (12).

Ultra-high conductivity in ordered block polymers: There is considerable interest in developing ordered, charge conducting polymeric materials for energy storage applications. Most of past work has considered block copolymers consisting of material that provides mechanical strength (e.g. PMMA), and a material that provides ionic conductivity (e.g. Li – PEO). We have developed a new process to introduced charge into pre-assembled block copolymers (13). In that process, which is depicted in the figure below, a neutral block copolymer (PS-P2VP) is pre-assembled on a surface, which may or may not include patterns to improve order, and after deposition, distinct chemical reaction are carried out to charge one of the blocks (PVP). Specifically, the P2VP domains are transformed into n-methyl pyridinium iodide ($NMP^+ I^-$) by exposure to methyl iodide vapor. Our work to date has demonstrated that we can achieve conductivities in such materials that are substantially higher than those accessible by traditional preparation routes, thereby opening new opportunities for applications in batteries and harvesting devices (14,15) that go beyond existing PEO-Li based materials.

Post nano-domain assembly functionalization and characterization of polymers for ionic conductivity

(A) Schematic representation of the post assembly vapor reaction which introduced ionic species into the P2VP domain (B) Experimental design for electrochemical characterization using interdigitated electrodes with large cross-sectional area for high statistic significance (C) Conductivity of the film as a function of degree of functionalization showing conductivity values comparable to commercial performances (D) Experimental SEM image showing the film following the MeI vapor reaction with the preserved nano-domain architecture.

Multimodal characterization of polymeric materials: For all of the applications outlined above and, more generally, for materials science and engineering, it is essential that new, multi-modal materials characterization techniques be developed that are capable of probing different aspects

of a sample by relying on different, complementary methods or tools. The data that emerge from such tools should be self-consistent, and it is desirable that as much information as possible be extracted from any given experiment. Such an approach has been demonstrated in our recent work, in the context of self-assembling polymeric materials, where theory and simulations provide the framework that is used to seamlessly mesh experimental data from two different scattering measurements. Specifically, the samples considered consist of diblock copolymers (BCP) that are self-assembled on chemically nano-patterned surfaces. The copolymers micro-phase separate into ordered lamellae with characteristic dimensions on the scale of tens of nanometers that are perfectly aligned by the substrate over macroscopic areas. As such, these aligned lamellar samples provide ideal standards with which to develop the formalism introduced in this work and, more generally, the concept of multimodal experimentation. The trajectories generated from simulations of physics-based models that impose a set of well-defined thermodynamic and boundary conditions (5-7) are compared to experimental data from scattering experiments, namely critical-dimension small angle x-ray scattering and grazing-incidence small-angle x-ray scattering that are sensitive to different characteristics of the films. An optimal combination of model parameters is then identified by resorting to an evolutionary computation approach. Through this process, we have been able to examine the effect of polymer asymmetry, geometry, and surface chemical pattern on block copolymer morphology and the corresponding scattering intensity profiles. The outcomes of the proposed analysis compare favorably with images generated by 3D tunneling electron microscopy tomography (14), serving to validate the merit of the ideas proposed in this project. We anticipate that the formalism developed here will be adapted by users for a wide range of applications, serving to usher a new era of materials research in which multiple and often demanding experiments are conducted simultaneously with theory and simulation to interrogate materials at unprecedented levels of detail.

Future Plans

Moving forward, our immediate plans are focused on the following three issues:

(1) Understanding the role of molecular architecture and charge distribution in charge-driven block polymer assembly, including the structure, rheology and the dynamics of assembly.

(2) Understanding the origin of ultra-high conductivity in pre-assembled charged block copolymers, and the effects of order on that conductivity.

(3) Extend our proposed multimodal and evolutionary optimization characterization strategy to a broader class of experiments and polymeric materials.

References

(1) S. L. Perry, L. Leon, K. Q. Hoffmann, M. J. Kade, D. Priftis, K. A. Black, D. Wong, R. A. Klein, C. F. Pierce III, K. O. Margossian, J. K. Whitmer, J. Qin, J. J. de Pablo,

M. Tirrell, (2015) Chirality-selected phase behavior in ionic polypeptide complexes, *Nature Comm,* 6, 6052 | DOI: 10.1038/ncomms7052.

(2) K. Q. Hoffmann, S. L. Perry, L. Leon, D. Priftis, M. Tirrell and J. J. de Pablo, (2015) A molecular view of the role of chirality in charge driven polypeptide complexation, *Soft Matter*, 11, 1525–1538.

(3) Robert Farina, Nicolas Laugel, Jing Yu, and Matthew Tirrell, (2015) Reversible Adhesion with Polyelectrolyte Brushes Tailored via the Uptake and Release of Trivalent Lanthanum Ions, *J. Phys. Chem. C*, 119, 14805−14814.

(4) Dimitrios Priftis, Lorraine Leon, Ziyuan Song, Sarah L. Perry, Khatcher O. Margossian, Anna Tropnikova, Jianjun Cheng, and Matthew Tirrell, (2015) Self-Assembly of a-Helical Polypeptides Driven by Complex Coacervation, *Angew. Chem. Int. Ed.*, 54, 11128 –11132.

(5) Qin, Jian and de Pablo, Juan J., "Ordering Transition in Salt-Doped Diblock Copolymers," *Macromolecules*, 49, 3630-3638 (2016).

(6) Ramirez-Hernandez, Abelardo; Peters, Brandon L.; Andreev, Marat; Schieber, Jay D. ; de Pablo, Juan J."A multichain polymer slip-spring model with fluctuating number of entanglements for linear and nonlinear rheology," *Journal of Chemical Physics*, 143, 24, 243147 (2015). DOI: 10.1063/1.4936878

(7) Hur, Su-Mi; Thapar, Vikram; Ramirez-Hernandez, Abelardo; Khaira, Gurdaman; Segal-Peretz, Tamar; Rincon-Delgadillo, Paulina A.; Li, Weihua; Muller, Marcus; Nealey, Paul F.; de Pablo, Juan J., "Molecular pathways for defect annihilation in directed self-assembly," *Proceedings National Academy of Sciences*, 112, 46, 14144-14149 (2015). DOI: 10.1073/pnas.1508225112

(8) Hinckley, Daniel M.; de Pablo, Juan J., "Coarse-Grained Ions for Nucleic Acid Modeling," *Journal of Chemical Physics*, 11, 5436-5446 (2015). DOI: 10.1021/acs.jctc.5b00341

(9) Whitmer, Jonathan K.; Fluitt, Aaron M.; Antony, Lucas; Qin, Jian; McGovern, Michael; de Pablo, Juan J., "Sculpting bespoke mountains: Determining free energies with basis expansions," *Journal of Chemical Physics*, 143, 4, 044101 (2015). DOI: 10.1063/1.4927147

(10) Hur, Su-Mi; Onses, M. Serdar; Ramirez-Hernandez, Abelardo; Nealey, P.F.; Rogers, J.A.; de Pablo, J.J. "Interplay of Surface Energy and Bulk Thermodynamic Forces in Ordered Block Copolymer Droplets", *Macromolecules*, 2015, 48, 4717-4723.

(11) Hernandez-Ortiz, Juan P.; de Pablo, Juan J., (2015) Self-consistent description of electrokinetic phenomena in particle-based simulations" *J. Chem. Phys.*, 143, 014108.

(12) Qin, Jian ; Li, Jiyuan; Lee, Victor; Jaeger, Heinrich; de Pablo, Juan J.; Freed, Karl F., "A theory of interactions between polarizable dielectric spheres," *Journal of Colloid and Interface Science*, 469, 237-241 (2016). DOI: 10.1016/j.jcis.2016.02.033

(13)   C.G. Arges, Y. Kambe, H.S. Suh, L.E. Ocola, and P.F. Nealey, "Perpendicularly Aligned, Anion Conducting Nanochannels in Block Copolymer Electrolyte Films," *Chemistry of Materials*, 2016, DOI: 10.1021/acs.chemmater.5b04452

(14)   Segal-Peretz, Tamar; Winterstein, Jonathan; Doxastakis, Manolis; Ramirez-Hernandez, , Abelardo; Biswas, Mahua; Ren, Jiaxing; Suh, Hyo Seon; Darling, Seth B.; Liddle, J. Alexander; Elam, Jeffrey W.;.de Pablo, Juan J.; Zaluzec, Nestor J.; Nealey, Paul F, "Characterizing the Three-Dimensional Structure of Block Copolymers via Sequential Infiltration Synthesis and Scanning Transmission Electron Tomography," *ACS Nano,* 9, 5, 5333-5347 (2015). DOI: 10.1021/acsnano.5b01013

(15)   Jorge W. Mok , Yen-Hao Lin , Kevin G. Yager , Aditya D. Mohite , Wanyi Nie , Seth B. Darling, Youngmin Lee , Enrique Gomez , David Gosztola , Richard D. Schaller , and Rafael Verduzco (2015), "Linking Group Influences Charge Separation and Recombination in All-Conjugated Block Copolymer Photovoltaics," *Adv. Func. Mat.*, 25, 5578–5585.

(16)   Chen, W.; Liu, F.; Dyck, O. E.; Duscher, G.; Chen, H.; Dadmun, M. D.; You, W.; Qiao, Q.; Xiao, Z. Huang, J.; Ma, W.; Ade, H. Keum, J. K.; Rondinone, A. J.; More, K. L.; Chen J., (2015) Nanophase Separation in Organic Solar Cells in Organic Solar Cells: Materials, Devices, Interfaces and Modeling, Q. Qiao and K. Iniewski, Editors, *CRC Press*. 2015.

Publications

(17)   Freeman, G.S., Lequieu, J.P., Hinckley, D.M., Whitmer, J.K. and de Pablo, J.J. (2014) DNA Shape Dominates Sequence Affinity in Nucleosome Formation. *Physical Review Letters*, 113, 168101.

(18)   Li, W., Nealey, P.F., de Pablo, J.J. and Mueller, M. (2014) Defect Removal in the Course of Directed Self-Assembly is Facilitated in the Vicinity of the Order-Disorder Transition. Physical Review Letters, 113.

(19)   Whitmer, J.K., Chiu, C.-c., Joshi, A.A. and de Pablo, J.J. (2014) Basis Function Sampling: A New Paradigm for Material Property Computation. *Physical Review Letters,* 113, 168301.

(20)   Onses, M.S., Ramirez-Hernandez, A., Hur, S.-M., Sutanto, E., Williamson, L., Alleyne, A.G., Nealey, P.F., de Pablo, J.J. and Rogers, J.A. (2014) Block Copolymer Assembly on Nanoscale Patterns of Polymer Brushes Formed by Electrohydrodynamic Jet Printing. *Acs Nano*, 8, 6606-6613.

(21)   Priftis, D., Xia, X., Margossian, K.O., Perry, S.L., Leon, L., Qin, J., de Pablo, J.J. and Tirrell, M. (2014) Ternary, Tunable Polyelectrolyte Complex Fluids Driven by Complex Coacervation. *Macromolecules*, 47, 3076-3085.

(22)   Qin, J., Priftis, D., Farina, R., Perry, S.L., Leon, L., Whitmer, J., Hoffmann, K., Tirrell, M. and de Pablo, J.J. (2014) Interfacial Tension of Polyelectrolyte Complex Coacervate Phases. *Acs Macro Letters*, 3, 565-568.

(23) Ramirez-Hernandez, A., Suh, H.S., Nealey, P.F. and de Pablo, J.J. (2014) Control of Directed Self-Assembly in Block Polymers by Polymeric Topcoats. *Macromolecules*, 47, 3520-3527.

(24) Hur, S.-M., Khaira, G.S., Ramírez-Hernández, A., Müller, M., Nealey, P.F. and de Pablo, J.J. (2015) "Simulation of Solvent Reduction in Block Copolymer Films by Solvent Annealing". ACS Macro Letters, 4, 11-15.

(25) Perry, Sarah L.; Li, Yue; Priftis, Dimitrios; M. Tirrell, (2014) The Effect of Salt on the Complex Coacervation of Vinyl Polyelectrolytes, *Polymers*, 6, 1756-1772.

(26) Hur, Su-Mi; Onses, M. Serdar; Ramirez-Hernandez, Abelardo; Nealey, P.F.; Rogers, J.A.; de Pablo, J.J. "Interplay of Surface Energy and Bulk Thermodynamic Forces in Ordered Block Copolymer Droplets", *Macromolecules,* 2015, 48, 4717-4723.

(27) Dylan Kipp, Jorge Mok, Joseph Strzalka, Seth B. Darling, Venkat Ganesan, and Rafael Verduzco, (2015), Rational Design of Thermally Stable, Bicontinuous Donor/Acceptor Morphologies with Conjugated Block Copolymer Additives, *Macro Lett.*, 4, 867−871.

(28) Yang, Y.; Chen, W.; Dou, L.; Chang, W.-H.; Duan, H.-S.; Bob, B.; Li, G.; Yang, Y., (2015) "Molecular Compatibility Enabling High-Performance Multiple Donor Bulk Heterojunction Solar Cells", *Nat. Photon*., 9, 190-198.

(29) Lu, L.; Xu, T.; Chen, W.; Landry, E. S.; Yu, Y., (2014) "Ternary Blend Polymer Solar Cells with Power Conversion Efficiency of 8.22%", *Nat. Photon*. 2014, 8, 716-722.

(30) Shao, M.; Keum, J.; Chen, J. H.; He, Y. J.; Chen, W.; Browning, J. F.; Jakowski, J.; Sumpter, B. G.; Ivanov, I. N.; Ma, Y. Z.; Rouleau, C. M.; Smith, S. C.; Geohegan, D. B.; Hong, K. L.; Xiao, K. "The isotopic effects of deuteration on optoelectronic properties of conducting polymers", *Nat. Commun*. 2014, 5, 4180.

(31) Gao, J.; Chen, W.; Dou, L.; Chen, C.-C.; Chang, W.-H.; Liu, Y.; Li, G.; Yang, Y. "Elucidating Double

(32) Aggregation Mechanisms in the Morphology Optimization of Diketopyrrolopyrrole-Based Narrow Bandgap Polymer Solar Cells". *Adv. Mater*. 2014, 26, 3142–3147.

(33) Gao, J.; Dou, L.; Chen, W.; Chen, C.-C.; Guo, X.; You, J.; Bob, B.; Chang, W.-H.; Strzalka, J.; Wang, C.; Li, G.; Yang, Y. "Improving Structural Order for a High-Performance Diketopyrrolopyrrole-Based Polymer Solar Cell with a Thick Active Layer". *Adv. Energy Mater*. 2014, 4, 1300739.

(34) Wen, J.; Miller, D. J.; Zaluzec, N. J. ; Chen, W.; Darling, S. B.; Xu, T.; He, F.; Yu L. "Direct Visualization of Hierarchical Nanomorphologies in Polymer-Fullerene Bulk Heterojunction Solar Cells Using Chromatic Aberration-Corrected Transmission Electron Microscopy", *Microscopy and Microanalysis* 2014, 20, 1507-1513.

(35) Jung, I. H.; Lo, W.-Y.; Jang, J.; Chen, W.; Zhao, D.; Landry, E. S.; Lu, L.;
Talapin, D. V.; Yu L. "Synthesis and Search for Design Principles of New Electron
Accepting Polymers for All-Polymer Solar Cells", *Chem. Mater*. 2014, 26,
3450−3459.

(36) Lu, L.; Chen, W.; Xu, T.; Yu, Y., (2015) "High-performance ternary blend
polymer solar cells involving both energy transfer and hole relay processes", *Nat.
Commun*., 6, 7327.

(37) Jung, I. H.; Zhao, D.; Jang, J.; Chen, W.; Landry, E. S.; Lu, L.; Talapin, D. V.;
Yu, Y. 2015, "Development and Structure/Property Relationship of New Electron
Accepting Polymers Based on Thieno[2',3':4,5]pyrido[2,3-g]thieno[3,2-c]quinoline-
4,10-dione for All-Polymer Solar Cells", *Chem. Mater*., 27, 5941–5948.

(38) Das, S.; Keum, J. K.; Browning, J. F.; Gu, G.; Yang, B.; Dyck, O.; Do, C.; Chen,
W.; Chen, J.; Ivanov, I. N.; Hong, K.; Rondinone, A. J.; Joshi, P. C.; Geohegan, D.
B.; Duscherd, G.; Xiao K., (2015) "Correlating high power conversion efficiency of
PTB7:PC71BM inverted organic solar cells with nanoscale structures", *Nanoscale*, 7,
15576-15583.

Fundamental Charge Transfer Processes in Stable Free-Radical Organic Polymer Systems

Principal Investigator: Thomas Gennett, Principle Scientist
National Renewable Energy Laboratory (NREL)
15013 Denver West Parkway, Golden, CO 80401-3305
thomas.gennett@nrel.gov

Program Scope:

Isotropic, non-conjugated polymeric materials with stable pendant radical groups are a unique class of electroactive materials that have emerged as potentially deployable materials for energy storage. These polymers facilitate remarkably rapid and reversible charge transfer processes in both pure and hybrid materials. The novel mechanism is dominated by inter-molecular electron-transfer at the radical site, which is in contrast to the more common semiconducting and conducting polymer systems. The focus of this project is to advance the fundamental understanding of the structure-property relationships associated with the mechanism(s) of electron transfer and ion transport, along with associated interfacial mass-transfer processes that impact the charge-transfer processes of organic free-radical polymeric redox active materials.

Our work consists of three tasks; 1) An analytical study of the relationship between structure and charge transfer dynamics; 2) the use of computational tools to develop predictive mechanistic models of charge transfer within the system; 3) organic synthesis directed to define specific physio-chemical properties. These tasks were approached in an integrated, iterative manner to determine the critical factors for the understanding of the important

Figure 1. Model compound (4-oxo-TEMPO) and polymer structures (PTMA, PTMA-X, PNNS) investigated

structure-property relationships. Specifically, the project involves chemical synthesis, electro-chemistry, spectroscopy and theoretical modeling of a series of stable organic radical materials. Initially, we focused on the 2,2,6,6-tetramethylpiperidine-N-oxyl (TEMPO) organic radical moiety incorporated into a complex materials set of poly(4-methacryloyloxy-2,2,6,6-tetramethylpiperidine-N-oxyl) (PTMA) and have expanded our recent efforts to include poly[4-(nitronylnitroxyl)styrene] (PNNS).

Our work was very successful as we established the charge-transfer mechanisms of a series of the TEMPO-containing macromolecules with varying chain lengths and side-chain compositions. As shown in Figure 1, we have investigated the model compound, 4-oxo-2,2,6,6-tetramethylpiperidine-N-oxyl (4-oxo-TEMPO), and compared the results to those for non-cross-linked and cross-linked PTMA oligomers and polymers with: (i) various oligomer chain-lengths; and (ii) controlled densities of the TEMPO radical moieties along the chain (i.e. with some TEMPO-methacrylate units replaced by methyl methacrylate).
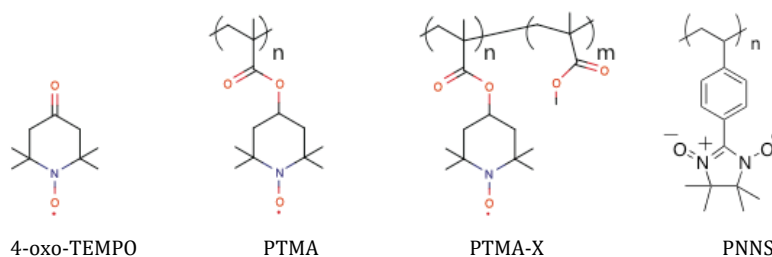
Recent Progress

We have made significant progress in the advancement of the controlled-synthesis of various PTMA materials. These efforts have allowed for a detailed series of electrochemical and spectro-electrochemical (Electron Paramagnetic Resonance, Photoluminescence, Raman and UV-Vis spectroscopies) characterizations of the materials series in various redox states. Furthermore, through theoretical modeling, the possible effects of packing on electron-transport mechanisms of the PTMA materials were predicted. The first-generation theoretical packing morphologies were modeled using classical molecular dynamics simulations and the electronic coupling matrix element between each radical site was then calculated. The following summarizes some of our most recent efforts with a more detailed explanation of results to be presented at the BES Materials Chemistry Principal Investigators' meeting.

Our initial synthetic efforts focused on developing strategies to alter the fundamental charge transport phenomena in the nitroxide radical polymers through structure control. For example we systematically changed the radical density within the polymers by introducing "blanks", or monomers not bearing any nitroxide radical. Several series of copolymers and oligomers bearing 20, 40, 60, 80, and 100 mol % of the radical moiety were synthesized. Recently, through the application of a new synthetic scheme, we have unprecedented access to well-defined nitroxide radical-containing polymers with tunable compositions, architectures, and cross-linking/grafting densities. This technique has allowed us to synthesize a series of nitroxide radical polymers to systematically study the effect of ionic motion in these materials as a function of their glass transition temperature. Specifically:

- A scheme to protect/deprotect nitroxide radicals was developed for cross-linked materials and implemented for the first time in an energy storage device
- Using this technique, a series of nitroxide radical polymers were designed to have dramatically different glass transition temperatures by either (1) incorporating butyl acrylate comonomers into the backbone or (2) by incorporating the nitroxide functionality at the terminus of a long alkyl chain
- Ion transport could now be systematically probed as a function of changes in the energetics of molecular motion in these materials.
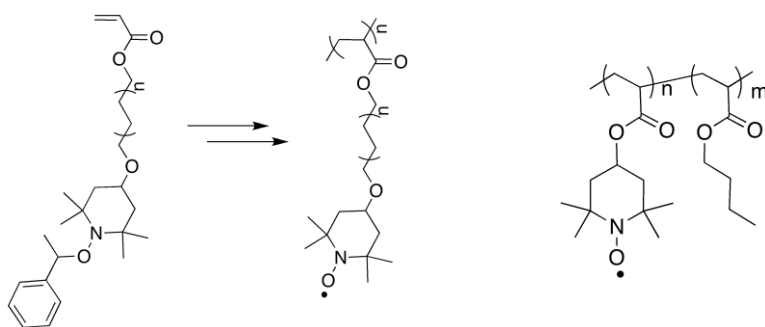

Figure 2: (Left) Polymerization and deprotection of 1-phenylethyl protected nitroxide radical to generate polymers with tunable ionic motion depending on alkyl chain length. (Right) A second class of materials enabled with this synthetic technique that have a tunable composition and hence tunable ionic motion.

We recently showed that the lowest energy conformation/morphology for the polymer material matrix in PTMA is when nitroxide radicals "find" each other and align both inter- and intra-molecular radical-radical associations. Changing the oligomer length and density of redox active species on the backbone allowed us to alter charge transfer rates by controlling this closest approach, fully consistent with our theoretical predictions (Figure 3.). Our work was specific to the PTMA system and we expect that further conformational and charge-transfer mechanism control is possible via steric control from the molecular structure to the meso-scale. Our preliminary EpR results on a new series of TEMPO-Framework materials will be presented.

Figure 3: Dependence of radical-radical spacing on the TEMPO concentration. Our data indicate that above a critical concentration (~60%), the radical-radical distance is constant regardless of phase.
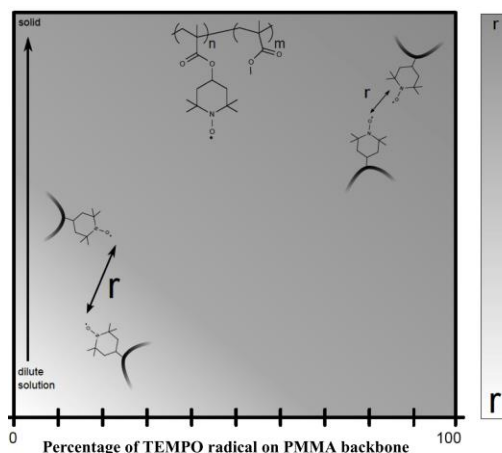
Interestingly, spin-echo EPR experiments illustrate that the density of radical pendant groups on the backbone alters the radical-radical coupling of the polymer. In the solid state we observed that the self-exchange radical-radical interaction is faster than 50 ns regardless of radical density; however, in solution the spin echo experiments show <50 ns radical-radical spin interactions for PTMA-100. For the PTMA-20, these species were slow enough to illustrate that we have different sets of radical-radical spin interactions in the lower radical-density materials. Cyclic voltammetry and ac impedance spectroscopy, also illustrated the existence of two distinct electron-transfer processes for PTMA-20, as compared to PTMA-100.

Recently, we utilized spectroelectrochemical techniques in order to study the rates of charge transfer in a different stable radical polymer system, poly-nitronyl nitroxide (PNNS). By employing such kinetic experiments, we were specifically able to determine rate constants for the diffusion of various counter-ions through PNNS solid-state films, an architecture which most closely resembles a functional electrode stack. PNNS was chosen for our study of ion-diffusion through the radical polymer system because this material exhibits a strong absorption coefficient and allows for measurement in the concentration regime conducive for electrochemical studies (typically up to 10 mM). Additionally, favorable pseudo-crosslinking conditions available to the PNNS radical polymer system allowed for ease of film processing. Through potential modulated spectroscopies we were able to understand the redox performance of PNNS as a function of counter-ion size within the "neat" polymer film. In these experiments the electroactive material shows preference towards the intercalation of the smallest anion, BF_4^-. These ions were capable of deeper film penetration and therefore increased radical oxidation throughout the film. However, with increased charge density reduction experiments suggest that ion-pairing caused a 2-step process for BF_4^- deintercalation as compared to PF_6^- or ClO_4^-.

Within our theoretical efforts, the suite of programs we created allowed us to generate large-scale molecular dynamics simulation of nitroxide polymer materials that was incorporated into a high-throughput python based code, Simulation Toolkit for Renewable Energy Advanced Molecular Modeling (STREAMM) (now available free on-line). This code is comprised of a simulation engine to: combine monomer units to create oligomers of a desired length; replicate them into a simulation cell with a specified solvent concentration if desired; generate input files for LAMMPS or GROMACS molecular dynamics (MD) simulations; extract molecules from MD simulations for electronic structure calculations. Automating this process has helped us to set up and run molecular dynamics simulations of organic radical materials more efficiently.

Through atomistic molecular dynamics simulations of the structure and morphology of polymer films we were able to establish that inter-TEMPO separations are controlled by steric repulsions between methyl groups that dictate the inter- and intra- molecular packing within the various PTMA materials. Electron spin resonance (CW X-band) evaluation of the radical-polymer local environment in both liquid and solid state indicates that the majority of radicals participate in multiple interactions, regardless of TEMPO radical fraction. Furthermore the approximate radical-radical distances calculated from the hyperfine splitting in the solid-state spectra, ~5 Å, correlates well with our theoretical predictions. Recently, we performed molecular dynamics simulations to understand the interaction PTMA and an electrolyte solution consisting of acetonitrile and the BF_4^- electrolyte anion. We found that the large spacing between polymer backbones caused by the radical-containing pendant groups means that although polymer film swells modestly with the absorption of 10% by mass of acetonitrile, the spacing between radical-containing groups that governs electron transfer within the film is unchanged. We also simulated film/electrolyte structures in different states of charge (SOC): 25%, 50%, 75% and 100% of the radical sites converted into cations with equal numbers of BF_4^- counterions included. At each SOC the structure of PTMA, the solvent and the counter ions was examined and the binding of the anion to the nitroxide cation site was found to be on the order of 10's of meV, that varies with SOC. In addition, we found that the cation state is stabilized by the presence of a nearby anion by approximately 1.4 eV which implies a stabilization that leads to the experimentally observed underpotential for reduction of PTMA in $LiBF_4$ (discharge reaction).

Summary: In summary, we have shown that we can control the radical density that is accessible to inter- and intra- molecular electron-hopping through changes in the polymer backbone. We have established that the materials properties of the polymer radical matrix (e.g., cross-linking) do not drastically alter the charge transfer rates but that we can control rates as needed to investigate interfacial processes via modifications of the redox-active group density (PTMA-X) on the polymer backbone. We successfully demonstrated the utility of an iterative experiment/theory loop in the understanding of our electrochemical, EPR and fluorescence quenching studies. Finally we have established that while mechanisms are similar in various polymer-radical systems, they can vary significantly depending on electrolyte compostion and polymer backbone.

Publications:
Spectroelectrochemical Studies of Ion Transfer in Organic Radical-Containing Polymer Films,
Barbara K. Hughes, Wade A. Braunecker, Justin C. Johnson, Rachelle Ihily, Thomas Gennett,
Manuscript awaiting institute approval for submission.

Molecular dynamics simulation study of film structure and conductivity of a nitroxyl-radical containing polymer energy storage material in the presence of electrolyte;
Travis W. Kemper, Thomas Gennett, and Ross E. Larsen
Manuscript awaiting institute approval for submission.

Close Packing of Nitroxide Radicals in Stable Organic Radical Polymeric Materials
Bobela, David C.; Hughes, Barbara K.; Braunecker, Wade A.; Kemper, Travis W.; Larsen, Ross E.; Gennett, Thomas, Journal of Physical Chemistry Letters (2015), 6(8), 1414-1419.

Close packing of radicals in the stable radical polymer, PTMA
Bobela, David C.; Hughes, Barbara; Braunecker, Wade; Larsen, Ross; Kemper, Travis; Gennett, Thomas
Preprints - American Chemical Society, Division of Energy & Fuels (2015), 60(1), 458-459.

Density of States and the Role of Energetic Disorder in Charge Transport in an Organic Radical Polymer in the Solid State   Kemper, Travis W.; Larsen, Ross E.; Gennett, Thomas
Journal of Physical Chemistry C (2015), 119(37), 21369-21375.

Fundamental charge transfer processes in stable free-radical organic polymer systems
Hughes, Barbara; Kemper, Travis; Braunecker, Wade; Larsen, Ross; Bobela, David; Gennett, Thomas
Preprints - American Chemical Society, Division of Energy & Fuels (2015), 60(1), 460-461.

Spectroelectrochemical studies of charge transfer processes in stable nitroxyl radical-containing polymers
Hughes, Barbara K.; Braunecker, Wade; Johnson, Justin C.; Ferguson, Andrew J.; Gennett, Thomas
Preprints - American Chemical Society, Division of Energy & Fuels (2015), 60(1), 408-409.

Quenching of the Perylene Fluorophore by Stable Nitroxide Radical-Containing Macromolecules
Hughes, Barbara K.; Braunecker, Wade A.; Ferguson, Andrew J.; Kemper, Travis W.; Larsen, Ross E.;
Gennett, Thomas Journal of Physical Chemistry B (2014), 118(43), 12541-12548.

Relationship between Molecular Structure and Electron Transfer in a Polymeric Nitroxyl-Radical Energy Storage Material Kemper, Travis W.; Larsen, Ross E.; Gennett, Thomas Journal of Physical Chemistry C (2014), 118(31), 17213-17220.

Patents
Thomas Gennett et.al, *Hybrid Radical Energy storage device and method of making*, April 26, 2016, patent #9,324,992

Thomas Gennett et.al., *Hybrid radical energy storage devices*, January 27, 2015, patent #8,940,444

"Giant" Nanocrystal Quantum Dots: Ideal Platforms for Intrinsic and Extrinsic Manipulation of Carrier-Recombination Processes

Dr. Jennifer A. Hollingsworth and Dr. Han Htoon, Materials Physics & Applications Division: Center for Integrated Nanotechnologies, Los Alamos National Laboratory, Los Alamos, NM

Program Scope

Solid-state lighting (SSL) has the potential to replace less efficient and robust lighting technologies, such as incandescent and fluorescent lamps. Significant inroads into the general-lighting markets have been made in recent years as light-emitting diodes (LEDs) find consumer acceptance. However, significant science challenges remain to be addressed to achieve *disruptive advances* in SSL. Existing technologies suffer from a combination of flaws: non-optimal efficiencies and/or manufacturing/materials costs, and insufficient access to a full-spectrum 'color palette,' resulting in poor color quality and spectral efficiencies. To address these challenges, a transformation in our understanding of and, thereby, our ability to control the processes underlying radiative recombination of electron and hole charge carriers is needed.

We have proposed that semiconductor nanostructures are ideal *platforms for understanding* such fundamental processes, as well as important potential *solutions* to achieving the required control over exciton→photon conversion pathways. For this reason, we have studied a novel class of optical nanomaterial – the "giant" or core/thick-shell nanocrystal quantum dot (g-NQD). As a result of their nanoscale structure, g-NQDs exhibit unique photophysical and chemical behaviors – non-blinking, non-photobleaching, suppressed non-radiative Auger recom-bination, and minimal self-reabsorption stemming from a large effective Stokes shift. Through an experimental and theoretical exploration of g-NQD "nanoengineering," we have developed basic design principles for how nanoscale heterostructures can be synthetically tuned to alter the interplay between between fundamental radiative and nonradiative carrier-recombination processes. We have established CdSe/CdS g-NQDs as uniquely functional "building blocks" for SSL, which has led to an applied program focusing on red-phosphor development. Here, in contrast, we aim to understand the underlying processes influencing exciton lifecycles as these relate both to intrinsic phenomena and interactions with an external environment. We do so through three Research Goals: (1) Defining nanoscale structure-function relationships via developing advanced correlated structure:properties characterization and combinatorial chemistry strategies; (2) Understanding and using intrinsic (core/shell structure) and extrinsic (g-NQD/metal or g-NQD/dielectric interactions) effects to control carrier-recombination at the level of single to a few emitted photons, and (3) Establishing conditions for enhanced multi-photon emission and mesoscale cooperative effects in electromagnetic-field-enhanced g-NQD assemblies.

Recent Progress

Research Goal 1: Defining nanoscale structure:function relations. With our collaborators at Vanderbilt Un., we have developed an approach to perform advanced single-nanostructure optical spectroscopies (Raman, PL, time-resolved PL, photon correlation spectroscopy, etc.) and transmission electron microscopy techniques on the same set of individual g-NQDs.[1] Fig. 1 shows the first direct correlation of a PL time trace, decay curve and 2nd order photon correlation function with the atomic composition of the same g-NQD. This is accomplished by performing optical experiments on the g-NQDs spread on a SiN membrane, where the g-NQDs are later located in TEM with the help of markers. The development allowed us, for example, to determine that, unlike for standard NQDs, g-NQD QY is not determined by a dark fraction, but instead by g-NQD charging.[1]
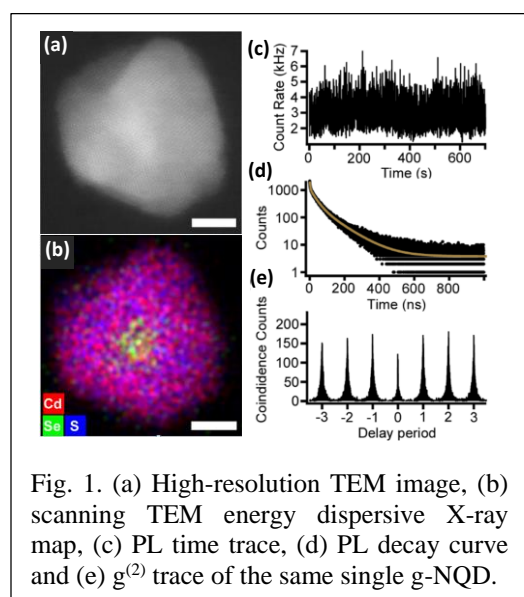

Fig. 1. (a) High-resolution TEM image, (b) scanning TEM energy dispersive X-ray map, (c) PL time trace, (d) PL decay curve and (e) $g^{(2)}$ trace of the same single g-NQD.

Research Goal 2: Intrinsic control: nanoscale-architecture engineering. Through a systematic investigation of the reaction parameters controlling the Successive Ionic Layer Adsorption and Reaction (SILAR) synthesis of thick-shell CdSe/CdS core/shell NQDs, we previously realized a *complete suppression of g-NQD blinking*, as well as a clear structure:function correlation showing a common volume threshold for non-blinking behavior[2] and the strong influence of core size on biexciton quantum yield (QY).[3] Recently, based on our hypothesis that in addition to core size and shell thickness, electronic structure is a key parameter responsible for the unusual g-NQD properties,[4,5] we used effective mass approximations to identify potential new g-NQDs.

Guided by the modeling, we targeted the synthesis of "inverted" quasi type-II CdSe/ZnSe and type II ZnSe/CdS g-NQDs. We successfully overcame challenges to thick-shell synthesis – interfacial alloying and cation exchange. The resulting new nanostructures exhibited unusual single-NQD properties, with CdSe/ZnSe principally emitting from dim "gray" states but having *high two-exciton (biexciton) emission efficiencies* and ZnSe/CdS possessing characteristic g-NQD blinking suppression, but only if shelling was accompanied by *partial* cation exchange.[6]

Extrinsic control: hybrid systems. Toward extrinsic control over fundamental and quantum optical processes, we coupled g-NQDs to Au gap-bar antenna. Using this construct, we investigated individual g-NQD-antenna couples by correlated optical spectroscopy-SEM imaging. Our study revealed that (a) the plasmonic field of the antenna has no effect on Auger recombination of biexcitons[7] and (b) the fringe field of a metal-dielectric-metal nanopatch antenna can provide up to factor of 15 enhancement to the g-NQD radiative recombination rate of the gQD.[8] Beyond enhancing radiative decays, our study on small g-NQD cluster-nanoantenna

couples revealed for the first time that the plasmonic field of gold nano-antenna can induce coupling between two g-NQDs separated by more than 30 nm, forcing them to behave as a single quantum emitter, i.e., like a NQD molecule, which we propose is a potential path toward quantum optical devices (Fig. 2).[9]
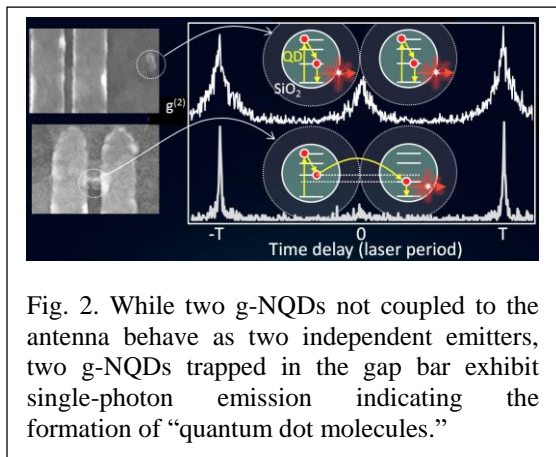

Fig. 2. While two g-NQDs not coupled to the antenna behave as two independent emitters, two g-NQDs trapped in the gap bar exhibit single-photon emission indicating the formation of "quantum dot molecules."

Research Goal 3

Enhanced multi-photon emission in down-conversion light-emitting devices (LEDs). Previously, we demonstrated novel g-NQD advantages in both down-conversion and direct-injection LEDs benchmarked against conventional core/shell NQDs.[10,11] As a basis for our future applied research, we more recently elucidated two important aspects of our advanced g-NQDs (chemistry and photophysics developed as part of this BES program) as down-conversion phosphors: (1) Complete retention of solution-phase QY in the solid-state and resulting near-unity (>85%) down-conversion efficiencies, and (2) Significantly enhanced efficiency and stability under high photon-flux.[12]

Future Plans

Research Goal 1: In a recent review article,[13] E. M. Chan estimated that the development of a hypothetical new nanomaterial requires ~100 reactions to be performed, or 3-12 months assuming reaction times of 1 h and the ability to conduct 2 reactions per day. The situation for g-NQD development is somewhat more grave. The 'workflow' (reaction process) that affords the most interesting single-dot optical properties, i.e., 100% blinking suppression. etc., entails long shell anneal times. Therefore, reactions where 16 monolayers of shell are grown can take ~6 days to complete. This is in large part due to interruptions in the workflow resulting from reliance on human operators for manual addition of shell precursors, which is 'paused' outside the hours of the typical workday. Progress is still possible, as selection of reaction 'process' and g-NQD 'formulation' parameters is based on effective "mining" of existing NQD literature, the g-NQD structure:function correlations we have begun to establish and recent attempts to better integrate theory and modeling. Nevertheless, clear opportunity exists for genuinely rapid evolution of g-NQD properties and development of new systems through "combinatorial" strategies for synthesis and characterization. To this end, we developed a reactor system for automated parallel synthesis of g-NQDs, and will target future work to establishing combinatorial-chemistry optimization and discovery work-flows. We will continue to work with external collaborators to definitively assess g-NQD structure-function relationships, using the knowledge to establish definitive "nanoengineering" design principles and significantly advancing the state-of-the-art in correlated characterization methodologies in doing so. *Research Goal 2:* We will extend our studies of core/shell g-NQDs to include multiple-shell structures and asymmetric structures in the context of intrinsic manipulation of carrier recombination processes, e.g., for the novel result

of suppressed two and three-color emission (unpublished submitted work). We will extend our exploration of external electromagnetic field manipulation of exciton/multi-exciton competitions and g-NQD/g-NQD quantum-coupling enhancement. The proposed novel hybrid structures will be achieved synthetically or established through a range of lithographic techniques, including direct-write pen-and-ink strategies. *Research Goal 3:* We will extend our studies of g-NQD/g-NQD through-field interactions to mesoscale many-emitter assemblies.

References

1. Orfield, N. J. et al. *ACS Nano* **2016***, 10*, 1960-1968.
2. Ghosh, Y. et al. *J. Am. Chem. Soc.* **2012**, *134*, 9634-9643.
3. Mangum, B. D. et al. *Nanoscale* **2014**, *6*, 3712-3720.
4. Hollingsworth, J. A. (*Invited Review Article) Chem. Mater.* **2013***, 25*, 1318-1331.
5. Dennis, A. M. et al. *Nano Lett.* **2012** *12*, 5545-5551.
6. Acharya, K. P. et al. *J. Am. Chem. Soc.* **2015**, *137*, 3755-3758.
7. Wang, F. et al. *Nanoscale* **2015**, *7*, 9387-9393.
8. Wang, F. et al. *Sci. Rep.* **2015**, 5, 14313.
9. Wang, F. et al. *Small* **2015**, *11*, 5176.
10. Kundu, J. et al. *Nano Lett.*, **2012**, *12*, 3031-3037.
11. Pal, B.N. et al. *Nano Lett.* **2012**, *12*, 331.
12. Hanson, C. J. et al. *ACS Appl. Mater. Interfaces* **2015**, *7*, 13125-13130.
13. Chan, E. M. *Chem. Soc. Rev.* **2015**, 44, 1653-1679.

Publications

References **1, 3, 6, 7, 8, 9, 12 above** and
1. Hartsfield, T. et al. *ACS Photonics* **2016**, DOI: 10.1021/acsphotonics.6b00151.
2. Sampat, S. et al. *ACS Photonics* **2016**, *3*, 708-715.
3. Sampat, S. et al. *ACS Photonics* **2015**, *2*, 1505-1512.
4. Karan, N. S. et al. *Chem. Sci.* **2015**, *6*, 2224-2236.
5. Paulite, M. et al. *J. Phys. Chem. Lett.* **2015**, *6*, 706-711.
6. Gao, Y. et al. *Adv. Optical Mater.* **2015**, *3*, 39-43.
7. Hollingsworth, J. A., Htoon, H., Piryatinski, A., Götzinger, S., Sandoghdar, V. (Invited Review) *MRS Bull.* **2015**, *40*, 768.
8. Devore, M. S. et al. *Proc. SPIE 9338*: Colloidal Nanoparticles for Biomedical Applications X., 933812 (2015) DOI:10.1117/12.2082943.
9. Chu, X.-L. et al. *Optica* **2014**, 1, 203-208.
10. Mangum, B. D. et al. *Small* **2014**, 14, 2892-2901.
11. Hollingsworth, J. A. *Coordin. Chem. Rev.* (*Invited Review Article*) **2014**, *263-64*, 197-216.

Rational Synthesis of Superconductors

Mercouri G. Kanatzidis, Materials Science Division, Argonne National Laboratory
Duck Young Chung, Materials Science Division, Argonne National Laboratory

Program Scope

This program emphasizes the synthesis of novel electronic materials and fuels new synergies with several condensed matter physics groups at MSD/ANL. This ambitious collaborative research generates: a) a rational concept for new material design aiming at emerging superconductivity, b) new insights in controlling structural/electronic instabilities in complex materials, c) new synthesis and crystal growth techniques for advanced electronic materials, and d) Fermi surface tuning accompanied by judicious doping which may drive the phase from a normal state to a superconducting state. Our long-term vision is to develop a more complete picture of how materials with superconducting properties can be discovered. We target specific two-dimensional lattices as structural motifs with charge or spin density waves. These can signify that a material is on the verge of an electronic instability, which if properly disrupted, may permit the emergence of superconductivity. The classes of interest include $REMX_2$, $REMX_3$, $RETe_2$, and $RETe_3$ (RE = rare-earth element, M = transition or main-group metal, X = P, As, Sb, Bi). Chemical tuning of properties will be accomplished with alkaline-earth, transition metals, and other main group elements (Ga, Sn, Se), respectively. Novel compounds may also be derived from the series $(REMX_3)_m(REM_3X_2)_n$ and $A(AM_4Te_{3+x})_n(RETe_2)_m(RETe_3)_k$ (A = alkali metal), as two examples of metallic systems and $Cs_4[Bi_{2n+4}Te_{3n+6}]$, $AM_{3+m}Te_{5+m}$, and $(MSe)_n(Bi_2Se_3)_m$, as semiconductor examples. Even if superconductivity does not emerge, these will provide fundamental insights into a wealth of physical phenomena such as charge and spin density waves, phase transitions, magnetic interactions in low-dimensional systems, as well as thermodynamics, kinetics and stability limits of hierarchical structures.

Recent Progress

Exploratory Synthesis of New Phases Targeting New Superconductors: As continued effort, we explored metal chalcogenides, pnictides, borides, and germanides and discovered very unusual compounds with rare electronic and magnetic features.

- A series of semiconductors $OsPn_2$ (Pn = P, As, Sb) is the first instance of single crystals grown by use of metal fluxes. These compounds are found in n-type or p-type indirect narrow band semiconductors depending on the doping state.
- A new iron oxychalcogende (CaO)(FeSe) with a quasi-two-dimensional network with unique combination of O^{2-} and Se^{2-} anions in the same FeSeO layer was synthesized.
- A series of new complex boride crystals of $LaOs_2Al_2B$, $La_2Os_2AlB_2$, $CeRu_2Al_2B$, $La_2Re_3B_7$, and $La_3Re_2B_5$ using La/Ni eutectic metal flux were grown and characterized. $LaOs_2Al_2B$ and $La_2Os_2AlB_2$ have linear T-shaped and squarer planar geometries of the boron atoms in the structure, which is uncommon in known boron compounds. The metallic $CeRu_2Al_2B$ compound is a Kondo-like metallic system with antiferromagnetic and

ferromagnetic transitions at low temperature. $La_2Re_3B_7$ and $La_3Re_2B_5$ are metallic and feature with extensive boron− boron bonding in the structure.

- $(BaF)_2Fe_{2-x}Q_3$ (Q = S, Se) is a novel compound system exhibiting anomalous magnetic properties that are correlated with defects in the Fe-sublattice, indicating that internal defects in $Fe_{2-x}Q_3$ layers play an important role in dictating the magnetic properties of the compound.

- Crystals of the p-type ternary metallic polygermanide $LaPtGe_2$ was grown for the first time. $LaPtGe_2$ exhibits p-type metallic behavior and unlike other compounds with PbO-type layers it does not show superconductivity.

- AF Kondo-lattice $CePd_{1-x}Bi_2$ was obtained from Bi metal flux. The results of resistivity, magnetoresistance, and Hall effect jointly reveal a conventional-metal behavior above 75K and a strong interplay between Kondo and CEF effects below 75 K. However the heavy-fermion superconductivity occurred by the Fermi-surface reconstruction and the magnetic ordering induced by RKKY interaction as in $CeCu_2Si_2$ have no chance to emerge in this compound.

- $[Pb_2BiS_3][AuTe2]$ known as the naturally occurring mineral buckhornite was synthesized. The compound has extremely large anisotropy, $\Gamma = \rho_c/\rho_{ab} \approx 10^4$, comparable to those of the benchmark 2D materials graphite and $Bi_2Sr_2CaCu_2O_{6+\delta}$. The electronic structure features linear band dispersion at the Fermi level and ultrahigh Fermi velocities of 10^6 m/s, which are virtually identical to those of graphene (Figure 1). Our results provide a novel candidate for a monolayer platform to investigate emerging electronic properties.
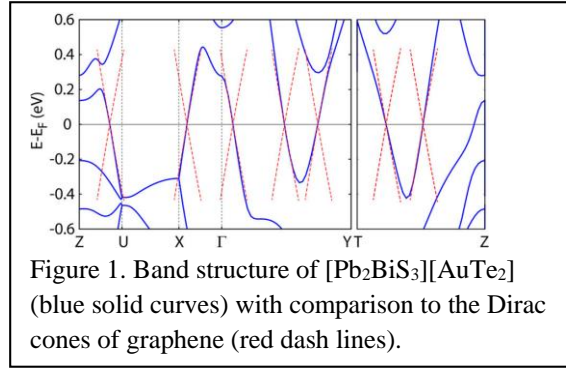
Figure 1. Band structure of $[Pb_2BiS_3][AuTe2]$ (blue solid curves) with comparison to the Dirac cones of graphene (red dash lines).

Detailed investigation of superconductivity and superconducting phase identification in the narrow gap semiconducting system: A 2D homologous series of alkali metal bismuth chalcogenides, intrinsically the valence precise intrinsic narrow gap semiconductors were investigated. We discovered superconductivity near 3 K in the semimetallic $RbBi_{11/3}Te_6$ and $AM_mBi_3Q_{5+m}$ (m = 1,2), (A = Cs, Rb; M = Pb, Sn; Q = Se, Te) by doping alkali metal or chalcogens.

Synthesis of high quality superconductors and Construction of Phase Diagram: For the 122 iron arsenide superconducting systems, we have refined the synthesis procedures and successfully generated high quality samples with precise compositions in both polycrystalline and single crystal across the entire phase diagram of alkaline earth (AE) alkali metal (A) iron arsenide ($AE_{1-x}A_xFe_2As_2$) including $Ba_{1-x}Na_xFe_2As_2$, $Sr_{1-x}Na_xFe_2As_2$, $Ca_{1-x}Na_xFe_2As_2$, $BaFe_2(As_{1-x}P_x)_2$ as well as other combinations that we published in the past years.

- This work enabled collaboration with FWP 58701 to discover multiple exotic magnetic features of iron arsenide superconductors by neutron and x-ray diffraction study. The recent discovery of coexistence of C4 symmetry phase with superconducting region in the $Sr_{1-x}Na_xFe_2As_2$ phase diagram proposed the double Q model supported by coexistence of magnetic and non-magnetic phases observed in Mössbauer spectroscopy (Figure 2). The results were published in Nature Physics.
- From the x-ray and neutron diffraction on $Ba_{1-x}K_xFe_2As_2$, we found the formation of a low-temperature minority magnetic tetragonal phase in $Ba_{0.76}K_{0.24}Fe_2As_2$ in addition to the majority magnetic, orthorhombic phase. The tetragonal magnetic phase is a universal feature of the hole-doped iron-based superconductors. The observations suggest that in this regime the energy levels of the $C2$ and $C4$ symmetric magnetic phases are very close.
- High quality $Cs_xFe_{2-y}Se_2$ single crystals were grown using an elaborate multistep synthesis technique. We demonstrate the existence of a superconducting dome with Tc smoothly evolving as a function of the nominal iron valence. From extensive structural studies using x-ray single-crystal diffraction, we found the complex structures of the majority 245 phase exhibiting both Fe- and Cs-ordered vacancies and also the superstructure of the minority three-dimensional Cs vacancy ordered LT122 phase.
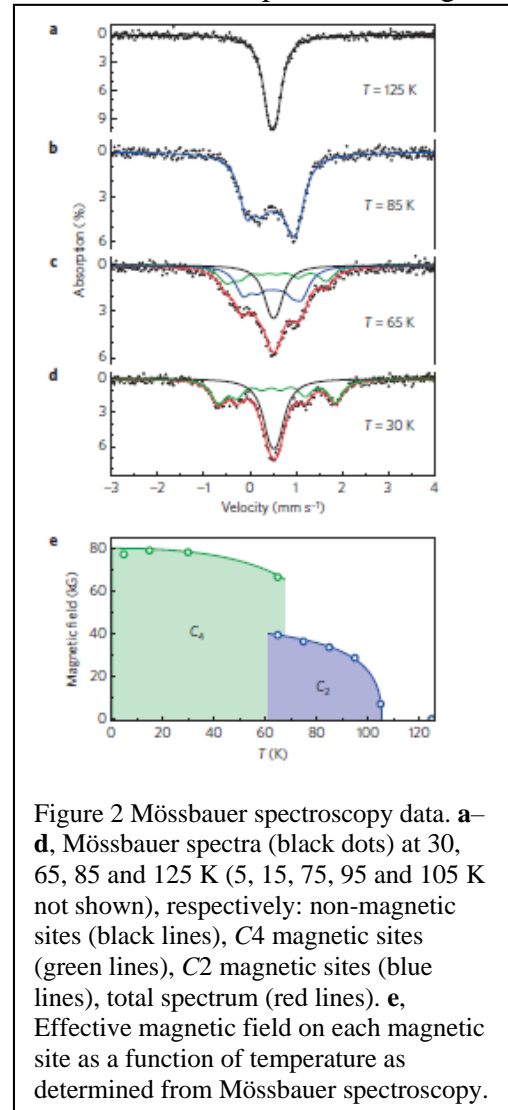
Figure 2 Mössbauer spectroscopy data. **a–d**, Mössbauer spectra (black dots) at 30, 65, 85 and 125 K (5, 15, 75, 95 and 105 K not shown), respectively: non-magnetic sites (black lines), $C4$ magnetic sites (green lines), $C2$ magnetic sites (blue lines), total spectrum (red lines). **e**, Effective magnetic field on each magnetic site as a function of temperature as determined from Mössbauer spectroscopy.

Future Plans

We plan to synthesize materials with a high degree of structural and compositional freedom and chemical/electronic complexity with which to investigate (a) density-wave instabilities (spin and charge), and their suppression through chemical doping in order to generate superconductivity that may emerge from phase competition, and (b) how narrow energy band gaps and facile doping properties could lead to a superconducting state. In the former we investigate low-dimensional intermetallics exhibiting magnetic interactions and spin density waves. In the latter we investigate narrow band ternary and quaternary chalcogenide phases comprising heavy elements such as lead, bismuth, selenium and tellurium. We use a conceptually robust tool in designing, predicting and creating sequences of structurally related materials.

We will explore the following class of complex pnictides (i.e. phosphides, arsenides, antimonides) that feature spin density wave states, intermetallic alloys, and narrow gap semiconductors, searching for new superconductors.

1. We are searching for superconductivity in two-dimensional compounds with square lattice. This includes compounds with pnicogen or chalcogen 2D nets such as $REQX$, $REMX_2$, $REMX_3$ systems (RE = rare earth metals; Q = chalcogen; X = pnicogen), $(AM\text{Te})_n(RE\text{Te}_3)_m$, $A(AM_4\text{Te}_{3+x})_n(RE\text{Te}_3)_m$, $A(AM_4\text{Te}_{3+x})_n(RE\text{Te}_2)_m(RE\text{Te}_3)_k$ (A = alkali metals).

2. The pressure (mechanical or chemical) induced superconductivity can also be realized by intercalation of two different layers. The systems to explore are $(RE\text{O})_n(A)_m(\text{Fe}Pn)_{n+m}$ and $(RE\text{O})_n(AE)_{m/2}(\text{Fe}Pn)_{n+m}$ (Pn = P, As, Sb, Bi) that can be considered as intergrowth structures between the parent $(RE\text{O})(\text{Fe}Pn)$ and $A\text{Fe}Pn$ fragments. In this series the PbO-type FePn slab stays intact.

Figure 3. Phase diagram of Pd$_x$HoTe$_3$ as function of Pd doping, presenting intercalation-induced superconductivity.

3. Intergrowth of LaTe$_3$ and FeTe, MnTe, FeSe, or KMnSe$_2$ will also be investigated. These compounds possess active superconducting layer (structurally anti-PbO type), magnetic and non-magnetic layer, and/or elemental Pn nets that CDW can be induced will be explored. Figure 3 is an example of superconductivity induced by intercalation (doping) of Pd metal in HoTe$_3$ in which Pd intercalation disturb the CDW Te net.

4. Copper and silver chalcogenides exhibit many interesting phenomena including superconductivity, superionic conductivity, phase transitions and high carrier mobilities. By adding alkali metal ions, 2-D metal-chalcogenide layers can be created and the reduced dimensionality can then induce new properties. We investigate KCu$_3$Se$_2$ and KAg$_3$Se$_2$ which are isostructural, narrow band gap semiconductors. KAg$_3$Se$_2$ exhibits high

Figure 4. 2-D structure of KM_3Se$_2$ (M = Cu, Ag).

electron mobility and a high temperature phase transition (on-set ~800 K) that is consistent with sublattice melting observed in superionic conductors. The copper analogue shows no high temperature phase transition, but complex resistivity behavior below room temperature, potentially indicating the formation of a charge density wave. Determination of the high temperature structure of KAg$_3$Se$_2$ will also be investigated. Further, the effects of doping and solid solution K(Ag$_{1-x}$Cu$_x$)$_3$Se$_2$ are also elucidated.

Publications

1. *"Mixed Valent NaCu$_4$Se$_3$: A Two–Dimensional Metal"* Mihai Sturza, Daniel E. Bugaris, Christos D. Malliakas, Fei Han, Duck Young Chung, and Mercouri G. Kanatzidis *Inorg. Chem.* **2016,** 55, 4884-4890.

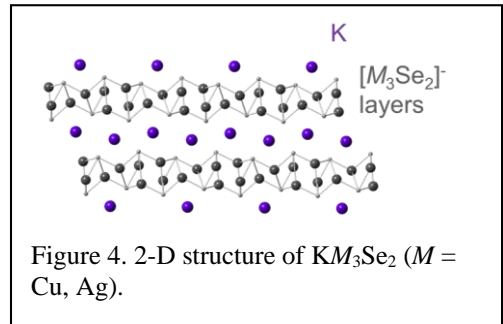2. *"Detailed magnetic and structural analysis mapping a robust magnetic C4 dome in Sr$_{1-x}$Na$_x$Fe$_2$As$_2$"* K. M. Taddei, J. M. Allred, D. E. Bugaris, S. Lapidus, M. J. Krogstad, R. Stadel, H. Claus, D. Y. Chung, M. G. Kanatzidis, S. Rosenkranz, R. Osborn, and O. Chmaissem *Phys. Rev. B* **2016**, *93*, 134510-1-12.

3. *"LaBiS$_3$: An n-Type Semiconductor"* Fei Han, Huimei Liu, Christos D. Malliakas, Mihai Sturza, Duck Young Chung, Xiangang Wan, and Mercouri G. Kanatzidis *Inorg. Chem.* **2016** *55*, 3547–3552.

4. *"Synthesis, Structure, and Complex Magnetism of MIr$_2$In$_8$ (M= Eu, Sr)"* Nicholas P Calta, Sergey L. Bud'ko, Alexandra P Rodriguez, Fei Han, Duck Young Chung, Mercouri G Kanatzidis *Inorg. Chem.* **2016**, *55*, 3128-3135.

5. *"Metallic Borides, La$_2$Re$_3$B$_7$ and La$_3$Re$_2$B$_5$, Featuring Extensive Boron-Boron Bonding"* Bugaris, Daniel; Malliakas, Christos; Chung, Duck Young; Kanatzidis, Mercouri *Inorg. Chem.* **2016**, *55*, 1664-73.

6. *"Hf$_3$Fe$_4$Sn$_4$ and Hf$_9$Fe$_{4-x}$Sn$_{10+x}$: Two stannide intermetallics with low-dimensional iron sublattices"* Nicholas P. Calta, Mercouri G. Kanatzidis *J. Solid State Chem.* **2016**, *236* 130–137.

7. *"Double-Q spin-density wave in iron arsenide superconductors"* J. M. Allred, K. M. Taddei, D. E. Bugaris, M. J. Krogstad, S. H.Lapidus, D. Y. Chung, H. Claus, M. G. Kanatzidis, D. E. Brown, J. Kang,R. M. Fernandes, I. Eremin, S. Rosenkranz, O. Chmaissem, and R. Osborn *Nature Physics* **2016,** 12, 493-498.

8. *"The magnetic structure of NiS$_{2-x}$Se$_x$"* Yano, S.; Louca, D.; Chatterjee, U.; Bugaris, D.E.; Chung, D.Y.; Peng, L.; Grayson, M.; Kanatzidis, M.G. *Phys. Rev. B* **2016** 93, 024409-6.

9. *"Design of active and stable Co–Mo–Sx chalcogels as pH-universal catalysts for the hydrogen evolution reaction"* Jakub Staszak-Jirkovský, Christos D. Malliakas, Pietro P. Lopes, Nemanja Danilovic, Subrahmanyam S. Kota, Kee-Chul Chang, Bostjan Genorio, Dusan Strmcnik, Vojislav R. Stamenkovic, Mercouri G. Kanatzidis and Nenad M. Markovic *Nature Materials* **2015**, *15*, 197-203.

10. *"Tetragonal magnetic phase in Ba$_{1-x}$K$_x$Fe$_2$As$_2$ from x-ray and neutron diffraction"* J. M. Allred, S. Avci, D. Y. Chung, H. Claus, D. D. Khalyavin, P. Manuel, K. M. Taddei, M. G. Kanatzidis, S. Rosenkranz, R. Osborn, and O. Chmaissem arXiv:1505.01433v1, *Phys. Rev. B* **2015,** *92,* 094515-5.

11. *"Cesium Vacancy Ordering in Phase Separated Cs$_x$Fe$_{2-y}$Se$_2$ Single Crystals"* K.M. Taddei, M. Sturza, D.Y. Chung, H.B. Cao, H. Claus, M.G. Kanatzidis, S. Rosenkranz, R. Osborn, O. Chmaissem *Phys. Rev. B* **2015,** 92**,** 094505.

12. *"Crystal Growth, Structures, and Properties of the Complex Borides, LaOs$_2$Al$_2$B and La$_2$Os$_2$AlB$_2$"* Bugaris, D.E.; Han, F.; Im, J.; Chung, D.Y.; Freeman, A.J.; Kanatzidis, M.G. *Inorg. Chem.* **2015**, 54, 8049−8057.

13. *"(CaO)(FeSe): A Layered Wide Gap Oxychalcogenide Semiconductor"* Fei Han, Christos D. Malliakas, Mihai Sturza, Duck Young Chung, and Mercouri G. Kanatzidis *Chem. Mater.* **2015**, *27*, 5695–5701.

14. *"Antiferromagnetic Kondo-lattice in the layered compound CePd$_{1-x}$Bi$_2$ and comparison to the superconductor LaPd$_{1-x}$Bi$_2$"* Fei Han, Xiangang Wan, Daniel Phelan, Constantinos

C. Stoumpos, Mihai Sturza, Christos D. Malliakas, Qing'an Li, Tian-Heng Han, Qingbiao Zhao, Duck Young Chung, and Mercouri G. Kanatzidis *Phys. Rev. B* **2015**, *92,* 045112-8.

15. "*Tuning the magnetic properties of new layered iron chalcogenides (BaF)$_2$Fe$_{2-x}$Q3 (Q = S, Se) by changing the defect concentration on the iron sublattice*" Sturza, Mihai; Allred, Jared; Malliakas, Christos; Bugaris, Daniel; Han, Fei; Chung, Duck Young; Kanatzidis, Mercouri *Chem. Mater.*, **2015**, *27*, 3280-90.

16. *"Flux crystal growth of the ternary polygermanide, LaPtGe$_2$, a p-type metal*" Daniel E. Bugaris, Mihai Sturza, Fei Han, Jino Im, Duck Young Chung, Arthur J. Freeman, Mercouri G. Kanatzidis *Eur. J. Inorg. Chem.* **2015,** *2015*, 2164-72.

17. *"Phase-Change Behavior and Nonlinear Optical Second and Third Harmonic Generation of the One-Dimensional K$_{(1−x)}$Cs$_x$PSe$_6$ and Metastable β-CsPSe$_6$"* Alyssa S. Haynes, Felix O. Saouma, Calford O. Otieno, Daniel J. Clark, Daniel P. Shoemaker, Joon I. Jang, and Mercouri G. Kanatzidis Chem. Mater. **2015**, *27*, 1837−1846.

18. "*Two-dimensional Mineral [Pb$_2$BiS$_3$][AuTe$_2$]: High mobility Charge Carriers in Single-atom-thick Layers*" Fang, Lei; Im, Jino; Stoumpos, Constantinos; Shi, Fengyuan; Dravid, Vinayak; Leroux, Maxime; Freeman, Arthur; Kwok, Wai-Kwong; Chung, Duck Young; Kanatzidis, Mercouri *J. Amer. Chem. Soc.*, **2014,** *137*, 2311-7.

19. "*NaCu$_6$Se$_4$: A layered compound with Mixed Valency and Metallic Properties*" Mihai Sturza, Christos D. Malliakas, Daniel E. Bugaris, Fei Han, Duck Young Chung, and Mercouri G. Kanatzidis *Inorg. Chem.* **2014**, *53*, 12191−12198.

20. "*Low lattice thermal conductivity in Pb$_5$Bi$_6$Se$_{14}$, Pb$_3$Bi$_2$S$_6$, and PbBi$_2$S$_4$: promising thermoelectric materials in the cannizzarite, lillianite, and galenobismuthite homologous series*" Michihiro Ohta, Duck Young Chung, Masaru Kunii and Mercouri G. Kanatzidis *J. Mater. Chem. A,* **2014**, *2*, 20048–20058.

21. "*Coincident structural and magnetic order in BaFe$_2$(As$_{1-x}$P$_x$)$_2$ revealed by high-resolution neutron diffraction*" J. M. Allred, K. M. Taddei, D. E. Bugaris, S. Avci, D.Y. Chung, H. Claus, C. dela Cruz, M. G. Kanatzidis, O. Chmaissem, S. Rosenkranz, and R. Osborn *Phys. Rev. B.* **2014**, *90*, 104513.

22. *"Crystal Growth and Characterization of the Narrow Band Gap Semiconductors OsPn$_2$ (Pn = P, As, Sb)"* Bugaris, Daniel; Malliakas, Christos; Shoemaker, Daniel; Do, Dat Thanh ; Chung, Duck Young; Mahanti, Subhendra D.; Kanatzidis, Mercouri *Inorg. Chem.* **2014**, *53*, 9959-9968.

23. "*In Situ Studies of A Platform for Metastable Inorganic Crystal Growth and Materials Discovery*" Daniel P. Shoemaker, Yung-Jin Hu, Duck Young Chung, Gregory J. Halder, Peter J. Chupas, L. Soderholm, J. F. Mitchell, and Mercouri G. Kanatzidis *Proc. Natl. Acad. Sci. U.S.A.*, **2014**, 111, 10922-10927.

24. *"Dirac Fermions and Superconductivity in the Homologous Structures (Ag$_x$Pb$_{1-x}$Se)$_5$(Bi$_2$Se$_3$)$_{3m}$, m = 1, 2"* L. Fang, C. C. Stoumpos, Y. Jia, A. Glatz, D. Y. Chung, H. Claus, U. Welp, W.-K. Kwok, and M. G. Kanatzidis *Phys. Rev. B.* **2014**, *90*, 020504(R)-1-5.

25. **"*Four High-Temperature Ferromagnets in the Hf–Fe–Sn System"* Nicholas P. Calta, Melanie C. Francisco, Christos D. Malliakas, John A. Schlueter, Mercouri G. Kanatzidis *Chem. Mater.*, **2014**, *26*, 6827-6837.

Energy and Fuels from Multifunctional Electrochemical Interfaces

Nenad M. Markovic (coordinator) and Vojislav R. Stamenkovic

Program Scope

This FWP is an interdisciplinary, atomic/molecular level approach, integrating both experimental- and- computational-based methodologies to design, synthesize, and characterize EC interfaces with tailored properties, with a specific focus on addressing closed-loop energy/chemical/environmental cycles based on water, carbon, and lithium. Two fold strategies isused: *(i)* first is based on *materials-by-design strategy*, involving transferring the knowledge gained from the single crystalline materials and thin metal films to nanoscale materials; and *(ii)* the second relies on the *double-layer-by-design strategy*, bearing precise organization of multiple functionalities of the electrolyte components at the sub-nano-scale regime that is operating in the double layer. The range of materials and electrolytes that is explored by these two strategies is broad, involving metals, metal/metal-oxides, pure oxides, sulfur-based and carbon-based materials as well as aqueous electrolytes with a wide pH range and organic solvents that are traditionally used in the battery systems. The methods used are diverse, ranging from ex situ and in situ optical methods to microscopy-based structural probes to synchrotron-based techniques and classical

Fig. 1. Bridging aqueous and organic electrochemical interfaces

electrochemical methods. Advancing in fundamental understanding of the reaction mechanisms and kinetics involved on well-characterized metal, oxide, and metal/metal-oxide materials in both aqueous-based and organic-based environments is critical in our quest to learn how to design efficient, stable and selective electrochemical systems that are needed by our society.

Recent Progress
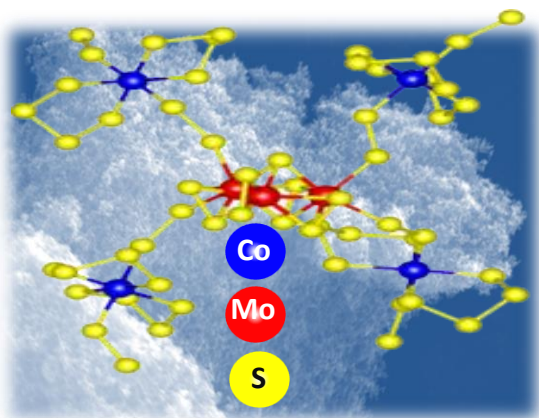
Figure 2 pH universal materials for the HER.

Research activities from the last two years resulted in total of 21 published articles. The unique strength of this program is particularly reflected in eight articles published in high impact journals such as Science, Nature Publishing Group and Angewandte Chemie. Research highlights from some of these articles are summarized below.

CoMoSx as unique pH catalyst for the HER: Three of the fundamental catalytic limitations that have plagued the electrochemical production of hydrogen for decades still remain: low efficiency, short lifetime of catalysts and a lack of low-cost materials. Recently, we have addressed these three challenges by establishing

and exploring an intimate functional link between the reactivity and stability of crystalline (CoS_2 and MoS_2) and amorphous (CoS_x and MoS_x) hydrogen evolution catalysts. We propose that Co^{2+} and Mo^{4+} centers promote the initial discharge of water (alkaline solutions) or hydronium ions (acid solutions). We establish that although CoS_x materials are more active than MoS_x they are also less stable, suggesting that the active sites are defects formed after dissolution of Co and Mo cations. By combining the higher activity of CoS_x building blocks with the higher stability of MoS_x units into a compact and robust $CoMoS_x$ structure, we are able to design a low-cost alternative to noble metal catalysts for efficient electrocatalytic production of hydrogen in both alkaline and acidic environments[1].

Electrochemistry on oxide single crystals: In developing cost-effective complex oxide materials for the oxygen evolution reaction, it is critical to establish the missing links between structure and function at the atomic level. The fundamental practical implications of the relationship on any oxide surface are prerequisite to the design of new stable and active materials. Recently, we have reported an intimate relationship between the stability and reactivity of oxide catalysts in exploring the reaction on strontium ruthenate ($SrRuO_3$) single crystal thin films in alkaline environments [2]. We determine that for $SrRuO_3$ films with the same conductance, the degree of stability, decreasing in the order (001)>(110)>(111), is inversely proportional to the activity. Both stability and reactivity are governed by the potential-induced transformation of stable Ru^{4+} to unstable $Ru^{n>4+}$. This ordered(Ru^{4+})-to-disordered($Ru^{n>4+}$) transition and the development of active sites for the reaction are determined by a synergy between electronic and morphological effects in the higher energy.
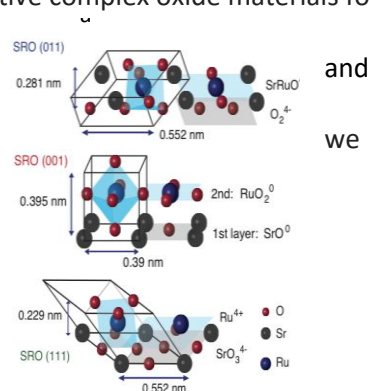
Figure 3. Schematics of SRO(hkl) for probing relationships between activity and stability .

Water as a promotor and catalysts: Water and oxygen electrochemistry lies at the heart of interfacial processes controlling energy transformations in fuel cells, electrolyzers, and batteries. Here, by comparing results for the ORR obtained in alkaline aqueous media to those obtained in ultra-dry organic electrolytes with known amounts of H_2O added intentionally, we propose a new rationale in which water itself plays an important role in determining the reaction kinetics. This effect derives from the formation of $HO_{ad}\cdots H_2O$ (aqueous solutions) and $LiO_2\cdots H_2O$ (organic solvents) complexes that place water in a configurationally favorable position for proton transfer to weakly adsorbed intermediates. We also find that even at low concentrations (<10 ppm), water acts simultaneously as a promoter and as a *catalyst* in the production of Li_2O_2, regenerating itself through a sequence of steps that include the formation and recombination of H^+ and OH^-. We conclude that although the binding energy between metal surfaces and oxygen intermediates is an important descriptor in electrocatalysis, understanding the role of water as a proton-donor reactant may explain many anomalous features in electrocatalysis at metal-liquid interfaces.

Figure 1. Activated water model

Future Plans

We plane to develop *in situ* spectroscopic methods that can detect adsorbed hydroxide oxide species and in particular, "activated water" (OH_{ad}---H-OH). That also assumes

efforts that are aimed at exploring the true nature of interactions between covalently bonded adsorbates and non-covalent forces that operate mainly in the double layer. We also plane to establish establishing functional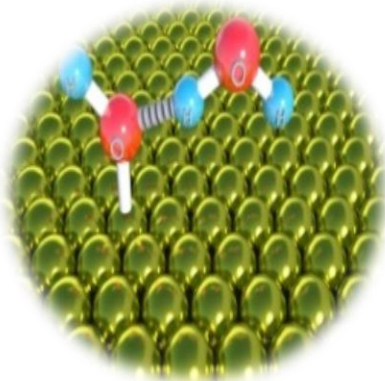 links between stability and activity at atomic and molecular levels Links between the electrochemistry in aqueous and organic electrolytes will be used to define a new landscape of parameters that govern interfacial vs. bulk properties, synthesis, metal deposition, corrosion, formation of SEI, intercalation, diffusion of ions, degradation of organic electrolytes and many other physicochemical properties of materials and electrolytes. The development of *in situ* methods for exploring interfaces in organic environments will quickly be followed by exploring new chemistries that will ultimately determine the future of energy storage systems. Last, but not least, we will explore further common descriptors that can unify electrochemistry of the water cycle with electrochemistry of the carbon cycle and the nitrogen cycle; a topic with broad-based scientific significance and enormous technological importance.

References

[1]   J. S. Jirkovsky,[1] C. D. Malliakas, P. P. Lopes, Nemanja Danilovic, S. S. Kota, K-C Chang, B. Genorio, D. Strmcnik, V. R. Stamenkovic, M. G. Kanatzidis, N. M. Markovic; "Design of Active and Stable Co-Mo-S$_x$ Chalcogels as pH-universal Catalyst for the Hydrogen Evolution Reaction"; *Nature Materials,* **15** (2016)197-202.

[2]   S. Chang, N. Danilovic, K. Chang, R. Subbaraman, A. Paulikas, D. Fong, M. Highland, P. Baldo, V. Stamenkovic, J. Freeland, J. Eastman,N. M. Markovic; "Functional Links between Stability and Reactivity of Strontium Ruthinate Single Crystals during Oxygen   Evolution"; *Nature Communication*, **5** (2014) 1-9.

[3]   J. S. Jirkovský, R. Subbaraman, D. Strmcnik, K. L. Harrison, R. Assary, O. Frank, L. Kobr, G. K. H. Wiberg, B. Genorio, J. G. Connell, P. P. Lopes, V. R. Stamenkovic, L. Curtiss, K. R. Zavadil, N. M. Markovic; "Water as a Promoter and Catalyst for Dioxygen Electrochemistry in Aqueous and Organic media, *ACS Catalysis*, **5**(2015)6600-6607.

Publications

1.   P.P Lopes, D. Strmcnik, D. Tripkovic, J.G. Connell, V.R. Stamenkovic and N.M. Markovic, "Relationships between Atomic Level Surface Structure and Activity/Stability of Platinum Surface atoms in Aqueous Environments" *ACS Catalysis*, **6** (2016) 2536-2544.

2.   D. Li, H Lv, Y. Kang, N.M. Markovic and V.R Stamenkovic, "Recent Advances in the Development of the Oxygen reduction reaction for Low Temperature Fuel cell"; *Anneal Rewires Chemical and Biochemical Engineering* , 2016.08o615-034526.

3.   H. Lv, D. Li, D. Strmcnik, A.P. Paulikas, N.M. Markovic and V.R Stamenkovic, "Recent Advances in the Design of Tailored Nanomaterials for Efficient Oxygen Reduction Reaction"; *Nano Energy*, DOI.org/10.1016/j.nanoen.2016.04.017..

5. D. Strmcnik, P. P. Lopes, B. Genorio, V. R. Stamenkovic and N. M. Markovic, "Design Principles for Hydrogen Evolution Reaction Catalysts Materials"; *Nano Energy*, DOI.org/10.1016/j.nanoen.2016.04.017.

6. B. Genorio, J. S. Jirkovsky, R. S. Assary, J. G. Connell, D. Strmcnik, C. E. Diesendruck, P. P. Lopes, V. R. Stamenkovic, J. S. Moore, L. A. Curtiss, and N. M. Markovic, " Superoxide (Electro)chemistry on Well-defined Surfaces in Organic Solvents"; *J. Phys. Chem. C* (2016). DOI:10.1021/acs.jpcc.5b12230.

7. M. Chi, C. Wang, Y. Lei, G. Wang, D. Li, K. L. More, A. Lupini, L. F. Allard, N.M. Markovic and V. R. Stamenkovic, "Surface Faceting and Elemental Diffusion Behavior at Atomic Scale for Alloy Nanoparticles During in situ Annealing"; *Nature Communication*, **6** (2015) 8925, DOI: 10.1038/ncomms9925.

8. C. Chen, Y, Kang, Z. Huo, Z. Zhu, W. Huang, H. Xin, J. Snayder, D. Li, J. Herron, M. Mavrikakis, M. Chi, K. More, Y. Li, N.M. Markovic, G. Somorjai, P. Yang, and V. R. Stamenkovic, Highly Crystalline Multimetallic Nanoframes with Three-dimensional Electrocatalytic Surfaces"; *Science,* **343** (2014)1339-1343.

9. J. S. Jirkovsky,[1] C. D. Malliakas, P. P. Lopes, Nemanja Danilovic, S. S. Kota, K-C Chang, B. Genorio, D. Strmcnik, V. R. Stamenkovic, M. G. Kanatzidis, N. M. Markovic; "Design of Active and Stable Co-Mo-S_x Chalcogels as pH-universal Catalyst for the Hydrogen Evolution Reaction"; *Nature Materials,* **15** (2016)197-202.

10. J. S. Jirkovský, R. Subbaraman, D. Strmcnik, K. L. Harrison, R. Assary, O. Frank, L. Kobr, G. K. H. Wiberg, B. Genorio, J. G. Connell, P. P. Lopes, V. R. Stamenkovic, L. Curtiss, K. R. Zavadil, N. M. Markovic; "Water as a Promoter and Catalyst for Dioxygen Electrochemistry in Aqueous and Organic media, *ACS Catalysis*, **5**(2015)6600-6607.

11. P. P. Lopes, D. Strmcnik, J. S.-Jirkovisky, J. G. Connell, V. Stamenkovic, N. M. Markovic: "Double Layer Effects in Electrocatalysis: the Oxygen Reduction Reaction and Ethanol Oxidation Reaction on Au(111), Pt(111) and Ir(111) in Alkaline Media Containing Na and Li Cations; *Catalysis Today*, http://dx.doi.org/10.1016/j.cattod.2015.09.010.

12. D. Strmcnik, D. Li, P. P. Lopes, D. Tripkovic, K. Kodama, V. R. Stamenkovic, N. M. Markovic; "When Small is Big: the Role of Impurities in Electrocatalysis; *Topics in Catalysis*, **58,** 1174–1180 (2015)..

13. E. G. Ciapina, P. P Lopez, R. Subbaraman, E. Ticianelli, V. Stamenkovic, D. Strmcnik, N. M. Markovic; "Surface Spectators and their Role in Relationships between Activity and Selectivity of the Oxygen Reduction Reaction in Acid Environments; *Electrochemistry Communications*, **670** (2015) 30-33.

14. S. Chang, J. Connell, N. Danilovic, R. Subbaraman, K. C. Chankg, V. R. Stamenkovic, N.M Markovic; "Activity-Stability Relationships in the Surface Electrochemistry of the Oxygen Evolution Reaction"; *Faraday Discussions*, 176. DOI:10.1039/C4FD00134F 4.61.

15. D. Li, C. Wang, D. Strmcnik, D. Tripkovic, X Sun, Y. Kang, M. Chi, J. Snyder, D. van der Vliet, Y Tsai, V. R. Stamenkovic, S. Sun, N. M. Markovic; "Functional Links between Pt Single Crystal Morphology and Nanoparticles with Different Size and Shape; the Oxygen Reduction Reaction Case; *Energy Environ. Sci.*, **7**(2014)4061-4069.

16. K. Kodama, Y. Morimoto, D. Strmcnik, N. M. Markovic; "Role of Noncovalent Interactions on CO Bulk Oxidation on Pt Single Crystal Electrodes in Alkaline Electrolytes"; *Electroch. Acta*, **152** (2014) 38-42.

17. N. Danilovic, R. Subbaraman, K. Chang, S. Chang, Y. Kang, J. Snyder, A. Paulikas, D. Strmcnik, Y. Kim, D. Myers, V. R. Stamenkovic, N. M. Markovic**; "**Using Surface Segregation to Design Stable Ru-Ir Oxides for the OER in Acidic Environments; *Angew. Chem. Inter. Ed*, DOI: 10.1002/anie.201406455R1

18. S. Chang, J. Connell, N. Danilovic, R. Subbaraman, K-C Chang, V. R. Stamenkovic, N. M. Markovic**; "**Activity-Stability Relationships in the Surface Electrochemistry of the Oxygen Evolution Reaction; *Faraday Transactions*, DOI: 10.1039/c4fd00134f

19. Y. Grunder, N. M. Markovic, P. Thomson, and C. Lucas; "Temperature Effects on the Atomic Structure and Kinetics in Single Crystal Electrochemistry"; *Surface Science*, DOI: 10.1016/j.susc.201406.022

20. N. Danilovic, R. Subbaraman, K-C Chang, S. Chang, Y. Kang, J. Snyder, A. Paulikas, D. Strmcnik, Y. Kim, D. Myers, V. Stamenkovic, N.M. Markovic**,** Activity-Stability Trends for the OER on Monometallic Oxides in Acidic Environments"; *J. Phys. Chem. Lett.*, **5** (2014) 2014-2478.

21. S. Chang, N. Danilovic, K. Chang, R. Subbaraman, A. Paulikas, D. Fong, M. Highland, P. Baldo, V. Stamenkovic, J. Freeland, J. Eastman,N. M. Markovic; "Functional Links between Stability and Reactivity of Strontium Ruthinate Single Crystals during Oxygen   Evolution"; *Nature Communication*, **5** (2014) 1-9.

Diamondoid Science and Applications

Nicholas A. Melosh,[1] Jeremy Dahl,[1] Peter R. Schreiner,[2] Zhi-Xun Shen,[1] Steven Chu,[1] Jelena Vuckovic[1]

[1]SIMES, SLAC National Accelerator Laboratory, Palo Alto CA

[2]University of Giessen, Germany

Program Scope

Diamondoids represent a new class of materials bridging the gap between nanodiamond and organic molecules. This crossover gives them diamond-like properties such as negative electron affinity, and exceptionally strong van der Waals attractions combined with atomically-precise structures and ultrahigh purity. Diamondoids thus present an intriguing system to explore the properties and applications of diamond at unprecedentedly small scales. Structurally, diamondoids are carbon-based nanomaterials consisting of 1-2 nanometer, fully hydrogen-terminated diamond particles (Fig 1). Unlike their conjugated counterparts, graphene or carbon nanotubes, the carbon atoms in diamondoids are sp^3 hybridized, leading to unique electronic and mechanical properties. Diamondoids behave much like small molecules, with atomic-level uniformity, flexible chemical functionalization, and systematic series of sizes, shapes and chiralities. At the same time diamondoids offer more mechanical and chemical stability than other small molecules, and vastly superior size and shape control compared to inorganic nanoparticles.

This program explores and develops diamondoids as a new class of functional nanomaterials based upon their unique electronic, mechanical, and structural properties. This includes diamondoid isolation from petroleum, chemical functionalization, and molecular assembly, as well as electronic, optical and theoretical characterization. We have currently focused on three areas of research: synthesis, direct self-assembly, and seeding nano-diamond growth.
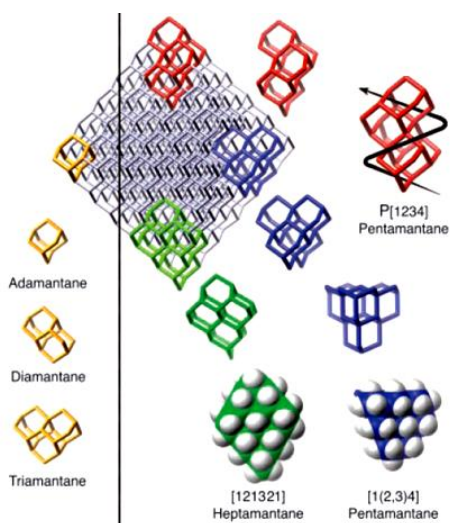
Fig 1. Molecular structures of diamondoids

Recent Progress

Diamondoids have unique electronic and emissive properties due to their combination of negative electron affinity and rigid structure. We recently reported self-assembled monolayers to create electron emitters with low work function, high stability and monochromaticity.(1) We discovered that monolayer diamondoid coatings can reduce the surface work function of gold by ~3 eV, representing the largest work-function reduction

by organic molecules. Experimental and computational results indicate that the diamondoid radical cations, stabilized by their cage-like structures, are responsible for this effect (Fig 2). Furthermore, we developed a generic approach to enhance the stability of the diamondoid coatings with monolayer graphene coverage. The atomically-thin graphene provides a robust diffusion barrier to inhibit the dissociation of surface-attached diamondoids, while allowing electron transmission with little scattering. Using this strategy, we created diamondoid-based photoelectron emitters with kinetic energy distribution less than 20 meV, by far the narrowest energy dispersion observed in diamond-based electron sources. Moreover, these graphene-protected diamondoid emitters can be operated at room temperature with enhanced long-term stability against both thermal and irradiation disruptions. These recent developments, combined with the negative electron affinity and strong electron-phonon coupling in diamondoid, provide a new paradigm to design monochromatic electron sources with high robustness, compact structure and low energy consumption.

Diamondoids are also unique for their true diamond structure that can serve as a homogeneous nucleation site for diamond nucleation and growth. Diamondoid seeding followed by diamond CVD can form high purity, ~10 nm nanoparticles or ultra-

Fig 2. (a) Cationic positive charge on the diamondoid led to increased local emission. (b) Field emission current increased 13,000x with the 6-tetramantane addition.(2)

high seeding density thin films. The small size and high purity makes these ideal candidates for controlling and manipulating optical and quantum coherence through active color centers in diamond. We have exploited the diamondoid's purity and controlled nanoparticle growth to produce high-quality, optically active Silicon-Vacancy (SiV) centers in diamond nanoparticles and thin films on both homoepitaxial and heteroepitaxial structures (2). Diamondoid seeded growth was effective at promoting diamond nucleation and growth on substrates where growth is usually limited, and appears to have low defect densities based upon the SiV lifetimes.

Diamondoids can also be used to direct organic-inorganic hybrid assembly as a powerful approach to synthesize one-dimensional (1D) nanomaterials. Formation of one-dimensional structures as nanowires, nanorods and coordination polymers can be induced by surfactants or metal-organic framework (MOF) linkers. These materials, however, usually lack electrical conductivity due to their amorphous nature, or the existence of organic bridging molecules hampering the conduction pathway. We recently developed the
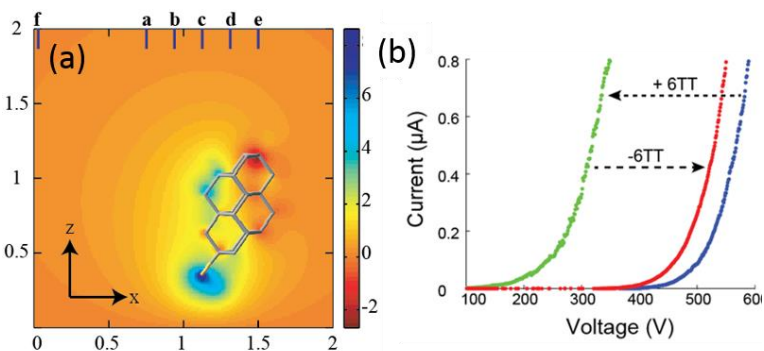
synthesis, and solved the structures of highly crystalline metal organic chalcogenide (MOC) core-shell nanowires with electrical conductivity. Unlike traditional MOF materials, these hybrid structures have solid, electrically-conductive inorganic cores with three-atom cross-sections, representing the smallest possible nanowire. The atomic structures of these ultrasmall nanowires were directed by the strongly-interacting, rigid-cage 'diamondoid' molecules. Density functional theory (DFT) computations show that the strong dispersive interaction between diamondoids dictates a *cis* configuration of the diamondoid sidegroups in the oligomer nuclei, affording a wide access cone for precursor attachment and axial elongation of the nanowires. This novel 'face-on' growth mechanism is in clear contrast to the 'edge-on' growth in most 1D hybrid materials. The structure of the inorganic core can be altered by tailoring the competition between steric repulsion and van der Waals attraction though the choice of diamondoid sizes and shapes, allowing for the modulation of optical and electronic properties without changing the inorganic composition. The diamondoid directed assembly can be applied to a wide variety of semiconductors, superconductors and topological insulators such as cadmium sulfide, bismuth selenide and iron selenide. Our discovery highlights a previously unexplored regime of structure directing agents compared with traditional surfactants, block copolymers or metal-organic framework linkers, and opens up a new approach to create 1D nanostructures with ultra-small dimensions, atomic-scale structural control, wide material choices and tailorable properties.

Future Plans

Among developing further methods for preparation of an even broader variety of functional diamondoid derivatives, we also plan to prepare a variety of diamondoid-carbon nanotube (CNTs) adducts and / or hybrids with small graphene models such as pyrene. These adducts will be thoroughly characterized chemically and physically (especially I/V curves) with a keen eye on single-molecule electronics and the dependence on the size, shape, attachment geometry, and functionalization of the diamondoids.

Given the success of the self-assembly of chalcogen materials from thiol and selenol modified diamondoids we will continue to explore these reactions. These materials fall into a new class of two-dimensional tessellated materials that have been rolled up into tube- or wire like structures. Using the diamondoid thiols as a building block we will explore which of the 3 primary and 7 secondary tessellation constructs are synthetically accessible. These may reveal new electronic and optical properties, similar to the chemical synthetic production of graphene ribbons.

We will also pursue diamond growth using different size and structure diamondoids as seed particles, and explore which defects can be controllably introduced into different size nanoparticles. We hope to achieve N-V and Si-V centers in sub 5nm diameter diamond particles, which have only been previously observed in meteoritic nanodiamond. We will investigate the ultimate stability limit for these defects and measure their environmental

stability and emission yield.

References

(1) Ultra-low effective work functions from diamondoid modified surfaces. Functionalized Nanodiamonds, part 51. Karthik T. Narasimha, Chenhao Ge, Jason D. Fabbri, William Clay, Boryslav A. Tkachenko, Andrey A. Fokin, Peter R. Schreiner, Jeremy E. Dahl, Robert M. K. Carlson, Z. X. Shen, Nicholas A. Melosh. *Nature Nanotech.* **2016**, *11*, 267–272. DOI: 10.1038/nnano.2015.277

(2) Hybrid group IV nanophotonic structures incorporating diamond silicon-vacancy color centers. Functionalized Nanodiamonds, part 52. Jingyuan Linda Zhang, Hitoshi Ishiwata, Thomas M. Babinec, Marina Radulaski, Kai Müller, Konstantinos G. Lagoudakis, Jeremy E. P. Dahl, Robert Edgington, Veronique Souliére, Gabriel Ferro, Andrey A. Fokin, Peter R. Schreiner, Zhi-Xun Shen,* Nick Melosh,* and Jelena Vukovic* *Nano Lett.* **2016**, *15*, 212–217. DOI: 10.1021/acs.nanolett.5b03515

Publications

1. Ultra-low effective work functions from diamondoid modified surfaces. Functionalized Nanodiamonds, part 51. Karthik T. Narasimha, Chenhao Ge, Jason D. Fabbri, William Clay, Boryslav A. Tkachenko, Andrey A. Fokin, Peter R. Schreiner, Jeremy E. Dahl, Robert M. K. Carlson, Z. X. Shen, Nicholas A. Melosh. *Nature Nanotech.* **2016**, *11*, 267–272. DOI: 10.1038/nnano.2015.277

2. Hybrid group IV nanophotonic structures incorporating diamond silicon-vacancy color centers. Functionalized Nanodiamonds, part 52. Jingyuan Linda Zhang, Hitoshi Ishiwata, Thomas M. Babinec, Marina Radulaski, Kai Müller, Konstantinos G. Lagoudakis, Jeremy E. P. Dahl, Robert Edgington, Veronique Souliére, Gabriel Ferro, Andrey A. Fokin, Peter R. Schreiner, Zhi-Xun Shen,* Nick Melosh,* and Jelena Vukovic* *Nano Lett.* **2016**, *15*, 212–217. DOI: 10.1021/acs.nanolett.5b03515

3. Unexpectedly stable primary diamondoid phosphines. Functionalized Nanodiamonds, part 56. Oana Moncea, Maria A. Gunawan, Didier Poinsot, Hélène Cattey, Jonathan Becker, Raisa I. Yurchenko, Ekaterina D. Butova, Heike Hausmann, Marina Šekutor, Andrey A. Fokin,* Jean-Cyrille Hierso,* and Peter R. Schreiner* *J. Org. Chem.* **2016**, *81*, DOI: 10.1021/acs.joc

4. [2](1,3)Adamantano[2]-(2,7)pyrenophane, a Hydrocarbon with a Large Dipole Moment. Functionalized Nanodiamonds, part 55. Paul Kahl, Jan P. Wagner, Ciro Balestrieri, Jonathan Becker, Heike Hausmann, Graham J. Bodwell, and Peter R. Schreiner* *Angew. Chem. Int. Ed.* **2016**, *55*, accepted for publication. DOI: 10.1002/anie.2016

5. Template Synthesis of Linear Chain Nanodiamond Inside Carbon Nanotubes from Bridgehead-Halogenated Diamantane. Functionalized Nanodiamonds, part 50. Yusuke Nakanishi, Haruka Omachi, Natalie A. Fokina, Ryo Kitaura, Peter R. Schreiner, Jeremy E. P. Dahl, Robert M. K. Carlson, and Hisanori Shinohara* *Angew. Chem. Int. Ed.* **2015**, *54*, 10802–10806. DOI: 10.1002/anie.201504904.

6. Transition metal complexes with cage-opened diamondoidtetracyclo[7.3.1.1^{4,14}.0^{2,7}]tetra-deca-6,11-diene. Functionalized Nanodiamonds, part 49. Lars Valentin, Anja Henss, Boryslav A. Tkachenko, Andrey A. Fokin, Peter R. Schreiner, Sabine Becker, Christian Würtele, and Siegfried Schindler* *J. Coord. Chem.* **2015**, *68*, 3295–3301. DOI: 10.1080/00958972.2015.1071802

7. The Functionalization of Nanodiamonds (*Diamondoids*) as key Parameter of the Easily Controlled Self-Assembly in Micro- and Nanocrystals from the Vapor Phase. Functionalized Nanodiamonds, part 46. Functionalized Nanodiamonds, part 43. Maria A. Gunawan, Didier Poinsot, Bruno Domenichini, Sébastien Chevalier, Céline Dirand, Andrey A. Fokin, Peter R. Schreiner,* and Jean-Cyrille Hierso,* *Nanoscale* **2015**, *8*, 1956–1962. DOI: 10.1039/C4NR04442H. Open Access.

8. Toward an Understanding of Diamond sp^2-Defects with Unsaturated Diamondoid Oligomer Models. Tatyana S. Zhuk, Tatyana Koso, Alexander E. Pashenko, Ngo Trung Hoc, Vladimir N. Rodionov, Michael Serafin, Peter R. Schreiner* and Andrey A Fokin* *J. Am. Chem. Soc.* **2015**, *137*, in press. DOI: 10.1021/jacs.5b01555

9. Unconventional Molecule-Resolved Current Rectification in Diamondoid-Fullerene Hybrids. Functionalized Nanodiamonds, part 44. Jason C. Randel, Francis C. Niestemski, Andrés R. Botello-Mendez, Warren Mar, Georges Ndabashimiye, Sorin Melinte, Jeremy E. P. Dahl, Robert M. K. Carlson, Ekaterina D. Butova, Andrey A. Fokin, Peter R. Schreiner, Jean-Christophe Charlier, and Hari C. Manoharan* *Nature Commun.* **2014**, *5*, 4877. DOI: 10.1038/ncomms5877. Open Access.

10. The Functionalization of Nanodiamonds (*Diamondoids*) as key Parameter of the Easily Controlled Self-Assembly in Micro- and Nanocrystals from the Vapor Phase. Functionalized Nanodiamonds, part 43. Maria A. Gunawan, Didier Poinsot, Bruno Domenichini, Sébastien Chevalier, Céline Dirand, Andrey A. Fokin, Peter R. Schreiner,* and Jean-Cyrille Hierso,* *Nanoscale* **2015**, *8*, 1956–1962. DOI: 10.1039/C4NR04442H. Open Access.

11. Selective Preparation of Diamondoid Phosphonates. Functionalized Nanodiamonds, part 44. Andrey A. Fokin,* Raisa I. Yurchenko, Boryslav A. Tkachenko, Natalie A. Fokina, Maria A. Gunawan, Didier Poinsot, Jeremy E. P. Dahl, Robert M. K. Carlson, Michael Serafin, Hélène Cattey, Jean-Cyrille Hierso,* and Peter R. Schreiner* *J. Org. Chem.* **2014**, *79*, 5369–5373. DOI: 10.1021/jo500793m

12. Functionalization of Homodiamantane: Oxygen Insertion Reactions Without Rearrangement with Dimethyldioxirane. Functionalized Nanodiamonds, part 42. Andrey A. Fokin,* Tanya S. Zhuk, Alexander E. Pashenko, Valeriy V. Osipov, Pavel A. Gunchenko, Michael Serafin, Peter R. Schreiner,* *J. Org. Chem.* **2014**, *79,* 1861–1866. DOI: 10.1021/jo4026594

13. Effects of molecular structures of carbon-based molecules on bio-lubrication. Zhou, Y., et al., Carbon, **2015**, *8*, 132-138.

14. A Novel Phase of Li15Si4 Synthesized under Pressure. Zeng, Z., et al., Advanced Energy Materials, 2015: in press.

15. Laser-induced fluorescence of free diamondoid molecules. Richter, R., et al,. *Physical Chemistry Chemical Physics*, **2015**, *17*, 4739-4749.

Innovative Complex and Metal-Rich Materials

Anja-Verena Mudring, Qisheng Lin, Gerd Meyer, Gordon J. Miller, Srinivasa Thimmaiah,

Ames Laboratory, Ames, IA 50011

Program Scope

This program combines experiment with theory to uncover and ultimately design new families of solids that are especially rich in a wide variety of metallic elements. These families include valence networks (Zintl-type), densely packed and cluster-based (Hume-Rothery-type) structures, as well as the emerging polar intermetallics, which involve both clusters and networks. Besides materials discovery, this FWP strives to understand the factors that stabilize metal-rich phases by combining exploratory synthesis, temperature-dependent structure determinations, and first principles electronic structure theory to examine structure-composition-property relationships for complex materials as related to both practical and fundamental issues, e.g., thermoelectric, magnetocaloric, catalytic, and magnetic behavior

Recent Progress

During the past year, this FWP continued investigation of Au-rich complex polar intermetallics in the Ae/R-Au-Tr (Ae = alkaline earth; R = rare earth; Tr = Group 13 metals) systems. For low electron/atom (e/a) values, new modifications of $NaZn_{13}$-related $Ba(Au,Al)_{12-13}$, $Ba(Au,Ga)_{12-13}$, $Eu(Au,Ga)_{12}$ and $Eu(Au, Al)_{12}$ compounds were discovered. Dependence of the structure type on both cation and anion sizes, valence electron concentration, and atomic distributions were investigated. $Ba(Au,Al)_{12-13}$, $Ba(Au,Ga)_{12-13}$ show complete disorder of Au and Ga in the anion sites and the highest symmetry for all compositions and anion ratios. $Eu(Au,Ga)_{12}$ exhibits distortion to tetragonal symmetry with partial ordering of the anion sites, whereas $Eu(Au,Al)_{12}$ is completely ordered and the lowest symmetric representative of the group. Electronic structure calculations revealed the strong preference of Au−Tr heteroatomic bonding and its importance for their structural stabilities. Both Eu compounds order ferromagnetically at temperatures around 10K. When the cation percentage is slightly increased, new representatives of the family with hexagonal, diamond-type Au networks, including $BaAu_5Ga_2$, $BaAu_{4.3}Ga_{2.7}$, $BaAu_{4.5}Ga_{2.4}$, $EuAu_{4.8}Ga_{2.2}$ and $Eu_{1.1}Au_{4.4}Ga_{2.2}$, were discovered. $BaAu_5Ga_2$ crystallizes in an unprecedented structure type, and together with $BaAu_4Ga_3$ and $EuAu_4Ga_3$ also published this year, show remarkable disorder among cations (Ba or Eu) and anion clusters (Au and Ga) in a single crystallographic position. In addition, new members of the Eu-Au-In system, viz., $EuAu_{0.46}In_{1.54}$, $EuAu_{4+x}In_{2-x}$ and $Eu_5Au_{17.3}In_{4.7}$, were discovered and structurally characterized. $Eu_5Au_{17.3}In_{4.7}$ is

a one-dimensional intergrowth of significant structural features of $EuAu_{0.46}In_{1.54}$ (hexagonal-diamond net of Au and In) and $EuAu_{4+x}In_{2-x}$ ($(Au/In)_8$ square prisms).

Tsai-type approximants to quasicrystals, structures we have studied for several years, have stimulated renewed interest with regards to magnetism arising from the arrangement of localized magnetic moments on an icosahedral cluster. Spin glass behavior is often observed for quasicrystal approximants, and magnetic ordering is rare due to the geometry frustrated magnetism. We have discovered and structurally characterized a series of 1/1-1/1-1/1 quasicrystal approximants in the R-Au-Ga (R = Pr, Tb, Er) systems and found surprising long-range magnetic ordering phenomena that can be tuned by varying the Au:Ga molar ratio (Figure 1). All 1/1-1/1-1/1 approximants have the common formula of $R_{\sim3}(Au_xGa_{18.5-x})$. Subtle differences lie in the occupation of specific atomic sites. Magnetic susceptibility measurements reveal paramagnetic $Pr_3Au_{12}Ga_6$ becomes antiferromagnetic with $\Theta = -5.7$ K. $Tb_3Au_{10}Ga_8$ is also antiferromagnetic ($\Theta = -17.3$ K), but shows strong spin-glass behavior below 2.5 K. In contrast, $Tb_3Au_{12}Ga_6$ shows long-range ordering at 5.1 K, which is believed to be ferrimagnetic considering the cluster geometry.

Exploratory syntheses in the transition-metal-rich regions revealed the existence of an isocompositional series EuT_5In (T = Ni, Cu, Ag, Au). $EuNi_5In$ shows an ability to absorb hydrogen under very mild condition leading to further structural and magnetic changes. Both, $EuNi_5In$ and $EuNi_5InH_{1.5}$, exhibit pseudo 2D Kagomé nets of Ni tetrahedra and Eu in the mixed valence state. A systematic investigation of the neighboring transition metal systems proved the existence of the isostructural specimen with Cu, similar structural motifs with Ag and completely different structure with Au. $EuAg_5In$ crystallizes in the $CeCu_6$ structure type and orders antiferromagnetically, while $EuAu_5In$ belongs to $YbMo_2Al_4$ type and ferromagnetically. Both compounds together with $EuCu_5In$ exhibit Eu in the oxidation state +II in contrast to $EuNi_5In$. Triple magnetocaloric effect has been discovered in $EuCu_5In$ making this compound an interesting example for both fundamental research and practical applications.

The Gd-Au-Sb system has been explored using both arc melting and high temperature furnaces for self-flux reactions with low melting components. Our results show that the $Gd_{14}Ag_{51}$ structure type is present in the system allowing Sb substitutions on the silver sites forming $Gd_{14}Au_{45}Sb_6$. A compositionally close compound Gd_3Au_9Sb containing unique Au_9 clusters has been obtained The R_3Au_9M phase appears stable for heavier rare earth elements (Gd, Tb, Ho, and Dy) whereas the $R_{14}Au_{45}M_6$ phase favors lighter rare earths (Ce, Pr, Nd, Gd) with Gd appearing to be the crossing point of stability for this system.

Lithiation of binary polar intermetallics continues to yield fruitful results and is proving to be a practical route for novel complex intermetallics with low e/a values. Although "$CaZn_4$" does not occur within the Ca-Zn binary phase diagram (Figure 2), we have discovered two new Ca-Li-Zn phases with compositions close to $Ca(Li,Zn)_4$. Both phases exhibit close structural relationship to the two $Ca(Li,Zn)_{\sim5}$ intergrowth structures discovered in the previous year.[1] Cubic $Ca_6Li_xZn_{23-x}$ crystallizes with acentric symmetry, featuring *fcc* packing of Ca_6 octahedra and (Zn,Li)-centered $(Zn,Li)_8$ cubes. This new structure type contrasts remarkably to the centric Th_6Mn_{23}-type by

chemical ordering and coloring of tetrahedra with one set of tetrahedra defined by Zn_4, and the other by mixed $(Zn,Li)_4$. Hexagonal $Ca_3Li_{1.81}Zn_{10.33}$ contains a framework of face-shared $(Zn,Li)_{12}$ icosahedral chains bridgegd by 4-bonded Zn atoms, whereas the Ca atoms form triangular units. The presence of Li in these two phases was confirmed by ^7Li NMR spectra.

Systematic reexamination of the structure, atomic distribution, and homogeneity range of the distorted γ-brass type phase Mn_5Al_8 continued to yield new insights about the interplay among valence electron concentration, vacancy formation, and structural stability in complex metallic alloys. Distorted γ-brasses are usually stabilized for higher *vec* values than cubic phases; by mixing zero-valent, $4d^{10}$ Pd into these Mn-Al phases, new ferromagnetic compounds $Mn_{1−x}Pd_xAl$ (0 .1 ≤ x ≤ 0.3) were obtained. These phases adopt simple CsCl-type structures, and their Curie temperatures decrease with increasing Pd content. In addition, we also discovered new phases related to both cubic γ-brass and β-Mn type structures in the Mn-Zn and Mn-Al systems and are studying their electronic structures (Figure 3). Single crystals of $Mn_{5±x}Al_{8∓x}$ phases were grown using Sn-flux.

During our search for novel 3d/4f ferromagnetics, we discovered an unprecedented structure type, $Pr_7Co_2Ge_4$, which features a packing of Co_4Ge_6 clusters with $H_4N_4O_2$-like structure and tetrahedra of rare earth metals. Since $Pr_5Co_2Ge_3$ contains ethylene-like Co_2Ge_4 and polyacene-like Co_4Ge_2 clusters and Pr_3CoGe_2 contains $CoGe_2$ chains, these three examples offer an exciting "playground" to investigate the magnetic behavior in polar intermetallics as from extended nets to metal-organic-like molecular fragments. Magnetic susceptibility measurements show long-range magnetic ordering at 19 K and a positive Weiss temperature of 16 K. Considering the frustrated geometry for rare earth metals, and the unsaturated magnetic moment up to 5.5 T, ferrimagnetic ordering and staging effects are possible, but need higher magnetic field measurement. The effective magnetic moment is slightly larger than expected, possibly arising from 3d/4f exchange interactions.

During the past year, this FWP also actively collaborates with other FWPs in the Ames Laboratory. Some achievements include: (a) discovery of a series of Au-rich compounds $R_3Au_7Sn_3$ (R = Y, La-Nd, Sm, Gd-Tm, Lu); (b) structural characterization of Gd_3Ni_2 and the solid solution $Gd_3Co_xNi_{1-x}$; (c) characterization of new high-T_C ferromagnets based on MnBi doped with small amount (<10 *at.*%) of transition metals; (d) crystal structure characterizations of ferromagnetic ZrMnP, HfMnP, and Fe_5B_2P; the complex twinned structures of $RMg_xCu_{17−x}$ (R = Y, Dy);[2] and the series $R_{2−x}Mg_{1+x}Co_9$ (R = Ce, Gd, Dy), which exhibit large magnetic anisotropies, (e) discovery and characterization of binary compounds R_3Pd_5 (R = Sc, Y, Gd-Lu) and (f) investigation of complex quaternary intermetallics $R_2TAl_xTt_y$. (R = Ce, Pr; T = Co, Pt, Ir; Tt = Si, Ge), (f) contributed to the search for new superconductors by providing reliable structural data and insights for crystal synthesis, including $Bi_2Rh_{3.5}S_2$, its low-temperature phase $Bi_2Rh_3S_2$[3], $Rh_{2.25}InS$,[4] and $CaKFe_4As_4$,[5] (g) analyzed the complex structure of $R_2Pt_6Al_{15}$ (R = Nd, Gd, Er).[6]

Future Plans

Research efforts will continue to tune the magnetic properties of Tsai-type quasicrystal approximants. Work will include systematic variation of R and Tr elements, as well as introducing 3d metals Fe, Co, and Ni.

Significant efforts will focus on the R-Co(Ni)-Ge(Si, Sn) systems to explore the generality of molecular analogues to organic molecules formed in R-rich polar intermetallics. Magnetic properties will be examined so that structure- composition-property relationships can be established for these new materials.

Research on the new quaternary mixed Eu($T1T2$)$_5$In (T = Cu, Ag, Au, etc) phases will be dedicated to the evaluation of their formation and stability ranges in close relationship with their physical properties tuning. The connection between magnetic and magnetocaloric properties of these new phases and their compositions and structures will be estimated.

A few rare-earth rich gold-containing analogues of the Mo$_5$B$_2$Si structure type have been reported recently[7,8] and the current research resulted in a new example Gd$_5$Au$_2$Sn. Synthetic efforts will been made in order to obtain wide range of compositionally related representatives and compare the effects of different rare earths and group 13-15 elements on the structural and physical properties of this type with the main focus on magnetic and magnetocaloric applications.

References

(1)   Lin, Q.; Zhu, R.; Miller, G. J. *Inorg Chem* 2016, *55*, 5041-5050.
(2)   Kong, T.; Meier, W. R.; Lin, Q. S.; Saunders, S. M.; Bud'ko, S. L.; Flint, R.; Canfield, P. C. *Phys. Rev. B* 2016.
(3)   Kaluarachchi, U. S.; Xie, W.; Lin, Q.; Taufour, V.; Bud'ko, S. L.; Miller, G. J.; Canfield, P. C. *Phys. Rev. B* 2015, *91*, 174513.
(4)   Kaluarachchi, U. S.; Lin, Q.; Xie, W.; Taufour, V.; Bud'ko, S. L.; Miller, G. J.; Canfield, P. C. *Physical Review B* 2016, *93*, 094524.
(5)   Mou, D.; Kong, T.; Meier, W. R.; Lochner, F.; Wang, L.-L.; Lin, Q. S.; Wu, Y.; Bud'ko, S. L.; Eremin, I.; Johnson, D.; Canfield, P.; Kaminski, A. *Phys. Rev. Lett.* 2016, *submitted*.
(6)   Manni, S.; Lin, Q. S.; Bud'ko, S. L.; Canfield, P. C. *Phys. Rev. B* 2016.
(7)   Verbovytsky, Y.; Latka, K. *Journal of Alloys and Compounds* 2007, *438*, L4-L6.
(8)   Verbovytsky, Y.; Latka, K.; Pacyna, A. *Journal of Alloys and Compounds* 2007, *442*, 337-340.

Publications

2016

A. Provino, V. Smetana, D. Paudyal, K. A. Gschneidner, A.-V. Mudring, V. K. Pecharsky, P. Manfrinetti and M. Putti "Gd$_3$Ni$_2$ and Gd$_3$Co$_x$Ni$_{2-x}$: magnetism and unexpected Co/Ni

crystallographic ordering," *Journal of the Material Chemistry C*, **4**, 6078-6089, (2016). 10.1039/C6TC01035K

D. Mou, T. Kong, W. R Meier, F. Lochner, L.-L. Wang, Q. S. Lin, Y.Wu, S. L Bud'ko, I. Eremin, DD Johnson, PC Canfield, A. Kaminski, "Enhancement of the superconducting gap by nesting in $CaKFe_4As_4$-a new high temperature superconductor", arXiv preprint arXiv:1606.05643

U. S. Kaluarachchi, Q. S. Lin, W. W. Xie, V. Taufour, S. L. Bud'ko, G. J. Miller, and P. C. Canfield, "Superconducting Properties of $Rh_9In_4S_4$ Single Crystals," *Physical Review B*, **93**, 094524 (2016). 10.1103/PhysRevB.93.094524

T. N. Lamichhane, V. Taufour, S. Thimmaiah, D. S. Parker, S. L. Bud'ko, and P. C. Canfield, "A Study of the Physical Properties of Single Crystalline Fe_5B_2P," *Journal of Magnetism and Magnetic Materials*, **401**, 525-531 (2016). 10.1016/j.jmmm.2015.10.088

Q. S. Lin, R. Zhu, and G. J. Miller, "Tuning Complexity by Lithiation: A Family of Intergrowth Structures Using Condensed Hypho-Icosahedra in the Li-Doped Ca-Zn System," *Inorganic Chemistry*, **55**, 5041-5050 (2016). 10.1021/acs.inorgchem.6b00612

2015

V. Smetana, S. Steinberg, Y. Mudryk, V. Pecharsky, G. J. Miller, and A.-V. Mudring, "Cation-Poor Complex Metallic Alloys in Ba(Eu)–Au–Al(Ga) Systems: Identifying the Keys That Control Structural Arrangements and Atom Distributions at the Atomic Level," *Inorganic Chemistry*, **54**, 10296-10308 (2015). 10.1021/acs.inorgchem.5b01633

U. S. Kaluarachchi, W. W. Xie, Q. S. Lin, V. Taufour, S. L. Bud'ko, G. J. Miller, and P. C. Canfield, "Superconductivity Versus Structural Phase Transition in the Closely Related $Bi_2Rh_{3.5}S_2$ and $Bi_2Rh_3S_2$," *Physical Review B*, **91**, 174513 (2015). 10.1103/PhysRevB.91.174513

Q. S. Lin, "Lithiation-Induced Zinc Clustering of Zn_3, Zn_{12}, and Zn_{-18} Units in Zintl-Like $Ca_{\sim30}Li_{3+x}Zn_{60-x}$ (x=0.44-1.38)," *Inorganic Chemistry*, **54**, 922-929 (2015). 10.1021/ic502326j

Q. S. Lin, V. Taufour, Y. M. Zhang, M. Wood, T. Drtina, S. L. Bud'ko, P. C. Canfield, and G. J. Miller, "Oxygen Trapped by Rare Earth Tetrahedral Clusters in Nd_4FeOS_6: Crystal Structure, Electronic Structure, and Magnetic Properties," *Journal of Solid State Chemistry*, **229**, 41-48 (2015). 10.1016/j.jssc.2015.05.020

Q. S. Lin, Y. M. Zhang, V. Taufour, T. N. Lamichhane, S. L. Bud'ko, P. C. Canfield, K. Dennis, and G. Miller, "On the Structure and Stability of $BaAl_4$-Type Ordered Derivatives in the Sr-Au-

Sn System for the 600 Degrees C Section," *Zeitschrift fuer Anorganische und Allgemeine Chemie*, **641**, 375-382 (2015). 10.1002/zaac.201400549

J. Liu, W. Xie, K. A. G. Jr, G. J. Miller, and V. K. Pecharsky, "Spin-Glass Behavior in a Giant Unit Cell Compound $Tb_{117}Fe_{52}Ge_{113.8(1)}$," *Journal of Physics: Condensed Matter*, **26**, 416003 (2014). 10.1088/0953-8984/26/41/416003.

G. J. Miller, G. Meyer, and A. V. Mudring, "Corbett Special Issue Editorial," *Inorganic Chemistry*, **54**, 705-706 (2015). 10.1021/ic5026125

A. Provino, S. Steinberg, V. Smetana, R. Kulkarni, S. K. Dhar, P. Manfrinetti, and A. V. Mudring, "Gold-Rich $R_3Au_7Sn_3$: Establishing the Interdependence between Electronic Features and Physical Properties," *Journal of Materials Chemistry C*, **3**, 8311-8321 (2015). 10.1039/c5tc00884k

V. Smetana, S. Steinberg, N. Card, A. V. Mudring, and G. J. Miller, "Crystal Structure and Bonding in $BaAu_5Ga_2$ and $AeAu_{4+x}Ga_{3-x}$ (Ae = Ba and Eu): Hexagonal Diamond-Type Au Frameworks and Remarkable Cation/Anion Partitioning in the Ae-Au-Ga Systems," *Inorganic Chemistry*, **54**, 1010-1018 (2015). 10.1021/ic502402y

S. Steinberg, N. Card, and A.-V. Mudring, "From the Ternary $Eu(Au/In)_2$ and $EuAu_4(Au/In)_2$ with Remarkable Au/in Distributions to a New Structure Type: The Gold-Rich $Eu_5Au_{16}(Au/In)_6$ Structure," *Inorganic Chemistry*, **54**, 8187-8196 (2015). 10.1021/acs.inorgchem.5b00257

V. Taufour, S. Thimmaiah, S. March, S. Saunders, K. W. Sun, T. N. Lamichhane, M. J. Kramer, S. L. Bud'ko, and P. C. Canfield, "Structural and Ferromagnetic Properties of an Orthorhombic Phase of MnBi Stabilized with Rh Additions," *Physical Review Applied*, **4**, 014021 (2015). 10.1103/PhysRevApplied.4.014021

S. Thimmaiah and G. J. Miller, "Influence of Valence Electron Concentration on Laves Phases: Structures and Phase Stability of Pseudo-Binary $MgZn_{2-x}Pd_x$," *Zeitschrift für anorganische und allgemeine Chemie*, **641**, 1486-1494 (2015). 10.1002/zaac.201500197

W. Xie, J. Liu, V. Pecharsky, and G. J. Miller, "Γ-Brasses with Spontaneous Magnetization: Atom Site Preferences and Magnetism in the Fe-Zn and Fe-Pd-Zn Phase Spaces," *Zeitschrift für anorganische und allgemeine Chemie*, **641**, 270-278 (2015). 10.1002/zaac.201400539

Nuclear Magnetic Resonance

Alexander Pines
Materials Sciences Division
Lawrence Berkeley National Laboratory

Program Scope

Nuclear Magnetic Resonance (NMR) techniques yield chemical and structural information of unparalleled specificity through experiments that do not perturb the natural state of the object under study. When NMR is combined with magnetic field gradients, this rich spectral information can be resolved as a function of space and time. The resulting Magnetic Resonance Imaging (MRI) experiment is a kind of "chemical microscope" which peers into opaque objects to elucidate the structure and dynamics within. The NMR Program, under Alexander Pines' leadership, pursues transformational theoretical, methodological, and technological advances in magnetic resonance. Our historical contributions include a set of NMR methods and technologies now critical to the application of magnetic resonance in solid materials ranging from proteins to battery electrodes; more recent contributions include the combination of microfluidic technologies with NMR for portable NMR applications; zero field and low field NMR and MRI; techniques for enhancing the sensitivity of NMR through combination of optical methods and magnetic resonance; and, finally, xenon-based molecular sensing.

Recent Progress

The optically pumped nitrogen-vacancy (NV-) defect center in diamond, with almost complete electron spin polarization at room temperature, suggests promising applications for the polarization of nuclear spins both inside and outside the diamond. Such polarization may be achieved independently of the use of high magnetic field, cryogenic temperature, and application of strong high frequency microwaves. We have recently demonstrated the use of room temperature dynamic nuclear polarization (DNP) to unlock an efficient, internal polarization transfer mechanism for bulk nuclear spins in diamond.

We report a new device that allows direct observation of hyperpolarized gas spectra in viscous and aligned media. Our method provides two orders of magnitude signal enhancement compared to standard xenon-129 studies of liquid crystals, which use isotopically pure, thermally - polarized xenon and higher external fields. We also observe, for the first time, a xenon spectrum in pf1 bacteriophage, an aqueous liquid crystal that is too viscous for gas bubbling. This device fits into a standard NMR tube and is constructed from commercially available materials, so any lab equipped for hyperpolarized gas production can use this technique immediately. This work has implications affecting a broad range of communities, from those who have used thermally polarized xenon for liquid crystal characterization and phase transition studies to the biosensing and imaging communities, who seek to use hyperpolarized gases to image biological systems that are viscous or prone to destruction by agitation. This study also opens the doors to determining whether xenon's sensitivity to local molecular order can be exploited for enhancement of molecular detection for biologically - relevant molecules

In order to bring ^{129}Xe NMR into the field, we have developed a new relaxation based sensing technique. While ^{129}Xe NMR can be used to detect proteins and other molecules with targeted sensors, these sensors work by changing the chemical shift of ^{129}Xe upon binding to their target. This reliance on chemical shift makes a strong magnetic field necessary for conventional ^{129}Xe experiments. These strong magnetic fields require extremely large magnets, making ^{129}Xe NMR inconvenient in some cases. To avoid using these magnets, we have developed a new sensing technique that uses the change in the relaxation time of xenon to detect targets with a sensor. When a sensor binds to its target, its rotational correlation time changes. This means that the rotational correlation time of ^{129}Xe will also change when in enters the sensor, increasing the relaxation rate of ^{129}Xe inside the sensor. This change in relaxation rate inside the sensor is sufficiently large to alter the relaxation rate of the entire ^{129}Xe population. Therefore, the presence of the target can be determined by measuring the bulk relaxation rate of ^{129}Xe when a sensor is added to a solution possibly containing its target. Unlike chemical shift based techniques, ^{129}Xe relaxometry can be performed at any magnetic field.

Future Plans

The grand intellectual and fundamental challenges associated with materials chemistry require analytical methods that are non-destructive, sensitive to molecular motion and dynamics, and allow for the structural analysis of condensed. We propose to develop nuclear magnetic resonance (NMR) and related methods to transform its applicability towards the study of materials, with early emphasis on nanoporous interfaces, surfaces, catalysts, defects, and chemically targeted sites. We will supersede the limitations of equilibrium NMR by exploiting artificial atom nitrogen-vacancy (NV) defects in diamond to generate hyperpolarized angular momentum then transfer it across interfaces. We will employ synthetic materials to develop new molecular probes that can target NMR methods to the interfaces, defects, and surfaces of nanoporous materials so as to image and monitor chemical transformations and molecular dynamics in multiphase systems, thereby informing accurate theory and simulation for rapid screening of new nanoporous materials. We will eschew requirements for large NMR magnets required for NMR will be mitigated as we further develop lower field and optical detection methods including zero-field NMR as quantum-fingerprinting tools for materials and chemical analysis. In this way will will enable in operando NMR towards the study of multiple time and length scales in active nanoporous materials. This work will be accomplished by an interdisciplinary team consisting of physical and materials chemistry senior scientist and professor Alexander Pines (MSD, UCB Chemistry), bioorganic chemistry senior scientist and professor Matthew Francis (MSD, UCB Chemistry), and chemical engineering senior scientist and professor Jeffrey Reimer (MSD, UCB Chemical and Biomolecular Engineering) who have made contributions to fundamental science, technology, and human capital in academia, federal laboratories, industry and government.

Publications

1. Nuclear magnetic resonance at millitesla fields using a zero-field spectrometer. *Journal of the American Chemical Society*. Sjolander, T. F, Tayler, M.C.D., Budker, D. & Pines, A. (Submitted, Not Published)

2. 129Xe NMR Relaxation-Based Macromolecular Sensing. *JACS Communication*. Gomes, M.D., Dao, P., Jeong, K., Slack, C.C., Vassiliou., C.C, Francis., M.B., Wemmer, D., & Pines, A. (Submitted, Not Published)

3. Transition-Selective Pulses in Zero-Field Nuclear Magnetic Resonance. *The Journal of Physical Chemistry*, *A* , **120 (25)**, pp 4343–4348, **DOI:** 10.1021/acs.jpca.6b04017 (2016) Sjolander, T. F, Tayler, M.C.D., King, J. P., Budker, D. & Pines, A.

4. Non-Disruptive Dissolution of Hp-129Xe into Viscous Aqueous and Organic Liquid Crystalline Environments. *Angewandte Chemie* **55(15)**:4666-70. **DOI:** 10.1002/anie.201511539 (2016) Truxal, A.E., Slack, C.C., Gomes M.D., Vassiliou, C.C., Wemmer, D.E., & Pines A.

5. Rotaxane-mediated suppression and activation of cucurbit[6]uril for molecular detection by 129Xe hyperCEST NMR, *ChemComm*, DOI: 10.1039/C5CC10410F (2016) Finbloom, J.A., Slack, C.C., Bruns, C.J., Jeong, K., Wemmer ,D.E., Pines, A. & Francis M.B.

6. Measurement of untruncated nuclear spin interactions via zero- to ultralow-field nuclear magnetic resonance, *Physical Review B*, **92(22)**. DOI: 10.1103/PhysRevB.92.220202 (2015), Blanchard, J. W., Sjolander, T. F. ; King, J. P., Ledbetter, M. P., Levine, E. H., Bajaj, V. S. ; Budker, D. & Pines, A.

7. Investigation of DOTA-Metal Chelation Effects on 129Xe Chemical Shift. *ChemPhysChem,* **16(17)** 3573–3577 DOI: 10.1002/cphc.201500806 (2015). Jeong, K., Slack, C.C., Vassiliou, C.C., Dao, P., Gomes, M.D., Kennedy, D.J., Truxal, A.E., Sperling, L.J., Francis, M.B., Wemmer, D.E. & Pines, A.

8. Room temperature in situ nuclear spin hyperpolarization from optically pumped nitrogen vacancy centers in diamond. *Nature Communications*, **6**: 8965 (2015), King JP, Jeong K, Vassiliou CC, Shin CS, Page RH, Avalos CE, Wang H-J, & Pines A.

9. Zero-field nuclear magnetic resonance spectroscopy of viscous liquids, *Journal of Magnetic Resonance*, **250**, 1-6. Doi:10.1016/j.jmr.2014.10.012 (2015) Shimizu, Y., Blanchard, J.W., Pustelny, S., Saielli, G., Bagno, A., Ledbetter, M.P., Budker, D., and Pines, A.

10. Gradient-free microfluidic flow labeling using thin magnetic films and remotely detected MRI, Journal of Magnetic Resonance, 249, 135-140 (2014), Halpern-Manners, N.W., Kennedy, D.J., Trease, D.R., Teisseyre, T.Z., Malecek, N.S., Pines, A., and Bajaj, V.S. (Cover Article)

Hydroxide Conductors for Energy Conversion Devices

Bryan Pivovar

Chemistry and Nanoscience Center, National Renewable Energy Laboratory, Golden, Colorado 80401, 303-275-3809, bryan.pivovar@nrel.gov

Program Scope

The present lack of stable, high performance, hydroxide conducting anion exchange membranes (AEMs) is a key limitation for several extremely promising energy conversion and storage systems and development of such materials is critical if the true potential of these technologies is to be realized. The main goal of this project is to evaluate and understand the factors that govern the stability of quaternary ammonium cationic group, linkage, and tether components of polymer electrolyte anion exchange membranes towards development of novel AEM materials with improved stability. Degradation routes and stability of quaternary ammonium cationic groups bound to perfluorinated polymer backbones is of particular interest. Our previous work within this space focused on evaluating the stability of benzyltrimethylammonium and imidazolium cationic groups as well as establishment of an applied and novel method to evaluate and quantify cation stability under conditions representative of those experienced by AEM materials during device operation. We have since expanded our focus to include not only the stability of cationic groups themselves but also their linkage and tether structure. The stability of AEM materials depends on several factors including the structure of cationic groups as well as tethers and covalent linkages. Using a combined experimental and computational approach we have been developing structure-function-property relationships that have resulted in notable increases in stability and development of improved AEM materials. More specifically, by preparing series of model ammonium cations with varying linkage, tether, and cationic group structure and evaluating their stability using our established method we have identified key degradation routes and problematic structures as well as key structural features that perturb degradation and improve stability. Computational modeling focused on our library of model cations has afforded further understanding of relevant degradation methods. Overall, our work represents a systematic progression of identification of optimized covalent linkage, tether and cationic group structure for improved stability.

Recent Progress

We have designed and synthesized series of model cationic compounds for evaluation of degradation routes and stability of cationic groups, tethers and linkers. We have prepared and performed degradation studies on a series of fluorinated and non-fluorinated sulfonamide-based model compounds (shown in Figure 1). Figure 1 clearly shows that increasing the length of the alkyl spacer leads to significantly improved durability, and that perfluorinated tethers have

lower durability than non-perfluorinated materials. These model compound studies have facilitated investigation of the influence of polymer backbones (perfluorinated vs. non-fluorinated), tether length, and linker structure on the routes of degradation and overall stability

We have employed our previously developed method (1) to study the degradation routes and stability of several new model cations. We have shown that β-hydrogen acidity is strongly influenced by tether length and properties of sulfur bound alkyl group (aliphatic vs. perfluoroalkyl).For a particular series of model compounds representing AEM materials with perfluorinated polymer backbones containing cationic functionality bound via sulfonamide linkages, we have demonstrated significant increases in stability of the cationic group (~30X). By varying tether length/structure
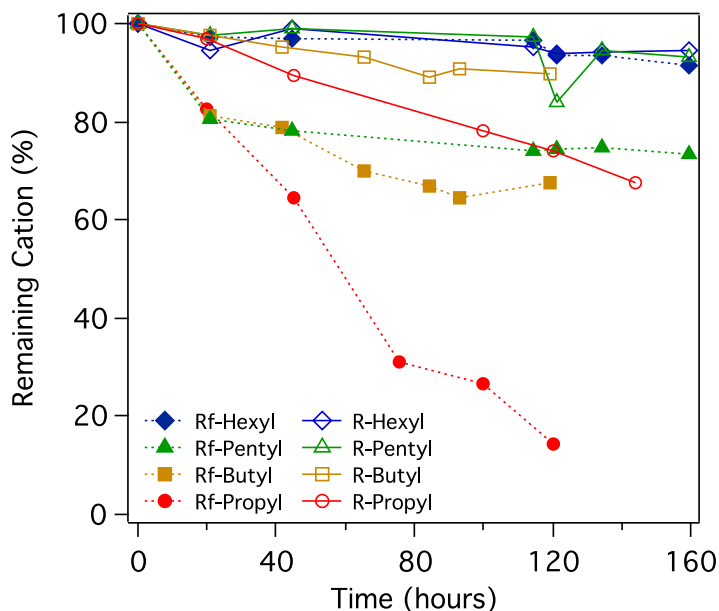

Figure 1: Comparison of degradation rates of perfluorinated (Rf) and non-perfluorinated (R) cations as a function of alkyl linkage length.

we have perturbed certain key degradation methods and identified tethers optimized for maximum stability. We have identified optimal tether length and structure for elimination of unfavorable interactions between polymer backbone/covalent linkage that result in degradation

Using combined experimental and computational approach we have developed key structure-function-property relationships for improving stability of AEM materials. By applying trends and information obtained from our series of
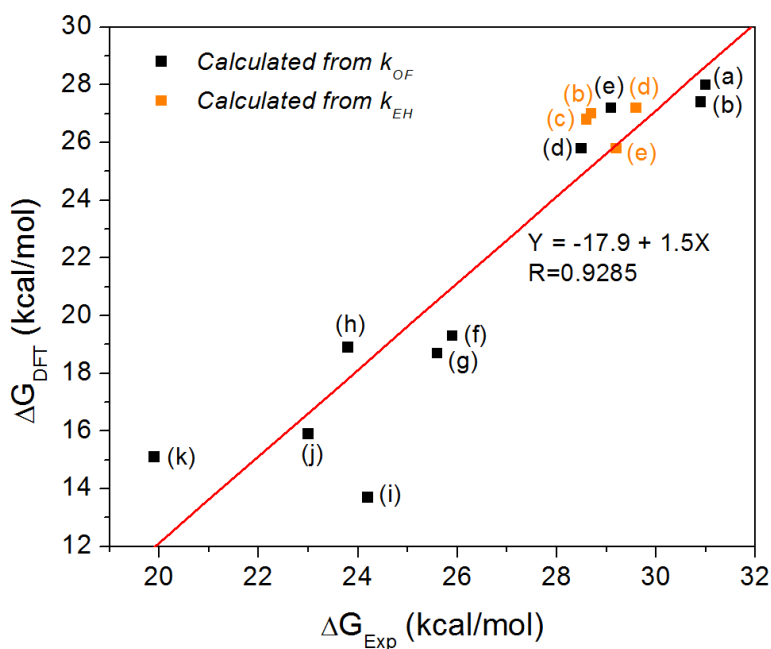

Figure 2: Experimentally measured ΔG vs. DFT calculated ΔG for phosphonium cations synthesized at U. of Delaware.

degradation studies we have identified several new model cation targets designed to perturb key

degradation routes. We have also interacted with Professor's from Penn State University (Mike Hickner), Colorado School of Mines (Dan Knauss), Rensselaer Polytechnic Institute (Chulsung Bae) and University of Delaware (Yushan Yan) to probe cations for degradation applying both computational and experimental tools. Figure 2 shows an example of work done with University of Delaware comparing computational derived degradation barriers to those obtained experimentally.

Future Plans

Continue collaborations with other leading researchers on cation and tether degradation studies

Expand work on tether strategies, including combined experimental and computational studies
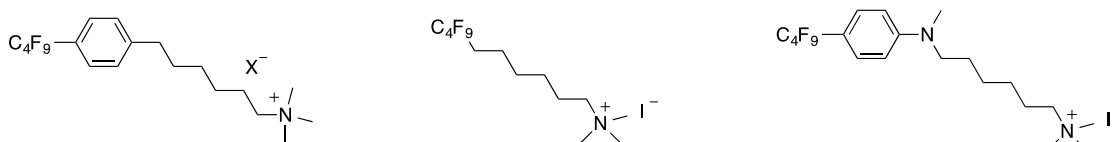
Correlation of free cation studies with polymer based degradation

References

1. Matthew R Sturgeon, Clay S. Macomber, Chaiwat Engtrakul, Hai Long, and Bryan S Pivovar, "Hydroxide Based Benzyltrimethylammonium Degradation: Quantification of Rates and Degradation Technique Development," J. Electrochem. Soc., 162 (4) F366-F372 (2015).

Publications

Matthew R. Sturgeon, Hai Long, Andrew M. Park, and Bryan S. Pivovar, "Advancements in Anion Exchange Membrane Cations," ECS Transactions, 69 (17) 377-383 (2015) doi:10.1149/06917.0377ecst

Matthew R Sturgeon, Clay S. Macomber, Chaiwat Engtrakul, Hai Long, and Bryan S Pivovar, "Hydroxide Based Benzyltrimethylammonium Degradation: Quantification of Rates and Degradation Technique Development," J. Electrochem. Soc., 162 (4) F366-F372 (2015). doi:10.1149/2.0271504jes

Hai Long and Bryan S. Pivovar, "Hydroxide Degradation Pathways for Substituted Benzyltrimethyl Ammonium: A DFT Study," ECS Electrochem. Lett. 2015 4(1): F13-F16; doi:10.1149/2.0041501eel

Hai Long Matthew R Sturgeon, Clay S. Macomber, Chaiwat Engtrakul, and Bryan S Pivovar, "Baseline BTMA Degradation as a Standard for Cationic Degradation in AEMFCs," ECS Trans. 2014 64(3): 1201-1209; doi:10.1149/06403.1201ecs

Hai Long and Bryan Pivovar, "Computational Modeling of Degradation of Substituted Benzyltrimethyl Ammonium," ECS Trans. 2014 64(3): 1211-1219; doi:10.1149/06403.1211ecst

Hai Long and Bryan Pivovar, Hydroxide Degradation Pathways for Imidazolium Cations: A DFT Study, J. Phys. Chem. C, 2014, v.118, p.9880-9888.

Chemical and Mechanical Properties of Surfaces, Interfaces and Nanostructures

Miquel B. Salmeron, Gabor A. Somorjai, Peidong Yang

Materials Sciences Division, LBNL, and Department of Chemistry, Berkeley, CA 94720-7300

Program Scope

We perform molecular level studies of surfaces and interfaces with gases, liquids and solids, focusing on structure, adsorption, and reactions, to obtain a fundamental understanding of the mechanisms that govern the physical and chemical properties of materials for applications to tribology, catalysis, solar energy, fuel cells and energy storage. To achieve a fundamental understanding we synthesize and use single crystals and nanoparticles of controlled size, shape and composition. An important activity of the program is the development of instruments and methods that make possible synthesis of nanoparticles, and microscopy and spectroscopy studies of interfaces in ambient gas pressures and liquids. These include sum frequency generation (SFG) vibrational spectroscopy, high-pressure scanning tunneling microscopy (HP-STM) and synchrotron-based techniques, such as ambient pressure x-ray photoelectron spectroscopy (APPES, also known as AP-XPS), and x-ray absorption spectroscopy (XAS). Today our APPES has been commercialized by SPECS in Germany [1], and Scienta in Sweden [2]. Today it has been implemented in many laboratories and Synchrotrons worldwide.

Recent Progress

Solid-gas interfaces: CO oxidation on low Miller-Index surfaces of Cu.

Using HPSTM and APXPS we have studied the CO oxidation reactions on low Miller-index Cu surfaces. Oxygen binds strongly to Cu forming ordered structures at room temperature. When the oxygen covered surface is exposed to CO the O structures remain unaltered during reaction as long as enough O remains on the surface. At room temperature the $CO + O_{ads} \rightarrow CO_2$ reaction rate is one order of magnitude higher on Cu(111) than on Cu(100), and two orders of magnitude higher than on Cu(110). By measuring the CO and O coverage with XPS as a function of time and temperature we obtained apparent activation energies of 0.24 eV for Cu(111), 0.29 eV for Cu(100), and 0.51 eV for Cu(110), with the difference correlating with the oxygen binding energy, with higher binding corresponding to lower rate. In all surfaces however the transition state has similar energy. XAS and APXPS showed that in a $CO + O_2$ mixture in the pressure range of 10-300 mTorr at 298-413

Fig.1. STM images of Cu(111) showing structural changes under CO gas. The flat, chemically inactive surface stable in UHV (top), decomposes into clusters upon CO adsorption. The clusters remain after removing the CO gas, leaving a highly active surface for reactions involving water. The APXPS results (right), show the facile dissociation of water on the cluster-covered

K, the Cu(111) surface was a mixture of Cu and Cu_2O, but CuO was never observed under the reaction conditions. This finding clarifies the chemical nature of the active surface for CO oxidation, which has been debated in the catalysis literature. [3,4]
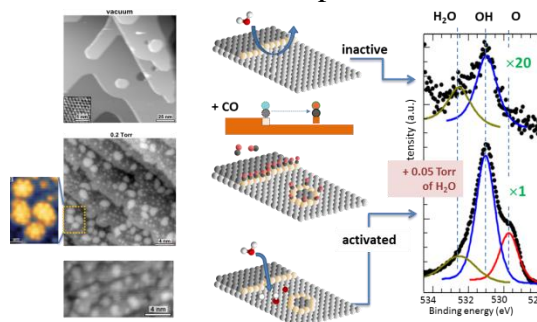
We also found that in the presence of pure CO the structure of three Cu surfaces changes drastically, with the initially clean and flat surface decomposing into clusters decorated by CO adsorbed on the edge atoms [5]. On Cu(111) the clusters are hexagonal in shape (Fig. 1). Calculations show that cluster formation is driven by: (a) the energy gain from CO binding on low coordination Cu atoms; (b) weakening of Cu-Cu binding by adsorbed CO; (c) increased mobility due to the weakened Cu-Cu binding energy. These findings point to a new paradigm applicable to all metal surfaces where restructuring will occur when these conditions are met. In the Cu(111) case, we found that removing the gas phase CO, the restructured surface is highly reactive towards water dissociation. The result is remarkable because the flat Cu(111) surface is very inactive and stays clean in the presence of H_2O even at pressures of 1 Torr.

Nanoparticle synthesis

Pt Nanoparticles in Mesoporous Oxides

Macroporous Al_2O_3, TiO_2, Nb_2O_5, Ta_2O_5, and ZrO_2 were synthesized through a hard-templating approach by removing polystyrene beads in a composite. The oxides had pore sizes greater than 300 nm to incorporate Pt metal nanoparticles capped with PVP (Fig. 2). They are ideal catalysts to investigate size- and support-dependent Pt catalytic selectivity and reaction mechanism in n-hexane isomerization. With Nb_2O_5 and Ta_2O_5 supports, the production of C6 isomers was increased selectively,

Fig.2. (a) Preparation of macroporous oxides using polymer templates, and TEM images of polystyrene beads template (b), and resulting Al_2O_3 replicas with macropores (c). (d) Pt nanoparticle-supported macroporous Al_2O_3 catalysts (d).

due to the effect of strong metal support interaction (SMSI). *In situ* XRD and ambient pressure X-ray photoelectron spectroscopy (APXPS) measurements showed that the oxidation states of Nb_2O_5 and Ta_2O_5 do not change under H_2 or O_2 at temperatures of 360^oC.

CeO₂-Pt@mSiO₂ 3D Tandem catalysts for ethylene hydroformylation

Tandem catalysts are a powerful concept in heterogeneous catalysis where two spatially arranged metal-oxide interfaces in a single nanostructure catalyze sequential chemical conversions. We demonstrated this with the ethylene hydroformylation reaction, where the first chemical conversion is the production of hydrogen and carbon from methanol, followed by ethylene hydroformylation. We have synthesized a new generation of tandem catalysts consisting of CeO_2-Pt core-shell particles in a mesoporous silica shell using a new approach described in ref, [6]. The two interfaces are Pt/CeO_2 and Pt/SiO_2, the former for methanol decomposition to produce CO and H_2, the latter to catalyze ethylene hydroformylation with CO and H_2 [7].

Pt₃Ni Nanoframes

We developed a unique synthesis method of hollow structures, which we called nanoframes (Fig. 3) [8]. It involves the reduction of Pt and Ni precursors in oleyl-amine to form $PtNi_3$ dodecahedrons. A Pt-rich phase segregated to the edges while the interior phase was Ni-rich.
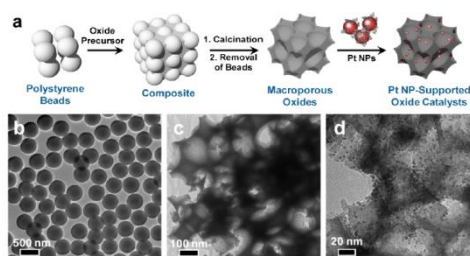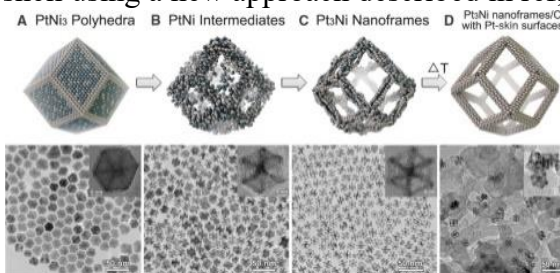
Fig. 3. Schematic and TEM images of $PtNi_3$ rhombic dodecahedron (A) evolving through an intermediate (B) to the Pt_3Ni nanoframe (C). Annealing treatment induce Pt-skin formation on the nanoframe (D).

The segregation allowed for the Ni-rich phase to be spontaneously corroded in air while the Pt-rich phase remained. The resulting structure was a hollow nanoframe with edges of approx. 2 nm in diameter and Pt_3Ni composition. We have shown that these nanoframes are ideal catalyst for the oxygen reduction reaction (ORR), in hydrogen proton exchange membrane fuel cells [9]. The nanoframes demonstrated significant activity enhancement over both PtNi nanoparticles and Pt/C catalysts for ORR. The high surface area three-dimensional structure of the nanoframe allows for efficient use of expensive Pt.

Solid-liquid interfaces

Isopropanol Oxidation on Pt nanoparticles at the solid-liquid and solid-gas interface

We studied the isopropanol oxidation to acetone on Pt nanoparticles in the liquid and gas phases. Using Sum Frequency Generation (SFG) we found that at the solid-liquid interface the reaction is two orders of magnitude slower than at the solid-gas interface, while catalytic activity increased with particle size for both liquid and gas phase reactions. Water substantially promotes isopropanol reactivity in the liquid phase but inhibits it in the gas phase. The results were explained as a result of different orientations of the alcohol molecule, as determined from SFG and DFT calculations. In the gas phase, the isopropyl group is lying down on the Pt surface, while in the liquid phase it is tilted and rotated. The differences in orientation may be responsible for the observed distinctive kinetics of the liquid phase and gas-phase reactions. [10]

The structure of water at the Au-liquid interface and the effect of applied bias

With the new techniques developed in our program we study structure and reactions at the solid-liquid interface using x-ray absorption spectroscopy (XAS). A cell with a 100 nm thick SiN membrane separates the electrode and electrolyte from the vacuum chamber. The working electrode is a thin film evaporated on back side of the membrane. A chopper modulates the incoming x-ray beam intensity to enable lock-in amplifier separation of the total electron yield XAS detected at the gold electrode from electrochemical currents (Fig. 4). With it we determined the molecular structure of water near gold electrodes as a function of bias. The spectra revealed that interfacial water molecules (within ~1 nm) have a different H-bonding structure than in the bulk. Comparison of XAS with first principles calculations revealed that ~50% of the molecules lie flat on the surface with saturated hydrogen bonds, while a significant fraction with broken hydrogen bonds does not contribute to the XAS spectrum because their core-excited states are delocalized due to coupling with the gold. At negative bias the population of flat lying molecules with broken hydrogen bonds increases, producing a spectrum similar to that of bulk water. [11]

Fig. 4. Left: Cell for XAS studies of solid-liquid interfaces. Right: X-ray absorption spectra at the O K-edge of water under open circuit. Right: (a) Total fluorescence yield (TFY) spectrum, reflecting bulk water; (b) Total electron yield XAS, reflecting interfacial water (within ~ 1nm of the Au electrode). (c) TEY XAS of water after covering the gold surface with a ($C_{16}SH$) monolayer. DFT calculated spectra are shown below.
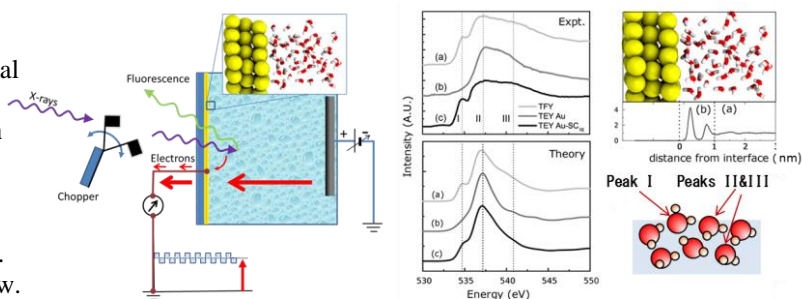
Future Plans

a) Solid-gas interfaces: reaction studies on model single crystal catalysts.

A new STM will be built to extend the pressure range of our current HP-STM to higher pressure (> 2 atm.), and temperatures of few hundred degrees C. We will apply it to studies of Fischer-Tropsch, ammonia synthesis, and other reactions. We will also study the reactions of CO_2 on Cu, Co, and Ni allow crystals, focusing on the adsorption of CO_2, a key reaction step in many reactions, including the reverse water gas shift ($CO_2 + H_2 \leftrightarrow CO + H_2O$), and methanol synthesis.

b) Synthesis, Characterization, and Chemical Properties of Nanoparticles
- We will synthesize 2-10 nm size bimetallic nanoparticles and study their activity and selectivity.
- We will synthesize nanoparticles decorated Metal-Organic Frameworks (MOFs)
- We will expand our studies of ternary metal nanoframes for enhanced ORR Stability

c) Solid-liquid interfaces

We will bench-mark our XAS approach by studying reactions on Pt electrodes extensively studied in the past in H_2SO_4 (aq.). We also plan to make extensive use of a new electron transparent graphene membrane scheme (Fig. 4) for XPS studies. We will focus on CO_2 reactions in gas and in water using bicarbonate solutes (to produce CO_3H^+). The formation of alcohol products will be studied by XPS. Preliminary results show that our instrument is sensitive to gases at pressures from Torr to several atmospheres (Fig. 4).
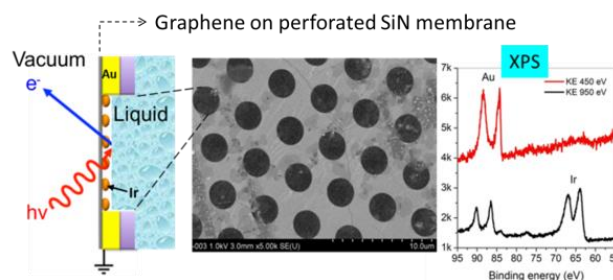

Fig. 4. Cell for XPS studies. A graphene membrane covers an array of 1 μm holes separating the cell from the Synchrotron beam line. Right: XPS of Ir clusters deposited on the membrane in water.

References

[1] http://www.specs.de/cms/front_content.php?idcat=269
[2] http://www.scientaomicron.com/en/products/354/1179
[3] B. Eren, G. Somorjai, M. Salmeron, et al. *J. Phys. Chem. C.* 119, 14669 (2015).
[4] B. Eren, C. Heine, H. Bluhm, G. Somorjai, M. Salmeron. *JACS.* 137, 11186 (2015).
[5] B. Eren, G. Somorjai, M. Salmeron, et al. *Science* 351, 475 (2016).
[6] S. Naito, M. Tanimoto. *J. Chem. Soc., Chem. Commun.* 1403 (1989).
[7] S.H. Joo, P. Yang, G.A. Somorjai, et al. *Nat. Mat.* 8, 126 (2009).
[8] C. Chen, G. Somorjai, P. Yang, et al. *Science*, 343 (2014) 1139-1343.
[9] V.R. Stamenkovic, et al. *Science*, 315 (2007) 493.
[10] H. Wang et al. *J. Am. Chem. Soc.* 136, 10515-10520 (2014)
[11] J. J. Velasco-Velez, M. Salmeron, et al. *Science.* 346, 831 (2014).

Publications (2014-2016)

1. Chen Chen, Yijin Kang, Ziyang Huo, Zhongwei Zhu, Wenyu Huang, Huolin Xin, Joshua D. Snyder, Dongguo Li, Jeffrey A. Herron, Manos Mavrakis, Miaofang Chi, Karren L. More, Yadong Li, Nenad M. Markovic, Gabor A. Somorjai, Peidong Yang and Vojislav R. Stamenkovic, "Highly Crystalline Multimetallic Nanoframes with Three-Dimensional Electrocatalytic Surfaces", Science, 343, 1339, 2014.

2. Kwangjin An, Selim Alayoglu, Nathan Musselwhite, Kyungsu Na and Gabor A. Somorjai. "Designed Catalysts from Pt Nanoparticle-Supported on Macroporous Oxides for Selective Isomerization of n-hexane". J. Am. Chem. Soc. 136, 6830 (2014).

3. G. Melaet, S. Alayoglu, Cheng-Shiuan Li, Walter T. Ralston, Kwangjin An, N. Musselwhite, B. Kalkan and G.A. Somorjai, "Evidence of Highly Active Co Oxide Catalyst for the Fischer-Tropsch Synthesis and CO_2 Hydrogenation", J. Am. Chem. Soc. 136, 2260 (2014).

4. Zhongwei Zhu, Cedric Barroo, L. Lichtenstein, Baran Eren, Cheng-Hao Wu, Baohua Mao, Thierry Visart de Bocarme, Zhi Liu, Norbert Kruse, Miquel Salmeron, Gabor A. Somorjai. "Influence of Step Geometry on the Reconstruction of Stepped Platinum Surfaces Under Ethylene and CO". J. Phys. Chem. Lett. 5, 2626-2631 (2014).

5. Hailiang Wang, Andras Sapi, Christopher Thompson, Fudong Liu, Danylo Zherebetskyy, James krier, Lindsay Carl, Xiaojun Cai, Lin-Wang Wang, Gabor A. Somorjai. "Dramatically Different Kinetics and Mechanism at Solid/Liquid and Solid/Gas Interfaces for Catalytic Isopropanol Oxidation over Size-Controlled Platinum Nanoparticles". J. Am. Chem. Soc. 136, 10515-10520 (2014).

6. James M. Krier, William D. Michalak, Xiaojun Cai, Lindsay Carl, Kyriakos Komvopoulos and Gabor A. Somorjai. Sum Frequency Generation Vibrational Spectroscopy Study of 1,3-Butadiene Hydrogenation on 4 nm $Pt@SiO_2$, $Pd@SiO_2$ and $Rh@SiO_2$ Core-Shell Catalysts". Nano Letters, 15, 39-44 (2014).

7. Sabine Maier, Ingeborg Stass, Jorge I. Cerda, Miquel Salmeron. "Unveiling the mechanism of water partial dissociation on Ru(0001) via variable temperature scanning tunneling microscopy and density functional theory". Phys. Rev. Letters. 112, 126101 (2014).

8. Juan Velasco-Velez, Cheng-Hao Wu, Bo-Yao Wang, Yinghui Sun, Yuegang Zhang, Jinghua Guo, Miquel Salmeron. "Polarized X-ray Absorption Spectroscopy Observation of Electronic and Structural Changes of CVD Graphene in Contact with Water". J. Phys. Chem. C. 118, 25456 (2014).

9. J. J. Velasco-Velez, C. H. Wu, Tod A. Pascal, L. F. Wan, J.-H. Guo, D. Prendergast, and Miquel B. Salmeron. "The structure of interfacial water on gold electrodes studied by x-ray absorption spectroscopy" Science. 346, 831 (2014).

10. Hyunsoo Lee, Yabing Qi, Sangku Kwon, Miquel Salmeron, and Jeong Young Park. "Large changes of graphene conductivity as a function of lattice orientation between stacked layers". Nanotechnology. 26, 015702 (2015).

11. Baran Eren, Leonid Lichtenstein, Cheng Hao Wu, Hendrik Bluhm, Gabor A. Somorjai, and Miquel Salmeron. "Reaction of CO with pre-adsorbed Oxygen on Low-Index Copper Surfaces: An Ambient Pressure X-ray Photoelectron Spectroscopy and Scanning Tunneling Microscopy Study". J. Phys. Chem. C. 119 (2015).

12. S. Maier, I. Stass, X. Feng, A. Sisto, A. Zayak, J.B. Neaton, and M. Salmeron. "Dehydrogenation of ammonia on Ru(0001) by electronic excitation". J. Phys. Chem. C. 119, 10520 (2015).

13. Xiaofeng Feng, Jason Wu, Alexis Bell, Miquel Salmeron. "An Atomic-Scale View of the Nucleation and Growth of Graphene Islands on Pt Surfaces". J. Phys. Chem. C. 119, 7124 (2015).

14. Xiaofeng Feng, J.I. Cerdá, and M. Salmeron. "Orientation-Dependent Interaction between CO_2 Molecules Adsorbed on Ru(0001)". J. Phys. Chem. Lett. 6, 1780 (2015).

15. Kwangjin An and Gabor A. Somorjai. "Nanocatalysis I: Synthesis of Metal and Bimetallic Nanoarticles and porous Oxides and Their Catalytic Reaction Studies". Cat. Lett. 145, 233-248 (2015).

16. Hui-Ling Han, Gerome Melaet, Selim Alayoglu, Gabor A. Somorjai. "In Situ Microscopy and Spectroscopy Applied to Surfaces at Work". ChemCatChem 7, 3625-3638 (2015).

17. Baran Eren, Christian Heine, Hendrik Bluhm, Gabor A. Somorjai, Miquel Salmeron. "Catalyst Chemical State during CO Oxidation Reaction on Cu(111) Studied with Ambient-Pressure X-ray Photoelectron Spectroscopy and Near Edge X-ray Adsorption Fine Structure Spectroscopy". J. Am. Chem. Soc 137, 11186 (2015).

18. Barbara A. J. Lechner, Youngsoon Kim, Peter J. Feibelman, Graeme Henkelman, Heon Kang, Miquel Salmeron. "Solvation and reaction of ammonia in molecularly thin water films". J. Phys. Chem. C. 119, 23052 (2015).

19. Cheng Hao Wu, Robert S. Weatherup, and Miquel B. Salmeron. "Probing the Solid/Liquid Interface in situ with X-rays: Old Methods, New Tricks". Phys. Chem. Chem. Phys. 17, 30229 (2015).

20. Sabine Maier, Miquel Salmeron. "How does water wet a surface?". Accts. Chem. Res. 48, 2783-2790 (2015). DOI 10.1021/acs.accounts.5b00214

22. N. Becknell, C. Zheng, C. Chen, Y. Yu, P. Yang. "Synthesis of $PtCo_3$ Polyhedral Nanoparticles and Evolution to Pt_3Co Nanoframes". Surf. Sci. 2015.

23. N. Becknell, Y. Kang, C. Chen, J. Resasco, N. Kornienko, J. Guo, N. M. Markovic, G.A. Somorjai, V.R. Stamenkovic, P. Yang. "Atomic Structure of Pt_3Ni Nanoframe Electrocatalysts by In situ XAS". JACS, 2015, 137(50), 15817.

24. Hyunsoo Lee, Han-Bo-Ram Lee, Sangku Kwon, Miquel Salmeron, Jeong Y. Park. "Internal and External Atomic Steps in Graphite Exhibit Dramatically Different Physical and Chemical Properties". ACS Nano. 9 (4), 3814-3819 (2015).

25. Cheng Hao Wu, Baran Eren, and Miquel B. Salmeron. "Structure and dynamics of reactant coadsorption on single crystal model catalysts by HP-STM and AP-XPS: a mini review". Topics in Catalysis. 2015. DOI: 10.1007/s11244-015-0527-1

26. N. Kornienko, Y. Zhao, C. S. Kley, C. Zhu, D. Kim, S. Lin, C. J. Chang, O. M. Yaghi, P. Yang. Metal-Organic Frameworks for Electrocatalytic Reduction of Carbon Dioxide. J. Am. Chem. Soc., 2015, 137, 14129.

27. Baran Eren, Danylo Zherebetskyy, Laerte L. Patera, Cheng Hao Wu, Hendrik Bluhm, Cristina Africh, Lin-Wang Wang, Gabor A. Somorjai, Miquel Salmeron. "Activation of Cu(111) surface by decomposition into nanoclusters driven by CO adsorption". Science 351, 475-478, 2016.

28. Sabine Maier, Barbara A. J. Lechner, Gabor A. Somorjai, and Miquel Salmeron. "Growth and Structure of the First Layers of Ice on Ru(0001) and Pt(111)". J. Am. Chem. Soc. 2016. DOI: 10.1021/jacs.5b13133

29. Zongqiang Pang, Stefan Duerrbeck, Chao Shun Kha, Erminald Bertel, Gabor Somorjai, Miquel Salmeron. "Adsorption and reactions of water on oxygen pre-covered Cu(110)". J. Phys. Chem. C. (2016). DOI:10.1021/acs.jpcc.6b0214

30. Baran Eren, Zongyuan Liu, Dario Stacchiola, Gabor Somorjai, Miquel Salmeron. "Structural Changes of Cu(110) and Cu(110)-(2×1)-O Surfaces under Carbon Monoxide in the Torr Pressure Range Studied with Scanning Tunneling Microscopy and Infrared Reflection Absorption Spectroscopy". J. Phys. Chem. C. (2016). DOI:10.1021/acs.jpcc.6b0214

31. Robert Weatherup, Baran Eren, Yibo Hao, Hendrik Bluhm, Miquel Salmeron. "Graphene Membranes for Atmospheric Pressure Photoelectron Spectroscopy". J. Phys. Chem. Letters. 7, 1622–1627 (2016).

32. Baran Eren, Danylo Zherebetskyy, Yibo Hao, Laerte L. Patera, Lin-Wang Wang, Gabor A. Somorjai, Miquel Salmeron. "One-dimensional Nanoclustering of the Cu(100) Surface under CO Gas in the mbar Pressure Range". Surf. Sci. (2016). DOI: 10.1016/j.susc.2016.04.016

Organic/inorganic Nanocomposites

Ting Xu, Paul Alivisatos, Yi Liu, Robert Ritchie, Miquel Salmeron, Lin-wang Wang
Lawrence Berkeley National Laboratory

Program Scope

Organic/inorganic nanocomposite can synergize advantages from both soft and hard material arenas. Our central hypothesis is that once we gain control over the spatial arrangement of each building block and the inter-component coupling in hybrid systems, it is possible to manipulate energy flow and transformation in different forms and access properties never seen before. Our long-term goal is to understand the principle governing the interfaces between the organic and inorganic building blocks and their co-assembly to generate hierarchically structured nanocomposites that can be incorporated into functional devices. Specifically, our team focuses on: (1) achieving structural control in supramolecular nanocomposite and polymer-grafted NP (PGNP) blends with single particle precision in bulk and in thin films; (2) developing nanoparticle (NP)'s passivation ligands using organic molecules, polymers and newly found 2-D materials to fundamentally understand and control the NP/ligand interface; and (3) in parallel, understanding the chemistry-structure-property relationship in nanocomposite with an initial focus on the optical, electronic and opto-mechanical properties.

Recent Progress

(1) <u>Structural Control</u> Nanocomposites based on NPs and polymers allow access to scalable, processible, technologically relevant hierarchical structures for both organic and inorganic components than other approaches. With successes in nanocomposites, we systematically investigated the phase behavior of spherical NP-based supramolecular nanocomposite in thin films; developed approaches to macroscopically align NP assemblies; quantified the kinetics and pathway of assembly process; and optimized the assembly kinetics to obtain ordered nanocomposite thin films in 1 minute. Guided assembly of nanocomposite could achieve macroscopically aligned 3-D NP arrays, more than 10 layers of NP chains (**Figure 1**). When the nanocomposites form nanowires, diverse 3-D NP

Fig.1. Nanocomposite thin film on a patterned surface. The supramolecular system adjusts its structure to accommodate incommensurability.

assemblies including single, double and triple helices and stacked NP rings can be obtained by varying NP loading to realize optical properties. These results indicated that the effects from the incommensurability in the supramolecular system can be quite different from that in block copolymer, opening opportunities to diversify NP assemblies. We also studied nanocomposites based on low-symmetry NPs (e.g. nanorod and nanodisc) and functional small molecules to build foundation to incorporate NPs with tailored organic/inorganic interface.
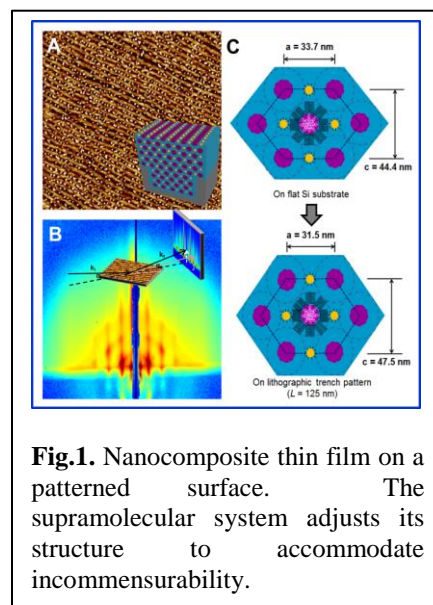
In order to narrow gap between the obtainable NP assembly and the needs to obtain novel properties, we investigated assemblies of polymer-grafted NPs. Different 3-D BNSLs were prepared by varying the stoichiometry of the constituent PGNPs, independent of the NP core size.

Figure 2. Schematics and TEM images of several examples of AB-type binary superlattices from a binary polymer-passivated NP mixture.

The structure of 3-D BNSLs was further tuned by varying the size ratio of PGNPs. Thus, PGNP opened a new strategy to use polymers to guide the assembly of multiple NPs into superlattices with precise structure and surface chemistry.
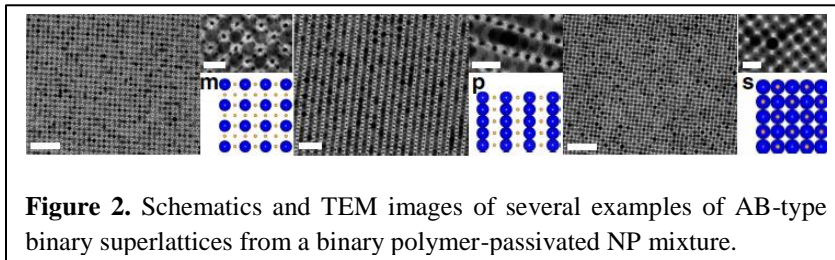
(2) <u>Organic/inorganic Interface: Fundamental and Control</u> The versatile surface chemistry of NPs allows precise tailoring of their electronic properties. There is little understanding of the influence of surface ligands, dopants, defects, and impurities on the electronic structure of NPs. We have carried out systematic *ab initio* electronic structure calculations to model the passivated surface structures of PbS NPs (**Figure 3**). The presence of small hydroxyl ligands at the NP surface is necessary, alongside with the oleate ligands. This has provided the first atomistic model of the structure and NP surface passivation by uncovering the until now controversial role of surface hydroxyl ions. We have further studied the effects of imperfection or defects in the passivation layer or in the interior of nanocrystals. Ionic vacancies (either inside the NPs or at the surface passivating layer) do not induce in-gap electronic states (IGS, states inside the bandgap). This finding explains why the II-VI NCs are so successful in optical applications, since they are tolerant to structural defects. Furthermore, we employed time-resolved KPFM to analyze the hysteresis behavior of charge injection and transport in monolayers of PbS NPs, thus providing a direct measure of the transient behavior of carrier density, which helps clarify the mechanism of charge trapping. We have utilized organic semiconductors with ligating groups for effective resonant alignment with NP surface states. Thin-film transistor measurements indicated a much enhanced field effect mobility for holes and
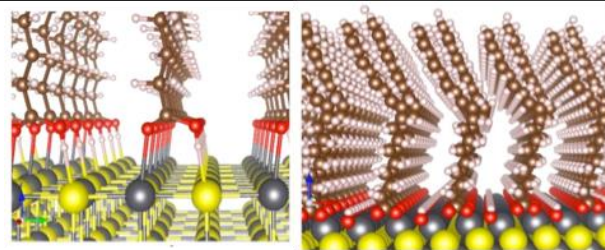

Figure 3. DFT calculated PbS surface passivation by oleate and hydroxyl ligands. Left: (001) and Right: (111) surface).
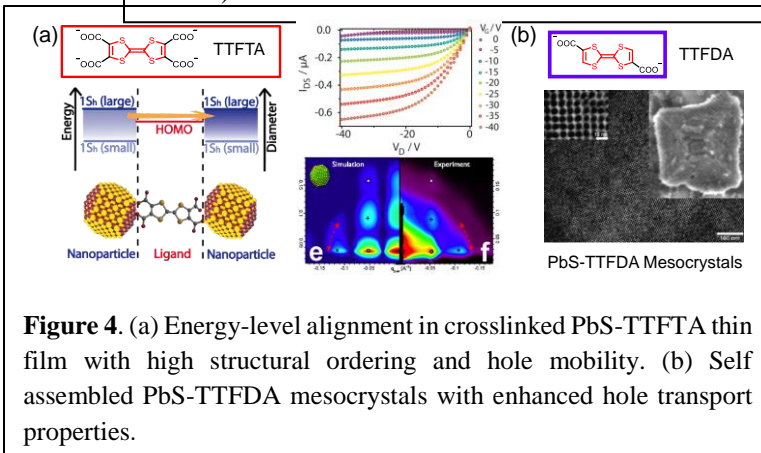

Figure 4. (a) Energy-level alignment in crosslinked PbS-TTFTA thin film with high structural ordering and hole mobility. (b) Self assembled PbS-TTFDA mesocrystals with enhanced hole transport properties.

suppressed mobility for electrons in the hybrid thin film, attributable to a near-resonant alignment of the NP and NP ligand (**Figure 4**).

(3) Explore functional nanocomposites: one example Rational design of composites with optimized mechanical properties requires understanding of how stresses are transferred across the filler/polymer interface. Upon incorporation of tetrapod quantum dots (tQDs) into a polymeric matrix, we showed that tQD acts as an *in situ* fluorescent stress sensor. The tQDs optically probe the stress relaxation and cyclic deformation/hysteresis of the polymer composites without changing its inherent mechanical behavior.

Future Plans

Our previous studies enabled us to develop generalized design principles to achieve structural control and to modulate organic/inorganic interfaces. These studies have been developed using versatile model systems where the building blocks can be substituted when needed. We propose to focus on specific combination of building blocks toward functional nanocomposites capable of inter-converting various forms of energy, such as light, electrical, mechanical, and chemical energy. Specifically, intrigued by recent developments in perovskite NPs we plan to investigate the use of these materials as functional nanocomposites.

(1) Structural Control Fabrication of NP-based metamaterial requires a better library of NP assemblies with improved structural diversity. Supramolecular approach is advantageous in terms of versatility, accuracy, processibility and scalability; however, the morphologies obtained so far are governed by the supramolecule's phase diagram. In comparison with block copolymers (BCP), the energy landscape of supramolecules is more complex and order-order transitions (OOTs) are commonly seen. To complete morphological transition, the BCP or the supramolecule goes through metastable states that are often mediated by microdomain fluctuations. NPs have been shown to effectively stabilize defects in BCP. We hypothesize that if the NP size is comparable to the fluctuation wavelength, the NP incorporation can effectively stabilize the fluctuation and thus, the metastable state. Successes in doing so would also effectively flatten the energy landscape of the supramolecular system. We plan to understand the effects of the NP incorporation on these metastable transition states of supramolecule and experimentally generate novel NP assemblies unseen to date. This capability, in conjunction with the solution processibility, scalability and rapid fabrication of supramolecular nanocomposite, will overcome a critical bottleneck to develop nanocomposites toward functional materials.

The newly designed PGNP blends further expanded the feasibility to diversify the NP assemblies accessible in nanocomposites. Systematic studies to elucidate design principle of PGNP-based assembly are critical to realize the full potential of PGNP. The softness of the PGNP adds another dimension in the phase diagram of NP assemblies and offers good tunability to the resultant assembly. The rigidity of polymer ligand can be readily tailored via the degree of polymerization, persistence length and polymer architecture. Their self-assembly behavior could

be quite different from what has been shown for superlattices from NP mixtures and for colloids. Once we gain some insights, we plan to extend these studies to functional polymers.

(2) <u>Organic/inorganic Interface: Fundamental and Control</u> Developing an efficient material that can convert electrical energy to optical energy or optical to electrical energy, depends greatly upon our understanding of how charge propagates within the composite. By better understanding charge migration, one can design a more efficient LED (electrical to optical) or solar cell (optical to electrical). Our team has clearly demonstrated our ability to probe defects and traps on the NP surface that is essential for charge transfer in the NP films. We aim to further develop a deep molecular level understanding of the charge transfer in assembled nanocomposite systems based on the newly discovered perovskite NPs, as well as NP-2D material composites. Different from other NPs studied before, the perovskites are ionic and have many unique features different from NPs based on covalent II-VI and III-V semiconductors. Preliminary DFT calculations showed that the unpassivated and nonpolar (100) and (110) surfaces of $CsPbBr_3$ have low formation energies, and will not induce in-gap-states in the NP. Nevertheless, neutral ligands including conjugated molecules, can still bind strongly with the surface (e.g., the calculated carboxyl group binding energy is about 0.5 eV). This separation between electronic structure passivation and neutral ligand binding provide more flexibility to manipulate the surface chemistry and electron coupling. Guided by these modeling results, semiconducting organic small molecule ligands and polymers with desired energy levels will be synthesized for coupling with a range of colloidal perovskite NPs. Through thorough characterization of surfaces and synthetic modifications of both organic and inorganic constituents, we aim at determining the atomic details of ligand attachment to NP surfaces, NP surface electronic states, and dissociation of photo-generated excitons at the interface.

(3) <u>Explore functional nanocomposites: one example</u> With developments in last funding cycle, we plan to select specific systems to evaluate chemistry-structure-property relationship. Specifically, we will focus on four subtasks: (a) optical conversion in ucnp-based supramolecular nanocomposite; (b) probing energy transfer dynamics in bnsls; (c) strain-dependent optical properties of luminescent nanocrystals and (4) optical-mechanical coupling: actuation and sensing in a hydrogel-nanoparticle hybrid**.**

Publications:

1. Zhang, Y.; Zherebetskyy, D.; Bronstein, N. D.; Barja, S.; Lichtenstein, L.; Schuppisser, D.; Wang, L. W.; Alivisatos, A. P.; Salmeron, M.; "Charge Percolation Pathways Guided by Defects in Quantum Dot Solids," *Nano Letters,* **2015**, 15, 3249.
2. Zhang, Y.; Chen, Q.; Alivisatos, A. P.; Salmeron, M.; "Dynamic Charge Carrier Trapping in Quantum Dot Field Effect Transistors," *Nano Letters* **2015**, 15, 4657.
3. He, B.; Dai, J.; Zherebetskyy, D.; Chen, T. L.; Zhang, B. A.; Teat, S. J.; Zhang, Q.; Wang, L. W.; Liu, Y.; "A Divergent Route to Core- and Peripherally Functionalized Diazacoronenes that Act as Colorimetric and Fluorescence Proton Sensors," *Chemical Science*, **2015**, 6, 3180.

4. Kao, J.; Xu, T.; "Nanoparticle Assemblies in Supramolecular Nanocomposite Thin Films: Concentration Dependence," *Journal of American Chemical Society,* **2015**, 137, 6356.

5. Thorkelsson, K.; Bai, P.; Xu, T.; "Self-Assembly and Applications of Anisotropic Nanomaterials: A Review," *Nano Today,* **2015**, 10, 48.

6. Zhang, Y.; Zherebetskyy, D.; Bronstein, N. D.; Barja, S.; Lichtenstein, L.; Alivisatos, A. P.; Wang, L. W.; Salmeron, M.; "Molecular Oxygen Induced in-Gap States in PbS Quantum Dots," *ACS Nano,* **2015**, 9, 10445.

7. Raja, S. N.; Olson, A. C. K.; Limaye, A. M.; Thorkelsson, K.; Luong, A. J.; Lin, L.; Ritchie, R. O.; Xu, T.; Alivisatos, A. P.; "Influence of Three-dimensional Nanoparticle Branching on the Young's Modulus of Nanocomposites: Effect of Interface Orientation", *Proceedings of the National Academy of Sciences,* **2015**, 112, 6533.

8. He, B.; Zhang, B. A.; Liu, F.; Navarro, A.; Fernández-Liencres, M. P.; Lu, R.; Lo, K.; Chen, T. L.; Russell, T. P.; Liu Y.; *ACS Applied Material Interface*, **2015**, 7, 20034.

9. Zhang, Y.; Pluchery, O.; Caillard, L.; Lamic-Humblot, A.; Casale, S.; Chabal, Y. J.; Salmeron M.; "Sensing the Charge State of Single Gold Nanoparticles via Work Function Measurements", *Nano Letters*, **2015**, 15, 51.

10. Zherebetskyy, D.; Zhang, Y.; Salmerson, M.; Wang, L.W.; "Tolerance of intrinsic defects in PbS quantum dots", *J. Physical Chemistry Letter*, **2015**, 6, 4711.

11. Andre, A.; Zherebetskyy, D.; Haifi, D.; He, B.; Khoshkhoo, M.S.; Jankowski, M.; Chassee, T.; Wang, L.W.; Schreiber, F.; Salleo, A.; Liu, Y.; Scheele, M.; "Toward conductive mesoscrystalline assemblies: PbS nanocrystals cross-linked with tetrathiafulavalene Dicarboxylate", *Chemistry of Materials*, **2015**, 27, 8105.

12. Ye, X. C.; Zhu, C. H.; Ercius, P.; Raja, S. N.; He, B.; Jones, M. R.; Hauwiller, M. R.; Liu, Y.; Xu, T.; Alivisatos, A. P.; Structural diversity in binary superlattices self-assembled from polymer-grafted nanocrystals. *Nature Communication*, **2015**, 6, 10052.

13. Rancatore, B.; Kim, B. S.; Mauldin, C.; Fréchet, J.; Xu, T.; "Organic Semiconductor-Containing Supramolecules: Effect of Small Molecule Crystallization and Molecular Packing", *Macromolecules*, **2016**, 49, 833.

14. Lee, K. H.; Bai, P.; Rancatore, B. J.; He, B.; Liu, Y.; Xu, T.; "Improved Hierarchical Ordering in Supramolecules via Symmetrically Bi-functionalized Organic Semiconductor", *Macromolecules*, **2016**, 49, 2639.

15. He, B.; Neo, W. T.; Chen, T. L.; Klivansky, L.; Wang, H.; Tan T.; Teat, S. J.; Xu, J.; Liu, Y. "Low Bandgap Conjugated Polymers Based on a Novel Bay-Annulated Indigo (BAI) Acceptor as Highly Stable Electrochromic Materials", *ACS Sustainable Chemistry & Engineering,* **2016**, *4*, 2797.

16. Rojo, M. M.; Zhang, Y. J.; Manzano, C. V.; Alvaro, R.; Gooth, J.; Salmeron, M.; González, M. M.; "Spatial potential ripples of azimuthal surface modes in topological insulator Bi2Te3 nanowires", *Scientific Reports*, **2016**, 6, 19014.

17. He, B.; Zherebetskyy, D.; Wang, H.; Kolaczkowski, M. A.; Klivansky, L. M.; Tan, T.; Wang, L. W.; Liu, Y. "Rational Tuning of the High Energy Visible Light Absorption for Panchromatic Small Molecules by a Two-Dimensional Conjugation Approach", *Chemical Science*, **2016**, in press. DOI: 10.1039/C6SC00428H.

18. Kang, J.; Wang, L. W.; "Robust band gap of TiS3 nanofilms", *Physical Chemistry Chemical Physics.* **2016**, in press. DOI: 10.1039/c6cp01125j.

19. Rancatore, B.; Bai, P.; Xu, T.; "Organic Semiconductor-Based Supramolecular Nanocomposites", *Macromolecules*, **2016**, 49, 4155.

20. Zhang, Y. J.; Hellebusch, D. J.; Bronstein, N. D.; Ko, C.; Ogletree, D. F.; Salmeron, M.; Alivisatos, A. P., *Nature Communication*, **2016**, 7, 11924.

UNIVERSITY GRANT PROJECTS

High Efficiency Biomimetic Organic Solar Cells

M.A. Baldo, *Dept. of Electrical Engineering and Computer Science, MIT*
T. Van Voorhis, *Dept. of Chemistry, MIT*

Program Scope

Charge transfer (CT) states govern both charge generation and recombination losses in organic solar cells. Consisting of bound electron-hole pairs located on separate molecules, CT states are formed at donor-acceptor interfaces after the dissociation of excitons or from the recombination of charge.

CT states are also the basis of the latest generation of organic light emitting devices (OLEDs). Because they are not as tightly bound as typical molecular excitons, CT states behave more like inorganic quantum dots.

Fig. 1. CT states mediate the conversion between charge and localized excitons. They are crucial to the operation of solar cells and the latest generation of organic light emitting devices.

They exhibit small splitting between their bright and dark spin states, such that thermal activation can allow ~100% of CT excitations to emit light. No heavy metal is required. Consequently, CT state emitters are promising for low cost, high efficiency lighting.
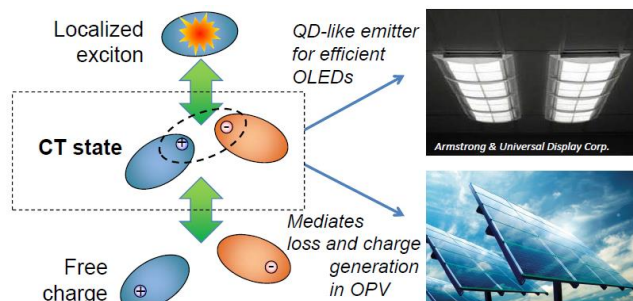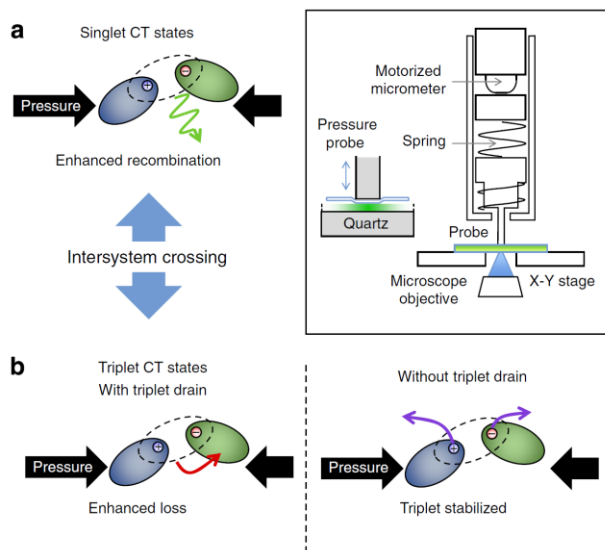

Fig. 1. Schematic of charge transfer state dynamics under pressure. Expected changes in (a) singlet and (b) triplet CT states as a function of their size and the presence of a triplet quenching 'drain'. Inset. The measurement apparatus used to apply pressure. Van Voorhis & Baldo, Nature Communications (2015)

Our focus is studying the optimum size of CT states and understanding the spin mixing processes that contribute to light emission. These two phenomena are crucial to the rational design of CT states in solar cells and light emitting devices.

Recent Progress: We highlight four recent papers with particular focus on spin dynamics in CT states.

1. *Van Voorhis, Baldo, et al.* Nature Communications (2015): A long term goal of our work in this program has been to demonstrate OPVs that are spin-protected against recombination by exploiting the inability of triplet CT states to recombine to the singlet ground state. Here, we examined recombination losses as a function of spin and the electron-hole spacing in fluorescent charge transfer states, including direct monitoring of both singlet and triplet charge transfer state dynamics. Using external

pressure to modulate molecular spacing, we demonstrated that large donor-acceptor separations minimize back transfer from the charge transfer state to a low-lying triplet exciton 'drain' or the ground state. The triplet drain quenches triplet charge transfer states that would otherwise be spin-protected against recombination, and switches the most efficient origin of the photocurrent from triplets to singlets. Our conclusion was that future organic solar cell designs should focus on raising the energy of triplet excitons to better utilize triplet charge transfer mediated photocurrent generation or increasing the donor-acceptor spacing in order to minimize recombination losses.

2. *Van Voorhis, Baldo, et al.* Nature Materials (2015): This second highlighted study was the completion of several years of work directed towards a key controversy in the field. Previous reports have described CT state dissociation into free charge that is both dependent[1] and independent[2] of the initial energy of the CT state. A particular puzzle is the apparent efficient generation of photocurrent from relaxed and tightly bound CT states[3]. We studied the dynamics of tightly bound CT states in a TADF-derived donor-acceptor blend that is amorphous, with localized CT states that are fluorescent, allowing direct observation of CT state dynamics[4].
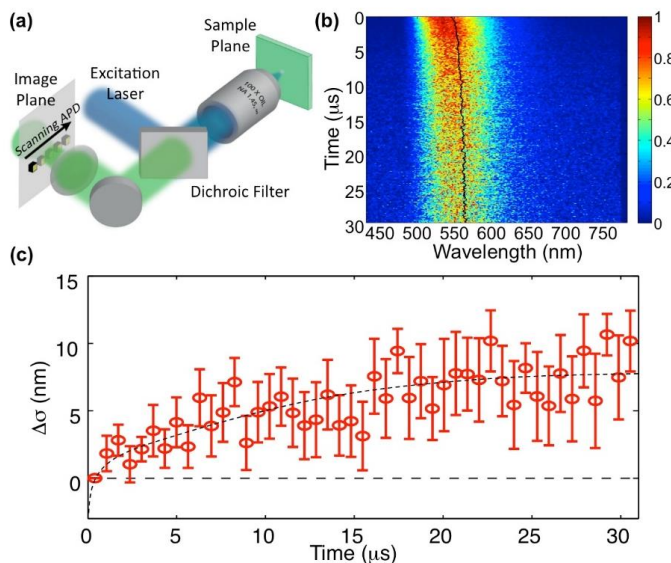

Fig. 2. (a) Setup of the scanning optical microscope for diffusion imaging measurements. **(b)** Streak camera measurement of charge transfer state emission showing red shift in peak emission wavelength. **(c)** Extracted CT state diffusion. Van Voorhis & ı̇re Materials (2015).
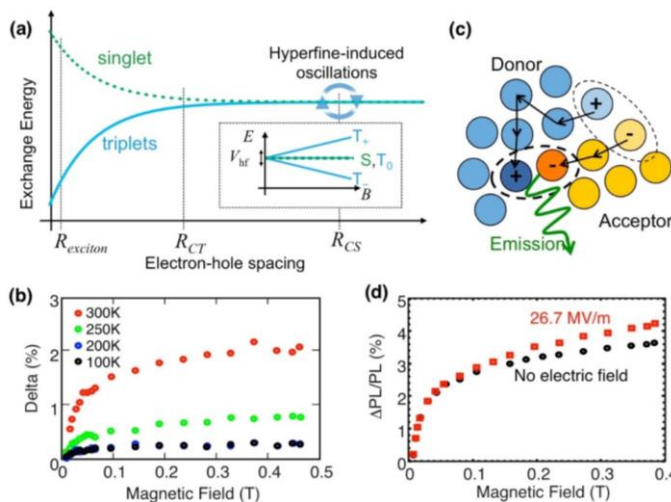

Fig. 3. (a) Energy schematic of singlet-triplet energy splitting as a function of electron-hole spacing. **(inset)** Schematic of Zeeman splitting due to external magnetic field in relation to hyperfine coupling V_{hf}. **(b)** The temperature dependence of the magnetic field modulation of CT state PL. The magnitude of the change in PL decreases at lower temperature, indicating magnetic field-dependent hyperfine mediated intersystem crossing decreases with lower thermal energy. However, change in the shape of the magnetic field dependence is not observed over this range of temperatures. **(c)** Illustration of stretching effect on CT state dynamics and spectral diffusion. **(d)** Bulk heterojunction device sample under magnetic field at open-circuit and closed-circuit, demonstrating that application of an electric field distorts the size of the CT state. Van Voorhis & Baldo, Nature Materials (2015).

Using a custom-built microscope, we performed perhaps the first direct imaging of CT motion, observing diffusion over distances of 5-10 nm. The other notable result of this study was our investigation into how the CT states move. We found signatures of a novel, 'inchworm'- type

process, where the CT extends and then compresses as the electron and hole move asynchronously through the blend. There would be too much binding energy for this process to occur with excitons, but in CT states only a few kT are required to allow the stretching. It is important to stress that the CT state remains bound, but we see evidence of the variation in electron-hole spacing in the magnetic field characteristic.

3. *Baldo, Van Voorhis, et al.* Journal of Physical Chemistry C (2015): We examined our model of CT splitting and reformation in the context of exciplex-based TADF emitters. Through analysis of the magnetic field dependence of the transient photoluminescence, we were able to conclusively demonstrate that the TADF mechanism in these exciplexes relies on charge separation followed by reformation to achieve reverse intersystem crossing.
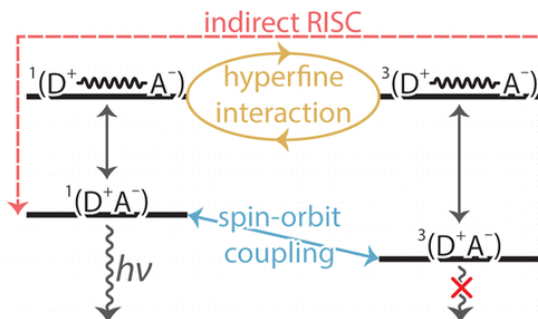

Fig. 4. The mechanism of indirect reverse intersystem crossing in exciplex TADF dyes. Van Voorhis and Baldo, J. Phys Chem C (2015)

4. (Partial support only) *Baldo, et al*. Nature Materials (2016): A computational screening guided by machine learning techniques in the Aspuru-Guzik group at Harvard identified several attractive TADF candidates. We built devices and demonstrated efficiencies as high as 22%. But note the efficiency roll off with current density suggestive of unsolved bimolecular annihilation in this system; see Fig. 5c.
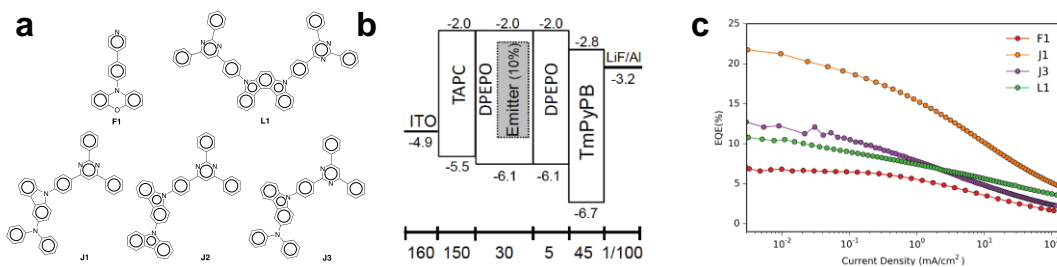

Fig. 5. (a) New TADF candidates. (b) Device structures. (c) External quantum efficiencies as a function of current density. Baldo, Aspuru-Guzik, et al. Nature Materials (2016).

Future plans: Bimolecular Interactions in Organic Semiconductors: Hot charge, Hot excitons, Efficiency Droop, and Instability

Interactions between multiple excited states are a leading cause of efficiency losses in organic semiconductor devices. Prominent examples include the high brightness efficiency 'droop' that limits the use of organic materials in solid state lighting. Such bimolecular interactions generate 'hot' states' - nonequilibrium excitations that quickly relax by dissipating vibrational or electronic energy. In addition to their role in efficiency losses, hot states are suspected of involvement in device degradation, an especially important concern for organic solar cells and light emitting devices.

We will pursue a joint theory-experiment collaboration to understand and manage bimolecular interactions in organic semiconductors. Major goals include the development of mean-field steady-state theory to model and account for fluctuations in microscopic bimolecular interaction rates. Understanding fluctuations in bimolecular processes is crucial to determine the impact of rare processes such as potential degradation pathways. We also plan to test a theory of degradation in organic light emitting devices. Based on this theory we identify the exciton lifetime as the key experiment target. We will perform non-perturbative probes that allow us to modify the exciton lifetime of a given material without altering any bulk or device-specific electrical properties. This is achieved using coupling to surface plasmons. Our non-perturbative probes will be used to experimentally confirm dominant bimolecular interaction pathways by observing their dependence on exciton lifetimes. Finally, we will build and characterize new structures for stable organic light emitting devices, especially the blue emitters that presently limit the operational stability of organic solid state lighting.

References

1. T. M. Clarke, J. R. Durrant, Charge photogeneration in organic solar cells. *Chemical Reviews* **110**, 6736-6767 (2010).
2. J. Lee, K. Vandewal, S. R. Yost, M. E. Bahlke, L. Goris, M. A. Baldo, J. V. Manca, T. Van Voorhi, Charge transfer state versus hot exciton dissociation in polymer-fullerene blended solar cells. *Journal of the American Chemical Society* **132**, 11878-11880 (2010).
3. M. Muntwiler, Q. Yang, W. A. Tisdale, X. Y. Zhu, Coulomb barrier for charge separation at an organic semiconductor interface. *Physical Review Letters* **101**, 1-4 (2008).
4. K. Goushi, K. Yoshida, K. Sato, C. Adachi, Organic light-emitting diodes employing efficient reverse intersystem crossing for triplet-to-singlet state conversion. *Nature Photonics* **6**, 253-258 (2012).

Publications supported under this program

1. T.C. Wu, D.N. Congreve, and M.A. Baldo, Solid State Photon Upconversion Utilizing Thermally-Activated-Delayed-Fluorescence Molecules as Triplet Sensitizer, APL 107 031103 (2015).
2. W. Chang, D. N. Congreve, E. Hontz, M. E. Bahlke, D. P. McMahon, S. Reineke, T. C. Wu, V. Bulović, T. Van Voorhis, M. A. Baldo, Spin-dependent charge transfer state design rules in organic photovoltaics. *Nat Commun* **6**, 6415 (2015).
3. P. B. Deotare, W. Chang, E. Hontz, D. N. Congreve, L. Shi, P. D. Reusswig, B. Modtland, M. E. Bahlke, C. K. Lee, A. P. Willard, V. Bulovic, T. Van Voorhis, M. A. Baldo, Nanoscale transport of charge-transfer states in organic donor-acceptor blends. *Nat Mater* **14**, 1130-1134 (2015).
4. E. Hontz, W. Chang, D. N. Congreve, V. Bulović, M. A. Baldo, T. Van Voorhis, The Role of Electron–Hole Separation in Thermally Activated Delayed Fluorescence in Donor–Acceptor Blends. *The Journal of Physical Chemistry C* **119**, 25591-25597 (2015).
5. Rafael Gómez-Bombarelli, Jorge Aguilera-Iparraguirre, Timothy D. Hirzel, David Duvenaud, Dougal Maclaurin, Martin A. Blood-Forsythe, Hyun Sik Chae, Markus Einzinger, Dong-Gwang Ha, Tony Wu, Georgios Markopoulos, Soonok Jeon, Hosuk Kang, Hiroshi Miyazaki, Masaki Numata, Sunghan Kim, Wenliang Huang, Seong Ik Hong, Marc Baldo, Ryan P Adams, Alán Aspuru-Guzik, Design of efficient molecular organic light-emitting diodes by a high-throughput virtual screening and experimental approach. *Nat Mater* accepted (2016).

Novel Pnictides with *d*- and *f*-Metals as Prospective Materials for Thermal Energy Conversion

P.I. Prof. Svilen Bobev, Department of Chemistry and Biochemistry, University of Delaware, Newark DE 19716

Program Scope

Our work is aimed at new knowledge by synthesis and thorough characterization (structure and properties) of NOVEL compounds with NOVEL properties. The study presented herein focuses on synthetically very challenging antimonides. These compounds are narrow-gap semiconductors and exhibit intermediate properties between those of typical insulators and typical metals. Such structural characteristics provide unique combination of charge/heat transfer properties [1].

Recent Progress

We have recently (simultaneous to other ongoing activities) embarked on studies of the rare-earth metal substituted series $Ca_{14-x}RE_xMnSb_{11}$ (RE = La–Nd, Sm, Gd–Dy; $x \approx 1$). This detailed investigation demonstrates that the exchange of trivalent RE^{3+} for Ca^{2+} is facile, allowing for compositions with x approaching or even exceeding 1 to be attained. The effects of the electron doping on the structure and electrical properties of the electron deficient $Ca_{14}MnSb_{11}$ host are discussed. Bulk magnetization measurements reveal the onsets of spontaneous ordering at relatively high temperatures, despite the high dilution of unpaired *d*- and/or *f*-electrons, which may suggest clustering and the formation of microscopic magnetic domains.
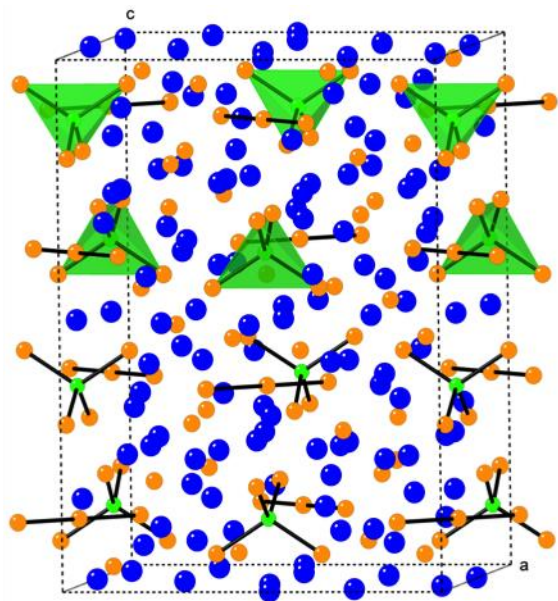
All newly synthesized $Ca_{14-x}RE_xMnSb_{11}$ (RE = La–Nd, Sm, Gd–Dy; $x \approx 1$) are isotypic. Their overall structure is a substitutional derivate of $Ca_{14}MnSb_{11}$. This bonding arrangement is well known (Figure 1), asymmetric unit of this complex structure ($Ca_{14}AlSb_{11}$ structure type, Pearson index *tI*208) consists of nine independent crystallographic sites [2]. The Mn atom occupies a single site with symmetry $\overline{4}$, and is tetrahedrally

Figure 1. General view of the tetragonal crystal structure of $Ca_{14-x}RE_xMnSb_{11}$. The Mn atoms centering the Sb tetrahedra are shown in green. The Ca/*RE*, and the Sb atoms are shown in blue, and orange, respectively.

bonded to four Sb atoms forming distorted tetrahedral $MnSb_4$ units (Figure 1). There are four Sb sites, of which, Sb2 are the ligands to the Mn atom, while Sb1 and Sb4 form the $[Sb_3]^{7-}$ linear polyanion. Antimony atoms labeled Sb3 are isolated, surrounded by six cations. There are four sites for the Ca atoms and rare-earth metal atoms substitute Ca on all sites in a statistical manner. The coordination environment can be loosely described as distorted octahedral (Figure 2).
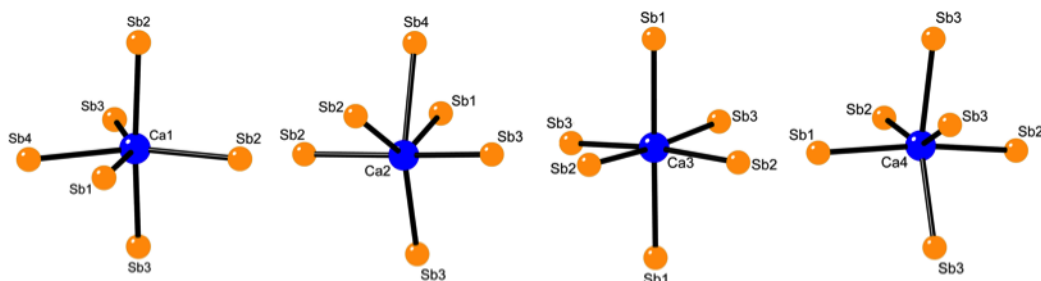

Figure 2. General view of the local coordination environment of the Ca/*RE* atoms.

We also draw attention to the fact that the distribution of the rare-earth metals on the four Ca varies, therefore, there are some other anomalies in the relative decrease in the *c*−constant vs the *a*−constant. For example, let us consider more carefully $Ca_{14}MnSb_{11}$ and $Ca_{12.99(3)}La_{1.01}MnSb_{11}$. The corresponding covalent radii of elemental Ca and La according to Pauling are 1.736 Å and 1.690 Å, respectively. Thus, it is not surprising that the unit cell volume of $Ca_{14}MnSb_{11}$ is 6249 Å^3, while the La−substituted compound has a 16 Å^3 smaller unit cell volume, 6233 Å^3 to be exact (i.e., 0.25%). While the overall volume decrease may be dismissed as statistically insignificant, the decrease in the *a*−constant (16.783 Å vs 16.739 Å) is clearly offset by the *increase* in the *c*−constant (22.188 Å vs 22.245 Å). This divergence becomes even more pronounced if $Ca_{14}MnSb_{11}$ and $Ca_{13.08(1)}Ce_{0.92}MnSb_{11}$ are considered alongside. Notice that the covalent radius of elemental Ce according to Pauling is even smaller, 1.646 Å, yet again, the decrease in the *a*−constant (now 16.704 Å) is compensated by further *increase* in the *c*−constant (22.298 Å). These findings cannot be rationalized based on elemental radii alone, and become even more obscured if one considers the corresponding ionic radii from Shannon— for the same coordination number, the ionic radii of Ca^{2+}, La^{3+}, and Ce^{3+} (based on their fluoride salts) are 1.14 Å, 1.17 Å, and 1.15 Å, respectively.

Theoretically, replacement of one Ca^{2+} by one RE^{3+} cation is expected to fill the single hole in the $[MnSb_4]^{9-}$ tetrahedral unit, thereby making these compounds semiconductors, akin to $Ca_{14}AlSb_{11}$ (the parent $Ca_{14}MnSb_{11}$ is heavily doped *p*-type conductor). The synthesized polycrystalline materials show unusual electric transport properties—all samples exhibit semiconducting/insulating behavior indicating the successful electron doping (via replacement of Ca^{2+} by RE^{3+} in $Ca_{14}MnSb_{11}$). The activation energies, estimated from the linear fits of the lnρ vs 1/T plots, using the Arrhenius equation, were found to be dependent on both the content and the nature and substituting rare-earth metal. These results indicate that the properties can be continuously varied, hence, these materials could be of relevance to the development of new

thermoelectrics. From a more fundamental point of view, the established structural relationships can provide some logical and reasonable predictions for possible new compounds in the targeted systems, their likely structures and potential properties.

Future Plans

Future thermopower and Hall effect studies will be needed to fully understand the interplay of concentration and nature of charge carriers with *RE* substitution. The magnetic responses of the newly synthesized samples show rich low temperature physics and hint at complex magnetic couplings, evidenced in the variation of T_C on the type of *RE* atoms Additional synthetic/structural work, coupled with neutron diffraction and precise magnetization experiment will be needed in order to unravel the origins of the unusual magnetic coupling in these materials. Preparations for such work are currently being pursued.

References

[1]   "CRC Handbook of Thermoelectrics", Rowe, D. M. (Ed.), CRC Press, 1995.

[2]   P. Villars, L. D. Calvert (Eds.), Pearson's Handbook of Crystallographic Data for Intermetallic Compounds, 2nd Ed., American Society for Metals, Materials Park, OH, USA 1991.

Publications

(in reverse order; *the names of the contributing undergraduate researchers are <u>underlined</u>*)

14. "*On the Extended Series of Quaternary Zintl Phases Ca₁₃REMnSb₁₁ (RE = La−Nd, Sm, Gd−Dy)*"
    Prakash, J.; Stoyko, S.; <u>Voss, L.</u>; **Bobev, S.** *Eur. J. Inorg. Chem.* **2016**, in print; *doi: 10.1002/ejic.201600306.*

13. "*Synthesis and Structural Characterization of the New Clathrates K₈Cd₄Ge₄₂, Rb₈Cd₄Ge₄₂, and Cs₈Cd₄Ge₄₂*"
    Schäfer, M. C.; **Bobev, S.** *Materials* **2016**, *9*, 236 – *doi: 10.3390/ma9040236* (themed issue *Inorganic Clathrate Materials*)

12. "*The New Zintl Phases Eu₂₁Cd₄Sb₁₈ and Eu₂₁Mn₄Sb₁₈*"
    Wang, Y.; <u>Darone, G. M.</u>; **Bobev, S.** *J. Solid State Chem.* **2016**, *238*, 303 – *doi: 10.1016/ j.jssc.2016.03.044.*

11. "*Synthesis, Crystal and Electronic Structures of the Pnictides AE₃TrPn₃ (AE = Sr, Ba; Tr = Al, Ga; Pn = P, As)*"
    Stoyko, S.; <u>Voss, L.</u>; He, H.; **Bobev, S.** *Crystals* **2015**, *5*, 433 – *doi: 10.3390/cryst5040433.*

10. "*Synthesis, Crystal and Electronic Structure of the Quaternary Sulfides Ln₂CuMS₅ (Ln = La, Ce; M = Sb, Bi)*"
    Kussainova, A. M.; Akselrud, L. G.; Suen, N-T.; <u>Voss, L.</u>; Stoyko, S.; **Bobev, S.** *J. Solid State Chem.* **2016**, *233*, 269 – *doi: 10.1016/j.jssc.2015.10.039.*

9. "*Synthesis and Structure Determination of Seven Ternary Bismuthides. Crystal Chemistry of the RELi$_3$Bi$_2$ Family (RE = La–Nd, Sm, Gd, Tb)*"
Prakash, J.; Schäfer, M. C.; **Bobev, S.** *Acta Cryst.* **2015**, *C71*, 894 – *doi:10.1107/ S2053229615016393.*

8. "*Ba and Sr Binary Phosphides: Synthesis, Crystal Structures, and Bonding Analysis*"
Dolyniuk, J.; He, H.; Ivanov, A.; Boldyrev, A.; **Bobev, S.**; Kovnir, K. *Inorg. Chem.* **2015**, *54*, 8608 – *doi:10.1021/acs.inorgchem.5b01253.*

7. "*Non-stoichiometric Compositions Arising from Synergistic Electronic and Size Effects. Syntheses, Crystal Chemistry and Electronic Properties of the A$_{14}$Cd$_{1+x}$Pn$_{11}$ Compounds (0 ≤ x ≤ 0.3; A = Sr, Eu; Pn = As, Sb)*"
Makongo, J. P. A.; Darone, G. M.; Xia, S.-Q.; **Bobev, S.** *J. Mater. Chem. C* **2015**, *3*, 10388 *doi: 10.1039/C5TC01605C* (themed issue *The Chemistry of Thermoelectric Materials*).

6. "*New Insights into the Application of the Valence Rules in Zintl Phases—Crystal and Electronic Structures of Ba$_7$Ga$_4$P$_9$, Ba$_7$Ga$_4$As$_9$, Ba$_7$Al$_4$Sb$_9$, Ba$_6$CaAl$_4$Sb$_9$, and Ba$_6$CaGa$_4$Sb$_9$*"
He, H.; Stoyko, S.; **Bobev, S.** *J. Solid State Chem.* **2016**, *236*, 116 – *doi: 10.1016/j.jssc. 2015.07.015* (themed issue *Crystal Growth*).

5. "*Synthesis, Crystal Structures, and Physical Properties of the New Zintl Phases A$_{21}$Zn$_4$Pn$_{18}$ (A = Ca, Eu; Pn = As, Sb)—Versatile Arrangements of [ZnPn$_4$] Tetrahedra*"
Suen, N.-T.; Wang, Y.; **Bobev, S.** *J. Solid State Chem.* **2015**, *227*, 204 – *doi: 10.1016/ j.jssc.2015.03.031.*

4. "*Synthesis, Structure, Thermoelectric Properties, and Band Gaps of Alkali Metal Containing Type-I Clathrates: A$_8$Ga$_8$Si$_{38}$ (A = K, Rb, Cs) and K$_8$Al$_8$Si$_{38}$*"
Sui, F.; He, H.; **Bobev, S.**; Zhao, J.; Osterloh, F.; Kauzlarich, S. *Chem. Mater.* **2015**, *27*, 2812 – *doi: 10.1021/cm504436v.*

3. "*Quaternary Pnictides with Complex, Non-centrosymmetric Structures. Synthesis and Structural Characterization of the New Zintl Phases Na$_{11}$Ca$_2$Al$_3$Sb$_8$, Na$_4$CaGaSb$_3$ and Na$_{15}$Ca$_3$In$_5$Sb$_{12}$*"
Wang, Y.; Stoyko, S.; **Bobev, S.** *Inorg. Chem.* **2015**, *54*, 1931 – *doi: 10.1021/ic502822v.*

2. "*Structural Variability vs Structural Flexibility. A Case Study of Eu$_9$Cd$_{4+x}$Sb$_9$ and Ca$_9$Mn$_{4+x}$Sb$_9$ (x ≈ 1/2)*"
Liu, X.-C.; Wu, Z.; Xia, S.-Q.; Tao, X.-T. **Bobev, S.** *Inorg. Chem.* **2015**, *54*, 947 – *doi: 10.1021/ic5023505* (special issue *dedicated to the memory of Prof. John D. Corbett*).

1. "*Synthesis and Crystal Chemistry of New Ternary Pnictides Containing Lithium—Adding Structural Complexity One Step at a Time*"
Schäfer, M. C.; Suen, N.-T.; **Bobev, S.** *Dalton Trans.* **2014**, *43*, 16889 – *doi:10.1039/c4dt02220.*

Programming Function via Soft Materials

Paul Braun, Randy Ewoldt, Steve Granick, Jimmy Hsia, Xiuling Li, Jeff Moore, Ralph Nuzzo, John Rogers, Ken Schweizer, Frederick Seitz Materials Research Laboratory, University of Illinois at Urbana-Champaign, Urbana, IL, USA

Program Scope

The Programming Function via Soft Materials (PFvSM) team is developing, understanding, and applying, in energy-relevant contexts, new classes of responsive materials with functionalities that derive from and/or exploit structural dynamics from the nanometer to mesoscopic to continuum scale. As elementary units we are employing function-encoded colloids, nanoparticles, large mesh fibrillar gels, deterministically fabricated networks, and their hybrid mixtures. We are employing top-down methods to create larger scale systems with a 3-dimensional spatial organization of the material components engineered to provide useful functional behaviors. The scientific and technological outputs of the cluster's research are providing new approaches to challenging problems in basic energy science relevant to energy harvesting, transport, and storage. To achieve these goals the cluster has brought together a team organized into two synergistic thrusts.

1) Reconfigurable and Dynamic Assemblies – are being realized using a suite of responsive colloids and nanoparticles of various shapes, sizes, softness, and chemistry created via chemical synthesis, cluster assembly and mechanical instabilities. The particles are being assembled, under quiescent and nonequilibrium conditions, to create dynamically and reversibly reconfigurable percolated networks with unique mechanical, electrical and/or ionic conductivity properties, both in suspension and in the presence of fibrillar polymer gels as guiding internal fields.

2) Responsive 3D Mesoscale Networks – which exploit residual and mismatch stress to "mechanically synthesize" deterministic functional networks of diverse chemistries and geometries including fractal motifs with energy-centric applications including energy harvesting and energy storage. Mesoscale networks with characteristic dimensions ranging from 100s of nm to 10s of micrometers are being formed via a combined experimental and modeling effort from both high performance semiconductor materials and photodefinable polymers.

Recent Progress

During the current grant period the cluster team established new foundational understandings of the equilibrium and field-driven assembly and dynamics of patchy spherical and rod-like colloids in the suspension, crystal, glass and plastic crystal states, exploited our colloidal concepts to fabricate novel hierarchically architectured battery electrodes with superb properties, created a mechanically triggerable shape-changing colloidal system, explored massively

reconfigurable colloidal assembly of energy conducting microstructures directed by quenched large mesh fibril biopolymer networks, developed new synthesis methods for the living polymerization of fibrils, created and applied new experimental and modeling methods to extract and understand the onset of mechanical nonlinearities in soft materials, and elucidated strong collective non-hydrodynamic behavior on the large length scales required for attaining continuum behavior in colloidal suspensions and entangled biopolymer networks. Following are a few specific highlights.

We created the first predictive replica integral equation statistical mechanical theory for the thermodynamic properties, structure, and conductivity of large mesh-colloid systems[1] based on a two-step "quenched-annealed" (QA) protocol. A large mesh percolated network composed of randomly arranged long, thin rigid rods (composed of elementary spherical interaction sites) is first formed with sufficiently strong "crosslinks" that it does not reorganize temporally or upon particle addition. It thus
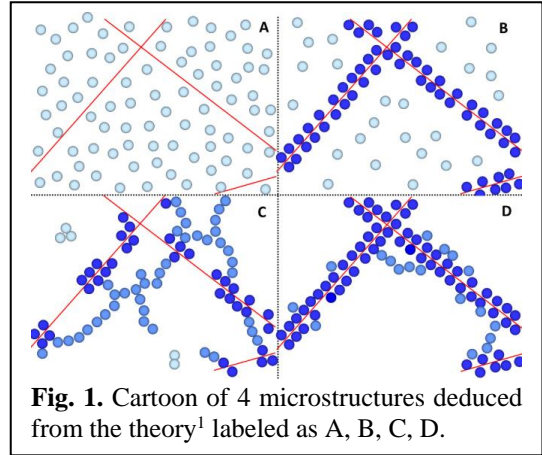

Fig. 1. Cartoon of 4 microstructures deduced from the theory[1] labeled as A, B, C, D.

serves as a template for colloids which are inserted into the network and equilibrated. This approach avoids undesirable macroscopic colloid-polymer phase separation that often occurs for fully annealed 2-component systems composed of structurally disparate objects. The minimal model involves a large parameter space: 4 structural length scales (rod thickness, d, rod length, L, colloid diameter, D, and network mesh size, ξ), colloid volume fraction (η), and two competing, short range attractive interactions, colloid-colloid fluid (F-F) and colloid-template (F-T), characterized by chemically-specific contact attraction strengths (in units of thermal energy) of ε_{FF} and ε_{FT}, respectively. The theory predicts the statistical microstructure (Fig. 1) as encoded in the F-F and F-T pair correlation functions in real and Fourier (structure factors) space over all length scales. From this, colloid percolation and thermodynamic properties can be calculated. By combining our theory with effective medium transport methods,[2,3] the hopping-controlled electrical conductivity is predicted, and design rules to realize a massive and abrupt insulator-metal transition have been
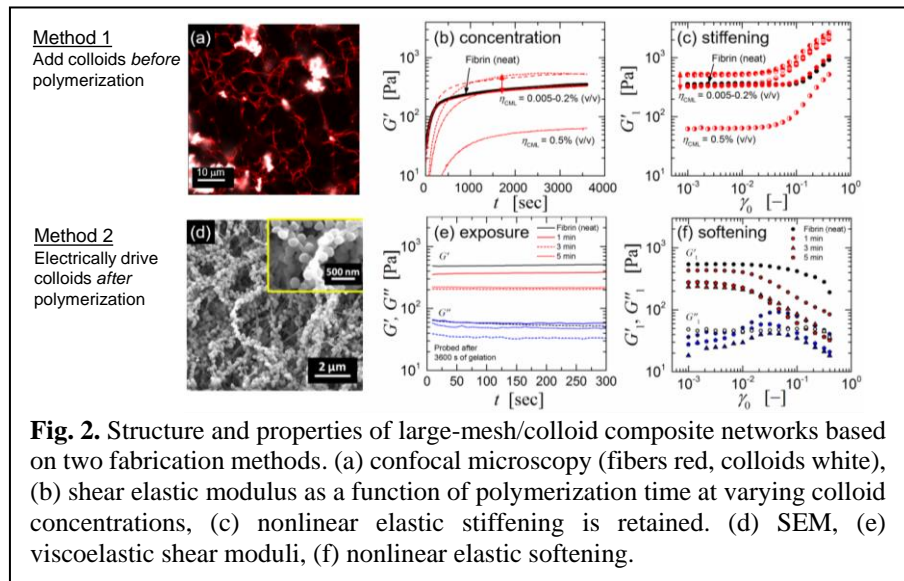

Fig. 2. Structure and properties of large-mesh/colloid composite networks based on two fabrication methods. (a) confocal microscopy (fibers red, colloids white), (b) shear elastic modulus as a function of polymerization time at varying colloid concentrations, (c) nonlinear elastic stiffening is retained. (d) SEM, (e) viscoelastic shear moduli, (f) nonlinear elastic softening.

elucidated.[1] Thermodynamic properties such as the bulk modulus also undergo dramatic changes. As a model material to investigate the underlying physics, we employed the well-studied biopolymer gel network of bovine fibrin,[4,5] which is composed of very long fibrils of thickness d~20-40 nm that form controllable meshes of diameter ξ~1-10 µm. Carboxylate modified polystyrene/latex (CML) particles (D~200 nm diameter) were used as a model colloid. The corresponding hybrid composites thus obey the theoretically identified design inequalities $L > \xi >> D >> d$. Based on this set of hybrid systems, we have explored both the responsive templating of colloid microstructure, and strongly nonlinear mechanics where small applied strains trigger large changes in material elasticity (fibrin networks are strain stiffening). Two scenarios for realizing CML colloid-fibrin composites and their resultant properties are described in Fig. 2.

Over the past three years, the team demonstrated the ability to rationally design and create functional and responsive structures by exploiting residual, mismatch, and externally applied stresses to "mechanically synthesize" deterministic functional networks of diverse chemistries and geometries including fractal motifs. These networks have been designed to respond to local chemical and electrical stimuli, form electrically active devices, provide exceptionally strain tolerant electrical conductors, and serve as active elements of new dynamic-mechanical actuating and energy harvesting hybrid materials. The team developed powerful routes to diverse classes of 3D architectures in advanced materials, with characteristic dimensions from nanometers to centimeters and areas that span square centimeters or more.[6-9] The approach relies on schemes originally conceived by the team, in which geometric transformation of preformed 2D precursor micro/nanostructures and/or devices lead to extended 3D layouts by controlled processes of substrate-induced compressive buckling. Our group conducted combined experimental and theoretical studies of more than forty representative geometries, from single and multiple helices, toroids and conical spirals to constructs that resemble spherical baskets, cuboid cages, raised platforms, starbursts, flowers, scaffolds, fences and frameworks, to reveal the underlying science and to establish the core capabilities. Isolated, nested and/or interconnected collections of these and other building blocks distributed across large areas yield 3D mesoscale networks with single and/or multiple level arrangements (Figure 3). Materials examples range from device-grade monocrystalline silicon to metals, and dielectrics and heterogeneous combinations of these, in 3D forms that can be dynamically adjusted by mechanically. The collective results establish unique possibilities for wide-ranging classes of 3D mesosystems as engineered analogs to chemically synthesized gels. Extensions of these concepts allow manipulation of membranes, ribbons and wires into hierarchical structures, with great versatility in design, with length scales that can span orders of magnitude. Areas of potential impact
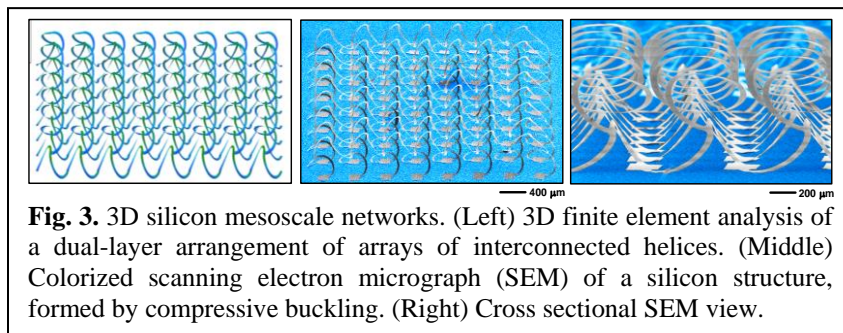

Fig. 3. 3D silicon mesoscale networks. (Left) 3D finite element analysis of a dual-layer arrangement of arrays of interconnected helices. (Middle) Colorized scanning electron micrograph (SEM) of a silicon structure, formed by compressive buckling. (Right) Cross sectional SEM view.

include high performance large area concentrator photovoltaics, and battery electrodes explicitly internally designed to optimize mechanical strain, ion diffusion, and electron transport.

Future Plans

We believe the time is right to deeply address the basic science of equilibrium and nonequilibrium assembly within the emerging paradigm of functional and dynamically reconfigurable building blocks. The acquired fundamental understandings will offer novel opportunities for transformational progress in materials chemistry. Over the next grant period, we plan an integrated research program to address this frontier scientific opportunity. The program elements we have identified include:

- *Multiscale self-assembly for mesoscopic control of materials properties*. The science of organization of mesoscopic soft matter (colloids, nanoparticles, polymers, fibrillar networks) that via free energy minimization lead to complex hierarchies usefully impacting material properties, e.g., energy transport and mechanics.
- *Dynamics of multiscale materials assembly*. The science of the complex, and potentially programmable, temporal evolution during the assembly and disassembly of multiscale materials, including kinetic trapping in nonequilibrium states with distinct bulk properties.
- *Mesoscale and programmable material dynamics*. The science of dynamical assembly systems in which the nature of forces change in time via either external (e.g., pH, temperature, irradiance, strain, flow) or internal (e.g., reactions occurring when constituents contact) effects.
- *Driven mesoscale assembly*. The science enabling the construction of complex hierarchical/multiscale materials that exhibit stable and useful forms of organization that arise only as a consequence of energetic processes occurring within them.

References

(1)   Jadrich, R. B.; Schweizer, K. S. *Phys Rev Lett* **2014**, *113*, 208302.
(2)   Ambrosetti, G.; Balberg, I.; Grimaldi, C. *Physical Review B* **2010**, *82*, 134201.
(3)   Grimaldi, C. *EPL (Europhysics Letters)* **2011**, *96*, 36004.
(4)   Fukada, E.; Kaibara, M. *Thrombosis Research* **1976**, *8, Supplement 2*, 49.
(5)   Copley, A. L.; King, R. G.; Scheinthal, B. M. *Biorheology* **1970**, *7*, 81.
(6)   Abdullah, A. M.; Nan, K.; Rogers, J. A.; Hsia, K. J. *Extreme Mechanics Letters* **2016**, *7*, 34.
(7)   Liu, Y.; Yan, Z.; Lin, Q.; Guo, X.; Han, M.; Nan, K.; Hwang, K.-C.; Huang, Y.; Zhang, Y. H.; Rogers, J. A. *Adv Funct Mater* **2015**, *26*, 2909.
(8)   Zhang, Y. H.; Yan, Z.; Nan, K. W.; Xiao, D. Q.; Liu, Y. H.; Luan, H. W.; Fu, H. R.; Wang, X. Z.; Yang, Q. L.; Wang, J. C.; Ren, W.; Si, H. Z.; Liu, F.; Yang, L. H.; Li, H. J.; Wang, J. T.; Guo, X. L.; Luo, H. Y.; Wang, L.; Huang, Y. G.; Rogers, J. A. *P Natl Acad Sci USA* **2015**, *112*, 11757.
(9)   Xu, S.; Yan, Z.; Jang, K.-I.; Huang, W.; Fu, H.; Kim, J.; Wei, Z.; Flavin, M.; McCracken, J.; Wang, R.; Badea, A.; Liu, Y.; Xiao, D.; Zhou, G.; Lee, J.; Chung, H. U.; Cheng, H.; Ren, W.; Banks, A.; Li, X.; Paik, U.; Nuzzo, R. G.; Huang, Y.; Zhang, Y.; Rogers, J. A. *Science* **2015**, *347*, 154.

Publications (2014-present)

(1)   Bharadwaj, N. A.; Ewoldt, R. H., The general low-frequency prediction for asymptotically nonlinear material functions in oscillatory shear, *J Rheol* **2014**, *58*, 891-910.

(2)   Braun, P. V.; Nuzzo, R. G., Batteries: Knowing when small is better, *Nat Nanotechnol* **2014**, *9*, 962-963.

(3)   Chaudhary, K.; Juarez, J. J.; Chen, Q.; Granick, S.; Lewis, J. A., Reconfigurable assemblies of Janus rods in AC electric fields, *Soft Matter* **2014**, *10*, 1320-1324.

(4)   Dagdeviren, C.; Su, Y. W.; Joe, P.; Yona, R.; Liu, Y. H.; Kim, Y. S.; Huang, Y. A.; Damadoran, A. R.; Xia, J.; Martin, L. W.; Huang, Y. G.; Rogers, J. A., Conformable amplified lead zirconate titanate sensors with enhanced piezoelectric response for cutaneous pressure monitoring, *Nat Commun* **2014**, *5*.

(5)   Dagdeviren, C.; Yang, B. D.; Su, Y. W.; Tran, P. L.; Joe, P.; Anderson, E.; Xia, J.; Doraiswamy, V.; Dehdashti, B.; Feng, X.; Lu, B. W.; Poston, R.; Khalpey, Z.; Ghaffari, R.; Huang, Y. G.; Slepian, M. J.; Rogers, J. A., Conformal piezoelectric energy harvesting and storage from motions of the heart, lung, and diaphragm, *P Natl Acad Sci USA* **2014**, *111*, 1927-1932.

(6)   Escabi, M. A.; Read, H. L.; Viventi, J.; Kim, D. H.; Higgins, N. C.; Storace, D. A.; Liu, A. S. K.; Gifford, A. M.; Burke, J. F.; Campisi, M.; Kim, Y. S.; Avrin, A. E.; Van der Spiegel, J.; Huang, Y. G.; Li, M.; Wu, J.; Rogers, J. A.; Litt, B.; Cohen, Y. E., A high-density, high-channel count, multiplexed mu ECoG array for auditory-cortex recordings, *J Neurophysiol* **2014**, *112*, 1566-1583.

(7)   Fan, J. A.; Yeo, W. H.; Su, Y. W.; Hattori, Y.; Lee, W.; Jung, S. Y.; Zhang, Y. H.; Liu, Z. J.; Cheng, H. Y.; Falgout, L.; Bajema, M.; Coleman, T.; Gregoire, D.; Larsen, R. J.; Huang, Y. G.; Rogers, J. A., Fractal design concepts for stretchable electronics, *Nat Commun* **2014**, *5*, 3266.

(8)   Fu, M.; Chaudhary, K.; Lange, J. G.; Kim, H. S.; Juarez, J. J.; Lewis, J. A.; Braun, P. V., Anisotropic Colloidal Templating of 3D Ceramic, Semiconducting, Metallic, and Polymeric Architectures, *Adv Mater* **2014**, *26*, 1740-1745.

(9)   Hattori, Y.; Falgout, L.; Lee, W.; Jung, S. Y.; Poon, E.; Lee, J. W.; Na, I.; Geisler, A.; Sadhwani, D.; Zhang, Y. H.; Su, Y. W.; Wang, X. Q.; Liu, Z. J.; Xia, J.; Cheng, H. Y.; Webb, R. C.; Bonifas, A. P.; Won, P.; Jeong, J. W.; Jang, K. I.; Song, Y. M.; Nardone, B.; Nodzenski, M.; Fan, J. A.; Huang, Y. G.; West, D. P.; Paller, A. S.; Alam, M.; Yeo, W. H.; Rogers, J. A., Multifunctional Skin-Like Electronics for Quantitative, Clinical Monitoring of Cutaneous Wound Healing, *Adv Healthc Mater* **2014**, *3*, 1597-1607.

(10)   Huang, W.; Koric, S.; Yu, X.; Hsia, K. J.; Li, X. L., Precision Structural Engineering of Self-Rolled-up 3D Nanomembranes Guided by Transient Quasi-Static FEM Modeling, *Nano Lett* **2014**, *14*, 6293-6297.

(11)   Jadrich, R. B.; Schweizer, K. S., Directing Colloidal Assembly and a Metal-Insulator Transition Using a Quench-Disordered Porous Rod Template, *Phys Rev Lett* **2014**, *113*, 208302.

(12)   Jeong, J. W.; Kim, M. K.; Cheng, H. Y.; Yeo, W. H.; Huang, X.; Liu, Y. H.; Zhang, Y. H.; Huang, Y. G.; Rogers, J. A., Capacitive Epidermal Electronics for Electrically Safe, Long-Term Electrophysiological Measurements, *Adv Healthc Mater* **2014**, *3*, 642-648.

(13)   Jiang, S.; Yan, J.; Whitmer, J. K.; Anthony, S. M.; Luijten, E.; Granick, S., Orientationally Glassy Crystals of Janus Spheres, *Phys Rev Lett* **2014**, *112*.

(14)   Kim, J.; Kim, H. S.; Choi, J. H.; Jeon, H.; Yoon, Y.; Liu, J.; Park, J. G.; Braun, P. V., Epitaxial Growth of Three-Dimensionally Mesostructured Single-Crystalline Cu2O via Templated Electrodeposition, *Chem Mater* **2014**, *26*, 7051-7058.

(15)   Kim, S. K.; Koo, H. J.; Lee, A.; Braun, P. V., Selective Wetting-Induced Micro-Electrode Patterning for Flexible Micro-Supercapacitors, *Adv Mater* **2014**, *26*, 5108-5112.

(16)   Kim, T. I.; Lee, S. H.; Li, Y. H.; Shi, Y.; Shin, G.; Lee, S. D.; Huang, Y.; Rogers, J. A.; Yu, J. S., Temperature- and size-dependent characteristics in ultrathin inorganic light-emitting diodes assembled by transfer printing, *Appl Phys Lett* **2014**, *104*.

(17)   King, J. T.; Yu, C. Q.; Wilson, W. L.; Granick, S., Super-Resolution Study of Polymer Mobility Fluctuations near c*, *Acs Nano* **2014**, *8*, 8802-8809.

(18)   Koo, H. J.; Kim, S. K.; Braun, P. V., Facile fabrication of graphene composite microwires via drying-induced size reduction of hydrogel filaments, *Rsc Adv* **2014**, *4*, 20927-20931.

(19)   Liu, J. Y.; Zhang, H. G.; Wang, J. J.; Cho, J.; Pikul, J. H.; Epstein, E. S.; Huang, X. J.; Liu, J. H.; King, W. P.; Braun, P. V., Hydrothermal Fabrication of Three-Dimensional Secondary Battery Anodes, *Adv Mater* **2014**, *26*, 7096-+.

(20)   Madhukar, A.; Perlitz, D.; Grigola, M.; Gai, D. H.; Hsia, K. J., Bistable characteristics of thick-walled axisymmetric domes, *Int J Solids Struct* **2014**, *51*, 2590-2597.

(21)   Mohseni, P. K.; Behnam, A.; Wood, J. D.; Zhao, X.; Yu, K. J.; Wang, N. C.; Rockett, A.; Rogers, J. A.; Lyding, J. W.; Pop, E.; Li, X. L., Monolithic III-V Nanowire Solar Cells on Graphene via Direct van der Waals Epitaxy, *Adv Mater* **2014**, *26*, 3755-3760.

(22)   Ning, H.; Krueger, N. A.; Sheng, X.; Keurn, H.; Zhang, C.; Choquette, K. D.; Li, X. L.; Kim, S.; Rogers, J. A.; Braun, P. V., Transfer-Printing of Tunable Porous Silicon Microcavities with Embedded Emitters, *Acs Photonics* **2014**, *1*, 1144-1150.

(23)   Shin, H.; Schweizer, K. S., Theory of two-dimensional self-assembly of Janus colloids: crystallization and orientational ordering, *Soft Matter* **2014**, *10*, 262-274.

(24)   Song, Y.; Cheng, P. N.; Zhu, L. J.; Moore, E. G.; Moore, J. S., Multivalent Macromolecules Redirect Nucleation-Dependent Fibrillar Assembly into Discrete Nanostructures, *J Am Chem Soc* **2014**, *136*, 5233-5236.

(25)   Xu, Z. D.; Yao, Y.; Brueckner, E. P.; Li, L. F.; Jiang, J.; Nuzzo, R. G.; Liu, G. L., Black silicon solar thin-film microcells integrating top nanocone structures for broadband and omnidirectional light-trapping, *Nanotechnology* **2014**, *25*.

(26)   Bassett, K. P.; Mohseni, P. K.; Li, X. L., Evolution of GaAs nanowire geometry in selective area epitaxy, *Appl Phys Lett* **2015**, *106*.

(27)   Bharadwaj, N. A.; Ewoldt, R. H., Constitutive model fingerprints in medium-amplitude oscillatory shear, *J Rheol* **2015**, *59*, 557-592.

(28)   Bharadwaj, N. A.; Ewoldt, R. H., Single-point parallel disk correction for asymptotically nonlinear oscillatory shear, *Rheol Acta* **2015**, *54*, 223-233.

(29)   Dagdeviren, C.; Shi, Y.; Joe, P.; Ghaffari, R.; Balooch, G.; Usgaonkar, K.; Gur, O.; Tran, P. L.; Crosby, J. R.; Meyer, M.; Su, Y. W.; Webb, R. C.; Tedesco, A. S.; Slepian, M. J.; Huang, Y. G.; Rogers, J. A., Conformal piezoelectric systems for clinical and experimental characterization of soft tissue biomechanics, *Nat Mater* **2015**, *14*, 728-+.

(30)   Dell, Z. E.; Schweizer, K. S., Microscopic Theory for the Role of Attractive Forces in the Dynamics of Supercooled Liquids, *Phys Rev Lett* **2015**, *115*, 205702.

(31)   Dell, Z. E.; Tsang, B.; Jiang, L. X.; Granick, S.; Schweizer, K. S., Correlated two-particle diffusion in dense colloidal suspensions at early times: Theory and comparison to experiment, *Phys Rev E* **2015**, *92*, 052304.

(32)   Epstein, E.; Yoon, J.; Madhukar, A.; Hsia, K. J.; Braun, P. V., Colloidal Particles that Rapidly Change Shape via Elastic Instabilities, *Small* **2015**, *11*, 6051-6057.

(33)   Glazer, M. P. B.; Cho, J.; Almer, J.; Okasinski, J.; Braun, P. V.; Dunand, D. C., In Operando Strain Measurement of Bicontinuous Silicon-Coated Nickel Inverse Opal Anodes for Li-Ion Batteries, *Adv Energy Mater* **2015**, *5*, 1500466.

(34)   Goodman, M. D.; Kim, S.; Tatsuda, N.; Yano, K.; Braun, P. V., Enhanced Secondary Battery Anodes Based on Si and Fe3O4 Nanoparticle Infilled Monodisperse Carbon Starburst Colloidal Crystals, *Particle & Particle Systems Characterization* **2015**, *32*, 928-933.

(35)   He, J.; Nuzzo, R. G.; Rogers, J. A., Inorganic Materials and Assembly Techniques for Flexible and Stretchable Electronics, *P Ieee* **2015**, *103*, 619-632.

(36)   Jang, K. I.; Chung, H. U.; Xu, S.; Lee, C. H.; Luan, H. W.; Jeong, J.; Cheng, H. Y.; Kim, G. T.; Han, S. Y.; Lee, J. W.; Kim, J.; Cho, M.; Miao, F. X.; Yang, Y. Y.; Jung, H. N.; Flavin, M.; Liu, H.; Kong, G. W.; Yu, K. J.; Rhee, S. I.; Chung, J.; Kim, B.; Kwak, J. W.; Yun, M. H.; Kim, J. Y.; Song, Y. M.; Paik, U.; Zhang, Y. H.; Huang, Y.; Rogers, J. A., Soft network composite materials with deterministic and bio-inspired designs, *Nat Commun* **2015**, *6*.

(37)   Jeong, J. W.; McCall, J. G.; Shin, G.; Zhang, Y. H.; Al-Hasani, R.; Kim, M.; Li, S.; Sim, J. Y.; Jang, K. I.; Shi, Y.; Hong, D. Y.; Liu, Y. H.; Schmitz, G. P.; Xia, L.; He, Z. B.; Gamble, P.; Ray, W. Z.; Huang, Y. G.; Bruchas, M. R.; Rogers, J. A., Wireless Optofluidic Systems for Programmable In Vivo Pharmacology and Optogenetics, *Cell* **2015**, *162*, 662-674.

(38)   Kim, S. K.; Jung, E.; Goodman, M. D.; Schweizer, K. S.; Tatsuda, N.; Yano, K.; Braun, P. V., Self-Assembly of Monodisperse Starburst Carbon Spheres into Hierarchically Organized Nanostructured Supercapacitor Electrodes, *Acs Appl Mater Inter* **2015**, *7*, 9128-9133.

(39)   Lee, C. H.; Ma, Y. J.; Jang, K. I.; Banks, A.; Pan, T.; Feng, X.; Kim, J. S.; Kang, D.; Raj, M. S.; McGrane, B. L.; Morey, B.; Wang, X. Y.; Ghaffari, R.; Huang, Y. G.; Rogers, J. A., Soft Core/Shell Packages for Stretchable Electronics, *Adv Funct Mater* **2015**, *25*, 3698-3704.

(40)   Liu, J.; Wang, J.; Kim, J.; Ning, H.; Pan, Z.; Kelly, S. J.; Epstein, E. S.; Huang, X.; Liu, J.; Braun, P. V., High Full-Electrode Basis Capacity Template-Free 3D Nanocomposite Secondary Battery Anodes, *Small* **2015**, *11*, 6265-6271.

(41)   Liu, J. Y.; Kelly, S. J.; Epstein, E. S.; Pan, Z.; Huang, X. J.; Liu, J. H.; Braun, P. V., Three-dimensionally scaffolded Co3O4 nanosheet anodes with high rate performance, *J Power Sources* **2015**, *299*, 40-48.

(42)   Liu, J. Y.; Li, N.; Goodman, M. D.; Zhang, H. G.; Epstein, E. S.; Huang, B.; Pan, Z.; Kim, J.; Choi, J. H.; Huang, X. J.; Liu, J. H.; Hsia, K. J.; Dillon, S. J.; Braun, P. V., Mechanically and Chemically Robust Sandwich-Structured C@Si@C Nanotube Array Li-Ion Battery Anodes, *Acs Nano* **2015**, *9*, 1985-1994.

(43)   Motala, M. J.; Perlitz, D.; Daly, C. M.; Yuan, P.; Nuzzo, R. G.; Hsia, K. J., Programming matter through strain, *Extreme Mechanics Letters* **2015**, *3*, 8-16.

(44)   Ning, H. L.; Pikul, J. H.; Zhang, R. Y.; Li, X. J.; Xu, S.; Wang, J. J.; Rogers, J. A.; King, W. P.; Braun, P. V., Holographic patterning of high-performance on-chip 3D lithium-ion microbatteries, *P Natl Acad Sci USA* **2015**, *112*, 6573-6578.

(45)   Norton, J. J. S.; Lee, D. S.; Lee, J. W.; Lee, W.; Kwon, O.; Won, P.; Jung, S. Y.; Cheng, H. Y.; Jeong, J. W.; Akce, A.; Umunna, S.; Na, I.; Kwon, Y. H.; Wang, X. Q.; Liu, Z. J.; Paik, U.; Huang, Y. G.; Bretl, T.; Yeo, W. H.; Rogers, J. A., Soft, curved electrode systems capable of

integration on the auricle as a persistent brain-computer interface, *P Natl Acad Sci USA* **2015**, *112*, 3920-3925.

(46)   Santos, C. J. E.; Nelson, A. Z.; Mendoza, E.; Ewoldt, R. H.; Kriven, W. M., Design and fabrication of ceramic beads by the vibration method, *J Eur Ceram Soc* **2015**, *35*, 3587-3594.

(47)   Shi, Y.; Dagdeviren, C.; Rogers, J. A.; Gao, C. F.; Huang, Y., An Analytic Model for Skin Modulus Measurement Via Conformal Piezoelectric Systems, *J Appl Mech-T Asme* **2015**, *82*.

(48)   Wang, J. J.; Zhou, H.; Nanda, J.; Braun, P. V., Three-Dimensionally Mesostructured Fe2O3 Electrodes with Good Rate Performance and Reduced Voltage Hysteresis, *Chem Mater* **2015**, *27*, 2803-2811.

(49)   Wang, S. D.; Huang, Y. G.; Rogers, J. A., Mechanical Designs for Inorganic Stretchable Circuits in Soft Electronics, *Ieee T Comp Pack Man* **2015**, *5*, 1201-1218.

(50)   Xu, S.; Yan, Z.; Jang, K.-I.; Huang, W.; Fu, H.; Kim, J.; Wei, Z.; Flavin, M.; McCracken, J.; Wang, R.; Badea, A.; Liu, Y.; Xiao, D.; Zhou, G.; Lee, J.; Chung, H. U.; Cheng, H.; Ren, W.; Banks, A.; Li, X.; Paik, U.; Nuzzo, R. G.; Huang, Y.; Zhang, Y.; Rogers, J. A., Assembly of micro/nanomaterials into complex, three-dimensional architectures by compressive buckling, *Science* **2015**, *347*, 154-159.

(51)   Yamamoto, U.; Schweizer, K. S., Microscopic Theory of the Long-Time Diffusivity and Intermediate-Time Anomalous Transport of a Nanoparticle in Polymer Melts, *Macromolecules* **2015**, *48*, 152-163.

(52)   Yan, J.; Bae, S. C.; Granick, S., Colloidal Superstructures Programmed into Magnetic Janus Particles, *Adv Mater* **2015**, *27*, 874-879.

(53)   Yan, J.; Bae, S. C.; Granick, S., Rotating crystals of magnetic Janus colloids, *Soft Matter* **2015**, *11*, 147-153.

(54)   Yu, C. J.; Yuan, P. X.; Erickson, E. M.; Daly, C. M.; Rogers, J. A.; Nuzzo, R. G., Oxygen reduction reaction induced pH-responsive chemo-mechanical hydrogel actuators, *Soft Matter* **2015**, *11*, 7953-7959.

(55)   Yu, X.; Arbabi, E.; Goddard, L. L.; Li, X.; Chen, X., Monolithically integrated self-rolled-up microtube-based vertical coupler for three-dimensional photonic integration, *Appl Phys Lett* **2015**, *107*, 031102.

(56)   Zhang, J.; Luijten, E.; Granick, S., Toward Design Rules of Directional Janus Colloidal Assembly, *Annu Rev Phys Chem* **2015**, *66*, 581-600.

(57)   Zhang, Y. H.; Yan, Z.; Nan, K. W.; Xiao, D. Q.; Liu, Y. H.; Luan, H. W.; Fu, H. R.; Wang, X. Z.; Yang, Q. L.; Wang, J. C.; Ren, W.; Si, H. Z.; Liu, F.; Yang, L. H.; Li, H. J.; Wang, J. T.; Guo, X. L.; Luo, H. Y.; Wang, L.; Huang, Y. G.; Rogers, J. A., A mechanically driven form of Kirigami as a route to 3D mesostructures in micro/nanomembranes, *P Natl Acad Sci USA* **2015**, *112*, 11757-11764.

(58)   Zhu, L. J.; Song, Y.; Cheng, P. N.; Moore, J. S., Molecular Design for Dual Modulation Effect of Amyloid Protein Aggregation, *J Am Chem Soc* **2015**, *137*, 8062-8068.

(59)   Abdullah, A. M.; Nan, K.; Rogers, J. A.; Hsia, K. J., Mismatch Strain Programmed Shape Transformation of Curved Bilayer-Flexible Support Assembly, *Extreme Mechanics Letters* **2016**, *7*, 34-41.

(60)   Kim, S.-K.; Cho, J.; Moore, J. S.; Park, H. S.; Braun, P. V., High-Performance Mesostructured Organic Hybrid Pseudocapacitor Electrodes, *Adv Funct Mater* **2016**, *26*, 903-910.

(61)   Liu, Y.; Yan, Z.; Lin, Q.; Guo, X.; Han, M.; Nan, K.; Hwang, K.-C.; Huang, Y.; Zhang, Y. H.; Rogers, J. A., Guided Formation of Three-Dimensional Helical Mesostructures: Analytical Modeling and Experimental Validation, *Adv Funct Mater* **2016**, *26*, 2909-2918.

(62)   Pikul, J. H.; Liu, J.; Braun, P. V.; King, W. P., Integration of high capacity materials into interdigitated mesostructured electrodes for high energy and high power density primary microbatteries, *J Power Sources* **2016**, *315*, 308-315.

(63)   Yan, Z.; Zhang, F.; Wang, J.; Liu, F.; Guo, X.; Nan, K.; Lin, Q.; Gao, M.; Xiao, D.; Shi, Y.; Qiu, Y.; Luan, H.; Kim, J. H.; Wang, Y.; Luo, H.; Han, M.; Huang, Y.; Zhang, Y.; Rogers, J. A., Controlled Mechanical Buckling for Origami-Inspired Construction of 3D Microstructures in Advanced Materials, *Adv Funct Mater* **2016**, *26*, 2629-2639.

(64)   Zhang, H.; Shi, T.; Wetzel, D. J.; Nuzzo, R. G.; Braun, P. V., 3D Scaffolded Nickel–Tin Li-Ion Anodes with Enhanced Cyclability, *Adv Mater* **2016**, *28*, 742-747.

(65)   Zhang, J.; Yan, J.; Granick, S., Directed Self-Assembly Pathways of Active Colloidal Clusters, *Angewandte Chemie International Edition* **2016**, *55*, 5166-5169.

Low-Temperature Chemical Routes to Functional Complex Oxide Nanocrystals

Richard L. Brutchey
Department of Chemistry, University of Southern California, Los Angeles, CA 90089 USA

Program Scope

Despite over thirty years of developments in the field of nanomaterials chemistry, there are still only a limited number of ways to rationally synthesize these materials. In 2004, a DOE-sponsored Grand Challenge workshop on *Nanoscience Research for Energy Needs* recommended "developing, understanding, and optimizing synthesis methods for . . . [the] production of nanomaterials" as being a foundational and vital nanoscience research theme for energy applications. To address challenges such as these, more robust and general strategies are needed for the synthesis of high quality nanocrystals (with a focus on small size, well-defined composition, and controlled surface chemistry). While there has been a great deal of progress over the past 25 years in the synthesis of high quality II-VI and lead-salt IV-VI colloidal semiconductor nanocrystals, there has been much less success in the synthesis of nanocrystals of other materials families, such as complex metal oxide and halide nanocrystals. Using a materials chemistry approach, we are executing basic research in the area of complex oxide and halide nanocrystals that can ultimately impact energy applications with three specific objectives:

(1) Leverage solution based methods to synthesize more compositionally complex oxide and halide nanocrystals, in order to tune properties through synthetic compositional control.
(2) Perform high-level structural characterization of the resulting complex oxide and halide nanocrystals to establish structure-property relationships at the nanoscale as a function of size and/or composition.
(3) Assess the functionality of the resulting nanocrystals.

Good progress on these objectives has been achieved since September 2014.

Recent Progress

1. Low-temperature synthesis of complex scheelite-structured nanocrystals. The scheelite ABO_4 (A = Ca, Sr, Ba, Pb and B = Mo, W) family of materials has attracted considerable interest in the areas of energy storage and conversion, in part because of their excellent chemical and thermal stability. The classic solid-state synthesis of these materials, where crystallization is induced via mechanical mixing of ACO_3 and BO_3 followed by high temperature sintering, typically requires temperatures ≥ 1000 ˚C.[1] Poor mixing can result in phase segregation in such multinary systems, and the intrinsic high vapor pressure of the MoO_3 and WO_3 precursors can lead to compositional inhomogeneity and nonstoichiometry at reaction temperatures exceeding 800 ˚C.[2] Furthermore, it has previously been shown that useful properties of scheelite-structured materials can be tuned by varying the A-site cation in $A_{1-x}A'_xBO_4$ solid solutions;[3] however, under high temperature synthesis conditions, some systems (e.g., CaWO₄-SrWO₄) have narrow regions of one phase, solid solution stability upon cooling.[4] This provides impetus to explore the synthesis and compositional homogeneity of $A_{1-x}A'_xWO_4$ solid solutions under kinetically controlled, low temperature conditions.

We prepared a series of compositionally complex scheelite nanocrystals of the formula $A_{1-x}A'_xWO_4$ (A = Ca, Sr, Ba) under benign synthesis conditions using our vapor diffusion sol-gel method. Discrete nanocrystals with sub-20 nm diameters were obtained after kinetically controlled hydrolysis and polycondensation at room temperature, followed by composition-dependent thermal aging at ≤ 60 ˚C. Rietveld analysis of X-ray diffraction data (**Fig. 1**) and
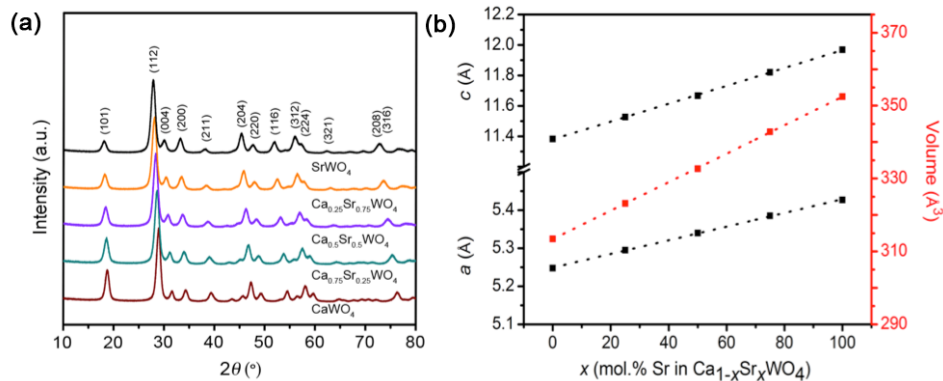
Fig. 1 Powder XRD patterns for (a) $Ca_{1-x}Sr_xWO_4$ nanocrystal solid solutions. (b) Lattice parameters (*a* and *c*) and unit cell volumes. Dotted lines are a guides-to-the-eye.

Raman spectroscopy verified the synthesis of continuous and phase-pure nanocrystal solid solutions across the entire composition space for both $Ca_{1-x}Sr_xWO_4$ and $Sr_{1-x}Ba_xWO_4$, where $0 \leq x \leq 1$. Elemental analysis by X-ray photoelectron and energy dispersive X-ray spectroscopies demonstrated excellent agreement between the nominal and experimentally determined elemental stoichiometries and illustrated good spatial elemental homogeneity within these nanocrystals synthesized under benign conditions.

2. Temperature-dependent local structure of CaMoO4 nanocrystals. Scheelite oxides of the formula AMO_4 (A = Ca, Sr, Ba; M = Mo, W) have proven to be a significant class of cryogenic scintillation detectors.[5] Structural studies performed on scheelite oxides have primarily focused on the effects of high temperature and/or pressure on bulk materials (e.g., phase transitions, thermal expansion, compressibility). To date, however, very little is known about the structure of AMO_4 materials at low temperatures, or on the nanoscale for that matter.

While Rietveld analysis provides structural information on the length scale of Bragg diffraction, pair distribution function (PDF) analysis is a total scattering technique (i.e., Bragg and diffuse scattering) that can resolve atomic pair arrangements on the Å scale. It has been shown in scheelites that changes brought on by chemical substitution and/or temperature should be accommodated through geometric distortions of the AO_8 dodecahedra, as opposed to affecting the rigid MoO_4 units. Our group previously used a dual-space approach, whereby Rietveld and PDF analysis were applied to synchrotron X-ray total scattering data,[6] to show that an anomalous contraction of Mo–O distances observed by Rietveld with A-site substitution was found to be the result of orientational disorder induced by random rotations of the MoO_4 tetrahedra (i.e., rotational disorder). Here, we exploit this dual-space approach on temperature-dependent synchrotron X-ray total scattering data (11-ID-B, Argonne National Laboratory) collected on 10-nm $CaMoO_4$ nanocrystals from 90–480 K to gain insight into the temperature dependence of the observed rotational disorder. Despite all relevant parameters associated with the average structure (Rietveld) showing nearly linear behavior with temperature, the local structure (PDF) exhibited a pronounced transition between 151 and 163 K. In this region, the two distinct Ca–O bond distances were found to strongly diverge from each other, resulting in a significant increase in the bond distance distortion index (**Fig. 2**). The origin of this divergence is attributed to the thermal activation of random MoO_4 tetrahedral rotations across the scheelite lattice, which may have structure-property ramifications for these materials as cryogenic scintillation detectors.

3. Crystal structure of colloidal CsPbBr3 nanocrystals. Since the discovery that halide perovskites with the formula AMX_3 (where, A = $CH_3NH_3^+$ or Cs^+; M = Pb^{2+} or Sn^{2+}; X = Cl^-, Br^-, I^-, or a combination thereof) can function as absorber layers and electron transport materials in high-efficiency thin film solar cells, there has been intense interest the structure-property relationships of this material. More recently, nanocrystals of $CsPbX_3$ have been prepared via
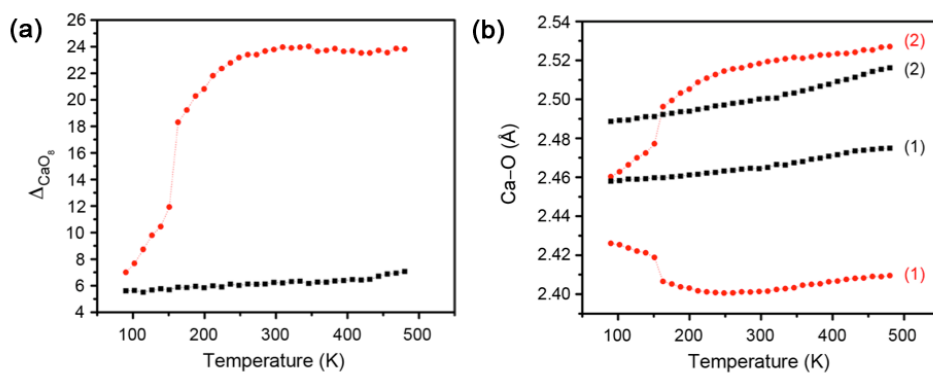
Fig. 2 (a) Ca–O distances and (b) bond length distortion indices extracted from Rietveld (black symbols) and PDF (red symbols) analysis of the X-ray total scattering data for $CaMoO_4$ nanocrystals from 90–480 K. Each unique Ca–O bond distance in (b) is denoted with a number in parentheses.

colloidal methods.[7] This approach yields monodisperse nanocrystals, with sharp optical absorption edges and extremely efficient photoluminescence (PL), possessing a narrow spectral width. The PL can be tuned from the near-UV into the near-IR by controlling the size of the particles and the identity of the halides. These optical properties make haldie peroskite nanocrystals particularly attractive for use in optical devices. In order to intelligently tune the optical properties of these nanocrystals, it is crucial to understand their structure-property relationships, which in turn depends on knowing the crystal structure. At room temperature, bulk $CsPbBr_3$ has been shown to possess a thermodynamically preferred orthorhombic structure with the space group *Pnma* by X-ray diffraction.[8] Previous reports based on benchtop X-ray diffraction are conflicting as to whether the correct crystal structure of $CsPbBr_3$ nanocrystals is cubic[7,9] or orthorhombic.[10]

Synchrotron X-ray scattering measurements were performed on bulk and $CsPbBr_3$ nanocrystal samples at room temperature using the 11-ID-B instrument at Argonne National Laboratory. Rietveld refinements were performed on the Bragg diffraction data using two crystal structures: a structure with the cubic space group $Pm\overline{3}m$ which exists as a high temperature polymorph for bulk $CsPbBr_3$ and a structure with the orthorhombic space group *Pnma* which is the thermodynamically preferred, room temperature structure. The orthorhombic distortion leads to the splitting of the single Br position in the cubic structure into two crystallographically distinct positions. In refinements for both bulk $CsPbBr_3$ and 12.5 nm $CsPbBr_3$ nanocrystals, splitting of the Br position is accompanied by a substantial reduction in the isotropic thermal displacement parameter for Br

Fig. 3 PDF extracted from synchrotron X-ray total scattering data collected on colloidal 12.5 nm $CsPbBr_3$ nanocrystals. The red and blue lines indicate cubic and orthorhombic model fits to the PDF, respectively. The lines at the bottom of the panels indicate the difference between the PDF and the fit.

(from $U_{iso} = 0.1263(4)$ $Å^2$ to $U_{iso} = 0.0356(3)$ $Å^2$ and $U_{iso} = 0.007(4)$ $Å^2$ for 12.5 nm nanocrystals). This reduction in the isotropic thermal parameter strongly indicates the presence of a symmetry-lowering distortion involving Pb-Br octahedra in both bulk $CsPbBr_3$ and $CsPbBr_3$
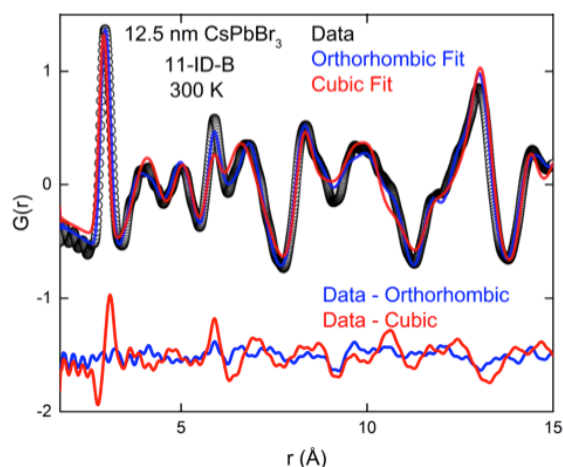
nanocrystals. The X-ray total scattering data were used to generate PDFs, and these were fit with the same cubic and orthorhombic space groups in order to investigate the structure of the materials on the Å scale (**Fig. 3**). The orthorhombic model provides quantitatively better fits to the PDF, especially in the length scale of 5.8 Å $< r <$ 7.0 Å. This region corresponds to Br–Br interatomic distances in the perovskite structure that are strongly affected by rotation of the $PbBr_6$ octahedra that generate the orthorhombic structure from the cubic structure. Taken together, we believe that that these results definitively resolve the question of the correct crystal structure of $CsPbBr_3$ nanocrystals. Because bulk $CsPbBr_3$ with the same orthorhombic crystal structure displays negligible room temperature photoluminescence, this result suggests that the efficient photoluminescence of these $CsPbBr_3$ nanocrystals results not from structural effects but rather from other factors such as passivation or strain.

Future Plans

(1) Leverage our vapor diffusion sol-gel method to synthesize compositionally controlled, doped scheelite nanocrystals at low temperatures. Focus will be placed on doping these nanocrystals with two rare earth elements to give dual emission nanocrystals with high quantum yields.

(2) Explore the solution-phase synthesis of $Fe_2(MO_4)_3$ nanomaterials, where M = Mo or W. Using a combination of synchrotron X-ray and neutron diffraction and PDF analysis, we will create a structural understanding of the differences between electrochemical lithium and sodium intercalation into these anti-NASICON structures.

(3) Probe the local structure of $APbX_3$ nanocrystals as a function of A-site cation (Cs^+ or $MeNH_3^+$) or halide (Cl^-, Br^-, or I^-). The dielectric properties of the halide perovskite nanocrystals will be tested and subsequently applied toward polymer nanocomposites for dielectric capacitors.

References

1. G. Blasse and L. H. Brixner, *Chem. Phys. Lett.*, 1990, **173**, 409.
2. L. Wöhler and O. Balz, *Z. Elektrochem.*, 1921, **27**, 415.
3. R. Oeder, A. Sharmann and D. Schaw, *J. Cryst. Growth*, 1980, **49**, 349.
4. L. L. Y. Chang, *Am. Mineral.*, 1967, **52**, 427.
5. V. B. Mikhailik, H. Kraus, G. Miller, M. S. Mykhaylyk and D. Wahl, *J. Appl. Phys.*, 2005, **97**, 083523.
6. F. A. Rabuffetti, S. P. Culver, L. Suescun and R. L. Brutchey, *Inorg. Chem.*, 2014, **53**, 1056.
7. L. Protesescu, S. Yakunin, M. I. Bodnarchuk, F. Krieg, R. Caputo, C. H. Hendon, R. X. Yang, A. Walsh, M. V. Kovalenko, *Nano Lett.,* 2015, **15**, 3692.
8. C. C. Stoumpos, C. D. Malliakas, J. A. Peters, Z. Liu, M. Sebastian, J. Im, T. C. Chasapis, A. C. Wibowo, D. Y. Chung, A. J. Freeman, B. W. Wessels, M. G. Kanatzidis, *Cryst. Growth Des.*, 2013, **13**, 2722.
9. D. Zhang, S. W. Eaton, Y. Yu, L. Dou, P. Yang, *J. Am. Chem. Soc.* 2015, **137**, 9230.
10. A. Swarnkar; R. Chulliyil, V. K. Ravi, M. Irfanullah, A. Chowdhury, A. Nag, *Angew. Chem. Int. Ed.*, 2015, **54**, 15424.

Publications

1. Culver, S. P.; Stepanov, V.; Mecklenburg, M.; Takahashi, S.; Brutchey, R. L. Low-Temperature Synthesis and Characterization of Lanthanide-Doped $BaTiO_3$ Nanocrystals. *Chemical Communications* **2014**, *50*, 3480-3483.

2.   Culver, S. P.; Greaney, M. J.; Tinoco, A.; Brutchey, R. L. Low-Temperature Synthesis of Homogeneous Solid Solutions of Scheelite-Structured $Ca_{1-x}Sr_xWO_4$ and $Sr_{1-x}Ba_xWO_4$ Nanocrystals. *Dalton Transactions* **2015**, *44*, 15042-15048.
3.   Cottingham, P.; Brutchey, R. L. On the Crystal Structure of Colloidally Prepared $CsPbBr_3$ Quantum Dots. *Chemical Communications* **2016**, *52*, 5246-5249.
4.   Culver, S. P.; Brutchey, R. L. Thermally Activated Rotational Disorder in $CaMoO_4$ Nanocrystals. *CrystEngComm* **2016**, *in press*. **DOI:** 10.1039/C6CE00673F

Synthesizing New Metal Organic Frameworks with Tailored Physical and Chemical Properties

Yves J. Chabal, University of Texas at Dallas
Jing Li, Rutgers University
Timo Thonhauser, Wake Forest University

Program Scope

The aim of this program is to develop a fundamental understanding of the interaction of guest molecules in porous metal organic framework (MOF) materials, using a combination of novel synthesis, *ab initio* modeling, and characterization. In particular, we combine high-pressure/low-temperature *in-situ* infrared (IR) absorption and Raman measurements with gas adsorption-desorption experiments and calculations based on density functional theory. Our goal is to study molecular adsorption, diffusion, and reactions in different MOF materials, with a particular emphasis on their effect on the physical and chemical properties of the MOF host materials. The short-term impact of the proposed work is the control and understanding of common MOF systems, with important impact on applications and industrial processes from gas storage and sequestration to catalysis and sensors. The long-term impacts are the development of (i) theoretical and experimental methods to gain a fundamental understanding of molecular interactions within MOFs, and (ii) new guidelines to synthesize microporous MOFs with tailored physical and chemical properties.

Recent Progress

a) *Surface molecular barrier for enhanced and selective adsorption and release of gases in MOFs [1]* – In contrast to efforts that enhance gas adsorption in MOFs by increasing their binding energy, we have shown that ethylenediamine (EDA) can be used to form a monolayer-thick cap that can effectively retain weakly adsorbed molecules (CO, CO_2, SO_2 C_2H_4) or prevent their penetration (see Figure 1). We further showed that water molecules diffuse through the same EDA barrier without hindrance and can fully displace these small molecules out of the MOF altogether at room temperature. This unexpected selectivity, as explained by *ab initio* modeling, is attributed to hydrogen bonding of water to the terminal amine network, which opens a space for water molecules to pass through. These findings not only provide a means for trapping gases inside MOF at atmospheric conditions without having to synthetically increase their binding energy within the MOFs, but also suggest a new concept to develop future selective membranes for adsorption in porous materials.
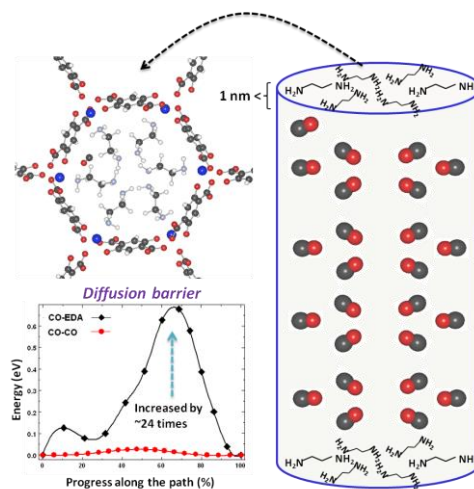

Figure 1. Capping MOF-74 with an EDA monolayer to trap small molecules.

b) *Understanding and controlling water stability of MOF-74 [2]* – MOFs in general, and MOF-74 in particular, have promising properties for many technologically important processes.

However, their instability under humid conditions severely restricts practical use. We have shown that this instability and the accompanying reduction of the CO_2 uptake capacity of MOF-74 under humid conditions originate in the water dissociation reaction $H_2O \rightarrow OH+H$ at the metal centers. After this dissociation, the OH groups coordinate to the metal centers, explaining the reduction in the MOF's CO_2 uptake capacity. This reduction thus strongly depends on the catalytic activity of MOF-74 towards the water dissociation reaction. We further showed that—while the water molecules themselves only have a negligible effect on the crystal structure of MOF-74—the OH and H products of the dissociation reaction significantly weaken the MOF framework and lead to the observed crystal structure breakdown. With this knowledge, we proposed a way to suppress this particular reaction by modifying the MOF-74 structure to increase the water dissociation energy barrier and thus control the stability of the system under humid conditions.

c) *Chemistry in confined spaces: Reactivity of the Zn-MOF-74 channels [3]* – Using IR spectroscopy combined with *ab initio* methods we studied reactions of H_2O and CO inside the confined spaces of Zn-MOF-74 channels. We showed that, once the water dissociation reaction $H_2O \rightarrow OH+H$ takes place at the metal centers, the addition of 40 Torr of CO at 200°C starts the production of formic acid via $OH+H+CO \rightarrow HCO_2H$. Our detailed

Figure 2. Formic acid catalysis in MOF-74.

analysis shows that the overall reaction $H_2O+CO \rightarrow HCO_2H$ takes place in the confinement of MOF-74 without an external catalyst (see Figure 2). This discovery has important consequences: It opens the door to a new set of catalytic reactions inside the channels of the MOF-74 system, it suggests that a recovery of the MOF's adsorption capacity is possible after it has been exposed to water, and it produces the important industrial feedstock formic acid. We also showed that the water dissociation reaction can be precisely controlled by the addition of the noble gas He [4]. Elucidating the entire reaction process with *ab initio* methods and IR spectroscopy, we proved that the interaction between water molecules is critical to the formation of water clusters (see Figure 3), reducing the dissociation barrier by up to 37% and thus influencing the reaction significantly. Since the water dissociation reaction is the cause of the structural instability of MOF-74 in the presence of water, our finding of the reaction mechanism lays the groundwork for designing water stable versions of MOF-74 as well as understanding water-related phenomena in MOFs in general.
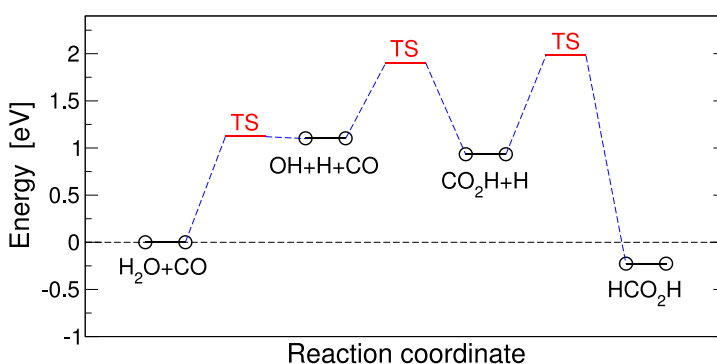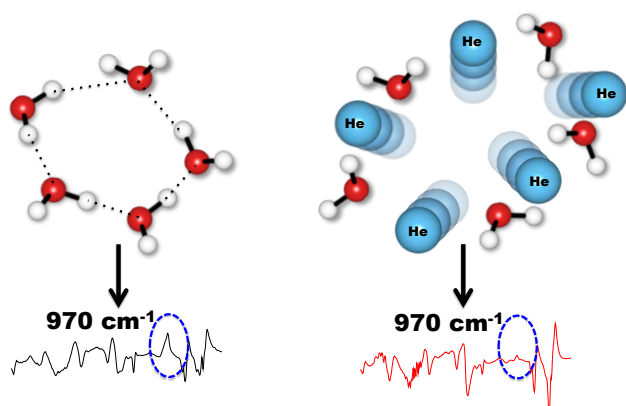

Figure 3. Formation of water clusters inside MOF-74, which significantly lower the water dissociation barrier. Helium provides a simple means to prevent the cluster formation and thus control the water dissociation rate.

d) *Spin signature of nonlocal correlation binding in metal organic frameworks [5]* – We have developed a proper nonempirical spin-density formalism for the theoretical description of van der Waals interactions within density functional theory. We showed that this generalized spin-density functional, termed svdW-DF, is firmly rooted in the single-particle nature of exchange. We investigated in detail the role of spin in the nonlocal correlation driven adsorption of H_2 and CO_2 in Mn-MOF-74, Fe-MOF-74, Co-MOF-74, and Ni-MOF74. In all cases, we found that spin plays a significant role during the adsorption process despite the general weakness of the molecular-magnetic responses. The case of CO_2 adsorption in Ni-MOF-74 is particularly interesting, as the inclusion of spin effects results in an increased attraction, opposite to what the diamagnetic nature of CO_2 would suggest. We explain this counterintuitive result, tracking the behavior to a coincidental hybridization of the O p states with the Ni d states in the down-spin channel. More generally, by providing insight on nonlocal correlation in concert with spin effects, our nonempirical svdW-DF method opens the door for a deeper understanding of weak nonlocal magnetic interactions, essential for an accurate theoretical description of the chemistry of many materials.

e) *Strongly luminescent metal-organic framework for effective detection of mycotoxins [6]* – We designed and synthesized a new luminescent metal-organic framework (LMOF). LMOF-241 is highly porous and emits strong blue light with high efficiency (see Figure 4). We demonstrated for the first time that very fast and extremely sensitive optical detection can be achieved, making use of the fluorescence quenching of a LMOF material. The compound is responsive to Aflatoxin B1 at parts-per-billion level, which makes it the best performing luminescence-based chemical sensor to date. We studied the electronic properties of LMOF-241 and selected mycotoxins, as well as the extent of mycotoxin-LMOF interactions, involving electron and energy transfer mechanisms.
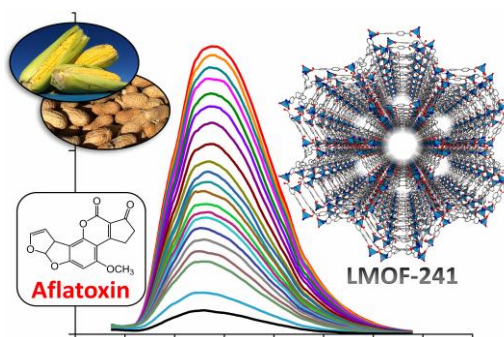

Figure 4. LMOF-241, capable of efficiently detecting and differentiating several major Aflatoxins and Ochratoxin A via fluorescence quenching. The detection limit for AFB1 is estimated to be 46 ppb, significantly better than 300 ppb, the tolerance level set by the FDA for corn and peanut feeds for beef cattle.

f) *Highly efficient luminescent metal organic frameworks for simultaneous detection and removal of heavy metals from water [7]* – We developed an isoreticular series of LMOFs by incorporating functionally diverse linkers and a molecular fluorophore into the Zn-containing structures. LMOF-261, -262, and -263 are three-dimensional, four-fold interpenetrated network structures that crystallize in body-centered tetragonal crystal system (space group *I*4$_1$/a). We have carried out a systematic study to analyze and compare their interactions with heavy metal ions. LMOF-263 exhibits impressive water stability, coupled with high porosity and strong luminescence, making it an excellent candidate as a fluorescent chemical sensor and adsorbent for aqueous contaminants. It is extremely responsive to toxic heavy metals, at a parts-per-billion level (3.3 ppb Hg^{2+}, 19.7 ppb Pb^{2+}) and exhibits a highly selective uptake for toxic heavy metals (Hg^{2+}, Pb^{2+}, Cd^{2+}) over light metals (Ca^{2+}, Mg^{2+}), with a maximum capacity of 380 mg Hg^{2+}/g. This work addresses issues in water remediation by employing a material that has high performances in both the detection and removal of toxic metals from contaminated water.

Future Plans

We plan to design new MOFs with targeted functionality, structures, and stability using a precursor approach in which secondary building units are preformed as soluble metal carboxylate clusters, and to (a) elucidate the diffusion and interaction of small molecules inside these MOFs; (b) investigate the diffusion process of metal salts in solution with the ultimate motivation to provide a platform for nanoparticle synthesis, and (c) determine which aspects of the MOF and/or adsorbed guest molecules govern a MOF's optical, electrical, and mechanical properties which in turn will guide directed and optimized synthesis.

References

[1] K. Tan, S. Zuluaga, E. M. A. Fuentes-Fernandez, E. C. Mattson, J. F. Veyan, H. Wang, J. Li, T. Thonhauser, and Y. J. Chabal, *Surface molecular barrier for enhanced and selective adsorption and release of gases in metal organic frameworks*, Nature Materials (2016), under review (submitted Jan. 2016).

[2] S. Zuluaga, E. M. A. Fuentes-Fernandez, K. Tan, F. Xu, J. Li, Y. J. Chabal, and T. Thonhauser, *Understanding and controlling water stability of MOF-74*, J. Mater. Chem. A **4**, 5176 (2016).

[3] S. Zuluaga, E. M. A. Fuentes-Fernandez, K. Tan, C. A. Arter, J. Li, Y. J. Chabal, and T. Thonhauser, *Chemistry in confined spaces: Reactivity of the Zn-MOF-74 channels*, J. Mater. Chem. A (2016), under review (submitted May 2016).

[4] S. Zuluaga, E. M. A. Fuentes-Fernandez, K. Tan, J. Li, and Yves J. Chabal, and T. Thonhauser, *Cluster assisted water dissociation mechanism in MOF-74 and controlling it using helium*, J. Mater. Chem. A (2016), under review.

[5] T. Thonhauser, S. Zuluaga, C. A. Arter, K. Berland, E. Schröder, and P. Hyldgaard, *Spin signature of nonlocal correlation binding in metal-organic frameworks*, Phys. Rev. Lett. **115**, 136402 (2015).

[6] Z. C. Hu, W. P. Lustig, J. M. Zhang, C. Zheng, H. Wang, S. J. Teat, Q. H. Gong, N. D. Rudd, and J. Li, *Effective detection of mycotoxins by a highly luminescent metal-organic framework*, J. Am. Chem. Soc. **137**, 16209 (2015).

[7] N. D. Rudd, H. Wang, E. M. A. Fuentes-Fernandez, S. J. Teat, F. Chen, G. Hall, Y. J. Chabal, and J. Li, *A highly efficient luminescent metal-organic framework for simultaneous detection and removal of heavy metals from water*, J. Am. Chem. Soc. (2016), under review.

DOE Sponsored Publications in the Last Two Years (5/2014 – 5/2016)

1. S. Zuluaga, E. M. A. Fuentes-Fernandez, K. Tan, F. Xu, J. Li, Y. J. Chabal, and T. Thonhauser, *Understanding and controlling water stability of MOF-74,* J. Mater. Chem. A **4**, 5176 (2016).

2. H. Wang, J. J. Peng, and J. Li, *Ligand functionalization in metal-organic frameworks for enhanced carbon dioxide adsorption*, The Chemical Record, (2016), early view, invited Personal Account. DOI: 10.1002/tcr.201500307

3. H. H. Wu, C. G. Thibault, H. Wang, K. A. Cychosz, M. Thommes, and J. Li, *Effect of temperature on hydrogen and carbon dioxide adsorption hysteresis in an ultramicroporous MOF*, Micopor. Mesopor. Mat. **219**, 186 (2016).

4. B. Banerjee, H. Wang, Q. H. Gong, J. Jagiello, H. H. Wu, W. R. Woerner, A. M. Plonka, T. J. Emge, D. H. Olson, J. B. Parise, and J. Li, *Direct structural evidence of commensurate-to-incommensurate transition of hydrocarbon adsorption in a microporous metal organic framework,* Chem. Sci. **7**, 759, (2016).

5. A. M. Plonka, X. Y. Chen, H. Wang, W. R. Woerner, B. Banerjee, R. Krishna, J. Li, and J. B. Parise, *Light hydrocarbons adsorption mechanisms in two Ca-based microporous metal organic frameworks*, Chem. Mater. **28**, 1636 (2016).

6. T. Thonhauser, S. Zuluaga, C. A. Arter, K. Berland, E. Schröder, and P. Hyldgaard, *Spin signature of nonlocal correlation binding in metal-organic frameworks,* Phys. Rev. Lett. **115**, 136402 (2015).

7. B. J. Deibert, J. M. Zhang, P. F. Smith, K. W. Chapman, S. Rangan, D. Banerjee, K. Tan, H. Wang, N. Pasquale, F. Chen, K. B. Lee, G. C. Dismukes, Y. J. Chabal, and J. Li, *Highly active 'polytype-birnessite' MnO_x water oxidation catalyst formed in-situ from $Mn^{II}_4O_4$ MOF precursor: Structural investigation of an amorphous catalyst*, Chem. Eur. J. **21**, 13218 (2015).

8. K. Tan, S. Zuluaga, Y. Gao, Q. Gong, N. Nijem, J. Li, T. Thonhauser, and Y. J. Chabal, *Competitive co-adsorption of CO_2 with H_2O, NH_3, SO_2, NO, NO_2, N_2, O_2, CH_4 in M-MOF-74 (M = Mg, Co, Ni): The role of hydrogen bonding*, Chem. Mater. **27**, 2203 (2015).

9. Z. C. Hu, W. P. Lustig, J. M. Zhang, C. Zheng, H. Wang, S. J. Teat, Q. H. Gong, N. D. Rudd, and J. Li, *Effective detection of mycotoxins by a highly luminescent metal-organic framework*, J. Am. Chem. Soc. **137**, 16209 (2015).

10. P. Canepa, K. Tan, Y. J. Du, H. B. Lu, Y. J. Chabal, and T. Thonhauser, *Structural, elastic, thermal, and electronic responses of small-molecule-loaded metal-organic framework materials*, J. Mater. Chem. **3**, 986 (2015), selected as "HOT" article for 2015.

11. S. Zuluaga, L.-H. Liu, N. Shafiq, S. M. Rupich, J.-F. Veyan, Y. J. Chabal, and T. Thonhauser, *Structural band-gap tuning in g-C_3N_4*, Phys. Chem. Chem. Phys. **17**, 957 (2015).

12. K. Tan, N. Nijem, Y. Gao, S. Zuluaga, J. Li, T. Thonhauser, and Y. J. Chabal, *Water interaction in metal organic framework,* Cryst. Eng. Comm. **17**, 247 (2015).

13. D. Banerjee, H. Wang, B. J. Deibert, and J. Li, *Alkaline earth metal based metal-organic frameworks: Synthesis, properties, and applications, in The Chemistry of Metal-Organic Frameworks,* Edited by Stefan Kaskel (Wiley-VCH, 2015).

14. F. Xu, H. Wang, S. J. Teat, W. Liu, Q. B. Xia, Z. Li, and J. Li, *Synthesis, structure and enhanced photoluminescence properties of two robust, water stable calcium and magnesium coordination networks,* Dalton Transac. **44**, 20459, (2015).

15. Z. Hu, K. Tan, H. Wang, Y. Zhao, C. Zheng, D. Banerjee, Q. Gong, T. J. Emge, Y. J. Chabal, and J. Li, *Effective sensing of RDX via instant and selective detection of ketone vapors*, Chem. Sci. **5**, 4873 (2014).

16. D. Banerjee, Z. C. Hu, and J. Li, *Luminescent metal-organic frameworks as explosive sensors*, Dalton Trans. **43**, 10668 (2014), invited perspective, top 20 most accessed Dalton Transactions articles in 2014.

17. K. Tan, S. Zuluaga, Q. Gong, J. Li, T. Thonhauser, and Y. J. Chabal, *Water reaction mechanism in metal organic frameworks with coordinatively unsaturated metal ions: MOF-74*, Chem. Mater. **26**, 6886 (2014).

18. N. Nijem and Y. J. Chabal, *Adsorbate interactions in metal organic frameworks studied by vibrational spectroscopy,* Comments on Inorg. Chem. **34**, 78 (2014), invited review.

Functionalization of Metal-Organic Frameworks - polyMOFs

Seth M. Cohen, University of California, San Diego

Program Scope

The scope of our program is on the functionalization of metal-organic frameworks (MOFs) for energy relevant applications. This includes the development of postsynthetic methods, such as postsynthetic modification (PSM) and postsynthetic exchange (PSE) to make MOF materials that can act as catalysts for hydrogen evolution or carbon dioxide reduction. In another direction, the functionalization/integration of MOFs with polymer architectures has revealed a new class of materials we refer to as polyMOFs. This abstract will focus on progress in this new area of MOF research, at the intersection of soft and hard materials.

Recent Progress

Preparation of porous materials from 1-dimensional polymers is challenging because the packing of polymer chains results in a dense, non-porous arrangement. In our recent work, we demonstrate the transformation of an amorphous, linear, non-porous, flexible organic polymer into a 3-dimensional, highly porous, crystalline solid, as the organic component of a metal-organic framework (MOF, Figure 1). A polymer with aromatic dicarboxylic acids in the backbone functioned as a polymer-ligand upon annealing with Zn(II) – generating a polymer-metal-organic-framework (polyMOF). These materials uproot the dogma that MOFs must be prepared from small, rigid ligands. Similarly, polyMOFs contradict conventional polymer chemistry by demonstrating that linear and amorphous polymers can be readily coaxed into a highly crystalline, porous, 3-dimensional

Figure 1. A linear, amorphous polymer (*right*) can be combined with metal ions (in this example Zn^{2+}, *middle*) to generate a polymer+MOF hybrid material termed a polyMOF. SEM images of polyMOFs (left) show they can form polycrystalline particles, but other morphologies, such as films, have also been obtained.

structure via coordination chemistry. More recently, we have shown that the polyMOF concept is compatible with MOFs that rely on a bridging coligand strategy. These findings demonstrating that polyMOFs are compatible with additional MOF architectures besides that of the first set of IRMOF-1 type polyMOF structures we described in our first study. Gas sorption studies revealed that co-ligand polyMOF materials exhibited relatively high CO_2 sorption but
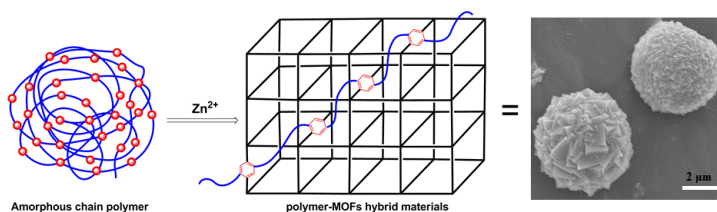
very low N_2 sorption, making them promising materials for separations. Moreover, these polyMOFs demonstrated exceptional water stability attributed to the hydrophobicity of polymer ligands as well as the cross-linking of the polymer chains within the MOF. Overall, the polyMOF strategy shows promise as a new class of materials that bridge the gap between polymers and porous solids.

Future Plans

We are continuing to explore and expand the scope of polyMOFs. We are exploring the effects of polymer architecture, metal ion source, reaction conditions, and the like to define what polymers can be used to form polyMOFs and what MOF architectures are compatible with polyMOFs. We are also examining the use of block copolymers to form polyMOFs in order to achieve polyMOF materials with polymer-like processing properties, but high surface areas reminiscent of MOFs.

References

See list of publications below.

Publications

1. Marco Taddei, Ferdinando Costantino, Riccardo Vivani, Stefano Sabatini, Sang-Ho Lim, and Seth M. Cohen, "The Use of a Rigid Tritopic Phosphonic Ligand for the Synthesis of a Robust Honeycomb-like Layered Zirconium Phosphonate Framework" *Chem. Commun.* **2014**, *50*, 5737-5740. DOI: 10.1039/C4CC01253D

2. Corinne A. Allen and Seth M. Cohen, "Exploration of Chemically Crosslinked Metal-organic Frameworks" *Inorg. Chem.* **2014**, *53*, 7014-7019. DOI: 10.1021/IC500951B

3. Phuong V. Dau and Seth M. Cohen, "Modulating H_2 Sorption in Metal-organic Frameworks via Ordered Functional Groups" *Chem. Commun.* **2014**, *50*, 12154-12157. DOI: 10.1039/C4CC05265J

4. JaeWook Shin, Min Kim, Jordi Cirera, Shawn Chen, Gregory Halder, Thomas A. Yersak, Francesco Paesani, Seth M. Cohen, and Ying Shirley Meng, "MIL-101(Fe) as a Lithium-ion Battery Electrode Material: Relaxation and Intercalation Mechanism During Lithium Insertion" *J. Mater. Chem. A* **2015**, *3*, 4738-4744. DOI: 10.1039/C4TA06694D

5. Yeob Lee, Sangjun Kim, Jeung Ku Kang, and Seth M. Cohen, "Photocatalytic CO_2 reduction by a mixed metal (Zr/Ti), mixed ligand metal-organic framework under visible light irradiation" *Chem. Commun.* **2015**, *51*, 5735-5738. DOI: 10.1039/C5CC00686D

6. Zhenjie Zhang, Ha Thi Hoang Nguyen, Stephen A. Miller, and Seth M. Cohen, "polyMOFs: A New Class of Interconvertible Polymer-MOF Hybrid Materials" *Angew. Chem. Int. Ed.* **2015**, *54*, 6152-6157. DOI: 10.1002/ANIE.201504077.

7. Yeob Lee, Sangjun Kim, Honghan Fei, Jeung Ku Kang*, and Seth M. Cohen*, "Photocatalytic CO2 Reduction Using Visible Light by Metal-monocatecholato Species in a Metal-organic Framework" *Chem. Commun*. **2015**, *51*, 16549-16552. DOI: 10.1039/C5CC04506A.

8. Zhenjie Zhang, Ha Thi Hoang Nguyen, Stephen A. Miller, Ann Ploskonka, Jared DeCoste, and Seth M. Cohen*, "polyMOFs as Water Tolerant Materials for Selective Carbon Dioxide Separations" *J. Am. Chem. Soc*. **2016**, *138*, 920-925. DOI: 10.1021/JACS.5B11034.

9. Teng-Hao Chen, Andreas Schneemann, Roland A. Fischer, and Seth M. Cohen*, "Metal−organic Frameworks Constructed from Crown Ether-based 1,4-Benzenedicarboxylic Acid Derivatives" *Dalton Trans*. **2016**, *45*, 3063-3069. DOI: 10.1039/C5DT04316F.

Design of Next Generation Thermoelectrics

Vinayak P. Dravid, PI
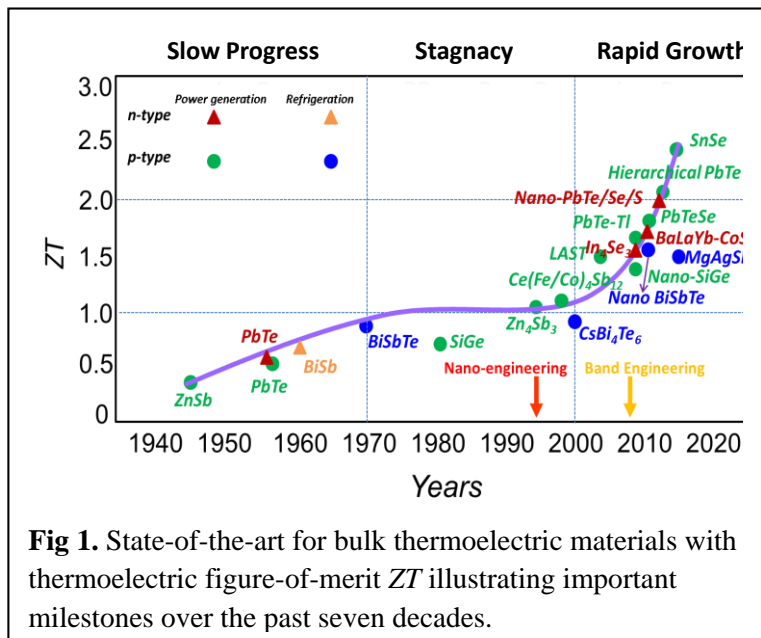**Mercouri Kanatzidis; co-PI**
Christopher Wolverton, co-PI
Northwestern University, Evanston, IL 60208

Program Scope

About two thirds of utilized energy in the world is lost; most of it in the form of waste heat. Thermoelectricity can make use of such lost heat by reversible conversion of a temperature gradient to electricity through the Seebeck effect. Fundamentally, it represents a microscopic process involving the transport and complex interplay between charge carriers and lattice vibrations, or phonons, in a solid. Thermoelectric materials present a unique opportunity to convert even a small fraction of such massive lost thermal energy to useful electricity.[1,2] Thermoelectric materials embody remarkably complex yet elegant scientific concepts of electron and thermal transport in converting a thermal gradient to electrical energy.

The efficiency for conversion of heat to electricity is determined by the dimensionless figure of merit $ZT = (\sigma \cdot S^2/\kappa)T$, where σ is the electrical conductivity, S is the Seebeck coefficient, κ the thermal conductivity, and T the absolute temperature. The figure of merit represents a fascinating dichotomy of "*contraindicated*" behavior. An increase in power factor (σS^2), for example by enhancing the electrical conductivity, typically increases thermal conductivity. Thus, innovative strategies are required that can independently tailor the power factor and thermal conductivity. Indeed, the design of a new generation of thermoelectrics will require filling knowledge and scientific gaps. This project involves a multidisciplinary team and focuses on the science of understanding the origin of the thermoelectric figure of merit and the complex interplay among the thermoelectric parameters. The project team has significantly contributed to the recent "*renaissance*" of the field of thermoelectricity by introducing innovative scientific concepts to enhance the figure of merit, ZT, as depicted in Fig. 1.[3,4]

The project team has achieved substantial reductions in thermal conductivity through innovative "*all-length-scale*" architecturing of nanostructured thermoelectrics.[4] We have also introduced new materials that exhibit intrinsically low thermal conductivities as in the layered SnSe system.[5] However, even with amorphous limit for thermal conductivity, increase in resultant ZT is likely to be rather small. On the other hand, innovative strategies for enhancing the power factor have been few and far between. We have argued that the field of thermoelectrics needs new bold guidance on how the

Fig 1. State-of-the-art for bulk thermoelectric materials with thermoelectric figure-of-merit *ZT* illustrating important milestones over the past seven decades.

power factor can be further enhanced in the existing leading materials, especially enhancements from the Seebeck coefficient. Our team has been at the vanguard at these developments and has collectively contributed to the field with new ideas and innovative approaches.

This research program primarily focuses on the scientific concepts surrounding increases in the power factor as the primary driver for increase in power factor. The research strategies revolve around valence band convergence, retention of carrier mobility through minimization of band energy offsets between matrix and precipitates, band engineering to increase the number of bands contributing to the transport. Certainly, we also employ strategies for reduction in thermal conductivity in conjunction with power factor enhancement, thereby contributing to potentially even higher ZT than currently achieved. The key scientific challenges which require a synergistic and collaborative approach include: a) insights into the collective mechanisms of charge and phonon transport across the atomic, nano- and mesoscale levels. b) potential integration of all of the ZT-enhancing mechanisms simultaneously and synergistically into a single material system, and c) understanding of precipitate nucleation and microstructural evolution of these systems.

The Year-I progress included tangible advances along all fronts; with peer reviewed publications comprising multiple members of the project team in high-impact journals and other relevant metrics for evaluation of progress. Some examples are outlined below.

Recent Progress: The project team has made substantial progress in Year-I of the grant. Our collaborative work has resulted in world-record breaking ZT through innovative panoscopic all-length-scale architecturing of thermoelectrics.We have also recognized that the biggest gains in thermoelectric efficiency must come from enhancement in power factor. Our recent work involved alloying lead, tin and germanium chalcogenides which significantly modify both of the valence and conduction bands to achieve band convergence in the electronic structure. Coupled to the control over nanostructured phases and interfaces, we have identified fertile ground for innovations through a combined theoretical and experimental undertaking of chalcogenides.

Lead, tin and germanium chalcogenides have an intriguing valence band configuration. In addition to the normal so-called light hole band at the L point of the highly symmetric Brillouin zone there is a second valence (so called heavy hole band) band (Σ) which lies energetically below it. Recent efforts to modify the valence band structure of SnTe with the aim to influence its Seebeck coefficient have been successful.[6,7] Specifically that Cd, Hg, Mg, and Mn doping in SnTe could enhance the Seebeck coefficient of SnTe by means of pushing the two valence bands closer in energy, i.e., band convergence. An alternative way is to introduce additional impurity states (resonant levels) near the Fermi level by guest atom alloying, as implemented in p-type Tl-doped PbTe and In-doped SnTe and n-type Al-doped PbSe.[8] As effective as modifying the band structure is, in terms of improving the electronic transport properties, the phonon transport is unaltered or only mildly influenced via point defect scattering by these small impurities. This makes sense because the atomic mass and radius contrasts between Sn and the doping elements are usually fairly small, while strong point defect scattering of phonons usually requires a significant difference in atomic properties between the host and guest atoms.

We have also extended these ideas to the SnTe system. We have unraveled the coexistence of two beneficial effects by In2Te3 alloying with SnTe: (i) a significant decrease of lattice thermal conductivity due to the strong vacancy phonon scattering between the host Sn atoms of SnTe and the guest structural vacancies of In2Te3, and an additional interfacial scattering by In-rich nanostructures; (ii) a considerable enhancement of Seebeck coefficient because of the resonant levels inside the valence bands of SnTe introduced by indium. As a consequence, the thermoelectric figure of merit ZT of SnTe is largely increased by In2Te3 alloying, with the

maximum value reaching ~0.9 around 923 K which is 50% improvement over the pristine SnTe. Together with its high average ZT of ~0.67 in the temperature range of 300–923 K and nontoxic constitute elements, In2Te3-alloyed SnTe holds great promise as a robust material for high-temperature thermoelectric power generation.[8]

We have demonstrated a thermoelectric figure of merit ZT of ~2.5 at ~923 K by the cumulative integration of several performance enhancing concepts in a single material system. [9,10] Using non-equilibrium processing hole-doped samples of PbTe can be heavily alloyed with SrTe well beyond its thermodynamic solubility limit of < 1 mol%. The much higher levels of Sr alloyed into the PbTe matrix widen the band gap and create convergence of the two valence bands of PbTe, greatly boosting the power factors. Exceeding the solubility limit endotaxial SrTe nanostructures are present, which produce extremely low lattice thermal conductivity but preserve high hole mobilities because of the matrix/precipitate valence band alignment.

It has been shown in past that SnSe exhibits one of the lowest lattice thermal conductivities known for crystalline materials (< 0.4 Wm−1K−1 at 923K) and even without any doping, it exhibits record high ZTs along the b- and c- crystallographic directions at 723-973K. Unlike the facile doping behavior of Pb-based rock salt chalcogenides, doping SnSe is challenging because of the layered anisotropic structure where each SnSe layer is two atoms thin and the locally distorted bonding around the Sn and Se atoms. We recently overcome this challenge to demonstrate successful hole doping in SnSe single crystals using Na as an effective acceptor.[11] The hole doped SnSe (b axis) outperforms most of the current p-type materials at 300-773K. The high PF and ZT give the highest "device" ZT (ZTdev) from 300-773K, of ~1.34.[11]

Stimulated by the high ZT in hole doped SnSe, we turned attention to analogous isovalent compounds, namely, GeSe and GeS.[12] It is known that the GeSe low temperature phase has a Pnma space group, while the high temperature rocksalt phase has a transition temperature of 853 K. For GeS, the low temperature and high temperature phases are respectively in Pnma and Cmcm space groups with a transition temperature of 863 K. Since the transition temperatures are relatively high and our aim is to improve thermoelectric performance over a broad temperature range from 300 K, we then mainly focus on the low temperature Pnma phases of GeSe and GeS. We used first-principles based methods to calculate all relevant physical properties to evaluate the figure of merit ZT and predict that the calculated ZT of GeSe is higher even than the record-setting SnSe, given the same hole concentration in the two compounds. The Pnma structure of high purity GeSe with perfect stoichiometry has been demonstrated by microscopy observations.

Future Plans: The ongoing and future plans will pursue power factor enhancement strategies, while exploring unusual layered systems such as SnSe and analogs. We continue to address the key unanswered scientific questions, which are being pursued in the context of chalcogenide systems: How can we modify the electronic structure of the matrix materials to enhance the Seebeck coefficient and power factor? How can we tailor the nanostructured phase to maintain high mobility of charge carriers? Embedded in this question is the need to understand the structural, chemical and electronic structural parameters that control doping behavior in these materials. How can we achieve all of the above and still simultaneously lower the thermal conductivity? In addition, we will look into: a) insights into the collective mechanisms of charge and phonon transport across the atomic, nano- and mesoscale levels; b) potential integration of all of the ZT-enhancing mechanisms simultaneously and synergistically into a single material system; and c) the nucleation of precipitates and microstructural evolution. The ongoing and future work will continue along the three interconnected scientific thrusts, which reflect the evolution towards superior performing thermoelectric systems. We tackle the following scientific

objectives for the enhancement of the power factor in chalcogenides: *(i) Band-engineering by leveraging multi-band strategies to enhance Seebeck coefficient:* By manipulating the band structure of thermoelectric chalcogenides via alloying, we systematically examine the possibility of bringing the multiple bands (near the Fermi level) closer in energy to achieve band degeneracy, thereby enhancing the Seebeck coefficients. *(ii) Band-alignment between the second phases and matrix:* Charge scattering across the matrix- precipitate interfaces deteriorates carrier mobilities and power factors in nanostructured systems. Understanding the physical factors that affect band alignment and charge mobilities is critical in predicting and selecting the optimal second phases. *(iii) Nucleation and evolution of nanostructures:* Through the understanding of nucleation/evolution of nanostructures, we optimize matrix and precipitate phases to enable microstructure-electronic structure correlation.

References:

1) Bell, L. E. Cooling, Heating, Generation Power, and Recovering Waste Heat with Thermoelectric systems, *Science* **2008**, *321*, 1457-1461.
2) Snyder, G. J.; Toberer, E. S. Complex thermoelectric materials, *Nat. Matls* **2008**, *7*, 105-114.
3) Zhao, L. D.; Dravid, V. P.; Kanatzidis, M. G. The panoscopic approach to high performance thermoelectrics, *Energy & Environmental Science* **2014**, *7*, 251-268.
4) Biswas, K.; He, J.; Blum, I. D.; Wu, C. I.; Hogan, T. P.; Seidman, D. N.; Dravid, V. P.; Kanatzidis, M. G. High-performance bulk thermoelectrics with all-scale hierarchical architectures, *Nature* **2012**, *489*, 414-418.
5) Zhao, L. D.; Lo, S. H.; Zhang, Y. S.; Sun, H.; Tan, G. J.; Uher, C.; Wolverton, C.; Dravid, V. P.; Kanatzidis, M. G. Ultralow thermal conductivity and high thermoelectric figure of merit in SnSe crystals, *Nature* **2014**, *508*, 373
6) Zhao, L.-D.; Zhang, X.; Wu, H.; Tan, G.; Pei, Y.; Xiao, Y.; Chang, C.; Wu, D.; Chi, H.; Zheng, L.; Gong, S.; Uher, C.; He, J.; Kanatzidis, M. G., Enhanced Thermoelectric Properties in the Counter-Doped SnTe System with Strained Endotaxial SrTe. J. Am. Chem. Soc. 2016, 138, (7), 2366-2373.
7) Zeier, W. G.; Zevalkink, A.; Gibbs, Z. M.; Hautier, G.; Kanatzidis, M. G.; Snyder, G. J., Thinking Like a Chemist: Intuition in Thermoelectric Materials. Angewandte Chemie (International ed. in English) 2016, 55, (24), 6826-41.
8) Tan, G.; Zeier, W. G.; Shi, F.; Wang, P.; Snyder, G. J.; Dravid, V. P.; Kanatzidis, M. G., High Thermoelectric Performance SnTe-In$_2$Te$_3$ Solid Solutions Enabled by Resonant Levels and Strong Vacancy Phonon Scattering. Chem. Mater. 2015, 27, (22), 7801-7811.
9) Hu, X.; Jood, P.; Ohta, M.; Kunii, M.; Nagase, K.; Nishiate, H.; Kanatzidis, M. G.; Yamamoto, A., Power generation from nanostructured PbTe-based thermoelectrics: development from materials to modules. Energy Environ. Sci. 2016, 9, (2), 517-529.
10) Tan, G.; Shi, F; Hao, S.; Zhao, L-D.;Chi, H.; Zhang, X.;Uher, C.; Wolverton, C.; Dravid, V. P.; Kanatzidis, M. G. Non-equilibrium processing leads to record high thermoelectric figure of merit in PbTe-SrTe. Nat. Commun. Accepted, in-press (2016)
11) Zhao, L.-D.; Tan, G.; Hao, S.; He, J.; Pei, Y.; Chi; Wang, H.; Gong.; Xu, H.; Dravid, V. P.; Uher, C.; Snyder, J.; Wolverton, C.; Kanatzidis, M. G., Ultrahigh power factor & performance in hole-doped single-crystal SnSe; Science (2016), 351, 6269, 141-144.
12) Hao, S.; Shi, F.; Dravid, V. P.; Kanatzidis, M. G.; Wolverton, C., Computational Prediction of High Thermoelectric Performance in Hole Doped Layered GeSe. Chem. Mater. 2016, 28, (9), 3218-3226.

Publications Supported by DOE-BES Grant No.: DE-SC0014520

Year-I: September 1, 2015 – August 31, 2016

1. Zheng, G.; Su, X.; Li, X.; Liang, T.; Xie, H.; She, X.; Yan, Y.; Uher, C.; Kanatzidis, M. G.; Tang, X., Toward High-Thermoelectric-Performance Large-Size Nanostructured BiSbTe Alloys via Optimization of Sintering-Temperature Distribution. Adv. Energy Mater. 2016, 1600595.

2. Zhao, L.-D.; Zhang, X.; Wu, H.; Tan, G.; Pei, Y.; Xiao, Y.; Chang, C.; Wu, D.; Chi, H.; Zheng, L.; Gong, S.; Uher, C.; He, J.; Kanatzidis, M. G., Enhanced Thermoelectric Properties in the Counter-Doped SnTe System with Strained Endotaxial SrTe. J. Am. Chem. Soc. 2016, 138, (7), 2366-2373.

3. Zhao, L.-D.; Tan, G.; Hao, S.; He, J.; Pei, Y.; Chi, H.; Wang, H.; Gong, S.; Xu, H.; Dravid, V. P.; Uher, C.; Snyder, G. J.; Wolverton, C.; Kanatzidis, M. G., Ultrahigh power factor and thermoelectric performance in hole-doped single-crystal SnSe. Science 2016, 351, (6269), 141-144.

4. Zeier, W. G.; Zevalkink, A.; Gibbs, Z. M.; Hautier, G.; Kanatzidis, M. G.; Snyder, G. J., Thinking Like a Chemist: Intuition in Thermoelectric Materials. Angewandte Chemie (International ed. in English) 2016, 55, (24), 6826-41.

5. Tan, G.; Zeier, W. G.; Shi, F.; Wang, P.; Snyder, G. J.; Dravid, V. P.; Kanatzidis, M. G., High Thermoelectric Performance SnTe-In$_2$Te$_3$ Solid Solutions Enabled by Resonant Levels and Strong Vacancy Phonon Scattering. Chem. Mater. 2015, 27, (22), 7801-7811.

6. Ioannidou, C.; Lioutas, C. B.; Frangis, N.; Girard, S. N.; Kanatzidis, M. G., Analysis and Implications of Structural Complexity in Low Lattice Thermal Conductivity High Thermoelectric Performance PbTe–PbSnS$_2$ Composites. Chem. Mater. 2016, 28, (11), 3771-3777.

7.   Hu, X.; Jood, P.; Ohta, M.; Kunii, M.; Nagase, K.; Nishiate, H.; Kanatzidis, M. G.; Yamamoto, A., Power generation from nanostructured PbTe-based thermoelectrics: comprehensive development from materials to modules. Energy Environ. Sci. 2016, 9, (2), 517-529.

8. Hong, M.; Chasapis, T. C.; Chen, Z.-G.; Yang, L.; Kanatzidis, M. G.; Snyder, G. J.; Zou, J., n-Type Bi$_2$Te$_{3-x}$Se$_x$ Nanoplates with Enhanced Thermoelectric Efficiency Driven by Wide-Frequency Phonon Scatterings and Synergistic Carrier Scatterings. Acs Nano 2016, 10, (4), 4719-4727.

9. Hao, S.; Shi, F.; Dravid, V. P.; Kanatzidis, M. G.; Wolverton, C., Computational Prediction of High Thermoelectric Performance in Hole Doped Layered GeSe. Chem. Mater. 2016, 28, (9), 3218-3226.

10. Hanson, E. D.; Shi, F.; Chasapis, T. C.; Kanatzidis, M. G.; Dravid, V. P., Two-dimensional bismuth-rich nanosheets through the evaporative thinning of Se-doped Bi_2Te_3. J. Cryst. Growth 2016, 436, 138-144.

11. Ahn, K.; Kong, H.; Uher, C.; Kanatzidis, M. G., Thermoelectric properties of p-type $Ag_{1-x}(Pb_{1-y}Sn_y)mSb_{1-z}Te_{m+2}$. J. Solid State Chem. doi:10.1016/j.jssc.2016.03.018.

12. Tan, G.; Shi, F; Hao, S.; Zhao, L-D.;Chi, H.; Zhang, X.;Uher, C.; Wolverton, C.; Dravid, V. P.; Kanatzidis, M. G. Non-equilibrium processing leads to record high thermoelectric figure of merit in PbTe-SrTe. Nat. Commun. 2016. Accepted, in Press.

Scalable Growth and Charge Transport Properties of Perovskite Microplate Crystal Array

Xiangfeng Duan, University of California, Los Angeles
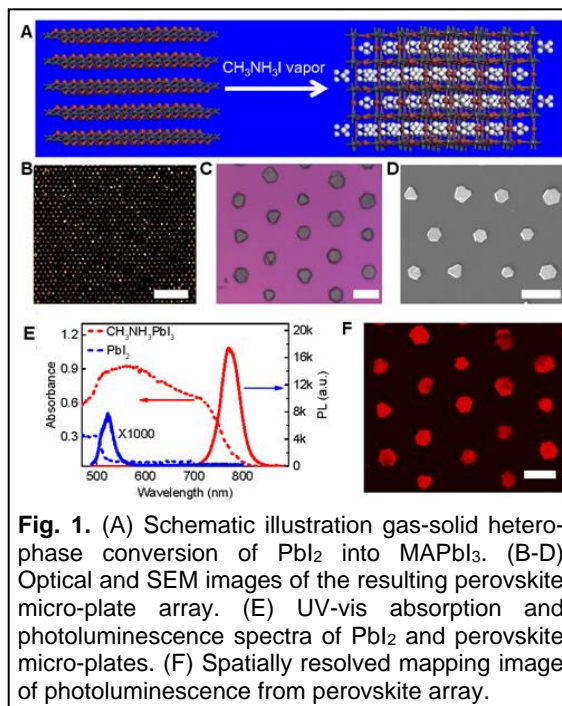
Program Scope

This research program aims to design and synthesize multi-heterostructures integrating light harvesting antenna with effective redox nanocatalysts, to probe the charge generation, separation and transport in such heterostructures, and to investigate their potential for energy harvesting.

Recent Progress

Our recent efforts focus on the growth of high quality perovskite crystals and fundamental investigations of the charge generation and transport, and the stability of these highly efficient light-harvesting materials. Methylammonium lead iodide perovskite has attracted intensive interest for diverse optoelectronic applications. However, most studies to date have been limited to bulk thin films, which are plagued with considerable hysteresis and poor stability and difficult to implement for integrated device arrays due to their incompatibility with typical lithography processes. The ability to use lithography to pattern electronic materials has been essential for the integrated electronic/optoelectronic systems. However, soluble in various solvents, the perovskite materials are not compatible with typical lithographic process and thus cannot be easily patterned into discrete device arrays. This represents an urgent challenge faced by the perovskite community to further advance this field. To this end, we developed a strategy for the scalable growth of large arrays of perovskite micro-plates as a new material platform for fundamental investigation of the electronic and optical properties and for creating independently addressable electronic and optoelectronic device array.

1. Wafer-scale growth of perovskite micro-plate crystals arrays

To produce regular arrays of perovskite crystals, lead iodide (PbI_2) micro-plates were first grown on a substrate with pre-patterned surface functionalization to control the nucleation and growth process to produce microplate arrays with variable lattice arrangements. The prepared PbI_2 microplates can be converted to methylammonium lead iodide perovskite through a gas-solid hetero-phase intercalation process under methylammonium iodide vapor (Fig. 1A). Compared to the conventional liquid-solid based conversion in organic solvents, gas-solid based intercalation could prevent the chemical dissolution of PbI_2 and perovskite crystals in organic solvents and well retain the morphology and crystalline quality of the perovskite micro-plates. The optical microscopy, SEM and TEM images of the converted perovskites show similar hexagonal plate shape with clean surface (Fig. 1B-D), suggesting the conversion from PbI_2 to perovskite does not significantly change the overall crystal morphology. Optical studies show that the PbI_2 crystals exhibit an absorption edge at

Fig. 1. (A) Schematic illustration gas-solid hetero-phase conversion of PbI_2 into $MAPbI_3$. (B-D) Optical and SEM images of the resulting perovskite micro-plate array. (E) UV-vis absorption and photoluminescence spectra of PbI_2 and perovskite micro-plates. (F) Spatially resolved mapping image of photoluminescence from perovskite array.

around 525 nm and a photoluminescence (PL) peak at 522 nm (Fig. 1E). In comparison, the converted perovskite crystals exhibit an absorption edge at around 800 nm (Fig. 2E. Importantly, the converted perovskite crystals exhibit a very strong room temperature PL peak at around 770 nm (Fig. 2E) that is more than 3 orders of magnitude stronger than that in the PbI_2 crystals, indicating high crystalline quality and excellent PL efficiency of the perovskite crystals. A photoluminescence mapping of the prepared perovskite crystal array further shows strong photoluminescence emission from the entire perovskite crystal arrays (Fig. 1F). Together, our study demonstrate the first successful growth of patterned perovskite crystal array, which can be readily used for creating integrated device arrays for both the fundamental studies and potential optoelectronic applications.

2. Fundamental charge transport properties in perovskite microplates

The controllable growth of perovskite crystals on pre-defined electrodes can readily enable us to create functional devices and probe the intrinsic charge transport properties of the perovskite materials, which remains elusive in bulk polycrystalline thin films due to the variability in spin-coating process and extensive grain boundary scattering and trapping. To this end, we have explored the micro-plate as the semiconducting channel of a field effect transistor (FET) on SiO_2/Si substrate (Fig. 2A). A set of representative output curves of a crystal perovskite FET under various gate voltages show typical transistor characteristics (Fig. 2B). The transfer characteristics show dominant n-type behavior (Fig. 2C). Slight p-type behavior is also observed at high negative gate voltage regime, indicating ambipolar characteristics. Similar to what commonly seen in literature, our devices also show considerable hysteresis under large gate swing, which has been attributed to the field induced ion drift, ferroelectric and/or trap state filling effects in perovskite. The maximum on/off ratio (I_{on}/I_{off}) is nearly six orders of magnitude, which is better than recently reported polycrystalline thin film perovskite transistors (Fig. 2C). The field-effect electron mobility can reach up to ~2.3 cm^2/Vs (backward sweeping) and ~1 cm^2/Vs (forward sweeping) at 77 K, both of which are much better than the best value reported in polycrystalline perovskite thin films ($< 10^{-1}$ cm^2/Vs at 77 K) prepared by spin coating method.
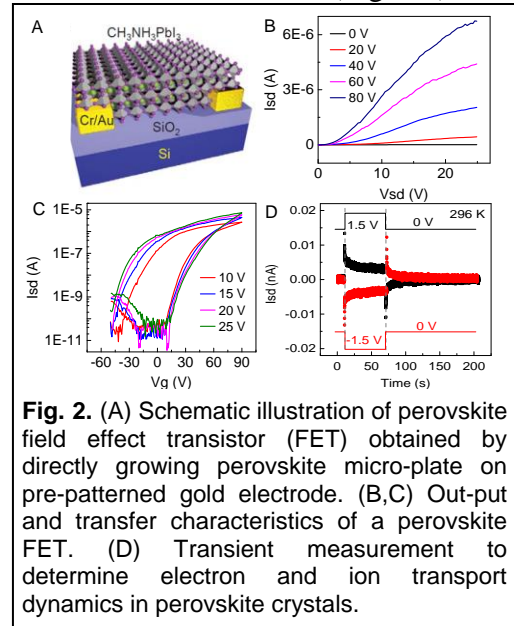

Fig. 2. (A) Schematic illustration of perovskite field effect transistor (FET) obtained by directly growing perovskite micro-plate on pre-patterned gold electrode. (B,C) Out-put and transfer characteristics of a perovskite FET. (D) Transient measurement to determine electron and ion transport dynamics in perovskite crystals.

To further probe the electronic and ionic transport dynamics and how they impact each other in perovskite materials and correlate with the hysteresis, we have conducted a systematic investigation of the electronic and ionic transport dynamics in organolead halide perovskite microplate crystals and thin films using temperature dependent transient response measurements upon the application and removal of an external bias, and experimentally determine the ion-induced electric potential across the device channel (Fig. 2D). Our study reveals that ionic and electronic conduction coexist in perovskite devices. Although the ionic conduction contributes negligible current to the total current, it can fundamentally affect the electronic transport process. It is found that both the electronic and ionic transport are thermally activated. The extracted activation energy for electronic transport in microplates (70 meV) is much smaller than that in

thin films (430 meV), while the activation energy for ionic transport in microplates (210 meV) is considerably larger than that in thin films (90 meV). These studies suggest that the electronic transport easier but ions migrate harder in the microplates than in thin films, demonstrating that the crystalline quality and grain boundaries can fundamentally modify electronic and ionic transport in perovskites. Importantly, we demonstrate that both the ion motion and source-drain IV hysteresis can be greatly suppressed or eliminated in nearly single crystalline microplates due to greatly reduced grain boundaries and better crystalline quality. Together, these studies clearly demonstrate the high quality and unique advantages of the perovskite micro-plate crystals compared with typical polycrystalline thin films. These findings offer valuable insight on the electronic and ionic transport dynamics in organolead halide perovskites, which is critical for optimizing perovskite devices with reduced hysteresis and improved stability and efficiency.

3. Size dependent optical and electronic properties of perovskite microplates

The crystalline size could significantly influence the optical and charge transport properties of perovskite materials. The orthorhombic-to-tetragonal phase transition in lead iodide perovskite can significantly alter its optical, electrical properties and influence the performance of perovskite solar cells and other optoelectronic applications. However, there is no systematic investigation of size dependent optical and charge transport properties in perovskite materials. The size dependent phase transition in $MAPbI_3$ remains elusive. To this end, we have conducted the first systematic investigation of size
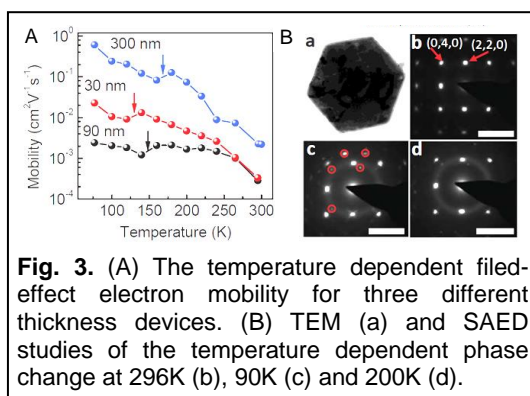

Fig. 3. (A) The temperature dependent filed-effect electron mobility for three different thickness devices. (B) TEM (a) and SAED studies of the temperature dependent phase change at 296K (b), 90K (c) and 200K (d).

dependent structural phase transitions in individual $MAPbI_3$ microplate crystals by using temperature dependent charge transport measurements, PL spectroscopy, and TEM and electron diffraction. Our studies of individual perovskite microplate crystals with variable thickness demonstrate that the phase transition temperature decreases with reducing microplate thickness, as evidenced by non-continuity in the temperature dependent field-effect mobility (Fig. 3A) and the extra emission peak in temperature dependent PL spectra. The phase transition was further directly confirmed by the temperature dependent selected area electron diffraction studies (Fig. 3B). The sudden decrease of field mobility around phase transition temperature and the presence of hysteresis loop in the temperature dependent field-effect mobility confirm that the orthorhombic-to-tetragonal phase transition is a first-order solid-solid phase transition. Our findings offers valuable fundamental insight on the temperature dependent structural, optical and charge transport properties of lead iodide perovskites, and can greatly impact future exploration of novel electronic and optoelectronic devices from these materials.

4. Optoelectronic device array from perovskite microplate array

The ability to control crystal nucleation and growth on the predefined sites can readily allow us to directly grow the perovskite crystals onto the pre-patterned electrodes to form functional devices. A large array of two-probe devices can be obtained with each pair of the probe electrodes bridged by a singlet perovskite crystal (Fig. 4A). Electrical measurements of these two-probe devices show nearly zero dark current, and a nearly linear current-voltage (I-V) behavior under illumination (Fig. 4B), indicating excellent photo-response of the perovskite crystals. The photocurrent-to-dark ratio of our devices can reach up to 3 orders of magnitude.

The responsivity, defined as the ratio of the photocurrent to the incident light power, was calculated to be ~7 A/W with the corresponding photocurrent gain of around 18. The response speed of our devices is characterized by a rising time and a falling time of ~500 μs (Fig. 4C, inset), which is limited by our measurement capability. The photocurrent increases with the increasing incident light power, and shows a sub-linear dependence on the light power (Fig. 4C).

With the precise control of the micro-crystal location and high device yield, it is possible to create large photo-detector arrays. To this end, we have created a large scale 100 (10×10) photo-detector array on a transparent glass substrate and placed a 'U' shape mask on the back of the glass substrate so that the incident light can only reach the area in the transparent "U" region (Fig. 4D). Photo-response measurement of the entire arrays indicates that almost all the devices that are exposed to the "U" shaped light illumination show a clear photocurrent response with 92 % device yield (Fig. 4E). A spatially resolved map of the photocurrent amplitude generated by the photo-detector arrays clearly shows a "U" shaped photo-response area (Fig. 4F), demonstrating that such two-terminal device arrays can function as effective photo-imaging arrays. These studies demonstrate an important step toward the integrated device applications based on the individual perovskite crystals.
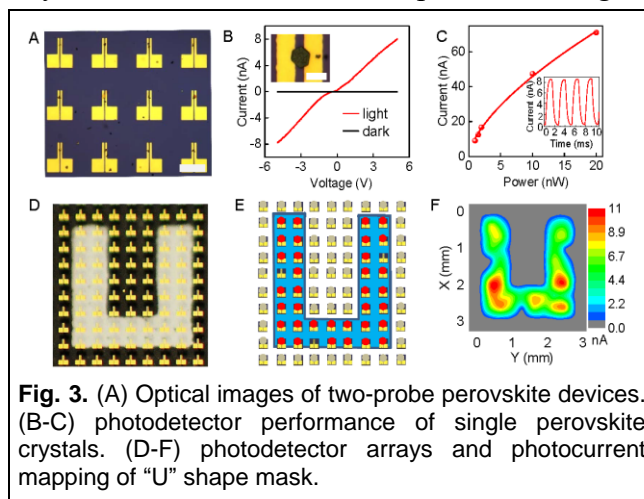

Fig. 3. (A) Optical images of two-probe perovskite devices. (B-C) photodetector performance of single perovskite crystals. (D-F) photodetector arrays and photocurrent mapping of "U" shape mask.

Together, our study presents the first successful patterned growth of large arrays of perovskite crystals, and represents a critical advancement in controllably producing patterned perovskite. The ability to grow high quality perovskite crystals with controlled dimension and precisely place them at specific positions can thus provide a powerful new material platform for fundamental investigation of the intrinsic electronic and optoelectronic properties of perovskite materials, and open up exciting opportunities for exploring perovskite arrays for diverse (opto)electronic systems such as transistors, light emitting diodes, laser diodes, photo-detectors, solar cells and solar fuel generation systems.

Future Plans

We will continue to probe the intrinsic optical and electronic properties of perovskite materials and to understand/improve their stability issue. In particular, we will use in situ TEM to probe the conversion of PbI_2 into perovskite and the degradation of perovskite under various stimuli, including heat, moisture and light. We will also explore various types of perovskite materials for improved electronic properties or stability.

Publications

1. D. Li, H. Wu, H. Cheng, G. Wang, Y. Huang, and X. Duan, Electronic and Ionic Transport Dynamics in Organolead Halide Perovskites, *ACS Nano,* **2016** (revised).

2. D. Li, G. Wang, H. Cheng, C. Chen, H. Wu, Y. Liu, Y. Huang and X. Duan, "Size Dependent Phase Transition in Methylammonium Lead Iodide Perovskite Microplate Crystals", *Nature Communications,* **2016,** 7:11330.

3. H. Cheng, G. Wang, D. Li, Q. He, A. Yin, Y. Liu, H. Wu, M. Ding, Y. Huang and X. Duan, "Van Der Waals Heterojunction Devices Based on Organohalide Perovskites and Two-Dimensional Materials", *Nano Letters,* **2016**, 16, 367-373.

4. Z. Zhao, X. Huang, M. Li, G. Wang, C. Lee, E. Zhu, X. Duan, and Y. Huang. Synthesis of Stable Shape-Controlled Catalytically Active β‑Palladium Hydride. J. *Am. Chem. Soc.* **2015**, 137, 15672−15675

5. G. Wang, D. Li, H. Cheng, Y. Li, C. Chen, A. Yin, Z. Zhao, Z. Lin, H. Wu, Q. He, M. Ding, Y. Liu, Y. Huang and X. Duan, "Wafer Scale Growth of Perovskite Single Crystal Arrays for Functional Electronics and Optoelectronics", *Science Advances*, **2015**, 1, e1500613.

6. G. Wang, X. Xiao, W. Li, Z. Lin, Z. Zhao, C. Chen, C. Wang, Y. Li, X. Huang, L. Miao, C. Jiang, Y. Huang and X. Duan, "Significantly Enhanced Visible Light Photoelectrochemical Activity in TiO_2 Nanowire Arrays by Nitrogen Implantation", **2015**, *Nano Letters,* **2015,**15, 4692-4698.

7. X. Zhong, G. Wang, B. Papandrea, M. Li, Y. Xu, Y. Chen, C.-Y. Chen, H. Zhou, T. Xue, Y. Li, D. Li, Y. Huang and X. Duan, Reduced Graphene-Oxide/Silicon Nanowire Heterostructures with Enhanced Photoactivity and Superior Photoelectrochemical Stability. *Nano Res.* **2015**, 8, 2850-2858.

8. X. Huang, Z. Zhao, L. Cao, Y. Chen, E. Zhu, Z. Lin, M. Li, A. Yan, A. Zettl, Y. Wang, X. Duan, T. Mueller and Y. Huang, High Performance for the Oxygen Reduction Reaction with Transition-Metal-Doped Pt_3Ni Octahedra, *Science* **2015,** 348,1230-124.

9. B. Volosskiy, K. Niwa, Y. Chen, Z. Zhao, N. O. Weiss, X. Zhong, M. Ding, C. Lee, Y. Huang and X. F. Duan, Metal-Organic Framework Templated Synthesis of Ultrathin, Well-Aligned Metallic Nanowires, *ACS Nano*, **2015**, 9, 3044-3049. (Published)

10. L. Ruan, H. Dakhel, C. Lee, Y. Li, X. Duan, H. Heinz, and Y. Huang, A Rational Biomimetic Approach to Structure Defect Generation in Colloidal Nanocrystals, *ACS Nano*, **2014**, 8, 6934-6944.

Molecular Magnets Based on a Modular Approach: Investigation of Coupling, Anisotropy, and Electronic Factors on Bistability

PI: Kim R. Dunbar

Program Scope

This research is directed at understanding the role of magnetic anisotropy in determining the blocking temperatures of molecular magnets. These goals are achieved primarily by exploiting strong first-order spin-orbit coupling and anisotropic exchange interactions in cyanide and organocyanide complexes of lanthanide and transition metals. A modular approach to designing homologous series of compounds has led to families of structurally related molecules with the same geometrical arrangement of spin centers and this approach continues to be very fruitful. We are targeting families of mononuclear compounds of transition metal ions that display bistability in spite of the few number of spins that they possess.

Recent Progress

In order to explore the properties of Single Molecule Magnets (SMMs) that contain a single transition metal ion as opposed to polynuclear complexes, we prepared the family of isostructural Co^{II} mononuclear complexes $[Co(TPMA)X](Y)_n$ ($X = CH_3CN$, $Y = (BF_4)^-$, $n = 2$; $X = Y = [Cl]^-$, $[Br]^-$, $[I]^-$, $n = 1$; TPMA = tris(2-pyridylmethyl)amine), **Figure 1**, in which the Co^{II} center is in a five-coordinate trigonal bipyramidal geometry. We discovered two phases of the
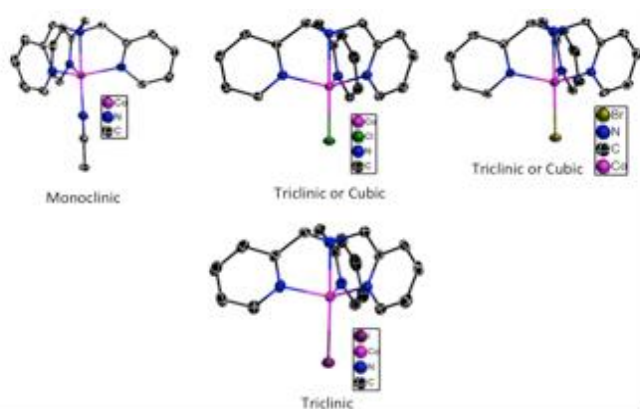

Figure 1. Structures of the $[Co(TPMA)X](Y)_n$ family. Ellipsoids are drawn at the 50% probability level. H atoms and the counterions have been omitted for the sake of clarity.

$[Co(TPMA)Cl]Cl$ and $[Co(TPMA)Br]Br$ analogs, namely a triclinic and cubic phase. The higher symmetry cubic phases display vastly improved SMM behavior as compared to the triclinic phases. The pseudo- or strict 3-fold symmetry of the molecules is sufficient to minimize transverse anisotropy which is detrimental to SMM behavior. SMM behavior is observed in those members of the family in which the intermolecular Co-Co distance is approximately 8 Å, while those members of the family for which this distance is significantly less than 8 Å do not exhibit SMM behavior (**Table 1**). What is most intriguing is that there is no evidence of a transition to a quantum tunneling regime above 1.8 K, which is highly unusual. These complexes show only thermal relaxation effects above 1.8 K. In tandem with the

experimental results, we carried out theoretical *ab initio* calculations on all members of the family. The zero-field splitting parameters obtained from magnetization measurements correlate well with those determined by computational methods (Table 2). It has been determined that the ground state and excited states of all of the members of this family are highly multi-configurational, with as many as five different determinants contributing significantly to the wave function of a given electronic state of the system. This work is being submitted to the *Journal of the American Chemical Society* as a full paper.

Table 1. Bond distances and angles for the members of the [Co(TPMA)X]$^{1+/2+}$ family obtained from the single crystal X-ray structures.

Compound	Co-X (Å)[a]	Co-N$_{py}$ plane (Å)[b]	N$_{py}$-Co-N$_{py}$ (°)[c]	Co-N$_{py}$ (Å)[d]	Co-N$_{am}$ (Å)[e]	Co-Co (Å)[f]
[Co(TPMA)(CH$_3$CN)] (BF$_4$)$_2$	2.037(17)	0.395	115.9	2.0378	2.1705(16)	7.863
[Co(TPMA)Cl]Cl triclinic	2.2707	0.435	115.6	2.058	2.193	6.119
[Co(TPMA)Cl]Cl cubic	2.277(12)	0.459	115.21(4)	2.068(2)	2.214(3)	7.951
[Co(TPMA)Br]Br triclinic	2.4151	0.436	114.9	2.061	2.200	6.289
[Co(TPMA)Br]Br cubic	2.427(16)	0.455	115.30(8)	2.068(4)	2.214(7)	8.079
[Co(TPMA)I]I triclinic	2.645	0.452	115.40	2.071	2.194	6.601

[a]distance between the Co^{II} ion and the coordinated CH$_3$CN/halide ion.
[b]distance the Co^{II} ion projects out of the mean plane of the three pyridine N atoms of TPMA.
[c]average angle formed by two of the three pyridine N atoms of TPMA and the Co^{II} ion.
[d]average distance between the Co^{II} ion and the pyridine N atoms of TPMA.
[e]distance between the Co^{II} ion and the bridgehead amine N atom of TPMA.
[f]closest intermolecular Co-Co distance.

In an effort to more fully understand the effects of geometry on magnetic properties, we also studied two Co^{II} complexes with trigonal antiprismatic geometry, [Co^{II}(Tpm)$_2$][ClO$_4$]$_2$ (**1**, Tpm = tris(pyrazol-1-yl)methane) and [Co^{II}(Tpm)$_2$][BPh$_4$]$_2$·2MeCN (**2**), the first such study of its kind. The scheme of the d orbitals splitting is showed in **Figure 2a**, which is expected to give rise to a large anisotropy. The static susceptibility and *ab initio* calculations (CASSCF and NEVPT2) confirm the anisotropy with an energy difference between ground and excited Kramers' doublets of approximately 200 cm^{-1}.

AC magnetic susceptibility data were collected as a function of both temperature and frequency in the presence and absence of an applied external dc field. Under a zero DC field, no out-of-phase AC signal was observed. Under applied DC fields, both complexes display typical slow relaxation of the magnetization. Importantly, after a very detailed analysis of the dynamic

Table 2. Experimental and theoretical zero-field splitting parameters for members of the [Co(TPMA)X](Y)$_n$ family

Compound	Data	g_{xx}	g_{yy}	g_{zz}	D (cm^{-1})	E (cm^{-1})	Co-Co distance (Å)	Ueff/k$_b$ (K)
CH$_3$CN	M-T/M-H		2.38*		9.63	0.008	7.863	20.4
	NEVPT2	2.14	2.18	2.20	8.86	0.97		
Cl⁻ triclinic	M-T/M-H		2.30*		-8.10	0.0004	6.119	--
	NEVPT2	2.17	2.17	2.24	-7.47	0.45		
Cl⁻ cubic	M-T/M-H		2.24*		-8.57	0.0006	7.951	~20
	NEVPT2	2.18	2.18	2.25	-8.63	0.0		
Br⁻ triclinic	M-T/M-H		2.41*		-7.59	0.001	6.289	--
	NEVPT2	2.18	2.18	2.20	-4.83	0.39		
Br⁻ cubic	M-T/M-H		2.23*		-7.24	0.0004	8.079	17.2
	NEVPT2	2.18	2.18	2.23	-5.30	0.0		
I⁻ triclinic	M-T/M-H		2.41*		-8.21	0.0006	6.601	--
	NEVPT2	2.18	2.19	2.22	-2.97	0.65		

*g_{iso}

susceptibility measurements, we concluded that an Orbach process is not responsible for the observed relaxation of the spin because the fit to an Arrhenius equation gives rise to energy barriers of 30-40 cm^{-1} and, as determined by static suscept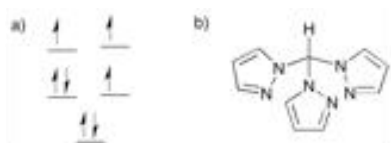ibility and *ab initio* calculations, there is no real state at that energy. Previously the spin relaxation of other mononuclear SMMs has been fitted considering direct, Raman, tunneling, and/or Orbach processes. First we analyzed the high temperature region. The large energy difference between states should lead to a very slow relaxation time (slower than the measurable relaxation times with the ac measurements that are possible with our SQUID). If the energy difference between the states is larger than the Debye temperature, the Raman term will be the principal one at high temperature with a negligible Orbach process. Secondly, we analyzed the lower temperature region. For both compounds, τ^{-1} is larger at lower fields. These results indicate that the predominant process is tunneling because the opposite trend is expected for a direct process (τ^{-1} is

Figure 2. a) Scheme of the orbital splitting. b) Tpm ligand.
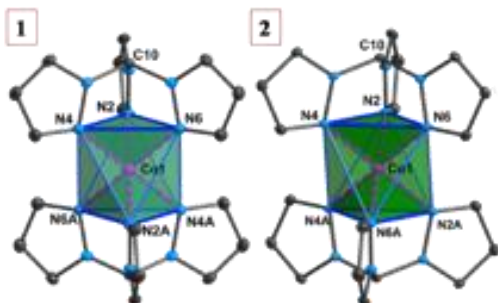
Figure 3. Molecular structure of the [Co(Tpm)$_2$]$^{2+}$ complexes.

proportional to H^4 for Kramers′ ions). Taking this aspect into consideration and to avoid the over-parameterization of the curves, we modeled the dependence of τ^{-1} with temperature using Equation 1, which considers just tunneling and Raman terms.

$$(1)$$

Figure 4 shows the best fit using Equation 1 while constraining the B parameter to the minimum value of τ^{-1}. The obtained parameters are B = 184 and 0 s^{-1} at 500 and 3000 Oe respectively, C = 0.0117 s^{-1} K^{-n} and n = 6.65 for **1** and B = 17.3, 9.9 and 0.9 s^{-1} at 300, 500 and 1500 Oe respectively, C = 0.0011 s^{-1} K^{-n} and n is 7.18 for **2**. From these parameters one can deduce that, for an optimal field, the tunneling is essentially negligible and that the exponent for the Raman term in both cases is very close to 7. The Raman coefficient for **1** is one order of magnitude larger than for **2**, a reflection of how a change in counterion modifies the spin-lattice Raman process. When we move from a smaller anion (ClO_4^-) to a larger one (BPh_4^-) there is an (i) increase in the distance between Co^{II} centers which reduces the dipolar interactions, and (ii) a change in the crystal packing and chemical environment of the SMM unit. In both of the complexes

Figure 4. Dependence of τ^{-1} with T for compounds **1** and **2** under different dc fields.

we have seen that tunneling is the predominant process at low temperature (whereas for other Co^{II} mononuclear SMMs the low temperature behavior is attributed to direct processes). In addition, the change in the crystal packing and chemical environment due to the larger anion leads to a decrease in the Raman parameter (C).

Future Plans

A deeper understanding of relaxation processes in small molecule SMMs will allow us to tune this effect with the appropriate selection of the chemical environment. It is not unreasonable to expect that further modifications of this geometry may result in a compound with an extremely high barrier as observed for other geometries. Ongoing efforts are being directed at designing new members of this family with different tripodal ligands and counterions to improve the magnetic properties and realize a system with zero-field slow relaxation. This work is in press as a full paper in *Chemical Science*.

Publications

1. A Single-Chain Magnet Tape Based on Hexacyanomanganate(III), Yuan-Zhu Zhang, Han-Hua Zhao, Edward Funck, and Kim R. Dunbar, *Angew.Chem.Int.Ed.* **2015**, *54*, 5583-5587. *Selected for Hot Topics*
2. A Trigonal-Pyramidal Erbium(III) Single-Molecule Magnet, Andrew J. Brown, Dawid Pinkowicz, Mohamed R. Saber, and Kim R. Dunbar, *Angew.Chem.Int.Ed*. **2015**, *54*, 5864-5868. *Selected for Hot Topics.*

3. Cyanide Single Molecule Magnets Exhibiting Reversible, Solvent Dependent "On" and "Off" Exchange Bias Behavior. Dawid Pinkowicz, Heather I. Southerland, Carolina Avendano, Andrey Prosvirin, Wolfgang Wernsdorfer, Kasper S. Pedersen, Jan Dreiser, Rodolphe Clerac and Kim R. Dunbar, *J. Am. Chem. Soc.*, **2015**, *137*, 14406-14422.
4. Magnetic Ordering in TCNQ-Based Metal-Organic Frameworks With Host-Guest Interactions, Xuan Zhang, Mohamed R. Saber, Andrey P. Prosvirin, Joseph H. Reibenspies, Lei Sun, Maria Ballesteros-Rivas, Hanhua Zhao, Kim R. Dunbar submitted to themed issue on 'Molecular Magnetism' *Inorganic Chemistry Frontiers*, **2015**, *2*, 904-911.
5. A cobalt(II) spin-crossover compound with partially charged TCNQ radicals and an anomalous conducting behavior, Zhang, X.; Wang, Z.-X.; Xie, H.; Li, M.-X.; Woods, T. J.; Dunbar, K. R. *Chem. Sci.* **2016**, *7*, 1569-1574.
6. Self-Assembly of Organocyanide Dianions and Metal–Organic Macrocycles into Polymeric Architectures Including an Unprecedented Quadruple Helical Aperiodic Structure, Zhang, X.; Zhao, H.; Palatinus, L.; Gagnon, K. J.; Bacsa, J.; Dunbar, K. R. *Cryst. Growth Des.* **2016**, *16*, 1805-1811.
7. Structural distortions of the spin-crossover material [Co(pyterpy)$_2$](TCNQ)$_2$ mediated by supramolecular interactions, Zhang, X.; Xie, H.; Ballesteros-Rivas, M.; Wang, Z.-X.; Dunbar, K. R. *J. Mater. Chem. C.* **2015**, *3*, 9292-9298
8. Metal–Organic Frameworks as Platforms for the Controlled Nanostructuring of Single-Molecule Magnets, Aulakh, D.; Pyser, J. B.; Zhang, X.; Yakovenko, A. A.; Dunbar, K. R.; Wriedt, M. *J. Am. Chem. Soc.* **2015**, *137*, 9254-9257.
9. Trigonal Antiprismatic Co(II) Single Molecule Magnets with Large Uniaxial Anisotropies: Importance of Raman and Tunneling Mechanisms. Y.-Z. Zhang, S. Gómez-Coca A. J. Brown, M. R. Saber, X. Zhang, K. R. Dunbar. *Chem. Sci.*, **2016**, *in press*.

Pore Space Engineering and Functionalization in Porous Metal-Organic Framework Materials

PI: Pingyun Feng
Department of Chemistry and Materials Science Engineering, University of California, Riverside, CA 92521

Program Scope

The overall objective of this project is to develop new synthetic strategies to synthesize advanced porous materials with geometrical features and chemical functionalities useful for gas storage and separation including CO_2 sequestration. Specific aims of this project are:

- Develop new synthetic strategies to generate novel active binding sites on metal ions and ligands to enhance gas uptake capacity and solid-gas interactions for increased gas uptake near ambient conditions;

- Design synthetic strategies that allow creation of novel heterometallic systems with greatly enhanced stability and gas sorption properties such as tunable binding affinity and high gas uptake capacity;

- Develop synthetic methods to create porous frameworks with architectural features such as partitioned pore space for the optimum size match with gas molecules;

- Fully characterize thermal and chemical stability, gas (e.g., CH_4, CO_2, N_2, and H_2) sorption properties, and crystal structures of new porous materials. Crystal structure analysis is an important part in the development of new materials because it allows us to identify compositional and structural features that correlate with such properties and can reveal previously unseen compositional and structural patterns that may lead to new or improved design strategies and more advanced materials.

Recent Progress

With the support from Materials Chemistry, Materials Sciences and Engineering Division, Office of Basic Energy Sciences, we have made significant progresses on the proposed project. The following summarizes several important contributions from PI's group.

(1) A New Pore Partition Strategy for Dramatic Tuning on Gas Uptake Capacity

A new pore-space-partition strategy has been developed by PI's group. It is named as symmetry matching regulated ligand insertion (Figure 1). The strategy entails the insertion of a

secondary ligand (L2, also called pore-partitioning ligand) into a primary framework. Its success depends on the symmetry and size matching between L2 and the symmetry of framework coordination sites and dimension of channels. In this study, MIL-88 type structures were selected as the prototype framework to demonstrate this strategy. In MIL-88, the metals in the trimeric clusters are terminated by pendant ligands (such as water, halide, or acetate) on three axial positions. These pendant groups can be removed, leaving potential open metal sites. Furthermore, on each layer parallel to the crystallographic *ab* plane, three such open metal sites from three different trimers adopt three-fold (**C₃**) symmetry and point to the center of hexagonal channels (Figure 1a). Such geometric features make it possible to fit in planar tritopic ligands with C_3 symmetry, which can bond to all three open metal sites simultaneously. In this work, we examined our strategy with select ligands including 2,4,6-tri(4-pyridyl)-1,3,5-triazine (**TPT**).
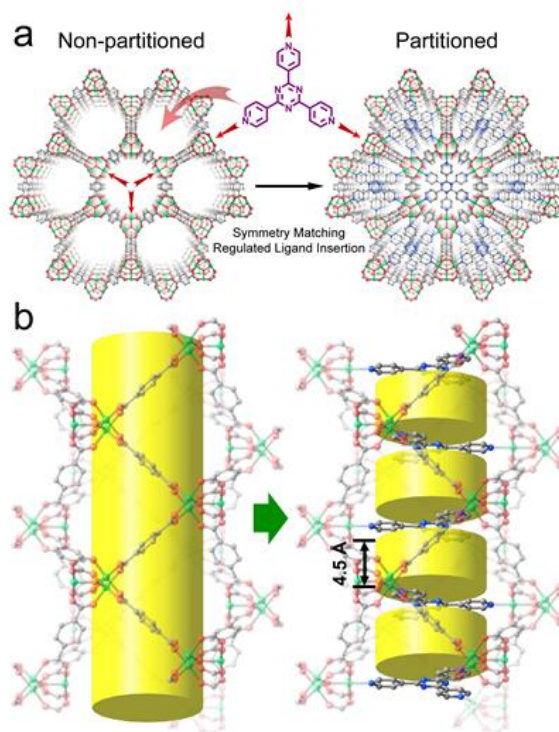

Figure 1. Illustration of pore space partition through symmetry matching regulated ligand insertion. (a) Viewed along c axis and (b) Side view of the channels showing the cylindrical channel before and after partition. (green: Ni, red: O, blue: N, grey: C)

MIL-88 frameworks are flexible and well known for their giant swelling effect due to the loss or gain of guest species.[1] Such flexibility intrinsic in MIL-88 structural type relaxes the size-matching requirement and makes it easier to select a C_3 symmetrical ligand to fit in the channel. Thus, MIL-88 provides an ideal platform to test our pore space partition strategy.

We demonstrate that through a ligand insertion pore space partition strategy, we can create crystalline porous materials (CPMs) with superior CO_2 uptake capacity.[2] The results demonstrate the power of our new pore space partition strategy. Through this strategy, fine tailoring of the pore properties can be achieved. This opens up numerous opportunities to tune the functionalities and properties of the materials.

(2) The record-breaking heat of adsorption for CO_2 in porous solids with Lewis acid sites: unprecedented combinations of heterometallic ions

In this project, a family of heterometallic MOFs with systematic and unprecedented combinations of trivalent (In^{3+}, Ga^{3+}, Fe^{3+}, V^{3+} and Sc^{3+}) and divalent metals (Mg^{2+}, Mn^{2+}, Co^{2+} and Ni^{2+}) have been achieved. The eight combinations between M^{3+} and M^{2+} were achieved for

trimeric [M(II)$_2$M(III)(μ_3-OH)(COO)$_6$] clusters, leading to the formation of a series of MOFs (denoted here as CPM-200-In/Mg, In/Ni, In/Co, In/Mn, Ga/Mg, Fe/Mg, V/Mg, Sc/Mg) (Figure 2). Impressively, in new heterometallic MOFs synthesized by the PI's group, the isosteric heat of adsorption can be systematically tuned from -16.4 kJ/mol for CPM-200-Sc/Mg to -79.6 kJ/mol for CPM-200-V/Mg.[3] The value of -79.6 kJ/mol is the strongest interaction with CO_2 by MOFs with Lewis acid sites. The synergistic effects of heterometals bestow CPM-200s with the highest CO_2 uptake capacity among known heterometallic MOFs and place them in striking distance of the all-time CO_2 uptake record.
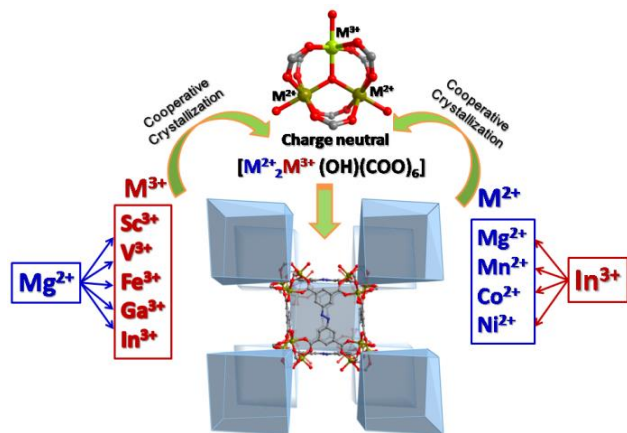
Figure 2. Realized M^{2+} and M^{3+} combinations for CPM-200s in this study.

(3)   The most exotic heterometallic systems leading to record-breaking properties

The PI's group has developed a large family of porous materials in heterometallic systems with different structure types and demonstrated a powerful platform for the development of new CPMs and control of their gas sorption properties. This platform can accommodate an exceptionally large variety of organic ligands and homo- or hetero-metallic clusters (Figure 3), which allows for extraordinary tunability in gas sorption properties. Even without any strong binding sites, most members of this platform synthesized here exhibit exceptionally high gas uptake capacity. The CO_2 uptake capacity of 232.3 cm^3/g (45.6 wt.%) at 273 K and 1 bar is the

Figure 3. The pacs platform based on a partitioned structure type shown in Figure 1 allows a variety of chemical compositions and record-breaking CO_2 uptake capacity at 273K.

highest among porous materials under the same conditions. Impressively, such extraordinary high capacity is accomplished with an isosteric heat of adsorption (Q_{st}) as low as 20 kJ/mol for CO_2, which could bring a distinct economic advantage because of the significantly reduced energy consumption for activation and regeneration of adsorbents.
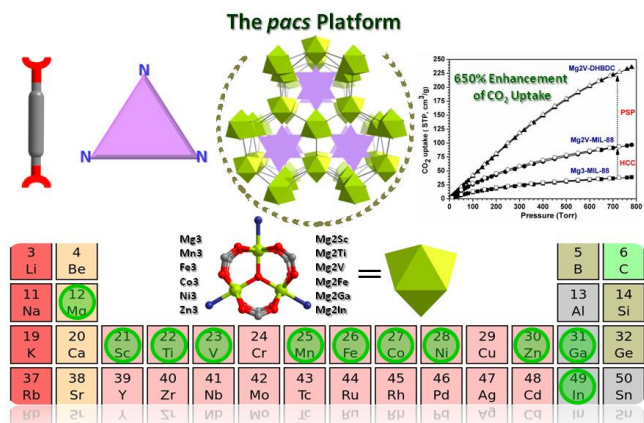
Future Plans

● To extend our success in the CPM-200 type platform to other trimer-containing platforms and to further improve their gas adsorption properties and selectivities.

● To further develop new heterometallic materials with dissimilar metal types. In addition to achieve new M^{3+}/M^{2+} combinations, materials with different M^{3+}/M^{2+} ratios will be developed. Their properties and ligands effects will be systematically studied.

● To develop new pore space partitioning strategies with diverse new chemistry approaches.

References

(1)   Serre, C.; Mellot-Draznieks, C.; Surble, S.; Audebrand, N.; Filinchuk, Y.; Ferey, G. Role of Solvent-Host Interactions That Lead to Very Large Swelling of Hybrid Frameworks. Science 2007, 315, 1828-1831.

(2)   Zhao, X.; Bu, X.; Zhai, Q.; Tran, H.; Feng, P. Pore Space Partition by Symmetry-Matching Regulated Ligand Insertion and Dramatic Tuning on Carbon Dioxide Uptake, J. Am. Chem. Soc. **2015**, 137, 1396-1399.

(3)   Zhai, Quan-Guo; Bu, Xianhui; Mao, Chengyu; Zhao, Xiang; Feng, Pingyun, Systematic and Dramatic Tuning on Gas Sorption Performance in Heterometallic MOFs, J. Am. Chem. Soc. 2016, 138, 2524-2527.

Publications

Publications wholly supported by DOE-BES under award no. DE-FG02-13ER46972 since 2014

(1)   Zhao, X.; Mao, C.; Bu, X.; Feng, P. Direct Observation of Two Types of Proton Conduction Tunnels Co-existing in A New Porous Indium-Organic Framework, Chem. Mater. **2014**, 26, 2492-2495. dx.doi.org/10.1021/cm500473f
(2)   Zhao, X.; Bu, X.; Zhai, Q.; Tran, H.; Feng, P. Pore Space Partition by Symmetry-Matching Regulated Ligand Insertion and Dramatic Tuning on Carbon Dioxide Uptake, J. Am. Chem. Soc. **2015**, 137, 1396-1399. DOI: 10.1021/ja512137t
(3)   Lin, Q.; Bu, X.; Kong, A.; Mao, C.; Zhao, X.; Bu, F.; Feng, P. New Heterometallic Zirconium Metalloporphyrin Frameworks and Their Heteroatom-Activated High-Surface-Area Carbon Derivatives, J. Am. Chem. Soc. **2015**, 137, 2235-2238. DOI: 10.1021/jacs.5b00076

(4)   Wang, Y.; Kong, A.; Chen, X.; Lin, Q.; Feng, P. Efficient Oxygen Electroreduction: Hierarchical Porous Fe-N-doped Hollow Carbon Nanoshells, ACS Catalysis **2015**, 5, 3887-3893. DOI: 10.1021/acscatal.5b00530

(5)   Lin, Q.; Bu, X.; Kong, A.; Mao, C.; Bu, F.; Feng, P. Heterometal-Embedded Organic Conjugate Frameworks from Alternating Monomeric Iron and Cobalt Metalloporphyrins and Their Application in Design of Porous Carbon Catalysts, Adv. Mater. **2015**, 27, 3431-3436. DOI: 10.1002/adma.201500727

(6)   Sasan, K.; Kong, A.; Wang, Y.; Mao, C.; Zhai, Q.; Feng, P. From Hemoglobin to Porous N-S-Fe-Doped Carbon for Efficient Oxygen Electroreduction, J. Phys. Chem. C **2015**, 119, 13545-13550. DOI: 10.1021/acs.jpcc.5b04017

(7)   Mao, C.; Kong, A.; Wang, Y.; Bu, X.; Feng, P. MIL-100 Derived Nitrogen-Embodied Carbon Shells Embedded with Iron Nanoparticles, Nanoscale **2015**, 7, 10817-10822. DOI: 10.1039/c5nr02346g

(8)   Zhai, Q.; Mao, C.; Zhao, X.; Lin, Q.; Bu, F.; Chen, X.; Bu, X.; Feng, P. Cooperative Crystallization of Heterometallic Indium-Chromium Metal-Organic Polyhedra and Their Fast Proton Conductivity, Angew. Chem. Int. Ed. **2015**, 54, 7886-7890. DOI: 10.1002/anie.201503095.

(9)   Bu, F.; Lin, Q.; Zhai, Q.; Bu, X.; Feng, P. Charge-Tunable Indium-Organic Frameworks Built from Cationic, Anionic, and Neutral Building Blocks, Dalton Trans. **2015**, 44,16671-16674. DOI: 10.1039/c5dt02861b

(10)   Zhai, Q.; Bai, N.; Li, S.; Bu, X.; Feng, P. Design of Pore Size and Functionality in Pillar-Layered Zn-Triazolate-Dicarboxylate Frameworks and Their High CO2/CH4 and C2 Hydrocarbons/CH4 Selectivity, Inorg. Chem., **2015**, 54, 9862-9868. DOI: 10.1021/acs.inorgchem.5b01611

(11)   Zhai, Q.; Bu, X.; Zhao, X.; Mao, C.; Bu, F.; Chen, X.; Feng, P. "Advancing Magnesium-Organic Porous Materials through New Magnesium Cluster Chemistry" Cryst. Growth Des. **2016**, 16, DOI: 10.1021/acs.cgd.5b01297

(12)   Zhai, Quan-Guo; Bu, Xianhui; Mao, Chengyu; Zhao, Xiang; Feng, Pingyun, Systematic and Dramatic Tuning on Gas Sorption Performance in Heterometallic MOFs, J. Am. Chem. Soc. 2016, 138, 2524-2527.. DOI: 10.1021/jacs.5b13491

Publications supported primarily by DOE-BES , under award no. DE-FG02-13ER46972.

(13)   Koroush, S.; Lin, Q.; Mao, C.; Feng, P. Incorporation of Iron Hydrogenase Active Site into Highly Stable Metal-Organic Framework for Photocatalytic Hydrogen Generation, Chem. Commun. **2014**, 50, 10390-10393. DOI: 10.1039/C4CC03946G

(14)   Mao, C.; Kudla, R. A.; Zuo, F.; Zhao, X.; Mueller, L. J.; Bu, X.; Feng, P. Anion Stripping as a General Method to Create Cationic Porous Framework with Mobile Anions, J. Am. Chem. Soc. **2014**, 136, 7579-7582. dx.doi.org/10.1021/ja5030723

(15)   Kong, A.; Lin, Q.; Mao, C.; Bu, X.; Feng, P. Efficient oxygen reduction by nanocomposites of heterometallic carbide and nitrogen-enriched carbon derived from the cobalt-encapsulated indium-MOF, Chem. Commun., **2014**, 50, 15619-15622. DOI: 10.1039/c4cc06867j

(16)   Kong, A.; Mao, C.; Lin, Q.; Wei, X.; Bu, X.; Feng, P. From cage-in-cage MOF to N-doped and Co-nanoparticle-embedded carbon for oxygen reduction reaction, Dalton Trans., **2015**, 44,6748. DOI: 10.1039/c4dt03726j

(17)   Kong, Aiguo; Mao, Chengyu; Wang, Yuan; Lin, Qipu; Bu, Xianhui; Feng; Pingyun, Hierarchically Porous Few-layer Porphyrinic Carbon Nanosheets Formed by VOx-Templating Method for High-Efficiency Oxygen Electroreduction, J. Mater. Chem. A **2016**, 4, 7305-7312. DOI: 10.1039/c6ta00154h.

Atomically Defined Doping of Graphene Nanoribbons for Mesoscale Electronics

Felix R Fischer

Department of Chemistry University of California Berkeley

Program Scope

The outstanding transformative potential of graphene, an infinite two-dimensional sheet of carbon atoms tightly packed into a honeycomb lattice, has been recognized mostly due to its exceptionally high charge-carrier mobility, thermal conductivity, and tensile strength.[1] These undeniably very desirable properties, however, represent only a very small facet of the true potential of all-sp^2 carbon materials and its promise to revolutionize the field of molecular electronics. Graphene's most unusual characteristics can be observed when the infinite macroscopic sheet is scaled down to nanometer dimensions.[2] While macroscopic objects largely obey classical physics, the properties and function of mesoscale objects are influenced by the laws of quantum mechanics. Graphene, for example, is a semimetal; its valence and conductance band overlap over a narrow range. Upon confining the two-dimensional carbon sheet to a narrow one-dimensional graphene nanoribbon (GNR), its energy states are quantized and give rise to a discrete bandgap. Control over this well-defined and tunable bandgap is a prerequisite for the seamless integration of semiconducting GNRs into advanced electronic circuits. Along with the tunable band gap GNRs most unusual properties, e.g. the theoretically predicted edge-magnetism and the exceptionally high spin-coherence, are intimately linked to quantum mechanical boundary conditions established by the dimension, symmetry, and the edge-structure. Unfortunately, these complex structure-function relationships remain poorly understood. The exploration, realization, and implementation of these truly exotic properties rely on the development of innovative synthetic strategies that provide atomically precise control over the self-assembly of mesoscale objects. The central objective of this research is to develop the technology and the tools required to synthesize and to fine tune the physical properties of atomically defined graphene nanoribbons (GNR). Particular focus lies on controlling the absolute dimensions (length, width), the symmetry, and the doping pattern of mesoscale carbon materials with atomic precision. The innovative techniques and the expanded knowledge will be used to rationally tailor desired physical properties and function into nanometer-scale molecular electronic devices. We foresee the development of new functional electronic devices, e.g. transistors as logic gates in computing, data storage media based on electrically gated spin valves, or molecular amplifiers, all fabricated from readily available molecular building blocks into atomically defined GNRs. Specific goals of this project are: *(1)* To develop a complementary set of bottom-up strategies toward atomically defined GNRs from small molecule building blocks, *(2)* to tune the intrinsic band gap of semiconducting GNRs by controlled doping, *(3)* to devise a strategy to fabricate segmented GNRs featuring heterojunction architectures, *(4)* to identify mesoscale structure-performance relationships.

Recent Progress

(1) Site Specific Substitutional Boron-Doping of Semiconducting Armchair Graphene Nanoribbons: A fundamental requirement for the development of advanced electronic device architectures based on graphene nanoribbon (GNR) technology is the ability to modulate the band structure and charge carrier concentration by substituting specific carbon atoms in the hexagonal graphene lattice with p- or n-type dopant heteroatoms. As a major accomplishment during the current funding period we reported for the first time the atomically precise introduction of group III dopant atoms into bottom-up fabricated semiconducting armchair GNRs (AGNRs). Trigonal-planar B-atoms along the backbone of the GNR share an empty p-orbital with the extended π-band for dopant functionality. Scanning tunneling microscopy (STM) topography reveals a characteristic modulation of the local density of states along the backbone of the GNR that is superimposable with the expected position and concentration of dopant B-atoms. The periodicity of this topographic feature, 1.30 ± 0.05 nm, correlates with the expected spacing between boranthene units along the backbone of a B-7AGNR. In order to better understand the electronic effects of substitutive B-doping in B-7AGNRs we performed first-principles calculations based on the *GW* approximation and included the screening effects from the underlying Au(111) substrate. The DOS of both the valence (VB) and the conduction (CB) bands show significant contributions (~10%) from B-atoms. Comparing to the electronic structure of a pristine 7-AGNR,

substitutive B-doping along the backbone of a 7-AGNR introduces a deep acceptor band (CB) 0.8 eV above the valence band maximum. The theoretically predicted quasiparticle band gap of B-7AGNRs, 0.8 eV, is significantly smaller than that of the
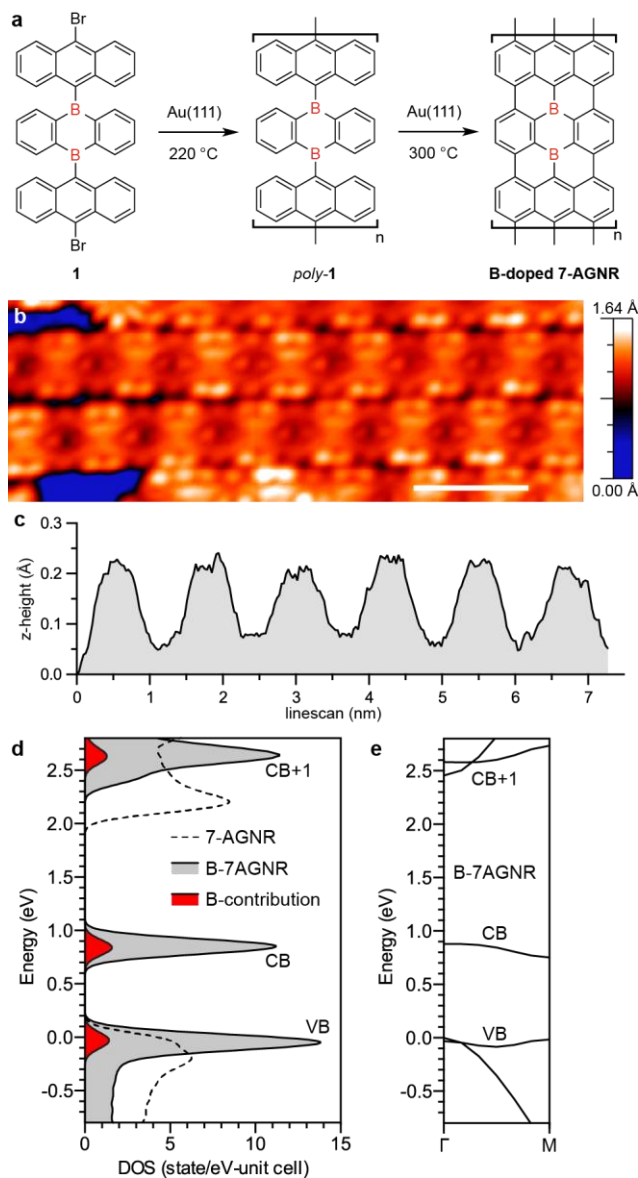
Figure 1 (a) Schematic representation of the bottom-up synthesis of B-7AGNRs. (b) fully cyclized B-7AGNRs (V_s = –0.1 V, I_t = 3 pA, T = 4.5 K). (c) Representative z-axis profile showing the characteristic height modulation along the long axis of a B-7AGNR. (d) Total density of states (DOS) for B-7AGNRs (grey) and contribution from B-atoms to the DOS (red). (e) Calculated quasiparticle band structure of B-7AGNRs.

undoped 7-AGNRs (~2.1 eV) calculated with the same method. This novel concept of site-specific substitutional doping along the backbone rather than the edges of of GNRs with group III heteroatoms will help pave the way toward the development of advanced functional device architectures based on GNR semiconductor technology.

(2) Surface-Assisted Synthesis of Peripentacene from 6,6'-Bipentacene Precursor: The unusual optical and electronic properties emerging from lateral quantum confinement effects in nanometer scale flakes of single-layer graphene has inspired the development of novel strategies and tools toward the rational synthesis of atomically defined nanographenes. Among these structures, polycyclic aromatic hydrocarbons (PAHs) featuring uniform edges, i.e. acenes or periacenes, represent privileged scaffolds. Their pursuit is further motivated by a fundamental interest in the exotic physical properties associated with atomically-defined finite boundary conditions in single-layer graphene. Recent resurgent interest in extended *n*-periacenes (**1** in Figure 2) has been spurred by theoretical calculations predicting an unusual electronic structure, a substantial decrease of the HOMO-LUMO gap upon extending the length of the *n*-periacene, and an antiferromagnetic ground state featuring spin localization along opposing zig-zag edges. As a major accomplishment during the current funding period we reported the first synthesis of peripentacene (**2** in Figure 2). Our strategy takes advantage of a surface-assisted cyclodehydrogenation of 6,6'-bipentacene (**2** in Figure 2) and its detailed characterization by STM and subnanometer-resolved ncAFM. The synthetic strategy makes use of a Staudinger type diazo-thioketone coupling, followed by a late-stage aromatization to give the metastable intermediate 6,6-bipentacene. Surface-assisted cyclodehydrogenation produces the peripentacene in excellent yields and high selectivity. This synthetic method has the potential to provide access to the experimental investigation of extended acenes predicted to exhibit exotic ground-state electronic configurations. Periacenes and related materials, long the subject of only theoretical investigation, are now more accessible for practical study and application.
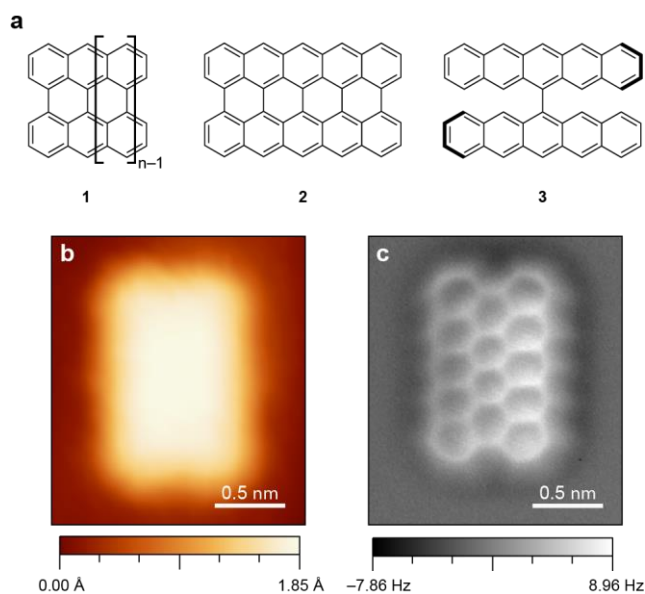

Figure 2 (a) Chemical structure of *n*-periacene (**1**), peripentacene (**2**), and 6,6'-bipentacene (**3**). (b) Constant-current STM image of **2**. (c) nc-AFM image of **2**.

(3) Bottom-up Synthesis of Sulfur-Doped Graphene Nanoribbons: Atomically precise edge-doping of GNRs has been used as a strategy to tune the relative alignment of the valence and the conduction band edges. This strategy is highly complementary to the width modulation of GNRs previously demonstrated by our group (controls the absolute size of the band gap) and

represents a structural tool that can be used to fine tune the alignment of energy levels across differentially doped segments in GNRs. As a major accomplishment during the current funding period we reported the bottom-up synthesis and characterization of atomically-precise N=13 armchair graphene nanoribbons (S-13-AGNRs) wherein alternating $(CH)_2$ groups lining the edges of the GNRs have been replaced by sulfur atoms. This alternative edge-doping pattern places one of the lone-pairs (having p-character) on trigonal planar S-atoms in full conjugation with the extended π-system of the 13-AGNR. Molecular precursors for S-13-AGNRs are derived from 10,10'-dibromo-9,9'-bisanthracene and feature (2-phenyl)thiophene substituents. Both scanning tunneling microscopy (STM) and scanning tunneling spectroscopy (STS) were used to investigate the structure and to probe the electronic states of the resulting S-13-AGNRs. STS measurements reveal a LUMO state (lowest unoccupied molecular orbital) for S-13-AGNRs at approximately the same energy as previously recorded for undoped 13-AGNRs. When compared to undoped 13-AGNRs, the density of states (DOS) associated with the LUMO in S-13-AGNR spans a significantly broader energy range. These results are consistent with ab-initio simulations of S-13-AGNRs that indicate a sulfur-induced increase in the energy separation between CB and CB+1 as well as between VB and VB–1 13-AGNR band edges (here CB refers to the conduction band and VB refers to the valance band).

Future Plans

We will expand our current focus on the design molecular precursors for GNRs that integrate our new concept of substitutional backbone-doping. This will include the integration of group V and group III elements at defined positions along the center of the GNRs. We will take advantage of this newly developed backbone doping strategy to assemble n-p-n and p-n-p junctions within segmented GNRs. We will develop solution-based strategies that enable the synthesis of graphene heterostructures integrating a molecule quantum dot at a defined position within a GNR. We will explore new structures both in solution as well as surface processed samples.

References

(1)   a) Novoselov, K.S.; Geim, A.K.; Morozov, S.V.; Jiang, D.; Dubonos, S.V.; Grigorieva, I.V.; Firsov, A.A., *Science* **2004**, *306*, 666. b) Novoselov, K.S.; Geim, A.K.; Morozov, S.V.; Jiang, D.; Katsnelson, M.I.; Grigorieva, I.V.; Dubonos, S.V.; Firsov, A.A., *Nature* **2005**, *438*, 197. c) Geim, A.K.; Novoselov, K.S., *Nat. Materials* **2007**, *6*, 183.
(2)   a) Tapaszto, L.; Dobrik, G.; Lambin, P.; Biro, L., *Nat. Nanotechnology* **2008**, *3*, 397. b) Man, M.Y.; Ozyilmaz, B.; Zhang, Y.; Kim, P., *Phys. Rev. Let.* **2007**, *98*, 206805(4).
Publications

(1)   Cloke, R. R.; Marangoni, T.; Nguyen, G. D.; Joshi, T.; Rizzo, D. J.; Bronner, C.; Cao, T.; Louie, S. G.; Crommie, M. F.; Fischer, F. R. *J. Am. Chem. Soc.* **2015**, *137*, 8872–8875.
(2)   Rogers, C.; Chen, C.; Pedramrazi, Z.; Omrani, A. A.; Tsai, H.-Z.; Jung, H. S.; Lin, S.; Crommie, M. F.; Fischer, F. R. *Angew. Chem. Int. Ed.* **2015**, *54*, 15143–15146.
(3)   Nguyen, G.; Toma, F.; Cao, T.; Pedramrazi, Z.; Chen, C.; Rizzo, D.; Joshi, T.; Bronner, C.; Chen, Y.-C.; Favaro, M.; Louie, S.; Fischer, F.; Crommie, M. *J. Phys. Chem.* **2016**, *120*, 2684–2687.

Toward the Rational Design of Glassy Polymers

Karl F. Freed, James Franck Institute & Department of Chemistry, University of Chicago

Program Scope

Glasses have found a plethora of applications since the dawn of civilization, and now they are present almost everywhere as plastics and other materials. Nevertheless, the development of a theory of glass-formation in polymeric systems poses one of the most fascinating and difficult challenges in soft matter physics from both scientific and technological perspectives. Relatively few theories of glass-formation exist on the molecular scale, which is the *sine qua non* for the successful elucidation of the universal characteristics of glass-formation and of the dependence of the physical properties of glass-formers (including "fragility," a measure of temperature sensitivity) on their molecular structure, molar mass, pressure, temperature, solvent and nanoparticle additives, geometrical confinement, etc.

The generalized entropy theory (GET) of glass-forming liquids is a combination of the Adam-Gibbs (AG) model for structural relaxation times and the lattice cluster theory (LCT) for the thermodynamics of polymer systems, rending the GET enormously wider in its scope and predictive power than any other existing theory, including, the classic Gibbs-DiMarzio (GD) approach. The unique position of the GET among theories of glass-formation in polymer fluids emerges from its underlying molecular based model that accounts for the complexities of monomer structure, chain connectivity, and chain semiflexibility. While the introduction of these three realistic molecular features of polymer chains into this statistical mechanical theory imparts significant algebraic complexity, the theory maintains conceptual simplicity, the necessary condition for its use in the design of advanced amorphous glassy polymer materials and the control of their properties, building upon our successes in theoretical modeling thermodynamic and dynamic properties of glass-forming polymer melts and partially miscible binary blends.

Recent Progress

A short list of the proposed extensions and application of the GET is proceeded by the description of a few of our recent advances in theoretical modeling thermodynamic and dynamic properties of glass-forming polymer melts and partially miscible binary blends.

A. Illustrative calculations of segmental relaxation times, fragility, and characteristic temperatures of glass-formation. Figure 1 presents our calculations of an "Angell plot" presenting the logarithm of the reduced segmental relaxation time $t(T)/t(T_g)$ as a function of the reciprocal of the reduced temperature $1/(T/T_g)$ over
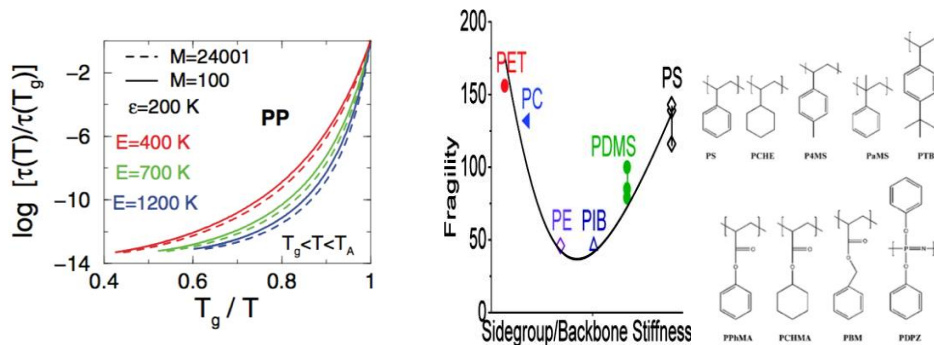
Figure 1 (left) A computed set of Angell plots of the logarithm of the temperature dependence of the reduced structural relaxation time vs. the inverse temperature, scaled by the glass transition temperature. Notice the change of ~ 14 orders of magnitude!

Figure 2 (middle) Data of Sokolov and coworkers verifying the prediction of the LCT that increasing the differences in the stiffness of the backbone and side groups enhances fragility.

Figure 3 (right) Pairs of similar monomers where one group (e.g., a ring) is stiff in one monomer while the other contains the corresponding flexible group. Figure 4. presents the data of Sokolov and coworkers for the shift in the glass transition temperature and fragility the respective polymers.

a temperature range above T_g for three model chains with poly(propylene) structures but different degrees of chain stiffness induced by the bending energies E = 400 K, 700 K, and 1200 K. Higher E corresponds to stiffer chains, increased packing frustration, larger free volume, elevated T_g, and finally increased fragility, a measure of the sensitivity of the dynamics of a material to temperature. Solid and dashed curves in Fig. 1, respectively, are for low and high
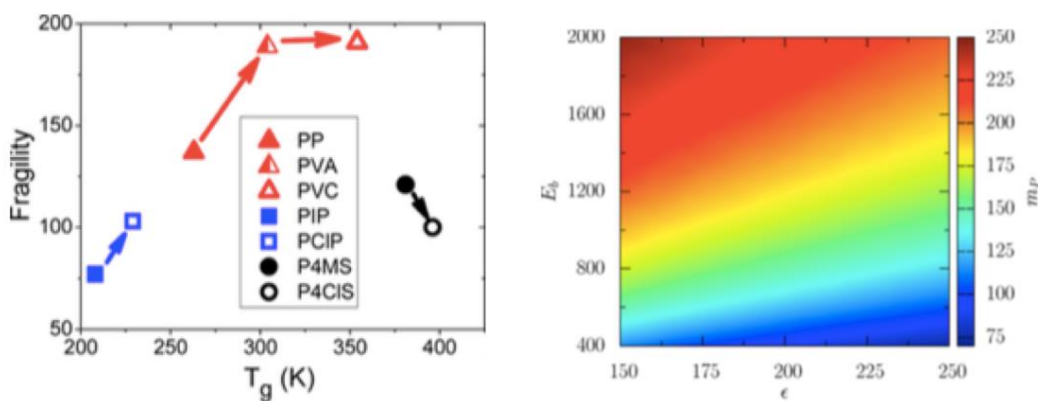
Figure 4. (left) Shifts in fragility and T_g for the pairs of polymers with monomers of Fig. 3. The data (Sokolov and coworkers) are inconsistent with GET predictions *if* only ε or E_{bend} differ between pairs.

molar mass polymers. Our calculations agree with the well-known general observation that fragility grows with the polymer molar mass. Exceptions to this rule of thumb appear for the unusual polyisobutylenes (PIB) whose density increases with temperature

but whose fragility diminishes. These experimental findings accord with the general prediction of the GET that better packing efficiency (i.e., higher density) implies a lower fragility and visa versa.

Our analysis also indicates that the thermodynamic fragility, introduced first by Sastry and coworkers, provides a good measure of fragility in the lower temperature regime ($T_g<T<T_c$).

B. The very important empirical Williams-Landell-Ferry (WLF) equation enables using the segmental relaxation time $\tau(T)$ of glass-forming materials to unify vast amounts of data for dielectric relaxation and stress relaxation over huge ranges of frequencies. The previous lack of a molecular basis for the WLF equation is remedied by determining the WLF parameters from the GET and by evaluating their dependence on monomer properties. The calculations cover temperatures over which the equally important Vogel-Fulcher-Tammann (VFT) equation is also valid, thereby also providing a molecular basis for the VFT equation. GET calculations yield universal VFT parameters for some systems because of similar interaction energies ε. The GET calculations also explain the often puzzling differences between the VFT and Kauzmann temperatures, T_{VFT} and T_0, as emerging when the local chain stiffness differs. Thus, T_{VFT} and T_0 only coincide in the limit of very fragile polymer glasses, but otherwise may differ appreciably.

C. The GET remains as the *only* molecular theory that describes the influence of monomer structure on properties of glass-formation of polymers, particularly, on the two quantities dictating how polymers can be processed, namely the glass transition temperature and the glass fragility parameter m_p (a measure of temperature sensitivity). Sokolov and coworkers have provided major experimental tests of the predictions by the GET of the molecular factors determining the glass-transition temperature and fragility. The first involves an example (Fig. 2) where Sokolov and coworkers verify the predictions of the GET that the fragility parameter is dependent of the relative stiffness of the backbone and side groups, while another example (Figs. 3 and 4) uncovers data indicating the need for lifting an inadequate approximation to enable the GET predictions to agree with the experiments (Fig. 5) and thereby provide deeper insight into the molecular factors determining the glass-transition temperature and fragility.

Sokolov has also tested GET predictions that increasing only the interaction energy ε elevates both T_g and m_p, but raising only the chain stiffness diminishes m_p but increases T_g. The experiments consider pairs of polymers whose monomers (depicted in Fig. 3) differ in the stiffness of a small portion of the monomer. The data exhibit counter examples to the GET predictions, such as for the pair of polymers displaying a shift in T_g but no change in m_p (red arrow, open triangles in Fig. 4.) However, experiments cannot simply modify the stiffness (E_{bend}) or interaction ε, and undoubtedly the pairs of monomers in Fig 3 have both stiffness and interaction altered to some degree. Contour plots in Fig. 5 present GET predictions of the joint interdependent variation of T_g and m_p with ε and E_{bend} that enables the GET to explain the data.

D. Some scientists view the Adam-Gibbs relation for the segmental relaxation time with skepticism, in part, due to the rather heuristic and semi-empirical nature of the original

arguments. Freed has recently derived the AG relation as an approximation to a general statistical mechanical formulation of transition state theory which predicts that the transition states for the cooperative relaxation have size distributions corresponding to an equilibrium self-assembling system. The new theory thus explains the previously enigmatic finding that the cooperatively rearranging string-like motions observed in computer simulations of glass-forming systems and in experiments for colloids remarkably have the predicted distribution. Thus, Freed's theory provides further support for stringlike motions being associated with the cooperative relaxation that is responsible from the enhanced relaxation times in glass-formers.

E. While fairly lengthy expressions for the configurational entropy emerge from the GET, a rather simple and compact analytic approximation (SGET) is derived for polymer melts. Thermodynamic properties for melts may be derived from the SGET with little added effort than required for Flory-Huggins theory, and illustrative calculations for T and m of model poly(n-α olefin) melts attest to the accuracy of the approximation.

Future Plans

1. Since the recent extensions of the GET (to specific interactions, sticky interactions, binary blends, etc.) have only been applied to the simplest examples, we plan more comprehensive studies, such as that in Fig. 5, to study the modification of T_g and m_p induced by the combined variation of monomer structure, multiple interaction energies in blends and sticky systems, chain architecture, e.g., diblock polymers, etc.

2. Monte Carlo simulations for selected models of polymer melts will be performed with standard polymer models (Lennard-Jones interactions, harmonic or FENE chains, etc., to test the GET variations of T_g and m_p in 1. that are inaccessible to experiment. Tests of the SGET will determine if this approximation can be used to enormously simplify the computations in 1.

3. Since our recent theory of the thermodynamic properties of thin, dense polymer films is insufficient to describe glass formations, after the needed extensions become available for the theory of films, the GET will be further developed to treat glass-formation in thin polymer films.

The goal of the research will be to develop guides enabling rational designing polymer glasses.

4. We will investigate applications of our polarization theory to areas of interest to DOE.

References

K. Kunal, et al., *Macromolecules* **41**, 7232 (2008).

R. Kumar, Phys. Chem. Chem. Phys. **15**, 4604 (2013).

K. F. Freed, J. Chem. Phys. **141**, 141102 (2014).

J. Qin, J. Li, V. Lee, H. Jaeger, J. de Pablo, K. Freed, J. Colloid & Interface Sci. **469**, 237 (2016).

Publications

1.   Perturbative Many-body Expansion for Electrostatic Energy and Field for System of Polarizable Charged Spherical Ions in a Dielectric Medium. K. F. Freed, J. Chem. Phys. **141**, 034115 (2014).

2.   Lattice Cluster Theory for Polymer Melts with Specific Interactions. W.-S. Xu and K. F. Freed, J. Chem. Phys. **141**, 044909 (2014). 7/30

3.   Influence of Cohesive Energy and Chain Stiffness on Polymer Glass Formation. W.-S. Xu and K. F. Freed, Macromolecules **47**, 6990 – 7 (2014). 9/18

4.   Towards First Principles Theory of Relaxation in Supercooled Liquids Formulated in Terms of Cooperative Motion. K. F. Freed, J. Chem. Phys. **141**, 141102 (2014). 10/10

5.   Advances in the generalized entropy theory of glass-formation in polymer melts. J. Dudowicz, J. F, Douglas, and K. F. Freed, J. Chem. Phys. . **141**, 234903 (2014). 12/18
6.   The Meaning of the "Universal" WLF Parameters of Glass-forming Polymer Liquids. J. Dudowicz, J. F, Douglas, and K. F. Freed, J. Chem. Phys. **142**, 014905 (2015). 1/7

7.   Generalized Entropy Theory of Glass Formation in Polymer Melts with Specific Interactions, W. S. Xu and K. F. Freed, Macromolecules **48**, 2333 (2015).
8.   The Simplified Generalized Entropy Theory of Glass-formation in Polymer Melts. K. F. Freed, J. Chem. Phys. **143**, 051102 (2015).

9.   Entropy Theory of Polymer Glass-Formation in Variable Spatial Dimension. W.-S. Xu, J. F. Douglas, and K. F. Freed, Adv. Chem. Phys. **161**, 443 (2016)

10.   A Theory of Interactions between Polarizable Dielectric Spheres. J. Qin, J. Li, V. Lee, H. Jaeger, J. de Pablo, K. Freed, J. Colloid & Interface Sci. **469**, 237 (2016).

Ordered Phases of Chiral Block Copolymers: Mesochiral, Periodic Nanostructures via Self-Assembly

Gregory M. Grason, Dept. of Polymer Science Engineering, University of Massachusetts Amherst; Edwin L. Thomas, Dept. of Materials Science and NanoEngineering, Rice University

Program Scope

This project aims to understand mechanisms and structural implications of chirality transfer from segment-scale chain-structure to mesoscale ordering in chiral diblock copolymer melts[1]. The project builds on i) recent observation—in chiral polylactic-acid (PLA)-based diblocks—of mesochiral cylinder morphologies [2] and ii) an new orientational self-consistent field (oSCF) theory framework for modeling chiral block copolymer melts[3, 4]. Under this overall aim, this collaborative theoretical and experimental project pursues 4 interrelated objectives:

1) *Develop and study "chiral nematic segment" model of diblock melts.* The project explores the hypothesis that mesochiral morphologies are stabilized by the interplay between the thermodynamics of domain formation in flexible diblocks and cholesteric twisting of chiral block segments. oSCF theory will predict the dependence or mesochiral domain structure and thermodynamics on parameters that characterize chiral structure and interactions of segments.

2) *Explore chiral block copolymer chemistries to characterize chiral parameters and connect theory and experiment.* Experiments will explore chiral diblocks beyond the current PLA-based systems, which will offer i) a means to quantify chiral ordering of homopolymer (independent of diblock assembly) and ii) an expanded window for observable mesochiral domain assembly.

3) *Image/quantify patterns of intra-domain segment/chain twist in mesochiral assemblies.* oSCF theory predicts that cholesteric ordering of segments within the chiral block domain underlies the chirality transfer mechanism[1]. The project explores novel high-resolution EM methods for directly imaging orientations of block- and segment- within self-assembled copolymer domains.

4) *Theoretically map chiral diblock melt phase diagram; and experimentally observe and characterize new mesochiral diblock morphologies.* The oSCF framework for chiral diblocks will predict conditions for mesochiral assembly, beyond the previously observed mesochiral cylinder phases, including the possibility of mesochiral networks or sphere packings. Theory will guide the design of new chiral diblocks and experimental study of yet unexplored regions and mesochiral ordered phases in the broader phase diagram of chiral diblocks.

 Recent Progress

Intra-domain nematic ordering in diblock assemblies - In a first application of a newly "nematic segment" oSCF theory of diblocks, we have analyzed the patterns of intra-domain nematic order of segments in microphase-separated morphologies. Liquid crystalline ordering of segments is
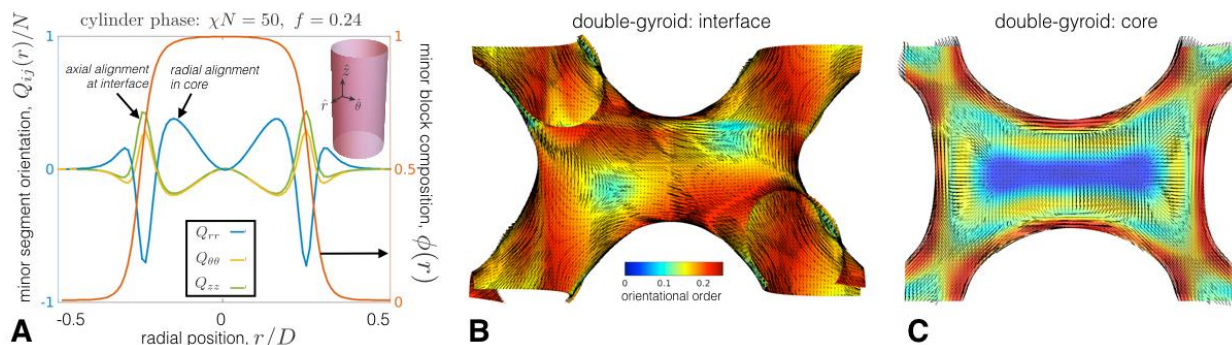
Figure 1 – (A) Profiles of the (biaxial) nematic order parameter of minor block segments of a cylinder-forming diblock copolymer. (B) and (C) depict the respective interfacial and core segment orientation profiles within tubular network, minor domains of a double-gyroid phase.

an unavoidable consequence of microphase-separation in block copolymers – even in the absence of strong orientational segment interactions — the patterns of segment orientation that underlie diblock morphologies is a surprisingly overlooked aspect of their structure. As a baseline for subsequent studies of chiral intra-domainsegment ordering, we considered first nematic ordering present in flexible chain models of diblocks with standard density (i.e. Flory-Huggins) interactions. Our oSCF model shows that generic orientation pattern underlies microphase-separation into all ordered states: segments at the inter-domain surface are strongly aligned *parallel* to the interface while deep in the "core" of the domain, this pattern transitions to a *normal* (or "homeotropic") orientation (Fig. 1A). Previous studies that have analyzed the *polar order* parameter of segments[3, 5], find that the normal orientation can be related to chain stretching in the brush-like domains, although the nature of interfacial orientation is completing missing in this description. Parallel segment orientation is known at interfaces of polymer blends[6, 7], although ours is the first study to our knowledge to show that both orientation patterns coexist within microphase-separated block copolymer domains.

Interfacial and "core" orientation patterns are strongly dependent on segregation strength, composition, and more profoundly, on the domain morphology. W show that the segment order parameter becomes biaxial at the interface of hexagonal and bicontinuous phases (Fig. 1B-C) due to their anisotropic surface curvature. We have developed an analytical argument to show that segments align along one of the principal directions of surface curvature (smallest curvature), leading to spatially organized patterns of orientation in even the standard diblock models. These results are critical to project aims, as they imply that drive for chirality will have distinct consequences for orientation near to and away from the interface, as well as for different morphologies. Beyond this application, these results may yield insights into performance and design of copolymer-based nanomaterials where segment anisotropy, and its spatial pattern, plays a key role in properties (e.g. transport, optical).

New chiral diblock chemistries - Work in collaboration with Rong-Ming Ho (Nat'l Tsing Hua Univ.) indicates preliminary progress in expanding the class of chiral diblocks capable of directing the mesochiral assembly of melts. Ho has developed a synthetic route to a new class of

chiral polymers, polycyclohexylglycolide (PCG). These polymers have a similar structure to PLA, with the methyl groups associated with chiral carbons replaced with bulkier carbon rings. CD measurements of the polymer in solution confirm chirality is maintained from the original mandelide monomers, and more perhaps significant, DSC shows the chiral PCG homopolymers do not crystallize over a 100° window above T_g. The bulkier side groups of PCG evidently suppress the competitor semi-crystalline state, which is a limitation for processing and characterizing mesochiral morphologies of PLA-based diblocks and homopolymers   At present, it is not yet clear whether the chiral PCG homopolymer exhibits chiral liquid crystalline ordering above T_g . To test whether chain chirality can propagate to the mesodomain assembly, Ho has synthesized chiral diblocks: poly(benzyl methacrylate)-b-poly(L-cyclohexylglycolide) (PBnMA-PLCG).   Preliminary TEM experiments of PBnMA-PLCG films show "arched" domain patterns in 2D TEM projections, characteristic of the helical cylinder phase (H*) observed in PLA-based diblocks.   Direct confirmation of the structure and handedness of a helical morphology has yet to be confirmed by EM tomography, but if the H* phase is confirmed, this would be the only second class of chiral chemistries shown to promote mesochiral domain formation in diblocks.

Future Plans

1) Phase behavior of the "chiral nematic segment" model of diblocks will be studied based on i) an weak-segregation theory (WST) and ii) pseudo-spectral implementation of oSCF theory in order to predect threshold composition and segregations for mesochiral domain formation and analyze the influence of chiral segment interactions on intra-domain segment profiles.

2) Mesochiral cylinder morphologies (H*) formed by chiral PS-PLA diblocks labeled with distinct-Z atoms at free chain ends and junctions (synthesized by collaborator B. Coughlin, UMass) will be imaged by high-resolution EM tomography to map contours of chain positions and extract mean block orientation as a probe for intra-domain cholesteric order.

3) Polarized optical microscopy and EM experiments will probe potentially chiral LC ordering of chiral PCG homopolymers and test chirality transfer to the apparent H* morphology it forms.

4) Experiments will test new classes of chiral diblocks based on block cholesterol side groups (synthesized by collaborator R. Kasi, UConn), where strong thermotropic cholesteric behavior may drive mesochiral domain formation (e.g. H* phase formation).

 References

1. Grason, G. M. "**Chirality Transfer in Block Copolymer Melts: Emerging Concepts**" *ACS Macro Letters* 4, no. 5 (2015): 526–532.

2. Ho, R.-M., Chiang, Y.-W., Chen, C.-K., Wang, H.-W., Hasegawa, H., Akasaka, S., Thomas, E. L., Burger, C., and Hsiao, B. S. "**Block Copolymers with a Twist.**" *Journal of the American Chemical Society* 131, no. 51 (2009): 18533–42.

3. Zhao, W., Russell, T. P., and Grason, G. M. "**Orientational Interactions in Block Copolymer Melts: Self-Consistent Field Theory.**" *The Journal of chemical physics* 137, no. 10 (2012): 104911.

4. Zhao, W., Russell, T., and Grason, G. "**Chirality in Block Copolymer Melts: Mesoscopic Helicity from Intersegment Twist**" *Physical Review Letters* 110, no. 5 (2013): 058301.

5. Jiang, Y. and Chen, J. Z. Y. "**Self-Consistent Field Theory and Numerical Scheme for Calculating the Phase Diagram of Wormlike Diblock Copolymers**" *Physical Review E* 88, no. 4 (2013): 042603,

6. Szleifer, I. and Widom, B. "**Structure and Tension of the Interface between Dilute Polymer Solutions**" *J. Chem. Phys.* 90, (1989):

7. Carton, J.-P. and Leibler, L. "**Density-Conformation Coupling in Macromolecular Systems: Polymer Interfaces**" *Journal de Physique* 51, no. 16 (1990): 1683–1691.

Transmetalation Reactions in the Syntheses of Phosphorescent Cyclometalates

Thomas G. Gray, Department of Chemistry, Case Western Reserve University

Program Scope

Work done under BES auspices focuses on the syntheses and characterization of cyclometalated complexes through transmetalation protocols. Complexes of iridium(III) and gold(III) have been emphasized. As part of this research, metallaboroxinato complexes have been encountered and investigated as the products of arrested transmetalation reactions. The new organometallics are triplet-state lumophores; they have been characterized by multinuclear NMR experiments, absorption and emission spectroscopies (including time-resolved emission), and X-ray diffraction crystallography.

Recent Progress

A. Terminal Fluoride Complexes of Iridium(III). Terminal fluoro complexes of the late transition metals are attractive precursors in metal-carbon bond-forming reactions.[1] The Gray research group has published the first examples of bis(cyclometalated) iridium(III) complexes bearing terminal fluoride ligands. A rational strategy for stabilizing nonbridging fluorides with second-sphere interactions was illustrated.

Reaction of fluoride bridged dimers with 3,5-dimethylpyrazole or similar hydrogen-bond donors yields mononuclear fluoro complexes, Scheme 1. The hydrogen-bond donating capacity of the incoming heterocycle is critical to the reaction's success. Control experiments with non-H-bond donor ligands returned unreacted starting materials. The crystal structure of a terminal fluoro complex appears as Figure 1. The Ir–F bond distance is 2.168(5) Å, which is longer than the few reported Ir^{III}–F bonds. This bond lengthening is attributed to hydrogen bonding to the adjacent 3,5-dimethylpyrazole ligand.
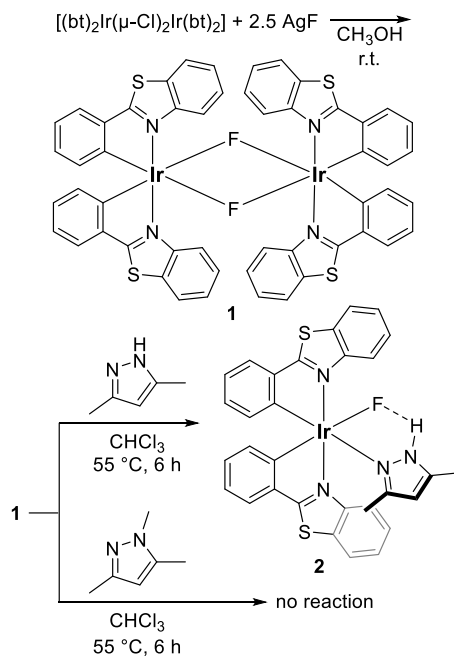
Scheme 1. Synthesis of a bis(cyclo-metalated)iridium(III) fluoride.
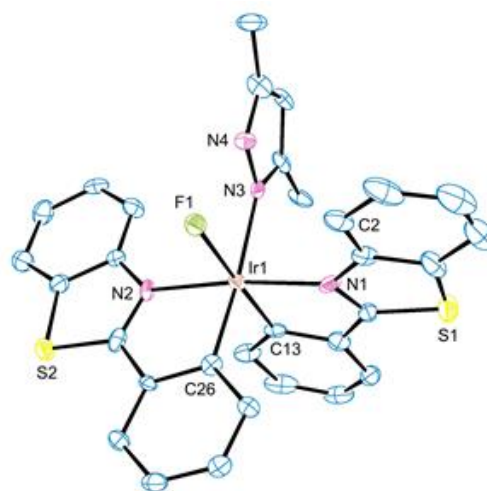
Figure 1. Crystal structure of fluoride complex **2** (50% probability, 100 K). Hydrogen atoms are omitted; unlabeled atoms are carbon.

The reactivity of terminal fluoride ligands was investigated. Bound fluoride reacts with C-, Si-, and S-based electrophiles. Reactions with functionalized organosilanes afford ligand substitution at iridium. Crystal structures of three products were published. Reactions also take place with electrophilic carbon and sulfur. These results prove that fluoride remains nucleophilic despite hydrogen-bonding and attachment to iridium.

Iridium(III) fluoride complexes luminesce at room temperature. Emission yields of 16–17% were measured relative to $[Ru(bpy)_3]^{2+}$. Radiative lifetimes are near 1 µs at 298 K.

B. Palladium-Catalyzed Suzuki-Miyaura Coupling of Gold(III). The Gray group has disclosed a *catalytic* protocol for carbon-gold(III) bond formation at room temperature. Examples appear in Table 1. Interaction of dichlorogold(III)

Table 1. Gold(III) products formed by palladium-catalyzed cross coupling. Catalytically formed C–Au bonds appear in red. Isolated yields shown.

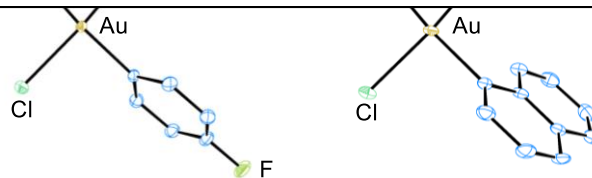*Six other examples, isolated yields 42–78%.*
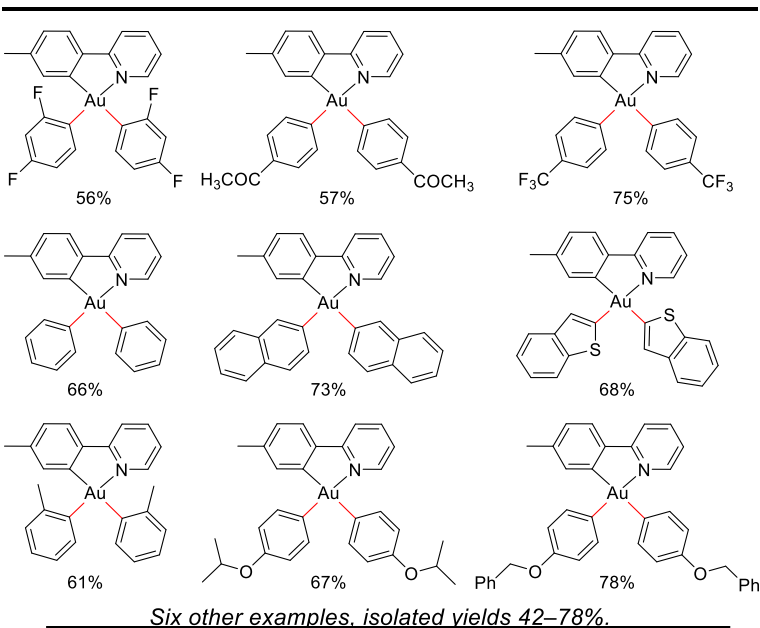
Figure 2. Crystal structures of two singly arylated gold(III) cyclometalates prepared in Suzuki-Miyaura coupling reactions. (50% probability, 100 K). Hydrogen atoms are omitted; unlabeled atoms are carbon.

complexes with arylboronic acids in the presence of palladium salts and a supporting base yields arylgold(III) products. Arylation is not observed without added palladium; reduction of gold(III) does not compete. Reaction conditions were devised that favor mono- or diarylations. Figure 2 shows crystal structures of two products of single arylation.

Table 1 collects some diarylated products and isolated yields. The reaction tolerates arylboronic acids with electron-withdrawing and -releasing substituents. A proposed mechanism appears in publication 72.

C. Boroxinato Complexes of Au(III). The results of Table 1 show that metal complexes are competent electrophiles in Suzuki-Miyaura cross coupling. The outcome is different when palladium and phosphines are omitted, and (trifluoroacetato)gold(III) precursors are used. *Trioxadiborrin complexes* form in arrested transmetalation reactions between cyclometalated
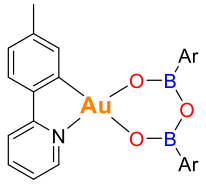

Scheme 2. Gold(III) boroxinato synthesis.

gold(III) reagents and boronic acids. Luminescent metallaboroxines were previously unknown, as were trioxadiborrins of gold in any oxidation state.
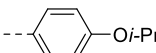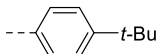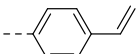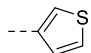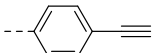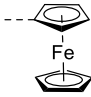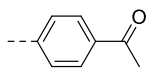
Reaction of (2-(p-tolyl)pyridyl)gold(III) trifluoroacetate[2] with (4-isopropoxyphenyl)-boronic acid in toluene with K_2CO_3 or KOtBu affords (trioxadiborrin)gold(III) product. Reaction conditions appear in Scheme 2. Table 2 compiles several new compounds and isolated yields. The reaction is insensitive to electron-withdrawing or -releasing aryl substituents. The crystal structure of one complex appears as Figure 3.

Trioxadiborrin complexes of cyclometalated Au(III) are luminescent. Shown in Figure 4 are optical spectra of a representative product. Room-temperature emission lifetimes are near 1.5 µs, and indicate triplet excited-state parentage. The trioxadiborrin aryl substituents show little effect on emission spectral profiles. (Trioxadiborrin)gold(III) species are ripe for exploration. They raise the prospect of unique optical properties that are exploitable in organic light-emitting diodes.

An extensive study of the bonding of gold(III) trioxadiborrins was undertaken with density-functional theory. Substituent effects are evaluated, and comparison is made to the cyclometalating 2-(p-tolyl)pyridine (tpy) ligand on gold. The tpy ligand binds more strongly than any trioxadiborrin ligand, and the two ligands bind competitively to gold. Trioxadiborrin ligands have larger binding enthalpies to gold than organic β-diketonate analogues. Fragment bond orders were partitioned into in-plane and out-of-plane contributions for a representative complex. In-plane bonding accounts for 88% of bonding between gold and the trioxadiborrin ligand. Spin-unrestricted triplet-state geometry optimizations find that the ten largest excited-state distortions all occur on the organic ligand. Triplet-state spin density resides almost wholly on the organic, cyclometalating ligand. The 77-K luminescence spectrum of a typical complex was reported. Time-dependent DFT and configuration interaction singles calculations (corrected for doubles excitations) overestimate the triplet-state energy by ~0.12 eV.

Table 2. Cyclometalated boroxinato complexes.

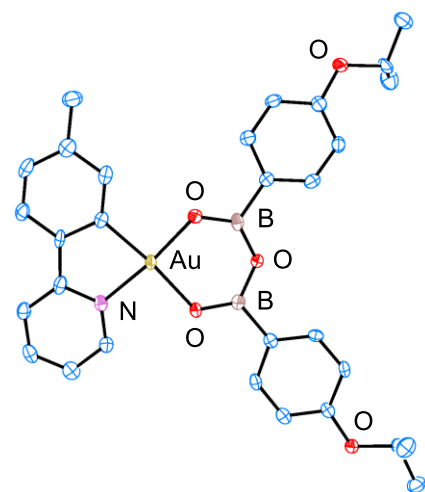| Ar	Yield	Ar	Yield
O*i*-Pr	68%	1-naphthyl	76%
t-Bu	74%	(styryl)	92%
(thienyl) S	77%	(ethynylphenyl)	76%
(ferrocenyl) Fe	72%	(acetylphenyl)	69%

Figure 3. Crystal structure (50%, 100 K) of a (boroxinato)gold(III) complex. Hydrogen atoms are omitted; unlabeled atoms are carbon.

157

Future Plans:

(1) Synthetic and photophysical investigations of platinum cyclometalates.
(2) Synthesis and photophysical characterization of a new class of luminescent gold(III) complexes accessed by oxidative addition.
(3) Synthesis of a family of gold(III) complexes having strong-field ligands that are expected to be triplet-state lumophores.
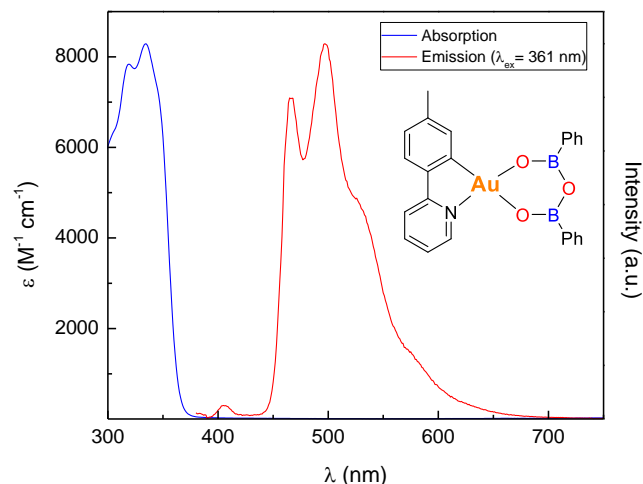(4) Characterization of new luminescent complexes by static and time-resolved emission spectroscopy and by electro-chemical measurements.

Figure 4. Absorption (blue) and emission (red) spectra of the inset complex in 2-methyl-tetrahydrofuran solution.

References

(1) Selected leading references: (a) Laitar, D. S.; Müller, P.; Gray, T. G.; Sadighi, J. P. *Organometallics* **2005**, *24*, 4503–4505; (b) Akana, J. A.; Bhattacharyya, K. X.; Müller, P.; Sadighi, J. P. *J. Am. Chem. Soc.* **2007**, *129*, 7736–7737; (c) Vela, J.; Smith, J. M.; Yu, Y.; Ketterer, N. A.; Flaschenriem, C. J.; Lachicotte, R. J.; Holland, P. L. *J. Am. Chem. Soc.* **2005**, *127*, 7857–7870; (d) Grushnin, V. V. *Acc. Chem. Res.* **2010**, *43*, 160–171; (e) Lee, D.-H.; Kwon, H. J.; Patel, B. P.; Liable-Sands, L. M.; Rheingold, A. L.; Crabtree, R. H. *Organometallics* **1999**, *18*, 1615–1621; (f) Patel, B. P.; Crabtree, R. H. *J. Am. Chem. Soc.* **1996**, *118*, 13105–13106.

(2) Langseth, E.; Görbitz, C. H.; Heyn, R. H.; Tilset, M. *Organometallics* **2012**, *31*, 6567–6571.

Publications 2015–2016

72. "Suzuki-Miyaura Coupling of Arylboronic Acids to Gold(III)," Maity, A.; Sulicz, A. N.; Deligonul, N.; Zeller, M.; Hunter, A. D.; Gray, T. G. *Chem. Sci.* **2015**, *6*, 981–986. DOI: 10.1039/c4sc02148g

74. "Fluoride Complexes of Cyclometalated Iridium(III)," Maity, A.; Stanek, R. J.; Anderson, B. L.; Zeller, M.; Hunter, A. D.; Moore, C. E.; Rheingold, A. L.; Gray, T. G. *Organometallics* **2015**, *34*, 109–120. DOI: 10.1021/om5009555.

75. "Cyclometalated (boroxinato)gold(III) complexes from arrested transmetalation," Browne, A. R.; Deligonul, N.; Anderson, B. L.; Zeller, M.; Hunter, A. D.; Gray, T. G. *Chem. Commun.* **2015**, *51*, 15800-15803. DOI: 10.1039/C5CC05200A

76. "Bonding and Reactivity of a Dicopper(I) μ-Boryl Cation." Wyss, C. M.; Bitting, J.; Bacsa, J.; Gray, T. G.; Sadighi, J. P. *Organometallics* **2016**, *35*, 71–74.

DOI: 10.1021/acs.organomet.5b00961

77. "Cyclometalated Gold(III) Trioxadiborrin Complexes: Studies of the Bonding and Excited States," Ayoub, N. A.; Browne, A. R.; Anderson, B. L.; Gray, T. G. *Dalton Trans.* **2016**, *45*, 3820-3830.   DOI:10.1039/C5DT04732C

78. "A tri-gold triazolide with long-lived luminescence," Heckler, J. E.; Anderson, B. L.; Gray, T. G. *J. Organomet. Chem.,* in press. DOI: 10.1016/j.jorganchem.2016.05.020

Designing Efficient Nanostructured Polymer Electrolytes Using Tapered Block Polymers - Joint Experiment and Theory Effort in Controlled Interface Design

Lisa M. Hall, The Ohio State University; Thomas H. Epps, III, University of Delaware

Program Scope

We are developing new interfacially modified (tapered) block polymers (BPs, see Figure 1) through a joint experimental and theoretical effort, focusing on self-assembly behavior, nanoscale network formation, and lithium ion transport in salt-doped systems.

Recent Progress

Taper Density Profiles in Self-Assembled Block Copolymers (Methods Development)

X-ray reflectivity (XRR) studies were conducted on uniform poly(isoprene-b-styrene) (I-S) [non-tapered] (126 nm), I-IS-S [normal tapered] (118 nm), and I-SI-S [inverse tapered] (126 nm) thin films. The profiles calculated from the XRR were modeled and showed good fits to the data (data not shown). Importantly, the interfacial roughness (indicative of interfacial width) could be resolved
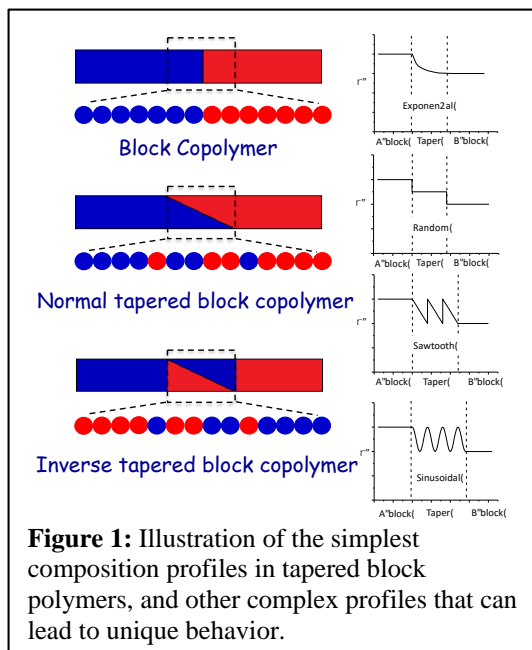

Figure 1: Illustration of the simplest composition profiles in tapered block polymers, and other complex profiles that can lead to unique behavior.
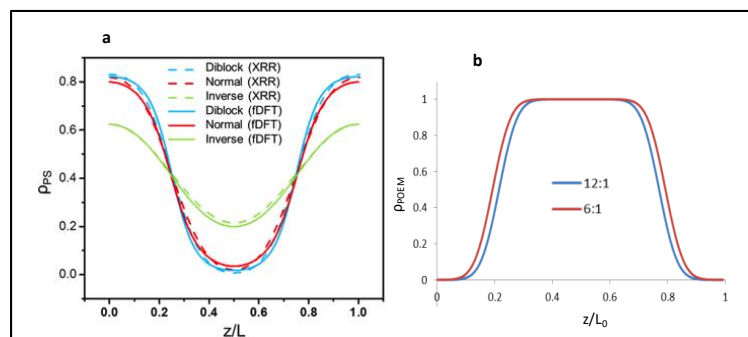
quantitatively. The average interfacial roughness for the I-S film was ~1.9 nm from our XRR fitting. There was a slight increase in the interfacial roughness in the I-IS-S film (~2.2 nm). The I-SI-S film showed a more significant increase of interfacial roughness to ~4.4 nm, which is expected as the I-SI-S possessed the largest miscibility. These interfacial characteristics could be plotted as lamellar density profiles as shown in Figure 2a. These experimental plots show excellent agreement with fluids density functional theory (fDFT) results; fDFT details are discussed

Figure 2. a) Lamellar density profile of PS *versus* perpendicular distance across the lamellae of width L at $\chi N \approx 14$ for symmetric ($f_A = f_B = 0.5$) systems for diblock, normal and inverse tapered BPs. Dashed lines are the profiles derived from XRR modeling, while solid lines are the profiles from fDFT calculations. b) Lamellar density profile of POEM domain versus perpendicular distance across the lamellae for a PS-POEM block copolymer with no tapering. The POEM domain is doped with lithium triflate salt at [EO]:[Li] of 12:1 and 6:1. As opposed to the PS-PI system in panel a, the more square-like profiles indicate a higher effective segregation strength and near-pure POEM/salt domains. We note that the 6:1 (higher salt) sample shows a sharper profile.

below. The normal tapered I-IS-S polymer had a similar density profile to the non-tapered diblock I-S, while the inverse tapered I-SI-S polymer demonstrated a wider interface and greater mixing within the defined PI and PS domains. We expected that the normal tapered interface has a relatively small effect for this system due to the modest BP molecular weight (low segregation strength regime), which leads to a comparable domain interface profile between the I-S and I-IS-S for short to moderate tapers. This behavior will change in the salt-doped materials of interest, poly(styrene-*b-oligo*-oxyethylene methacrylate (PS-POEM) doped with lithium triflate, as shown in the preliminary results in Figure 1b; however, the fitting procedure should remain nearly identical. Thus, these studies (published in *Macromolecules* 2016) provide a robust experimental/theoretical framework for the investigation of polymer electrolyte self-assembly. Further studies on the PS-POEM materials are currently in progress.

Fluids DFT calculations were performed to show density profiles and lamellar spacing as a function of segregation strength χN for 30%, 50%, and 70% normal and inverse tapered systems, using a Lennard-Jones potential cut off at a distance of 2.5σ (σ is the monomer diameter). As was seen in prior SCFT work, we found that 50% and 70% inverse tapered polymers have a relatively constant domain spacing as a function of χN due to competing effects of the polymers folding back and forth across the interface and also locally stretching with increasing segregation strength. In previous fDFT work, this trend also was found using a repulsive-only potential (cut off at $2^{1/6}\sigma$, such as in Ref. 1. Such shorter ranged potentials have been frequently used for more efficient calculations, especially in molecular dynamics (MD) simulations, and this generally leads to accurate results because, at a given density, the local liquid-like packing of monomers depends primarily on the repulsive part of the potential. However, when comparing fDFT to MD results, significantly better agreement was obtained by using the attractive potential, especially for inverse tapered systems. Because fDFT treats the interactions at the mean field level, its results for repulsive and attractive systems were relatively similar. The disagreement between fDFT and MD arises because the repulsive and attractive MD systems, compared based on a naive mapping of interaction parameter to χN, are quite different at strong segregation. This is because increasing the interaction parameter for the repulsive system, beyond some large value at which the monomers are barely overlapping, is ineffective in further increasing the segregation strength of the system. Additionally, the fDFT code Tramonto was updated to better treat longer chains, leading to the ability to perform calculations of N≈150 as shown in Figure 1a (these calculations also included the attractive potential).

Single-Ion Conducting Block Polymer Electrolytes for Tapering
Traditional block polymer electrolytes need lithium salts to be added to bestow conductivity to the system. In most of these systems, because the counter-ion is close in size to the lithium ion, both are able to diffuse across the electrolyte, which does not generate current. We also are designing and characterizing a single-ion block polymer electrolyte that can be incorporated into the taper geometry, in which the counter-ion is much larger than lithium ions; thus, the flow of ions across the electrolyte is heavily biased towards lithium ions. The productive ion motion can

Scheme 1. Synthetic scheme for the single-ion conducting block polymer electrolytes.
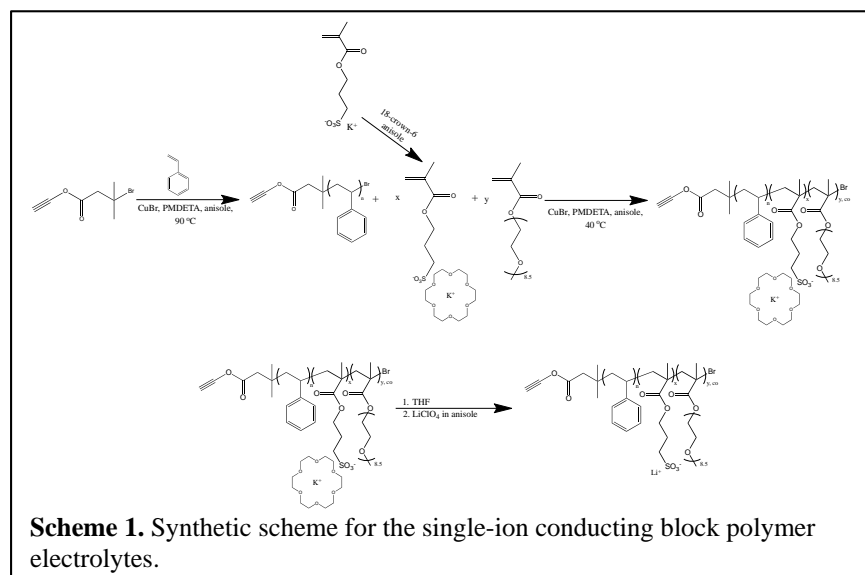
be quantified by the transference number.

The desired single-ion conducting monomers, 3-sulfopropyl methacrylate potassium salt [KSPM] have been incorporated into block polymers as shown in Scheme 1 (these monomer segments subsequently are converted to LiSPM). Tapering is controlled in these polymers through our well-established semi-batch (syringe-pump) method. These block polymers are able to assemble on nanometer length scales as indicated in Table 1.

We also are combining block polymer/homopolymer (A-B/A) blending with salt-doping to determine how homopolymer segregation within BP domains may influence the location of the enhanced mobility regions that are synergistic with Li$^+$ distributions. As shown in the Figure 3, in preliminary studies of PS-POEM blended with POEM, we have noted an increase in conductivity for LiTFSI, which segregates to the center of the domain, but not for lithium triflate, which spreads throughout the domain. Though these studies are preliminary, they provide rationale for the adaptation of Hall's

Table 1. Domain spacings of select PS-P(OEM-*co*-KSPM) BCPs.

	MW (g/mol)	f$_{PS}$	Doping ratio (EO:ion)	Domain spacing (nm)
PS-P(OEM-*stat*-KSPM)_6	30,000	.40	6:1	31
PS-P(OEM-*stat*-KSPM)_13	31,000	.39	13:1	31
PS-POEM	30,000	.40	13:1	48
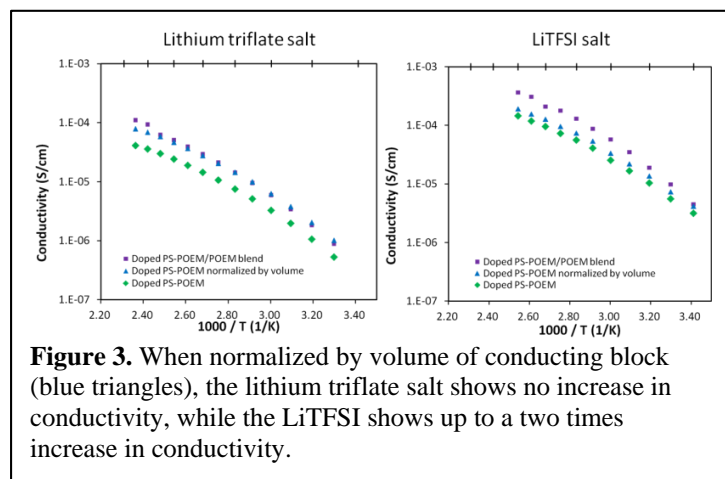
fDFT work to salt-doped materials as discussed below.

Obtaining accurate fDFT results for charged systems presents several challenges, especially in including the effects of ion aggregation/packing. Recent testing showed that the functionals used to treat correlations of ions that currently exist in Tramonto significantly underestimate the change in free energy that results

Figure 3. When normalized by volume of conducting block (blue triangles), the lithium triflate salt shows no increase in conductivity, while the LiTFSI shows up to a two times increase in conductivity.

from ion aggregation for the strongly charged systems of interest here. We are now using a new combination of fDFT and the polymer reference interaction site model (PRISM) theory. We

modeled AB diblock polymers of freely jointed chains of hard spheres, in which one of the A beads is charged, along with single bead counterions. PRISM calculations were performed on short A segments with a single charge, with the corresponding number of counterions, to generate correlation data for the fDFT calculations. The fDFT calculations then generate density profiles and free energies as a function of the whole chain connectivity, AB interaction parameter, ion solvation energy, and ionic strength and correlations. We predict that the effects of ion correlations lead to a significant change in the density profiles, as shown in Figure 4, and correspondingly this significantly alters phase behavior.
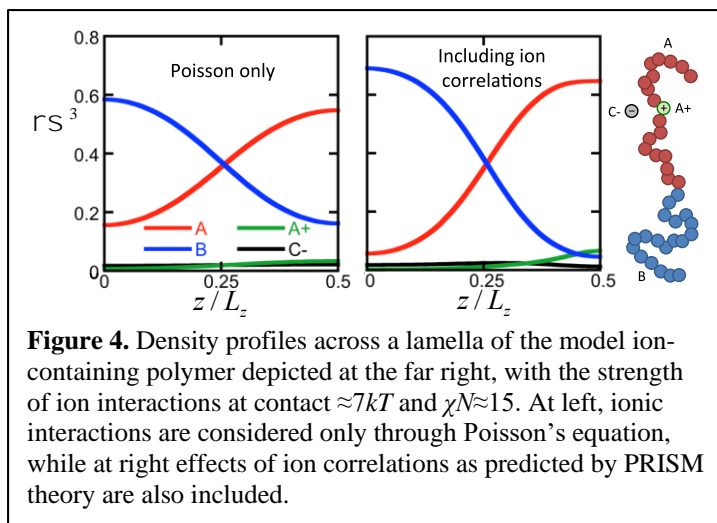

Figure 4. Density profiles across a lamella of the model ion-containing polymer depicted at the far right, with the strength of ion interactions at contact $\approx 7kT$ and $\chi N \approx 15$. At left, ionic interactions are considered only through Poisson's equation, while at right effects of ion correlations as predicted by PRISM theory are also included.

Future Plans

We plan to synthesize and characterize new tapered block copolymers with variations in molecular weight and taper profile and novel single-ion conducting tapered block copolymers in which the anion is tethered to the copolymer chain. The nanostructures and transport properties of these will be examined through X-ray scattering (SAXS, XRR), electron microscopy (TEM), neutron scattering (neutron reflectivity [NR]), differential scanning calorimetry (DSC), X-ray Photoelectron Spectroscopy (XPS with C_{60}^{+} sputtering), and impedance spectroscopy. Our recent results connecting XRR, DSC, and fDFT results in terms of density profiles establish the capability to gather quantitative insight regarding interfacial profiles in self-assembly of tapered systems and prepare us to consider geometries other than parallel lamellae. Also, we will use and validate a new combination of fDFT and PRISM theory, and compare to simulations and experiments. These methods are especially suited to systems where local monomer or ion packing is likely more important than for typical diblock copolymers, such as for tapered copolymers containing ions which we will study using this method, including adjusting the method after comparing with experimental data. Further, we will use the fDFT results to inform MD simulations of salt-doped tapered systems to probe salt transport in our materials.

References
1. Brown, J. R.; Seo, Y.; Hall, L. M. *The Journal of Chemical Physics* 2016 (144, 124904).

Publications
Brown, J. R.; Seo, Y.; Hall, L. M. *The Journal of Chemical Physics* **2016** (144, 124904) "Fluids Density Functional Theory and Initializing Molecular Dynamics Simulations of Block Copolymers"

Luo, M.; **Brown, J. R.;** Remy, R. A.; Scott, D. M.; Mackay, M. E.; **Hall, L. M.; Epps, T. H., III** *Macromolecules* **2016** (submitted) "Determination of Interfacial Mixing in Tapered Block Polymer Thin Films: Experimental and Theoretical Investigations"

Crystallization-driven assembly of conjugated-polymer-based nanostructures

Ryan C. Hayward, Department of Polymer Science & Engineering, University of Massachusetts Amherst

Program Scope

The goal of this project is to harness solution-state crystallization of conjugated polymers and small molecules to construct well-defined nanoscale building blocks that will facilitate fabrication of optoelectronic devices, especially photovoltaic cells, in scalable and cost-effective ways. We seek to ultimately control the organization, and therefore the electronic properties, of matter on length-scales spanning: (i) the molecular, to achieve highly crystalline semiconducting polymer-based materials capable of efficient charge transport, (ii) the nanoscale, to position electron donating and accepting materials with domain sizes comparable to exciton diffusion lengths (~ 10 nm) to facilitate charge separation, and (iii) the colloidal scale, such that well-defined crystalline nanoscale building blocks can be hierarchically organized into device layers with optimal structures.

Recent Progress

One major goal of our recent work has been to develop approaches to control nucleation, growth, and post-assembly modification of conjugated polymer nanowires. Notably, we have identified conditions under which supersaturated solutions of the p-type conjugated polymer poly(3-hexyl thiophene) (P3HT) remain kinetically stable over periods of several days, enabling the selective growth of oriented nanowires from surfaces that lower the energetic barrier to nucleation, in particular based on graphene [1]. Remarkably, the incorporation of up to ~ 20 mol % of hexyl thiophene comonomers bearing azido functionalities at the side-chain ends is found to have minimal effects on crystallization behavior or electronic properties of the polymers, thus allowing for post-assembly crosslinking and chemical modification of nanowires. We have exploited these copolymers to develop chemically and thermally robust nanowires that can be processed from high polarity "green" solvents such as alcohols and water [2].

A second theme has been the use of P3HT to control crystal morphology in blends with small molecule n-type semiconductors based on perylene diimide (PDI) derivatives. We previously reported on formation of 'shish-kebab' donor/acceptor nanocrystalline heterostructures consisting of a central PDI nanowire flanked by perpendicularly-oriented P3HT nanowires through a process of coupled crystal modification [3]. Very recently, we have found that globally aligned films of these heterostructures can be prepared through a simple capillary-assisted drop-casting method, providing a high degree of orientation of both PDI and P3HT phases. The resulting materials represent the first example of an 'orthogonal ambipolar semiconductor', i.e., showing directionally separated transport of electrons and holes, and open new opportunities in the design of organic electronic devices such as organic field effect transistors and nanowire sensors.
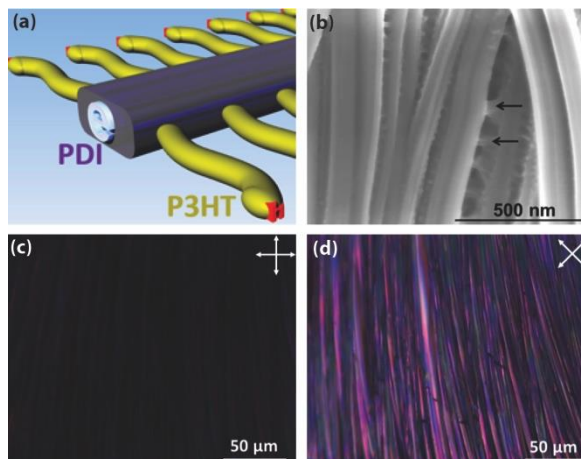

Figure 1. (a) Schematic illustration of P3HT/PDI hybrid shish-kebab structures; (b) Scanning electron micrograph of aligned shish-kebab films: arrows denote bundles of P3HT nanowires. (c-d) Polarized optical micrographs showing a high degree of orientation in aligned shish-kebab films.

Future Plans

Ongoing work and future plans include efforts to understand the influence of polymer molecular weight and regioregularity on surface-directed crystallization, alternative methods for alignment of shish-kebab heterostructures through flow-coating or magnetic fields, and the extension of each approach to other conjugated polymer systems with more attractive electronic properties.

References

[1] D.E. Acevedo-Cartagena, J. Zhu, E. Trabanino, E. Pentzer, T. Emrick, S.S. Nonnenmann, A.L. Briseno, R.C. Hayward, "Selective Nucleation of Poly(3-hexyl thiophene) Nanofibers on Multilayer Graphene Substrates" *ACS Macro Letters*, **4**, 483-487 (2015) DOI: 10.1021/acsmacrolett.5b00038

[2] H.J. Kim, M. Skinner, A.L. Briseno, T. Emrick, B.J. Kim, R.C. Hayward, "Water Processable Polythiophene Nanowires by Photo-crosslinking and Click-functionalization", *Nano Letters*, **15**, 5689-5695 (2015). DOI: 10.1021/acs.nanolett.5b01185

[3] L. Bu, E. Pentzer, F.A. Bokel, T. Emrick, R.C. Hayward, "Growth of poly(3-hexyl thiophene)/perylene tetracarboxydiimide donor/acceptor shish-kebab nanostructures by coupled crystal modification", *ACS Nano*, **6**,10924-10929 (2012).

Publications

H.J. Kim, M. Skinner, A.L. Briseno, T. Emrick, B.J. Kim, R.C. Hayward, "Water Processable Polythiophene Nanowires by Photo-crosslinking and Click-functionalization", *Nano Letters*, **15**, 5689-5695 (2015). DOI: 10.1021/acs.nanolett.5b01185

D.E. Acevedo-Cartagena, J. Zhu, E. Trabanino, E. Pentzer, T. Emrick, S.S. Nonnenmann, A.L. Briseno, R.C. Hayward, "Selective Nucleation of Poly(3-hexyl thiophene) Nanofibers on Multilayer Graphene Substrates" *ACS Macro Letters*, **4**, 483-487 (2015) DOI: 10.1021/acsmacrolett.5b00038

L. Bu, T.J. Dawson, R.C. Hayward, "Tailoring Ultrasound-Induced Growth of Perylene Diimide Nanowire Crystals from Solution by Modification with Poly(3-hexyl thiophene)", *ACS Nano*, **9**, 1878-1885 (2015) DOI: 10.1021/nn506795q

B.A.G. Hammer, M.A. Reyes-Martinez, F.A. Bokel, F. Liu, T.P. Russell, A.L. Briseno, R.C. Hayward, T. Emrick, "Robust Polythiophene Nanowires Cross-linked with Functional Fullerenes", *Journal of Materials Chemistry C*, **2**, 9674-9682 (2014). DOI: 10.1039/C4TC01898B

B.A.G. Hammer, M.A. Reyes-Martinez , F.K. Bokel , F. Liu , T.P. Russell , R.C. Hayward , A.L. Briseno , and T. Emrick, "Reversible, Self Cross-linking Nanowires from Thiol-Functionalized Polythiophene Diblock Copolymers", *ACS Applied Materials and Interfaces*, **6**, 7705-7711 (2014). DOI: 10.1021/am500976w

Project Title: **Relationships between the chemistry and physical interaction forces (adhesion, friction & lubrication) between closely apposed surfaces in liquids** (DOE Award number: DE-FG02-87ER 45331)

Jacob Israelachvili, Dept Chemical Engineering, Materials Department, and Materials Research Laboratory (MRL), University of California (UCSB), Santa Barbara, CA 93106.

Program Scope

1. Measure and characterize complex dynamic molecular interactions by continuing to apply and develop new experimental techniques to gain fundamental under-standings of the adhesion, friction, lubrication and particularly the initiation of wear (damage/failure) to

Fig. 1. (**A**) Adhesion and friction forces and wear mechanisms between "real" (rough or textured) surfaces as opposed to "ideal" molecularly smooth surfaces are being measured over 7 orders of magnitude of length and time (rate) scales, including (**B**) simultaneous visualization, control and measurement of electro-chemical reactions.

surfaces of engineering interest, that is, rough or micro-nano structured surfaces, and investigate the dynamics, i.e., the roles of rate and time, on these often non-equilibrium interactions (Fig. 1A).

2. Correlating chemistry with (physical) interaction forces by further developing and applying new experimental techniques for measuring the above interactions while *simultaneously* measuring and controlling the voltages and currents between or flowing through the solid-liquid interfaces to establish the (electro)chemical, e.g., dissolution and corrosion, reactions occurring at the interface (Fig. 1B).
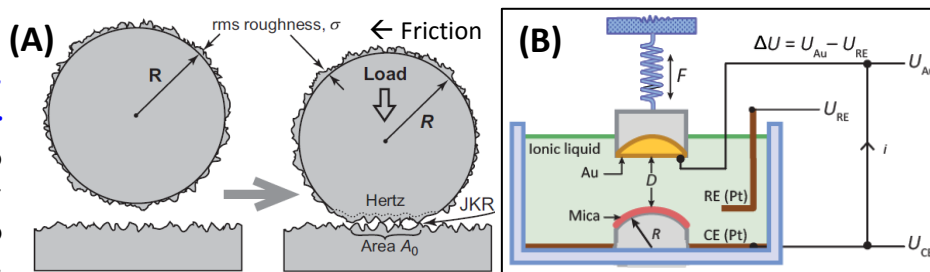
Recent Progress

Instrumental developments: new experimental techniques and applications

(1) Miniature SFA (Figs 2, ref. 1): A miniature "multimodal SFA" was developed (Fig. 2 left) and successfully tested that can be mounted on a microscope stage and perform force measurements simultaneously with *in situ* electro-chemical and spectroscopic studies, e.g., fluorescence (FL-SFA), dielectric, SPR, IR and X-ray imaging, as well as both top and bottom confocal imaging requiring large objectives. Figure 2 (right) shows our first use of the new FL-SFA in a fluorescence study of the interactions of organic and inorganic species, with simult-aneous imaging of their heterogeneous surfaces, e.g., with particles or microphase separated domains.
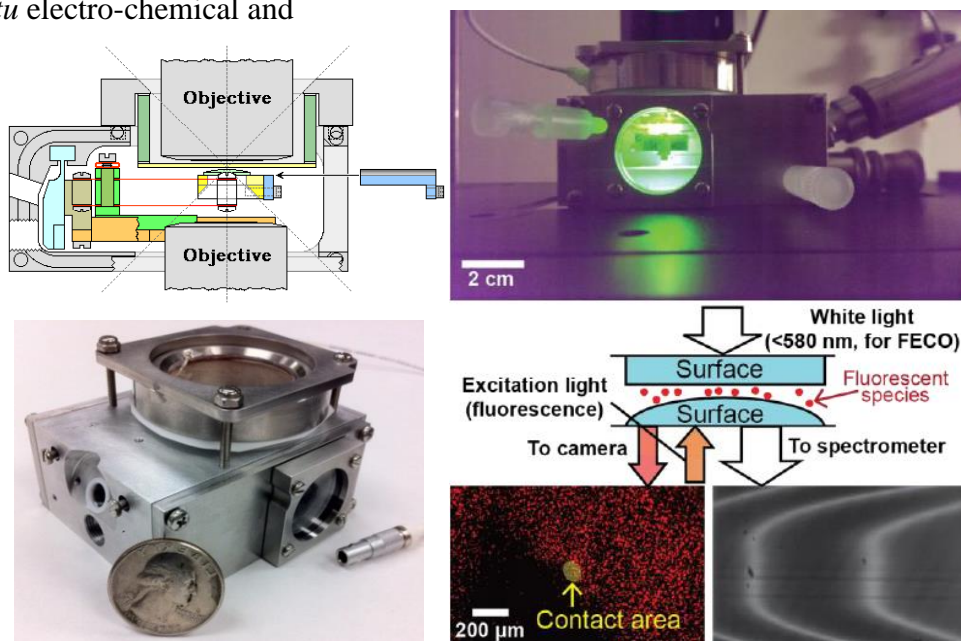

Fig. 2. Left: Schematic and photo of the new mini-multimodal SFA. Right: FL-SFA.

168

(2) *High-speed / high time-resolution friction attachment to the SFA (Fig. 3, ref. 2):*
The SFA 2000 with rotating disk lower surface attachment. Modifications will be made to allow for higher speeds, sensing friction forces in any lateral direction, and at very high time resolution. This attachment is being used in measurements of highly dynamic adhesion and friction forces, as described in some of the following projects.
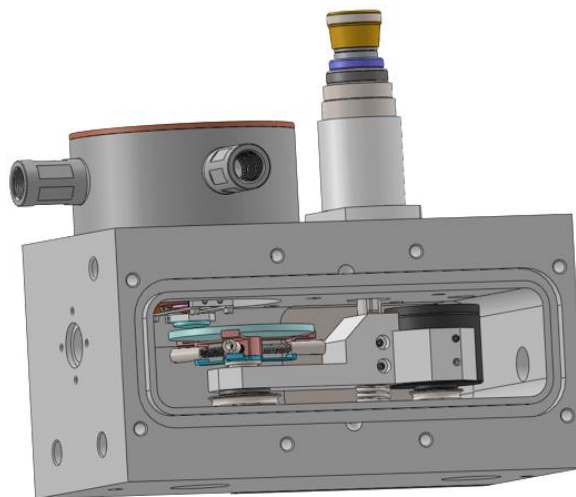
Fig. 3. SFA 2000 with new high speed rotating disk allowing for sliding speeds up to 15 m/s, and detecting friction 'transients, such as stick-slip and stiction spikes at high 0.1 ms resolution.

Mechanisms of surface wear during adhesion, friction and non-contact lubrication processes
(3) *Relationship between stick-slip ('intermittent') adhesion/detachment, frictional sliding, and surface damage/wear/failure mechanisms (Fig. 4, ref. 3):* Figure 4 shows various types of adhesion and friction measurements that give rise to 'intermittent' motion, e.g., regular, irregular or random
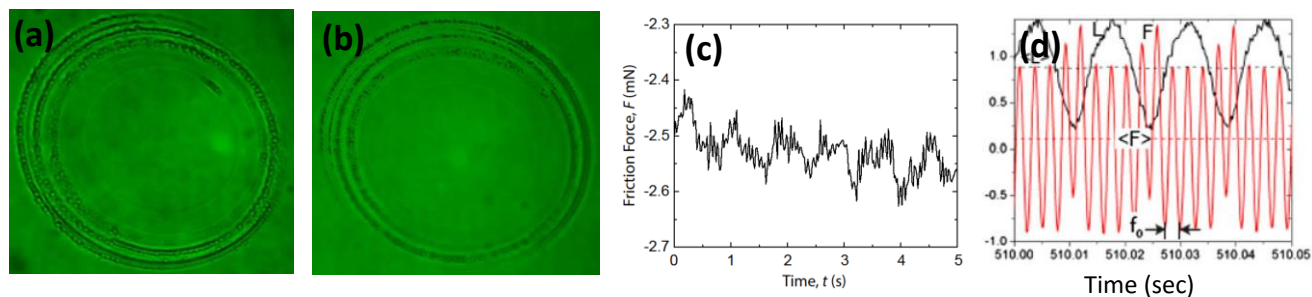

Fig. 4. (a, b) Mica surface (left) and polystyrene surface (right) after a smooth clean mica surface and a spherical smooth but viscoelastic PS surface were brought into contact and separated at a given separation rate. Stick-slip detachment was observed that involved material transfer of PS to the mica, leaving concentric rings on the mica (a) and complementary concentric depressions on the PS surface (b). **(c)** Stick-slip friction trace of a complex (multicomponent) lubricating oil sliding on a polymer surface showing two superimposed stick-slip 'spectra': low frequency, ~1.2 Hz, and high frequency, ~15 Hz. **(d)** High frequency friction-induced mechanical vibrations in a high speed (~15 m/s, 45 rpm) lubricated system. Note that these frictional responses (vibrations) are at the resonance frequency of the instrument (345 Hz), and are sinusoidal in shape which is quite different from the sawtooth 'spikes' characteristic of stick-slip friction.

stick-slip motion, or sinusoidal oscillations (vibrations). Each of these non-steady motions eventually cause surface damage: wear tracks, failure cracks, brittle or ductile behavior, or electrochemical corrosion or dissolution – described further below.

(4) *Corrosion damage (Fig. 5, ref. 4):* Using interference (FECO) and optical microscopy in an electrochemical (EC)-SFA we studied in real time the evolution of 'crevice' and 'pitting' corrosion of confined 30 nm thick Ni metal layers on mica substrates in sodium chloride (NaCl)
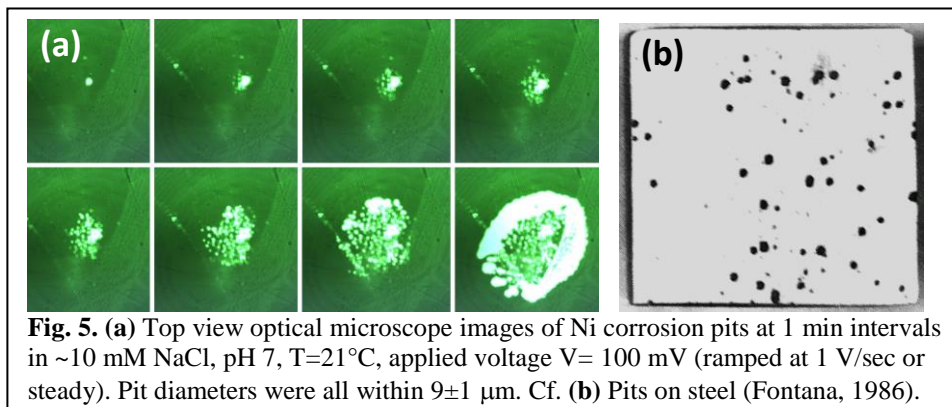

Fig. 5. (a) Top view optical microscope images of Ni corrosion pits at 1 min intervals in ~10 mM NaCl, pH 7, T=21°C, applied voltage V= 100 mV (ramped at 1 V/sec or steady). Pit diameters were all within 9±1 μm. Cf. **(b)** Pits on steel (Fontana, 1986).

solutions under different applied voltages, NaCl concentrations, and amounts of dissolved oxygen (a known enhancer of corrosion rates). Corrosion was initiated as preferential and self-catalyzed 'pitting corrosion' (inhomogeneous localized dissolution with the rapid formation of pits) inside the confined zone (Fig. 5A), and proceeded to develop differently inside and at the rim of the contact area, forming pits of surprisingly uniform diameter, 8-10 μm, and depth, ~10 nm (Fig. 5B, 5C). Our results reveal new highly detailed micro- and nano-scale insights into the initial corrosion mechanism for confined metal surfaces.

Fig. 5C

(5) *Cavitation damage (Fig. 6, ref. 5):*
It is well known that separating two surfaces rapidly in a liquid can cause cavitation, and that the explosive expansion of the bubble, as well as its equally explosive collapse onto a surface, can cause damage. Here we find that rapid vibration can cause surface damage even when surfaces are well separated in 3 of the 4 liquids studied, including water. Figure 6 shows FECO fringes of two curved mica surfaces of radius ~2 cm at a separation of ~400 nm under (A) static conditions, (B) as they are vibrated normally (amplitude ~10 nm, frequency f = 6.5 kHz) with no observable damage (but a strong offset, i.e., non-oscillatory, repulsion), and (C) after the frequency is increased to f = 8.5 kHz when spontaneous damage occurs, as can be readily seen both in the FECO fringes as well as under a normal optical microscope.
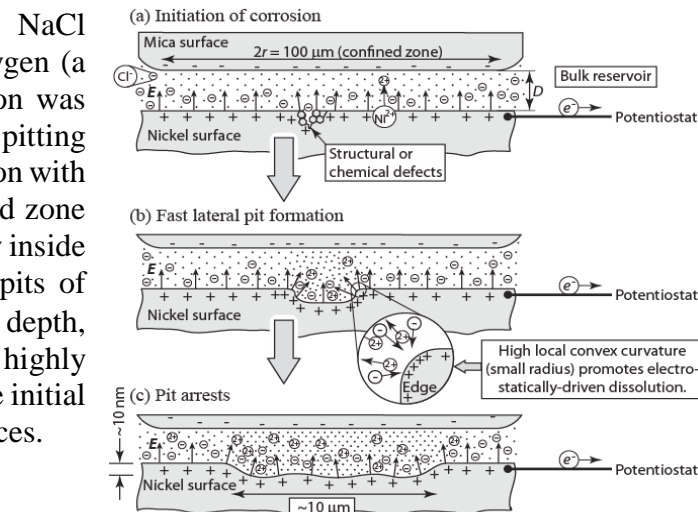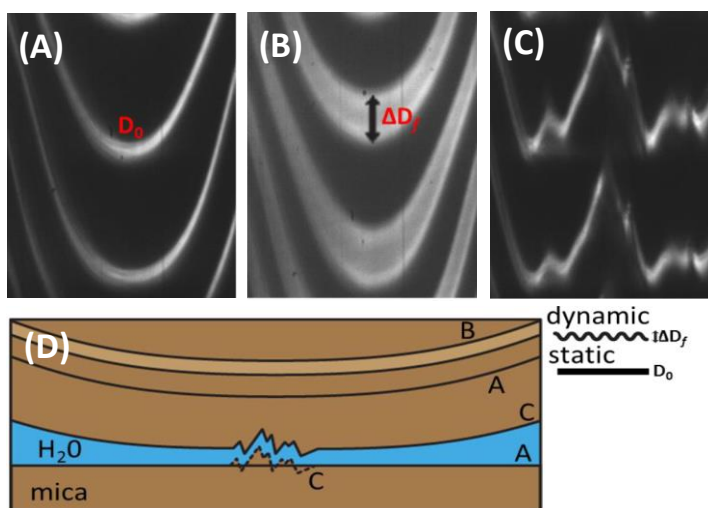

Fig. 6. **(A)** FECO fringes of undamaged surfaces ~10 nm apart; **(B)** still undamaged surfaces undergoing vibrations at $f \approx 6.5$ kHz; **(C)** damaged surfaces on increasing f to 8.5 kHz; **(D)** Schematics of **(A)-(C)**.

Studies with the Electrochemical SFA (EC-SFA): New insights into the molecular mechanisms of electrochemical reactions at solid-liquid-solid interfaces

(6) *Static and dynamic electronic properties of non-aqueous liquids ionic liquids (Fig. 7, ref. 6):* In this review article we seek to identify areas of consensus and contention regarding long-range surface forces in ionic liquids, and explore the mechanism of these forces. it is now clear that long-range surface forces are present for several ionic liquid/surface combinations, and that these exponential forces decay both with distance and temperature consistent with the predictions of the Poisson-Boltzmann equation for the 'double-layer' forces due to a dilute concentration of dissociated, i.e., 'free', rather than bound ions. Therefore, the majority of the ions are bound in ion pairs and do not contribute to the long-range double-layer forces. By analogy, water may be thought of as an ionic liquid in which 1 in 10^7 molecules are
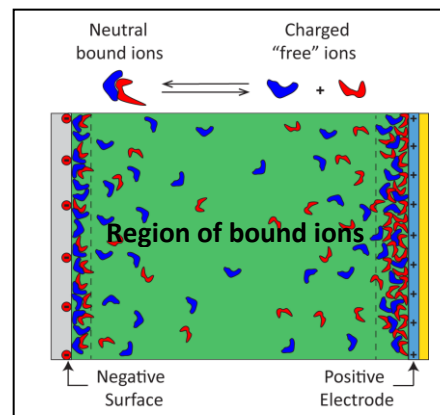

Fig. 7. Likely ionic distributions in ILs.

dissociated as H^+ and OH^- ions (pH 7), while the others are bound in the (highly polar) H_2O molecule. In the IL systems we have studied, less than 0.1% of the ions are 'free' to conduct, and therefore contribute to energy storage. We have also developed a model that quantitatively predicts the fraction of free and bound ions at any given temperature.

(7) ***Chemical Mechanical Polishing (CMP), cement hardening and related processes such as Pressure Solution in the morphogenesis of (geologic) rocks (Al-O-Si):*** Our current work has confirmed our earlier results showing that many polishing, contact reactions (e.g., Al-O-Al), and dissolution processes are not due to frictional abrasion or pressure, but to electrochemical reactions that depend on the close proximity, but not contact, of the interacting surfaces in the solution.

Future & Ongoing Plans (in addition to the above 7 sub-projects*)

♦ New metal and inorganic surfaces are being developed, of controlled isomorphism and roughness, including titania, calcite, alumina (sapphire) and silica, for nano-scale physico-chemical studies with the SFA and other techniques. *For example, this is also a continuation of project (7) above.

♦ Work is continuing on the dependence of surface forces (adhesion, stick-slip friction, wear, etc.) on changes in the structure (deformations, dissolution, corrosion, cavitation damage) of surfaces.

♦ Work on the spreading *liquids* on surfaces that give rise to deformations of initially smooth viscoelastic surfaces is also in progress.

♦ Work is continuing to investigate the molecular physico-chemical mechanisms of rehealing (self-healing) materials/surfaces that can regain their original mechanical properties (strength, toughness) after undergoing plastic deformations or failure.

References

1. **Real-time imaging and force-measurements to determine the interactions of gold nanoparticles and biomembranes.** Nicholas Cadirov, Kai Kristiansen, Zachariah Berkson, Stephen Donaldson, Jacob N. Israelachvili. *In preparation for Nature Communications*.
2. Manuscript in preparation: Tom Cristiani, et al………………..
3. **Adhesion and Detachment Mechanisms between Polymer and Solid Substrate Surfaces: Using Polystyrene-Mica as a Model System.** Hongbo Zeng, Jun Huang, Yu Tian, Lin Li, Matthew Tirrell, Jacob Israelachvili. Submitted to *Macromolecules*.
4. **Simultaneous interferometry and microscopy reveal unexpected Nickel corrosion dynamics in confined geometry**. Markus Valtiner, Claudia Merola, Hsiu-Wei Cheng, Kai Kristiansen, Howard Dobbs, Jacob Israelachvili, and Ying-Ju Chen. Submitted to the *Journal of the Electrochemical Society* (Corrosion Science and Technology section).
5. **Vibration-induced wear and damage of confined lubricant environments between mica surfaces.** Steven H. Donaldson, Howard A. Dobbs, Kai Kristiansen, Derek Chan, Jacob N. Israelachvili. *In preparation for Wear.*
6. **Long range surface forces across ionic liquids: controversies and opportunities.** Matthew A. Gebbie, Nicklas Hjalmarsson, Alexander M. Smith, Hua Li, Howard A. Dobbs, Alpha A. Lee, Xavier Banquy, Markus Valtiner, Gregory G. Warr, Jacob N. Israelachvili, Mark W. Rutland Susan Perkin, Rob Atkin. **Feature Article** for *Chemical Communications* (submission date: July 2016).
7. **Enhancing epoxy network toughness and reversibility with mussel-inspired catechol-Fe crosslinks.** Thomas Cristiani, Emmanouela Filippidi, Sungbaek Seo, Alessia Pallaoro, Neil Dolinski, Megan Valentine, Martin Moscovits, Herbert Waite, Jacob Israelachvili. In preparation for *Nature Materials*.

Publications supported by BES (2 years: mid 2014 – mid 2016)

1. **Surface-initiated self-healing of polymers in aqueous media.** B. Kollbe Ahn, Dong Woog Lee, Jacob Israelachvili, J. Herbert Waite. *Nature Materials* (2014) **13,** 862-872.

2. **Influence of molecular dipole orientations on long-range exponential interaction forces at hydrophobic contacts in aqueous solutions.** Kristiansen, Kai; Stock, Philipp; Baimpos, Theodoros; Raman, Sangeetha; Harada, Jaye; Israelachvili, Jacob; Valtiner, Markus. *ACS Nano* (2014) **8** (10) 10870-10877. PMID: 25289697.

3. **Contact time- and pH- dependent adhesion and cohesion of chitosan oligosaccharide coated surfaces.** Chanoong Lim; Dong Woog Lee; Jacob N. Israelachvili; YongSeok Jho; Dong Soo Hwang, *Carbohydrate Polymer* (2014) **117** 887-894.

4. **Stick-slip Friction of Gecko-Mimetic Flaps on Smooth and Rough Surfaces.** Saurabh Das, Nicholas Cadirov, Sathya Chary, Yair Kaufman, Jack Hogan, Kimberly L. Turner, and Jacob N. Israelachvili. *J. Roy. Soc. Interfaces* (2014) 12, 20141346.

5. **Simultaneous Measurements of Molecular Forces and Optical Properties of a Confined 5CB Liquid Crystal Film using a Surface Forces Apparatus (SFA).** Kai Kristiansen, Hongbo Zeng, Bruno Zappone, Jacob Israelachvili. *Langmuir* (2015) 31 (13), 3965–3972.

6. **Real time monitoring of aluminium crevice corrosion and its inhibition by vanadates with multiple beam interferometry in a surface forces apparatus.** Buddha Ratna Shrestha, Qingyun Hu, Theodoros Baimpos, Kai Kristiansen, Jacob Israelachvili, Markus Valtiner. *J. Electrochem. Soc.* (2015) 162 (7) C327-C332 (2015).

7. **Real time intermembrane force measurements and imaging of lipid domain morphology during hemifusion.** Dong Woog Lee, Kai Kristiansen, Stephen H. Donaldson, Jr., Nicholas Cadirov, Xavier Banquy, Jacob N. Israelachvili. *Nature Communications* (2015) 6, 7238, 1-8.

8. **Long-range electrostatic screening in ionic liquids.** Matthew A. Gebbie, Howard A. Dobbs, Markus Valtiner, Jacob N. Israelachvili. PNAS (2015) 112 (24) 7432–7437. PMID: 26040001.

9. **Adhesion and Detachment Mechanisms between Polymer and Solid Substrate Surfaces: Using Polystyrene-Mica as a Model System.** Hongbo Zeng, Jun Huang, Yu Tian, Lin Li, Matthew Tirrell, Jacob Israelachvili. Submitted to *Macromolecules* (2016).

10. **Simultaneous interferometry and microscopy reveal unexpected Nickel corrosion dynamics in confined geometry**. Markus Valtiner, Claudia Merola, Hsiu-Wei Cheng, Kai Kristiansen, Howard Dobbs, Jacob Israelachvili, and Ying-Ju Chen. Submitted to the *Journal of the Electrochemical Society* (*JEST* – Corrosion Science and Technology section).

Fundamental Studies of Charge Transfer in Nanoscale Heterostructures of Earth-Abundant Semiconductors for Solar Energy Conversion

Song Jin, John C. Wright, and Robert J. Hamers
Department of Chemistry, University of Wisconsin-Madison, Madison, Wisconsin 53706
(jin@chem.wisc.edu, wright@chem.wisc.edu, rjhamers@wisc.edu)

Program Scope

We create new earth-abundant semiconductor nanostructures of two families of materials, layered metal chalcogenides (MX_2) and lead halide perovskites, and their heterojunctions with well-defined chemistry and develop new coherent multidimensional spectroscopies and atomic force microscopy integrated with ultrafast spectroscopy that probe charge transport at the quantum mechanical level in nanoscale heterostructures. They provide the fundamental understanding required to enable transformative solar energy nanotechnologies.

Recent Progress

1. Growth of layer-controlled 2D MX_2 heterostructures via van der Waals epitaxy.

We have developed CVD growth of vertical heterostructures of 2D MX_2 materials by taking advantage of the van der Waals (vdW) epitaxy between different 2D layers. MoS_2, WS_2, and WSe_2 layers were grown uniformly onto microplates of SnS_2 (Fig. 1), TaS_2 and graphene, under mild CVD reaction conditions (< 500 ℃) using metal chloride and S(Se) precursors. SnS_2 is a less studied MX_2 semiconductor (band gap 2.1 eV) with similar layered structure. Large (>10 µm in width) single-crystal SnS_2 plates with a thickness of hundreds of nanometers and well-defined hexagonal shapes and smooth surfaces can be conveniently grown by sulfidizing fluorine-doped tin oxide (FTO) coated glass substrates or by CVD (Fig. 1A). Raman spectroscopy, transmission electron microscopy (TEM), and scanning transmission electron microscopy (STEM) with elemental mapping (Fig. 1B) confirmed that the respective MX_2 layers selectively and uniformly coat the basal planes of SnS_2 microplates. We have unequivocally characterized the heteroepitaxy by resolving the large-area Moiré patterns in TEM (Fig. 1D), which are the consequence of the lattice mismatch between different MX_2. Heteroepitaxy with such large mismatch of lattice constants (15% for MoS_2, 16% for WS_2, and 11% for WSe_2) is possible because the 2D layer structures have only weak vdW inter-layer interactions and thus
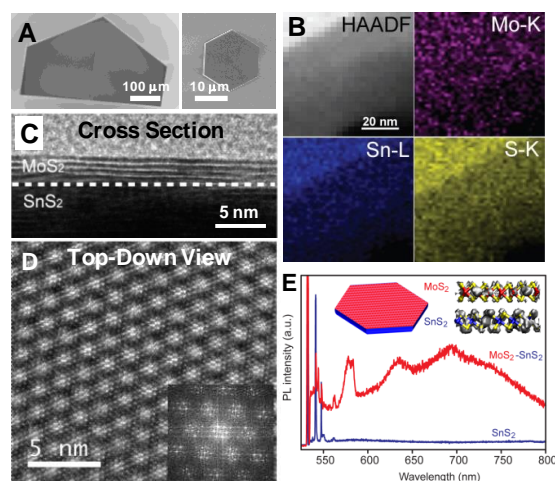

Fig. 1. Vertical (layer-by-layer) MX_2 heterostructructures. (A) SEM and (B) STEM elemental mapping of MoS_2 on SnS_2 plates; (C) Cross section and (D) top-down HRTEM and the FFT showing the Moiré fringes; (E) PL spectra and charge separation across the heterointerface (inset).

minimal strain. Furthermore, we have observed new photoluminescence (PL) peak at 578 nm in heterostructures of MoS$_2$-SnS$_2$ (Fig. 1). Electronic structure calculations showed that the new PL features arise from electronic coupling and charge separation between MoS$_2$ and SnS$_2$ layers. Our early synthesis yielded heterostructures of a few layers of MX$_2$; we have since refined the growth procedures so that we can now controllably grow mono-, bi-, tri-, or a few layers of MoS$_2$ on SnS$_2$, as verified by Raman and PL spectroscopy and cross-sectional TEM (data not shown). We are achieving a similar level of layer-controlled growth of MoSe$_2$ on SnSe$_2$. These results showed that we can exploit vdW epitaxy to realize novel 2D heterostructures. Intrinsically scalable CVD methods create structures that are important for future spectroscopic studies and device applications because manual mechanical transfer and stacking does not create epitaxic heterostructures. These MX$_2$ heterostructures will be studied as the model systems using CDMS for resolving quantum state dynamics and study the charge transfer at heterojunctions.

2. Controlled crystal growth of single-crystal lead halide perovskite nanostructures

Amidst the surging interest and the exciting progress in solar cells based on hybrid organic-inorganic lead halide perovskites, improved understanding and better control of the crystal growth of these materials and fundamental understanding of their photophysical properties could further boost their solar performance. We found that their formation can involve different pathways of either a conversion reaction at low precursor concentration or dissolution-recrystallization at high precursor concentration (Fig. 2B). We discovered a simple solution growth of single-crystal nanowires (NWs), nanorods, and nanoplates of MAPbI$_3$ (Fig. 2C-E) and other perovskites *via* the dissolution-recrystallization pathway by carefully tuning the supersaturation of crystal growth.

Fig. 2. (A) Crystal structure of perovskites. (B) Two growth pathways for MAPbI$_3$ formation in solution. (C-E) SEM images of single-crystal NWs and nanoplates of MAPbI$_3$ perovskite we grew from solution. (F) Emission spectra and (G) optical images of MAPbI$_3$ NWs photoexcited by increasing power demonstrating stimulated light emission (lasing), (H) time-resolved PL spectra of the MAPbI$_3$ NWs.

The remarkable performance of lead halide perovskites in solar cells can be attributed to the long carrier lifetimes and low non-radiative recombination rates, the same physical properties that are ideal for semiconductor lasers and other applications beyond photonics. In collaboration with Prof. Xiaoyang Zhu at Columbia University, we further demonstrated room temperature and wavelength tunable lasing from single crystal lead halide perovskite NWs (Fig. 2F,G) with low lasing thresholds, and high lasing quality factors, and near unity quantum yield. We have further
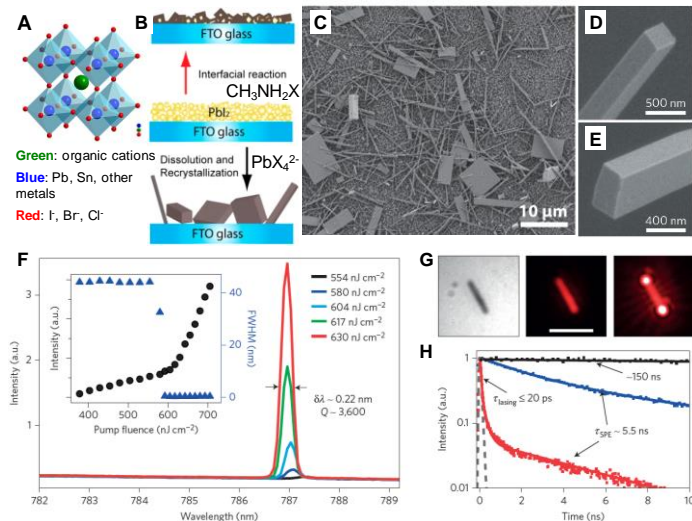
expanded the family of NWs to formamidinium lead halides (FAPbX$_3$) and all-inorganic cesium lead halides (CsPbX$_3$) and greatly enhanced the robustness of the lasing. Such record-setting lasing performance, coupled with facile solution growth of single-crystal nanowires and broad tunability of emission color from 420 nm to 824 nm using different perovskite stoichiometry, makes lead halide perovskites ideal materials for the development of nano-photonics and optoelectronic devices (such as LEDs), in parallel with the rapid development in photovoltaic technology from the same materials. This facile solution growth of single-crystal nanostructures of the diverse families of perovskite materials with different cations, anions, and dimensionality and different properties will enable many interesting device applications with high performance.

3. Coherent Multidimensional Spectroscopy (CMDS) of nanomaterials and heterostructures.

Our CMDS work includes development of new methods and applications for the materials described earlier. Light scattering interference was eliminated by dual chopping while temporal modulation between the scatter and signal was addressed by fibrillation of the delay times. The CMDS dimensionality was expanded to excitation fluence, coherence dephasing rate, and population lifetime to define many body effects. The multidimensional data set was visualized with movies that displayed 3D relationships. To maximize instrumental throughput, we automated the control of the motors controlling the frequency scanning of the optical parametric amplifiers (OPAs) and the compensation optics. We also integrated on-line fitting of multidimensional spectra of the OPA frequency dependence on the control motors in order to automate spectral calibration and eliminate artifacts introduced into the spectroscopy. The system now allows queuing so experiments can be performed continuously and controlled remotely.

CMDS methods characterized the four classes of materials described earlier: perovskites, dichalcogenides, hematite, and quantum dots. 2D spectra of MoS$_2$ showed a strong diagonal spectrum for delay times where fully coherent pathways drove coherences between excitonic and continuum states and a probe pulse excited an output coherence from the same states. No population relaxation occurred. A cross-peak also appeared between the A and B excitons because of the direct coupling between the states that was enforced by their common valence band state. Together, they form a multidimensional signature of MoS$_2$ quantum states. The 2D spectra changed completely for delay times with partially coherent pathways with intermediate populations. The spectra along the excitation dimension followed the absorption spectrum while the spectrum along the output coherence dimension showed just the A and B excitons. The complete set of data resolved the intra- and interband population relaxation dynamics and the rapid coherent dephasing dynamics. Population relaxation could be resolved by 2D spectra of the population lifetime dependence on excitation and output coherences. Similar work on hematite resolved the ultrafast coherent and incoherent dynamics of the charge carriers. Particularly interesting was the observation of spectral diffusion as excitation into higher k-vectors in the Brillouin zone relaxed to the band edge.

Our earlier work on PbSe quantum dots was expanded to include experiments where 2D transient absorption and transient grating where performed simultaneously so the two methods

could be related. Transient absorption depends only on the imaginary part of the third order susceptibility while transient grating depends on the real and imaginary parts. A 2D Kramers-Kronig transform of the transient absorption allowed a prediction of the real part of the susceptibility and therefore the transient grating spectra. Subtraction of the predicted and actual transient grating spectra revealed a broad spectral feature that was not in the transient absorption feature because this new feature had a strong and real nonlinear susceptibility.

Three types of spectroscopy were performed on thin film perovskites- CMDS, transient absorption, and transient fluorescence spectroscopy. The CMDS and transient absorption experiments defined the intra- and interband population relaxation dynamics as well as the coherent dephasing dynamics. It also revealed that the new feature observed at 480 nm was a second interband transition at a different point in the Brillouin zone. The transient fluorescence experiments were done at different fluences and rep rates. The transients at different fluences defined the rates but did not define the processes. The transients at different rep rates resulted in photodoping that changed the steady state concentration of different charge species and dynamical processes. A global analysis then defined the complete set of charge dynamics including geminate pair dissociation, exciton formation and dissociation, recombination, trapping and detrapping, Auger relaxation, and stimulated emission rates. The data and the fitted transients shown in the figure show the excellent agreement with theory.

Future Plans

We will continue developing synthetic methods for

Fig. 3. Experimental and theoretical fluorescence transients at eight different fluences and two repetition rates.

MX2 heterostructures and new chemistry to control the electronic structure and properties of 2D nanosheets, including ligand modifications. We are working on synthesizing new nanostructures of diverse lead halide perovskites and their nanostructures to study their photophysical properties and exploit potential applications. We will expand CMDS experiments to develop three-color, fully coherent experiments that can create multidimensional spectral signatures. The signatures are key to developing pump-CMDS probe experiments that have the selectivity required to distinguish components within the heterostructures and provide quantum state resolved charge dynamics over the multiple materials forming the heterostructures. Performing a global analysis of experiments with different fluences and rep rates will allow a complete analysis of the population and coherent dynamics of heterostructures on both ultrafast and long time scales.
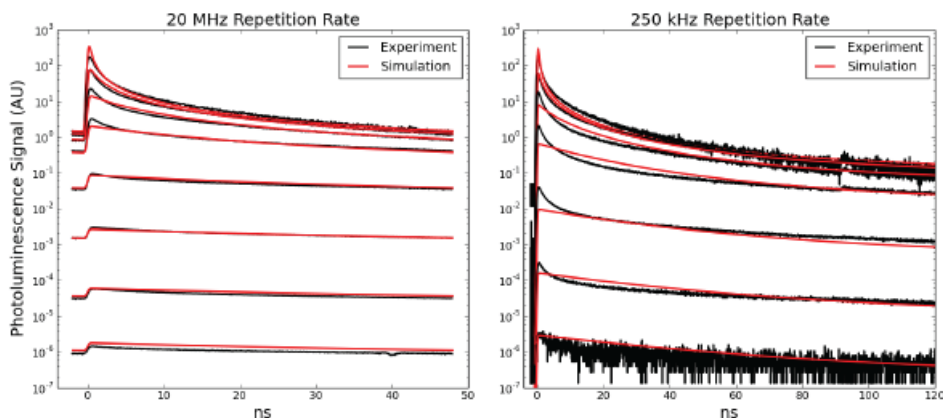
References (see the next section)

Publications

1. Zhang, X.; Meng, F.; Christianson, J. R.; Arroyo-Torres, C.; Lukowski, M. A.; Liang, D.; Schmidt, J. R.; Jin, S.; "Vertical Heterostructures of Layered Metal Chalcogenides by van der Waals Epitaxy" *Nano Letters* **2014**, *14*, 3047-3054. **DOI:** *10.1021/nl501000k.*

2. Faber, M. S.; Lukowski, M. A.; Ding, Q.; Kaiser, N. S.; Jin, S.; "Earth-Abundant Metal Pyrites (FeS$_2$, CoS$_2$, NiS$_2$, and Their Alloys) for Highly Efficient Hydrogen Evolution and Polysulfide Reduction Electrocatalysis" *J. Phys. Chem. C* **2014**, *118,* 21347–21356. **DOI:** 10.1021/jp506288w.

3. Faber, M. S.; Jin, S.; "Earth-Abundant Inorganic Electrocatalysts and Their Nanostructures for Energy Conversion Applications" *Energy Environ. Sci.,* **2014**, *7*, 3519-3542. **DOI:** 10.1039/C4EE01760A. (This is an invited Feature review)

4.* Cabán-Acevedo, M.; Kaiser, N. S.; English, C. R.; Liang, D.; Thompson, B. J.; Chen, H.-E.; Czech, K. J.; Wright, J.C.; Hamers, R. J.; Jin, S.; "Ionization of High-Density Deep Donor Defect States Explains the Low Photovoltage of Iron Pyrite Single Crystals" *J. Am. Chem. Soc.* **2014**, *136*, 17163-17179. DOI: 10.1021/ja509142w.

5.* Samad, L.; Cabán-Acevedo, M.; Shearer, M. J.; Park, K.; Hamers, R. J.; Jin, S.; "Direct Chemical Vapor Deposition Synthesis of Phase-Pure Iron Pyrite (FeS$_2$) Thin Films" *Chem. Mater.* **2015**, *27,* 3108–3114. **DOI:** 10.1021/acs.chemmater.5b00664.

6. Zhu, H.;[†] Fu, Y.;[†] Meng, F.; Wu, X.; Gong, Z.; Ding, Q.; Gustafsson, M. V.; Trinh, M. T.; Jin, S.; Zhu, X.-Y. Lead halide perovskite nanowire lasers with low lasing thresholds and high quality factors, *Nature Materials* **2015**, *14*, 636-642. DOI:10.1038/nmat4271. ([†] equally contributing first authors. Both Jin and Zhu are corresponding authors).

7. Fu, Y.; Meng, F.; Rowley, M. B.; Thompson, B. J.; Shearer, M. J.; Ma, D.; Hamers, R. J.; Wright, J. C.; Jin, S. "Solution Growth of Single Crystal Methylammonium Lead Halide Perovskite Nanostructures for Optoelectronic and Photovoltaic Applications" *J. Am. Chem. Soc.* **2015**, *137*, 5850-5818. DOI: 10.1021/jacs.5b02651.

8. Ding, Q.; Zhai, J.; Cabán-Acevedo, M.; Shearer, M. J.; Li, L.; Chang, H.-C.; Tsai, M.-L.; Ma, D.; Zhang, X.; Hamers, R. J.; He, J.-H.; Jin, S.; "Designing Efficient Solar-Driven Hydrogen Evolution Photocathodes Using Semi-Transparent MoQ$_x$Cl$_y$ (Q=S, Se) Catalysts on Si Micropyramids" *Adv. Mater.* **2015**, 27, 6511–6518. DOI: 10.1002/adma.201501884.

9. Zhuo, J.; Cabán-Acevedo, M.; Liang, H.; Samad, L.; Ding, Q.; Fu, Y.; Li, M.; Jin, S.; "High-Performance Electrocatalysis for Hydrogen Evolution Reaction Using Se-Doped Pyrite-Phase Nickel Diphosphide Nanostructure" *ACS Catal.* **2015**, *5*, 6355–6361. DOI: 10.1021/acscatal.5b01657.

10. Cabán-Acevedo, M.; Stone, M. L.; Schmidt, J. R.; Thomas, J. G.; Ding, Q.; Chang, H.-C.; Tsai, M.-L.; He, J.-H.; Jin, S.; "Efficient Hydrogen Evolution Catalysis Using Ternary Pyrite-Type Cobalt Phosphosulphide" *Nature Materials* **2015**, *14*, 1245-1251. DOI:10.1038/nmat4410.

11. Czech, K. J.; Thompson, B. J.; Kain, S.; Ding, Q.; Shearer, M. J.; Hamers, R. J.; Jin, S.; Wright, J. C.; "Measurement of Ultrafast Excitonic Dynamics of Few-Layer MoS$_2$ Using State-Selective Coherent Multidimensional Spectroscopy" *ACS Nano* **2015**, 12146–12157. **DOI:** 10.1021/acsnano.5b05198.

12. Fu, Y.;[†] Zhu, H.;[†] Schrader, A. W.; Liang, D.; Ding, Q.; Joshi, P.; Hwang, L.; Zhu, X.-Y.; Jin, S. Nanowire Lasers of Formamidinium Lead Halide Perovskites and Their Stabilized

Alloys with Improved Stability, *Nano Letters* **2016**, *16*, 1000-1008. **DOI:** 10.1021/acs.nanolett.5b04053. ([†] equally contributing first authors. Both Jin and Zhu are corresponding authors).

13. Samad, L.; Bladow, S. M.; Ding, Q.; Zhuo, J.; Jacobberger, R. M.; Arnold, M. S.; Jin, S.; "Layer-Controlled Chemical Vapor Deposition Growth of MoS_2 Vertical Heterostructures via van der Waals Epitaxy" *in revision*.

**Statically Polarized Polymer Heterostructures for Charge Carrier Density Control
in Energy-Relevant Semiconductors**

Howard E. Katz, Daniel H. Reich, Arthur E. Bragg, and N. Peter Armitage,
Johns Hopkins University, Baltimore, MD 21218

Program Scope

Active insulating polymers can enhance performance in applications such as information storage (nonvolatile electronic memory elements) and capture of mechanical energy (via piezoelectricity), and ameliorate deleterious effects of interfaces in devices such as transistors, light-emitting diodes, and solar cells, which are at the heart of integrated circuits, displays, and renewable power systems, respectively. Most of this work relies on single bulk polymer films, or even masks some polymer properties by including additional inorganic layers. There is little work on precisely positioning the charge-hosting sites at specific levels within films or on understanding the consequences of such positioning. There are further unrealized opportunities to use active insulators with traditionally inorganic semiconductors beyond transistors. This project utilizes new chemical approaches for static charge storage at arbitrary locations in insulating polymer films relative to film interfaces with organic and inorganic semiconductors. The main objectives of our work are to control the positioning and density of static charges within polymers at the smallest length scales possible, to understand the chemical structures responsible for these charges and synthesized new structures, to control the morphologies of the polymers in which the charges are embedded, and to uncover the fundamental mechanisms by which synthesized and charged insulating polymer films act upon semiconductors in components where energy conversion or usage is a major consideration.

We are synthesizing crosslinkable, nonpolar copolymers with covalently bound chargeable side chains, and spincoating separate layers of these polymers, any of which can contain chargeable side chains. We use representative insulating polymer backbones (polystyrene and fluorinated polymers), and electron donor (triarylamine), and electron acceptor (fullerene) functional groups. While transistors will continue to be used as analytical probes of the effects of charging functional groups in various positions in the devices, we are also investigating the interaction of the static charged polymers with other energy-relevant materials, such as polymer thermoelectric materials and other classes of materials displaying charge density-dependent physics such as topological insulators.

Multilayer morphologies are characterized with scanning probe spectroscopy and neutron scattering. Charge density-dependent characteristics of adjacent semiconductors, which now include organic transistor semiconductors, are measured as well. The neutron scattering work utilizes deuterium-labeling to distinguish adjacent but functionally distinct polystyrene layers. We have already used neutron scattering to show that polymer layers that we prepare are highly distinct. Static, time-resolved, and *in situ* optical spectroscopy is being introduced as a means of identifying charged species. Our overall vision for this project is a broadly applicable synthesis,

film formation, and characterization platform, along with fundamental understanding, that will provide charged dielectric heterostructures tuned for multiple energy-relevant purposes.

Recent Progress

Charged Polystyrene heterostructures in pentacene transistors. Organic transistor (OFET) gate insulators affect bias stress and threshold voltage (V_{th}), and charging them can preset the operating voltages and control bias stress. We designed and fabricated stacks of polystyrene (PS) layers, each with arbitrary concentrations of potentially chargeable functional groups.[1] Specific polymer structures are shown in Figure 1. Thermal crosslinking of benzocyclobutene subunits ensures layer integrity while keeping the layers free of polar functionality and small molecule byproducts. Neutron reflectivity (NR), scanning electron microscopy, and atomic force microscopy (AFM) showed that individual layer thicknesses varied systematically with polymer concentration in deposition solutions, and interfacial thicknesses ranged from 1.5-4 nm, independent of layer thickness, demonstrating formation of distinct layers with minimal roughness or intermixing. We compared V_{th} of pentacene transistors using the heterostructures as the only gate dielectrics (without any inorganic oxide in series with the heterostructures) before and after charging. Increased bias stress stability as evidenced by reduced V_{th} shift was seen in devices with trilayer dielectrics with electron donor-substituted PS as the middle layer compared to a dielectric made from unsubstituted PS. On the other hand, increased V_{th} shift was seen in many devices with bilayer dielectrics made with substituted PS as the top layer. We attribute the decreased V_{th} shift seen in trilayer devices to an increased dielectric polarization of the substituted PS in the middle layer that countered the charge trapping effect in the top layer. This demonstration establishes a method for utilizing vertical charge patterns for various electronics applications.
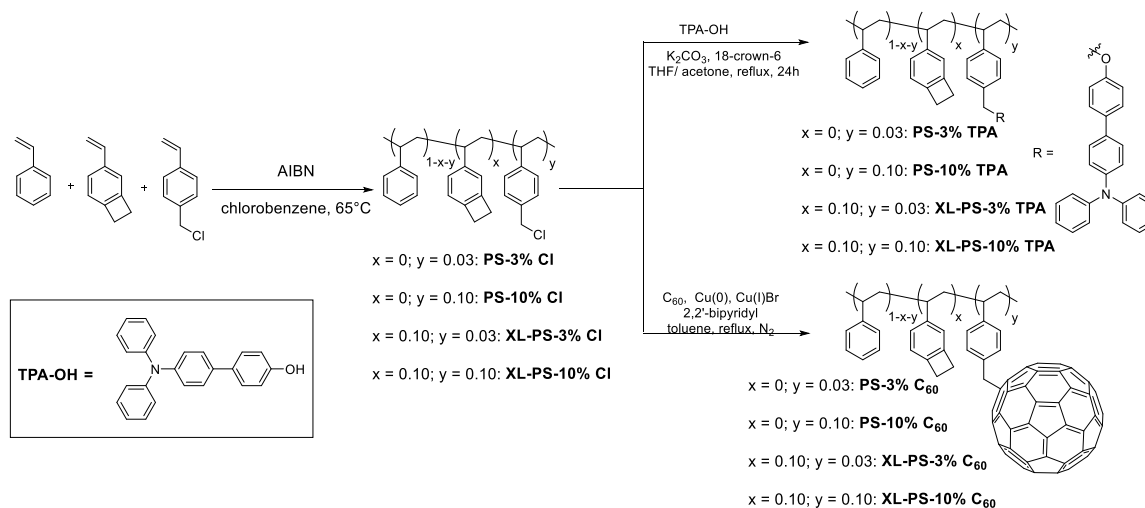

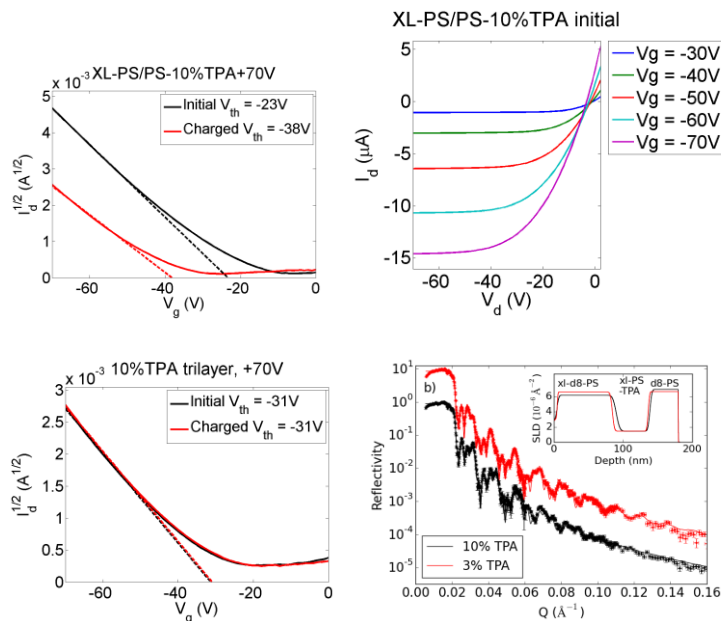Figure 1. Synthesis of crosslinkable and chargeable sidechain polystyrenes.

Figure 2. Top: V_{th} shift from sqrt drain current I_d vs. gate voltage V_g for a pentacene OFET with a bilayer XL-PS/PS-C_{60} gate dielectric (V_d held at -70V) with output curves also shown. "10%" indicates 10% substitution with C_{60}. Bottom left: An XL-PS/PS-TPA/PS trilayer OFET that was very stable to charging; the curves before and after charging are nearly superimposed. Bottom right: NR data for trilayers with layer structure XL-d8-PS/XL-PS-R/d8-PS, where R=3% TPA or 10% TPA. The upper trace was offset by a factor of 10 for clarity. Solid lines through the data are best-fit model curves. This modeling yields the scattering length density (SLD) profiles shown in the insets, where the zero of the depth axis is the top of the underlying Si.
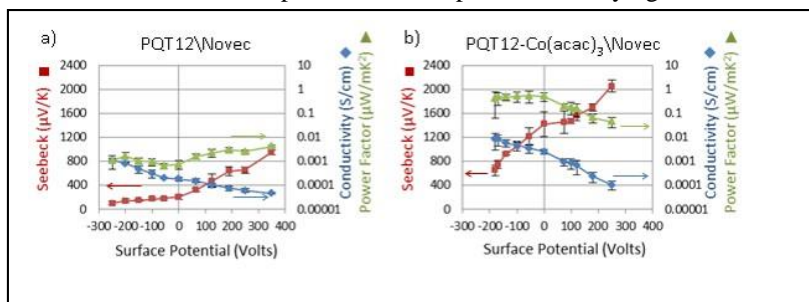

Figure 3. Seebeck coefficient (left y-axis, red squares), conductivity (right y-axis, blue diamonds), and power factor (right y-axis, green triangles) for composites comprising of a) PQT12 capped with Novec and b) PQT12-Co(acac)$_3$ capped with Novec, all as functions of the stored surface potential in Novec.

Transistor data are shown in Figure 2, representing extreme cases of a large V_{th} shift for chargeable groups adjacent to the pentacene and bias stress stabilization from chargeable groups in the interior layer of the dielectric. An NR dataset verifying the structure and good layer definition is also shown.

Charged dielectrics over thermoelectric polymers. TE properties of bulk materials have been modified in the past with a gate electrode to induce a field-effect. This tunability is important where desired performance cannot be obtained by the active material alone, or when minimum output voltages or conductivities are required, and has also resulted in contributions to the basic understanding of the relationship between charge carrier density and the S-σ tradeoff. Polymer-hosted static charge offers the combination of kinetic stability, all-solid-state configuration, and high absolute gating voltage even when the gate electrode is subsequently disconnected. Here, we gated thermoelectric devices based on the t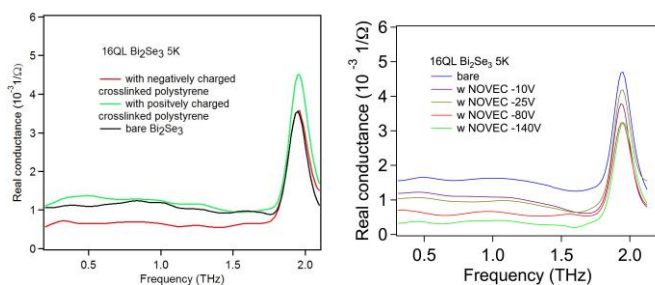hiophene polymer PQT12, with and without the solid dopant[2] Co(acac)$_3$ using the fluorinated polymer Novec as the nonvolatile dielectric (Figure 3). The Seebeck coefficients and electrical conductivities showed opposite dependences on static voltage, as expected. More importantly, this dependence was realized in an all-solid-state device for the first time without active operation of the gate electrode.[3]

Figure 4. Frequency-dependent conductance of Bi_2Se_3 affected by charging of overlying (a) polystyrene and (b) Novec.

Charged gates on Topological Insulators. We have demonstrated the effectiveness of a monolithic single-component charged electret in extracting charge carriers from bismuth selenide (Bi_2Se_3), a material believed to be a topological insulator; a new class of materials that host robust surface states that wrap an insulating bulk. Figure 4 shows THz spectra of three Bi_2Se_3 samples without, with negatively, and with positively charged polystyrene with crosslinkable side chains. We performed THz (alternating current) and DC Hall measurements on them. In the THz spectra there is a Drude component peaked at zero frequency and a phonon peak at ~1.9THz. The area below the Drude conductance is proportional to the carrier density over the effective mass. Lower area means lower carrier density. We can see Bi_2Se_3 with negatively charged polymers has the smallest area and the positively charged one has the highest area, indicating negatively charged polymers deplete the carrier density of surface states of Bi_2Se_3 while the positive one slightly increases the carrier density. This polarity is consistent with charge stored as a dipole, with one pole in the dielectric and the other pole in the Bi_2Se_3 or at its polymer interface, where electrons would be trapped. DC transport measurements reach the same conclusion. Even at room temperature, the sample with negatively charged polymer has low carrier density $2.4*10^{12}/cm^2$ and high mobility (~1100 cm^2/Vs). This is well into the topological regime where only surface state electrons are contributing, making room temperature application possible.[4]

Future Plans

Plans for the coming year include consideration of more hydrophobic electret polymers for all of the applications mentioned above, synthesis of more strongly electron donating or accepting side chain groups for dielectric polymers, introduction of spectroscopic markers to indicate charged subunit locations and structures, construction of apparatus to perform in situ spectroscopy of dielectrics during charging, and time-resolved spectroscopy after charging to interrogate properties of charged active moieties.

References

[1]Alley, O.J.; Plunkett, E.; Kale, T.S.; Guo, X.; McClintock, G.; Bhupathiraju, M.; Kirby, B.J.; Reich, D.H,; Katz, H.E. Macromolecules 49, 3478 (2016); [2]Ireland, R.M.; Liu, Y.; Xuo, X.; Cheng, Yu-Ting; Kola, S.; Wang, W.; Jones, T.; Yang, R.; Katz, H.E. Advanced Science 2, 1500015 (2015); [3]Ireland, R.M.; Jones, T.; West, J.E.; Katz, H.E., submitted. [4]Ireland, R.M.; Wu, L.; Saleha, M.; Oh, S.; Armitage, N.P.; Katz; H.E.; submitted.

Publications

Huang, W. Besar, K. Dulloor, P. Sinha, J. Martínez Hardigree, J.F. Pick, C. Swavola, J. Everett, A.E.. Frechette, J., Bevan, M.E. Katz, H.E., "Label-free Brain Injury Biomarker Detection Based on Highly Sensitive Large Area Organic Thin Film Transistor with Hybrid Coupling Layer" Chemical Science 5, 416-426 DOI: 10.1039/C3SC52638K (2014)

Jo, M.Y.; Bae, J.H; Lim, G.E.; Ha, Y.E.; Katz, H.E.; Kim, J.H. "Photovoltaic properties of low band gap polymer based on phenanthrene and diketopyrrolopyrrole" Synth. Met. 176 41-46 (2013)

Kola, S.; Kim, J.H.; Ireland, R.; Yeh, M-Y.; Smith, K.; Guo, W.; Katz, H.E. "Pyromellitic Diimide – Ethynylene Based Homopolymer Film as an N-Channel Organic Field-Effect Transistor Semiconductor" ACS Macro Letters, 2, 664-669 (2013).

Ireland, R.M.; Liu, Y.; Spalenka, J.; Jaiswal, S.; Fukumitsu, K.; Oishi, S.; Saito, H.; Ryosuke, M. Evans; P.; Katz, H.E. "Device isolation in hybrid field-effect transistors by semiconductor micropatterning using picosecond lasers" Phys. Rev. Applied 2, 044006 (2014).

Martinez Hardigree, J.F, Katz, H.E. "Through Thick and Thin: Tuning the Threshold Voltage in Organic Field-Effect Transistors" Accounts of Chemical Research, 47, 1369-1377 (2014).

Dawidczyk, T.J.; Martinez Hardigree, J.F.; Johns, T.L.; Ozgun, R.; Alley, O.; Andreou, A.G.; Markovic, N.; Katz, H.E. "Visualizing and Quantifying Charge Distributions Correlated to Threshold Voltage Shifts in Lateral Organic Transistors" ACS Nano, 8, 2714-272 (2014).

Yeh, M.L.; Wang, S.-Y.; Martinez Hardigree, J.F.; Podzorov, V.; Katz, H.E. "Effect of Side Chain Length on Film Structure and Electron Mobility of Core-Unsubstituted Pyromellitic Diimides and Enhanced Mobility of the Dibrominated Core Using the Optimized Side Chain" Journal of Materials Chemistry C, DOI: 10.1039/C4TC02611J (2015)

Ireland, R.M.; Liu, Y.; Xuo, X.; Cheng, Yu-Ting; Kola, S.; Wang, W.; Jones, T.; Yang, R.; Katz, H.E. "ZT > 0.1 Electron-Carrying Polymer Thermoelectric Composites with in-situ $SnCl_2$ Microstructure Growth". Advanced Science 2, 1500015 (2015).

Alley, O.J.; Plunkett, E.; Kale, T.S.; Guo, X.; McClintock, G.; Bhupathiraju, M.; Kirby, B.J.; Reich, D.H,; Katz, H.E. "Synthesis, Fabrication, and Heterostructure of Charged, Substituted Polystyrene Multilayer Dielectrics and Their Effects in Pentacene Transistors" Macromolecules 49, 3478 (2016).

Mesoscale Fragments of Crystalline Silicon by Chemical Synthesis

Rebekka S. Klausen (PI), Johns Hopkins University, Department of Chemistry, Baltimore, MD 21218

Program Scope

Silicon is the dominant semiconductor for both electronics and solar cells, suggesting opportunities for molecular and polymeric silicon in optoelectronic device applications. Such materials could combine the practical advantages of organic electronics, including solution processing, with the performance of inorganic semiconductors. The aim of this program is to develop an innovative synthetic approach towards mesoscale silicon architectures based on novel cyclic precursors inspired by fragments of the crystalline silicon lattice. The design and synthesis of chair-like cyclohexasilane monomers site-specifically labeled with functional groups for silane polymerization is described. Length-controlled polymerization and rational incorporation of organic and inorganic substituents is envisioned to control the optoelectronic properties of the polymer.

Recent Progress

Our efforts have focused on 1) understanding and controlling charge separation and transport in silicon materials and 2) the synthesis of the novel cyclosilane monomers, with a particular focus on routes emphasizing short step count, efficiency, and scalability.
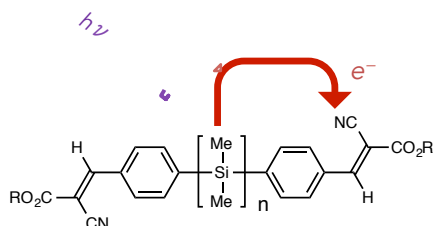
Figure 1. Photoinduced charge separation in molecular silicon σ-π hybrids.

Photoinduced Charge Separation. Two of the most fundamental steps in the function of an organic solar cell are photoinduced charge separation and charge transport. Recent work from my group has demonstrated that molecular silicon materials perform both of these fundamental actions.[1,2] These studies were conducted with a family of σ-π hybrid materials in which a chain of silicon atoms is capped with aromatic electron acceptors (Figure 1). The hybrid materials are brightly colored, while each parent component (an oligosilane and cyanovinylarene) is colorless. We hypothesized that the origin of the color is due to an intramolecular charge transfer. While steady-state spectroscopic characterization (IR and electronic) revealed that charge separation does not occur in the ground state, femtosecond stimulated Raman spectroscopy (FSRS) showed that the excited oligomers exhibited a series of intense resonantly enhanced features between 1000 and 1650 cm^{-1} that are consistent with reduction of the cyanovinyl C=C bond.[1] The intensity and position of this feature is dependent on the number of silicon atoms in the chain, implicating silicon as the electron donor. Insights from our work support the viability of molecular forms of silicon as photoresponsive materials in optoelectronic devices.

Charge Transport and Crystal Packing. A challenge in the application of molecular silicon materials is the lack of understanding of the fundamental intermolecular forces that lead to a close-packed material, as intermolecular distances in a crystal or thin film strongly influence charge transport. Towards addressing this challenge, we have shown that σ-π hybrid materials form close-packed crystalline thin films.[2] An intramolecular C-H-π interaction induces a gauche conformation in the molecule that allows two molecules to stack in an antiparallel fashion with a 3.44 Å intermolecular distance (Figure 2a). This value is comparable to the close distances observed in the best organic charge transport materials such as TIPS-pentacene (3.60 Å). We further show that this material forms highly oriented crystalline solution-deposited thin films (Figure 2b-c) and we measure hole mobilities up to 0.06 x 10^{-2} cm^2 V^{-1} s^{-1} in thin film transistors, a record-setting value for a device based on a silane active layer.
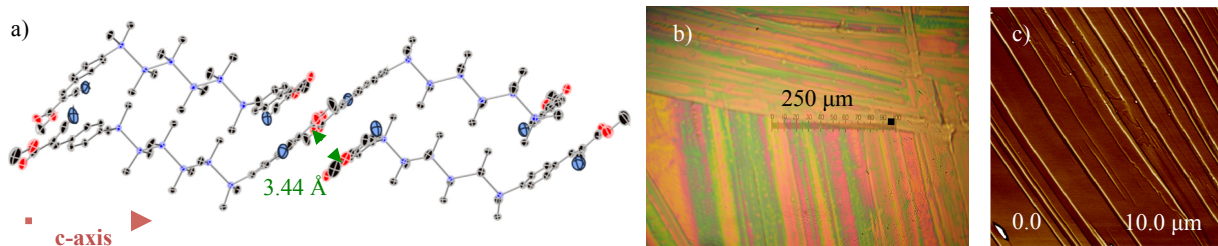

Figure 2. a) Crystal structure of σ-π hybrid material extended along the c-axis highlighting close packed structure. b) Optical and c) Atomic Force Microscopy images showing smooth and highly oriented crystalline thin films.

Cyclosilane Monomer Design. Our synthetic efforts prioritize short step count, efficiency, and scalability. These priorities reflect the demand for large quantities of material for polymerization and the importance of developing an inexpensive and energy-efficient alternative to silicon-based optoelectronic materials as the long energy payback time of silicon solar cells is attributed to the expensive and energy-intensive purification of semiconductor-grade silicon.[3] Key to our approach is the use of chloromethylsilanes which are derived from lower purity metallurgical grade silicon via the Müller-Rochow Direct Synthesis.[4]
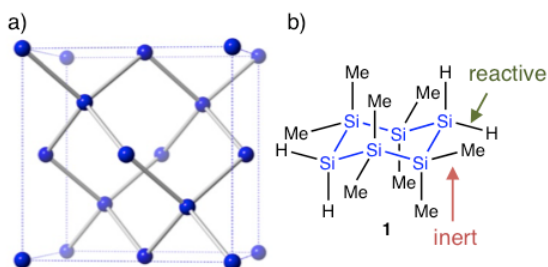

Figure 3. a) Crystalline Si lattice. b) Cyclosilane monomer **1**. Si-Me and Si-H bonds are labeled inert and reactive, respectively.

The core repeat unit of crystalline and nanocrystalline silicon is a six-membered ring of silicon atoms in a chair-like conformation (Figure 3a). We have designed a family of molecular precursors to low-dimensional silicon that contain the core chair-like cyclohexasilane motif and one example of such a precursor is shown in Figure 3b. The inert Si-Me groups ensure polymerization only initiates at the reactive Si-Cl or Si-H bonds and protect the silicon scaffold from oxidation. Chlorosilanes are polymerized by reducing Wurtz coupling conditions[5] and primary and secondary

silanes by early transition metallocenes by a dehydrocoupling mechanism.[6] We call this synthetic strategy molecular patterning, after our inspiration surface patterning, the practice of using an inert mask to determine the size and shape of a nanostructure.

Monomer Synthesis. While the simplest unfunctionalized molecular cyclosilane (dodecamethylcyclosilane, Si_6Me_{12}) is readily obtained as a byproduct of Wurtz polymerization of dichlorodimethylsilane (Me_2SiCl_2) and was first reported more than 50 years ago,[7] the preparation of site-specifically functionalized cyclosilanes is a significant challenge. We have developed an efficient synthesis of the novel 1,4-
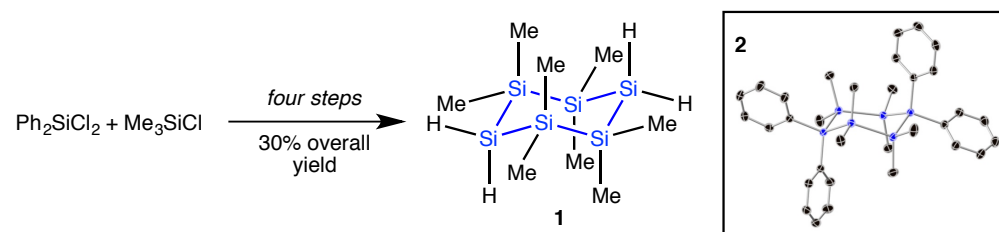
Figure 4. Four-step synthesis of **1** from Müller-Rochow Direct Synthesis products. Inset shows a crystal structure of **2**. Blue = silicon, black = carbon, hydrogens omitted for clarity.

difunctionalized cyclosilane **1** that proceeds in 30% overall yield in four steps from commercially available chlorotrimethylsilane (Me_3SiCl) and dichlorodiphenylsilane (Ph_2SiCl_2), both of which are products of the Müller-Rochow Direct Synthesis (Figure 4). A crystal structure of tetraphenylcyclosilane **2**, a synthetic intermediate, is shown in the inset.

Evidence for Chair Conformation. We provide evidence for a chair-like conformation in compound **1.** Precursor **2** is crystalline and a distorted chair-like conformation is observed in the crystal structure (inset, Figure 4). The chair conformation is also observed in solution, as demonstrated by NMR spectroscopy. Compound **1** in the chair conformation belongs to the C_{2h} point group, possessing a major C2 rotational axis, a mirror plane, and inversion symmetry. Rapid ring inversion (chair flipping) renders the diastereotopic axial and equatorial methyl groups equivalent, predicting a single methyl signal in the ^1H NMR spectrum. The room temperature ^1H NMR spectrum of **1** in benzene is consistent with the prediction.

Polysilane Passivation. Silicon's propensity towards surface oxidation is well known and the insulating native oxide layer is exploited in electronic devices including transistors.[8] However, in low-dimensional and nanoscale silicon systems, the increased surface area results in rapid oxidation with a corresponding degradation of semiconductor-like properties. Oxidation has been a particularly notable challenge in silicene characterization.[9] A general strategy to ensure polysilane surface passivation is required to explore the potential of freestanding nanoscale silicon for electronic applications. The autooxidation of poly(hydrosilanes) is attributed to the labile Si-H bond.[10] We have developed a general strategy for passivating these surface Si-H bonds through mild catalytic alkylation.

Future Plans

Our future plans are to develop length-controlled syntheses of novel polycyclosilanes and to incorporate donor and acceptor functionality towards the goal of accessing well-defined silicon polymers with controlled optoelectronic properties. Particular focus will be applied to developing silicon donor-acceptor polymers.

References

[1] Zhou, J.; Surampudi, S. K.; Bragg, A. E.; Klausen, R. S. "Photoinduced Charge Separation in Molecular Silicon." *Chem. Eur. J.* **2016**, *22*, 6204–6207.

[2] Surampudi, S.; Yeh, M.L.; Siegler, M. A.; Martinez Hardigree, J. F.; Kasl, T. A.; Katz, H. E.; and Klausen, R. S. "Increased carrier mobility in end-functionalized oligosilanes." *Chem. Sci.*, **2015**, *6*, 1905-1909.

[3] Peng, J.; Lu, L.; Yang, H. "Review of Life Cycle Assessment of Energy Payback and Greenhouse Gas Emission of Solar Photovoltaic Systems." *Renewable Sustainable Energy Rev.* **2013**, *19*, 255-274.

[4] Kalchauer, W.; Pachaly, B. *Handbook of Heterogeneous Catalysis*. Chapter 12.6. "Muller-Rochow Synthesis: The Direct Process to Methylchlorosilanes." 2635-2647.

[5] Miller, R. D.; Michl, J. "Polysilane high polymers." *Chem. Rev.*, **1989**, *89*, 1359–1410.

[6] Tilley, T. D. "The coordination polymerization of silanes to polysilanes by a "σ-bond metathesis" mechanism. Implications for linear chain growth." *Acc. Chem. Res.*, **1993**, *26*, 22–29.

[7] Burkhard, C. A. "Polydimethysilanes." *J. Am. Chem. Soc*. **1949**, *71*, 963–964.

[8] Doering, R., & Nishi, Y. (2008). Handbook of semiconductor manufacturing technology. 2nd ed. Boca Raton: CRC Press.

[9] Tao, L.; Cinquanta, E.; Chiappe, D.; Grazianetti, C.; Fanciulli, M.; Dubey, M.; Molle, A.; Akinwande, D. "Silicene field-effect transistors operating at room temperature." *Nature Nanotechnology* **2015**, *10*, 227–231.

[10] Chatgilialoglu ,C.; Guerrini , A.; Lucarini , M.; Pedulli , G. F.; Carrozza , P.; Da Roit , G.; Borzatta , V.; Lucchini, V. "Autoxidation of Poly(hydrosilane)s" *Organometallics*, **1998**, *17*, 2169–2176.

Publications

[1] Press, E. M.; Marro, E. A.; Surampudi, S. K.; Siegler, M. A.; Klausen, R. S. "Poly(Cyclosilane): A Polymer Inspired by Crystalline Silicon." *Organometallics*, submitted.

Synthesis and Single Crystals of Refractory Oxides of Lanthanides and Thorium
Joseph W. Kolis Department of Chemistry Clemson University
kjoseph@clemson.edu

Program Scope: This program encompasses the use of high temperature hydrothermal fluids to induce reaction and crystallization of a variety of refractory oxides. Previous work in our group identified reaction conditions that can mineralize otherwise completely insoluble and unreactive metal oxides. This enables both exploratory synthesis of new materials, as well as growth of single crystals for full structural characterization and physical property studies. We developed techniques for performing reactions in hydrothermal fluids at 700°C and 2 kbar pressure. A key component of this technology is the mineralizer. Typically in hydrothermal crystal growth the mineralizer is aqueous hydroxide or carbonate. It is used to induce solubilization of oxide feedstock and transport to a growth zone to form single crystals. If multiple metal ions are present in the feedstock, they can be co-solubilized and transported, performing chemical reactions as well as crystal growth in the process. This enables synthesis of many new phases, usually in the form of high quality single crystals. [1]

To address more refractory and insoluble oxides such as the rare earth sesquioxides (RE_2O_3), the tetravalent oxides MO_2, (M = Zr, Hf, Ce, and Th) and pentavalent oxides (Nb, Ta), simple aqueous base is often not sufficient to induce solubilization, reaction or transport. We found however that the use of fluorides, in conjunction with hydroxide, in aqueous base at temperatures near 700°C is often suitable to solubilize even the most recalcitrant oxides. This allows us to explore the chemistry, structure and properties of a number of oxides that are otherwise poorly unexplored. In many cases we can perform single crystal studies for the first time on such species. The initial target classes in this program are combinations of rare earth elements with tetravalent or pentavalent oxides. In these cases the research is motivated by several factors. For example the rare earth vanadates are excellent solid state laser hosts but have some suboptimal physical properties. Thus the examination of the corresponding niobates and tantalates seems worthwhile. In addition the fuller development of the rare earth silicates, -germinates and -stannates is also of interest since preliminary investigations by ourselves and others strongly suggests that the chemistry can be both extensive and interesting. Our goal in these efforts, in addition to identifying new materials, is to probe the limits of the mineralizers and thermal conditions. Obviously it is desirable to employ the least demanding reactions conditions required, but the systems are so refractory that the requirements of temperature pressure and mineralizer are not known to even an approximate degree in many cases. Thus an important component of this research is to find out what conditions are needed to induce reactivity and crystallization.

Recent Progress: As we initiated this project, one class of compounds we targeted in its first year, is the series of compounds based on $RENbO_4$ and $RETaO_4$. [2] We thought this approach would serve two purposes. It would continue to develop the mineralization chemistry of refractory rare earth oxides and also lead to potential new hosts for high power laser applications. We successfully grew a wide range of $RENbO_4$ single crystals at 700°C using strong alkali OH^- mineralizers. These grew in the traditional fergusonite

structure, but were of much higher quality, and did not suffer the multiple domain issues in crystals grown by traditional high temperature melt methods. Interestingly we also discovered that if the growth reactions were performed at slightly lower temperature (~650˚C), we isolated a series of hydroxide containing species, the identity of which is dependent on the reaction conditions. When using CsOH we isolated $CsNb_2O_5(OH)$ in the pyrochlore structure. When KOH was used we isolated the novel structure $K_3RENb_2O_7(OH)_2$ (RE = Y, Lu, Yb, Sc etc.) in good yield. Surprisingly these new structures represent the first alkali rare earth niobates to our knowledge. We believe they are only the tip of the iceberg for this class.

When the corresponding reactions are performed with the tantalates between 600-700˚C the binary oxides are only a minor product, and a whole new series of interesting metal hydroxides were isolated in high yield as extremely high quality crystals. (Fig. 1)

RE_2O_3 + 0.5 Ta_2O_5 → $RE_2TaO_5(OH)$ (RE = La, Pr, Nd)   30KOH/660˚C/2kbar
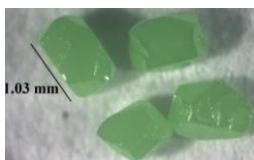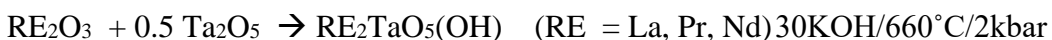
Figure 1. Example of products from hydrothermal reactions. Single crystals of $Pr_2TaO_5(OH)$ 1mm/edge.

With just a subtle change in stoichiometry an entirely different phase can be isolated.

1.5 RE_2O_3 + Ta_2O_5 → $RE_3Ta_2O_9(OH)$ (RE = La, Pr, Nd)   30KOH/660˚C/2kbar

Both compounds are new structure types with extremely complex structures. The $RE_2TaO_5(OH)$ phase has a complicated structure that does lend itself to easy description. It consists of two rare earth environments, a 2-D layer of edge shared polyhedral and chains of edge-shared polyhedral with both running parallel to the b-axis. Buried within that superstructure are a series of Ta_2O_{10} edge shared dimers. (Figure 2.)
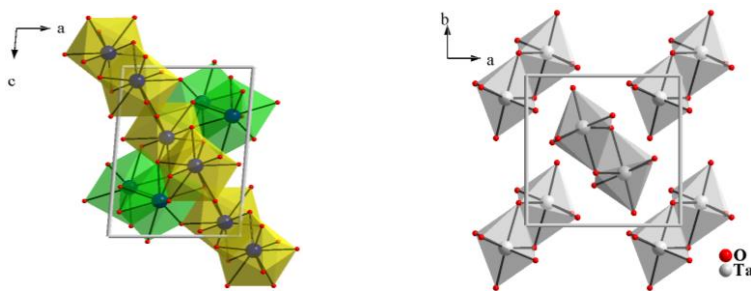

Figure 2. (Left) Infinite chains of edge sharing REO_9 polyhedra (green) and layers of edge sharing REO_9 polyhedra (yellow). (Right) Ta_2O_{10} dimers (gray) interspersed between the rare earth oxides chains.

The $RE_3Ta_2O_9(OH)$ phase also has a very intricate structure with double chains of edge-shared TaO_6 octahedra woven between complex layers of RE – oxide layers. (Figure 3)
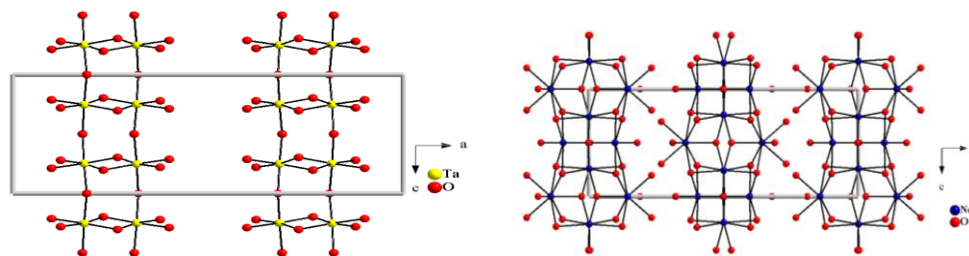
Figure 3. Structure of $RE_3Ta_2O_9(OH)$ showing double chains of TaO6 octahedra (left) and complex ReO$_8$ slabs (right)

In our initial foray into the rare earth titanates the hydrothermal chemistry also proved to be unexpectedly rich. In addition to the anticipated cubic pyrochlore single crystals of the smaller rare earths $(Sm-Lu)_2Ti_2O_7$,[3] we also obtained single crystals of the polar $P2_1$ monoclinic phase of the larger rare earths (e.g. $Pr_2Ti_2O_7$) in concentrated hydroxide mineralizer. However when lower concentrations of mineralizer were used we also obtained a series of structurally complex OH containing crystals. (Figure 4)

$$RE_2O_3 + 2\ TiO_2 \rightarrow RE_5TiO_4O_{15}(OH) \qquad 10KOH/700°C/2kbar$$
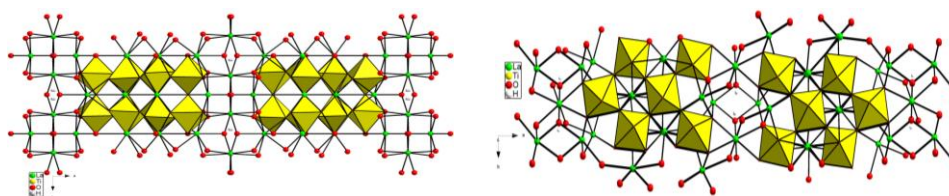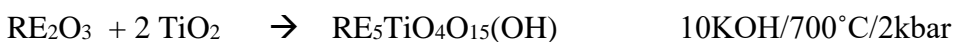
Figure 4. Structure of $RE_5TiO_4O_{15}(OH)$ with TiO$_6$ corner shared octahedral slabs (yellow) and edge shared REO$_8$ (green) polyhedral layers.

Clearly the scope of these reactions has not yet been developed and is part of our ongoing work. Opening up this extensive chemistry of hydroxyl containing metal solids was not anticipated but may be useful in that hydroxyl-containing tantalates and titanates show excellent photocatalysis behavior, including efficient photocatalytic water splitting. [4]

Future Plans: We are now expanding our work to tetravalent refractory oxides, with particular focus on ThO_2, CeO_2, HfO_2 and SnO_2 feedstocks. All are extremely recalcitrant, but are vacant shell representatives of different parts of the periodic table, actinides, lanthanides, d blocks and p-blocks respectively. Now that we are getting more knowledgeable about the chemistry of the oxides in the high temperature fluids, we can extend our studies to more intractable starting materials. The tetravalent oxides represent some of the most important materials in a wide variety of applications, including nuclear waste storage and oxide conductors. However they are among the least well studied in terms of single crystal structures. It is our long-term goal on this project to be able to extend the reaction chemistry over a broad range of tetravalent oxides.

An important avenue to the investigation of tetravalent oxides is the development of alternative mineralizers. We found that the MO_2 compounds are some of the most recalcitrant compounds known, and employing aqueous fluorides either alone or in conjunction with hydroxide, is often a good route to high quality single crystals. We are now extending that to other mineralizers. In particular we are beginning to explore the use of acidic fluorides as mineralizers. These are turning out to be extremely powerful and are capable of solubilizing even the most difficult oxides. The acids have their own set of experimental requirements however, and we are in the process of determining optimal conditions for reactions and crystal growth.

One important technical advance in our lab has been the development of higher temperature reactions. We recently set up technology that allows us to perform hydrothermal reactions up to 850°C using a variety of mineralizers. This is particularly important given our recent discoveries of a range of interesting OH containing compounds such as hydroxyl-tantalates as described above, with many others on the way. These were all prepared at or below 700°C, and we know that in many cases, higher temperature reactions can lead to metal oxides with no OH groups in the formula. It appears that we are on a bit of a thermal cusp, particularly in the case of tantalates. We hope that this new access to a higher temperature regime at 850°C will lead to pure metal oxides as opposed to the metal oxyhydroxides. In essence we can convert the hydroxide containing species to the anhydrous oxides at these higher temperatures. We suspect that this will prove to be the case with other metal oxide systems as well. This will make for a rich and interesting chemical series. This work will be explored in the next two years of the program.

References:

[1] "Bulk Single Crystal Growth from Hydrothermal Solution" C.D. McMillen, J.W. Kolis* Phil Trans B. **2012** 1-26

[2] "Hydrothermal Chemistry and Growth of Fergusonite-type $RENbO_4$ (RE=La-Lu, Y) Single Crystals and New Niobate Hydroxides" K. Fulle, C. D. McMillen, L. D. Sanjeewa, J. W. Kolis* Crystal Growth and Design **2016** submitted.

[3] "Structural and crystal chemical properties of rare-earth titanate pyrochlores" J.M. Farmer, L.A. Boatner, B.C. Chakoumakos, M-H. Du, M.J. Lance, C.J. Rawn, J.C. Bryan J. Alloys and Compounds 2014, 605, 63-70.

[4] "Photocatalytic Water Splitting in Ni Intercalated Ruddleson Popper Tantalate $H_2La_{2/3}Ta_2O_7$" K. Shimizu, S. Itoh, T. Hatamachi, T. Kodama, M. Sato, K. Toda Chem. Mater. 2005, 17, 5161-5166.

Publications from this grant:

"Hydrothermal Chemistry and Growth of Fergusonite-type $RENbO_4$ (RE=La-Lu, Y) Single Crystals and New Niobate Hydroxides" K. Fulle, C. D. McMillen, L. D. Sanjeewa, J. W. Kolis* <u>Crystal Growth and Design</u> **2016** submitted.

"Synthesis and Structural Relationships of New Rare Earth Titanate and Tantalate Hydroxides" K. Fulle, L.D. Sanjeewa, C.D. McMillen, J.W. Kolis Inorg. Chem. To be submitted.

"New Rare Earth Silicates" K. Fulle, L.D. Sanjeewa, C.D. McMillen, J.W. Kolis Acta Cryst. B To be submitted.

"Hydrothermal Synthesis of Rare Earth Germanates" K. Fulle, L.D. Sanjeewa, C.D. McMillen, J.W. Kolis J. Solid State Chem. In preparation

Unconventional clathrates based on transition metal pnictides

Kirill Kovnir

Department of Chemistry, University of California, Davis

Program Scope

Thermoelectrics (TEs) convert heat into electrical energy and vice versa. As such, they are promising materials for waste heat reduction or recovery, thus enhancing energy efficiency and diminishing our dependence on fossil fuels. The development of novel materials where charge and heat transport are partially de-coupled is a key factor for the next generation of TEs. This project seeks to develop a new class of bulk TE materials based on transition metal-pnicogen clathrates, pnicogen = P, As, Sb. Clathrate crystal structures have a three dimensional framework comprised of oversized transition metal- and pnicogen-based polyhedral cages that encapsulate guest cations. The rattling of guest cations provide effective scattering of heat carrying phonons while the host framework is responsible for transporting charge carriers. Transition metal-based clathrates have the following advantages over conventional clathrates that are based on Si, Ge, and Sn frameworks: i) a larger variety of framework topologies and cage shapes due to the flexibility of the transition metal and pnicogen local coordinations; ii) a higher tunability of the electronic properties via framework substitutions.

Recent Progress
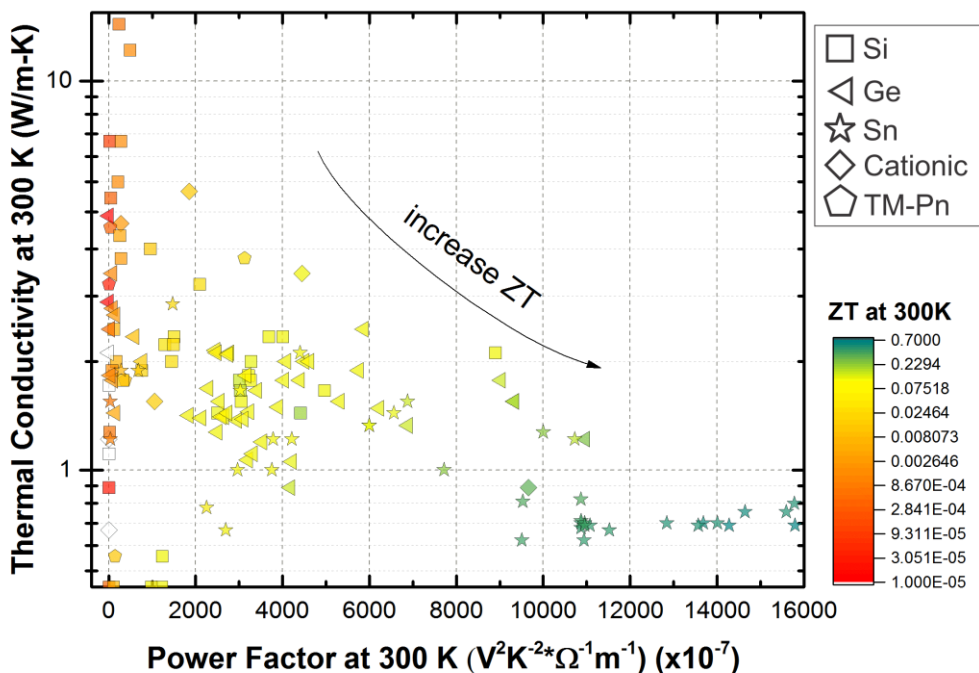
Properties of conventional clathrates

Figure 1. Room temperature thermal conductivities versus room temperature power factors ($S^2\sigma$). Si-based clathrates are shown as squares, Ge-based clathrates are shown as sideways triangles, Sn-based clathrates are stars, cationic clathrates are diamonds, and transition metal-pnicogen (TM-Pn) clathrates are pentagons. The colors of the shapes represent room temperature *ZT* values. Values increase logarithmically from red (0.00001) to yellow (0.1) to teal (0.7). Any ZTs below 0.00001 are shown as empty shapes.

A detailed analysis of most of the data published over several decades demonstrated that high thermoelectric figures of merit can be realized in clathrate materials. The vast majority of clathrates exhibit low thermal conductivities – a highly desirable trait for efficient thermoelectric materials (Figure 1). For the tetrel-based clathrates, a clear trend is observed: the highest thermoelectric efficiencies are observed for Sn-based clathrates, which exhibit the lowest thermal stabilities (Figure 2). On the other hand, thermally stable Si-based clathrates often exhibit only moderate efficiencies. We propose to search for more polar frameworks, such as those found in the tetrel-free clathrates. For example, transition metal-phosphides exhibit significantly higher thermal and chemical stabilities than Sn-based clathrates.
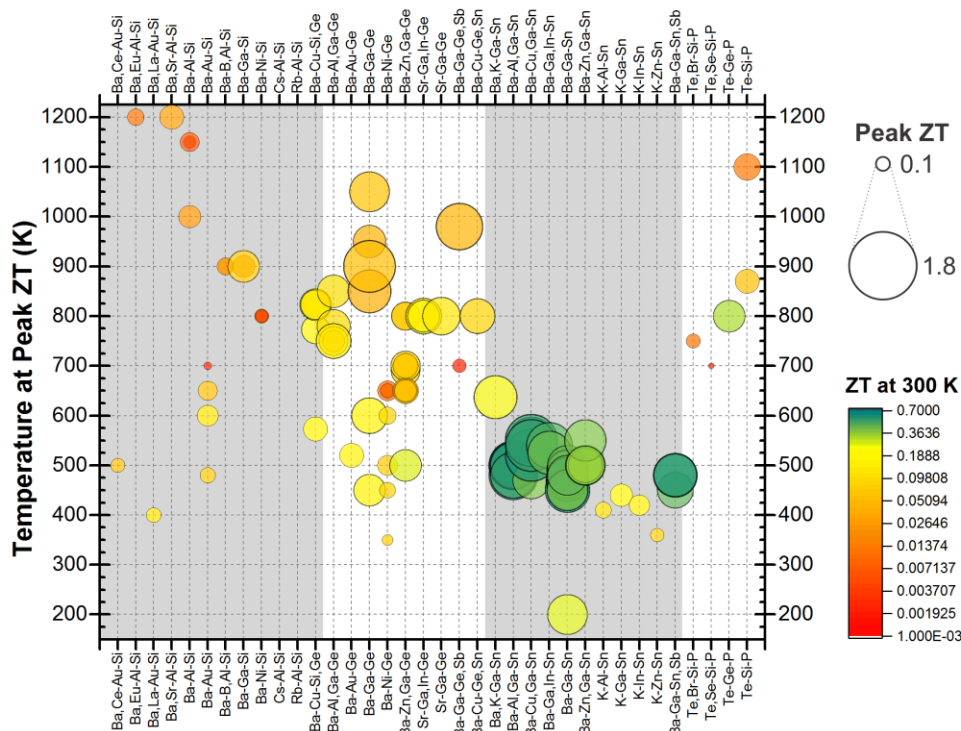

Figure 2. This figure relates room temperature *ZT* values to their corresponding maximum ZTs. The temperatures at which maximum *ZT* values are observed is shown for selected elemental systems. The sizes of the shapes correspond to the values of maximum *ZT*s at the indicated temperatures for the indicated systems. Additionally, the colors of the circles represent the room

temperature *ZT* values. Values increase logarithmically from red (0.00001) to yellow (0.1) to teal (0.7). Any *ZT*s below 0.00001 are shown as empty shapes.

Novel clathrate topologies

Three new nickel and copper polyphosphides, AM_2P_4 (A = Sr, Ba; M = Ni, Cu), were synthesized from elements and structurally characterized. The crystal structure is that of a clathrate type composed of M_8P_{16}, 14-faced polyhedral cages that encapsulate A^{2+} atoms. The crystal structures of each of the discussed transition metal-based clathrates are composed of unique polyhedra containing square faces. These structural fragments were predicted to be unstable for the conventional clathrates based on Si, Ge, and Sn. The crystal and electronic structures, chemical bonding, as well as the thermoelectric properties of this novel class of unconventional clathrates were characterized.
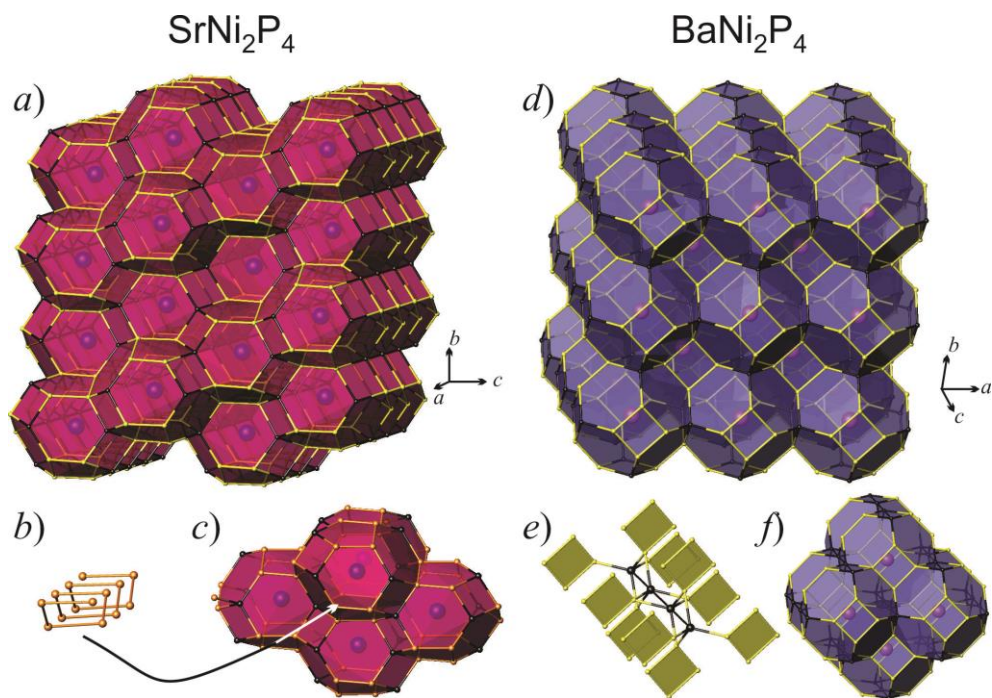

Figure 3. The crystal structures of $SrNi_2P_4$ and $BaNi_2P_4$ are shown on the left and right, respectively: a) and d) general views; b) a phosphorus chain and c) polyhedra around the chain in the crystal structure of $SrNi_2P_4$; as well as e) a Ni chain and f) polyhedra around the chain in the crystal structure of $BaNi_2P_4$. Ba and Sr: blue; Ni: black; P: yellow.

Future Plans

Over the previous years of this project we have shown that transition metal-phosphorus clathrates can be tuned by aliovalent substitution in the transition metal sublattice. On the model system, the clathrate $Ba_8Cu_{16}P_{30}$, we have shown that substitution of Zn for Cu results in not only the adjustment of the charge carrier concentration but also a change in the type of charge carriers

from holes to electrons. These adjustments resulted in the increase of ZT by more than an order of magnitude due to significant increase in the Seebeck thermopower and power factor. So far we have investigated only clathrates in the alkaline-earth metal – transition metal – phosphorus systems. In the future we will answer following fundamental questions::

- ❖ Can the heavier pnicogens, As and Sb, as well as larger alkali cations form Ni- and Cu-based clathrates?
- ❖ What factors, geometrical or electronic, define the topology of the cage and crystal structure of the transition metal-based clathrates?
- ❖ How will aliovalent substitution in the transition metal sublattice affect the structural and electronic properties of these compounds?
- ❖ What are the fundamental reasons for the unprecendently low lattice thermal conductivity in these phases?

Publications

1. Wang, J.; Kaseman, D.; Lee, K.; Sen, S.; Kovnir, K. Enclathration of X@La$_4$ tetrahedra in channels of Zn-P frameworks in La$_3$Zn$_4$P$_6$X (X = Cl, Br). *Chem. Mater.* **2016,** *DOI: 10.1021/acs.chemmater.6b01752*.

2. Lee, K.; Kamali, S.; Ericsson, T.; Bellard, M.; Kovnir, K. GeAs: Highly anisotropic van der Waals thermoelectric material. *Chem. Mater.* **2016,** *28,* 2776-2785.

3. Wang, J.; Lee, K.; Kovnir, K. Synthesis, crystal and electronic structure, and optical properties of two new chalcogenide-iodides: Ba$_3$Q$_4$I$_2$ (Q = S, Se). *Inorg. Chem. Front.* **2016,** *3,* 306-312.

4. Wang, J.; Greenfield, J.T.; Kovnir, K. Synthesis, Crystal Structure, and Magnetic Properties of Quaternary Iron Selenides: Ba$_2$FePnSe$_5$ (Pn = Sb, Bi). *J. Solid State Chem.* **2016,** *doi:10.1016/j.jssc.2015.12.030*.

5. Wang, J.; Kovnir, K. Elusive *β*-Zn$_8$Sb$_7$: A new zinc antimonide thermoelectric. *J. Amer. Chem. Soc.* **2015,** *137,* 12474-12477.

6. Wang, J.; Lee, K.; Kovnir, K. Synthesis, Crystal Structure, and Thermoelectric Properties of Two New Barium Antimony Selenides: Ba$_2$Sb$_2$Se$_5$ and Ba$_6$Sb$_7$Se$_{16.11}$. *J. Mater. Chem. C,* **2015,** *3,* 9811-9818.

7. Dolyniuk, J.; He, H.; Ivanov, A.; Boldyrev, A.; Bobev, S.; Kovnir, K. Ba and Sr Binary Phosphides: Synthesis, Crystal Structures, and Bonding Analysis. *Inorg. Chem.* **2015,** *54,* 8608-8616.

8. Dolyniuk, J.; Wang, J.; Lee, K.; Kovnir, K. Twisted Kelvin cells and truncated octahedral cages in the crystal structures of unconventional clathrates, AM$_2$P$_4$ (A = Sr, Ba; M = Cu, Ni). *Chem. Mater.* **2015,** *27,* 4476-4484.

9. Lee, K.; Kaseman, D.; Sen, S.; Hung, I.; Gan, Z.; Gerke, B.; Pottgen, R.; Feygenson, M.; Neuefeind, J.; Lebedev, O.I.; Kovnir, K. Intricate short-range ordering and strongly anisotropic transport properties of Li$_{1-x}$Sn$_{2+x}$As$_2$. *J. Amer. Chem. Soc.* **2015,** *137,* 3622-3630.

The Nature of Charge Storage in Nitroxide Radical Polymers

Jodie L. Lutkenhaus, Artie McFerrin Department of Chemical Engineering, Department of Materials Science & Engineering, Texas A&M University

Program Scope

Organic radical batteries (ORBs) are a potentially revolutionary means of energy storage in the post-Lithium-ion battery era.[1-3] As requirements in energy storage technologies have become increasingly more stringent (higher capacity, higher energy, higher power, cyclability, smaller form factor, safer, lower cost, sustainability), new materials and concepts are required. ORBs are particularly interesting because they are poised to comprehensively meet many of these needs. In recent years, a particular class of organic radical polymers, poly(2,2,6,6-tetramethylpiperidine-1-oxyl-4-yl methacrylate)s (PTMAs), have emerged as promising materials for ORBs. This polymer consists of an aliphatic backbone with nitroxide radical side groups. PTMA's high rate capability is unparalleled in comparison to conjugated polymers and lithium transition metal oxides, which leads to high power density and rate capability. To date, most investigations of PTMA and other similar nitroxide radical polymers have centered on its performance in a battery at the device level and have not probed deeper into the fundamentals of how charge is stored. The nature of charge storage in many ORB materials is not well understood, and this knowledge will become increasingly important as the field moves forward and expands. **Therefore, the main goal of this project is to establish how charge is stored in PTMAs and related hybrid electrodes.** On the most fundamental scientific level, it is of essential importance to understand how charge is stored, how electrons and ions transport, and how degradation proceeds in PTMA and its related hybrid electrodes. This forthcoming knowledge will have a broad impact in the understanding of the nature of charge storage in other organic radical polymers such as carbonyls and organodisulfides. Successful execution of these Objectives will generate a broad roadmap for the reaction mechanism in organic radical polymers, how PTMA participates in hybrid electrodes, and how organic radical polymers degrade. To this end, the three proposed Objectives are designed to establish this basic knowledge and are described as follows:

Objective 1: Elucidate the fundamental phenomena that govern charge storage in homopolymer PTMA.

Objective 2: Deduce the mechanism of charge storage in PTMA-based hybrid electrodes. This emerging class of hybrid electrode combines PTMA with conventional battery cathode transition metal oxides.

Objective 3: Determine chemical mechanisms for degradation resulting from repeated charge storage events.

This will be accomplished using *in situ* electrochemical quartz crystal microbalance with dissipation monitoring (QCM-D), electrochemical characterization (cyclic voltammetry, electrochemical impedance spectroscopy (EIS), materials characterization, and post-mortem analysis.

 Recent Progress

Our project began August 1, 2015, so our initial efforts have focused entirely on Objective 1: "Elucidate the fundamental phenomena that govern charge storage in homopolymer PTMA." Our activities have centered on synthesizing PTMA and establishing baseline behavior of homopolymer PTMA by electrochemical QCMD. This is of utmost importance because development of electrochemical QCMD as a viable characterization route will provide a strong platform to execute all Objectives in the project. **Thus, the major accomplishment for this period has been the demonstration of electrochemical QCMD of PTMA for the first time.[4]** We also report challenges that we have encountered along the way as the form our future path forward.

Figures 1-4 show a collection of data showing an example experiment in which the PTMA cathode is monitored using electrochemical QCMD. The electrode was cycled twice using cyclic voltammetry at a scan rate of 10 mV/s between 0 and 1 V vs. the quasi-Ag reference electrode in lithium perchlorate/propylene carbonate electrolyte mixture. Figure 1 shows a typical cyclic voltammogram, with half-wave potentials matching those expected for PTMA, thus validating the electrochemical approach of our setup. Figure 2 shows the trend in frequency change with respect to voltage. Sharp increases in frequency occur during both cathodic and anodic scans coinciding with the peaks observed in Figure 1's cyclic voltammogram. Therefore, it can be concluded that the changes in frequency are associated with large scale restructuring of the PTMA associated with reduction and oxidation of PTMA. Similarly, Figure 3 shows step-changes in dissipation associated with a softer state upon oxidation and a more rigid state upon reduction. This is consistent with plasticization of the PTMA as caused by an injection of a dopant anion upon the oxidation reaction. Using viscoelastic modeling of the raw data, changes in mass with respect to voltage were calculated, Figure 4. Large decreases in mass occur at the reduction and oxidation events; this may be interpreted as either dissolution of polymer at the redox event or else structural rearrangement caused by sequential expulsion and uptake of the solvated anion. The overall trend from 0 to 1 V, however is an increase in mass upon oxidation and *vice versa* for reduction. From Figure 4 and integration of the data shown in Figure 1, an estimation of the mass transferred per electron ($\Delta m/e$) can be obtained. This leads to a value of 0.446 mg/C, where the theoretical value is 1.03 mg/C. At a higher scan rate of 50 mV/s (Figure 5-8), $\Delta m/e$ increases to 0.626, suggesting an increased efficiency in charge transfer. Notably at

higher scan rate, the change in mass and dissipation lags behind the electrochemical current response. This suggests that mass transfer essentially occurs on a much longer time scale than electron transfer.
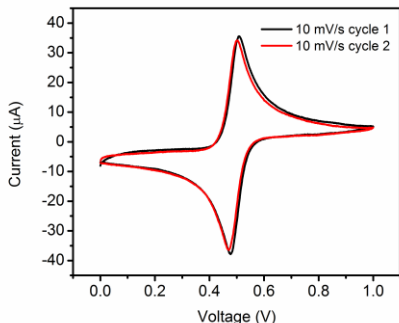

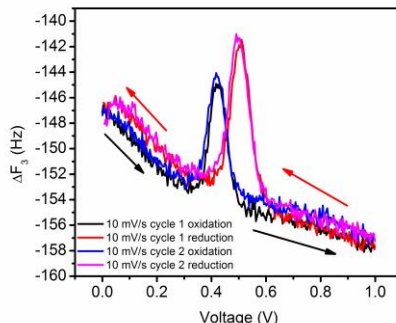Figure 1. Cyclic voltammogram of the PTMA coated sensor as the working electrode.

Figure 2. Variation of ΔF for the 3rd overtone with respect to voltage at 10 mV/s scan rate.
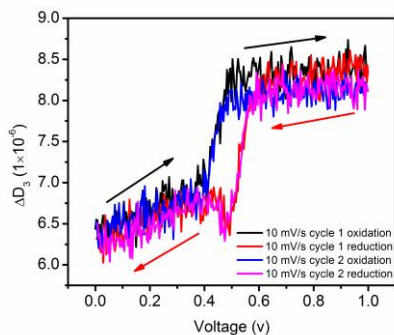
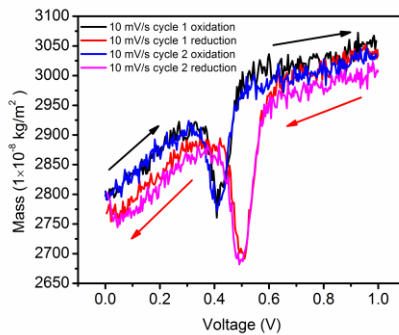Figure 3. Variation of ΔD for the 3rd overtone with respect to voltage at 10 mV/s scan rate.

Figure 4. Change of mass with respect to voltage at 10 mV/s scan rate.

In sum these results demonstrate that electrochemical QCMD is a viable technique for tracking changes in PTMA electrode mass during electrochemical interrogation. We are just beginning to establish the behavior of PTMA toward different electrolytes, paving the way for our future work.

Future Plans

In the next reporting period, we are going to continue with Objective 1 and move into Objective 2. As we continue with Objective 1, we will synthesize a crosslinkable PTMA to combat issues with PTMA dissolution into the electrolyte. Then, we will compare by

electrochemical QCM-D differences between crosslinked and uncrosslinked PTMA. Then, varying amounts of carbon and varying thicknesses will be investigated. As we move into Objective 2 in the next reporting period, we will first examine best practices in depositing PTMA/LiFePO$_4$ electrodes onto the QCM-D sensor and compare with standard coin cell measurements. Once baseline behavior is established, we will examine a variety of scan rates, discharge rates, compositions, and so on to elucidate how charge is stored and transferred in the hybrid electrode. *Acknowledgement: The work was supported by the grant DE-SC0014006; funded by the U.S. Department of Energy, Office of Science.*

References

1   Song, Z. & Zhou, H., Towards sustainable and versatile energy storage devices: an overview of organic electrode materials. *Energy & Environmental Science* 6 (8), 2280-2301 (2013).

2   Liang, Y., Tao, Z., & Chen, J., Organic Electrode Materials for Rechargeable Lithium Batteries. *Advanced Energy Materials* 2 (7), 742-769 (2012).

3   Mike, J.F. & Lutkenhaus, J.L., Recent Advances in Conjugated Polymer Energy Storage. *Journal of Polymer Science Part B-Polymer Physics* 51 (7), 468-480 (2013).

4   Wang, S. & Lutkenhaus, J.L., Quantitative Analysis of Mass Transport in Organic Radical Polymers. *In Preparation*.

Publications

None to report.

Materials and Interfacial Chemistry for Next-Generation Electrical Energy Storage

John Goodenough and Arumugam Manthiram, Materials Science and Engineering Program, University of Texas at Austin, Austin, TX 78712

1. Program Scope

There are three major applications for alkali-metal rechargeable batteries: (1) powering of hand-held devices, (2) powering of electric vehicles, and (3) stationary EES, central or distributed, of electric power delivered from alternative energy sources. Powering of hand-held devices does not compete with fossil fuels, which is why the Li-ion battery has become ubiquitous. However, the rechargeable Li-ion battery is assembled in the discharged state not only to avoid, for safety, the presence of lithium in the anode, but also to facilitate synthesis of a cathode that provides a high voltage. These batteries suffer from three principal drawbacks: (1) a slow rate of charge where it uses a carbon anode, (2) too small a volumetric energy-storage capacity, and (3) on the initial charge, an irreversible loss of Li^+ from the cathode in a solid-electrolyte interphase (SEI) that passivates an anode-electrolyte reaction. In a collaboration between the University of Texas at Austin (UT-Austin) and the Oak Ridge National Laboratory (ORNL), the fundamentals of electrode processes and strategies to alleviate each of these drawbacks separately are being investigated; we are also in a position to integrate the separate findings in the assembly and testing of full cells that promise to compete in performance and cost with the higher energy density stored in a fossil fuel. We present below the recent progress, and the work has led to 68 journal articles published and 7 articles submitted during the past 2 years.

2. Recent Progress

(a) The anode problem

The graphite anode used in today's Li-ion batteries (LIB) requires a slow charge to avoid lithium plating and has a low capacity of ~ 372 mAh/g. Moreover, the Na^+ ion is too large for a carbon anode in a Na-ion battery. There are two approaches to overcome the anode problem: develop (1) alloy nanocomposites that permit a fast charge and retain active particles unchanged by cycling and (2) solid electrolytes with surfaces that are wet by an alkali-metal anode.

Alloy anodes: We have focused on Sb-based alloy anodes for the first option. Sb has a Fermi energy 0.8 eV below that of lithium and a theoretical capacity of 660 mAh/g. However, alloys like those with Sb form an SEI in a liquid electrolyte and undergo large volume changes during charge/discharge cycling. We have demonstrated architectures that give small particles both electronic access to the current collector and ionic access to the electrolyte. Nanoparticle Li-ion and Na-ion carbon composites were synthesized with high-energy ball milling.[1] Extended cyclability to over 1,000 cycles along with a high rate capability has been demonstrated in both Li-ion and Na-ion cells with these composite anodes. In addition, in-depth thermal-stability measurements have shown that the heat generated per unit capacity for both Sb and Cu_2Sb at < 150 °C is ~ 37 % lower than that with graphite, demonstrating safety advantages.[2] Also, the

galvanostatic intermittent titration technique has shown that while the intermetallic NiSb, FeSb, and FeSb$_2$ alloys have a lithium diffusivity in the range of pure Sb, Cu$_2$Sb shows an order of magnitude higher lithium diffusivity due to the persistence of the Cu$_2$Sb phase during cycling.[3]

Alkali-metal anodes: A solid-electrolyte separator that is stable on contact with an alkali-metal anode would act as an SEI that would not rob Li$^+$ or Na$^+$ ions from the cathode. Reversible plating/stripping of an alkali-metal anode through a solid electrolyte may occur without the formation and growth of dendrites during plating if the alkali metal wets the surface of the solid-electrolyte. We began by investigating an oxide Li$^+$ conductor with the garnet framework. Although we were able to develop a Li$^+$ conductivity $\sigma_{Li} \approx 10^{-3}$ S/cm at room temperature, water absorption and dendrite penetration of the grain boundaries of this ceramic commonly occur unless the ceramic is fabricated as a dense solid with close contact between grains. Since large-area, thin ceramic membranes are fragile and not easily made dense over large areas, we abandoned this approach to investigate the use of low-cost gel-polymer/oxide composites that are mechanically robust and flexible.[4] These membranes, if loaded with Al$_2$O$_3$ or Sb$_2$O$_3$, were shown to block dendrites from both a metallic-lithium and a metallic-sodium anode. A poly(vinylidene fluoride – hexafluoropropylene) (PVDF-HFP) polymer deposited on glass-fiber paper absorbs a liquid electrolyte to provide fast alkali-ion transport; the flexible membrane is stable to 200 °C, and a Na half-cell assembled with the Na$_2$MnFe(CN)$_6$ cathode gave at 2C rate high coulombic efficiency. The plating of an alkali-metal without dendrites has been demonstrated.

(b) Insertion cathodes

With a collaboration between UT-Austin and ORNL, a combination of powder neutron and X-ray diffraction has been used to investigate the structure-property relationships of the α- and α_1- forms of the multivalent polyanion material Li$_2$VOPO$_4$.[5] The α_1-Li$_2$VOPO$_4$ displayed a surprising dependency upon reaction rate. At slower rates, the diffraction data indicate a single-phase solid-solution reaction whereas at higher rates, there is evidence for a combination of two-phase and solid-solution reactions. At higher rates, there is a kinetic limitation that leads to a buildup of lithium, followed by a discontinuous change in composition, characteristic of a two-phase reaction.

(c) Conversion cathodes

Sulfur or selenium cathodes: The main obstacles to realization of the potential high volumetric capacity and long cycle life of a S or Se cathode are: (1) the small size of the cathode S$_8$ or Se$_8$ molecules and their reaction products, Li$_2$S or Li$_2$Se, which are both insulators requiring deposition on an electronic conductor contacting the current collector; and (2) the solubility of intermediate Li$_2$S$_x$ or Li$_2$Se$_x$ products that can diffuse to the anode through the separator to poison the anode or to a surface from which they cannot be reconstituted, thus lending to capacity fade; and (3) a cathode architecture with too low a S or Se loading for a competitive volumetric energy density. To suppress the polysulfide diffusion, we have coated a polymer separator on the sulfur cathode side with a thin layer (< 0.2 mg cm^{-2}) of microporous carbon and polyethylene glycol (PEG).[6] The dissolved polysulfides are trapped by the carbon/PEG coating from which they can be reconstituted as starting molecules to give a long cycle life. A post-mortem analysis of the separator by scanning electron microscopy (SEM) combined with energy dispersive spectroscopic analysis after extended cycling reveals that most of the polysulfides are effectively trapped by the carbon/PEG coating. We have also developed carbon architectures and

sodiated Nafion polymer separators to suppress polysulfide migration in ambient-temperature sodium-sulfur batteries.[7]

Air cathodes: In order to have a high voltage air cathode with an aqueous catholyte, we need to have a solid electrolyte for a dual-electrolyte cell that is stable in an aprotic anolyte and an aqueous catholyte. We have demonstrated high rates of charge/discharge with dual-electrolyte cells and the solid electrolyte $Li_{1+x+y}Ti_{2-x}Al_xP_{3-y}Si_yO_{12}$ (**Fig. 1**). With the dual-electrolyte lithium-air cell strategy, we have developed a number of inexpensive catalysts: nitrogen-doped carbons for the oxygen reduction reaction (ORR) and spinel Co_3O_4 or $NiCo_2O_4$ for the oxygen evolution reaction (OER)[8,9] as well as ordered inter-metallic alloys.[10] These lithium-air cells fabricated with nitrogen-doped macro/meso/microporous carbon (macro/meso/micro-NC, a pore-in-pore structure) as the ORR catalyst and carbon-
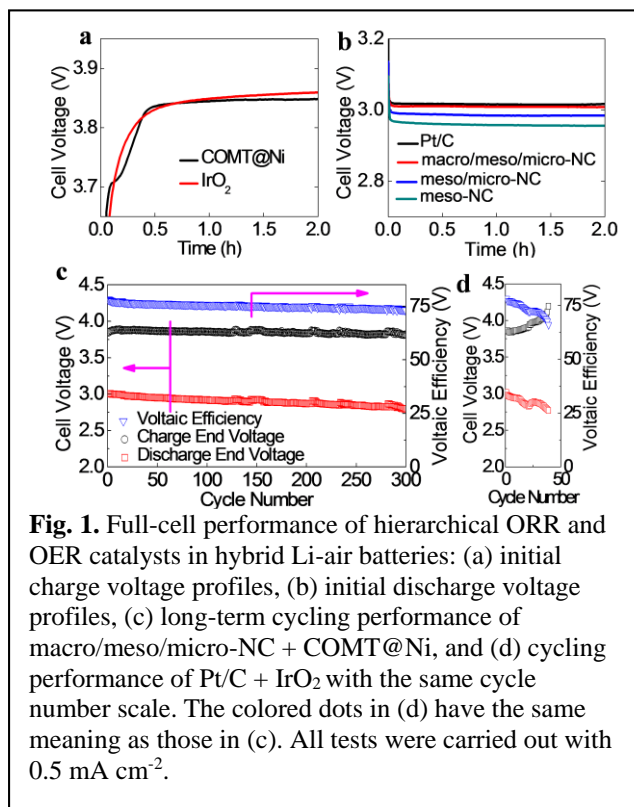

Fig. 1. Full-cell performance of hierarchical ORR and OER catalysts in hybrid Li-air batteries: (a) initial charge voltage profiles, (b) initial discharge voltage profiles, (c) long-term cycling performance of macro/meso/micro-NC + COMT@Ni, and (d) cycling performance of Pt/C + IrO$_2$ with the same cycle number scale. The colored dots in (d) have the same meaning as those in (c). All tests were carried out with 0.5 mA cm^{-2}.

free Co_3O_4 microtrepangs (a wire-in-wire structure) grown onto a nickel foam (COMT@Ni) as the OER catalyst with a decoupled ORR/OER-catalyst hybrid cell configuration exhibit superior cycle life with a lower overvoltage compared to that with the expensive Pt/C as the ORR catalyst and IrO$_2$ as the OER catalyst (**Fig. 1**).[9]

(d) Lithium-metal anode stabilization

The ultimate success of lithium-sulfur and hybrid lithium-air cells depends on the ability to cycle a lithium-metal anode effectively without encountering safety issues or poisoning by any polysulfide that migrates from the cathode to the anode. We have focused on utilizing additives to form a stable SEI layer *in situ* on the lithium-metal anode.[11] For example, addition of a small amount of copper acetate along with polysulfide to the lithium-anode side of a lithium-sulfur cell offers extended cyclability and a smooth lithium-metal surface without much corrosion even after 100 cycles. XPS analysis and EDS analysis show that copper acetate leads to the formation of a smooth Cu_2S and CuS layer on the lithium-metal surface, which prevents penetration of polysulfide into the bulk of the lithium-metal during cycling. In addition, by employing a specifically designed electrolyte and a combination of advanced time-of-flight – secondary ion mass spectroscopic (TOF-SIMS) analysis and X-ray diffraction, we have identified that the crystallinity of the impurity phases formed in the lithium-metal anode *via* chemical reactions with the electrolyte is the dominant factor involved in the degradation of lithium-metal anode in lithium-sulfur cells.[12]

3. Future Plans

Building on the above results, our future efforts are focused on the following:

- Glass and polymer electrolytes from which metallic lithium and/or sodium anodes can be plated without dendrite formation
- Conditioning of glass electrolytes containing electric dipoles by thermal treatment in an *ac* electric field
- Exploration of a supercapacitor with a solid glass electrolyte containing electric dipoles
- Development of all-solid-state Li and/or Na batteries of large capacity, energy density, and cycle life
- Lithium-sulfur and sodium-sulfur cells with a more efficient capture of polysulfides
- Li-air and Na-air cells with the exploration of efficient low-cost electrocatalysts
- Probing of interfacial chemistry with neutrons
- Phosphorous-based anodes for lithium-ion and sodium-ion batteries
- Soft chemistry synthesis approaches to assess multi-valent cation insertion chemistry

References

1. S.-O. Kim and A. Manthiram, "High-performance Zn–TiC–C Nanocomposite Alloy Anode with Exceptional Cycle Life for Lithium-ion Batteries," *ACS Applied Materials & Interfaces* **7**, 14801-14807 (2015).
2. E. Allcorn and A. Manthiram, "Thermal Stability of Sb and Cu_2Sb Anodes in Lithium-ion Batteries," *Journal of the Electrochemical Society* **162**, A1778-A1786 (2015).
3. E. Allcorn and A. Manthiram, "Lithium Diffusivity in Antimony-based Intermetallic and FeSb-TiC Composite Anodes as Measured by GITT," *Physical Chemistry Chemical Physics* **17**, 28837-28843 (2015).
4. H. C. Gao, B. Guo, J. Song, K. S. Park, and J. B. Goodenough, "A Composite Gel–Polymer/Glass–Fiber Electrolyte for Sodium-ion Batteries," *Advanced Energy Materials* 1402235 (2015).
5. G. He, C. A. Bridges, and A. Manthiram, "Crystal Chemistry of Electrochemically and Chemically Lithiated Layered alpha(I)-$LiVOPO_4$," *Chemistry of Materials* **27**, 6699-6707 (2015).
6. S.-H. Chung and A. Manthiram, "A Polyethylene Glycol-Wrapped Microporous Carbon Coating as a Polysulfide Trap for Utilizing Pure Sulfur Cathodes in Lithium-Sulfur Batteries," *Advanced Materials* **26**, 7352-7357 (2014).
7. A. Manthiram and X. Yu, "Ambient-temperature Sodium-sulfur Batteries," *Small* **11**, 2108-2114 (2015).
8. A. Manthiram and L. Li, "Hybrid and Aqueous Lithium-air Batteries," *Advanced Energy Materials* **5**, 1401302 (2015).
9. L. Li, C. Liu, G. He, D. Fan, and A. Manthiram, "Hierarchical Pore-in-pore and Wire-in-wire Catalysts for Rechargeable Zn- and Li-air Batteries with Ultra-long Cycle Life and High Cell Efficiency," *Energy and Environmental Science* **8**, 3274-3282 (2015).
10. Z. Cui, L. Li, A. Manthiram, and J. B. Goodenough, "Enhanced Cycling Stability of Hybrid Li-Air Batteries Enabled by Ordered Pd_3Fe Intermetallic Electrocatalyst," *Journal of the American Chemical Society* **137**, 7278-7281 (2015).
11. C. Zu and A. Manthiram, "Stabilized Lithium Surface in a Polysulfide-Rich Environment of Lithium-Sulfur Batteries," *Journal of Physical Chemistry Letters* **5**, 2522-2527 (2014).
12. C. Zu, A. Dolocan, and A. Manthiram, "Breaking down the Crystallinity: The Path for Advanced Lithium Batteries," *Advanced Energy Materials* **1501933**: 1-9 (2015). DOI: 10.1002/aenm.20150193.

LIST OF PUBLICATIONS DURING THE PAST 2 YEARS

Articles Published

1. J. B. Goodenough and A. Manthiram, "A Perspective on Electrical Energy Storage," *MRS Communications* **4**, 135-142 (2014). DOI: 10.1557/mrc.2014.36

2. I.-T. Kim, E. Allcorn, and A. Manthiram, "High-performance FeSb-TiC-C Nanocomposite Anodes for Sodium-ion Batteries," *Physical Chemistry Chemical Physics* **16**, 12884-12889 (2014). DOI: 10.1039/C4CP01240B

3. X. Yu and A. Manthiram, "Highly Reversible Room-temperature Sulfur/Long-chain Sodium Polysulfide Batteries," *Journal of Physical Chemistry Letters* **5**, 1943-1947 (2014). DOI: 10.1021/jz500848x

4. X. Yu and A. Manthiram, "Capacity Enhancement and Discharge Mechanisms of Room-temperature Sodium-sulfur Batteries," *ChemElectroChem* **1**, 1275-1280 (2014). DOI: 10.1002/celc.201402112

5. L. Li, S.-H. Cai, S. Dai, and A. Manthiram, "Advanced Hybrid Li-air Batteries with High-performance Mesoporous Nanocatalysts," *Energy & Environmental Science* **7**, 2630-2636 (2014). DOI: 10.1039/C4EE00814F

6. A. Manthiram, Y.-Z. Fu, S.-H. Chung, C. Zu, and Y.-S. Su, "Rechargeable Lithium-sulfur Batteries," *Chemical Reviews* **114**, 11751-11787 (2014). DOI: 10.1021/cr500062v

7. J.-H. Kim, A. Huq, M. Chi, N. P. W. Pieczonka, E. Lee, C. A. Bridges, M. Tessema, A. Manthiram, K. A. Persson, and B. R. Powell, "Integrated Nano-Domains of Disordered and Ordered Spinel Phases in $LiNi_{0.5}Mn_{1.5}O_4$ for Li-Ion Batteries," *Chemistry of Materials* **26**, 4377-4386 (2014). DOI: 10.1021/cm501203r

8. L. Li and A. Manthiram, "Decoupled Bifunctional Air Electrodes for High-performance Hybrid Lithium-air Batteries," *Nano Energy* **9**, 94-100 (2014). DOI: 10.1016/j.nanoen.2014.07.002

9. C. Zu and A. Manthiram, "High-performance Li/dissolved Polysulfide Batteries with an Advanced Cathode Structure Containing High Sulfur Loading," *Advanced Energy Materials* **4**, 1400897 (2014). DOI: 10.1002/aenm.201400897

10. C. Zu and A. Manthiram, "Stabilized Lithium-metal Surface in a Polysulfide-rich Environment of Lithium-sulfur Batteries," *Journal of Physical Chemistry Letters* **5**, 2522-2527 (2014). DOI: 10.1021/jz501352e

11. L. Li, Y.-Z. Fu, and A. Manthiram, "Imidazole-buffered Acidic Catholytes for Hybrid Li-air Batteries with High Practical Energy Density," *Electrochemistry Communications* **47**, 67-70 (2014). DOI: 10.1016/j.elecom.2014.07.027

12. I.-T. Kim, S.-O. Kim, and A. Manthiram, "Effect of TiC Addition on SnSb-C Composite Anodes for Sodium-ion Batteries," *Journal of Power Sources* **269**, 848-854 (2014). DOI: 10.1016/j.jpowsour.2014.07.081

13. S.-H. Chung and A. Manthiram, "A Polyethylene Glycol-wrapped Microporous Carbon Coating as a Polysulfide Trap for Utilizing Pure Sulfur Cathodes in Lithium-sulfur Batteries," *Advanced Materials* **26**, 7352-7357 (2014). DOI: 10.1002/adma.201402893

14. S.-H. Chung and A. Manthiram, "Eggshell-membrane-derived Polysulfide Absorbents for Highly Stable and Reversible Lithium-sulfur Cells," *ACS Sustainable Chemistry & Engineering* **2**, 2248-2252 (2014). DOI: 10.1021/sc500452j

15. X. Yu and A. Manthiram, "Room-temperature Sodium-sulfur Batteries with Liquid-phase Sodium Polysulfide Catholytes and Binder-free Multi-wall Carbon Nanotube (MWCNT) Fabric Electrodes," *Journal of Physical Chemistry C* **118**, 22952-22959 (2014). DOI: 10.1021/jp507655u

16. Z. Moorhead-Rosenberg, E. Allcorn, and A. Manthiram, "*In-situ* Mitigation of First-cycle Anode Irreversibility in a New Spinel / FeSb Lithium-ion Cell Enabled via a Microwave-assisted Chemical Lithiation Process," *Chemistry of Materials* **26**, 5905-5913 (2014). DOI: 10.1021/cm5024426

17. C. Zu, M. Klein, and A. Manthiram, "Activated Li_2S as a High-performance Cathode for Rechargeable Lithium-sulfur Batteries," *Journal of Physical Chemistry Letters* **5**, 3986-3991 (2014). DOI: 10.1021/jz5021108

18. K. L. Harrison, C. A. Bridges, C. U. Segre, C. D. Varnado, D. Applestone, C. W. Bielawski, M. P. Paranthaman, and A. Manthiram, "Chemical and Electrochemical Lithiation of $LiVOPO_4$ Cathodes for Lithium-ion Batteries," *Chemistry of Materials* **26**, 3849-3861 (2014). DOI: 10.1021/cm501588j

19. B. K. Guo, X. Q. Yu, X. G. Sun, M. F. Chi, Z. A. Qiao, J. Liu, Y. S. Hu, X. Q. Yang, J. B. Goodenough, and S. Dai, "A Long-life Lithium-ion battery with a Highly Porous $TiNb_2O_7$ Anode for Large-scale Electrical Energy Storage," *Energy & Environmental Science* **7**, 2220-2226 (2014). DOI: 10.1039/C4EE00508B

20. F. R. Beck, Y. Q. Cheng, Z. H. Bi, M. Feygenson, C. A. Bridges, Z. Moorhead-Rosenberg, A. Manthiram, J. B. Goodenough, M. P. Paranthaman, and A. Manivannan, "Neutron Diffraction and Electrochemical Studies of $Na_{0.79}CoO_2$ and $Na_{0.79}Co_{0.7}Mn_{0.3}O_2$ Cathodes for Sodium-ion Batteries," *Journal of the Electrochemical Society* **161**, A961-A967 (2014). DOI: 10.1149/2.025406jes

21. V. Augustyn and A. Manthiram, "Characterization of Layered Li*M*O_2 Oxides for the Oxygen Evolution Reaction in Metal-air Batteries," *ChemPlusChem* **80**, 422-427 (2015). DOI: 10.1002/cplu.201402107R1

22. A. Manthiram and L. Li, "Hybrid and Aqueous Lithium-air Batteries," *Advanced Energy Materials* **5**, 1401302: 1-17 (2015). DOI: 10.1002/aenm.201401302

23. S.-O. Kim and A. Manthiram, "A Facile, Low-cost Synthesis of High-performance Silicon-based Composite Anodes with High Tap Density for Lithium-ion Batteries," *Journal of Materials Chemistry A* **3**, 2399-2406 (2015). DOI: 10.1039/C4TA06113F

24. X. Yu and A. Manthiram, "Na_2S-carbon Nanotube Fabric Electrodes for Room Temperature Sodium-sulfur Batteries," *Chemistry – A European Journal* **21**, 4233-4237 (2015). DOI: 10.1002/chem.201405344

25. G. Zhou, Y. Zhao, C. Zu, and A. Manthiram, "Free-Standing TiO_2 Nanowire-Embedded Graphene Hybrid Membrane for Advanced Li/Dissolved Polysulfide Batteries," *Nano Energy* **12**, 240-249 (2015). DOI: 10/1016/j.nanoen.2014.12.029

26. L. Qie and A. Manthiram, "A Facile Layer-by-layer Approach for High-areal-capacity Sulfur Cathodes," *Advanced Materials* **27**, 1694-1700 (2015). DOI: 10.1002adma.201405698

27. E. Allcorn and A. Manthiram, "High-rate, High-density FeSb-TiC-C Nanocomposite Anodes for Lithium-ion Batteries," *Journal of Materials Chemistry A* **3**, 3891-3900 (2015). DOI: 10/1039/C4TA06869F

28. J. Leibowitz, E. Allcorn, and A. Manthiram, "SnSb-TiC-C Nanocomposite Alloy Anodes for Lithium-ion Batteries," *Journal of Power Sources* **279**, 549-554 (2015). DOI: 10.1016/j.jpowsour.2015.01.055

29. A. Manthiram, S.-H. Chung, and C. Zu, "Lithium-sulfur Batteries: Progress and Prospective," *Advanced Materials* **27**, 1980-2006 (2015). DOI: 10.1002/adma.201405115

30. N. Colligan, V. Augustyn, and A. Manthiram, "Evidence of Localized Lithium Removal in Layered and Lithiated Spinel $Li_{1-x}CoO_2$ ($0 \le x \le 0.9$) under Oxygen Evolution Reaction Conditions," *Journal of Physical Chemistry C* **119**, 2335-2340 (2015). DOI: 10.1021/jp511176j

31. I.-T. Kim, E. Allcorn, and A. Manthiram, "Cu_6Sn_5-TiC-C Nanocomposite Anodes for High-performance Sodium-ion Batteries," *Journal of Power Sources* **281**, 11-17 (2015). DOI: 10.1016/j.jpowsour.2015.01.163

32. C. Zu, L. Li, L. Qie, and A. Manthiram, "Expandable-graphite-derived Graphene for Next-generation Battery Chemistries," *Journal of Power Sources* **284**, 60-67 (2015). DOI: 10.1016/j.jpowsour.2015.03.009

33. A. Manthiram and X. Yu, "Ambient-temperature Sodium-sulfur Batteries," *Small* **11**, 2108-2114 (2015). DOI: 10/1002/smll.201403257

34. G. Zhou, Y. Zhao, and A. Manthiram, "Dual-confined Flexible Sulfur Cathodes Encapsulated in Nitrogen-doped Double-shelled Hollow Carbon Spheres and Wrapped with Graphene for Li-S Batteries," *Advanced Energy Materials* **5**, 1402263: 1-10 (2015). DOI: 10.1002/aenm.201402263

35. X. Yu and A. Manthiram, "Ambient-temperature Sodium-sulfur Batteries with a Sodiated Nafion Membrane and a Carbon Nanofiber-Activated Carbon Composite Electrode," *Advanced Energy Materials* **5**, 1500350: 1-6 (2015). DOI: 10.1002/aenm.201500350

36. S. Liu, L. Li, H. S. Ahn, and A. Manthiram, "Delineating the Roles of Co_3O_4 and N-doped Carbon Nanoweb (CNW) in Bifunctional Co_3O_4/CNW Catalysts for Oxygen Reduction and Oxygen Evolution Reactions," *Journal of Materials Chemistry A* **3**, 11615-11623 (2015). DOI: 10.1039/C5TA00661A

37. Z. Cui, L. Li, A. Manthiram, and J. B. Goodenough, "Enhanced Cycling Stability of Hybrid Li-Air Batteries Enabled by Ordered Pd_3Fe Intermetallic Electrocatalyst," *Journal of the American Chemical Society* **137**, 7278-7281 (2015). DOI: 10.1021/jacs.5b03865

38. S.-H. Chung, R. Singhal, V. Kalra, and A. Manthiram, "A Porous Carbon Mat as an Electrochemical Testing Platform for Investigating the Polysulfide Retention of Various Cathode Configurations in Li-S Cells," *Journal of Physical Chemistry Letters* **6**, 2163-2169 (2015). DOI: 10.1021/acs.jpclett.5b00927

39. E. Allcorn and A. Manthiram, "Thermal Stability of Sb and Cu_2Sb Anodes in Lithium-ion Batteries," *Journal of the Electrochemical Society* **162**, A1778-A1786 (2015). DOI: 10.1149/2.0331509jes

40. S.-H. Chung, P. Han, R. Singhal, V. Kalra, and A. Manthiram, "Electrochemically Stable Rechargeable Lithium-Sulfur Batteries with a Microporous Carbon Nanofiber Filter for Polysulfide," *Advanced Energy Materials* **5** (2015). DOI: 10.1002/aenm.201500738

41. S.-O. Kim and A. Manthiram, "High-performance Zn–TiC–C Nanocomposite Alloy Anode with Exceptional Cycle Life for Lithium-ion Batteries," *ACS Applied Materials & Interfaces* **7**, 14801-14807 (2015). DOI: 10.1021/acsami.5b03110

42. J. Leibowitz, E. Allcorn, and A. Manthiram, "$FeSn_2$-TiC Nanocomposite Alloy Anodes for Lithium Ion Batteries," *Journal of Power Sources* **295**, 125-130 (2015). DOI: 10.1016/j.jpowsour.2015.06.144

43. V. Augustyn, S. Therese, T. C. Turner, and A. Manthiram, "Nickel-Rich Layered $LiNi_{1-x}M_xO_2$ (M = Mn, Fe, and Co) Electrocatalysts with High Oxygen Evolution Reaction

Activity," *Journal of Materials Chemistry* **3**, 16604-16612 (2015). DOI: 10.1039/C5TA04637H

44. C.-H. Chang, S.-H. Chung, A. Manthiram, "Ultra-lightweight PANiNF/MWCNT-functionalized Separators with Synergistic Suppression of Polysulfide Migration for Li-S Batteries with Pure Sulfur Cathodes," *Journal of Materials Chemistry A* **3**, 18829-18834 (2015). DOI: 10.1039/C5TA05053G

45. Y. Zhao and A. Manthiram, "$Bi_{0.94}Sb_{1.06}S_3$ Nanorod Cluster Anodes for Sodium-ion Batteries: Enhanced Reversibility by the Synergistic Effect of the Bi_2S_3–Sb_2S_3 Solid Solution," *Chemistry of Materials* **27**, 6139-6145 (2015). DOI: 10.1021/acs.chemmater.5b02833

46. E. Allcorn, S. O. Kim, and A. Manthiram, "Thermal Stability of Active/Inactive Nanocomposite Anodes based on Cu_2Sb in Lithium-ion Batteries," *Journal of Power Sources* **299**, 501-508 (2015). DOI: 10.1016/j.jpowsour.2015.09.020

47. L. Li, C. Liu, G. He, D. Fan, and A. Manthiram, "Hierarchical Pore-in-pore and Wire-in-wire Catalysts for Rechargeable Zn- and Li-air Batteries with Ultra-long Cycle Life and High Cell Efficiency," *Energy and Environmental Science* **8**, 3274-3282 (2015). DOI: 10.1039/C5EE02616D

48. V. Augustyn and A. Manthiram, "Effects of Chemical versus Electrochemical Delithiation on the Oxygen Evolution Reaction Activity of Nickel-rich Layered Li*M*O_2," *Journal of Physical Chemistry Letters* **6**, 3787-3791 (2015). DOI: 10.1021/acs.jpclett.5b01538

49. G. He, C. A. Bridges, and A. Manthiram, "Crystal Chemistry of Electrochemically and Chemically Lithiated Layered α_I-LiVOPO_4," *Chemistry of Materials* **27**, 6699-6707 (2015).

50. J.-Y. Liao and A. Manthiram, "High-performance $Na_2Ti_2O_5$ Nanowire Arrays Coated with VS_2 Nanosheets for Sodium-ion Storage," *Nano Energy* **18**, 20-27 (2015). DOI: 10.1016/j.nanoen.2015.09.014

51. E. Allcorn and A. Manthiram, "Lithium Diffusivity in Antimony-based Intermetallic and FeSb-TiC Composite Anodes as Measured by GITT," *Physical Chemistry Chemical Physics* **17**, 28837-28843 (2015). DOI: 10.1039/C5CP04023J

52. S. Wan, X. G. Jiang, B. K. Guo, S. Dai, J. B. Goodenough, and X. G. Sun, "A Stable Fluorinated and Alkylated Lithium Malonatoborate Salt for Lithium Ion Battery Application," *Chemical Communications* **51**, 9817-9820 (2015). DOI: 10.1039/c5cc01428j

53. J. S. Zhang, Y. Bai, X. G. Sun, Y. C. Li, B. K. Guo, J. H. Chen, G. M. Veith, D. K. Hensley, M. P. Paranthaman, J. B. Goodenough, and S. Dai, "Superior Conductive Solid-like Electrolytes: Nanoconfining Liquids within the Hollow Structures," *Nano Letters* **15**, 3398-3402 (2015). DOI: 10.1021/acs.nanolett.5b00739

54. H. C. Gao, B. K. Guo, J. Song, K. Park, and J. B. Goodenough, "A Composite Gel-Polymer/Glass-Fiber Electrolyte for Sodium-ion Batteries," *Advanced Energy Materials* **5**, 1402235, **DOI:** 10.1002/aenm.201402235 (2015). DOI: 10.1002/aenm.201402235

55. C. Zu, A. Dolocan, and A. Manthiram, "Breaking down the Crystallinity: The Path for Advanced Lithium Batteries," *Advanced Energy Materials* **1501933**: 1-9 (2015). DOI: 10.1002/aenm.20150193

56. S.-H. Chung, C.-H. Chang, and A. Manthiram, "Robust, Ultra-tough Flexible Cathodes for High-energy Li-S Batteries," *Small* **DOI:** 10.1002/smll.201503167 (2015).

57. L. Li and A. Manthiram, "Long-life, High-Voltage Acidic Zn-air Batteries," *Advanced Energy Materials* **1502054**, 1-7 (2015). DOI: 10.1002/aenm.201502054

58. C.-H. Chang, S.-H. Chung, and A. Manthiram, "Effective Stabilization of High-loading Sulfur Cathode and Lithium-metal Anode in Li-S Batteries," *Small* **12**, 174-179 (2016). DOI: 10.1002/smll.201502505

59. J.-Y. Liao, B. De Luna, and A. Manthiram, "TiO$_2$-B Nanowire Arrays Coated with Layered MoS$_2$ Nanosheets for Lithium and Sodium Storage," *Journal of Materials Chemistry A* **4**, 801-806 (2016). DOI: 10.1039/C5TA07064C

60. Y. Li, M. P. Paranthaman, L. W. Gill, E. W. Hagaman, Y. Wang, A. P. Sokolov, S. Dai, C. Ma, M. Chi, G. M. Veith, A. Manthiram, and J. B. Goodenough, "Conduction below 100 °C in Nominal Li$_6$ZnNb$_4$O$_{14}$," *Journal of Materials Science* **51**, 854-860 (2016). DOI: 10.1007/s10853-015-9408-z

61. S. Liu, L. Li, N. A. Patterson, and A. Manthiram, "Morphological Transformations during *In-situ* Electrochemical Generation of 2-Dimensional Co$_3$O$_4$ Hexagonal Nanoplates," *Journal of the Electrochemical Society* **163**, A150-A155 (2016). DOI: 10.1149/2.0331602jes

62. X. Yu and A. Manthiram, "Performance Enhancement and Mechanistic Studies of Room-temperature Sodium-sulfur Batteries with a Carbon-coated Functional Nafion Separator and a Na$_2$S/Activated Carbon Nanofiber Cathode," *Chemistry of Materials* **28**, 896-905 (2016). DOI: 10.1021/acs.chemmater.5b04588 (2016)

63. K. A. Jarvis, C.-C. Wang, J. C. Knight, L. Rabenberg, A. Manthiram, and P. J. Ferreira, "Formation and Effect of Orientation Domains in Layered Oxide Cathodes of Lithium-ion Batteries," *Acta Materialia* **108**, 264-270 (2016).

64. S. O. Kim and A. Manthiram, "Facile Synthesis and Enhanced Sodium-storage Performance of Chemically Bonded CuP$_2$/C Hybrid Anode," *Chemical Communications* **52**, 4337-4340 (2016).

65. Y. Li, M. Parans Paranthaman, K. Akato, A. K. Naskar, A. M. Levine, R. J. Lee, S. O. Kim, J. Zhang, S. Dai, and A. Manthiram, "Tire-derived Carbon Composite Anodes for Sodium-ion Batteries," *Journal of Power Sources* **316**, 232-238 (2016).

66. C. Zu, L. Li, J. Guo, S. Wang, D. Fan, and A. Manthiram, "Understanding the Redox Obstacles in High Sulfur-loading Li-S Batteries and Design of an Advanced Gel Cathode, " *Journal of Physical Chemistry Letters* **7**, 1392-1399 (2016).

67. Z. Jiang, Z.-J. Jiang, T. Maiyalagan, and A. Manthiram, "Cobalt Oxide-coated N- and B-doped Graphene Hollow Spheres as a Bifunctional Electrocayalyst for Oxygen Reduction and Oxygen Evolution Reactions," *Journal of Materials Chemistry A* **4**, 5877-5889 (2016).

68. Z. Cui, C. Zu, W. Zhou, A. Manthiram, and J. B. Goodenough, "Mesoporous Titanium Nitride-enabled Highly Stable Lithium-Sulfur Batteries," *Advanced Materials* **DOI:** 10.1002/adma.201601382 (2016).

Articles Submitted

69. B. Guo, Z.-A. Qiao, G.-S. Xiao, J. Song, J. B. Goodenough, and S. Dai, "Highly Porous NaTi$_2$(PO$_4$)$_3$ Electrode with Ultra-High Rate and Long Life for Room-Temperature Sodium-ion Batteries," *Journal of the Electrochemical Society* (submitted).

70. J. H. Jang, E. Lee, P. Xiao, K. Park, I. Y. Kim, G. Henkelman, S.-J., Hwang, Y.-U. Kwon, and J. B. Goodenough, "Superior Oxygen Electrocatalysis on Novel RuSe$_x$ Nanoparticles for Rechargeable Air Cathodes," *Angewandte Chemie* (submitted).

71. W. Zhou, S. Wang, B. Xu, B.-C. Yu, S. Xin, K. Park, H. Duan, Y. Li, A. Manthiram, and J. B. Goodenough, "Polymer/Ceramic/Polymer Sandwich Electrolyte for All-solid-state Lithium Batteries," *Nano Energy* (submitted).

72. S.-M. Oh, P. Oh, S.-O. Kim, and A. Manthiram, "A Low-cost, Layered Na[$Cu_{0.2}$($Fe_{1/3}Mn_{2/3}$)$_{0.8}$]O_2 Cathode Assessed in a Full Cell with a P-Ti_2P-C Composite Anode for Sodium-ion Batteries," *Chemistry of Materials* (submitted).

73. A. Manthiram, "Electrical Energy Storage: Materials Challenges and Prospects," *MRS Bulletin* (submitted).

74. M. J. Klein, K. Goossens, C. W. Bielawski, and A. Manthiram, "Elucidating the Electrochemical Activity of Electrolyte-insoluble Polysulfide Species in Lithium-sulfur Batteries," *Journal of the Electrochemical Society* (submitted).

75. X. Yu and A. Manthiram, "Performance Enhancement and Mechanistic Studies of Magnesium-Sulfur (Mg-S) Batteries with an Advanced Cathode Structure," *Energy and Environmental Science* (submitted).

Leveraging Kinetic Control in the Assembly and Sorption Properties of Nanostructured Porous Materials

Principal Investigator: Adam J. Matzger
Co-Investigator: Antek G. Wong-Foy
Department of Chemistry and the Macromolecular Science and Engineering Program
University of Michigan, Ann Arbor, MI 48109-1055

Program Scope

The overarching theme of the program is to develop, understand, and deploy new methods for sorbent synthesis. The development of new high performance sorbents is critical for a variety of established (separations, purification) and emerging (hydrogen storage, carbon capture) technologies. Coordination polymers offer tremendous promise for such applications and complement greatly established materials such as zeolites and carbons. The specific goal of this program is to develop an understanding of how kinetic control elements can be leveraged to improve microporous coordination polymer (MCP) synthesis. A major issue is control over phase selection by manipulating the kinetic pathways leading to phase formation thereby affording access to advanced sorbents from simple feedstocks. In a second aspect of the work we are developing an approach to interface crystalline MCPs with soft materials, such as polymers, by leveraging some of our developments in the area of mixed linker MCPs.

Recent Progress

Using modulators to achieve phase-selective synthesis of Zr-based MCPs

Unlike traditional Zn- and Cu-based MCPs, Zr-based MCPs show significant tolerance to water and in fact are proving to be excellent desiccants for humid gas streams.[1] We have now demonstrated the synthesis of a 2-D Zr-based MCP, UMCM-309a, derived from H_3BTB by using aqueous HCl as the chemical modulator.[2] Structure elucidation of UMCM-309a (Figure 1) showed that it is non-
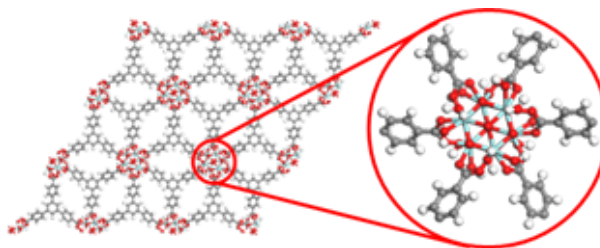
Figure 1. Structural model of UMCM-309a and expansion of a single Zr_6 cluster.

interpenetrated and is comprised of nominally planar $Zr_6(\mu_3\text{-}O)_4(\mu_3\text{-}OH)_4(CO_2)_6(OH)_6(H_2O)_6$ secondary building units (SBUs). UMCM-309a is stable in aqueous HCl solution for over four months. Based on the N_2 adsorption isotherm of UMCM-309a, the surface area (BET method) was 810 m^2/g which is comparable to UiO-66, a benchmark Zr-material.

While modulators are extensively used in Zr-based MCP synthesis to increase crystallinity, they are often assumed to be removed from the framework after washing with polar solvents such as DMF. Here a rare case was found where the modulator can be incorporated and subsequently removed to affect the interlayer spacing of the resulting solid. Using biphenyl-4-

carboxylic acid in place of aqueous HCl as the modulator generates a new material, UMCM-309c, with an interlayer spacing of 14.8 Å compared to 7.04 Å of UMCM-309a. From computational models, the drastic change in the interlayer spacing results from substituting the free hydroxyl groups of the Zr_6 cluster with the organic carboxylate modulator (Figure 2). The role of the modulator can be further controlled by treating the material with water/DMF mixture at 120 °C to remove biphenyl-4-carboxylate. After the treatment, UMCM-309c yields the parent UMCM-309a with the original interlayer spacing.
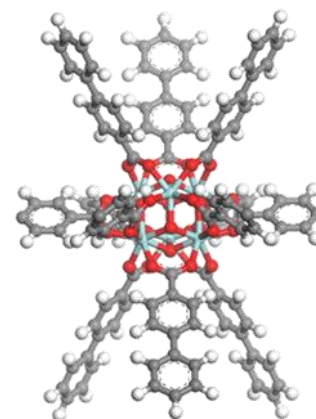
Figure 2. Model of biphenyl-4-carboxylate groups replacing the terminal OH and H_2O groups of the Zr_6 cluster.

Topological analysis of tetratopic linker-derived MCPs.

A geometric analysis of linker geometry and flexibility was performed in the context of achieving a method to predict the net topology of tetratopic-linker based Zr MCPs. Tetratopic linkers were categorized into tetrahedral, planar square or planar rectangular groups with an emphasis on linker flexibility (Figure 3). The combination of these three linker shapes and known Zr_6 SBUs generates a relatively small number of net topologies. A flow chart demonstrates this strategy and the resulti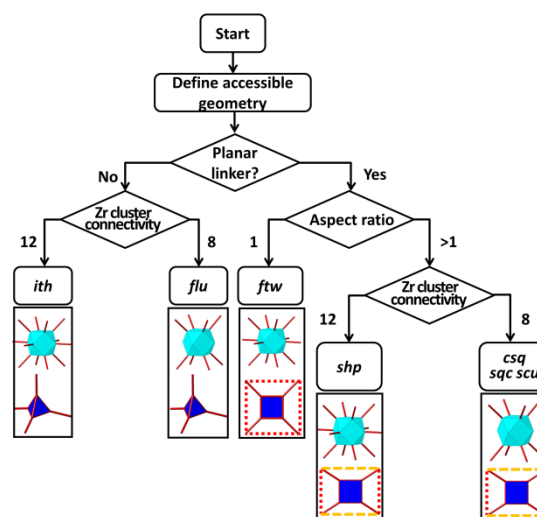ng predicted net topologies (Figure 4). To test this, all reported tetratopic-linker based Zr MCPs were analyzed according to Figure 4 and all predicted topologies matched well with literature results. More importantly, two new Zr MCPs (UMCM-312 and UMCM-313) were predicted based on tetratopic linkers known in the literature. These have subsequently been synthesized in our laboratory, and their topologies confirmed by single crystal X-ray diffraction studies as matchingpredictions.[3]

Figure 3. Classification of tetratopic linkers and mechanisms by which a flexible linker can access multiple geometries.

UMCM-312 contains a tetratopic linker utilizing a biphenyl core to target the shape of a tetrahedron (Figure 5). The two aryl rings in the biphenyl core exhibit a distorted tetrahedral shape with a dihedral angle of 29.9° matching our predication that the shape of this linker is best thought of as a tetrahedron for topological analysis. UMCM-313 takes advantage of a perylene based tetratopic linker to achieve a rectangular shape (Figure 6). An analysis of the crystal structure determined the topology to be

Figure 4. Topology prediction decision tree for designing tetratopic based Zr MCPs.

that of the ***csq*** net in agreement with our predictions, and unambiguously confirming our assignment of the linker as a rectangular. The successful prediction of these two new MCP nets demonstrates predictable topologies could be achieved by tuning the geometry of the linker. Moreover it highlights the importance of understanding linker flexibility (dynamics) thus setting the stage for some of the work proposed in the renewal period.

Polymer@MOF@MOF: "Grafting From" Atom Transfer Radical Polymerization for the synthesis of hybrid porous solids
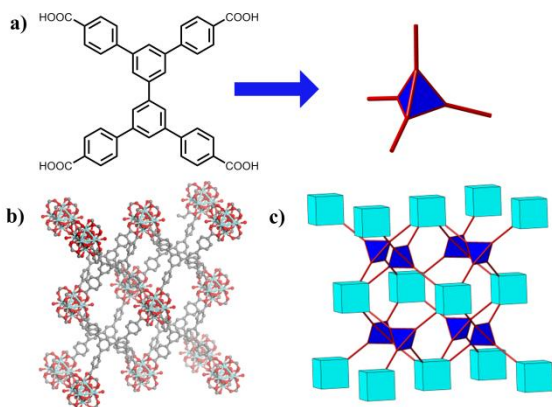
Figure 5. Structure of UMCM-312 a) Linker structure and its topology representation. b) Crystal structure of UMCM-312. c) Topology representation of ***flu*** topology.
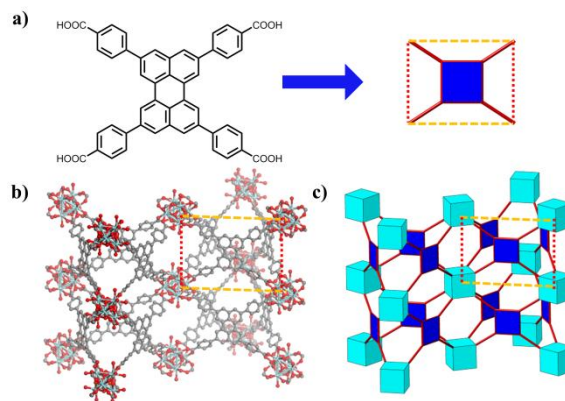
Figure 6. Structure of UMCM-313 a) Linker structure and its topology representation. b) Crystal structure of UMCM-313. c) Topology representation of ***csq*** topology.

Among soft materials, organic polymers possess properties difficult to achieve in crystalline materials. The effort of this second major focus area is to combine the properties of both classes of materials into a single entity; specifically, a hybrid polymer MCP architecture, in which polymer chains are covalently tethered to the outer shell of a core-shell MCP, which is termed polymer@MOF@MOF. The utilization of core-shell architecture enables controlling the extent to which polymer intrudes into the internal crystal pores. This strategy achieves polymer hybridization while maintaining the internal pore structure of the unfunctionalized MCP. Specifically, a shell of IRMOF-3, containing 2-aminoterephthalic was grown from the surface of MOF-5 to form IRMOF-3@MOF-5 (step a, Figure 7).[4] The initiator carrying sites can be incorporated into the IRMOF-3 outer shell through postsynthetic modification (PSM) by the reaction of amine groups in IRMOF-3 with 2-bromoisobutyric anhydride (step b, Figure 7). The resulting MCP is denoted as ICL@IRMOF-3@MOF-5 (initiator carrying linker@IRMOF-3@MOF-5). Polymerization reaction with methyl methacrylate as monomers was then carried out employing copper mediated atom transfer radical polymerization to yield the hybrid materials poly(methyl methacrylate)@IRMOF-3@MOF-5 (hereafter referred to as PMMA@IRMOF-3@MOF-5) (step c, Figure 7).

PXRD analysis of the MCPs obtained from each step confirms that the framework maintains its structure after shell formation, PSM, and polymer grafting. BET surface areas indicates that the MOF-5 core is intact and the porosity is accessible. Moreover, the depth of polymerization from the external surface of the MOF hybrid material was investigated by Raman microscopy. The polymer is found to extend to a depth of ~10 μm into the crystal which is equal to the depth of IRMOF-3 shell. These results demonstrate co-localization of shell and polymer consistent with the selective initiation of polymerization from the sites where the initiator-carrying linker is present. Hence, by modulating the

Figure 7. Synthetic route to PMMA@IRMOF-3@MOF-5 wherein the cubic MOF crystal is represented as an open book to show both the core and shell chemistry: (a) core-shell formation (b) PSM (c) ATRP with methyl methacrylate.

thickness of the initiator-carrying shell, the thickness of the polymer film can likewise be controlled.

Future Plans

The project period is over on 8/31/16 and future plans are turning primarily to work proposed in the renewal. The focus of the renewal is to understand and exploit the dynamic properties of coordination polymers. Most of the mechanistic insights will be gained with Raman spectroscopy *in situ* and *ex situ* during various treatments. We will also further develop the polymer-MCP hybrids under the current project with a new synthetic approach that is initiator free.

References

1. Guo, P.; Wong-Foy, A. G.; Matzger, A. J. Microporous Coordination Polymers as Efficient Sorbents for Air Dehumidification. *Langmuir*, **2014**, 30, 1921-1925.
2. Ma, J.; Wong-Foy, A. G.; Matzger, A. J., "The Role of Modulators in Controlling Layer Spacings in a Tritopic Linker Based Zirconium 2D Microporous Coordination Polymer" *Inorg. Chem.,* **2015**, *54*, 4591-4593.
3. Ma, J.; Tran, L. D.; Matzger, A. J., "Towards Topology Prediction in Zr-Based Microporous Coordination Polymers: the Role of Linker Geometry and Flexibility." *Cryst. Growth Des.* **2016**, ASAP.
4. McDonald, K. A.; Feldblyum, J. I.; Koh, K.; Wong-Foy, A. G.; Matzger, A. J., "Polymer@MOF@MOF: "grafting from" atom transfer radical polymerization for the synthesis of hybrid porous solids" *Chem. Commun.*, **2015**, *51*, 11994-11996.

Publications

Ma, J.; Tran, L. D.; Matzger, A. J., "Towards Topology Prediction in Zr-Based Microporous Coordination Polymers: the Role of Linker Geometry and Flexibility." *Cryst. Growth Des.* **2016**, ASAP.

Tran, L. D.; Ma, J.; Wong-Foy, A. G.; Matzger, A. J., "A Perylene-Based Microporous Coordination Polymer Interacts Selectively with Electron-Poor Aromatics" *Chem. Eur. J.,* **2016**, *22*, 5509-5513.

Ma, J.; Wong-Foy, A. G.; Matzger, A. J., "The Role of Modulators in Controlling Layer Spacings in a Tritopic Linker Based Zirconium 2D Microporous Coordination Polymer" *Inorg. Chem.,* **2015**, *54*, 4591-4593.

Dutta, A.; Koh, K.; Wong-Foy, A. G.; Matzger, A. J., "Porous Solids Arising from Synergistic and Competing Modes of Assembly: Combining Coordination Chemistry and Covalent Bond Formation" *Angew. Chemie Int. Ed.,* **2015**, *54*, 3983-3987.

Tran, L. D.; Feldblyum, J. I.; Wong-Foy, A. G.; Matzger, A. J., "Filling Pore Space in a Microporous Coordination Polymer to Improve Methane Storage Performance" *Langmuir*, **2015**, *31*, 2211-2217.

Barnard, R. A.; Dutta, A.; Schnobrich, J. K.; Morrison, C. N.; Ahn, S.; Matzger, A. J., "Two-Dimensional Crystals from Reduced Symmetry Analogues of Trimesic Acid" *Chem. Eur. J.*, **2015**, *21*, 5954–5961.

Guo, P.; Dutta, D.; Wong-Foy, A .G.; Gidley, D. W.; Matzger, A. J., "Water Sensitivity in Zn_4O-Based MOFs is Structure and History Dependent" *J. Am. Chem. Soc.*, **2015**, *137*, 2651-2657.

McDonald, K. A.; Feldblyum, J. I.; Koh, K.; Wong-Foy, A. G.; Matzger, A. J., "Polymer@MOF@MOF: "grafting from" atom transfer radical polymerization for the synthesis of hybrid porous solids" *Chem. Commun.*, **2015**, *51*, 11994-11996.

Dutta, A.; Ma, J.; Wong-Foy, A. G.; Matzger, A. J., "A non-regular layer arrangement of a pillared-layer coordination polymer: avoiding interpenetration via symmetry breaking at nodes" *Chem. Commun.*, **2015**, *51*, 13611-13614.

Dutta, A.; Wong-Foy, A. G.; Matzger, A. J., "Coordination Copolymerization of Three Carboxylate Linkers into a Pillared Layer Framework" *Chem. Sci.,* **2014***, 5*, 3729-3734.

Defect Tolerance to Intolerance in Perovskite Halide Semiconductors

James R. Neilson, Colorado State University, Department of Chemistry

Program Scope

The properties of conventional (*e.g.*, diamond-lattice based) semiconductors are very sensitive to the nature of defects; however, perovskite halides appear to be far less sensitive to defects, thus permitting the perovskites to be solution-deposited (*i.e.,* containing many defects) without significant consequence for utility. However, the underlying crystal chemistry that permits this defect tolerance is not yet well understood – for example, why is the nearly molecular, ionic crystal, Cs_2SnI_6, [1] as conductive as the three-dimensionally covalently-connected perovskite, $CsSnI_3$ [2]? Therefore, we have been interested in understanding why the inorganic perovskite halide lattice provides such advantageous electronic transport and efficient charge-separation characteristics, but with such insensitivity to crystalline imperfections, in contrast to silicon-related compound semiconductors.
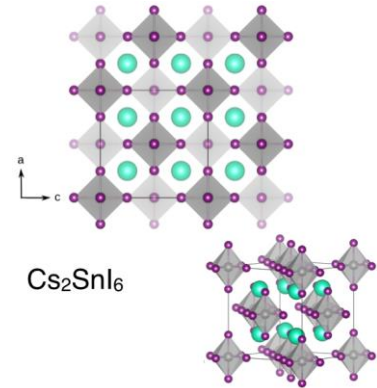
Cs_2SnI_6

Figure 1: Crystal structure of Cs_2SnI_6, a vacancy-ordered double perovskite halide

Recent Progress

The vacancy-ordered double perovskites provide an excellent platform with which to probe the structure/property relationships in these materials. We have prepared a series of compounds belonging to the solid-solution, $Cs_2Sn_{1-x}Te_xI_6$. The electronic properties undergo a drastic change upon substitution but with minimal change to the crystal structure. Hall measurements reveal a large concentration of mobile electrons in Cs_2SnI_6 (concentration ~ 5×10^{16} cm^{-3}, mobility ~ 9 cm^2 V^{-1} s^{-1}). However, after substitution of only 5% of the Sn with Te, we observe a precipitous drop in the conductivity, carrier concentration, and carrier mobility. Meanwhile, the crystal structures are virtually identical, as determined from high-resolution synchrotron X-ray diffraction (Advanced Photon Source), high resolution time-of-flight neutron diffraction (Spallation Neutron Source), and X-ray pair distribution function analysis. The only significant structural changes observed with Te substitution are a decrease in the I–I distance between neighboring octahedra, which theoretically should decrease the carrier masses, as supported by density functional calculations.
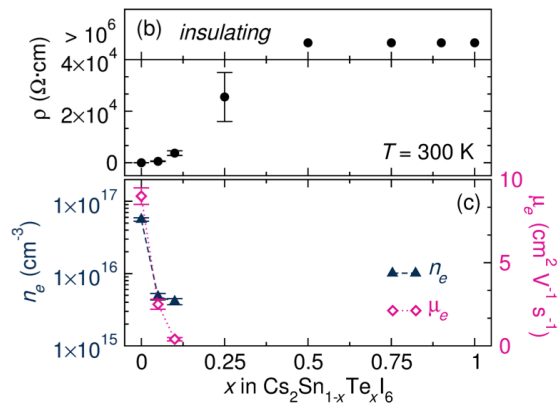

Figure 2: Resistivity, carrier concentration, and Hall mobility across the series of compounds, $Cs_2Sn_{1-x}Te_xI_6$.

Instead, the frontier electronic states undergo a significant change across the solid-solution, $Cs_2Sn_{1-x}Te_xI_6$. From density functional theory (DFT) calculations, Cs_2SnI_6 is a direct bandgap semiconductor whereas Cs_2TeI_6 is an indirect bandgap semiconductor. We calculate that the band structures are pinned at their valence band maxima, comprised predominately of I $5p$ states. In these compounds, iodine vacancies are the lowest-energy defect; the enthalpy of their formation is much lower in the case of Cs_2SnI_6. The energy levels of these defects are nearly in resonance with the conduction band, thus explaining the tolerance of this material to defects. However, these defects form in the gap for Cs_2TeI_6, thus localizing the decreased population of charge carriers, thus leading to defect intolerance. Together, these results define a clear relationship for obtaining defect tolerance in this now ubiquitous family of perovskite halide semiconductors through band structure engineering.

Future Plans

Our previous results have elucidated the electronic origins of defect tolerance in vacancy-ordered double perovskite halides. In our future work, we plan to further inform the materials design principles based upon their local structures and their dynamics in *hybrid inorganic-organic* perovskites and their defect-ordered analogs. Looking forward, we will place a specific emphasis on understanding the role and nature of electron-phonon coupling and what organic-inorganic interactions control phase stability in this family of functional materials.

References

[1] Lee, B.; Stoumpos, C. C.; Zhou, N.; Hao, F.; Malliakas, C.; Yeh, C.-Y.; Marks, T. J.; Kanatzidis, M. G.; Chang, R. P., *J. Am. Chem. Soc.,* 2014, *136*, 15379–15385.

[2] Chung, I.; Lee, B.; He, J.; Chang, R. P.; Kanatzidis, M. G., *Nature*, 2012, *485*(7399), 486-9.

Publications

N/A

Fundamental ion-association and acid-base behavior of aqueous species
May Nyman; Department of Chemistry, Oregon State University; Corvallis, OR 97331

Program Scope

The goal of this program is to use discrete metal-oxo clusters to understand fundamental aqueous ion-association, and how to exploit ion-association to develop new material forms in water. Atomic and molecular level ion-pairing and acid-base behavior in aqueous systems control important phenomena in both synthesis and nature. These include self-assembly and precipitation of ionic solids, electron-transfer reactions, separation chemistries, and growth of complex and novel forms of materials and lattices. Many successes in discovering and ultimately optimizing functional materials from water are based in trial-and-error, quasi-combinatorial approaches, and certainly luck; because behavior of aqueous systems is complex, dynamic and often unpredictable. This arises in part from the fact that the solvent (H_2O) is also the metal ligands, in the form of O^2, OH^- or H_2O. For a more deliberate approach to obtain functional materials from water, we need to understand the many factors that drive self-assembly, including ion association. Polyoxometalates (POMs), and other aqueous molecular metal oxo clusters, are ideal to study ion association. These clusters are charged (polyanions or polycations) and their interactions with counterions regulate their behavior in water including dissolution/precipitation, electron transfer, and catalytic function, and conversion to related materials. Discrete molecular clusters in water also serve as experimental and computational models for interactions at the metal oxide-water interface. They are small enough to provide a tractable computational model. They are molecular and absolute, so they yield clear and assignable spectra. We currently have two major foci of study within the realm of aqueous metal-oxo clusters to probe ion-association in water: 1) Probing Cs-POM interactions in water to delineate roles of frontier orbitals and covalent interactions between ions. 2) Unconventional 'covalent' counterions to isolate unprecedented metal-oxo clusters.

Recent Progress

Probing Cs-POM interactions in water to delineate roles of frontier orbitals and covalent interactions between ions. We have noted in a series of studies that alkali salts of Group V (Nb, Ta) POMs solubility trends Cs>Rb>K>>Na>>Li, while the trend for Group VI POMs (Mo, W) is opposite.(*1-4*) Group V POMs are very charge dense and Group VI POMs have low charge-density. Our hypothesis is that for charge-dense polyatomic anions such as the $[Nb_6O_{19}]^{8-}$ Lindqvist ion (**fig. 1**), the alkali cation is sufficiently neutralized by association with a single anion. Conversely, the POM anions become neutralized with bound cations and therefore are not attracted to one another by cation-mediated processes. On the other hand, the tungstate analogue $[W_6O_{19}]^{2-}$ will not associate so strongly with an alkali, and therefore the alkali will bridge to a second cluster, and this proceeds throughout the solution and initiates precipitation. However, charge-density only partially explains the trends, and we are exploring other factors, including covalency of interactions between Cs^+ and Group V POMs. Cs has frontier *f*-orbitals that presumably provide partial covalent bonding character. DOE has considerable motivation to understand Cs's solution behavior in a range of chemical environments because radioactive ^{137}Cs is contained in DOE nuclear waste tanks and has been released to the environment at Fukushima. Recently we have utilized 1) calorimetry to measure heat of dissolution and relate it to ion-association 2) [133]Cs NMR quadrupolar relaxation rates coupled with UV-vis spectroscopy to

measure ion-association and its effect on acid-base behaviour 3) X-ray scattering to probe ion-association induced structuring in solution.
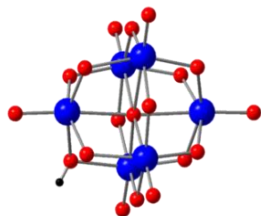

Fig 1. POM referred to as hexametalate, hexaniobate, hexatantalate, Lindqvist ion or $[H_xM_6O_{19}]^{x-8}$ (M=Nb,Ta; x=0-3). Blue spheres are Nb/Ta; red spheres are oxygen, black sphere is hydrogen
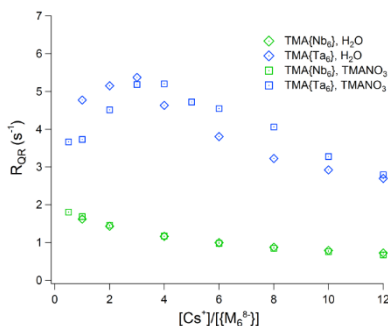

Fig. 2 (Above right) Quadrupolar relaxation rate (R_{QR}) of ^{133}Cs for 20 mmolar TMA salts of Nb_6O_{19} (green) and Ta_6O_{19} (blue) as a function of equivalents Cs added. Open circles are in water, open diamonds are in a 200 mmol TMA nitrate electrolyte solution
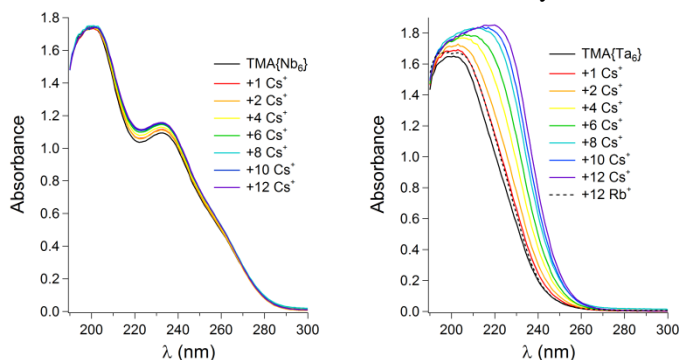
Figure 3. UV-vis absorption spectra of TMA salts of hexaniobate (left) and hexatantalate (right) with Cs added (up to 12 equivalents); and also 12 equivalents of Rb to hexatantalate for comparison (right).

Calorimetry Using calorimetry, we measured the dissolution energy for $[Nb_6O_{19}]^{8-}$ as a function of counterion (Li, K, Rb, Cs, TMA) and concentration in pure water and in parent hydroxide solutions.(*5*) These studies show clearly that ion association and protonation are concomitant, that deprotonation of the clusters is the most exothermic step of dissolution while disrupting lattice ion associations is the most endothermic. Additionally, $Cs_8[Nb_6O_{19}]$ dissolution has more concentration dependence than the other alkali salts, including Rb. This is surpising base on prior studies ,(*2, 6, 7*) and evidence of the unique partial coavalent character.

NMR and UV-vis spectroscopies We are currently exploiting the ^{133}Cs quadrupolar spin lattice relaxation time parameter, T_1, and its reciprocal relaxation rate, R_{QR} that is affected by asymmetric f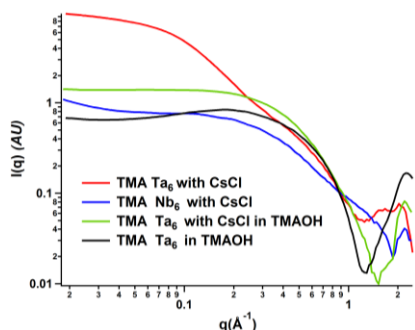ields produced by ion association. A faster R_{QR} correlates with more extensive ion association, and it represents an average of associated and non-associated Cs, since these populations are in rapid equilibrium. We found the ^{133}Cs R_{QR} for Cs salts of W-Nb and W-Ta POMs increased with increasing Group V:Group VI metal ratio. This is not surprising because higher charge density correlates with more ion-association. However, the considerably higher R_{QR} of Cs in contact with hexatantalate vs. hexaniobate was unexpected (**Fig. 2**). The R_{QR} for Cs in solution with hexatantalate increases for addition of up to ~4 Cs. UV-vis spectroscopy (**fig. 3**) of the same solutions (**fig. 2**) show that addition of Cs shifts the HOMO LUMO gap for hexatantalate but not for hexaniobate. There is maximum protonation of hexatantalate and hexaniobate upon dissolution,(*8*) and the added Cs replaces the protons for hexatantalate, but not hexaniobate.

Fig.4 SAXS of hexametalates with added base and/or Cs.

X-ray Scattering. Consistent with the differences between the Group V hexametalates noted above, preliminary SAXS (small-angle X-ray scattering) data also reveals that the hexatantalate undergoes considerable supramolecular structuring upon addition of Cs, while hexaniobate does not (**fig. 4**). Moreover, aging increased the structuring in both hexatantalate and hexaniobate solutions, but considerably more so for hexatantalate.

Unconventional 'covalent' counterions to isolate unprecedented metal-oxo clusters

Chemists and geochemists have been trying to isolate the Fe Keggin ion from water to understand its role as a prenucleation cluster to magnetite or ferrihydrite that also possess the Keggin-ion building block. Last year we isolated the elusive iron Keggin ion (formulated $[FeO_4Fe_{12}(OH)_{12}O_{12}TCA_{12}]^{17-}$ (TCA = trichloroacetate) from water by employing bismuth as a counterion. (denoted $Fe_{13}Bi_6TCA_{12}$; **fig. 5**).(*9*) It is our hypothesis that the highly-charged (and therefore unstable) cluster required suitably highly-charged counterions, such as trivalent bismuth. We showed by SAXS and TEM that 1) the six bismuth-cations capping the cluster are imperative for isolation of this reactive specie, and 2) the bismuth is readily removed upon re-dissolution in water, and the iron clusters rapidly rearrange and aggregate to form ferrihydrite. In a current study, we replace TCA with trifluoroacetate (TFA) and isolate a
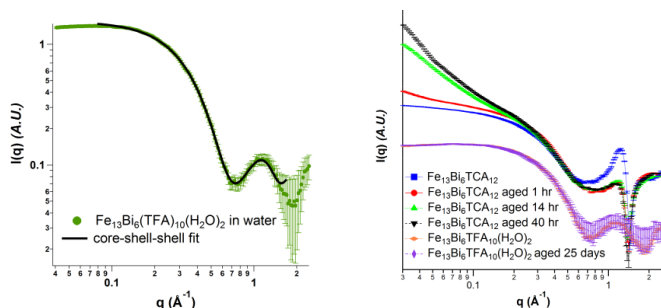

Figure 5. $Fe_{13}Bi_6TCA_{12}$ (left) and iron Keggin ion containing materials ferrihydrite (middle), and magnetite (right). The red polyhedral emphasize the Keggin unit.

Figure 6. (left) SAXS of $Fe_{13}Bi_6TFA_{10}(H_2O)_2$ in water with a core-shell-shell fit to the scattering data. (Right) Comparison of SAXS of $Fe_{13}Bi_6TFA_{10}(H_2O)_2$ and $Fe_{13}Bi_6TCA_{12}$ in acetone with aging. $Fe_{13}Bi_6TFA_{10}(H_2O)_2$ remains unchanged for 25 days. $Fe_{13}Bi_6TCA_{12}$ aggregates after one hr, initiated by dissociation of Bi.

similar cluster denoted $Fe_{13}Bi_6TFA_{10}(H_2O)_2$. The difference in solution behavior between the two clusters is remarkable—the latter cluster is indefinitely stable in water, and the bismuth cations remain bound to the cluster (**fig. 6**).

Future Plans

We will perform calorimetric studies on the series of hexatantalate clusters as a very sensitive probe of ion-association and protonation behavior. This will serve as another means to understand the difference between 2nd and 3rd row transition metal oxides, related to the lanthanide effect; and the profound differences we have observed thus far between hexatantalate and hexaniobate. We will also exploit calorimetry to understand the differences in stability

between the two Fe_{13} clusters, and their conversion to related iron oxide materials. We will continue to utilize the hexametalates as models for understanding ion-association in solution. The preliminary SAXS observations of the growth of large aggregates (**fig. 4**) are promising for direct imaging via TEM as a corroborative technique. Ultimately these studies will contribute to an understanding of how materials grow from water, and in particular the role of ionic associations. We are investigating the dynamic behavior of the ions using molecular dynamics and the role of covalency using DFT. Finally, we are exploring isolation of other metastable metal-oxo cluster systems using bismuth and other covalent counterions.

References

1. Y. Hou, M. Nyman, M. A. Rodriguez, Soluble Heteropolyniobates from the Bottom of Group IA. *Angew Chem Int Edit* 50, 12514 (2011).
2. M. Nyman *et al.*, Solid-state structures and solution behavior of alkali salts of the $[Nb_6O_{19}]^{(8-)}$ Lindqvist ion. *J Clust Sci* 17, 197 (Jun, 2006).
3. M. Nyman, P. C. Burns, A comprehensive comparison of transition-metal and actinyl polyoxometalates. *Chem Soc Rev* 41, 7354 (2012).
4. M. Nyman, Polyoxoniobate chemistry in the 21st century. *Dalton Transactions* 40, 8049 (2011).
5. D. J. Sures, S. K. Sahu, P. I. Molina, A. Navrotsky, M. Nyman, Distinctive Interactions of Cesium and Hexaniobate in Water. *ChemistrySelect* 1, (2016).
6. L. B. Fullmer, P. I. Molina, M. R. Antonio, M. Nyman, Contrasting ion-association behaviour of Ta and Nb polyoxometalates. *Dalton Transac.* 43, 15295 (2014).
7. M. R. Antonio, M. Nyman, T. M. Anderson, Direct Observation of Contact Ion-Pair Formation in Aqueous Solution. *Angew Chem Int Edit* 48, 6136 (2009).
8. L. B. Fullmer, R. H. Mansergh, L. N. Zakharov, D. A. Keszler, M. Nyman, Nb2O5 and Ta2O5 Thin Films from Polyoxometalate Precursors: A Single Proton Makes a Difference. *Cryst Growth Des* 15, 3885 (Aug, 2015).
9. O. Sadeghi, L. N. Zakharov, M. Nyman, Aqueous formation and manipulation of the iron-oxo Keggin ion. *Science* 347, 1359 (Mar 20, 2015).

Publications

—L. B. Fullmer, P. I. Molina, M. R. Antonio, M. Nyman, Contrasting ion-association behaviour of Ta and Nb polyoxometalates. *Dalton Transactions* **43**, 15295 (2014).
—P. I. Molina, D. J. Sures, P. Miro, L. N. Zakharov, M. Nyman, Bridging the opposite chemistries of tantalum and tungsten polyoxometalates. *Dalton Transactions* **44**, 15813 (2015).
—D. J. Sures, P. I. Molina, P. Miro, L. N. Zakharov, M. Nyman, Cesium salts of niobo-tungstate isopolyanions with intermediate group V-group VI character. *New J Chem* **40**, 928 (2016).
—D. J. Sures, S. K. Sahu, P. I. Molina, A. Navrotsky, M. Nyman, Distinctive Interactions of Cesium and Hexaniobate in Water. *ChemistrySelect* **1**, *in press* (2016).
—O. Sadeghi, L. N. Zakharov, M. Nyman, Aqueous formation and manipulation of the iron-oxo Keggin ion. *Science* **347**, 1359 (Mar 20, 2015).
—O. Sadeghi *et al.*, Chemical stabilization and electrochemical destabilization of the iron Keggin ion in water. *J Am Chem Soc in review*, (2016).
—N. A. G. Bandeira, O. Sadeghi, T.J. Woods, Y.Z. Zhang, J. Schnack, K. Dunbar, M. Nyman, C. Bo, An examination of the magnetic properties of homonuclear Fe(III) Keggin type polyoxometalates. *Inorganic chemistry in review*, (2016).

Engineering transport in confined environments of self-assembled stable radical polymers

Christopher Ober (PI), MS&E, Cornell University; Michael Flatté (Co-PI), P&A, ECE, U Iowa; Greg Fuchs (Co-PI), A&EP, Cornell University

Program Scope

We are focused on polymer-based stable radicals and are investigating the charge and spin transport behavior of these materials. Specific questions that are being addressed by this interdisciplinary research project include:

1. What are the fundamental mechanisms of electronic transport involving stable radical polymer materials?
2. How do stable radicals influence conductivity and charge storage in solid polymer films?
3. Can we use confinement and orientation imposed through block co-polymer self-assembly to influence the conductivity and charge storage?
4. Can we control the conductivity of stable radical polymers by introducing conjugation to the polymer backbone?
5. What is the role of electron spin in the electronic transport through these materials?

To address these questions, our research project brings together: i) synthesis and processing of stable radical polymers and copolymers combined with ii) the physical characterization of these new materials along with both electronic transport characterization, electron paramagnetic resonance measurements, and optical fluorescence spectroscopy. Finally, iii) theoretical and computational studies will play a key role in understanding the conduction process. This combination of approaches is aimed at establishing a fundamental and quantitative picture of electronic transport in these materials which to date remains incomplete.

Recent Progress

Synthesis of Block Copolymers Containing Stable Radicals and Fluorinated Groups

We are using tailored block copolymer architectures to separate, orient, and confine radical groups. Our approach has two attractive features. First, it provides a measure of physical property tuning of radical groups through self-assembly: orientation and confinement of the radical groups within the stable radical domains. This provides a "knob" to study the effects of these physical properties without changing the essential chemistry of the radical phase. Secondly, it provides a way to mix-and-match the properties of each microphase independently.

Block copolymers containing a radical block, such as poly(TEMPO-methacrylate) (denoted, PTMA) and a high χ parameter second block are of interest because they allow the study of charge transport of PTMA domains confined in a strongly phase separated, insulating matrix. The first polymer created to contain these two blocks was poly(TEMPO-methacrylate)-block-poly(2,2,2-trifluoroethyl methacrylate) (PTMA-b-PTFEMA) via atom transfer radical polymerization (ATRP) [1]. These polymers have the ability to phase separate into specific morphologies depending on their block to block ratios.

Following the creation of PTMA-b-PTFEMA, we have now prepared poly(TEMPO methacrylate)-b-poly(2,2,3,4,4-hexafluorobutyl methacrylate) via ATRP (*Scheme 1*). By systematically the increasing fluorination on these block copolymers, the effects between the

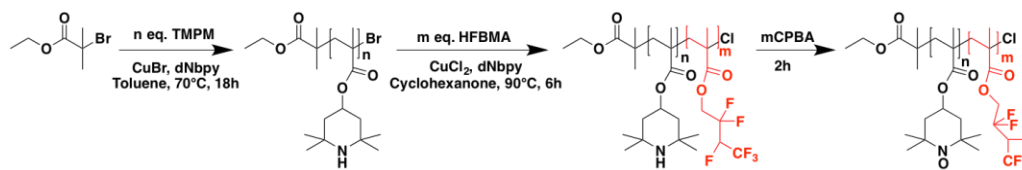degree of phase separation and confinement of the PTMA transport block are being studied further.

Figure 1. Synthesis route of PTMA-b-PTFEMA via ATRP

In order to create the PTMA–b-PTFEMA block copolymer described above with higher molecular weight and smaller dispersity, we used anionic polymerization because it allows better control of molecular weight and dispersity. This synthesis method is promising because dispersity was decreased below 1.15, which we expect will lead to more well-defined block copolymers. We are currently working on fractionating these polymers via preparatory GPC for further analysis, while also investigating other conditions in which to avoid bimodal characteristics.

Electronic Characterization of Radical Polymers

Over 50 samples of PTMA polymers have been synthesized and characterized. Initially, some samples were found to be conductive; however, conductivity was inconsistent and unstable, typically decaying to fully insulating over a period of hours to days. We note that this is in contrast to the previous theory [2] that expected intrinsic hopping-mediated conductivity in PTMA via their radical sites, and in contrast to the published results on PTMA conductivity fabricated with RAFT [3]. Note that different synthesis methods produce different radical yields, which may play a role in a hopping conductivity mechanism. To further investigate the discrepancy between our results and other published results, our team synthesized PTMA homopolymers using three methods: anionic polymerization, ATRP, and RAFT. We performed quantitative EPR measurements of our solution form PTMA materials using a conventional x-band EPR spectrometer. These measurements reveal that our PTMA has high radical concentrations (Table 1), supporting our preliminary

Table 1: Quantitative EPR of radical polymers by synthesis technique, showing radical content

Polymer	Synthesis	Radical yield (%)
PTMA homopolymer	Anionic	72
PTMA homopolymer	ATRP	97.5
PTMA homopolymer	RAFT	not yet meas.
P3HT-b-PTMA 6	GRIM, ATRP	27
P3HT-b-PTMA 10	GRIM, ATRP	33

conclusion that the theoretical suggestions of radical-site mediated hopping conductivity in PTMA is not viable as an intrinsic mechanism, and that reports of PTMA conductivity in the literature may originate from some unintentional doping, or some other mechanism that has yet to be identified. This study is still on-going.

Motivated by these conclusions, our team has begun synthesizing radical-containing polymers with conjugated blocks and backbones to introduce engineered conductivity. Poly(3-hexylthiophene) (P3HT) was adopted in this study due to its high conductivity, extensively stud-

ied self-assembly and versatile synthesis techniques. TEMPO is attached to the P3HT backbone via a spacer of selected length. Such materials reported before were synthesized via oxidation or electropolymerization of the TEMPO substituted thiophene (TEMPO-Th) monomer. We started by employing a post-functionalization strategy based on azide-functionalized poly(3-hexylthiophene) (P3HT-azide), which allows for subsequent functionalization with propargyl ether TEMPO using click chemistry (*Figure 2*).
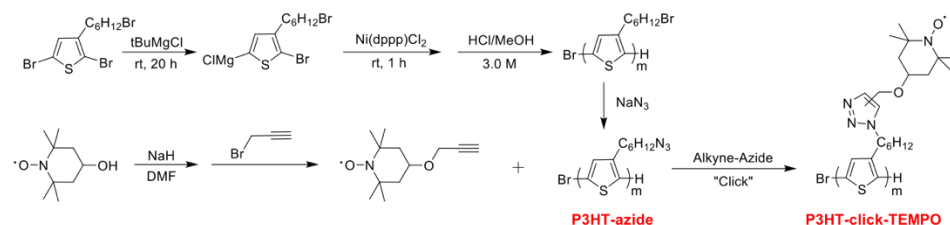

Figure 2. Synthesis Route of P3HT-click-TEMPO via GRIM and alkyne-azide click chemistry

We have now moved forward to improve the solubility of the P3HT-click-TEMPO, via copolymerization with thiophenes with soluble substituents, such as 3-hexylthiophene. As a result, we are currently working on obtaining more copolymers (such as random and diblock) with careful control on the copolymer structure. We are also working on polymerization of a bithiophene monomer, which is composed of 3-bromohexylthiophene and 3-hexylthiophene, to synthesize alternating polythiophenes with TEMPO substituents, while investigating the self-assembly and electrical properties of the resultant polymer.

EPR Characterization of Stable Radical Polymers

A key accomplishment of the research team this period is the development of multi-frequency, on-chip EPR capabilities for *in operando* measurement. To study the role of radicals in transport and charge storage, we have developed EPR that is well-matched to the planar form-factor of polymer films. In contrast to a conventional EPR spectrometer, we use a broadband coplanar waveguide to mediate microwave absorption, rather than a frequency specific resonator. This approach is more effective on solid polymer films than a conventional spectrometer, and it can be integrated with other measurements.

Another advantage of broadband, on-chip EPR characterization is it allows measurement at any frequency and field. In the coming period we plan to leverage this feature to study the magnetic-field dependent
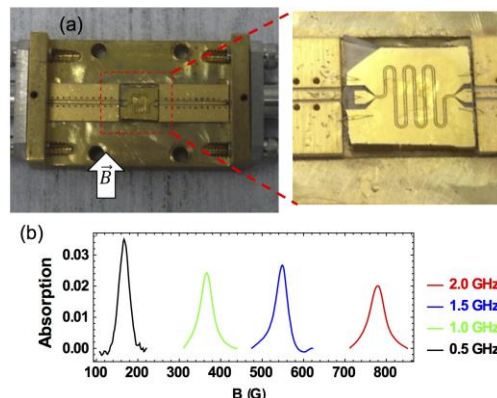

Figure 3. (a) On-chip EPR set-up with sample box. Coplanar waveguide meander couples broadband microwave power to the test polymer, which is spun or dropped on top. (b) Absorption spectra for PTMA as a function of magnetic field using different excitation frequencies.

ent linewidth, especially at low field <1 kG, as proposed by Flatté. These measurements can reveal the role of hyperfine fields in spin-dependent polaron conductivity, which has recently been revealed as an important mechanism in transport experiments of conjugated organic conductors [4]. Initial measurements (Figure 3) show field-dependent linewidth effects; however, it is unclear whether they are due to a magnetic field inhomogeneity or the intrinsic effect.

We are upgrading our EPR set-up to address this challenge.

We are also developing new theoretical understanding of radical polymer EPR lineshapes, going beyond "counting" radical spins to extracting information about the local radical environment and chemical environment. This provides a new handle on the electrical transport and spin-dependent transport properties of radical polymers, and how they depend upon the charge states of unpaired electron spins. The data strongly suggests that the three hyperfine multiplets due to the nitrogen near the radical are being affected by exchange when going from solution to film. We are also devising a model to understand the line width (T_2) considering dipolar and hyperfine effects.
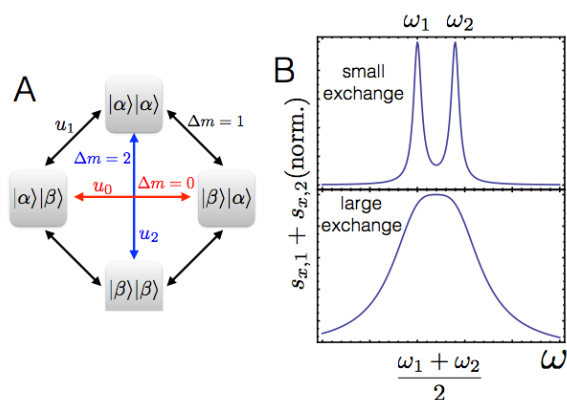
Figure 4: (a) Diagram of transverse spin populations and transitions. (b) Preliminary line shapes calculated from a simple model incorporating hyperfine, dipolar, and exchange interactions, which will be compared with experimental measurements by the other PI's to extract/compare with these quantities.

Future Plans

We expect to test the theoretical prediction of the observation of hyperfine multiplets in going from solution to solid state. Synthetic studies will continue as we develop new spin containing materials.

References

1. C. Liedel, A. Moehle, G. D. Fuchs and C. K. Ober, "Block Copolymers with Stable Radical and Fluorinated Groups by ATRP" *MRS Commun*. 5, 441-446 (2015)._

2. T. Kemper, R. E. Larsen, and T. Gennett, "Relationship between Molecular Structure and Electron- Transfer in a Polymeric Nitroxyl-Radical Energy Storage Material Relationship Between Molecular Structure and Electron Transfer in a Nitroxyl-radical Polymer Energy Storage Material" J. *Phys. Chem. C* 118, 17213 (2014).

3. A. G. Baradwaj, L. Rostro, and B. W. Boudouris, "On the Environmental and Electrical Bias Stability of Radical Polymer Conductors in the Solid State" *Macromol. Chem. Phys.* 217, 477 (2016).

4. Y. Wang, K. Sahin-Tiras, N. J. Harmon, M. Wohlgenannt, and M. E. Flatté, "Immense Magnetic Response of Exciplex Light Emission due to Correlated Spin-Charge Dynamics" *Phys. Rev.* X 6, 011011 (2016).

Publications

1. Y. Wang, K. Sahin-Tiras, N. J. Harmon, M. Wohlgenannt, and M. E. Flatté, "Immense Magnetic Response of Exciplex Light Emission due to Correlated Spin-Charge Dynamics" *Phys. Rev.* X 6, 011011 (2016).

Elucidating the Determinants of Alkali Ionic Conductivity in Oxide and Sulfide Frameworks

Shyue Ping Ong, University of California San Diego

Program Scope

The aim of this project is to conduct fundamental investigations into the structural and chemical factors that affect alkali conductivity in oxide and sulfide structural frameworks using a combination of automated first principles calculations and topological analysis. The factors that will initially be studied include the local environment of the alkali ion, the topology of the diffusion pathways, the cation and anion chemistry, and the alkali concentration and degree of disorder. Detailed investigations will be conducted into several prototypical structure types / chemistries of significant interest in energy storage, where we will attempt to answer some of the most pressing questions regarding alkali conductivity in these structure types / chemistries. The results of these detailed investigations will then be used as part of a broader study where datamining techniques will be used to extract insights into the relationships between structure, chemistry, and alkali ionic conductivity.

Recent Progress

Effect of Anion Doping on Conductivity of the $Li_3OCl_{1-x}Br_x$ Lithium-Rich Anti-Perovskite

The main aim of this effort is to elucidate the effect that the local environment of the alkali ion, the topology of the diffusion pathways, the cation and anion chemistry, and the alkali concentration and degree of disorder has on the conductivity. The lithium-rich anti-perovskites (LRAPs)[1] with formula Li_3OX, where X = Cl, Br, or a mixture of both halogens, present a particularly interesting candidate to carry out such a fundamental investigation. Despite their apparent structural simplicity (Figure 1), previous experimental and theoretical works[2,3] have yet to provide a coherent understanding of the impact that the halide environment have on the vacancy diffusion barriers and hence overall conductivity.
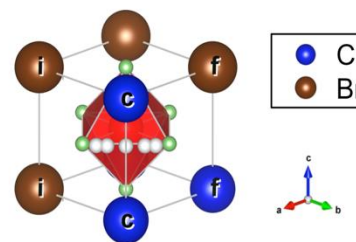

Figure 1: Crystal structure, vacancy diffusion pathway and local halide environment in the LRAP.

We have carried out a comprehensive analysis of Li^+ conductivity in the LRAPs using a combination of first principles calculations and percolation theory. We find that the Li_3OCl-Li_3OBr pseudo-binary system is characterized by low mixing energies, which indicate that halide disorder is likely at room temperature. Nudged elastic band (NEB) calculations find that a Cl-rich channel with Br-rich endpoints leads to low vacancy migration barriers in the LRAP structure (left subfigure of Figure 2). By incorporating the computed NEB barriers in a bond percolation model, we show that there are potentially higher conductivity $Li_3OCl_{1-x}Br_x$ structures near $0.235 < x < 0.395$ (right subfigure of Figure 2). These predicted were further confirmed using *ab initio* molecular dynamics (AIMD) simulations, which predict a higher conductivity for $Li_3OCl_{0.75}Br_{0.25}$ compared to $Li_3OCl_{0.5}Br_{0.5}$, the highest conductivity composition in the anti-perovskite chemistry identified experimentally thus far. Our work has shed important **insights into**

the fundamental tradeoffs of Br doping in the LRAP structure. Low levels of Br incorporation would increase the proportion of fast migration paths in the LRAP structure, but an excess of Br incorporation would lead to "choking" in the channels and decreased conductivity. This **approach that has surprising generality and may be extended for further composition optimization in other ionic conduction network topologies or chemistries**, e.g., perovskite oxygen-ion conductors of interest in solid-oxide fuel cells.

This work has been published in Chemistry of Materials.[4]
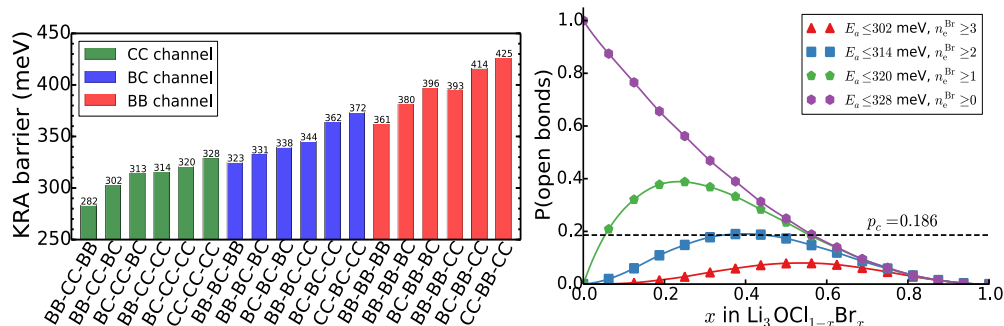
Figure 2: (left) NEB kinetically-resolved activation (KRA) barriers for vacancy migration for different local halide environments in the initial (i), channel (c) and final (f) sites. Labeling is based on a X_iX_i-X_cX_c-X_fX_f convention; (right) Probability of open bonds in $Li_3OCl_{1-x}Br_x$ at various Br concentrations. Each curve corresponds to a particular barrier cutoff. n^{Br}_e denotes the number of Br in the endpoints. The anti-perovskite bond percolation threshold is indicated by the black dashed line.

Performance limits of the $Li_7P_3S_{11}$ Superionic Conductor Electrolyte

The $Li_7P_3S_{11}$ (L7PS) glass-ceramic is a promising superionic conductor electrolyte (SCE) with an extremely high Li^+ conductivity of 17 mS cm^{-1},[5] which exceeds that of even traditional organic electrolytes. In collaboration with the Meng group, we have conducted a comprehensive first-principles and experimental investigation of the performance limits of this material.

The AIMD simulations predict that L7PS to have an ionic conductivity of 57 mS cm^{-1} at room temperature, far higher than the measured conductivities of 11.6 mS cm^{-1} and 1.3 mS cm^{-1} for the spark-plasma sintered (SPS) and cold-pressed L7PS samples respectively (see Figure 3). Our main conclusion is **that grain boundary conductivity is limiting the overall Li^+ conductivity in L7PS, and further optimization of overall conductivities should be**
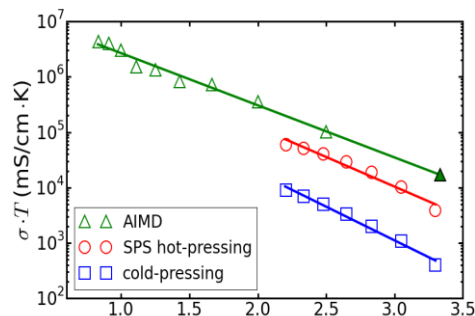

Figure 3. Arrhenius plots of L7PS obtained from AIMD simulations (green triangles) and conductivity measurements of cold pressed sample (blue squares) and SPS hot-pressed sample (red circles). The filled triangle corresponds to the linearly extrapolated room temperature conductivity from AIMD.

possible. Using Li probability density analysis, we show that Li^+ motions in this material are highly collective with 3D diffusion pathways and the flexing of the P_2S_7 ditetrahedra in the framework structure facilitates fast Li^+ diffusion.

Another interesting finding is that the products formed at the cathode-L7PS interface depends strongly on the cathode chemistry. Our first-principles calculations predict that the most common cathode material, $LiCoO_2$, tends to form poor electronic insulators with L7PS, which may not protect against propagation of the reaction front. On the other hand, the olivine $LiFePO_4$ and spinel $LiMn_2O_4$ cathodes form good electronic insulators close to the cathode-rich side of the interface, which can potentially passivate against further reaction. Future work will be conducted on understanding the implications of interfacial chemistry on Li^+ transport across the interface.

This work has been published in ACS Applied Materials & Interfaces.[6]

Universal relationship between alkali ion migration barrier and DFT "clearance" descriptor in the NASICON $AM_2(PO_4)_3$ materials

The NAtrium SuperIonic CONductor (NASICON) family of materials is one of the most well-known solid electrolytes with a 3D diffusion network and a good ionic conductivity at room temperature. We have performed a systematic study of Li and Na vacancy migration in the NASICON $AM_2(PO_4)_3$ materials (A = Li, Na; M = Ge, V, Ti, Sn, Hf and Zr) using NEB calculations. We have limited the scope of this study to purely M^{4+} cations and the same polymorph to avoid introducing alkali concentration and topology effects. The relevant diffusion mechanism explored is the migration of a single vacancy along the M1-M2-M1 sites in the NASICON framework (see Figure 4).
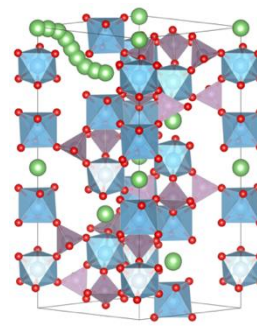

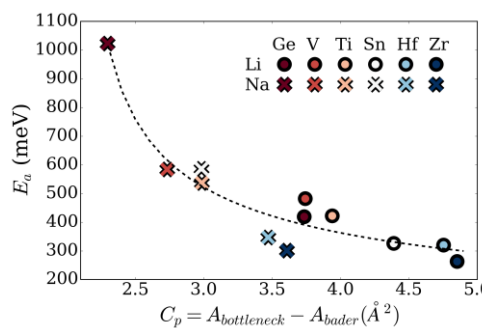**Figure 4.** Diffusion pathway of A^+ ion in $AM_2(PO_4)_3$.

Figure 5: Relationship between migration barrier and DFT "clearance" parameter (difference between bottleneck area and alkali Bader area).

The key finding from this work is that there is a universal relationship between alkali migration barriers and a DFT electronic "clearance" parameter, which is given by the difference between the bottleneck area of the diffusion pathway and the Bader area of the migrating alkali ion. Figure 5 shows this universal relationship. We may observe that regardless of cation or alkali chemistry, the migration barrier is described by the same "clearance" parameter. For Na NASICONs, the much larger Bader radius of Na^+ compared to Li^+ result in a high sensitivity of Na^+ migration barriers to cation M^{4+} radius. Generally, the smaller the cation M^{4+} radius, the smaller the bottleneck size, which in turns leads to a much sharper increase in migration barriers for Na^+ compared to for Li^+.

Future Plans

We will continue to further enhance our computational infrastructure to improve its robustness and power. In particular, we plan to modify our existing workflow software to take advantage of idle time at the Triton Shared Computing Center (TSCC) at UCSD, which would greatly expand the amount of computational resources available for this work.

In terms of methodology and algorithm development, we will optimize and automate our recently developed AIMD-NEB hybrid methodology for extracting diffusion properties of alkali superionic conductors.

We will extend our detailed investigations into other prototypical system types including the layered AMO_2 and AMS_2 as well as the perovskite $Li_{3x}La_{2/3-x}TiO_3$ materials that are of great interest in energy storage.

References

(1)   Zhao, Y.; Daemen, L. L. *Superionic Conductivity in Lithium-Rich Anti-Perovskites.*, J. Am. Chem. Soc., 2012, *134*, 15042–7, doi:10.1021/ja305709z.

(2)   Emly, A.; Kioupakis, E.; Van der Ven, A. *Phase Stability and Transport Mechanisms in Antiperovskite Li 3 OCl and Li 3 OBr Superionic Conductors*, Chem. Mater., 2013, 131126064324001, doi:10.1021/cm4016222.

(3)   Zhang, Y.; Zhao, Y.; Chen, C. *Ab initio study of the stabilities of and mechanism of superionic transport in lithium-rich antiperovskites*, Phys. Rev. B, 2013, *87*, 134303, doi:10.1103/PhysRevB.87.134303.

(4)   Deng, Z.; Radhakrishnan, B.; Ong, S. P. *Rational Composition Optimization of the Lithium-Rich Li 3 OCl 1- x Br x Anti-Perovskite Superionic Conductors*, Chem. Mater., 2015, *27*, 3749–3755, doi:10.1021/acs.chemmater.5b00988.

(5)   Seino, Y.; Ota, T.; Takada, K.; Hayashi, A.; Tatsumisago, M. *A sulphide lithium super ion conductor is superior to liquid ion conductors for use in rechargeable batteries*, Energy Environ. Sci., 2014, *7*, 627–631, doi:10.1039/C3EE41655K.

(6)   Chu, I.-H.; Nguyen, H.; Hy, S.; Lin, Y.-C.; Wang, Z.; Xu, Z.; Deng, Z.; Meng, Y. S.; Ong, S. P. *Insights into the Performance Limits of the Li7P3S11 Superionic Conductor: A Combined First-Principles and Experimental Study*, ACS Appl. Mater. Interfaces, 2016, *8*, 7843–7853, doi:10.1021/acsami.6b00833.

Publications

1.   Zhi Deng, Balachandran Radhakrishnan, and Shyue Ping Ong, "Rational Composition Optimization of the Lithium-Rich $Li_3OCl_{1-x}Br_x$ Anti-Perovskite Superionic Conductors", Chem. Mater., 2015, 27 (10), pp 3749–3755, doi:10.1021/acs.chemmater.5b00988.
2.   Zhi Deng, Yifei Mo, and Shyue Ping Ong, "Computational studies of solid-state alkali conduction in rechargeable alkali-ion batteries", NPG Asia Mater., 2016 8, e254, doi:10.1038/am.2016.7.
3.   Iek-Heng Chu, Han Nguyen, Sunny Hy, Yuh-Chieh Lin, Zhenbin Wang, Zihan Xu, Zhi Deng, Ying Shirley Meng and Shyue Ping Ong, "Insights into the Performance Limits of the $Li_7P_3S_{11}$ Superionic Conductor: A Combined First-Principles and Experimental Study", ACS Appl. Mater. Interfaces, 2016, 8 (12), pp 7843–7853, doi:10.1021/acsami.6b00833.

Activation of Hydrogen under Ambient Conditions by Main Group Molecules

PI: Philip P. Power, Department of Chemistry, University of California, Davis, California 95616.

Program Scope

The major objective of the research is the investigation of the reactions of H_2 and related species with element-hydrogen bonds, e.g. N-H, P-H, C-H, and Si-H, with main group molecules, and the determination of their reaction mechanisms. Current work involves:

(a) The continued investigation of the reactions of heavier main group 13 and 14 element open-shell species and cluster compounds with important small molecules such as H_2, NH_3, olefins, alkynes, CO, and CO_2. In addition, we are developing a greater focus on derivatives of the elements aluminum and silicon, where stable open-shell compounds are currently much scarcer.

(b) Establish proof of concept for the use of low valent heavier main group 13 and 14 compounds, especially their hydride derivatives, as hydrogenation or dehydrogenative coupling catalysts.

There are two major justifications for pursuing this research. The first is that the investigations provide fundamental information on the main group compounds and their reactions with industrially important small molecules under mild conditions. The second is the use of main group compounds in catalysis. Currently, many industrial catalysts are based on scarce and expensive transition metals. In contrast, main group elements, for example aluminum or silicon, are earth abundant, inexpensive, and offer obviously attractive alternatives.

Recent Progress

In addition to our work on the reactivity of unsaturated aluminum and silicon species[1] such as $Ar^{Pri_4}Al=AlAr^{Pri_4}$ and Ar^{Pri_4}-Si≡Si-Ar^{Pri_4} (Ar^{Pri_4} = C_6H_3-2,6(C_6H_3-2,6-Pr^i_2)$_2$) or main group clusters like $Sn_8(Ar^{Me_6})_4$ (Ar^{Me_6} = C_6H_3-2,6(C_6H_2-2,4,6-Me_3)$_2$)[2] with small molecules such as H_2, NH_2, CO, and CO_2, we have investigated the catalytic properties of low valent group 13 and 14 species.[3] We found that divalent tin species such as $\{Ar^{Me_6}Sn(\mu\text{-}OMe)\}_2$ (**1**)[4] or $\{Ar^{Pri_4}Sn(\mu\text{-}OMe)\}_2$ (**2**)[3] are precatalysts to the catalytically active tin(II) hydrides $\{Ar^{Me_6}Sn(H)\}_4$[2] or $\{Ar^{Pri_4}Sn(\mu\text{-}H)\}_2$[5] for the facile heterodehydrocoupling of a range of primary or secondary amines with pinacolborane (HBPin) to yield a wide variety of aminoboranes.[3]

Aminoboranes have a growing utility in modern synthetic chemistry as sources of iminium cations for the reductive amination of aldehydes, Mannich-type couplings of aldehydes, secondary amines, and silyl ketene acetals.[6,7] They have been synthesized by a variety of

methods via the action of silicon-nitrogen[8] and tin-hydrogen[9] bonds and haloboranes, salt metathesis of lithium amides with boron halides.[10]

Table 1: Amines dehydrocoupled with HBPin as catalyzed by **1** and **2**.

	Catalyst:	$\{Ar^{Me_6}Sn(\mu\text{-OMe})\}_2$ (**1**)			$\{Ar^{iPr_4}Sn(\mu\text{-OMe})\}_2$ (**2**)		
Amine	**Product**	**Reaction**	**t(h)**	**Conv. (%)**	**Reaction**	**t(h)**	**Conv. (%)**
nBuNH$_2$	PinBN(H)nBu	1a	10	99	1b	1	99
sBuNH$_2$	PinBN(H)sBu	2a	13	99	2b	48	30
Aniline	PinBN(H)Ph	3a	12	99	3b	2	99
4-Fluoroaniline	PinBN(H)(4-F-Ph)	4a	5	99	4b	1	99
4-Chloroaniline	PinBN(H)(4-Cl-Ph)	5a	9	99	5b	2	99
4-Bromoaniline	PinBN(H)(4-Br-Ph)	6a	9	99	6b	2	99
4-Ethylaniline	PinBN(H)(4-C$_2$H$_5$-Ph)	7a	26	95	7b	3	99
2,6-Diisopropylaniline	PinBN(H)Dipp	10a	78	70	10b	-	-
3,5-Dichloroaniline	PinBN(H)(3,5-Cl-Ph)	11a	7	99	11b	2	99
Et$_2$NH	PinBNEt$_2$	12a	9	99	12b	-	-
iPr$_2$NH	PinBNiPr$_2$	13a	10	99	13b	-	-
Cy$_2$NH	PinBNCy$_2$	14a	49	99	14b	-	-
Ph$_2$NH	PinBNPh$_2$	15a	100	15	15b	-	-
(Me$_3$Si)$_2$NH	No reaction	16a	-	-	16b	-	-
NH$_3$	PinBNH$_2$	17a	12*	99	17b	12*	99
PinBNH$_2$	(PinB)$_2$NH	18a	12*	99	18b	12*	99

Scheme 1: Catalytic cycles derived from redox-inactive bond-forming steps. E = Si, Ge, Sn; X = NR$_2$, OR; Y = BR$_2$, SiR$_3$; Z = O, NR.

Catalytic dehydrocoupling of amine-boranes R$_n$NH$_{3-n}$·BH$_3$ (n = 0, 1, 2) has been studied due to their potential use in hydrogen storage applications,[11] and are usually catalyzed by transition metal complexes to give oligoborazane products.[11,12] In main group chemistry, dehydrocouplings of pinacolborane with a range of primary and secondary amines with a Mg[13] or an Al complex[14] have been reported. We have now shown that the group 14 element complexes $\{Ar^{Me_6}Sn(\mu\text{-OMe})\}_2$ (**1**) and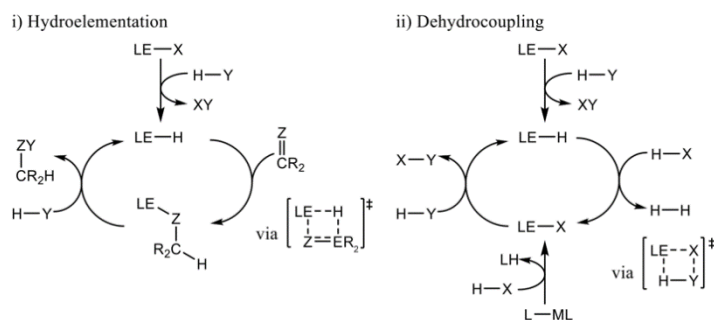 $\{Ar^{Pr_4}Sn(\mu\text{-OMe})\}_2$ (**2**) are precatalysts for the catalytic dehydrocoupling of a variety of amines (Table 1) via the generalized route in Scheme 1. We note that the steps in these reactions, as outlined in general terms in Scheme 1 (ii) are all redox-inactive. Also, the percentage conversion is quantitative in most cases, except where the amine is sterically-hindered as with Ph$_2$NH or (SiMe$_3$)$_2$NH. The reaction times and catalyst loadings (2 mol%) are shorter and lower than other
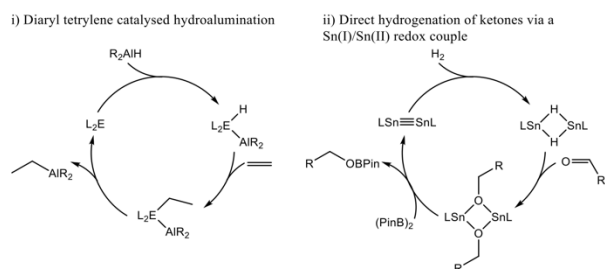
main group catalysts.[13,14] A further aspect of the reactions in Table 1 is that ammonia couples to produce a unique primary borylamine.

Future Plans

As noted above, the preponderance of work in catalysis by main group species has relied on bond activation without change in oxidation state. This is in contrast to transition metal work, which usually relies on oxidative addition and reductive elimination steps. Recently, a number of groups have shown that redox-active ion activation relying on P(III)/P(V) transformations are viable catalytic steps with reductive elimination allowing closure of this cycle.[15] Given the redox potential of the Sn(II)/Sn(IV) couple, it is remarkable that such reactivity had not been extended to group 14. However, our investigations have shown that reversible M-C bond insertion involving an Sn(II)/Sn(IV) can occur, as described in our recent publications.[16,17]

The products are tetravalent diaryl tetrylenes $E(Ar^{Me_6})_2(MMe_n)Me$ (E = Ge or Sn, M = Al or Ga, n = 2 or Zn, n = 1). The $E(Me_n)Me$ moiety reductively eliminates to yield $E(Ar^{Me_6})_2$ and $M(Me_{n+1})$. The use of such a reductive elimination in main group catalysis is obviously desirable. Thus, a cycle in which an M-X insertion step yields a ligand-supported

Scheme 1: Proposed redox-active catalytic cycles based on terphenyl supported tetrels. E = Ge, Sn; PinBH = $(Me_2CO)_2BH$.

$E(MMe_n)X$ fragment that can insert an unsaturated moiety such as ethylene could eliminate an M-C bond to yield a catalytic cycle (Scheme 2(i)). Initial work will investigate the insertion of dialkyl or diaryl tetrylenes into M-H bonds such as aluminum hydrides, and the viability of subsequent hydrometallation and reductive elimination to yield a net hydroalumination of alkenes. Further investigations will involve the use of a divalent metal hydride[5] (cf. Scheme 2(ii)) to introduce reductive metathesis steps into main group catalysis. Such a reaction involving loss of a strong E-X (e.g. E-O) bond to yield a low valent species is unknown in main group chemistry. The corresponding reduction step will involve metathetic reduction agents (e.g. HBPin) to allow regeneration of the low-valent species (e.g. the distannyne in Scheme 2(ii)).

References

1. J. Queen and P. P. Power. Unpublished work, 2015-2016.
2. P. Vasko, S. Wang, H. M. Tuononen, and P. P. Power. *Angewandte Chemie International Edition* **2015**, *54*, 3802-3807. http://dx.doi.org/10.1002/anie.201411595
3. J. D. Erickson, T. Y. Lai, D. J. Liptrot, and P. P. Power. *Chemical Communications* **2016**. Manuscript submitted.
4. J. D. Erickson, P. Vasko, R. D. Riparetti, J. C. Fettinger, H. M. Tuonenen, and P. P. Power. *Organometallics* **2015**, *34*, 5785-5791. http://dx.doi.org/10.1021/acs.organomet.5b00884

5. E. Rivard, R. C. Fischer, R. Wolf, Y. Peng, W. A. Merrill, N. D. Schley, Z. Zhu, L. Pu, J. C. Fettinger, S. J. Teat, I. Nowik, R. H. Herber, N. Takagi, S. Nagase and P. P. Power. *Journal of the American Chemical Society* **2007,** *129*, 16197-16208. http://dx.doi.org/10.1021/ja076453m

6. B. Singaram. *Heteroatom Chemistry* **1992**, *3*, 245-249. http://dx.doi.org/10.1002/hc.520030309

7. M. Suginome, T. Tanaka, and T. Hasui. *Synlett* **2006**, 1047. http://dx.doi.org/10.1055/s-2006-939070

8. J. F. Janik, C. K. Narula, E. G. Gulliver, E. N. Duesler, and R. T. Paine. *Inorganic Chemistry* **1988**, *27*, 1222-1227. http://dx.doi.org/10.1021/ic00280a026

9. H. Nöth, P. Otto, and W. Storch. *Chemische Berichte* **1986**, *119*, 2517-2530. http://dx.doi.org/10.1002/cber.19861190811

10. P. Wilfling, K. Schittelkopf, M. Flock, R. H. Herber, P. P. Power, and R. C. Fischer. *Organometallics* **2015**, *34*, 2222-2232. http://dx.doi.org/10.1021/om500946e

11. A. Staubitz, A. P. M. Robertson, and I. Manners. *Chemical Reviews* **2010**, *110*, 4079-4124. http://dx.doi.org/10.1021/cr100088b

12. C. M. Vogels, P. E. O'Connor, T. E. Phillips, K. J. Watson, M. P. Shaver, P. G. Hayes, and S. A. Westcott. *Canadian Journal of Chemistry* **2001**, *79*, 1898-1905. http://dx.doi.org/10.1139/v01-177

13. D. J. Liptrot, M. S. Hill, M. F. Mahon, and A. S. Wilson. *Angewandte Chemie International Edition* **2015**, *54*, 13362-13365. http://dx.doi.org/10.1002/anie.201505949

14. Z. Yang, M. Zhong, X. Ma, K. Nijesh, S. De, P. Parameswaran, and H. W. Roesky. *Journal of the American Chemical Society* **2016**, *138*, 2548-2551. http://dx.doi.org/10.1021/jacs.6b00032

15. (a) N. L. Dunn, M. Ha, and A. T. Radosevich. *Journal of the American Chemical Society* **2012**, *134*, 11330-11333. http://dx.doi.org/10.1021/ja302963p (b) S. M. McCarthy, Y-C. Lin, D. Devarajan, J. W. Chang, H. P. Yennawar, R. M. Rioux, D. H. Ess, and A. T. Radosevich. *Journal of the American Chemical Society* **2014**, *136*, 4640-4650. http://dx.doi.org/10.1021/ja412469e (c) W. Zhao, S. M. McCarthy, T. Y. Lai, H. P. Yennawar, and A. T. Radosevich. *Journal of the American Chemical Society* **2014**, *136*, 17634-17644. http://dx.doi.org/10.1021/ja510558d (d) T. P. Robinson, D. M. De Rosa, S. Aldridge, and J. M. Goicoechea. E–H Bond Activation of Ammonia and Water by a Geometrically Constrained Phosphorus(III) Compound. *Angewandte Chemie International Edition* **2015**, *54*, 13758-13763. http://dx.doi.org/10.1002/anie.201506998

16. J. D. Erickson, J. C. Fettinger, and P. P. Power. *Inorganic Chemistry* **2015**, *54*, 1940-1948. http://dx.doi.org/10.1021/ic502824w

17. J. D. Erickson, R. D. Riparetti, J. C. Fettinger, and P. P. Power. *Organometallics* **2016**; published ASAP. http://dx.doi.org/10.1021/acs.organomet.6b00344

Publications Supported by BES

1. C. E. Melton, J. W. Dube, P. J. Ragogna, J. C. Fettinger, and P. P. Power. Synthesis and Characterization of Primary Aluminum Parent Amides and Phosphides. *Organometallics*. **2014**, *33*, 329-337. http://dx.doi.org/10.1021/om4010675

2. F. Lips, J. C. Fettinger, A. Mansikkamäki, H. M. Tuononen, P. P. Power. Reversible Complexation of Ethylene by a Silylene. *Journal of the American Chemical Society*. **2014**, *136*, 634-637. http://dx.doi.org/10.1021/ja411951y

3. J. W. Dube, Z. D. Brown, C. A. Caputo, P. P. Power, and P. J. Ragogna. Activation of Gaseous PH_3 with Low Coordinate Diaryltetrylene Compounds. *Chemical Communications*. **2014**, 1944-1936. http://dx.doi.org/10.1039/C3CC48933G

4. J. W. Dube, C. M. E. Graham, C. L. B. Macdonald, Z. D. Brown, P. P. Power, and P. J. Ragogna. Reversible Photo-Induced Activation of White Phosphorus by Low Coordinate Main Group Compounds. *Chemistry - A European Journal.* **2014**, *20*, 6739-6744. http://dx.doi.org/10.1002/chem.201402031

5. F. Lips, J. D. Queen, J. C. Fettinger, and P. P. Power. Unusual Coordination of Tetrylenes to Molybdenum Carbonyl Fragments. *Chemical Communications.* **2014**, *50*, 5561-5564. http://dx.doi.org/10.1039/c4cc00999a

6. F. Lips, A. Mansikkamäki, J. C. Fettinger, H. M. Tuononen, and P. P. Power. Reactions of Alkenes and Alkynes with an Acyclic Silylene and Heavier Tetrylenes under Ambient Conditions. *Organometallics*. **2014**, *33*, 6253-6258. http://dx.doi.org/10.1021/om500947x

7. J. C. Fettinger, P. A. Gray, C. E. Melton, and P. P. Power. Hydroalumination of Alkenes and Alkynes by Primary Aluminum Hydrides Under Mild Conditions. *Organometallics.* **2014**, *33*, 6232-6240. http://dx.doi.org/10.1021/om500911f

8. J. D. Erickson, J. C. Fettinger, and P. P. Power. Reaction of a Germylene, Stannylene, or Plumbylene with Trimethylaluminum and Trimethylgallium: Insertion into Al–C or Ga–C Bonds, a Reversible Metal–Carbon Insertion Equilibrium, and a New Route to Diplumbenes. *Inorganic Chemistry*. **2015**, *54*, 1940-1948. http://dx.doi.org/10.1021/ic502824w

9. P. Vasko, S. Wang, H. M. Tuononen, and P. P. Power. Addition of Ethylene or Hydrogen to a Main Group Metal Cluster under Mild Conditions. *Angewandte Chemie International Edition*. **2015**, *54*, 3802-3807. http://dx.doi.org/10.1002/anie.201411595

10. P. Wilfling, K. Schittelkopf, M. Flock, R. H. Herber, P. P. Power, and R. C. Fischer. Influence of Ligand Modifications on Structural and Spectroscopic Properties in Terphenyl based Heavier Group 14 Carbene Homologues. *Organometallics*. **2015**, *34*, 2222-2232. http://dx.doi.org/10.1021/om500946e

11. J. D. Erickson, P. Vasko, R. D. Riparetti, J. C. Fettinger, H. M. Tuonenen, and P. P. Power. Reactions of *m*-Terphenyl Stabilized Germylene and Stannylene with Water and Methanol: Oxidative Addition versus Arene Elimination and Different Reaction Pathways for Alkyl and Aryl Substituted Species. *Organometallics*. **2015**, *34*, 5785-5791. http://dx.doi.org/10.1021/acs.organomet.5b00884

12. P. Vasko, A. Mansikkamäki, J. C. Fettinger, H. M. Tuonenen, and P. P. Power. Reaction of $LiAr^{Me6}$ ($Ar^{Me6} = C_6H_3$-2,6-$(C_6H_2$-2,4,6-$Me_3)_2$) with Indium(I)chloride Yields Three *m*-Terphenyl Stabilized Mixed-Valent Organoindium Subhalides. *Polyhedron.* **2016**, *103*, 164-171. http://dx.doi.org/10.1016/j.poly.2015.09.052

13. M. L. McCrea-Hendrick, C. A. Caputo, C. J. Roberts, J. C. Fettinger, H. M. Tuononen, and P. P. Power. The Reactions of Terphenyl Substituted Digallene $Ar^{iPr4}GaGaAr^{iPr4}$ (Ar^{iPr4} = C_6H_3-2,6-$(C_6H_3$-2,6-$^iPr_2)_2$) with Transition Metal Carbonyls and Theoretical Investigation of the Mechanism of Addition. *Organometallics*. **2016**, *35*, 579-588. http://dx.doi.org/10.1021/acs.organomet.5b00992

14. N. Y. Tashkandi, L. C. Pavelka, P. D. Boyle, P. P. Power, and K. M. Baines. Probing the mechanism of the addition of alkynes to digermynes. *Dalton Transactions*. **2016**, *45*, 7226-7230. http://dx.doi.org/10.1039/C6DT01015F

15. J. D. Erickson, R. D. Riparetti, J. C. Fettinger, and P. P. Power. Molecular Zinc Species with Ge-Zn and Sn-Zn Bonds: A Reversible Insertion of a Stannylene into a Zinc-Carbon Bond. *Organometallics*. **2016**; article ASAP. http://dx.doi.org/10.1021/acs.organomet.6b00344

Dielectric Ceramics in Nanosheet Form

Tina Salguero

Assistant Professor, Department of Chemistry, The University of Georgia

salguero@uga.edu

Program Scope

Nanosheets are characterized as being from one to several monolayers thick and up to tens of micrometers in lateral dimensions. The nanosheet morphology has several unique features that put it at the frontier of materials development, foremost the fact that nanosheets can combine remarkable, quantum effect-derived properties with large surface areas and the advantages of solution-based manipulation methods. To date, most well-defined nanosheets have been derived from lamellar materials via exfoliation processes; examples include selected perovskites, various transition metal oxides and chalcogenides, hexagonal boron nitride, and graphene. We are interested in materials for energy applications that go beyond these examples, specifically oxide-based materials. The challenge is that there is no bulk layered precursor that can be exfoliated to provide nanosheets of these materials. However, when this preparative hurdle is surmounted, the scientific rewards will be substantial. At a fundamental level, such nanosheets will provide an opportunity to better understand the properties of complex oxide compositions at a size regime down to one monolayer, as well as allow us to study the roles of surface functionalization and interface interactions. Our approach in this new area of two-dimensional nanomaterials encompasses synthesis, characterization, and deposition methods. Specifically we have the following three major goals: *(1) To develop innovative methodologies for preparing dielectric ceramics in nanosheet form.* The key first step is to prepare dielectric ceramics as nanosheets, a non-natural form of these materials. This synthetic challenge will require novel strategies and techniques encompassing solid-state inorganic chemistry as well as solution-based modification and processing. For example, one of our innovations is to apply topotactic chemical transformations to pre-existing nanosheet starting materials, which will enable us to prepare metal titanates $MTiO_3$ and ruthenates $MRuO_3$ in nanosheet form. We further plan to develop ways to scale-up the preparation of exceptional nanosheet materials as they are identified. *(2) To characterize the fundamental properties of dielectric ceramic nanosheets.* Our innovation is to use the unique combination of morphology and surface functionalization of monolayer-thick ceramic nanosheets to tune their dielectric properties. *(3) To process dielectric ceramic nanosheets via solution-based techniques.* We propose two ways to assemble and deposit nanosheet materials. The first is inkjet printing of nanosheet inks; because nanosheets typically exhibit liquid crystal properties, the solid components will be well-ordered when the

ink dries, which leads to high-quality (near crystalline) materials. The second way is to use dielectric ceramic nanosheets in the assembly of layered, hybrid, and composite macroscale materials. The concept of nanosheet building blocks is based on bottom-up assembly strategies that will allow us to create novel materials with dielectric ceramic nanosheet components. In addition, solution-based approaches will enable the preparation of macroscale samples on large and/or flexible substrates at ambient conditions.

Recent Progress

Work has focused on new synthetic methodologies to access nanosheets of diverse inorganic materials, including ternary metal oxides, metal fluorides, metal silicates, and metal phosphates. Additional work on metal carbonates has been related to studying the formation of metal oxides.

Ternary metal oxide nanosheets: One of our targets has been nanosheets of the Aurivillius-type layered oxides Bi_2MO_6. We developed a template approach to transform cesium tungstate nanosheets into Bi_2WO_6 nanosheets using *in situ* generated bismuth oxide hydroxide nanosheets. We have refined the approach using isolated bismuth oxide borate nanosheets. The reaction between cesium tungstate nanosheets and bismuth oxide borate nanosheets provides a higher quality Bi_2WO_6 nanosheet product. The control reactions using non-nanosheet precursors shows no templating effects and generates bulk Bi_2WO_6. In comparison, analogous reactions with Mo-based precursors like α-MoO_3 nanosheets proceed through a different mechanism involving dissolution-recrystallization, which destroys the template. In the process of tuning the reaction conditions to make bismuth oxide borate nanosheets, we discovered hydrothermal conditions to prepare boron sillenite $Bi_{24.5}BO_{38.25}$ microspheres (isostructural with γ-Bi_2O_3), which previously have been accessible via solely high temperature routes. Another targeted class of ternary oxide materials are the perovskite-type ABO_3 compositions with useful electronic properties. For example, we have prepared strontium manganite $SrMnO_3$ nanosheets from MnO_2 nanosheets using hydrothermal conditions. We optimized the method by evaluating concentration, temperature, time, and especially the type of MnO_2 nanosheet precursor, ranging from highly-crystalline samples made by crystal exfoliation to structually-defective MnO_2 made by in situ nanosheet formation from manganese sources like $KMnO_4$. Another example, $PbTiO3$, has more complex chemistry. We discovered that the layered compositions $PbTi_{0.8}O_{2.6}$ and $Pb_5O(OH)_2(CO_3)_3$ (also known as plumbonacrite) were intermediates in the formation of $PbTiO_3$ nanostructures from titanate nanosheet precursors under hydrothermal conditions. This key insight has led to a more detailed understanding of the mechanism of $PbTiO_3$ nanostructures in this system, as well as ways to control the course of the reaction, and consequently we have optimized the formation of sub-10 nm thick $PbTiO_3$ nanosheets.

Silicon oxide-based nanosheet precursors: With the intent of making silicate-based perovskites $ASiO_3$, interesting materials typically formed under high pressure conditions like the Earth's mantle and shocked meteorites, we targeted fluoride-stabilized siloxene $(Si_6H_xF_{12-x})_y$ by

reacting CaSi$_2$ with fluorinating agents. Although we tested a variety of highly-reactive fluorinating agents, the most significant reaction of CaSi$_2$ occurred with aqueous hydrofluoric acid. However, instead of a Si-based product, the product instead consists of CaF$_2$ nanosheets that form within CaSi$_2$ via interlayer confinement and templating effects. These CaF$_2$ nanosheets display very different reactivity with lanthanide ions compared to bulk or nanoparticulate CaF$_2$.

In particular, we found that the reaction of CaF$_2$ nanosheets with lanthanum ions under room temperature, aqueous condition yields LaF$_{3-2x}$O$_2$ nanoscrolls. This unique topochemical transformation also demonstrates a new scrolling mechanism based on strain induced by the substitution of O for F in the LaF$_3$ lattice.
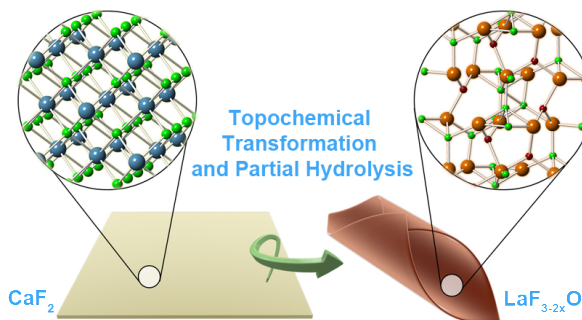
Metal silicate nanosheets: In collaboration with Prof. Joe Kolis at Clemson University, who has the lab facilities to conduct hydrothermal reactions at temperatures up to 650 °C, we successfully synthesized calcium copper tetrasilicate CaCuSi$_4$O$_{10}$, which can be exfoliated into monolayer metal silicate nanosheets with strong near infrared luminescent properties. We demonstrated solution processing in the form of spray coating and polymer composite formation for the scalable CaCuSi$_4$O$_{10}$ nanosheets. Studies in collaboration with Prof. Datta Late (CSIR National Chemical Laboratory, Pune, India) showed that ACuSi$_4$O$_{10}$ (A = Ca, Sr, Ba) nanosheets have remarkable double layer capacitance and electrochemical performance that indicate promise in supercapacitor applications. We also were successful at accessing the isostructural iron-based system BaFeSi$_4$O$_{10}$ (also known as the mineral gillespite) by an analogous hydrothermal approach, and the exfoliated nanosheets have potentially interesting magnetic properties due to the two dimensional Fe^{2+} network.
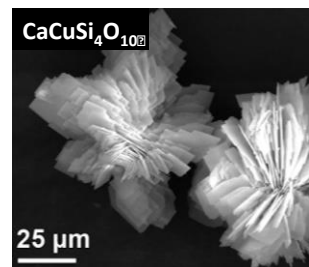
Metal carbonate nanoparticles: During our investigations of metal oxide nanosheet formation, we became more interested in the chemistry of ACO$_3$ nanoparticles. We have discovered a surprising polymorphism of SrCO$_3$ nanoparticles stabilized with methanol. Using infrared, Raman, and solid-state NMR spectroscopies with isotopically labeled samples, and in collaboration with computational materials scientist Prof. Scott Beckman at Washington State University, we have determined that the SrCO$_3$ nanoparticles are monoclinic. As part of these studies, we revisited research on the stabilization of BaCO$_3$ with sulfate ions from the 1980s. New characterization information using various spectroscopic techniques in combination with theory has allowed us to re-analyze and correct the structural interpretation of monoclinic BaCO$_3$. These alkaline earth metal carbonate systems are especially important for carbon sequestration applications, and the ability to tune carbonate polymorphs should play an important role in engineering such processes.

Metal phosphate nanosheets: We also applied the synthetic methodologies developed previously on this project to metal phosphate compositions, starting with manganese-based phosphates. We demonstrated access to lithium manganese phosphate $LiMnPO_4$ nanosheets directly from flowerlike micron-sized clusters of $LiMnPO_4$ or from a new polymorph of manganese orthophosphate $Mn_3(PO_4)_2$ with a novel open-framework structure. These materials have applications for lithium and sodium ion storage.

δ-$Mn_3(PO_4)_2$
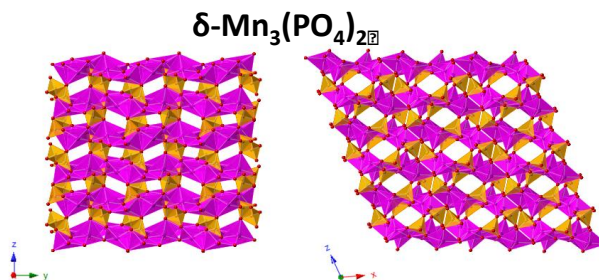
Future Plans

Ternary oxide nanosheets: Based on numerous observations that implicate the participation of atmospheric CO_2 in reactions that transform MO_2 nanosheets into ternary oxide nanosheets, we plan to carefully examine the impact of CO_2 by conducting these reactions under CO_2-free conditions as well as under CO_2-enriched conditions, especially using ^{13}C NMR and FTIR on ^{13}C-labeled products. In addition, we plan to characterize the magnetic properties of these nanosheets by Moessbauer and EPR spectroscopies at the National High Field Magnet Laboratory (FL). **Metal silicate-based nanosheets:** We plan to characterize the magnetic properties of $BaFeSi_4O_{10}$ crystals and exfoliated nanosheets by Moessbauer and EPR spectroscopies at the National High Field Magnet Laboratory. We also plan to expand the exfoliation and hydrothermal chemistries developed on this project to additional metal silicate compositions $BaMgSi_4O_{10}$ and $BaCrSi_4O_{10}$. **Metal phosphate-based nanosheets:** We plan to study the lithiation and sodiation properties of new metal phosphate-based nanosheets. To study the electrochemical properties of these materials, we will process them into battery electrodes for coin cells. **Metal carbonate chemistry:** In ongoing work we will be applying the synthetic methods and structural control lessons learned in prior work on alkaline earth metal carbonates to transition metal and main group metal carbonate systems.

Publications

"Hydrothermal Formation of Calcium Copper Tetrasilicate" Darrah Johnson-McDaniel, Sara Comer, Joseph W. Kolis and Tina T. Salguero, *Chemistry–A European Journal*, **2015**, 21, 17560.

″Two-Dimensional Structuring of Photocatalytic Bismuth-Based Metal Oxides" Tina T. Salguero, Timothy R. Pope, Gregory Neher, and Abigail Bruning, *Proceedings, American Chemical Society 249th National Meeting,* **2015**.

"Chromism of Bi_2WO_6 in Single Crystal and Nanosheet Forms," Timothy R. Pope, Melissa N. Lassig, Gregory Neher, Richard D. Weimar, Tina T. Salguero, *Journal of Materials Chemistry C*, invited contribution to the 2014 Emerging Investigators Issue, **2014**, *2*, 3223-3230.

Hybrid Halide Perovskites: Advancing Optoelectronic Materials [DE- SC-0012541]

Ram Seshadri, University of California Santa Barbara (Principal Investigator)
Michael Chabinyc, University of California Santa Barbara (Co-Investigator)
Fred Wudl, University of California Santa Barbara (Co-Investigator)
Mercouri Kanatzidis, Northwestern University (Co-Investigator)

Program Scope

A collaborative, multi-investigator approach is employed to address the emerging area of functional materials based on perovskite-halide–derived architectures. The recent explosion of interest in these functionally and architecturally diverse materials has been due to their potential as PV absorbers and sensitizers. However, while important, these applications represent only a small part of what these materials are capable of. Recent studies have revealed several important knowledge gaps in our understanding of these systems and raised a number of fundamental questions with regard to the prospects for developing innovative new variants with enhanced properties. In particular, there is the recognition that these materials exhibit useful yet contraindicated properties, or properties that usually do not coexist in the same material; metallic conductivity and band-edge luminescence, or high carrier mobility in combination with a large band gap. The assembled group of investigators bring together the necessary strengths to make fundamental contributions in new inorganic and hybrid perovskite halide material synthesis, structural characterization of single- and polycrystalline materials and thin films, property measurement, first-principles theoretical modeling of molecular and crystalline structure, and electronic structure. These studies will advance the fundamental science and establish structure–composition–property relations in this fascinating class of materials. Understanding the basic science of these materials, and developing new systems is expected to open up new domains of functional materials.

Recent Progress

The systems studied by us have proved to be an extremely fertile area of research. Some key aspects of our findings are highlighted here.

Figure 1: Absolute electronic energy levels for a number of bismuth halide compounds from ultraviolet photoemission and density functional theory.

Complex bismuth iodides: Continuing our investigation of promising lead-free alternative optoelectronic materials, we have correlated dimensionality of the crystal structure and size of the counter cation with absolute electronic energy levels in binary and ternary inorganic bismuth iodides *via* photoemission spectroscopy and density functional theory calculations (see accompanying **figure 1**).[1] Many of the methods that we employed for the electronic structure calculations were based on our prior work on related lead compounds.[2] Photovoltaic devices
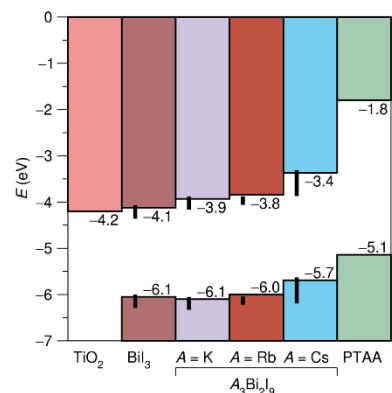
employing the binary BiI_3 as the active layer were fabricated, and their modest performance underscores the importance of band alignment.[3]

Fundamental studies of $CH_3NH_3PbI_3$ and related perovskites: To better understand the factors that imbue the canonical hybrid perovskite alloys with such remarkable optoelectronic performance, we have undertaken two basic studies to relate crystal chemistry to electronic transport and defect tolerance. The first is focused on the role of the organic molecular ion on the *A*-site of the perovskite: We have found, through dielectric and calorimetric measurements, the first evidence for an orientationally glassy state in $CH_3NH_3PbI_3$ and $HC(NH_2)_2PbI_3$ induced on cooling by the complex interaction between the polar, organic molecular cations and the anionic inorganic sublattice.[4] The second effort to relate crystal chemistry to transport and defect tolerance is focused on the importance of the lone pair-bearing divalent main group cation. Via synchrotron X-ray and neutron total scattering experiments, we have observed a locally distorted state in the perovskite $CsSnBr_3$ that emerges on warming as a consequence of dynamic, spatially incoherent lone pair stereochemical activity.

In order to investigate the operating mechanism of the key halide systems, *viz.* $CH_3NH_3PbI_3$, including the charge-transport properties, and to elucidate more general protocols and phenomena relevant for material design, field-effect transistors (FETs) were fabricated in a bottom-gate, top-contact (BGTC) architecture. Initial measurement attempts proved unsuccessful, with devices exhibiting low source-drain currents and no field-induced current modulation. However, at reduced temperatures we see functional devices emerge. We have hypothesized that mobile ions in the perovskite structure may be responsible for the absence of a field-effect in $CH_3NH_3PbI_3$ at room-temperature, with ions effectively screening the applied gate potential.[5]

New hybrids, including with functional organic cations: We have developed new hybrid, perovskite-related materials by investigating the inclusion of functional organic cations within heavy-metal halide matrices. Synergistic effects between organic and inorganic components have been established, that could form key components in future optoelectronic materials. One example is a new lead iodide halide networks stabilized by chains of tetrathiafulvalene

Figure 2: Crystal structure of $(TTF)Pb_2I_5$.

(TTF) radical cations.[6] A commensurate compound has the chemical formula $(TTF)Pb_2I_5$, with the crystal structure shown in **Figure 2.**

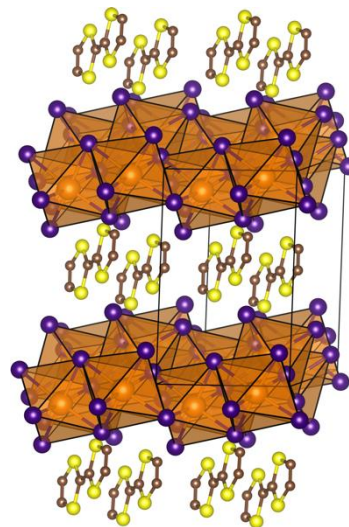We have also accomplished the large scale synthesis, crystal structure and optical characterization of the two-dimensional (2D) $[CH_3(CH_2)_3NH_3]_2(CH_3NH_3)_{n-1}Pb_nI_{3n+1}$ (n = 1, 2, 3, 4, ∞) perovskites, a family of layered compounds with tunable semiconductor characteristics. The band gaps of the series change progressively between 2.43 eV for the n = 1 member to 1.50 eV for $n = \infty$ adopting intermediate values of 2.17 eV (n = 2), 2.03 eV (n = 3) and 1.91 eV (n =

4) for those between the two compositional extrema. DFT calculations confirm this experimental trend and predict a direct band gap for all the members of the Ruddlesden-Popper series. The band gaps of higher n members indicate that these compounds can be used as efficient light absorbers in solar cells, offering better solution processability and good environmental stability. The compounds exhibit intense room-temperature photoluminescence with emission wavelengths consistent with their energy gaps, 2.35 eV ($n = 1$), 2.12 eV ($n = 2$), 2.01 eV ($n = 3$) and 1.90 eV ($n = 4$) and point to their potential use in light-emitting diodes. In addition, owing to the low dimensionality and the difference in dielectric properties between the organic spacers and the inorganic perovskite layers, these compounds are naturally occurring multiple quantum well structures which give rise to stable excitons at room temperature.[7]

A second accomplishment relates to the exploration of new systems. We have synthesized and characterized two series of two-dimensional halide perovskites, one with a monovalent benzylammonium (BZA) cation and the other with a divalent histammonium (HA) cation. The $(BZA)_2MI_4$ (M = Pb, Sn) crystallize in the orthorhombic space group *Pbca* while the $(HA)MI_4$ (M = Pb, Sn) crystallize in the Monoclinic space group $P2_1/n$. Compounds featuring BZA cation have larger band gaps than the HA ones due to the relatively smaller M–I–M angles, which were proven both experimentally and from DFT calculations. Band gaps of the solid solutions show an anomalous trend for both series. Optical and electronic properties (Figure 8) such as time-resolved fluorescence and resistivity are also under investigation for these compounds. Thin films of both series of compounds are also fabricated and the PXRD of the films show different orientations: the BZA films show same orientation as the bulk while HA films show the "perpendicular" film growth orientation, which is highly favorable for photovoltaic devices. The structure and properties are heavily influenced by the nature of the cations, which bring contrasting effect on the photovoltaic performances of these materials. This unique orientation of $HAPbI_4$ has proven to be beneficial to both the EQE and the device performance, showing a preliminary power conversion efficiency of 1.13%.[8]

Future Plans

We will continue, in the following year, to expand the fundamental understanding of these systems, and develop new chemistries for both stable Pb-containing compounds, and well as Pb-free compounds.

Publications

1. A. J. Lehner, D. H. Fabini, H. A. Evans, C.-A. Hébert, S. R. Smock, J. Hu, H. Wang, J. W. Zwanziger, M. L. Chabinyc, and R. Seshadri, Crystal and electronic structures of complex bismuth iodides $A_3Bi_2I_9$ (A = K, Rb, Cs) related to perovskite: Aiding the rational design of photovoltaics, *Chem. Mater.* **27** (2015) 7137–7148.
2. J. Brgoch, A. J. Lehner, M. L. Chabinyc, and R. Seshadri, Ab initio calculations of band gaps and absolute band positions of polymorphs of $RbPbI_3$ and $CsPbI_3$: Implications for main-group halide perovskite photovoltaics, *J. Phys. Chem. C.* **118** (2014) 27721–27727.

3. A. J. Lehner, H. Wang, D. H. Fabini, C. D. Liman, C.-A. Hébert, E. E. Perry, M. Wang, G. C. Bazan, M. L. Chabinyc, and R. Seshadri, Electronic structure and photovoltaic application of BiI_3, *Appl. Phys. Lett.* **107** (2015) 131109.

4. D. H. Fabini, T. Hogan, H. A. Evans, C. C. Stoumpos, M. G. Kanatzidis, and R. Seshadri, Dielectric and thermodynamic signatures of low temperature glassy dynamics in the hybrid perovskites $CH_3NH_3PbI_3$ and $HC(NH_2)_2PbI_3$, *J. Phys. Chem. Lett.* **7** (2016) 376–381.

5. J. G. Labram, D. H. Fabini, E. E. Perry, A. J. Lehner, H Wang, A. M. Glaudell, G. Wu, H. Evans, D. Buck, R. Cotta, L. Echegoyen, F. Wudl, R. Seshadri, and M. L. Chabinyc, Temperature-dependent polarization in field-effect transport and photovoltaic measurements of methylammonium lead iodide, *J. Phys. Chem. Lett.* **6** (2015) 3565–3571.

6. H. Evans, A. Lehner, J. Labram, D. Fabini, O. Barreda, S. Smock, G. Wu, M. Chabinyc, R. Seshadri, and F. Wudl, $(TTF)Pb_2I_5$: A radical cation-stabilized hybrid lead iodide with synergistic optoelectronic signatures. *Chem. Mater.* 28 (2016) 3607–3611.

7. C. Stoumpos, D. H. Cao, D. J. Clark, J. Young, J. M. Rondinelli, J. I. Jang, J. T. Hupp, and M. G. Kanatzidis, Ruddlesden-Popper hybrid lead iodide perovskite 2D homologous semiconductors, *Chem. Mater.* **28** (2016) 2952−2867.

8. D. A. Valverde-Chavez, C. S. Ponseca, C. C. Stoumpos, A. Yartsev, M. G. Kanatzidis, V. Sundstrom, and D. G. Cooke, Intrinsic femtosecond charge generation dynamics in single crystal $CH_3NH_3PbI_3$, *Energy Environ. Sci.* **8** (2015) 3700–3707.

9. C. Stoumpos, L. Frazer, D. J. Clark, Y. S. Kim, S. H. Rhim, A. J. Freeman, J. B. Ketterson, J. I. Jang, and M. G. Kanatzidis, Hybrid germanium iodide perovskite semiconductors: Active lone pairs, structural distortions, direct and indirect energy gaps, and strong nonlinear optical properties, *J. Am. Chem. Soc.* **137** (2015) 6804–6819.

Transition Metal Oxides Nanomaterials for Aqueous Electrochemical Energy Storage

Xiaowei Teng, Department of Chemical Engineering, University of New Hampshire

Program Scope

Supercapacitors, also called electrochemical rcapacitors or ultracapacitor, are a class of energy storage devices that fill the gap between high-energy-density batteries and high-power-density electrostatic capacitors. This project is to investigate the transition metal oxides for use as electrode materials for supercapacitors. Through the novel material syntheses, structural and functional characterizations, and synchrotron-/neutron-based measurements, the goals of the project are:

(i) Develop aqueous electrochemical energy storage (EES) devices using novel types of metal oxide nanomaterials that can be operated at the potential window beyond 1.23 V. A key technical challenge for ESS to rival the performance of lithium-ion batteries (LIBs) is the width of the electrical potential range. Aqueous EES devices usually operate at or below 1.2 V because the thermodynamically stable potential window of water is approximately 1.23 V. Beyond this limit the hydrogen evolution reaction (HER) and oxygen evolution reaction (OER) occur. However, a voltage window of 1.2 V is too narrow to achieve high energy density and power density. In the study of water electrolysis, many metals and metal oxides have shown a high overpotential to HER and/or OER, which is defined as the potential difference between the potentials experimentally observed for gas evolution and those determined at equilibrium states. Therefore, our primary goal of the project is to discover a new type of materials that are not only substantially inactive to HER and OER as electrodes for aqueous EES, but also highly active toward reversible charge‐storage of alkaline cation.

(ii) Develop novel types of metal oxide nanomaterials that can reversibly storage alkali cations in aqueous electrolyte via intercalation/deintercalation charge storage mechanism. The low energy density of the aqueous EES is not only due to the narrow workable potential window of aqueous electrolyte, but also due to the fact that electrochemical insertion and extraction of alkaline cations (especially Na- and K-ion) often cause large distortions of the host electrode materials due to its large ionic radius, and eventually leads to pulverization of the electrode and the degradation of the cell. Our approach to improve the energy density and stability of alkali aqueous EES can be improved through the design of layered electrode materials, from which the interlayer distance can afford nearly reversible insertion/extraction of alkali without causing structural degradation.

Recent Progress

Aqueous Energy Storage with 3.0 V Potential Window
A key technical challenge for aqueous electrochemical energy storage (EES) to rival the performance of lithium-ion batteries is the width of the electrical potential range. Aqueous EES devices usually operate at or below 1.23 V, beyond which the gas evolution reactions occur (decomposition of water). In the previous funding period we had demonstrated the synthesis, characterization and function test of a new type of monoclinic manganese oxide (Mn_5O_8) nanoparticles. Our results showed that Mn_5O_8, the *only* bivalence layered manganese oxide structure, can serve as a new generation of pseudocapacitor electrode materials for enabling a

stable potential window of 3.0 V for aqueous electrochemical energy storage, though its unique electrochemical properties has been largely overlooked in the past *fifty* years since its structure was first determined in 1965 (Nature, 207, 72, 1965). An aqueous symmetric full cell using such electrodes demonstrates a stable potential window of *3.0* V, and high energy and power performance with nearly 100% coulombic efficiency and 85% energy efficiency after *25,000* charge-discharge cycles. To our knowledge, this is the widest and the most stable potential window ever reported for an aqueous energy storage device. Our discovery has been filed as a provisional patent application in July 2014. In the current funding period (July 2015 to June 2016), the innovation of Mn_5O_8 materials has been converted into a full patent application in July 2015 (US Patent Application No. 14/737,823, pending). The PI has been working closely with UNH Innovation Services for the opportunities licensing and/or entrepreneurship for this innovation. Besides the technological breakthrough, the PI has conducted various analyses to obtain the fundamental understanding of superior Mn_5O_8 systems by employing synchrotron-based soft X-ray spectroscopy and density functional theory (DFT) calculations. The related results are summarized as following:
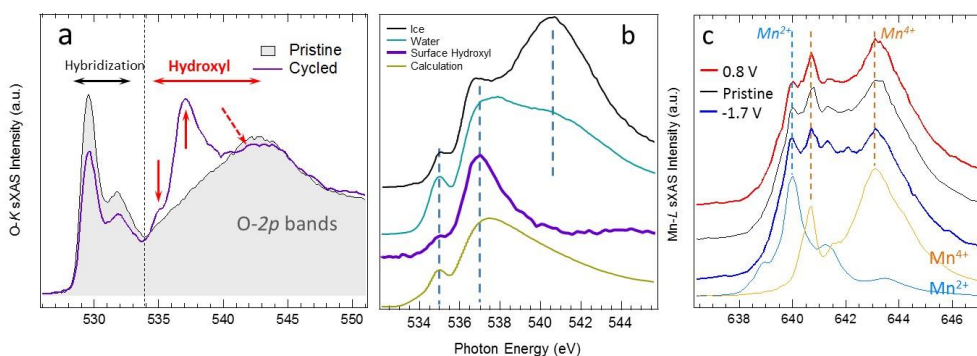
Figure 1. (a) O-K sXAS of Mn_5O_8 (pristine) and Mn_5O_8 electrode after two CV cycles between -1.7 V and 0.8 V. Features below 534 eV are from the hybridization of Mn-*3d* and O-*2p* states. The 535 and 537 eV peaks are fingerprints of the water "pre-peak" and "main peak". (b) A comparison of the O-K sXAS of the surface hydroxyl layer of Mn_5O_8 with water, ice, and one of the calculations with aligned H-bonds but lengthened O-O (3.50 and 3.00 Å) distances (*Science* **304**, 995, 2004). (c) Mn *L*-edge of Mn_5O_8 (pristine) and Mn_5O_8 at different electrochemical cycling stages along with references from MnO (blue) and Li_2MnO_3 (yellow).

(i)   Our soft X-ray absorption data from O-K edge and Mn-L edge, obtained from beamline 8.01 1 at the Advanced Light Source (ALS) of the Lawrence Berkeley National Lab (LBNL), revealed a well ordered ice-like surface hydroxyl layer that were only proposed in theory before (*Science* **304**, 995, 2004) (**Figure 1 a, b**).

(ii)   Interplay between Mn^{2+} terminated surface and special hydroxylated interphase accounted for the high overpotential (> 0.6 V) of Mn_5O_8 towards HER and OER, confirmed experimentally and theoretically, and therefore the stable 3.0 V potential window.

(iii) Our soft X-ray absorption data from Mn-L edge indicated that the unique bivalence ($Mn^{2+}_2Mn^{4+}_3O_8$) structure that enables two-electron charge transfer via Mn^{2+}/Mn^{4+} redox couple (**Figure 1c**).

Highly disordered V_2O_5 nanosheets for high capacity aqueous energy storage

In the current funding period, the PI and his research group has studied and developed report a new type of highly disordered vanadium-based electrode material for reversible K-ion storage in an aqueous electrolyte, which delivered 178 mAh/g of capacity in the half-cell with a scan rate of 5 mV/sec, corresponding to 0.87 electron charge per vanadium atom. A plausible electrode capacity of ~ 50 mAh/g was observed in a two-electrode symmetric full-cell after 2,000 cycles at a high current density of 2 A/g. Our results from neutron and synchrotron scattering showed that structured water intercalated between V-O layers play critical roles in stabilizing the disordered nanolayer structure, and benefiting the insertion and extraction of K-ion during charge-discharge process. These results will contribute to the exploration a large family of disordered layered structure from the earth-abundant elements in electrochemical energy storage applications. The related results are summarized as following:

(i) The disordered potassium intercalated vanadium oxide KVO nanosheets exhibited excellent gravimetric capacitance of 661 F/g, corresponding to a capacity of 178 mAh/g, at a scan rate of 5 mV/s from CV measurements. Given the fact that theoretical capacitance of $K_2V_2O_5$ is 205 mAh/g based on one charge transfer per vanadium atom, the reported capacitance (661 F/g) was equivalent of 0.87 electrons transfer per vanadium atom. Even at a high scan rate of 200 mV/s, disordered KVO retained significant amount of capacitance of 334 F/g (93 mAh/g), representing plausible 0.45 electrons transfer per vanadium atom. To the best of our knowledge, this is one of the highest storage capacities in aqueous phase ever reported not only among the vanadium oxide materials, but also among other metal oxide electrode based on intercalation charge storage mechanism. KVO nanosheets showed long-term stability upon cycling in symmetric full-cell tests. No obvious capacity decay was observed
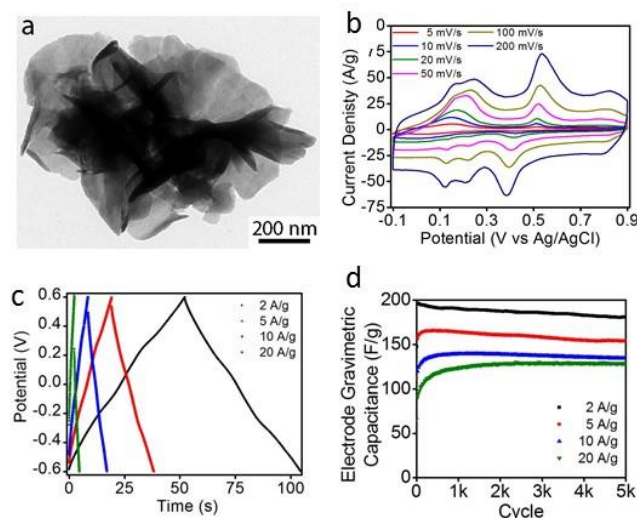

Figure 2. (a) TEM image of the disordered potassium intercalated vanadium oxide (KVO) nanosheets. (b) Electrochemical performance of KVO in half-cell cyclic voltammetry measurements at various scan rates from 5 to 200 mV/s. Electrochemical performance of KVO in full-cell, including (c) constant current galvanostitic charge-discharge curves at various current densities, and (d) the calculated electrode gravimetric capacities as a function of cycling numbers.

throughout 5,000 charge-discharge cycles, demonstrating excellent coloumbic efficiencies (~ 100%) (**Figure 2**)

(ii) Our neutron scattering data showed that interaction between KVO and water play important roles in stabilizing the KVO structure. Here we study the KVO and water (D_2O) interaction by total neutrons scattering experiments and the refinement of the Pair Distribution Function (PDF). As-made and hydrated KVO showed a similar monoclinic structure having potassium and water intercalated within V-O layers consisting of bi-layered [VO_6] octahedral units. Both materials showed large atomic displacement parameter in the direction of C axis, suggesting a disordered nature with a discernable turbostratic stacking of the layers, namely the dis-alignment

between adjacent V-O sheets. Albeit these similarities, neutron PDF shows a clear change in the local structure of the KVO upon water interaction (**Figure 3**), evidenced by a nearly threefold increase in intensity of O-H bond (r = 1Å). Various de-convoluted O-O peaks appear after water interaction in the range from 4 to 11 Å, resulting from the increased correlation between the oxygen atom in water (between the V-O layers) and the oxygen atoms comprised the [VO_6] (of the V-O layers).
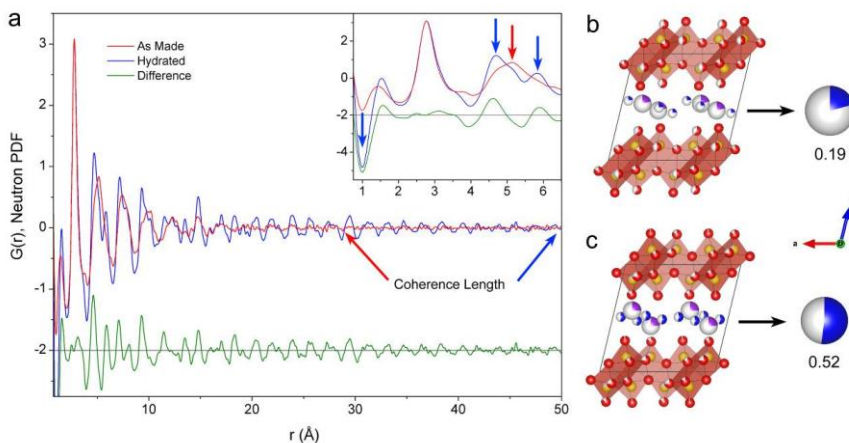

Figure 3. (a) Neutron pair distribution function (PDF) analyses of as-made KVO and KVO after interacting with water (D_2O). The fitting results show that (b) as-made KVO only has an O occupancy of 0.19 between V-O layers, while (c) hydrated KVO after D_2O interaction has an O occupancy of 0.52. In the refined crystal structure of KVO, the vanadium atoms are blue, the potassium atoms are purple, the oxygen atoms are red and gray represents vacancy.

Future Plans

(i)   PI will synthesize Na-doped Mn_5O_8 with controlled chemical compositions, and study the effect of the dopants on the capacitance of the resulting electrode material. Meanwhile, the effect of the dopants on the HER and OER will also be studied. The optimal materials will have enhanced the capacitance of energy storage, with uncompromised resistance to HER and OER to maintain the wide potential window of 3.0 V.

(ii)   PI will continue to study the influence of disordered structure, in the case of disorder V_2O_5 nanolayers, on the energy storage capacity and cycling life for aqueous energy storage. The outcome could help the design other types of disordered layered metal oxide nanostructure including MnO_2, TiO_2, MoO_3 and Nb_2O_5.

Publications

1) Teng, X.W., Charles, D. S., Shan, X.Q., Wu, Y. T., "*In Situ Studies of Charge-Storage Mechanism of Manganese Oxide Nanomaterials for Electrochemical Capacitors*",

Chapter in In "*Supercapacitors: Electrochemical Properties, Applications and Technologies*", Nova (2014)

2) Teng, X.W. *Manganese Oxide Compositions and their Use as Electrodes for Aqueous Phase Energy Storage Devices*, **U.S. Patent** Application No. 14/737,823, Pending (2015)

3) Charles, D. S., Teng, X.W.; *Vanadium Pentoxide Electrode for Aqueous Energy Storage: Understand Ionic Transport using Electrochemical, X-ray and Neutron Tools*, **Chapter** in "*Ion Batteries*", Intech (2016)

4) Shan, X., Charles D.S, Lei Y., Qiao R., Wang G., Yang W., Feygenson M., Su D., Teng, X.W. *Bivalence Mn_5O_8 with hydroxylated interphase drives for high-voltage aqueous sodium-ion storage*, **Nature Communication**, In Revision (2016)

5) Charles D.S,, Feygenson M., Xu, W., Teng, X.W. *Revealing the role of structural water in disordered vanadium oxide nanosheets for high capacity and high rate aqueous K-ion storage*, **Nature Materials**, In Review (2016)

Using Nanoporous Materials to Understand Kinetic Constraints in Pseudocapacitive Energy Storage

Sarah H. Tolbert, UCLA, Depts. of Chem. & Biochem. and Materials Sci. & Engineering

Program Scope

This project has three main goals. The first of these relates to understanding the fundamental nature of intercalation pseudocapacitance. Pseudocapacitive energy storage involves fast redox reactions and is typically found in nanostructured materials. While power densities in pseudocapacitive materials are not as high those observed in double layer capacitors, energy densities can be much higher, particularly when intercalation pseudocapacitance is involved. In such cases, intercalation over 2 – 50 nm can appear capacitive. Despite the exciting potential of pseudocapacitance to dramatically reduce charging times in Li^+ batteries, the fundamental rules governing intercalation pseudocapacitance remain poorly understood. In order to understand the underlying charge storage mechanisms in these systems, we specifically focus on the idea that in most battery materials, distinct phase transitions occur between lithiated and non-lithiated states, and phase transition kinetics can dominate the kinetics of Li^+ intercalation. The major goal of this project was to determine if suppression of such phase transitions in a variety of nanostructured materials is a key component of intercalation pseudocapacitance.

The second main goal of this DOE supported work focuses on the development of cathode materials for lithium ion pseudocapacitors that display intercalation pseudocapacitance. Anode materials for lithium ion batteries are generally in their stable thermodynamic state without lithium in the lattice, and as a result, many of these materials can be readily fabricated into nanoscale architectures that show high levels of intercalation pseudocapacitance. By contrast, cathode materials are in their stable state containing lithium, and the sol-gel chemistry of lithium and the need for high temperatures to produce cation ordering makes the synthesis of nanostructured cathodes more challenging. For this work, we have focused on lithium manganese oxide (LMO) with a goal of creating first thin film and then bulk porous powders that show high levels of intercalation pseudocapacitance at voltages suitable for cathode applications.

Our final goal again focuses on porous materials, this time aimed at understanding how porous structures can accommodate the deleterious large volume changes in high capacity alloying anodes. While porosity is clearly good for electrodes with large volume changes, some critical questions remained unanswered, in particular, the relationship between structural stability and the microstructure of these porous materials. We address this question using dealloyed nanoporous metals. Our model system is nanoporous tin (NP-Sn), as tin metal is abundant, environmental friendly, and exhibits high Li and Na storage capacities. We aim to tailor both the size and structure of the nanoscale ligaments to best accommodate volume change. We further aim to use X-ray imaging to directly see how porous grains deform upon Li intercalation.

Recent Progress

Pseudocapacitive charge storage has been demonstrated in numerous oxide based materials, but sulfide based materials are a relatively unexplored material landscape for this type of fast charge storage. MoS_2 is especially attractive for fast intercalation pseudocapacitance based charge storage because the interaction between Li-ions and the sulfide host-lattice should be weaker compared to an oxide-based lattice, which enables the possibility of extremely fast reaction kinetics. In addition, MoS_2 is also crystalographically ideal for pseudocapacitive charge storage because its large interatomic spacings should enable fast ion migration. In order to test these ideas, we synthesized

3-D ordered porous MoS2 thin films from polymer templated MoO2 materials. The thin film format was chosen to eliminate the need for conductive carbon additives or binders in order to isolate the effects of nanostructuring the MoS2. These MoS2 thin films possess ideal nano-architectures for pseudo-capacitive energy storage. The 10 nm pore walls provide short ion diffusion pathlengths, while the pore-voids allow good electrolyte accessibility to the electrochemically active walls. The combination of these structural factors leads to the extremely fast kinetics. Over 80% of the theoretical

Fig. 1. (a) SEM image of nanostructured MoS2 shows a network of agglomerated nanocrystals. (b) TEM further shows sub-50 nanometer primary particles with open access to the layer to allow facile ion insertion into the nanocrystal.

capacity can be accessed in only 20 seconds which is consistent with our quantitative analysis indicating that a high percentage of the charge storage is capacitor-like. Moreover, the cycling performance is extremely good as the capacity decrease over 10,000 cycles is only 13%. The paper on this work was distinguished as one of the five most highly downloaded articles in Advance Energy Mater. during February.

Utilizing the results of this ideal system, we created thick film nanostructured MoS2 based electrodes to study the structural mechanism of intercalation pseudocapcitance (MoS2 thin films are not amenable to in-situ diffraction studies due to their low mass loading). The nanostructured MoS2 used for this study was synthesized using similar methods to the thin films but starting with MoO2 nanocrystals. Structural analysis is shown in Figure 1. These electrodes were scaled-up to contain two-orders of magnitude more active material, while retaining the high level of pseudo-capacitance demonstrated in the thin film system. As a result, these thicker electrodes may be technologically important. This thicker electrode geometry can still be charged to more than 50% capacity in just 30 seconds, and cycles 3000 times with 80 % capacity retention. Using synchrotron based X-ray diffraction, we have discovered that the phase transit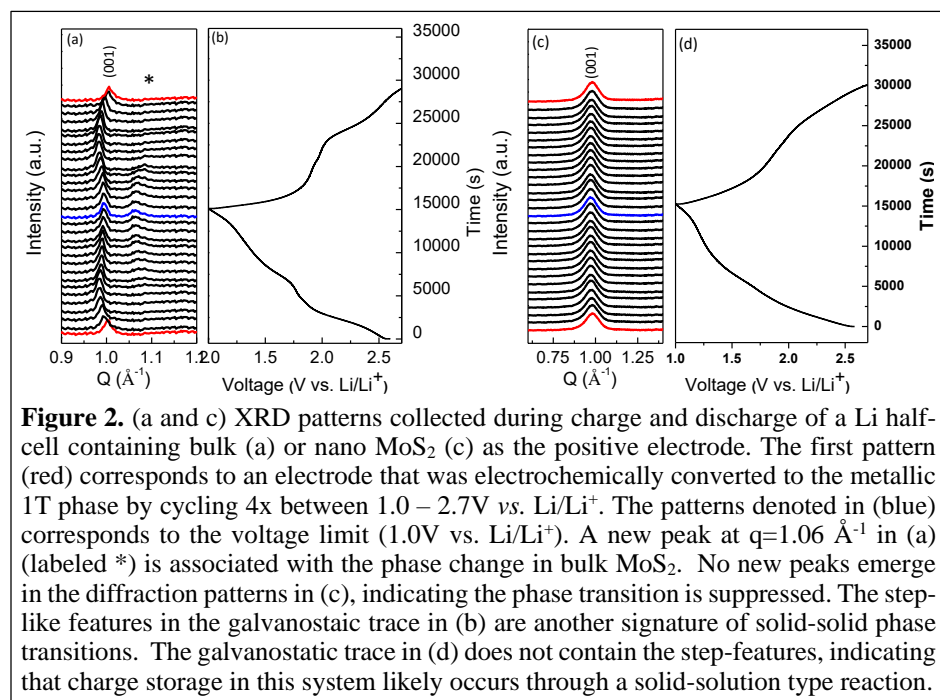ion seen in bulk micrometer size MoS2 particles are suppressed in this nanostructured form of MoS2 (Figure 2). In excellent agreement with our previous structural studies on TiS2 and MoO2, the suppression of phase transitions enables battery-like inter-calation reactions with capacitive type kinetics (intercalation pseudocapacitance).

We have also examined how the introduction of oxy-gen vacancies into

Figure 2. (a and c) XRD patterns collected during charge and discharge of a Li half-cell containing bulk (a) or nano MoS2 (c) as the positive electrode. The first pattern (red) corresponds to an electrode that was electrochemically converted to the metallic 1T phase by cycling 4x between 1.0 – 2.7V *vs.* Li/Li+. The patterns denoted in (blue) corresponds to the voltage limit (1.0V vs. Li/Li+). A new peak at q=1.06 Å^{-1} in (a) (labeled *) is associated with the phase change in bulk MoS2. No new peaks emerge in the diffraction patterns in (c), indicating the phase transition is suppressed. The step-like features in the galvanostaic trace in (b) are another signature of solid-solid phase transitions. The galvanostatic trace in (d) does not contain the step-features, indicating that charge storage in this system likely occurs through a solid-solution type reaction.

α-MoO$_3$ leads to improved electrochemical properties. The incorporation of oxygen vacancies leads to faster kinetics and greater reversibility of these energy storage reactions. Using ex-situ X-ray diffraction, we found that nanostructuring alone was not sufficient to suppress the charge induced phase transitions associated with MoO$_3$. However, we have found that phase transitions in MoO$_3$ can be suppressed through synthetic incorporation of oxygen vacancies. Therefore, we were able to compare the structural stability of two similarly nanostructured MoO$_3$ samples, which effectively allowed us to decouple the dominant effect leading to high levels of pseudocapacitance in this system: short ion diffusion lengths due to nanostructuring or phase transition suppression due to oxygen vacancies. Even though both materials had the same sized domains, the one that did not undergo a phase transformation was kinetically much faster, and showed much longer cycle lifetimes. It appears that, as our original hypothesis suggested, suppression of phase transformations is essential for fast intercalation pseudocapacitance. In addition, we have now demonstrated two methods to suppress Li intercalation induced phase transformations – nanostructuring and chemical modification.

In our work on pseudocapacitive cathode materials, we have developed methods to create both thin films and bulk powders of nanoporous LMO. The synthetic method begins with ligand free Mn$_3$O$_4$ nanocrystals which are assembled with amphiphilic diblock copolymers to produce nanoporous Mn$_3$O$_4$, either in thin film or powder form. These nanoporous materials are then converted to LMO through a solid state reaction with LiOH. The electrochemistry of the nanoporous films was examined directly after conversion, but size variation in the nanoporous powders was achieved by "flash" heating the samples for 1 minute at high temperature. Figure 3 shows SEM images of a typical thin film and of two nanoporous powders displaying 30 nm and 60 nm average crystallite sizes. The thin film samples showed kinetics indicative of intercalation pseudocapacitance, with significant capacity retention at very high C rates (figure 3). Powder samples built into traditional slurry electrodes showed somewhat slower kinetics, but samples with smaller domain sizes showed much better kinetics than samples with larger domains (figure 3). While the powder work is still in progress, the results clearly indicate that intercalation pseudocapacitance can be observed in cathode materials, and that these materials can be scaled to bulk slurry electrodes with at least partial retention of the favorable kinetics.
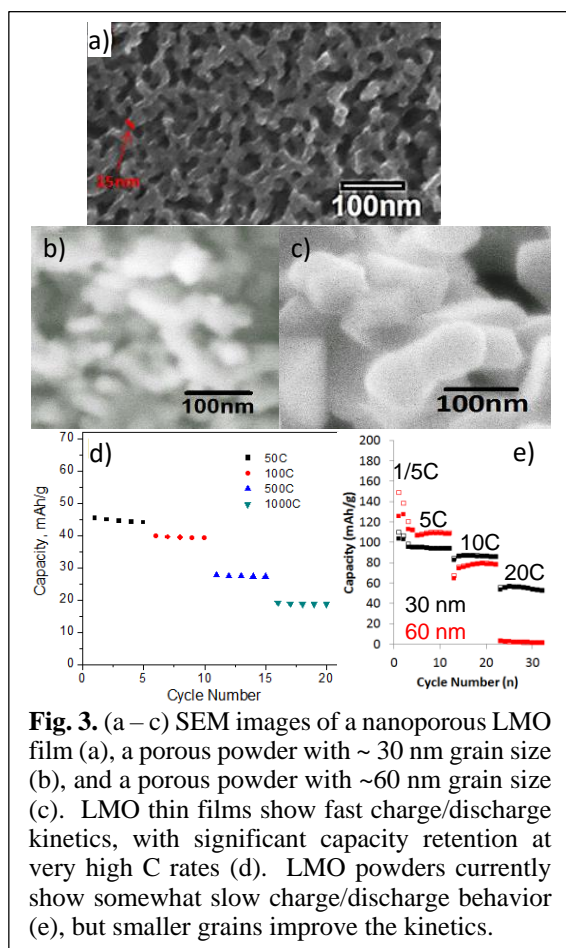

Fig. 3. (a – c) SEM images of a nanoporous LMO film (a), a porous powder with ~ 30 nm grain size (b), and a porous powder with ~60 nm grain size (c). LMO thin films show fast charge/discharge kinetics, with significant capacity retention at very high C rates (d). LMO powders currently show somewhat slow charge/discharge behavior (e), but smaller grains improve the kinetics.

For the NP-Sn work, we created porous materials with either nanowire or granular ligament morphologies using acetic acid and ammonium sulfate solutions, respectively, for dealloying. Figure 4a shows SEM micrographs of NP-Sn dealloyed in acetic acid to produce monolithic samples with an average ligament size of ~300 nm composed of randomly interconnected nanowires. In comparison, figure 4b shows SEM images of NP-Sn dealloyed in ammonium
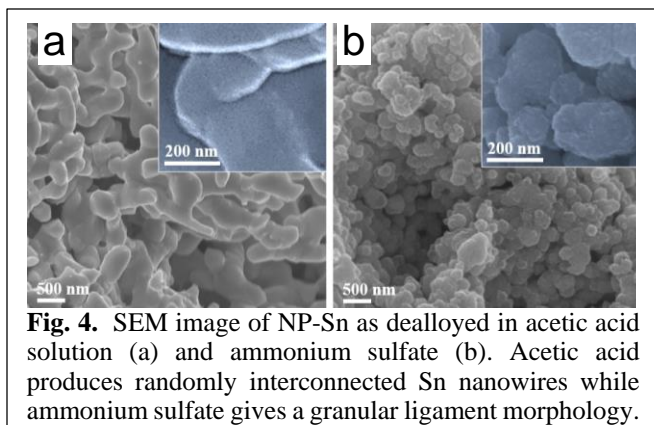
Fig. 4. SEM image of NP-Sn as dealloyed in acetic acid solution (a) and ammonium sulfate (b). Acetic acid produces randomly interconnected Sn nanowires while ammonium sulfate gives a granular ligament morphology.

sulfate. These samples are micrometer sized powders made up of porous grains (Fig. 2b). Further analysis shows that the nanoporous Sn pieces are made of clustered nanograins (inset Fig. 2b) and we refer to this as a granular ligament morphology. Interestingly, TEM (not shown) reveals that the ligaments are made of yet smaller nanograins, some of which are as small as 5 nm in diameter.

In long term galvanostatic cycling studies, both morphologies exhibit high capacities near 700 mAh/g, which is roughly twice that of graphitic carbon used in commercial Li-ion battery anodes. However, only the NP-Sn with granular ligament shows good stability, with a capacity retention of ~72% over 350 cycles at a current density of 250 mAh/g. This stability is unusual in Sn metal and is attributed to the multiscale granular morphology, which results in enhanced mechanical flexibility, and thus better accommodation of the lithiation-induced volume expansion.

To better understand this cycling stability, synchrotron-based Transmission X-Ray Microscopy (TXM) was used to monitor the volume change in NP-Sn with the granular ligament morphology during electrochemical cycling (Fig. 5). Bulk tin, which is used as a control, fails after ten cycles and expands by 120% during lithiation, mostly in the last

Figure 6. Dense tin (top) undergoes a large areal expansion, which leads to strain in the material followed by crack propagation. The NP-Sn with a granular morphology (bottom) expands less than dense tin.

stages of lithium intercalation. In contrast, granular NP-Sn only expanded by 20 percent, and does so much more gradually over the voltage range. In addition, granular NP-Sn has pores that remain open at the fully lithiated stage, allowing the electrolyte to fully access the active material.
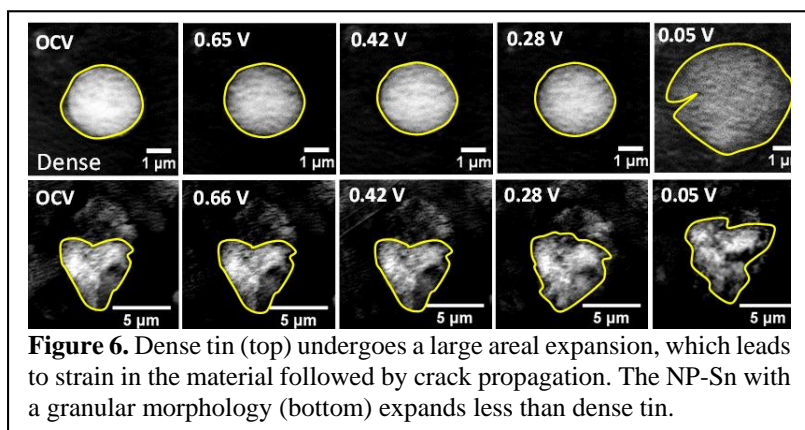
Future Plans

For fundamental studies of intercalation pseudocapacitance, we plan to focus on a range of oxide and sulfide materials cycled with Na and Mg ions. Na is much bigger in size and Mg typically shows stronger electrostatic interaction with the host. Na and Mg ion batteries are new emerging rechargeable battery systems and have gained tremendous attention due to their earth abundance and low cost. Unlike Li, Na usually intercalates by staging, meaning it first intercalates every other layer of the host material, then later fills the remaining layers. We plan to explore how differences in intercalation mechanism effect phase change suppression. Work on cathode materials will focus on improving performance in nanoporous LMO powders using control of pores size and crystallite faceting. We will also begin to examine nanostructured versions of other cathode materials.

Work on NP-Sn will use TXM to further understanding the interplay between pore geometry and cycling stability. Na ions will also be examined in combination with various pore geometries.

Publications

This grant has only been running for 9 months. A list of publications published or submitted during the past 9 months supported by BES is included below.

J.B. Cook, H.-S. Kim, Y. Yan, J.S. Ko, S. Robbennolt, B. Dunn, S.H. Tolbert, "Mesoporous MoS_2 as a Transition Metal Dichalcogenide Exhibiting Pseudocapacitive Li and Na-Ion Charge Storage." *Adv. Energy Mater.* **6**, 1501937 (2016). Doi: 10.1002/aenm.201501937.

E. Detsi**,** J.B. Cook**,** B.K. Lesel**,** C.L. Turner**,** Y.-L. Liang**,** S. Robbennolt, S.H. Tolbert "Mesoporous $Ni_{60}Fe_{30}Mn_{10}$-Alloy Based Metal/Metal Oxide Composite Thick Films As Highly Active and Robust Oxygen Evolution Catalysts." *Energy Environ. Sci.* **9,** 540-549 (2016). Doi: 10.1039/C5EE02509E.

B.K. Lesel, J. Ko, B. Dunn, S.H. Tolbert, "Mesoporous $Li_xMn_2O_4$ Thin Film Cathodes for Lithium Ion Pseudocapacitors." Submitted (2016).

J.B. Cook, E. Detsi, Y. Liu, Y.-L. Liang, H.-S. Kim, X. Petrissans, B. Dunn, S.H. Tolbert, "Nanoporous Tin With A Granular Hierarchical Ligament Morphology As A Highly Stable Li-Ion Battery Anode." Submitted (2016).

H.-S. Kim, J.B. Cook, H. Lin, S.H. Tolbert, V. Ozolins, B. Dunn, "Oxygen Vacancies Enhance Pseudocapacitive Charge Storage Properties of MoO_{x-3}." Submitted (2016).

J.B. Cook, H.-S. Kim, T.C. Lin, M. Lai, B. Dunn, S.H. Tolbert, "Pseudocapacitive Charge Storage in Thick Composite MoS_2 Nanocrystal Based Electrodes." Submitted (2016).

S.H. Tolbert, B. Dunn, J.B. Cook, H.-S. Kim, "Metal Chalcogenides for Pseudo capacitive Applications." US Provisional Patent Applications 62/259144. Submitted 11/24/2015.

S.H. Tolbert, E. Detsi, J.B. Cook, "Nanoporous Tin Powder for Energy Applications." US Provisional Patent Applications 62/242241. Submitted 10/15/2015.

Mesoscale Photophysical Properties of Anisotropic Hybrid Nanostructure Assemblies

Vladimir V. Tsukruk

Dean's Professor of Engineering, School of Materials Science and Engineering

Georgia Institute of Technology,

771 Ferst Dr., NW. Atlanta, GA 30332

Ph.: 404-894-6081; fax: 404-894-9140

vladimir@mse.gatech.edu ; http://polysurf.mse.gatech.edu/

Mostafa El-Sayed

Julius Brown Chair and Regents Professor

School of Chemistry and Biochemistry, Georgia Institute of Technology

770 State Street, Atlanta, GA 30332

phone: 404-894-0292, fax: 404-894-0294

http://www.chemistry.gatech.edu/faculty/elsayed/el-sayed.html

Program Scope

In this project, we focus on understanding the principles of non-covalent assembling of tunable functional hybrid (organic-inorganic) materials with various selected nanocrystals in order to control light-matter interactions by changing localized interfacial refractive properties, coupling parameters, or the ionic environment of surrounding media. We explore novel soft functional matrices with controlled physical (refractive indices) properties via the application of light (photochromic materials), mechanical stresses (elastomers), ionic environment (ionic liquids), and electrical potential (electrochromic polymers). These tunable functional matrices are used in conjunction with novel anisotropic inorganic nanostructures such as noble metal/metal alloy anisotropic nanostructures with complex optical properties (multiple LSPR modes) and quantum dots with light-emissive or absorbing properties in a broad spectral range from the UV to the NIR.

Recent Progress

Electrically Controlled Plasmonic Behavior of Gold Nanocube@Polyaniline Nanostructures: We demonstrate the electrically controllable plasmonic signature of hybrid core-shell polymer-metal nanostructures consisting of gold nanocubes (AuNCs) coated with electrochromic polyaniline (PANI) shells with precisely controlled shell thicknesses (Figure 1). A reversible tuning of the localized surface plasmon resonance (LSPR) peak of the AuNC core was obtained by applying an electrical potential that caused a reversible oxidation state change in the electroactive PANI nanoshell. A significant shift of the main LSPR peak was achieved (24

nm LSPR shift with 37 nm PANI shell). Furthermore, the PANI shell also acts as a spacer layer that prevents undesirable coupling between adjacent nanoparticles. Therefore, the unique properties of these core-shell structures facilitate the preservation of the original individual nanostructure signature and the suppression of strong plasmonic extinction in the near-infrared region of aggregated metal nanostructures.

Hybrid Electrochromic Materials with Large Electrical Modulation of Plasmonic Resonances: We present a rational approach to fabricating plasmonically active hybrid polymer−metal nanomaterials with tunable

Figure 1. a) Schematic diagram of electrically tunable AuNC@PANI core/shell nanostructures. b) The TEM image and c) UV-vis spectra of AuNC@PANI core/shell nanostructures.
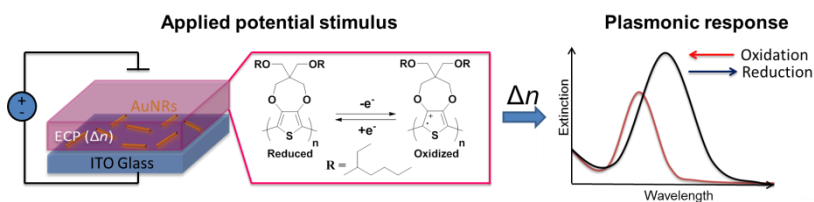
localized surface plasmon resonances (LSPRs) of noble metal nanostructures embedded in an electroactive polymer matrix. To maximize LSPR modulation, gold nanorods with a controlled aspect ratio, synthesized to provide high refractive index sensitivity, were combined with a solution-processable electroactive and electrochromic polymer (ECP): alkoxy-substituted poly(3,4-propylenedioxythiophene) (Figure 2). We fabricated ultrathin plasmonic electrochromic hybrid films consisting of gold nanorods and ECP that exhibited LSPR modulation of up to 25−30 nm with an applied electrical potential.

Figure 2. Schematic diagram for electrooptical plasmon modulation with hybrid gold nanorod/ECP nanomaterials.

Super-Radiant Plasmon Mode is More Efficient for SERS than the Sub-Radiant Mode in Highly Packed 2D Gold Nanocube Arrays: Plasmonic field coupling in highly packed plasmonic nanoparticle arrays is not localized due to the energy transport via the sub-radiant plasmon modes, which is formed in addition to the regular super-radiant plasmonic mode. Unlike the sub-radiant mode, the plasmon field of the super-radiant mode cannot extend over long distances since it decays radiatively with a shorter lifetime. The coupling of the plasmon fields of gold nanocubes (AuNCs) when organized into highly packed 2D arrays (Figure 3a) was examined experimentally by
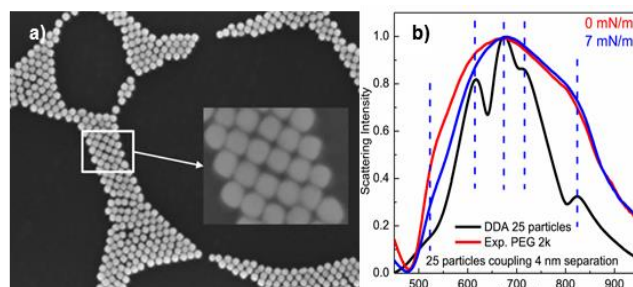

Figure 3. a) SEM image of an assembly of AuNCs functionalized with 6k molecular weight PEG. b) Experimental and DDA-calculated scattering spectra for arrays of AuNCs.

functionalizing AuNCs with polyethylene glycol (PEG). Multiple plasmon resonance optical peaks are observed for the AuNC arrays and are compared to those calculated using the discrete dipole approximation (Figure 3b). The Raman signal enhancement by the super-radiant plasmon mode was ultimately found to be one hundred fold greater than that of the sub-radiant plasmon mode.

Concurrent Reduction of Metal Ions by Multiple Reducing Agents Initiates the Asymmetric Growth of Metallic Nanoscrystals: The simultaneous multiple asymmetric reduction technique (SMART) was introduced to successfully prepare silver nanodisks (AgNDs) of controllable sizes within a few seconds. Silver ions are reduced and form nanodisks by two reducing agents of different strengths, rather than using the traditional kinetic controlled methods of slowing down the rate of the growth of the nanocrystal (Figure 4a). The SMART succeeded in the synthesis of silver nanodisks of different diameters that can be easily tuned in size from 26 to 47 nm but having similar thicknesses. An increase in the diameter of the AgNDs from 26 to 47 nm was accompanied by a red-shift in the plasmon spectrum of AgNDs of 158 nm (from 503 to 661 nm, Figure 4b).
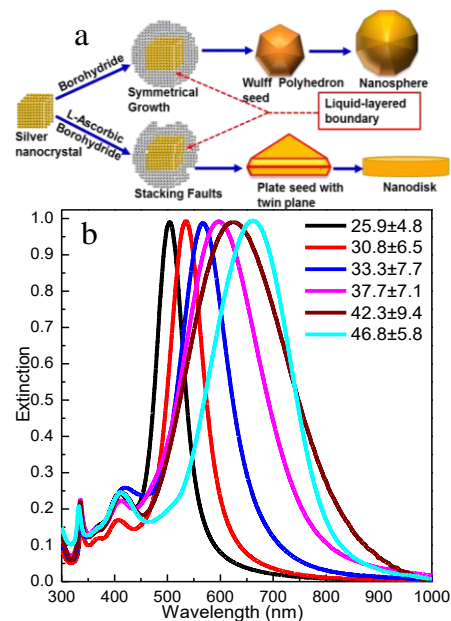
Figure 4. a) Schematic diagram of synthesis of AgNDs by SMART. b) Extinction spectrum of AgNDs with different diameters.

Polarized Optomechanical Response of Silver Nanodisc Monolayers on an Elastic Substrate Induced by Stretching: A monolayer assembly of silver nanodisks (AgNDs) was fabricated on the surface of a polydimethylsiloxane (PDMS) polymer substrate using the Langmuir–Blodgett technique.

Upon stretching the PDMS substrate, the localized surface plasmon resonance (LSPR) spectrum of the AgND monolayer is blue-shifted when the incident light excitation is polarized parallel to the stretching direction (Figure 5). Conversely, a red shift in the LSPR spectrum of the AgND monolayer is observed in the case of light polarization orthogonal to the stretching direction. The magnitude of the shift in the LSPR spectrum is proportional to the degree of stretching of the PDMS substrate. The different optical responses of the AgND assembly on the surface of stretched PDMS when excited with different polarization directions is due to the change in the strength of the plasmon field coupling, which is inversely proportional to the separation gap between the AgNDs.
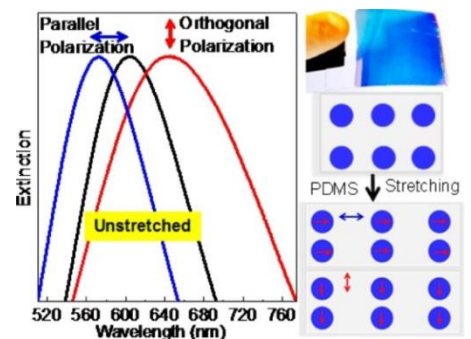

Figure 5. The extinction spectra of AgND monolayer deposited onto a flexible PDMS substrate. Upon stretching the substrate, the LSPR displays either a blue shift or redshift depending on the excitation polarization.

Future Plans

- Direct synthesis of electrically tunable core/shell nanostructures consisting of various electrochromic polymers and gold nanostructures
- Fabrication of responsive fluorescent nanostructures that react to stimuli such as a change in light polarization, temperature, or mechanical stress
- Preparation of vertically or horizontally aligned anisotropic nanoparticles on substrates by chemical growth of deposited nanoparticle monolayers
- Fabrication of plasmonic nanoparticle monolayers with different surface coverages deposited in a gradient manner on a substrate to for modulators and optical rulers

Recent Publications

(1) Jeon, J. W.; Ledin, P. A.; Geldmeier, J. A.; Ponder, J. F.; Mahmoud, M. A.; El-Sayed, M.; Reynolds, J. R.; Tsukruk, V. V., Electrically Controlled Plasmonic Behavior of Gold Nanocube@Polyaniline Nanostructures: Transparent Plasmonic Aggregates. *Chem. Mater.* **2016,** *28*, 2868-2881.

(2) Ledin, P. A.; Jeon, J. W.; Geldmeier, J. A.; Ponder, J. F.; Mahmoud, M. A.; El-Sayed, M.; Reynolds, J. R.; Tsukruk, V. V., Design of Hybrid Electrochromic Materials with Large Electrical Modulation of Plasmonic Resonances. *ACS Appl. Mater. Interfaces* **2016**, *8*, 13064−13075.

(3) R. Geryak, J. Geldmeier, K. Wallace, V. V. Tsukruk, Remote Giant Multispectral Plasmonic Shifts of Labile Hinged Nanorod Array via Magnetic Field, *Nano Lett.,* **2015**, *15*, 2679-2684.

(4) Ledin, P. A.; Russell, M.; Geldmeier, J. A.; Tkachenko, I. M.; Mahmoud, M. A.; Shevchenko, V.; El-Sayed, M.; Tsukruk, V. V., Light-Responsive Plasmonic Arrays Consisting of Silver Nanocubes and a Photoisomerizable Matrix. *ACS Appl. Mater. Interfaces* **2015**, *7*, 4902-4912.

(5) Konig, T. A. F.; Ledin, P. A.; Russell, M.; Geldmeier, G. A.; Mahmoud, M. A.; El-Sayed, M.; Tsukruk, V. V., Silver Nanocube Aggregation Gradient Materials in Search for Total Internal Reflection with High Phase Sensitivity. *Nanoscale*, **2015**, *7*, 5230-5239.

(6) Mahmoud, M. A., Polarized Optomechanical Response of Silver Nanodisc Monolayers on an Elastic Substrate Induced by Stretching. *J. Phys. Chem.* C **2015**, *119*, 19359-19366.

(7) Mahmoud, M. A., Simultaneous Reduction of Metal Ions by Multiple Reducing Agents Initiates the Asymmetric Growth of Metallic Nanocrystals. *Cryst. Growth Des.* **2015**, *15*, 4279–4286.

(8) Mahmoud, M. A., Super-Radiant Plasmon Mode is More Efficient for SERS than the Sub-radiant Mode in Highly Packed 2D Gold Nanocube Arrays. *J. Chem. Phys.* **2015**, *143*, 074703-074711.

(9) Hanske, C.; Tebbe, M.; Kuttner, C.; Bieber, V.; Tsukruk, V. V.; Chanana. M.; Konig, T. A. F.; Fery, A., Strongly Coupled Plasmonic Modes on Macroscopic Areas via Template-Assisted Colloidal Self-Assembly. *Nano Lett*. **2014**, *14*, 6863-6871.

(10) Geldmeier, J. A.; Konig, T. A. F.; Mahmoud, M. A.; El-Sayed, M.; Tsukruk, V. V., Tailoring the Plasmonic Modes of a Grating Nanocube Assembly to Achieve Broadband Absorption in the Visible Spectrum, *Adv. Funct. Mater.* **2014**, *24*, 6797-6805.

Functionalization of π-Extended Porphyrins and Their Applications in Dye-Sensitized Solar Cells

Hong Wang, Associate Professor, Department of Chemistry, Miami University

Lei Kerr, Professor, Department of Chemical and Paper Engineering, Miami University

Program Scope

Although known for decades, π-extended porphyrins remain largely unexplored due to synthetic limitations.[1-3] Functionalization of π-extended porphyrins had been very challenging. In order to open up π-extended porphyrins for much broader exploration, the Wang group has been engaged in developing new synthetic methodologies for π-extended porphyrins. We have developed a number of concise and versatile synthetic methods in the past several years.[4-6] The availability of these methods makes it possible to systematically design and synthesize a number of functionalized π-extended porphyrin systems.

The purpose of this project is threefold. First, new synthetic methods will be developed to further extend the porphyrin π-system. Second, β–functionalized push-pull π-extended porphyrins will be designed and synthesized using these methods. Third, push-pull π-extended porphyrins will be developed and evaluated as sensitizers for dye-sensitized solar cells (DSSCs).

Recent Progress

We have prepared a number of π-extended porphyrin systems in the past two years, including pentaquinone- and pentacene-fused diporphyrins, linear push-pull π-extended porphyrins, unsymmetrical push-pull π-extended porphyrins, and A2B2 push-pull π-extended porphyrins. Our study has shown that the introduction of different types of substituents to the porphyrin periphery makes a remarkable difference in the electrochemical and electronic properties of these porphyrins. In particular**,** unprecedented fluorescence properties were found for nitro-containing benzoporphyrins and pyridyl-bearing dibenzoporphyrins. A series of monobenzoporphyrins bearing different conjugated spacer groups, were designed and synthesized as sensitizers for dye-sensitized solar cells. These monobenzoporphyrins displayed significant linker group effect, demonstrating the exceptional tunability of monobenzoporphyrins. Dye-sensitized solar cells based on these monobenzoporphyrin dyes displayed a remarkable difference in power conversion efficiency (PCE). A monobenzoporphyrin bearing vinyl spacers achieved PCE of 5.2%, which is close to the PCE of the reference ruthenium N3 dye (6.9%) obtained under similar conditions.

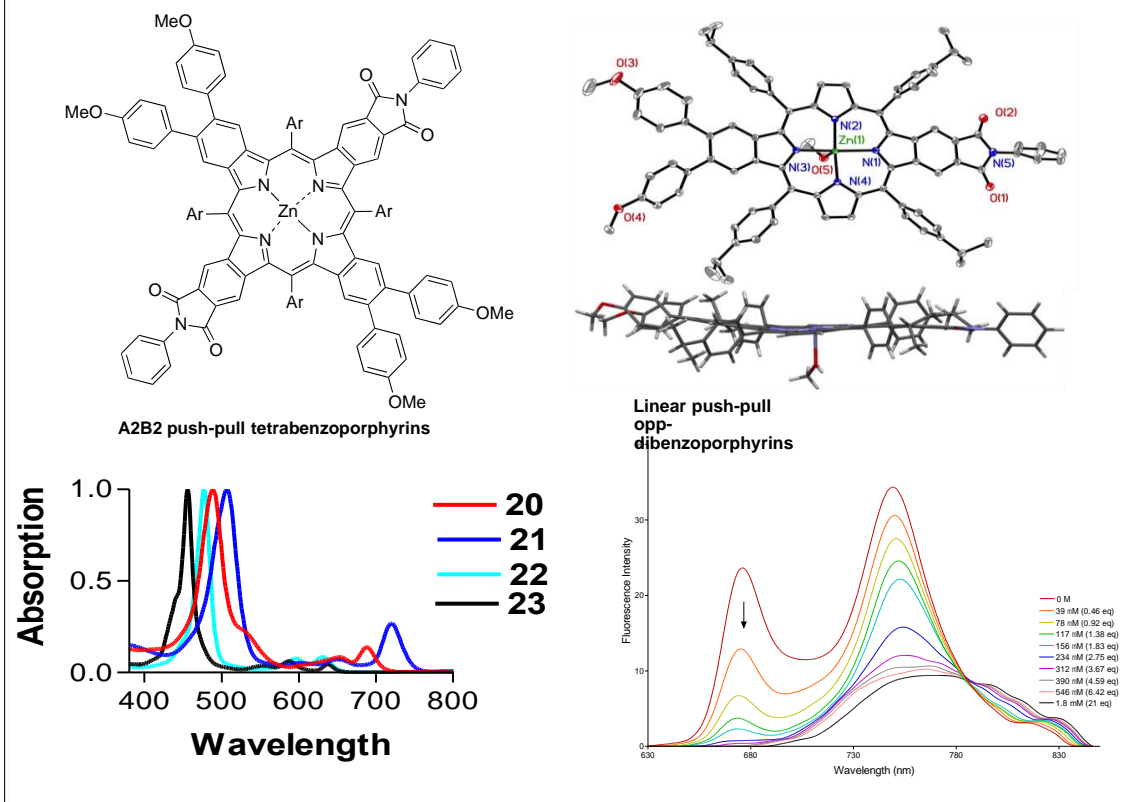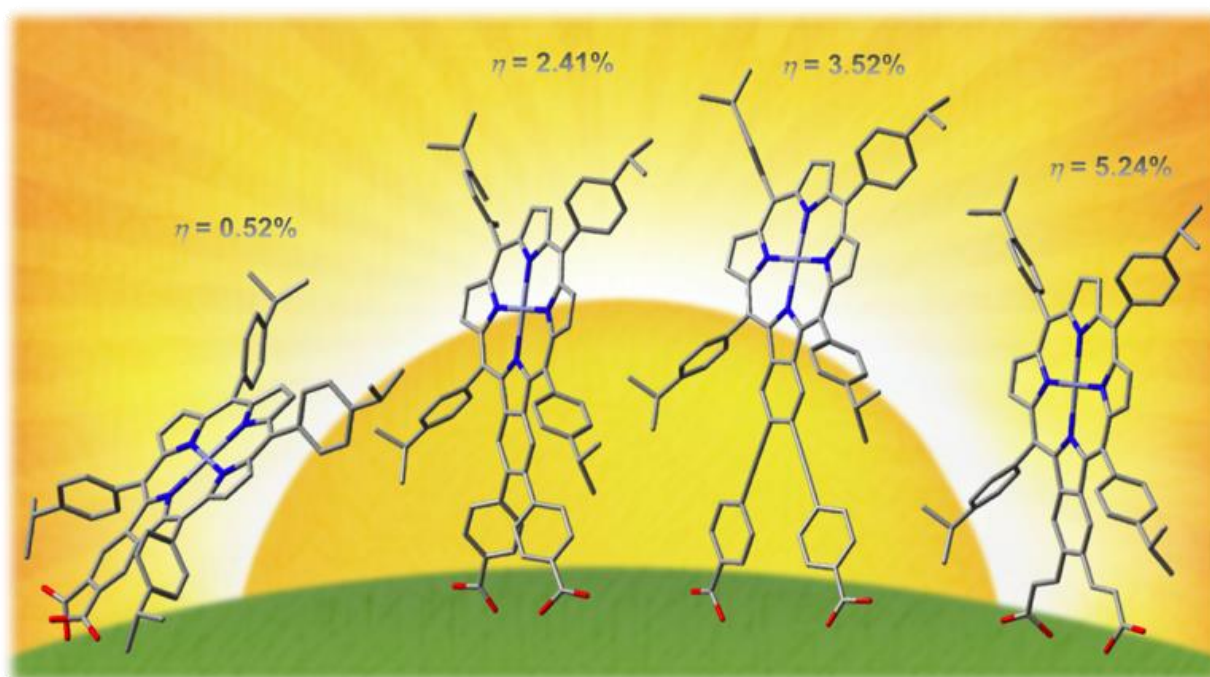Figure 1. Selected Examples of Push-Pull Pi-Extended Porphyrins

A2B2 push-pull tetrabenzoporphyrins

Linear push-pull opp-dibenzoporphyrins

Figure 2. Benzoporphyrins Bearing Different Conjugated Linker Groups as Sensitizers for Dye-Sensitized Solar Cells

$\eta = 0.52\%$

$\eta = 2.41\%$

$\eta = 3.52\%$

$\eta = 5.24\%$

Future Plans

1. We will continue working on methodology development to further extend the π-conjugation of porphyrin systems, including naphthalenoporphyrins, tetracenoporphyrins and pentacenoporphyrins.
2. We will design and synthesize new π-extended porphyrin systems with push-pull features. We will study the electronic properties of these compounds using UV-Vis spectroscopy, time-resolved and steady state fluorescence spectroscopy, cyclic voltammetry and DFT calculations.
3. We will design and synthesize new push-pull π-extended porphyrins as sensitizers for dye-sensitized solar cells. The performance of these porphyrins in dye-sensitized solar cells will be evaluated.

References

1. V. Cheprakov, M. A. Filatov, *J. Porphyrin Phthalocyanines* 2009, **13**, 291-303.
2. S. Banala, T. Ruhl, K. Wurst, B. Krautler, *Angew. Chem. Int. Ed.* 2009, **48**, 599-603.
3. S. Banala, R. G. Huber, T. Muller, M. Fechtel, K. R. Liedl, B. Krautler, *Chem. Commun.* 2012, **48**, 4359-4361.
4. R. Deshpande, L. Jiang, G. Schmidt, J. Rakovan, X. P. Wang, K. Wheeler, H. Wang, *Org. lett* 2009, **11**, 4251-4253
5. L. Jiang, R. A. Zaenglein, J. T. Engle, C. Mittal, C. S. Hartley, C. J. Ziegler, H. Wang, *Chem. Commun.* 2012, **48**, 6927-6929
6. L. Jiang, J. T. Engle, L. Sirk, C. S. Hartley, C. J. Ziegler, H. Wang, *Org. Lett*., 2011, **13**, 3020-3023.

Publications

1. Jiang, L.; Engle, J. T.; Zaenglein, R. A.; Matus, A.; Ziegler, C. J.; Wang, H.; Stillman, M. J., Pentacene-fused diporphyrins. *Chem. Eur. J.* **2014,** *20* (43), 13865-70. *Selected as **a hot paper** by the editors.*
2. R. G. W. Jinadasa, Y-Y Fang, S. Kumar, A. J. Osinski, X-Q Jiang, C. J. Ziegler, K. M. Kadish, H. Wang, "☐-Functionalized Push-Pull *Opp*-Dibenzoporphyrins", *J. Org. Chem,* **2015**, *80* (24), 12076–12087.
3. R. G. W. Jinadasa, Y-Y Fang, Y. Deng, R. Deshpande, X-Q Jiang, K. M. Kadish, H Wang, "Unsymmetrically functionalized benzoporphyrins", *RSC Adv.*, **2015**, 5, 51489-51492.
4. Raja Gabadage Jinadasa, Siddhartha Kumar, Hong Wang,* "*Push-Pull* Porphyrins: Synthesis, Properties and Applications", invited book chapter for Porphyrin Handbooks, 2016, in press.
5. B. Schmitz, B. Li, R. G. W Jinadasa, S. B. Lalvani, L. Kerr and H. Wang,* "Benzoporphyrins Bearing Pyridine or Pyridine-N-Oxide Anchoring Groups as

Sensitizers for Dye-Sensitized Solar Cell", invited manuscript, J. Porphyrins Phthalocyanines, invited manuscript, published on line.

6. R. G. Waruna Jinadasa, Bihong Li, Siddhartha Kumar, Benjamin Schmitz, Lei L. Kerr and Hong Wang. β-Functionalized benzoporphyrins as sensitizers for dye-sensitized solar cells. Submitted to ChemSusChem, under revision.

7. C. Frigerio, J. P. G. Santos, P. Quaresma, S. L. H. Rebelo, A. Gomes, P. Eaton, E. Pereira, P. A. Carvalho, J. A. Shelnutt, L. Jiang, H. Wang, and Craig J. Medforth, "Binary and Ternary Nanomaterials from Self-Assembly of an Octacationic Porphyrin with the Anionic Porphyrin TPPS", submitted to Chemistry of Materials.

Charge carrier dynamics in hybrid organic-inorganic semiconductors

Xiaoyang Zhu, Department of Chemistry, Columbia University

Program Scope

Recent discoveries of highly efficient solar cells based on hybrid organic-inorganic lead halide perovskites (HOIPs) have led to a surge in research activity on this class of hybrid organic-inorganic semiconductor materials. The high efficiency of solar cells has been attributed to the exceptionally long electron/hole diffusion lengths, a result of the low charge carrier trapping densities and, thus, low recombination rates. These properties also make lead halide perovskites an excellent material system for lasing. This project aims to initiate a fundamental research program at understanding intrinsic physical properties of lead halide perovskites in single crystal forms. This project focuses on charge carrier and exciton dynamics in (macro, micro, and nano) crystals of lead halide perovskites. The specific aims are: (1) To optimize the growth of high quality lead halide perovskite single crystals; to establish the valence band structure using angle-resolved photoemission spectroscopy, photophysical properties using absorption and photoluminescence spectroscopies, and carrier transport properties using time-resolved absorption and second harmonic generation microscopy; (2) To directly determine the electron relaxation and localization dynamics in the conduction band using time-resolved two-photon photoemission spectroscopy (TR-2PPE); to unambiguously establish the free carrier or excitonic nature of the initial optical excitation in perovskite single crystals based on the time-dependent parallel dispersions; To quantify surface charge carrier recombination rates using single crystal nanorod laser as sensitive probes; to quantify charge carrier trap densities on perovskite single crystal surfaces using laser-ARPES & TR-2PPE; to explore chemical strategies for the reduction of surface traps. The mechanistic studies on perovskite single crystals serve to establish fundamental limits on charge carrier generation, transport, surface/interface trapping, and recombination. This level of understanding will guide the imminent applications of lead halide perovskites and the development of design principles for new hybrid organic-inorganic semiconductors.

Recent Progress

The PI has made major progress on two fronts: the first is the discovery of the protected nature of charge carriers in HOIPs and the second on the successful demonstration of most efficient lasing from HOIPs nanowires.

The remarkable discoveries of highly efficient solar cells from hybrid organic-inorganic lead halide perovskites (HOIPs) have led to feverish research activities with no slow-down in sight. In this discussion, I will focus on unique physical properties of HOIPs that give rise to their exceptional carrier physics and optoelectronic performance. HOIPs, easily formed from solutions at room temperature, should contain a high density of structural defects. Surprisingly, photophysical and transport measurements reveal the behavior only expected for intrinsic and defect-free semiconductors. These properties include: (1) Inverse temperature dependence of

charge carrier mobility (μ) with a power law ($\mu \propto T^{-3/2}$) predicted for coherent transport, slowed down only by acoustic phonon scattering; (2) long carrier diffusion length ($\geq$ μm) and carrier lifetime ($\geq$ μs) that are unprecedented for a semiconductor with modest charge carrier mobility (μ ~ 1-100 cm^{2}V^{-1}s^{-1}); (3) low electron-hole recombination rate constant (10^{-10} cm^{3}s^{-1}) that rivals those of the purest direct bandgap semiconductors (e.g., GaAs). These observations suggest that charge carriers in HOIPs are protected from efficient scattering with charged defects or with each other.

Recent experiments in the PI's lab have revealed the carrier protection mechanism. In methylammonia lead iodide perovskite thin films, we discovered energetic electrons with excess energy $\langle E^* \rangle$ ~ 0.25 eV above the conduction band minimum, with concurrent hot fluorescence emission, and with pseudo electronic temperatures as high as 1900 K. The lifetime of energetic electrons is ~100 ps, which is $\geq 10^3$ time longer than those in conventional semiconductors. These results are confirmed in a comparative study of three single-crystal lead bromide perovskites: CH₃NH₃PbBr₃, CH(NH₂)₂PbBr₃, and CsPbBr₃. We observe hot fluorescence emission from energetic carriers with ~10^2 ps lifetimes in CH₃NH₃PbBr₃ or CH(NH₂)₂PbBr₃, but not in CsPbBr₃. The hot fluorescence is correlated with liquid-like molecular reorientational motions, suggesting that organic cations protect energetic carriers via solvation or large polaron formation on time scales competitive with ultrafast cooling. The long-lived energetic carriers may enable hot-carrier solar cells with efficiency exceeding the Shockley-Queisser limit.

All these exceptional properties may be explained by a large dipolar polaron model which comes from the established polaron physics since Landau but also borrows from well-known concepts of solvation in chemistry. Here we must distinguish a large polaron from a small polaron. The former is characterized by a size larger than unit cell dimension and originates mainly from the long-range Coulomb potential between an excess charge carrier and the ionic lattice. The latter features a size smaller than unit cell dimension and its formation is dominated by the short-range deformation potential. The size difference leads to drastically different transport properties. A large polaron moves coherently and its mobility depends inversely on temperature, while a small polaron moves via incoherent hopping from one localized site to another and is thermally activated. The formation of large polarons can occur on ultrafast time scales due to the reorientational motion (10^2 fs) of the organic cations and on slower time scales (> 1 ps) due to displacement motions

Fig. 1. Crystal structure of methylammonium (green) lead (grey) halide (purple) perovskite.

of the PbX₃⁻ network. The large polaron may provide the essential protection mechanisms to shield charge carriers from each other and from charged defects, giving rise to the exceptional photophysical and transport properties.
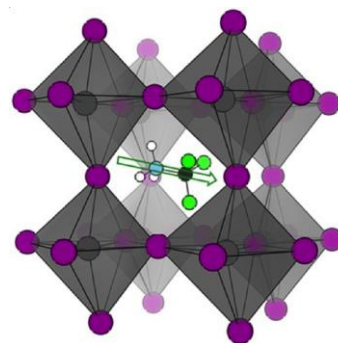
The second part of the PI's research program has been carried out in collaboration with Song Jin of the University of Wisconsin – Madison. The remarkable performance of lead halide perovskites in solar cells can be attributed to the long carrier lifetimes and low non-radiative recombination rates, the same physical properties that are ideal for semiconductor lasers. Here we show room temperature and wavelength tunable lasing from single crystal lead halide perovskite nanowires with very low lasing thresholds (220 nJ/cm2) and high quality factors (Q ~

3600). The lasing threshold corresponds to a charge carrier density as low as 1.5×10^{16} cm^{-3}. Kinetic analysis based on time-resolved fluorescence reveals little charge carrier trapping in these single crystal nanowires and gives estimated lasing quantum yields approaching 100%. Such lasing performance, coupled with the facile solution growth of single crystal nanowires and the broad stoichiometry-dependent tunability of emission color, makes lead halide perovskites ideal materials for the development of nano-photonics, in parallel with the rapid development in photovoltaics from the same materials. Most recently, we have extended the demonstration of most efficiency lasing to formamidinium lead halide perovskites and cesium lead halide perovskites with not only much improved stability and broad color tunability.

Future Plans

During the next funding period, the PI will focus on the nature of charge carrier protection in HOIP single crystals. Specifically, the PI will apply time-resolved optical Kerr effect spectroscopy to probe the liquid-like motions and dynamic disorder in HOIPs and to follow large polaron formation in the time domain. The PI will quantify large polaron formation dynamics using femtosecond spectroscopies and isotope effects. All these are aimed at developing a robust design principle for new semiconductor materials: introducing dynamic disorder and screening to make a defective semiconductor behave as a perfect one.

Publications

Haiming Zhu, Yongping Fu, Fei Meng, Xiaoxi Wu, Zizhou Gong, Qi Ding, Martin V. Gustafsson, M. Tuan Trinh, Song Jin, X.-Y. Zhu, "Lead halide perovskite nanowire lasers with low lasing thresholds and high quality factors," *Nature Mater.* **2015**, *14*, 636-642.

X. Wu, M. T. Trinh, D. Niesner, H. Zhu, Z. Norman, J. S. Owen, O. Yaffe, B. J. Kudisch, X.-Y. Zhu, "Trap States in Lead Iodide Perovskites," *J. Am. Chem. Soc.* **2015**, *137*, 2089–2096.

X.-Y. Zhu, V. Podzorov, "Charge carriers in hybrid organic-inorganic lead halide perovskites might be protected as large polarons," *J. Phys. Chem. Lett.* **2015**, *6*, 4758-4761.

Yongping Fu, Haiming Zhu, Alex Schrader, Dong Liang, Qi Ding, Leekyoung Hwang, X-Y. Zhu, Song Jin, "Nanowire lasers of formamidinium lead halide perovskites and their stabilized alloy s with improved stability," *Nano Lett.* **2016**, *16*, 1000-1008.

X.-Y. Zhu, "The perovskite fever and beyond," *Acct. Chem. Res.* **2016***, 49*, 355-356.

Daniel Niesner, Haiming Zhu, Kiyoshi Miyata, Prakriti Joshi, Tyler J. Evans, B. J. Kudisch, M. Tuan Trinh, M. Marks, X.-Y. Zhu, "Protected energetic electrons in hybrid organic-inorganic lead halide perovskite," *Nature Mater.* under review.

Yongping Fu, Haiming Zhu, Constantinos C. Stoumpos, Qi Ding, Jue Wang, Mercouri G. Kanatzidis, X-Y. Zhu, Song Jin, "Broad Wavelength Tunable Robust Lasing from Single-Crystal

Cesium Lead Halide Perovskites (CsPbX$_3$, X=Cl, Br, I) Nanowires," *J. Am. Chem. Soc.* under review.

Haiming Zhu, Kiyoshi Miyata, Yongping Fu, Jue Wang, Prakriti P. Joshi, Song Jin, X.-Y. Zhu, "Dipole Motion in a Crystalline Liquid Protects Energetic Carriers in Hybrid Perovskites," *Science,* under review.

H. T. Yi, X. Wu, X.-Y. Zhu, V. Podzorov, "Intrinsic charge transport across phase transitions in hybrid organo-inorganic perovskites," *Adv. Mater.* **2016**, *28*, in press.

**A Synthetic Strategy to Prepare New Complex Uranium- and Thorium-Containing Oxides:
Predictive Solid State Synthesis of New Composition using Radius Ratio Rules and
Materials Discovery based on Crystal Growth from High Temperature Solutions**

Hans-Conrad zur Loye
Department of Chemistry and Biochemistry
University of South Carolina

Program Scope

Our research continues to focus on expanding the boundaries of uranium(IV) and uranium(VI) oxide chemistry via two approaches: 1) the synthetic targeting of functional building blocks to create new uranium containing oxides, oxyhalides and fluorides and 2) a materials discovery approach based on single crystal growth from mild hydrothermal and from high temperature solutions to target new U(VI), U(IV) and the relatively uninvestigated U(III), containing materials. The integration of prediction and new synthetic approaches, in our opinion, is most likely to result in the discovery of new uranium containing compositions exhibiting complex structures and, potentially, new or enhanced properties. Moreover, the ability to prepare these new materials as high quality single crystals is extremely desirable for structure determination and physical property characterization.

Recent Progress

U(VI) containing silicates and salt-inclusion uranyl silicates

We have continued our work on the crystal growth of uranium containing silicates using mixed alkali halide fluxes. In particular, we have developed an enhanced flux growth technique for the growth of salt-inclusion uranyl silicates. Namely, by reducing the surface area to volume ratio of the reaction and using metal halide, as opposed to oxide, reaction precursors, we are able to target the synthesis of salt-inclusion phases. These phases contain a covalent uranyl silicate framework that contains voids occupied by ionic alkali halide lattices.

$K_4CaUSi_4O_{14}$

One example of one new silicate is $K_4CaUSi_4O_{14}$, which was grown from a KF-CaF_2 eutectic flux. This compound was found to crystallize in a new structure type related to the mineral Fresnoite, $Ba_2TiSi_2O_8$. This structure crystallizes with a 49-fold supercell and a subcell that can be solved in *P*-4*n*2. Shown in the adjacent figure, $K_4CaUSi_4O_{14}$ belongs to a family of compounds that

Relationship of the known Fresnoite type compounds
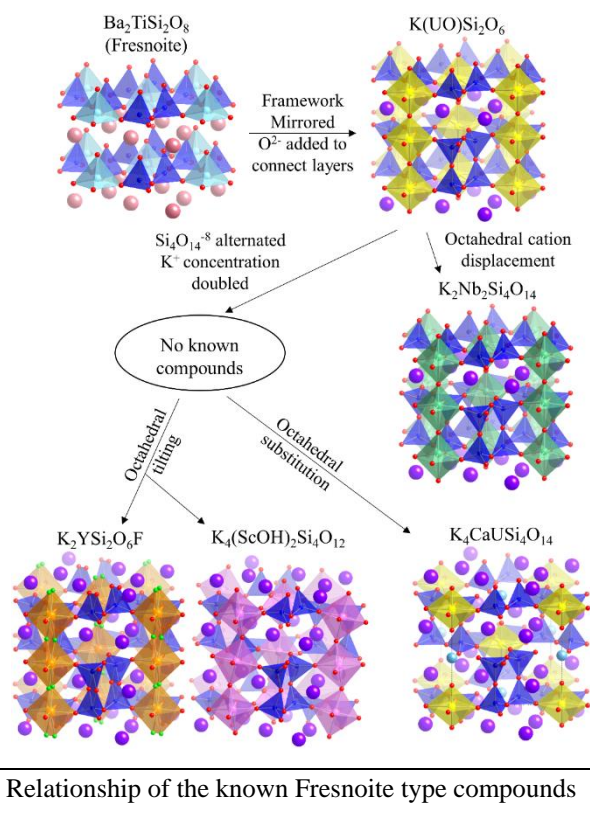
are conceptually obtained from Fresnoite by mirroring the framework. $K_4CaUSi_4O_{14}$ is unique from the rest of the family because Ca^{+2} cations substitute onto every other octahedral site. This substitution of a low valent cation onto the octahedral site serves to charge balance the U(VI) and allows for the uranyl oxygens to only further bond to low valent, K^+ and Ca^{+2}, cations. The substitution also leads the structure to be non-centrosymmetric and $K_4CaUSi_4O_{14}$ was found to be weakly SHG active.
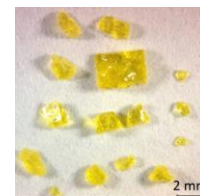
Single crystals of $K_4CaUSi_4O_{14}$

$[NaK_6F][(UO_2)_3(Si_2O_7)_2]$ and $[KK_6Cl][(UO_2)_3(Si_2O_7)_2]$
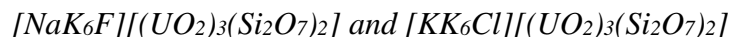
$[NaK_6F][(UO_2)_3(Si_2O_7)_2]$ and $[KK_6Cl][(UO_2)_3(Si_2O_7)_2]$ crystallize in the $[NaRb_6F][(UO_2)_3(Si_2O_7)_2]$ structure type with space group *Pnnm*. The two compounds were synthesized using mixed halide, NaF/KF or KF/KCl, flux. Importantly, the growth of $[NaK_6F][(UO_2)_3(Si_2O_7)_2]$ was found to be very reaction vessel dependent. While $[KK_6Cl][(UO_2)_3(Si_2O_7)_2]$ readily forms even in shallowly filled crucibles, $[NaK_6F][(UO_2)_3(Si_2O_7)_2]$ could only be grown in reactions which had a small surface area to volume ratio. In the $[AB_6X][(UO_2)_3(Si_2O_7)_2]$ structure, the uranyl silicate framework create channels in the *c* direction which are occupied by octahedral K_6X (X = F, Cl) salt inclusions. Both compounds exhibit the typical yellow-green luminescence of the uranyl group. However, the luminescent intensity of $[KK_6Cl][(UO_2)_3(Si_2O_7)_2]$ is much weaker, probably due to quenching by the Cl^- ion.

$K_{13}FU_6Si_8O_{40}$

Using the synthetic conditions developed for the growth of $[NaK_6F][(UO_2)_3(Si_2O_7)_2]$, we grew the first intergrowth uranyl silicate. $K_{13}FU_6Si_8O_{40}$ was growth from a KF/KBr flux and crystallizes in the space group $P2_12_12_1$. The structure consists of an *ABAB* stacking of two slabs related to known uranium silicates, highlighted by its structural formula $\{(K_5F)[(UO_2)_2O]_2(Si_4O_{12})\}\{K_8(UO_2)_2(Si_2O_7)_2\}$. The $\{(K_5F)[(UO_2)_2O]_2(Si_4O_{12})\}$ slab is related to our previously reported Cs_2USiO_6 and consists of uranyl silicate rings occupied by a K_5F salt-inclusion. The $\{K_8(UO_2)_2(Si_2O_7)_2\}$ slab is structurally related to the

Structure of $K_8(K_5F)U_6Si_8O_{40}$ with U (orange), Si (blue), K (purple), F (green), and O (red)

U(VI) slab of $[Na_9F_2][(UO_2)(UO_2)_2(Si_2O_7)_2]$. $K_{13}FU_6Si_8O_{40}$ luminesces intensely at room-temperature and its luminescence is influence by the unique bonding in the $[(UO_2)_2O]$ unit.

Cesium halide salt-inclusion uranyl silicates

Motivated by our success in growing potassium halide salt-inclusion uranyl silicates, we decided to target cesium halide salt-inclusion uranyl silicates. Cesium containing uranium compounds are particularly of interest as Cs is one of the most abundant fission products. Cesium containing salt-inclusion uranyl silicates could possibly be used as nuclear waste storage materials as they are capable of immobilizing multiple constituents of spent nuclear fuel. Our exploration of the U-Si-O-CsCl/CsF phase space led us to develop a second enhancement for the flux growth of salt-inclusion compounds, the use of halide precursors. Seen in the figure below, we have successfully grown four new salt-inclusion uranyl silicates, three of which could only be grown

using UF_4, as opposed to UO_2 or U_3O_8, as the uranium source. Several new compositions were prepared and their structures determined, including $[Cs_3F][(UO_2)(Si_4O_{10})]$, which crystallizes in the orthorhombic space group *Imma*. The structure contains channels within the uranyl silicate framework that are occupied by face sharing Cs_6F octahedra. $[Cs_2Cs_5F][(UO_2)_3(Si_2O_7)_2]$ crystallizes in the monoclinic space group $P2_1/n$. The structure contains the same uranyl silicate
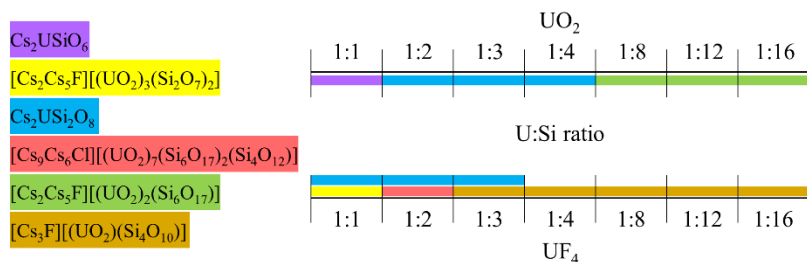
Uranyl silicate products of reactions with varying U:Si ratios using either UO_2 (top) or UF_4 (bottom) as the uranium source. Reaction products were determined by PXRD

framework as $[NaK_6F]$ $[(UO_2)_3(Si_2O_7)_2]$ and $[KK_6Cl]$ $[(UO_2)_3(Si_2O_7)_2]$, although it is monoclinically distorted. However, due to the large size of the Cs cations, the salt-inclusion has rotated and distorted to become a Cs_5F salt-inclusion. $[Cs_2Cs_5F]$ $[(UO_2)_2(Si_6O_{17})]$ crystallizes in the orthorhombic space group $P2_12_12$. The structure consists of a different uranyl silicate framework than $[Cs_2Cs_5F]$ $[(UO_2)_3(Si_2O_7)_2]$ but contains channels that are filled in a very similar fashion by the salt-inclusion, again Cs_5F. $[Cs_9Cs_6Cl][(UO_2)_7(Si_6O_{17})_2(Si_4O_{12})]$ crystallizes in the triclinic space group *P*-1. Following $K_{13}FU_6Si_8O_{40}$, it is the second example of a uranyl silicate containing more than one silicate motif. The structure contains both Si_6O_{17} chains and Si_4O_{12} squares, which combined with the uranyl units, create channels in which the octahedral Cs_6Cl salt-inclusion sits.
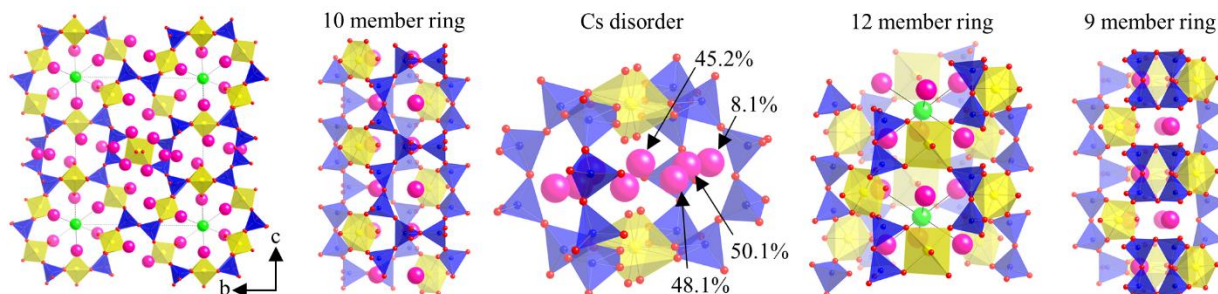
The structure of $[Cs_9Cs_6Cl][(UO_2)_7(Si_6O_{17})_2(Si_4O_{12})]$ (**4**) showing, from left to right, the view down the *a*-axis, the channel created by the 10-member ring, the environment around the disordered Cs sites, the channel created by the 12-member ring, and the channel created by the 9-member ring. Silicate polyhedra are shown in blue, uranium polyhedra in yellow, cesium atoms in pink, and fluorine atoms in green, and oxygen atoms in red.

Future Plans

Salt Inclusion Complexes: We have developed a successful methodology for preparing uranyl salt inclusion complexes and will pursue the synthesis and structural investigation of additional members. We have nice preliminary results that show scintillating behavior in these type of materials and we will further investigate their performance as a function of halide ion, anion, and crystal structure.

Complex Uranium Containing Fluorides: We have developed several methods for synthesizing new quaternary fluorides containing first row transition elements. We are now targeting more complex structures containing, in addition to 2nd and 3rd row transition elements, rare earth cations. Finally, with our new mild hydrothermal approach we should be able to systematically expand this work and create crystals of both compositionally known but not structurally characterized systems as well as of completely new systems.

Silicates: In addition to salt inclusion complexes we have synthesized several new silicates including some in new structure types. We will expand this to other tetragens and will focus on the incorporation of rare earth cations.

Publications

Morrison, G., Smith, M. D., zur Loye, H.-C., "Understanding the Formation of Salt-Inclusion Phases: An Enhanced Flux Growth Method for the Targeted Synthesis of Salt-Inclusion Cesium Halide Uranyl Silicates", DOI: 10.1021/jacs.6b03205. J. Am. Chem. Soc, **2016**, in print.

Grzechnik, A., Yeon, J., zur Loye, H.-C., Friese, K., "High-pressure behaviour of $Cs_2V_3O_8$", DOI:10.1016/j.jssc.2016.03.041J. Solid State Chem., **2016**, *238*, 252-258.

Morrison, G., Tran, T. T., Halasyamani, P. S., zur Loye, H.-C., "$K_8(K_5F)U_6Si_8O_{40}$: An Intergrowth Uranyl Silicate", DOI:10.1021/acs.inorgchem.6b00242. Inorg. Chem., **2016**, *55*, 3215-3217.

Yeon, J., Smith, M. D., Tapp, J., Möller, A., zur Loye, H.-C., "Mild Hydrothermal Crystal Growth of New Uranium(IV) Fluorides, $Na_{3.13}Mg_{1.43}U_6F_{30}$ and $Na_{2.50}Mn_{1.75}U_6F_{30}$: Structures, Optical and Magnetic Properties", DOI: 10.1016/j.jssc.2015.04.036. Special Issue on Crystal Growth. J. Solid State Chem., **2016**, *236*, 83-88.

Morrison, G., zur Loye, H.-C., "Flux Growth of $[NaK_6F][(UO_2)_3(Si_2O_7)_2]$ and $[KK_6Cl][(UO_2)_3(Si_2O_7)_2]$: The Effect of Surface Area to Volume Ratios on Reaction Products", DOI: doi.org/10.1021/acs.cgd.5b01408. Cryst. Growth Design, **2016**, *16*, 1294-1299.

Read, C. M., Smith, D. M., zur Loye, H.-C., "Synthesis, Crystal Structure, and Optical Properties of a New Complex Uranium Oxychloride, KUO_3Cl", DOI:10.1007/s10870-015-0612-0. J. Chem. Cryst. **2015**, *45*, 440-444.

Felder, J. B., Yeon, J., zur Loye, H.-C., "Synthesis of Anhydrous K_2TiOF_4 via a Mild Hydrothermal Method", DOI: 10.1016/j.solidstatesciences.2015.08.012. Solid State Sci., **2015**, *48*, 212-217.

Yeon, J., Felder, J. B., Smith, M. D., Morrison, G., zur Loye, H.-C., "Synthetic Strategies for New Vanadium Oxyfluorides Containing Novel Building Blocks: Structures of V(IV) and V(V) Containing $Sr_4V_3O_5F_{13}$, $Pb_7V_4O_8F_{18}$, $Pb_2VO_2F_5$, and Pb_2VOF_6", DOI:10.1039/c5ce01464f . CrystEngComm, **2015**, *17*, 8428-8440. *CrystEngComm* Hot Article.

Read, C. M., Morrison, G., Yeon, J., Smith, M. D., zur Loye, H.-C., "$A_2MnU_3O_{11}$ (A = K, Rb) and $Li_{3.2}Mn_{1.8}U_6O_{22}$: Three New Alkali-Metal Manganese Uranium(VI) Oxides Related to Natrotantite", DOI:10.1021/acs.inorgchem.5b01004. Inorg. Chem., **2015**, *54*, 6993-6999.

Morrison, G., Ramanantoanina, H., Urland, W., Smith, M. D., zur Loye, H.-C., "Flux Synthesis, Structure, Properties, and Theoretical Magnetic Study of Uranium (IV) Containing $A_2USi_6O_{15}$ (*A* = K, Rb) with an Intriguing Green-to-Purple, Crystal-to-Crystal Structural Transition in the K Analogue", DOI:10.1021/acs.inorgchem.5b00556. Inorg. Chem., **2015**, *54*, 5504-5511.

Morrison, G., Smith, M. D., Tran, T. T., Halasyamani, P. S., zur Loye, H.-C., "Synthesis and Structure of the New Pentanary Uranium (VI) Silicate, $K_4CaUSi_4O_{14}$, a Member of a Structural Family Related to Fresnoite", DOI: 10.1039/C5CE00504C. CrystEngComm, **2015**, *17*, 4218–4224.

Read, C. M., Gordon, E. E., Smith, M. D., Yeon, J., Morrison, G., Whangbo, M.-H., zur Loye, H.-C., "Synthesis of the Layered Quaternary Uranium Containing Oxide $Cs_2Mn_3U_6O_{22}$ and Characterization of its Magnetic Properties", DOI:10.1021/acs.inorgchem.5b00552. Inorg. Chem., **2015**, *54*, 5495-5503.

Read, C. M., Smith, M. D., Withers, R., zur Loye, H.-C., "Flux Crystal Growth and Optical Properties of Two Uranium-Containing Silicates: A_2USiO_6 (*A* = Cs, Rb)", DOI:10.1021/acs.inorgchem.5b00364. Inorg. Chem., **2015**, *54*, 4520–4525.

Yeon, J., Smith, M. D., Morrison, G., zur Loye, H.-C., "Trivalent Cation Controlled Phase Space of New U(IV) Fluorides, $Na_3MU_6F_{30}$ (M = Al^{3+}, Ga^{3+}, Ti^{3+}, V^{3+}, Cr^{3+}, Fe^{3+}): Mild Hydrothermal Synthesis Including an In Situ Reduction Step, Structures, Optical, and Magnetic Properties", DOI:10.1021/ic5030857. Inorg. Chem., **2015,** *54*, 2058-2066.

Morrison, G., Read, C. M., Smith, M. D., zur Loye, H.-C., "Flux Crystal Growth and Structural Analysis of Two Cesium Uranium Oxides, $Cs_{2.2}U_5O_{16}$ and $Cs_2U_4O_{13}$, Containing Multiple Cation-Cation Interactions", DOI:10.1039/c4ce02430c CrystEngComm,. **2015**, *17*, 1968-1974.

Morrison, G., zur Loye, H.-C., "Simple Correction for the Sample Shape and Radial Offset Effects on SQUID Magnetometers: Magnetic Measurements on Ln_2O_3 (*Ln* = Gd, Dy, Er) Standards", J. Solid State Chem., **2015**, *221*, 334-337.

Read, C. M., Smith, D. M., zur Loye, H.-C., "Single Crystal Growth and Structural Characterization of a Novel Mixed-Valent Ternary Uranium Oxide, $K_8U_7O_{24}$", DOI:10.1007/s10870-014-0555-x. J. Chem. Cryst., **2014**, *44*, 604-608.

POSTER SESSIONS

Soft Nanoparticles: Novel Additives for Polymer Matrices
        Vera Bocharova, Oak Ridge National Laboratory

Synthesizing New Metal Organic Frameworks with Tailored Physical and Chemical Properties
        Yves Chabal, University of Texas, Dallas

Two-Dimensional Chalcogenide Nanomaterials
        Yi Cui, SLAC

Cluster/Carbon Composite Materials for Energy
        Larry A. Curtiss, ANL

Fundamental Charge Transfer Processes in Stable Free-Radical Organic Polymer Systems
        Thomas Gennett, NREL

Transmetalation Reactions in the Syntheses of Phosphorescent Cyclometalates
        Thomas G. Gray, Case Western Reserve University

Using Tapering to Control Block Polymer Microstructure and Dynamics: Joint Theory and Experimental Effort
        Lisa Hall, Ohio State University

Crystallization-Driven Assembly of Conjugated-Polymer-Based Nanostructures
        Ryan C. Hayward, University of Massachusetts, Amherst

Statically Polarized Polymer Heterostructures for Charge Carrier Density Control in Energy-Relevant Semiconductors
        Howard Katz, Johns Hopkins University

Hydrothermal Synthesis and Structural Comparison of Novel Rare Earth Tantalates and Titanates: $Ln_2TaO_5(OH)$ (Ln = La, Pr), $Ln_3Ta_2O_9(OH)$ (Ln = Pr, Nd), and $Ln_5Ti_4O_{15}(OH)$ (Ln = La-Er)
        Joseph Kolis, Clemson University

The Nature of Charge Storage in Nitroxide Radical Polymers
        Jodie Lutkenhaus, Texas A&M University

Materials and Interfacial Chemistry for Next Generation Electrical Energy Storage
        Ram Manthiram, University of Texas, Austin and Sheng Dai, Oak Ridge National Laboratory

Diamondoid Science and Application: Conductive Solid-Core Metal-Organic Chalcogenide Nanowires and Enhanced Field Emission Sources
>   Nicholas Melosh, SLAC

Innovative and Complex Metal-Rich Materials
>   Anja Mudring, Ames Laboratory

Fundamental Ion-Association and Acid-Base Behavior of Aqueous Species
>   May Nyman, Oregon State University

Experimental and Computational Studies of Stable Radical Polymers in Confined Environments
>   Christopher Ober, Cornell University

Activation of Hydrogen under Ambient Conditions by Main Group Molecules
>   Philip P. Power, University of California, Davis

Transition Metal Oxides Nanomaterials for Aqueous Electrochemical Energy Storage
>   Xiaowei Teng, University of New Hampshire

Domain Interface Tomography and Chain Trajectories in Ordered Block* Polymer Microdomains
>   Ned Thomas, Rice University

Functionalization of π-Extended Porphyrins and Their Applications in Dye-Sensitized Solar Cells
>   Hong Wang, Miami University

POSTER SESSION 2 – Wednesday, July 13, 2016 4:30–6:00PM

High Efficiency Biomimetic Organic Solar Cells
>   Marc Baldo, MIT

Programming Function via Soft Materials
>   Paul Braun, University of Illinois at Urbana-Champaign

Clarifying the Structure of CsPb(Br,I)$_3$ Perovskite Quantum Dots
>   Richard Brutchey, University of Southern California

Design of Next Generation Thermoelectrics
>   Vinayak Dravid, Northwestern University

Scalable Growth of Perovskite Microplate Crystal Array and Their Charge Transport Properties
>   Xiangfeng Duan, UCLA

Toward the Rational Design of Glassy Polymers
>   Karl Freed, University of Chicago

"Giant" Nanocrystal Quantum Dots: Ideal Platforms for Intrinsic and Extrinsic Manipulation of Carrier-Recombination Processes
>   Jennifer A. Hollingsworth, Los Alamos National Laboratory

New Techniques for Measuring Diverse Static and Dynamic Physico-Chemical Interactions at the Sub Nano-, Micro-, and Macro-Scales
>   Jacob Israelachvili, University of California, Santa Barbara

Composite Organic and Topological Insulator Heterostructures
>   Howard Katz, Johns Hopkins University

Nuclear Magnetic Resonance (NMR) Program at LBNL
>   Jonathan King, Lawrence Berkeley National Laboratory

Unconventional Clathrates based on Transition Metal Pnictides
>   Kirill Kovnir, University of California, Davis

Defect Tolerance to Intolerance in Perovskite Halide Semiconductors
>   James R. Neilson, Colorado State University

Hydroxide Conductors for Energy Conversion Devices
    Bryan Pivovar, NREL

Dielectric Ceramics in Nanosheet Form
    Tina Salguero, University of Georgia

Chemical and Mechanical Properties of Surfaces, Interfaces and Nanostructures
    Miquel Salmeron, Lawrence Berkeley National Laboratory

Hybrid Halide Perovskites: Novel Materials with Contraindicated Properties
    Ram Seshadri, University of California, Santa Barbara

Surface Passivation and Surface States of Inorganic Nanocrystals
    Lin-wang Wang, Lawrence Berkeley National Laboratory

Toward Hierarchically Structured Nanocomposite
    Ting Xu, Lawrence Berkeley National Laboratory

Why Do Hybrid Lead-Halide Perovskites Behave as Defect-Free and Nonpolar Semiconductors?
    Xiaoyang Zhu, Columbia University

A Synthetic Strategy to Prepare New Complex Uranium- and Thorium-Containing Oxides: Predictive Solid State Synthesis of New Composition using Radius Ratio Rules and Materials Discovery based on Crystal Growth from High Temperature Solutions
    Hans-Conrad zur Loye, University of South Carolina

AUTHOR INDEX

279

PARTICIPANT LIST

Name	Organization	Email
Alivisatos,Paul	University of California, Berkeley	paul.alivisatos@berkeley.edu
Armitage,Norman	Johns Hopkins University	npa@pha.jhu.edu
Baldo,Marc	Massachusetts Institute of Technology	baldo@mit.edu
Bobev,Svilen	University of Delaware	bobev@udel.edu
Bocharova,Vera	Oak Ridge National Laboratory	bocharovav@ornl.gov
Bragg,Arthur	Johns Hopkins University	artbragg@jhu.edu
Braun,Paul	University of Illinois	pbraun@illinois.edu
Brutchey,Richard	University of Southern California	brutchey@usc.edu
Chen,Qian	University of Illinois, Urbana-Champaign	qchen20@illinois.edu
Cohen,Seth	University of California, San Diego	scohen@ucsd.edu
Cui,Yi	Stanford University	yicui@stanford.edu
Curtiss,Larry	Argonne National Laboratory	curtiss@anl.gov
Dadmun,Mark	Oak Ridge National Laboratory	dad@utk.edu
Dai,Sheng	Oak Ridge National Laboratory	dais@ornl.gov
De Yoreo,James	Pacific Northwest National Laboratory	james.deyoreo@pnnl.gov
Dravid,Vinayak	Northwestern University	v-dravid@northwestern.edu
Duan,Xiangfeng	University of California, Los Angeles	xduan@chem.ucla.edu
Dunbar,Kim	Texas A&M University	dunbar@mail.chem.tamu.edu
Epps,Thomas	University of Delaware	thepps@udel.edu
Feng,Pingyun	University of California, Riverside	pingyun.feng@ucr.edu
Fischer,Felix	University of California, Berkeley	ffischer@berkeley.edu
Fischer,Peter	Lawrence Berkeley National Laboratory	PJFischer@lbl.gov
Freed,Karl	University of Chicago	freed@uchicago.edu
Fuchs,Gregory	Cornell University	gdf9@cornell.edu
Gennett,Thomas	National Renewable Energy Laboratory	thomas.gennett@nrel.gov
Grason,Gregory	University of Massachusetts, Amherst	grason@mail.pse.umass.edu
Gray,Thomas	Case Western Reserve University	tgray@case.edu

Hall,Lisa	Ohio State University	hall.1004@osu.edu
Hayward,Ryan	University of Massachusetts, Amherst	rhayward@mail.pse.umass.edu
Henderson,Craig	U.S. Department of Energy	Craig.Henderson@science.doe.gov
Hollingsworth,Jennifer	Los Alamos National Laboratory	jenn@lanl.gov
Horton,Linda	U.S. Department of Energy	Linda.Horton@science.doe.gov
Israelachvili,Jacob	University of California, Santa Barbara	jacob@engineering.ucsb.edu
Jin,Song	University of Wisconsin, Madison	jin@chem.wisc.edu
Kanatzidis,Mercouri	Northwestern University	m-kanatzidis@northwestern.edu
Katz,Howard	Johns Hopkins University	hekatz@jhu.edu
King, Jonathan	Lawrence Berkeley National Laboratory	jpking@lbl.gov
Klausen,Rebekka	Johns Hopkins University	klausen@jhu.edu
Kolis,Joseph	Clemson University	kjoseph@clemson.edu
Kovnir,Kirill	University of California, Davis	kkovnir@ucdavis.edu
Li,Jing	Rutgers University	jingli@rutgers.edu
Lutkenhaus,Jodie	Texas A&M University	jodie.lutkenhaus@tamu.edu
Manthiram,Arumugam	University of Texas, Austin	rmanth@mail.utexas.edu
Markovic,Nenad	Argonne National Laboratory	nmmarkovic@anl.gov
Matzger,Adam	University of Michigan	matzger@umich.edu
Melosh,Nicholas	Stanford University	nmelosh@stanford.edu
Mudring,Anja-Verena	AMES Laboratory	mudring@iastate.edu
Nealey,Paul	Argonne National Lab/University of Chicago	nealey@uchicago.edu
Neilson,James	Colorado State University	james.neilson@colostate.edu
Nuzzo,Ralph	University of Illinois, Urbana-Champaign	r-nuzzo@illinois.edu
Nyman,May	Oregon State University	may.nyman@oregonstate.edu
Ober,Christopher	Cornell University	cko3@cornell.edu
Ong,Shyue Ping	University of California, San Diego	ongsp@eng.ucsd.edu
Pellin,Michael	Argonne National Laboratory	pellin@anl.gov
Pivovar,Bryan	National Renewable Energy Laboratory	bryan.pivovar@nrel.gov
Power,Philip	University of California	pppower@ucdavis.edu

Reich,Daniel	Johns Hopkins University	reich@jhu.edu
Salguero,Tina	University of Georgia	salguero@uga.edu
Salmeron,Miquel	Lawrence Berkeley National Laboratory	mbsalmeron@lbl.gov
Sarrao, John	Los Alamos National Laboratory	SARRAO@LANL.GOV
Schweizer,Kenneth	University of Illinois	kschweiz@illinois.edu
Sennett,Michael	U.S. Department of Energy	Michael.Sennett@science.doe.gov
Seshadri,Ram	University of California, Santa Barbara	seshadri@mrl.ucsb.edu
Somorjai,Gabor	Lawrence Berkeley National Laboratory	somorjai@berkeley.edu
Stamenkovic,Vojislav	Argonne National Laboratory	vrstamenkovic@anl.gov
Teng,Xiaowei	University of New Hampshire	xw.teng@unh.edu
Thomas,Edwin	Rice University	elt@rice.edu
Thonhauser,Timo	Wake Forest University	thonhauser@wfu.edu
Tirrell,Matthew	University of Chicago	mtirrell@uchicago.edu
Tolbert,Sarah	University of California, Los Angeles	tolbert@chem.ucla.edu
Tsukruk,Vladimir	Georgia Institute of Technology	vladimir@mse.gatech.edu
Wang,Hong	Miami University	wangh3@miamioh.edu
Wang,Lin-Wang	Lawrence Berkeley National Laboratory	lwwang@lbl.gov
Wright,John	University of Wisconsin, Madison	wright@chem.wisc.edu
Xu,Ting	University of California, Berkeley	Tingxu@berkeley.edu
Yuan,Hongtao	Stanford University	htyuan@stanford.edu
Zhu,Xiaoyang	Columbia University	xyzhu@columbia.edu
zur Loye,Hans-Conrad	University of South Carolina	zurloye@mailbox.sc.edu